MELCOR EVALUATION TECHNIQUES FOR GAS REDISTRIBUTION IN THE MHTGR REACTOR BUILDING FOLLOWING A DEPRESSURIZATION ACCIDENT SCENARIO

A Thesis

by

COLTEN ZACHARIAH BUENDEL

Submitted to the Graduate and Professional School of
Texas A&M University
in partial fulfillment of the requirements for the degree of

MASTER OF SCIENCE

Chair of Committee, Karen Kirkland
Committee Members, Maria King
Mark Kimber
Head of Department, Michael Nastasi

December 2021

Major Subject: Nuclear Engineering

ABSTRACT

A novel method of MELCOR model creation was used to produce 1/28th-scale and full-scale representations of the MHTGR reactor building to investigate the temporal and spatial movement of gas concentrations in support of a gas-cooled reactor safety study. The models were tested in a variety of coolant blowdown scenarios as a sensitivity study of the models. Simulation results compared favorably to expected trends seen in design documentation, a confirmation of model success. Further study of results found that little natural refill occurs in the models over the test period of 24 hours, as volumes are quickly voided with the blowdown of coolant, excluding scenarios were little blowdown occurred due to complex geometry. These models will be applied to guide the design of a planned experimental facility. The method of input creation, along with the models themselves, were thoroughly documented in the efforts for future research in this region.

DEDICATION

To my grandparents, Jack and Joann Bond, who pushed me to continue all my pursuits in life leading me to my continued higher education. Though you are both gone, your memory lives on in my continued education and my push to better myself.

ACKNOWLEDGEMENTS

I would like to first thank Dr. Karen Kirkland for her support and guidance through both my undergraduate and graduate career. She offered me a position in her research group that has guided me in furthering my education and pointing me in the direction I would like to look following gaining my degree. Without her belief in me I would not be in the position I am now.

I would also like to thank Dr. Mark Kimber and Dr. Maria King, who are the other members of my graduate advisory committee. I truly appreciate their time and technical advice, as well as their extensive comments and discussion of my work.

I would also like the profusely thank the MELCOR team at Sandia National Laboratories, for not only making the analysis code that forms the basis of this research but their quick and timely response to any posed questions or assistance. I would like to especially thank Chris Faucett who not only works on the MELCOR development team at SNL, but continues his education here at Texas A&M. He assisted me many times for what may have been to him been to him trivial questions but helped me greatly learn MELCOR intricacies and quirks, not to mention some late-night discussions that helped my models develop properly.

I would also like to thank my family for their support that they have given me throughout my higher education career, not only at the graduate level but as well as pushing me to continue during undergraduate when times were tough.

Finally, I would like to my girlfriend Alexis Ash. We first met my first month here at Texas A&M and since she has been at my side through both undergraduate and graduate school. She has been an invaluable help throughout our years together and has always backed me in bettering myself.

CONTRIBUTORS AND FUNDING SOURCES

Contributors

This thesis work was supervised by a thesis dissertation committee consisting of Professor Karen Kirkland and Professor Mark Kimber of the Department of Nuclear Engineering and Professor Maria King of the Department of Biological and Agricultural Engineering.

The dimensions provided for the model development in the Modeling Approach section were provided by Dr. Shripad Revankar of the School of Nuclear Engineering at Purdue University.

All other work conducted for this thesis was completed by the student independently.

Funding Sources

Graduate study was supported with funding from the US Department of Energy, Office of Nuclear Energy, for Federal Award Number DE-NE00008879 “Investigation of HTGR Reactor Building Response to a Break in Primary Coolant”. Purdue University is the Pass-Through Entity who subcontracted the project to TEES. This works content are solely the responsibility of the authors and do not necessarily represent the official views of the US Department of Energy, Office of Nuclear Energy and Purdue University.

NOMENCLATURE

2D	Two-Dimension
3D	Three-Dimension
ASME	American Society of Mechanical Engineers
CAD	Computer-Aided Design
CF	Control Function
CFD	Computational Fluid Dynamics
CPU	Central Processing Unit
CVH	Control Volume Hydrodynamics
DBE	Design Basis Event
DOE	Department of Energy
EQS	Equipment and Vent Shaft
EXEC	Executive
FL	Flow Path
GA	General Atomics
GT-MHR	Gas Turbine Modular Helium Reactor
HTGR	High-Temperature Gas Reactor
HVAC	Heating, Ventilation, and Air Conditioning
LWR	Light Water Reactors
MHTGR	Modular High-Temperature Gas Reactor
NCG	Noncondensible Gas
NGNP	Next Generation Nuclear Plant
NRC	Nuclear Regulatory Commission

PORV	Pressure-Operated Relief Valve
PRA	Probabilistic Risk Assessment
PSID	Preliminary Safety Information Document
PWR	Pressurized Water Reactor
RC	Reactor Cavity
RCCS	Reactor Cavity Cooling System
RPV	Reactor Pressure Vessel
RSC	Reserve Shutdown Control
SC-MHR	Steam Cycle Modular Helium Reactor
SGC	Steam Generator Cavity
SGV	Steam Generator Vessel
SMR	Small Modular Reactor
TMI	Three Mile Island
TRISO	Tri-structural Isotropic

TABLE OF CONTENTS

Page

LIST OF FIGURES

Page

LIST OF TABLES

Page

1. INTRODUCTION

Gas-cooled reactors, such as the Modular High Temperature Gas-Cooled Reactor (MHTGR) which is cooled by gaseous helium coolant, have been designed with large-scale containment structures similar to those employed by pressurized water reactors (PWR) reactors. In the condition of a blowdown following a break in the main coolant pressure boundary, high pressure and temperature helium would be vented into the reactor building structure where it would displace the present atmosphere. Post blowdown though, as refill of the reactor building atmosphere occurs from the outside environment, oxygen can potentially be drawn into the primary coolant system. If oxygen is of high enough concentration, and the nuclear core graphite is above oxidation temperature, the risk of oxidation reactions and oxygen burning increase greatly. A highly-exothermic combustion in the redistributed volumes becomes a safety concern.

MELCOR was chosen to simulate the reactor building and accident scenarios. While being a severe accident simulation code typically used in the evaluation of Light Water Reactors (LWRs), MELCOR capabilities have been expanded to better simulate High Temperature Gas-Cooled Reactors (HTGRs) by use of its system-level thermal hydraulics equations code basis. Previous research (Beeny and Vierow, 2015; Vierow et al., 2014) has shown the validity of MELCOR in simulation of HTGR abilities within the reactor pressure vessel (RPV) and within simplified reactor building volumes. As such, further work should be done to validate the ability of the code to handle accident scenarios of such reactors with more accurately modeled full reactor building volumes. The basis of this research was done as pursuant to a Department of Energy (DOE) project to better understand HTGR reactor building response to a primary coolant break, which is one of the most critical accident scenarios for a reactor to be tested under, a primary system break.

While originally conceived to be actively compared to data collected from an experimental test facility at Purdue University, the primary partner of the DOE project, complications due to the COVID-19 pandemic have led to delays in the experimental portions of the project. As such, the physical experimentation that was to be used in comparison to the simulation models will not be able to be used for MELCOR model validation. Instead, the reactor building model created herein will be put through a sensitivity study of the various components and layouts to determine their effect on accident progression. For this point, the "reactor building" will be identified as the silo structure containing the reactor and any connecting cavity until reaching the exterior atmosphere, an example of which can be seen in Fig. 1.1.

By providing an in-depth development process for a MELCOR input deck comprising of the full reactor building, in comparison to a simplistic volume, techniques are proposed for further research into reactor building response using MELCOR. The detailed thought process and creation path are also described with the expectation that the same development process can be adapted for other reactor buildings, with a focus mainly on HTGR reactors. This research is a first-of-a-kind application of MELCOR outside of its standard use-case with respect to both the complexity of the reactor building being simulated, and the tracking of specific gas species redistribution through the reactor building.

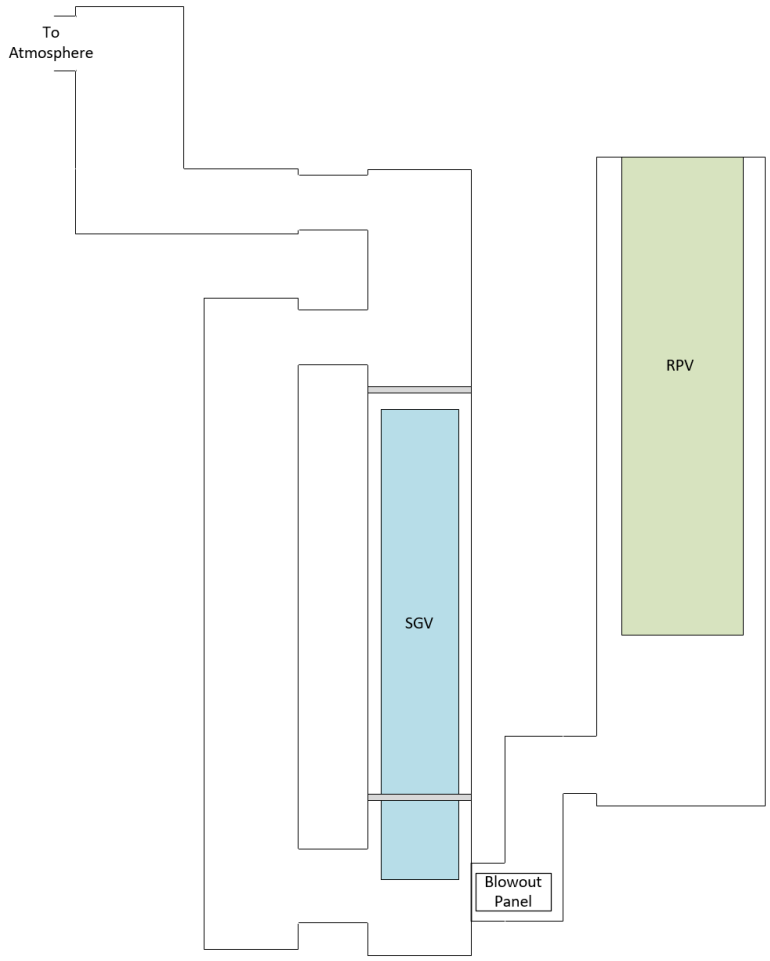

Fig. 1.1. Reactor Building Defined Space.

1.1 Thesis Objectives

The objectives set forth to be described in this thesis are the following:

- Develop modeling techniques for evaluating spatial and temporal gas concentrations in a gas-cooled reactor's reactor building structure.
- Implement into a reactor safety code and assess code capabilities ability for handling HTGR reactor building simulation in accident scenarios.
- Perform analysis to support the design and operation of an experimental facility to study oxygen concentrations throughout a scaled reactor building.

1.2 Significance of Work

The recent drive by the DOE to push reactor sizes smaller, in the range of Small Modular Reactors (SMRs), has created a new demand to look back at previous designs that fit those size and energy production levels. This has brought designs such as the General Atomics (GA) MHTGR back into the spotlight for research of feasibility as it has a smaller power rating but similar reactor building design as current reactors. This makes the reactor desirable for scalable reactor systems while also being contained within a below-grade silo. Being based on the standard two-loop heat transfer production model common in electricity production reactors keeps the reactor system familiar while also experiencing the benefits of the gas cooling of the reactor core. By creating a method where HTGR reactor buildings can be simulated accurately for depressurization scenarios with reinforcement from experimental data, this effort is intended to promote future endeavors to license and validate new reactor building designs.

Accurate analysis of spatial and temporal gas concentrations in large and complex volumes currently requires detailed and time-consuming techniques such as computational fluid dynamics (CFD). The analysis methodologies developed in this research for the reactor building will enable the first known simulations of gas concentrations in a reactor building by a systems-level reactor safety code, which has the ability to perform these simulations in a much more timely manner. As stated previously, research on gas diffusion in building atmospheres has been simulated through the use of CFD on experimental setups such as the PANDA facility, where striation of gas species is seen on large scale facilities (Paladino et al., 2010). CFD studies on HTGR reactor buildings have also been attempted, but to a much more simplified style of very limited and simplified geometries which do not show gas movement through a complex building geometry (Ham et al., 2013).

Research into loss of coolant accidents in reactor buildings has been performed very frequently for LWRs but not to a great extent for HTGRs. The typical specialization of reactor simulation codes does not lend greatly to dual capabilities of modeling an accurate reactor core and building that can properly show spatial changes of atmosphere. This has led to much research on the ability to link multiple codes in attempts to maintain a coherent simulation from reactor to building (Kang et al., 2021; Safarzadeh et al., 2021) with codes like TRACE, CONTAIN, RELAP5, and GOTHIC being interconnected to leverage their capabilities. Further evolutions of codes are allowing for greater individual capabilities in these regards, such as RELAP/SCDAPSIM and SPECTRA (Skolik et al., 2021; Stempniewicz, 2000), but they still approach the containment/reactor building in a much more simplified layout. MELCOR has previously been tested in comparison to CFD (Jeon et al., 2019) for gas redistribution in a LWR reactor primary coolant break, where it was shown to underestimate the diffusion of hydrogen from an LWR primary boundary break. While this research used a MELCOR approach similar to what is going to be done with this research, the LWR containment building lacks the complex flowing geometry of the HTGR reactor building being studied in this research.

Of the research comparable to the issue that is being approached in this research is that done of the NGNP reactor building, a later iteration on the MHTGR reactor being studied in this research (Haynes et al., 2017). This similar DOE-funded project approached the issue of a HTGR blowdown scenario in a similar manner to that of this research, but with a differing layout for flow of coolant in a blowdown scenario (Yang et al., 2018). The experimental setup of the project was simulated through the use of the GOTHIC code, where results were overall comparable with experimentally determined results of gas concentrations (Yildiz et al., 2018). The research being performed for this thesis will not only allow a further comparison between these individual reactor

designs but also the comparability of simulation codes, with GOTHIC being one of the few comparable codes to MELCOR that can simulate the gas flow of a HTGR blowdown through the reactor building, which is not possible on other systems-level accident codes like RELAP5.

Originality will come into the modeling by subdivision of key systems and structures to allow higher fidelity data to be collected about the reactor building than seen in previous research done with simulation codes. The benefits of this research will be analysis techniques that enable assessment of oxygen concentration in gas-cooled reactor buildings with sufficient accuracy to evaluate the design's safety characteristics, along with calculations that require less computational resources through the potential use a systems-level reactor safety code. Further, the new analysis techniques will be applied to support the design, construction, and operation of an experimental facility for high-fidelity measurements of oxygen concentrations in a scaled-down MHTGR reactor building at Purdue University that in the future will be able to be used for comparison to the simulation results presented in this research.

1.3 Technical Approach

MELCOR input decks were created for a $1/28^{th}$-scale experimental setup of the MHTGR reactor building designed by Purdue University, as well as for a model of the MHTGR following the same layout as the experimental setup but at full reactor scale. The primary source of reactor building information was provided by Purdue University from their scaling study to properly simulate the experimental setup, as well as the full-scale model. The Preliminary Safety Information Document (PSID) of the MHTGR also served as a major source of information for the input decks for operation conditions and primary coolant boundary break reference sizes.

Since reactor operation is not the major constituent of the research, focusing more on the reactor building response, the reactor pressure vessel is simplified down to a simple volume of

helium coolant at operating temperature and pressure. After iterations of initial models and input decks, the reactor building volumes were nodalized to gather more localized points of data for positions designated to be oxygen sensor locations in the experimental setup. Due to the lack experimental confirmation data or replicable scenarios in safety documentation, a sensitivity study will be performed by changing primary coolant boundary break locations and flow paths.

A custom testing regime was created to test both models under a variety of scenarios that include two different break locations, that are different sizes, and 3 different layout changes. Layout changes were made to force the flow through a variety of routes through the reactor building in an effort to determine the effect on the blowdown progression. A comparison of the two models' responses to the scenarios should help indicate any potential differences in the experimental setup and a true reactor building.

1.4 Thesis Overview

Chapter 2 gives an overview of the MHTGR general design and the design of its reactor building structure that is the basis of this research. Chapter 3 describes the features of MELCOR being used in the research and their functions, mechanics, and concepts. Chapter 4 gives a basic overview of the process that was used to process and create the input decks behind this research, with sufficient detail to enable the process to be repeated and applied to other HTGR designs. Chapter 4 continues by describing the collation of information, design of models, and implementation into code of the MELCOR input decks for the MHTGR for the purposes of this research. Chapter 5 outlines the testing methodology created to test the models under various conditions for the sensitivity study. Chapter 6 presents the results gathered from the MELCOR simulations tested under the developed methodology and discusses the data that was found in relation to the known results and comparisons to baseline simulations, differing scales, and

different tested scenarios. Chapter 7 develops the conclusions garnered from the research and proposes expansions and recommendations for continuing research of similar purpose. The appendices included in the conclusion of the paper will describe in tabular format the input deck information for comparison and replication of the evaluated scenarios as well as inclusion of any result figures excluded from Chapter 6.

2. MHTGR DESCRIPTION

2.1 Brief History of MHTGR

Increased demand from utilities led to the formation of the Gas Cooled Reactor Associates (GCRA) following the post nuclear market collapse of the mid 1970's to explore the commercialization of the gas-cooled reactors that had been successfully demonstrated with Peach Bottom 1 and Fort St. Vrain, even with its many issues and extensive downtime (Williams et al., 1994). This led to the creation of designs like the MHTGR, which is a reactor concept that was created by GA starting in the early 1980's. In 1986 the PSID of the MHTGR was submitted to the Nuclear Regulatory Commission (NRC) for approval.

The base MHTGR design has since went through many iterations including a 450 MW expanded version of the base 350 MW design, the Gas Turbine Modular Helium Reactor (GT-MHR), and the Steam Cycle Modular Helium Reactor (SC-MHR) which was chosen for the Next Generation Nuclear Plant (NGNP) project. These designs have come from experience gained by the US nuclear industry and worldwide partners on the creation and operation of gas-cooled reactors. In the US specifically, the design, construction, and operation of the before-mentioned Peach Bottom 1 and Fort St. Vrain was used as the basis for the design of the MHTGR. Peach Bottom 1 was an experimental helium-cooled prismatic core reactor with a 40 MW_e output located in Peach Bottom Township, Pennsylvania. It operated successfully from June 1967 to its shutdown in October 1974 due to successful demonstration of gas cooled commercialized reactors (Williams et al., 1994). The success of Peach Bottom 1 led to the creation of the Fort St. Vrain near Platteville, Colorado, the first, and only, commercialized gas-cooled reactor in the US. Fort St. Vrain was also a helium-cooled prismatic core reactor but with a much larger 330 MW_e output. During its operation period, from 1976 to 1989, it was plagued with a number of first adopter issues that

eventually were corrected and the reactor enjoyed a period of high uptime near its closure, which was early due to costly issues being discovered during maintenance (Brey, 1991).

With the nearly 20 years of domestic commercial operating gas cooled reactor experience, as well as experience from gas-cooled reactors around the world, gas-cooled reactors have become a hot topic for consideration in the current energy market. Even through the differing iterations across the preceding decades that have changed the MHTGR, its base concept as a modular gas-cooled reactor system remains the core of those designs. The design, which is much different than the large-scale, large electrical output reactors that are in use currently, opts for a smaller output from units that could modularly be added and linked as demand grew. This modular building system fits the current push for the DOE for smaller scaled reactors that can be placed in more remote locations without large-scale infrastructure need and even factory production.

2.2 MHTGR Objectives

The MHTGR was designed to be one of the first commercially viable, passively safe reactors to be the next generation of nuclear reactors to transition from the LWR's of the period, which are still operating to this day. The largest boon of the new designs of the time were the passive safety that they afforded, which in the time of post Three Mile Island (TMI), was of critical importance to an industry and nation fearful of the extent of a nuclear accident and release. Designed with features that could activate and operate with no operator interaction needed, along with features without active equipment, led to a safer design with inherent accident tolerance and safety.

By removing required operator action in the event progression, the human factor element in accident progression is eliminated because operator error and the inherent delay of human interaction are negated. Also, the removal or decreased reliance on active equipment, those with

mechanically moving parts and/or relying on a power source, increases the reliability of safety systems in accident scenarios by removing modes of failure for moving components. These hands-free safety systems make the MHTGR desirable close to 40 years after its initial design.

2.3 MHTGR Design General Description

The MHTGR has many of the same features as basic High-Temperature Gas Reactors (HTGRs) including graphite moderator, ceramic Tri-structural Isotropic (TRISO) fuel, and a gaseous coolant (helium in this case). It incorporates several passive safety features to further increase the safety of operation, and the modular design makes it economically scalable to a desired size. Even though this design is currently nearing 40 years old, the MHGTR is receiving renewed attention for its feature set, size, and modularity.

Many of the before-mentioned features of HTGRs are some of the MHTGRs biggest safety features. The helium coolant is inert and single-phase and cannot undergo flashing or phase change, no pumping cavitation or fluid level measurements are required, and the coolant has no chemical reactions with core materials leading to no undesirable effects such as oxidation heating or hydrogen production. The TRISO fuel used by the MHTGR is made with its own containment layer so that the fission products produced are not released, making the fuel much hardier against high fuel temperatures that could be seen in accident scenarios, decreasing the possibility of fuel failure. Finally, the graphite core of the reactor works in conjunction with the TRISO fuel and provides a wide thermal margin between operation and damage temperatures. The graphite core gives the reactor a large heat capacity and the low power density of operation gives the reactor very slow and deliberate temperature transients. With these safety features, combined with the uninsulated reactor vessel, the MHTGR is stated to be able to suffer a complete loss of coolant and forced circulation and keep its fuel under temperature levels of large fuel failure due to the core’s

ability to retain heat and disperse it to the reactor building environment slowly through the natural processes of conduction, convection, and radiation (General Atomics,1.3-6,1986).

2.3.1 Reactor Vessels, Core Layout, and Coolant Flow

The reactor core is of prismatic design utilizing an inner and outer reflector region to achieve its 350 MW_e power rating, as with no central reflector it would only be able to produce roughly 250 MW_e (General Atomics,4.1-7,1986). The standard active core layout can be seen in Fig. 2.1, where the inner and outer reflector regions are shown, as well as the control rod layout. All standard operation control rods are contained within the graphite elements of the core except the reserve shutdown control (RSC) rods which directly insert into fuel elements.

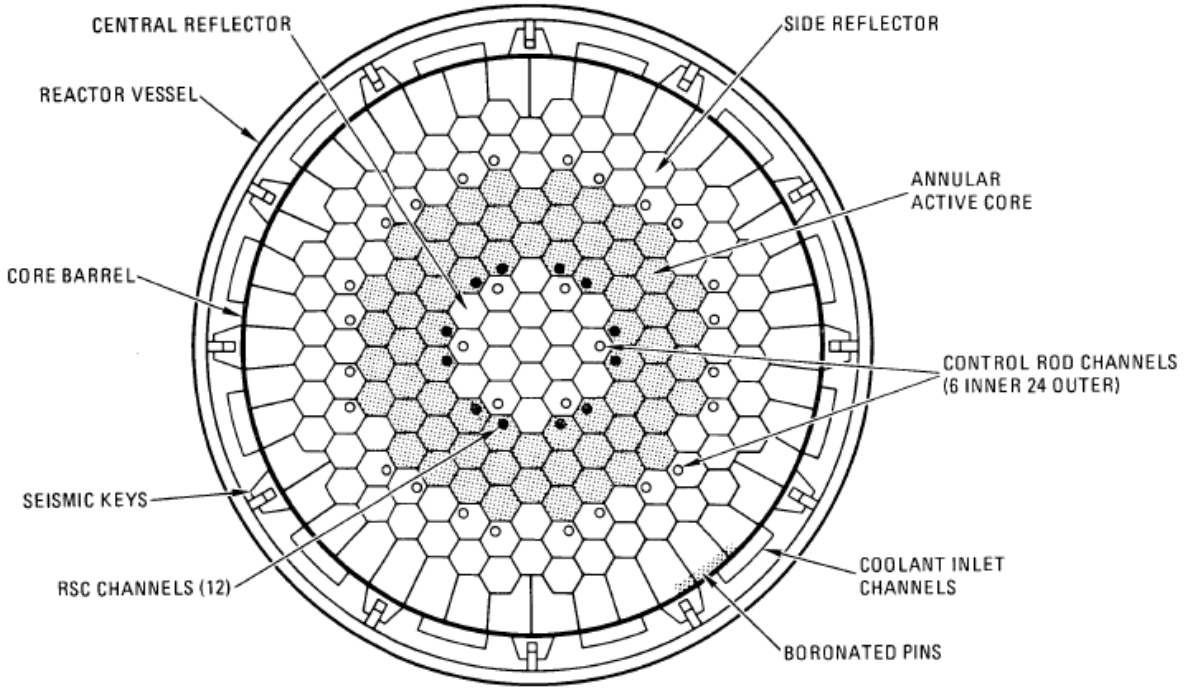

Fig. 2.1. Reactor Core Layout. Reprinted from (General Atomics, 1986).

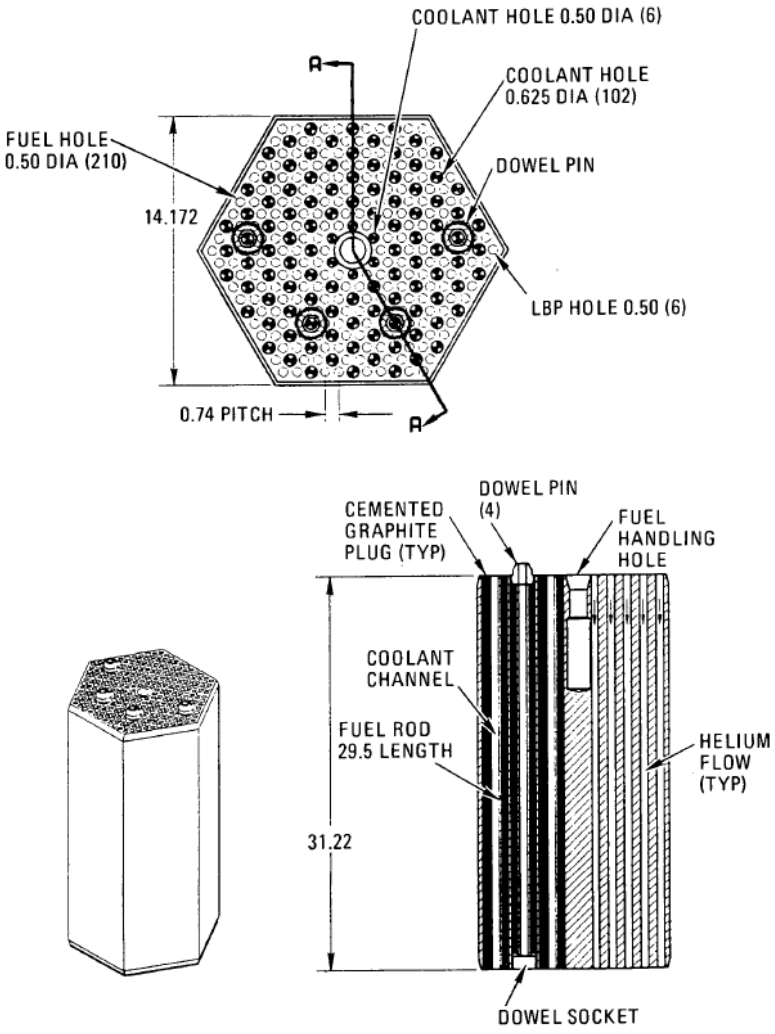

Fig. 2.2. Fuel Element. Reprinted from (General Atomics, 1986).

Each core element is hexagonal in shape with differing layouts if the element contains control rods, or if they are fuel or reflector elements. Fig. 2.2 illustrates the design of a standard fuel element. In the reactor core, fuel elements are stacked in columns 10 units high for the active region (General Atomics,4.1-7,1986), seen in Fig. 2.3. The graphite type used throughout the majority of the core is composed of H-451 graphite, but the lower plenum structure is made of 2020 graphite.

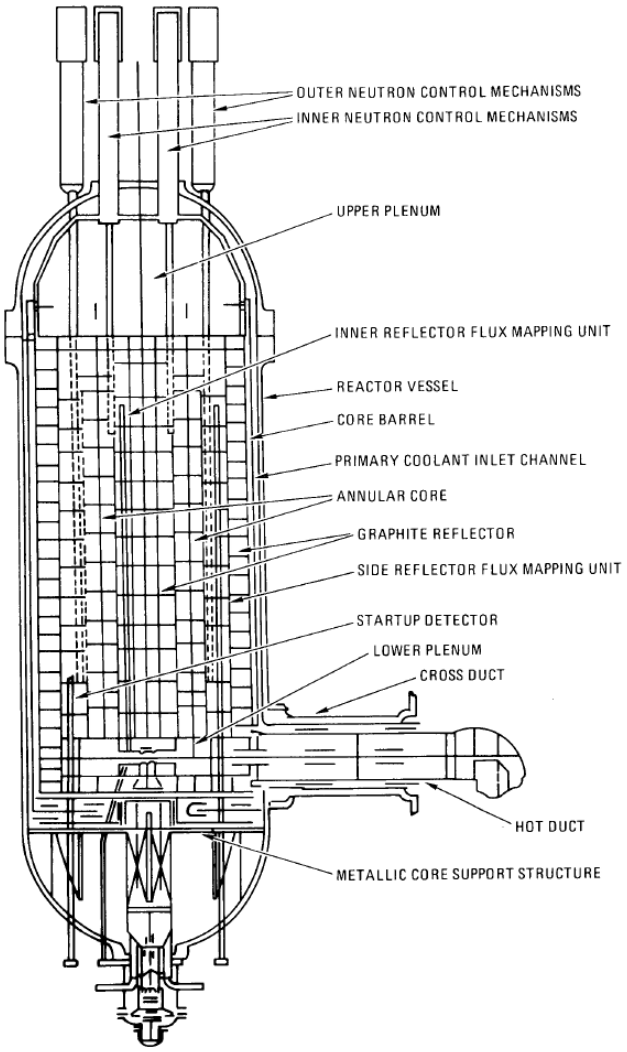

Fig. 2.3. Reactor Core Vertical Layout. Reprinted from (General Atomics, 1986).

The MHTGR primary coolant system is contained within a setup of two cross connected vessels, one containing the reactor core and the other containing the steam generator system, which can be seen in Fig. 2.4. The cross connection between the two vessels is an annular tube allowing the flow of coolant in both directions. The wall between the flowing coolant paths is insulated to prevent heating of the coolant by regeneration before it flows into the core. Both vessels are to be made of steel to meet the American Society of Mechanical Engineers (ASME) code for its operation conditions and lifetime.

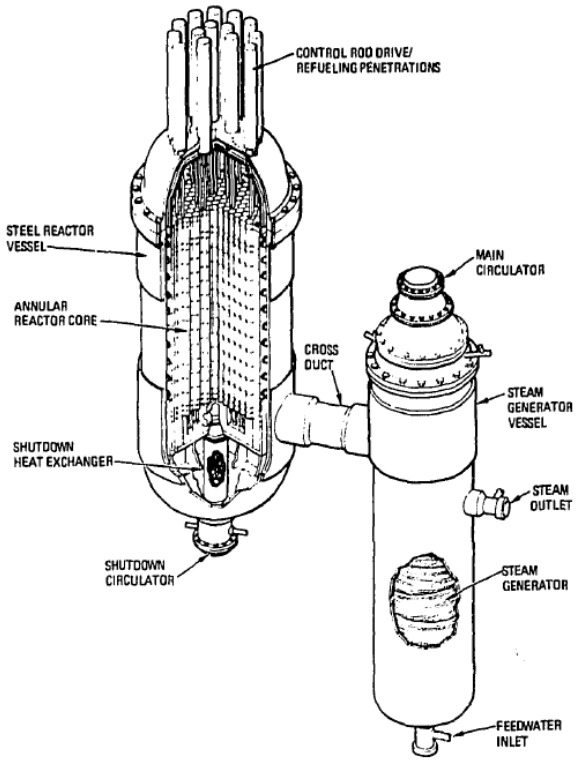

Fig. 2.4. Vessel Layout and Connections. Reprinted from (General Atomics, 1986).

The general flow path for coolant follows much the same flow path as a standard two-loop reactor. Beginning with the cooled coolant in the top of the steam generator with the main circulator, the coolant flows down and through the outer annulus of the crossduct to the RPV. Once in the RPV the coolant flows up and around the outer core containing the core inlet flow channels making its way to the RPV upper plenum. From the upper plenum, the coolant is pulled through the upper graphite through coolant channels and through the active core region where heat is transferred to the coolant from the heated graphite. Heated coolant flows out of the bottom graphite blocks where it turns and flows through the center of the crossduct, which is insulated to prevent regeneration of the cooled coolant. The heated coolant makes a turn downwards when it reaches the inner steam generator inlet plenum where it flows over the helical secondary coolant tubes containing water to be heated to steam. The primary coolant makes a 180 degree turn once it reaches the bottom steam generator plenum where it flows up the outer vessel and back to the main

circulator. An overview of the coolant flow is seen in Fig. 2.5, which has been enhanced with arrows giving general temperature variation based on color.

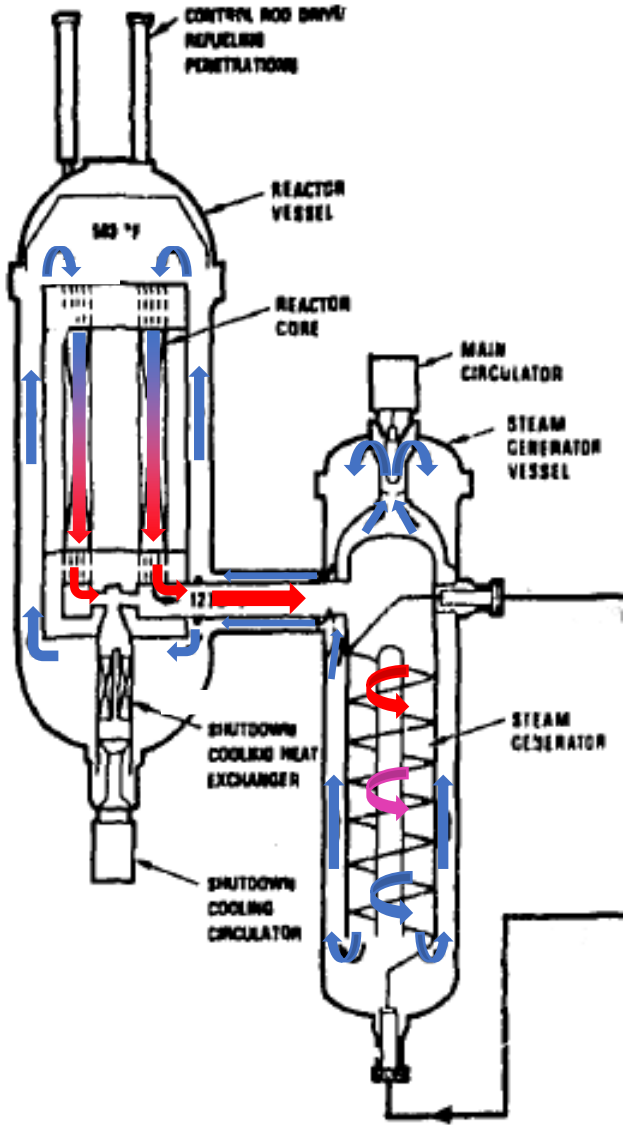

Fig. 2.5. Primary System Coolant Flow Paths, Enhanced with Colored Arrows. Reprinted from (General Atomics, 1986).

2.3.2 Reactor Building Layout and Modularity

Each MHTGR reactor system is contained in a below-grade concrete silo which is covered above-grade by a structure which can house multiple reactor silos as well as the steam turbine systems, as seen in Fig. 2.6. This figure gives an excerpt of the plot plan of the standard design

plant for the MHTGR with a focus on the reactor buildings. In the figure, the circles with the 1 indicator are the individual MHTGR silos with the large building containing the silos, indicated by the 3 and 4, being the reactor auxiliary building, which contains all the fuel handing equipment for all the reactors in a single space. The individual MHTGR steam generators are linked to their turbines housed in the building, indicated by 23, by a below grade system of steam pipes and return feedwater pipes, indicated by 2.

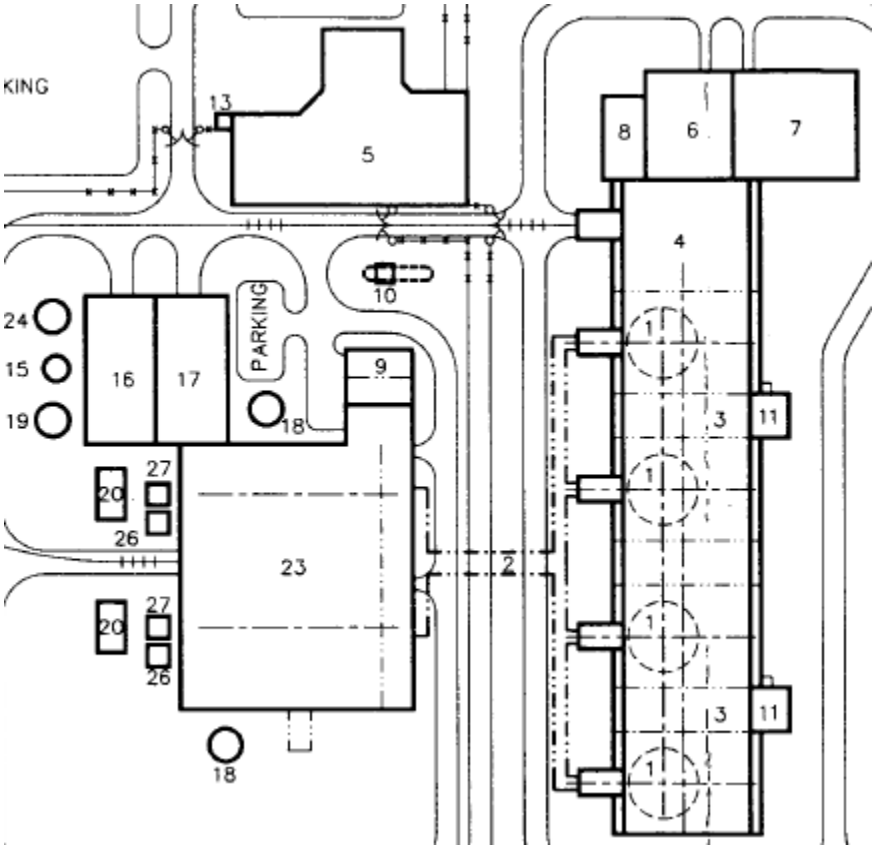

Fig. 2.6. Reactor Plant Layout. Reprinted from (General Atomics, 1986).

The MHTGR is modular in its design by allowing multiple reactors to be hooked into a central system of turbines to generate electricity. Reactors are paired into groups of 2 that feed steam to a singular turbine to produce electricity. The basic plant design is a setup of 4 MHTGR reactors setup with 2 turbines to provide 1400 MW_e. This design can be scaled down or up though lending to its value in remote or even large-scale applications.

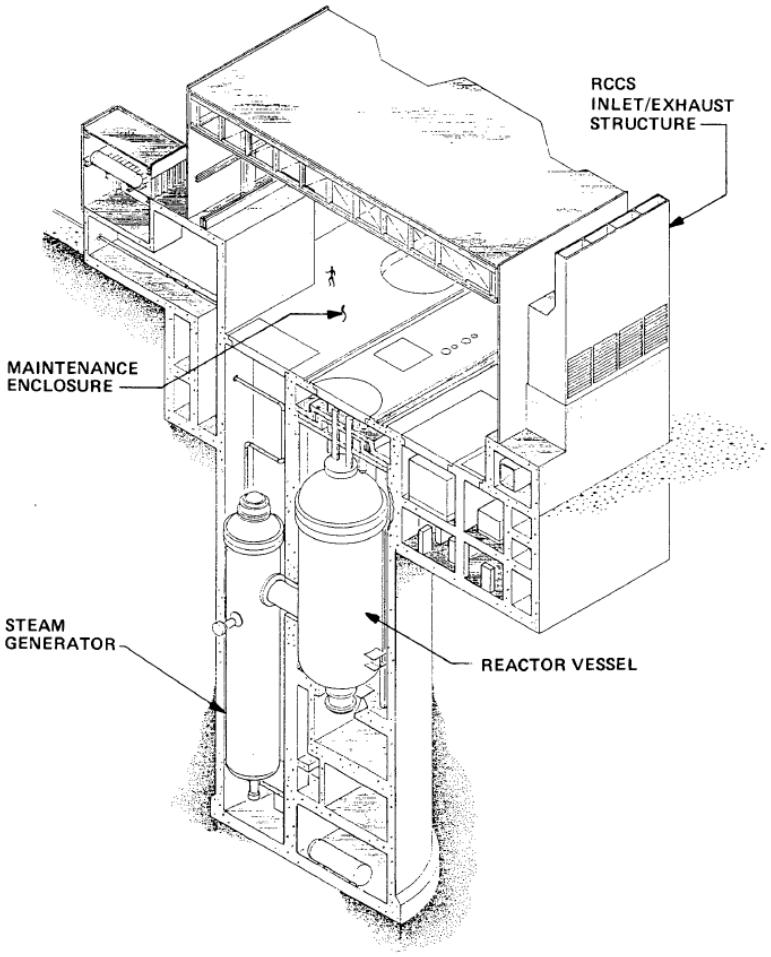

Fig. 2.7. Reactor Building Layout of MHTGR. Reprinted from (General Atomics, 1986).

The MHTGR utilizes a below-grade silo that is compartmentalized, containing the primary coolant system as well as the steam generator, seen in Fig. 2.7. The below-grade design of the reactor building reduces the probability of a break in containment from outside sources, such as earthquakes or other natural causes. This can be seen as a viable alternative to the large above ground containment structures of current LWRs due to the use of TRISO which would contain any postulated release within the layers of the fuel particles.

Both the reactor cavity and the steam generator cavity have their respective vessel mounted within the cavity by a series of structural supports. The reactor cavity is linked to the steam generator cavity by a labyrinth tunnel which prevents potential neutron streaming from the reactor

cavity in the event of an accident. The steam generator cavity has additional metal plates near the bottom and top of the cavity that subdivide the cavity into 3 major regions. The side ventilation and equipment shaft permit flow between the subdivided sections of the steam generator cavity allowing for a connected environment. From the top of the steam generator cavity an upper vent, which is U-shaped to prevent possible radiation streaming, connects to a further upper vent above grade. The upper vent contains louvers connecting the reactor building to the outside environment (General Atomics,6.1-1,1986).

2.3.3 Reactor Building Circulation and Ventilation Control

Standard circulation of reactor building atmosphere is handled by the Heating, Ventilation, and Air Conditioning (HVAC) system which provides air circulation for the reactor building. Reactor building atmosphere from the HVAC system flows from areas of low radiation potential to areas of high radiation potential then out of a monitored stack for release to the atmosphere. If the monitored stack detects radiation the stack is closed and the HVAC output is passed through air filter trains to remove radioactive particles from the released air. Air handling by the HVAC system is contained within a single unit for two reactor buildings, silos and above auxiliary buildings.

Air circulated through the reactor building is kept as once-through to ensure the removal of any potential radioactivity and to prevent potential buildup in areas of recirculation. The reactor and steam generator cavities are isolated during general operation of the reactor but can be purged and circulated during reactor shutdown. Any continuously accessible portions of the reactor building are kept fully circulated with once-through air. The steam generator cavity during normal operation is isolated but functions with a cooling unit, part of the HVAC system, that cools the concrete and supports of the cavity. The reactor cavity is isolated from the other reactor building

cavities to limit the spread of released Ar-41 during normal operation of the reactor. Also, since the RPV is uninsulated, removing HVAC circulation of the cavity removes unnecessary strain on the system. The HVAC system would only be used in the reactor cavity to purge the cavity atmosphere for shutdown operations. Standard cooling of the reactor cavity is handled by the Reactor Cavity Cooling System (RCCS) (General Atomics,9.1-121,1986).

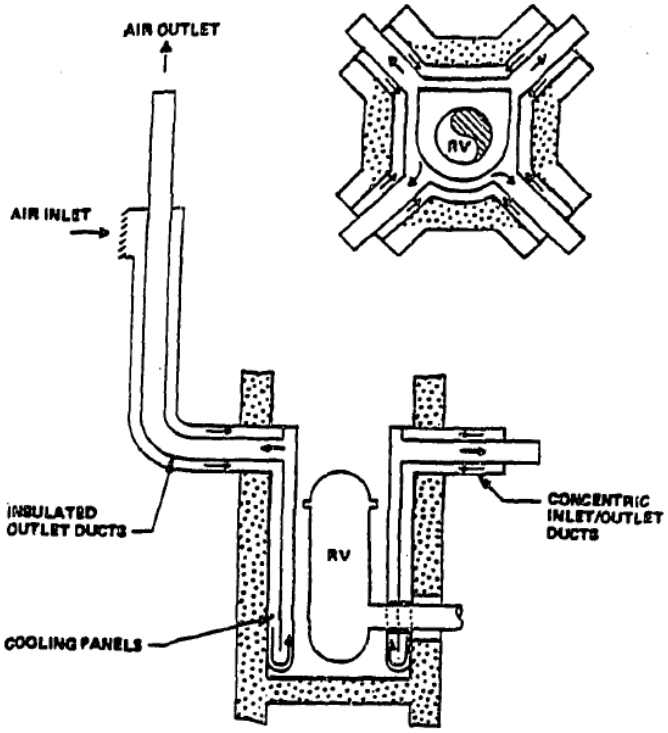

Fig. 2.8. RCCS Layout. Reprinted from (General Atomics, 1986).

The RCCS is a natural air circulation cooling system built into the reactor cavity to provide cooling to the cavity and reactor, which is seen in Fig. 2.8. The system uses a number of cooling panels and associated ductwork to transfer heat to environmental air that is circulated due to the natural convection of the heat transferred to it. The system keeps the concrete walls of the cavity cooled during standard operation but is also a critical safety system in case of a loss of coolant accident. The reactor vessel would conduct a large amount of heat from the core which would be transferred via radiation and convection to the cavity atmosphere, which the RCCS would then be

able to transfer to the external atmosphere safely. The heating of air in the inner RCCS duct causes it to rise where it can exit the system which causes air to be drawn into the inlet of the system, providing a naturally circulating system to cool the reactor cavity and the reactor itself (General Atomics,5.5-1,1986).

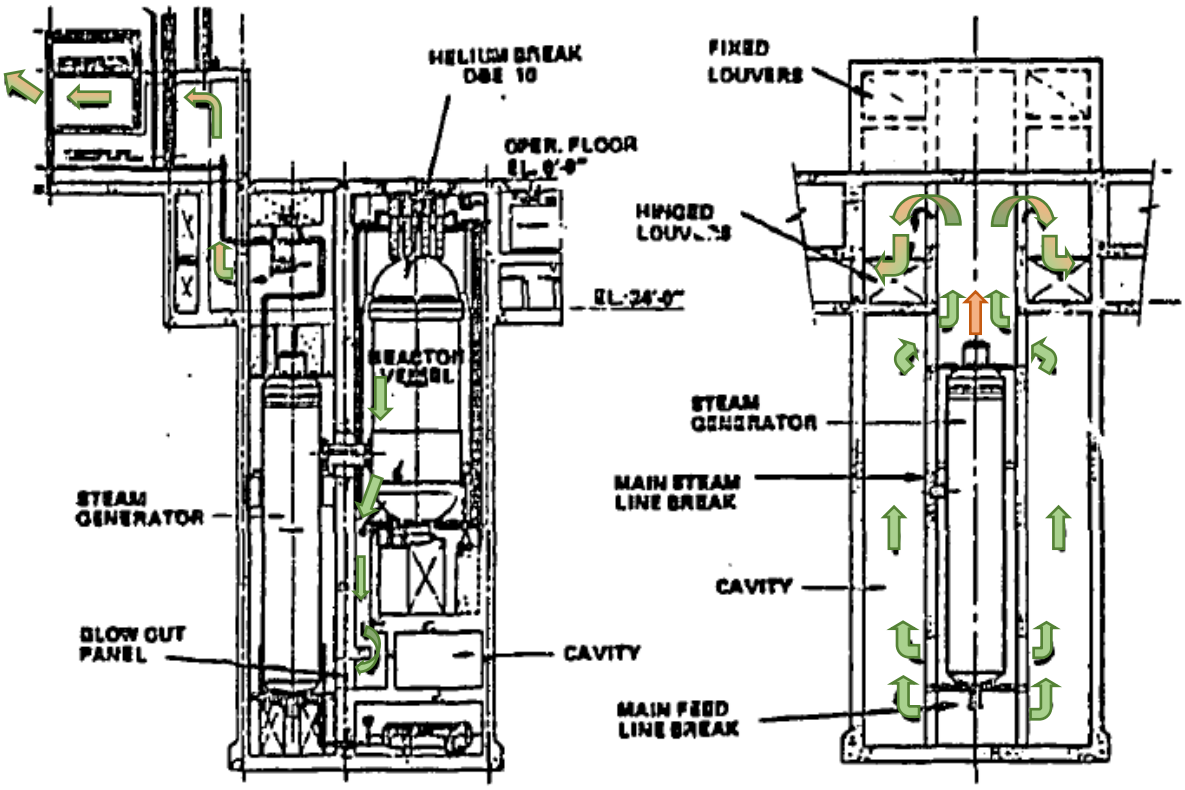

Fig. 2.9. Reactor Building Blowdown Flow Paths. Reprinted from (General Atomics, 1986).

In the case of a coolant release and blowdown scenario, Fig. 2.9 illustrates the standard blowdown pathway through the reactor building, with the green arrows indicating the RPV primary coolant boundary break and orange arrows indicating a pressure operated relief valve (PORV) failure from the steam generator vessel (SGV). Beginning with a break in the primary coolant pressure boundary of the RPV, the general flow of helium coolant will be forced down into a labyrinth connection. The connection leaves the bottom of reactor cavity and leads to s-tunnel connection to the steam generator cavity. This connection is ended by a blowout panel at

the labyrinth connection to the steam generator cavity that isolates the reactor cavity from the other reactor building cavities. The blowout panel is set to isolate the reactor cavity during normal operation but is set to fail and open the pathway between the reactor and steam generator cavity with the initial pressure wave from a blowdown scenario.

Since the steam generator cavity is divided and isolated during standard operation, direct flow rise in the central cavity is not possible. To handle the blowdown flow, the steam generator cavity is flanked with equipment and vent shafts that run up the silo allowing flow to bypass and leave the central portion of the cavity and enter the upper portion. The upper portion of the steam generator cavity is then linked into a vent network that leads to the external atmosphere. The initial portion of the vent system consists of a u-shaped labyrinth connection to prevent radiation streaming but also hinged louvers that are normally closed for standard operation but can be opened to create a flow path into the vent system. After the hinged louvers, the blowdown atmosphere would then rise into an upper vent where it could flow through a fixed louver to the external environment.

3. MELCOR CODE DESCRIPTION

3.1 Introduction

MELCOR is a systems-level severe accident analysis code that has been under development and use for almost 40 years by Sandia National Laboratories for the NRC. When originally conceived in 1982, the code was designed as a Probabilistic Risk Assessment (PRA) code for quick and flexible simulation for assessing reactors. Through the preceding decades, the code has been thoroughly developed and expanded through the inclusions of specialized smaller codes and models that currently allow it to simulate a reactor to the point of a radioactive release. The code has progressed to the point of thermo-hydraulic simulation of coolant systems and cavities (reactor building, buildings, etc.), heat transfer through solid bodies, radionuclide source term generation, and even exotic cooling simulation (gas or salt cooling).

MELCOR in its current state, version 2.2, is split into 23 different packages that can be individually called to suit the needs of individual model development without the need to have unwanted processing slowing simulations. On top of individually callable packages, users are able to input parameters for constants in inputs which is a rarity in most analysis codes as they are hardwired into calculation equations. For referencing, the code has an extensive documentation describing individual input cards, as well as their variables, with examples as necessary showing entire input cards. The documentation also has extensive background information on the equations and principles that guide the individual packages and provides the basis for simulation accuracy. As the code is still under development, it continues to evolve to the ever-changing reactor market with the simulation of HTGRs and liquid metal cooled reactors being valid for simulation using the code.

3.2 Code Process

Execution of a MELCOR simulation is a joint process from two separate executable files, MELGEN and MELCOR. Fig. 3.1 shows the general code process overview of the standard MELCOR operation and use, from input to output. MELGEN takes the users input, a file containing input cards from individual packages, and checks for syntax or user errors. If the input file passes these checks, it is processed into an initial restart file which can then be used in the true simulation and which contains all the initial conditions to be used.

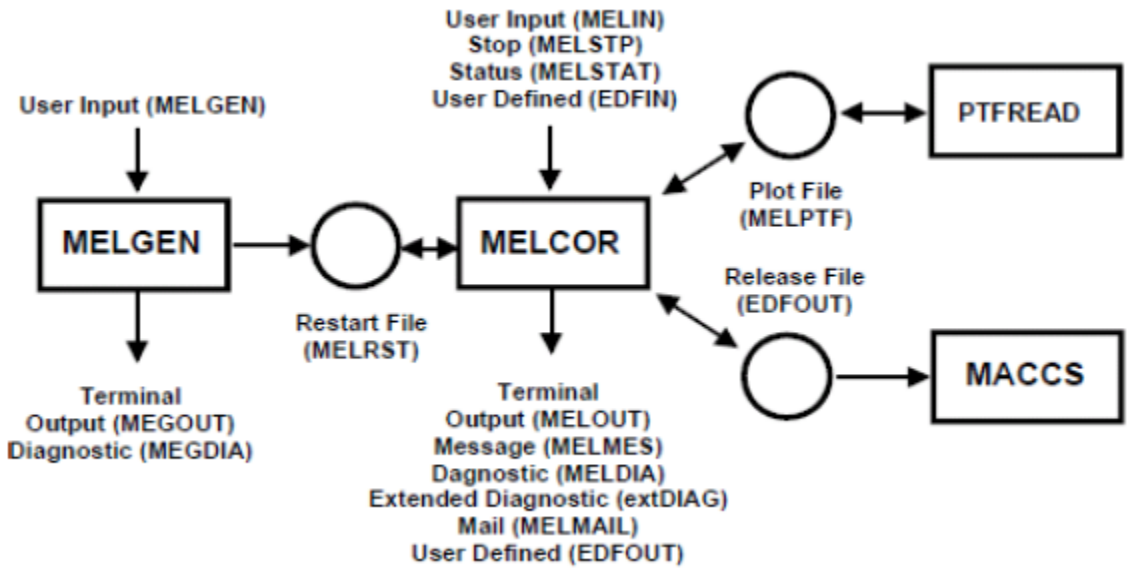

Fig. 3.1. MELCOR Progression Diagram. Reprinted from (Humphries et al., 2017b).

MELCOR then takes this initial restart file and progresses it through the user defined time allocation defined in the input file. At the end of the defined time period, MELCOR compiles various defined output files to be used in the exploration of its results. Results can be presented as a standard text output file, a plotting file which can be imported into Microsoft Excel, PTFRead, for quick tabular and plotted results, and even a source file of released radiation that can be used by the associated program MELCOR Accident Consequence Code System, MACCS, to determine the spread of radiation in the case of a containment breach.

3.3 Code Package Description and Concepts

MELCOR is a suite of 23 individual code packages, each with a specific purpose of use, including reactor core phenomena, thermal hydraulic phenomena, and even specific containment system functions like sprays, recombiners, and condensers. For the purpose of this research five of these packages were used, Noncondensible Gas (NCG), Control Volume Hydrodynamics (CVH), Flow Path (FL), Control Function (CF), and Executive (EXEC) packages. Of the five packages, CVH and FL are the primary workhorses of the models to be constructed in this research and as such will be described in greater detail in following sections. NCG, CF, and EXEC will be described in shorter details in the following paragraphs.

The NCG package is a support package that is used to define noncondensible gases for further use throughout other packages, such as CVH. Common gases are defined naturally within the code with default values, but custom gases can be defined by user input of set properties and default gas properties can be edited to suit a user's need. All gases defined by this package, default and user defined, are modelled as ideal gases to determine their properties for the simulation.

The CF package is a support package that is used to create user defined functions that can perform a number of features within a simulation. Functions defined in this package are used in a variety of other packages where they are used to control functions like valve opening/closing, pump operations, and reactor operation control. This package has a wide operability to read simulation information, such as control volume pressures, temperatures, water content, and pool levels, which can be integrated into the function for control of the model. A majority of standard FORTRAN and elementary mathematics functions are available to be introduced into the individual control functions for customization to a user's desire.

The EXEC package is the overall control and execution package for MELGEN and MELCOR. This package allows the defining of output files to be created, limits placed on the simulation on a computation standpoint, and the definition of the time progression through the calculations. Within this package, the definition of stepping of time and subsequent calculations is performed, allowing users control over the progression of their simulation. This package bridges MELGEN and MELCOR within the users defined input for an input deck.

3.3.1 CVH Description

CVH is first of the two critical MELCOR packages that allows the code to process and simulate the progression of thermal-hydraulic behavior in both liquids and gases. CVH allows the user to define a volume on its elevation, physical volume, and thermal hydraulic properties. The volumes created in this package can be used to model any desirable flowing volume for the code to interpret, from reactor building cavities, duct work, pressure vessels, piping between vessels, and even the cooling channels within the reactor core. Each volume is filled with mass in the form of "pool" liquids and "atmosphere" gases which are dynamic in their properties for the purpose of the of the simulation outside of the user defined initial conditions. All dynamic materials in a simulation reside within the CVH volumes, along with their associated energy. When a volume contains both a pool and atmosphere, pressure is averaged over the entirety of the volume while individual temperatures are given for the pool and atmosphere. For the purpose of this research though, and any volumes that contain only an atmosphere, a single pressure and temperature are given as an average of the entire volume.

Volumes are constructed primarily based on primary elevation values with associated volumes to build a volume table across the elevation of the volume, all of which are two dimensional in implementation. Fig. 3.2 shows the conversion mindset between a true spatial

volume and the volume-altitude table used in calculations. Creation of a volume occurs with the defining of a set of elevations defining the bottom and the top elevations of the volume, with the potential inclusion of intermediate elevations for complex geometries. Volumes are then defined for each point in elevation, with the initial lowest elevation being zero volume, and each elevation point following the initial being the total volume from the bottom most elevation or the volume from the previous elevation step. Elevations used for defining volumes are shared across all volumes of the model and as such need to be planned before creation. A set "zero" elevation is usually defined as the bottom most elevation of the model or the bottom most elevation of the critical location being studied. Elevations in a negative direction are allowed to accommodate centralized "zero" elevations.

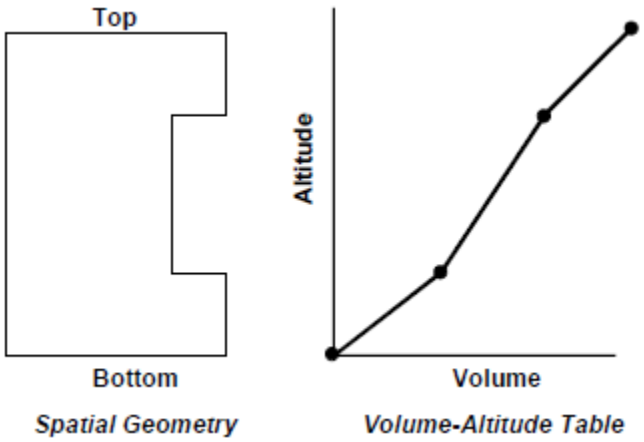

Fig. 3.2. Spatial Volume and Volume-Altitude Table Comparison. Reprinted from (Humphries et al., 2017a).

As previously stated, initial thermodynamic conditions of volumes are set by the user in their input deck creation of the CVH volume. These properties are to be updated across simulation steps by solving linearized-implicit finite difference equations to update changes to mass, momentum, and energy within each volume (Humphries et al., 2017a). Volumes can be created with alternate conditions though, as only in active volumes are the thermohydraulic properties

actively calculated. Alternatively, volumes can be set to be time-independent, with properties that are initially set in the input with function created variables to control property values which can be used for sink or source volumes in testing.

Nodalization of volumes is not handled directly by the code but by the users input and creation of volumes. Volumes can be created to handle the entirety of a room with a single volume or be brought into a nodalized state with multiple volumes being created to cover the overall volume of the room across a group of associated CVH volumes. Nodalization can be as fine as a user desires, though as models become more complex with nodalization, computation time does increase. Nodalization should be kept to appropriate levels to get the desired results and be able to see the warranted phenomena, within a respectable computation time.

3.3.2 FL Description

FL is second of the two critical MELCOR packages that allows the code to process and simulate the progression of thermal-hydraulic behavior in both liquids and gases. FL facilitates the transport of hydrodynamic materials between the individual volumes created by the CVH package, controlling the flow of mass and momentum between volumes. Flow paths created by this package have no implicit volume in of themselves as their purpose is to only facilitate the transfer mass and energy between volumes. Due to this specification, all flow paths specified in this research are simple surface flow paths that have no inherent volume but connect two adjacent CVH volumes.

Flow paths are defined by their “junctions”, which are elevation based like the CVH volume creation method. Each flow path connects a “from” volume to a “to” volume with appropriate parameters such as flow area, hydraulic diameter, and open fraction. Losses are accounted for over the length of a flow path even though they do not represent true volumes through the use of simulated losses from friction due to surface roughness and form loss. Flow

path transfer while connecting volumes in a set direction, can undergo countercurrent flow and flow in a reverse direction.

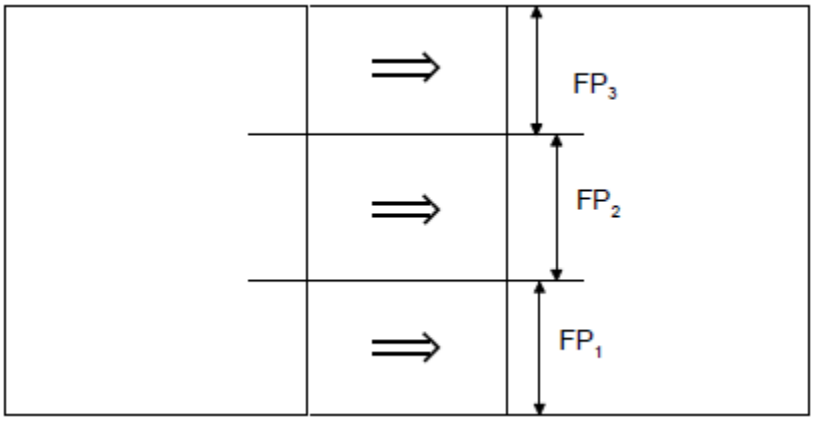

Fig. 3.3. Multiple Flow Path Connection. Reprinted from (Humphries et al., 2017a).

Complex flow path creation can be performed by linking a single pair of CVH volumes with multiple parallel flow paths which equate the total interface area of the volumes, which helps augment the finite difference limit in calculations. Fig. 3.3 illustrates the complex pairing of two volumes with multiple flow paths, a method which has potentially been shown to alleviate natural flow calculations between volumes. Methods like this can be used to further simulations past simple one-dimensional flow into the range of approximating two- or three-dimensional flow by complex pairing of volumes. This does have its limitations though as flow paths only carry one-dimensional momentum information and CVH volumes have no inherent momentum, leading to no possibility of multidimensional flow effects being possible from the advection of momentum (Humphries et al., 2017a).

4. INPUT DEVELOPMENT

4.1 Modelling Approach

Generating a model capable of MELCOR simulation requires development of an approach to represent the physical system within the capabilities and functions of the code. Models are not able to be finely-nodalized, depth bound representations of a physical geometries as done in CFD, instead requiring simplification to 2D representations and layouts. While a majority of volumes can simply be modelled in their physical form due to their simple cylindrical or rectangular dimensions, mirrored or complex geometries need to be simplified to be represented properly in the 2D model.

In a majority of model creation cases, information used in the creation of models for reactor building testing will have to be compiled from design documentation of reactors and their reactor buildings. The primary design documentation of a reactor, such as a PSID, should provide detailed enough information to create an operable model. More detailed design documentation may not be available during the modeling attempts such as detailed schematics and elevation charts due to the early or theoretical designs of the reactors and reactor buildings being simulated.

The initial step in starting the modelling process is gathering and interpreting information on the design being simulated. Relative design information such as dimensions, connection pathways, components, and operation parameters need to be compiled with detailed information to be used for implementation in the model. From this collected information, data should be complied and tabulated for quick access and sorted in a logical manner for input deck creation and use. Relevant data pertaining to the specific desired simulation will be of most importance and should be collected and tabularized for use. Outside of the design documentation, component documentation may need to be referenced to get more accurate information on the performance

characteristics of relevant components or simulation work done on similar designs for methods of proper implementation. Non-important systems should not have information collected and should be ignored in the creation of models and inputs deck as they will waste computing time during simulation runs and would not provide relevant information.

Important modeling decisions must be made during the model creation process such as how to break down cavities into constituent volumes and how to combine complex depth spatial volumes down to 2D forms that would be used by MELCOR. When initially creating a layout of the volumes, possible complex depth volumes must be simplified down to 2D representations. This can be done by a number of methods including overlapping unconnected volumes or creating simplified unified volumes that consist of a number of complex volumes combined. When using unified volumes precautions must be taken to ensure that tracking volumes are being combined in the proper manner to ensure a correct simulation.

These decisions also expand, for example, to decisions on how the large size of the reactor building volumes can be simulated for each cavity through the use of various methods. A cavity may be left as a single large volume, and results of a simulation of this method will give averaged results over the entire cavity. This is useful for volumes of small size or less supposed significance. Alternatively, a cavity can be split into a number of individual volumes that are freely connected to give a more nodalized set of data for each individual cavity. This is important when considering things such as test setups incorporating instrumentation at various points in a singular cavity.

Once cavities have been decided upon, along with their nodalization, the composition of each volume must be defined. The elemental composition of each volume must be defined along with initial parameters, such as humidity, temperature, and pressure. Connections must then be described to designate their layout and flow connections. Parameters such as connection areas,

open percentages, and hydraulic diameter must be defined for each connection between individual volumes, for both large cavity volumes and each nodalized volume that used to subdivide large cavities for more discrete results, known as flow paths.

Following the layout of reactor building volumes and connections, venting structures and controls must be defined. Flow limiters such as louvers and blowout panels can be defined using control functions guiding flow path operation under conditions of system aspects. At this stage of the model development, components that drive flow in a reactor building may also be implemented, such as air circulation systems, if they are going to be used in a simulation.

Implementation of loss of coolant accident scenarios can be done through the use of a combination of flow paths and control functions. Flow paths may be setup in critical locations of primary coolant boundary breaks but set to being closed normally allowing standard operation of the model during initial stages of a run or when other aspects are being tested. When a particular scenario is looking to be tested the flow path can be opened through the use a control function allowing the blowdown progression to occur with a wide variety of initiating conditions. Multiple scenarios can be combined in a single input deck or spread across different input decks.

4.2 Models and Spreadsheets

To begin the modelling approach for the MHTGR, a scaling study of the reactor building was provided by project colleagues from Purdue University (Revankar, 2020). In the study they translated the full-scale reactor building into a simplified model that was then scaled down to a $1/28^{th}$-scale facsimile. The $1/28^{th}$-scale model was then to be used in an experimental setup for real world testing and confirmation of results to be gathered from the simulation of the reactor building. The process of MELCOR input deck creation started with the design of simplified layout models to designate the major volumes and their connections for the input deck. The initial layout was

taken from design mockups created in computer-aided design (CAD) software for the scaled experimental setup to be used in the planning and creation of pressure vessels. The layout of the cavities and connection ports were applied to a simplified 2D design figure, which is shown in Fig. 4.1. This initial design figure was created to gain a sense of the overall layout of the reactor building to be implemented into the input deck without a general sense of dimensions.

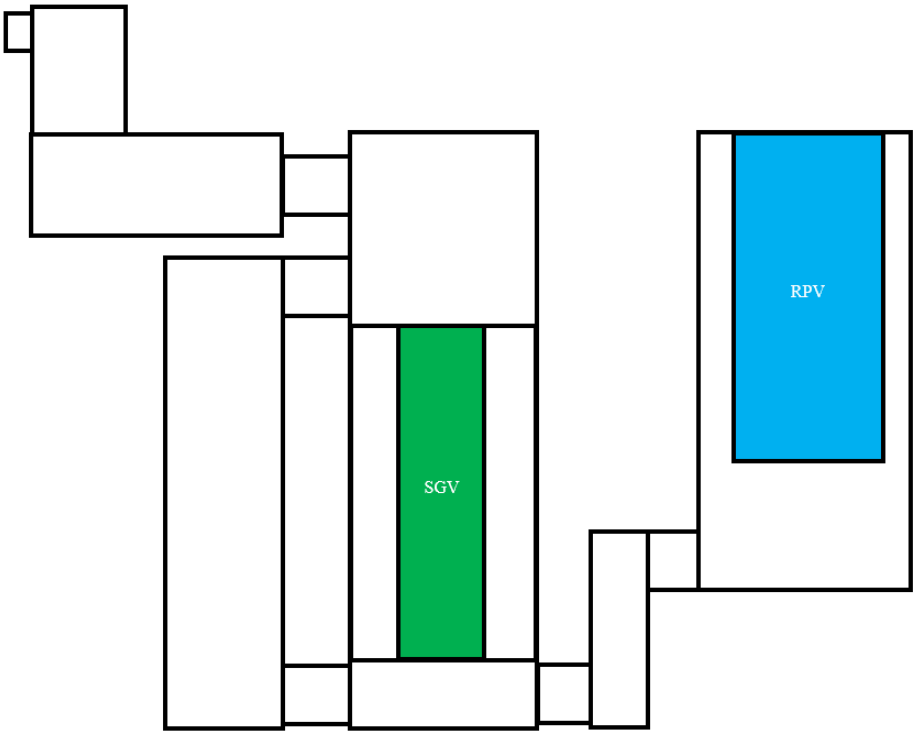

Fig. 4.1. Simplified Layout of MHTGR Reactor Building.

Using the scaling study performed by Purdue University, elevations were then given to cavities in the simplified design figure, indicating their elevations at critical points to be used in the input deck. Height values from the provided spreadsheet documentation of the scaling study and the CAD models were used to determine an overall elevation model of the layout. The initial elevation model was created with imperial measurements at the 1/28th-scale that matches the experimental model CAD mockups, which is seen in Fig. 4.2.

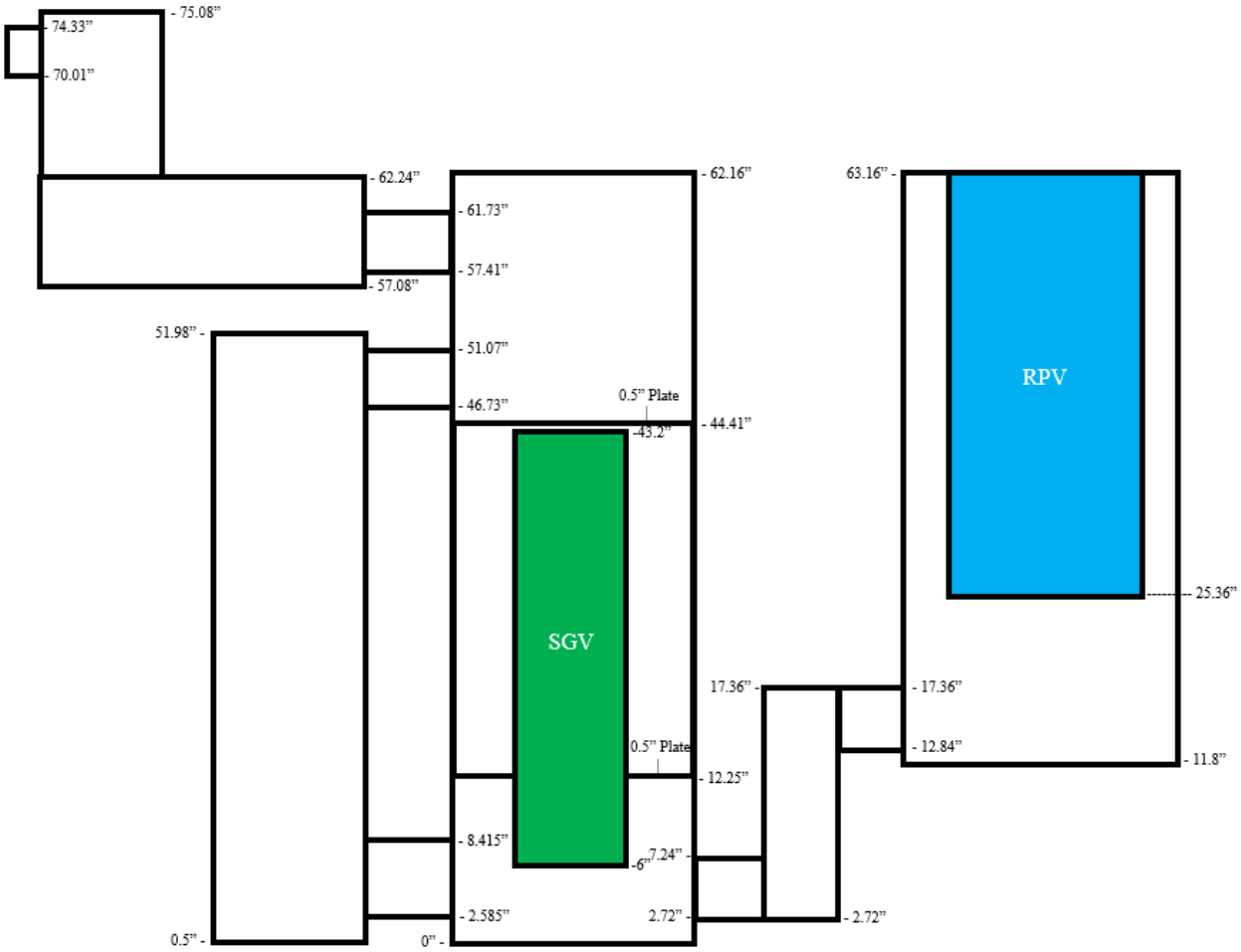

Fig. 4.2. Imperial 1/28th-Scale Elevation Model.

As MELCOR handles all dimensions with metric dimensions, the imperial 1/28th-scale model was then converted to metric measurements, seen in Fig. 4.3. At this point, as well, the cavities to be used in the input deck modeling were initially labeled to show the subdivision of the major regions of the volumes of the input deck. This model would become the basis for the original MELCOR model that was used for initial testing for a working model.

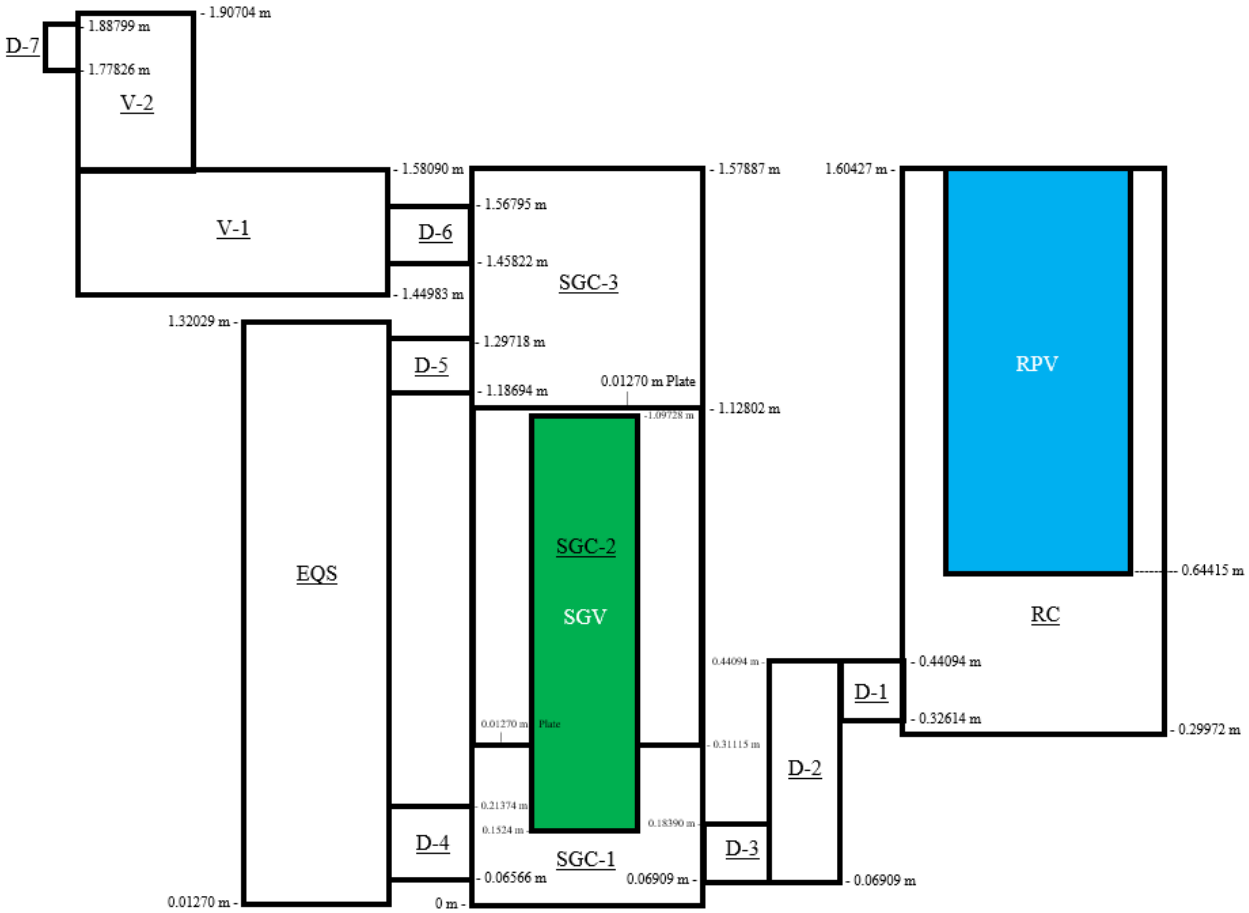

Fig. 4.3. Metric 1/28th-Scale Elevation Model.

A comparison model was then created by scaling the 1/28th model back to full size so that it could be used for simulation comparisons between the two models to confirm the accuracy of the scaled model. The full-scale elevation model, seen in Fig. 4.4, was used for the initial MELCOR full-scale input deck. Of the three models that were created, only the two models with metric dimensions, 1/28th-scale and full-scale, were maintained for further use due to MELCORs use of metric dimensions. All further work was done to both scale models to ensure consistency between the models and to allow for more accurate and reliable future model comparisons.

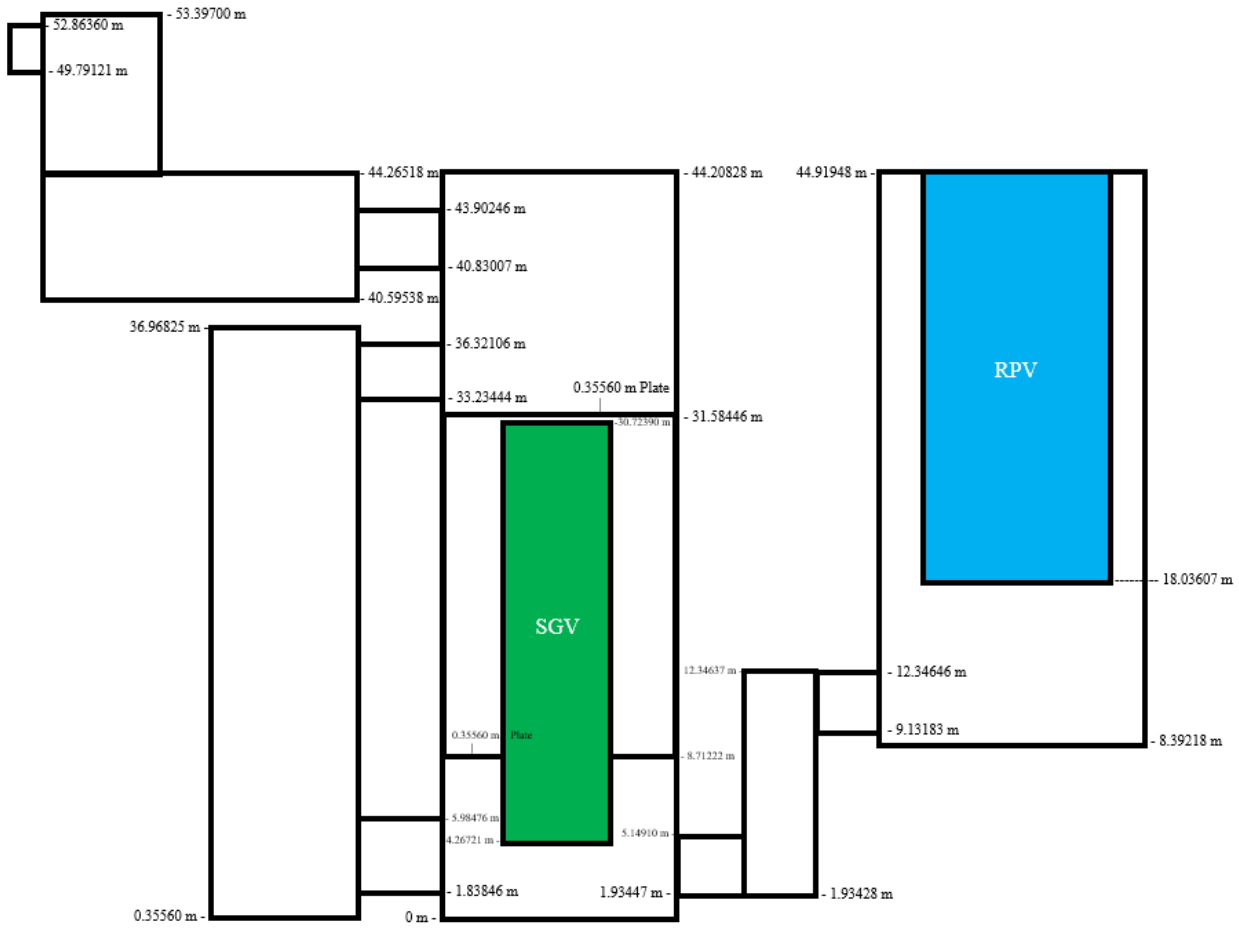

Fig. 4.4. Metric Full-Scale Elevation Model.

Following the basic elevation model creation, a spreadsheet was created compiling the dimensions of each cavity and connection in a singular location for both scales, which allowed for simple conversion between the scales of the models. The 3D dimensions (width, depth, and height) were used to calculate the overall volumes and elevation characteristics for each cavity to use in the creation of the MELCOR input decks. This spreadsheet was used to track the major elevation points in the models, including the top and bottom of cavities and top and bottom of vessels contained in the cavities.

Junction heights were then calculated in the spread sheet for the connecting volumes between the larger cavity volumes. The flow between individual volumes were split into dual flow

paths due to limitations with the handling of flow in single time steps. As flow paths can only handle flow in a single direction during a time step, all flow path connections between individual volumes in the model were split into two separate flow paths to allow for countercurrent flow during a single time step, if needed. When there is no mixing, the flow in both flow paths can travel in the same direction. This approach allows for the mixing of the reactor building atmosphere gas species between volumes, displacement, and refilling of the reactor building following blowdown.

The top, bottom, and middle elevations were calculated for horizontal junctions between volumes to specify the two regions of flow for the individual flow paths. The mid-point elevation of each region, the respective one-quarter and three-quarter elevations of the overall connection, were calculated to give the middle elevation of each flow path. The middle elevation of the upper flow path is at the three-quarter elevation for the overall connection and the middle elevation of the lower flow path is at the one-quarter elevation of the overall connection. The area of each flow path was calculated, being half of the overall connection area, and the hydraulic diameter of the overall junction was calculated for the final flow path parameters for use in the input deck creation.

Following a period of preliminary testing of the models, nodalization of the models was performed to gather more accurate results at specific locations in the reactor building. An initial nodalization was planned with the layout seen in Fig. 4.5. In the initial nodalization, all volumes were broken into vertical bands of the original volumes in mostly equal amounts, excluding the regions surrounding connections where bands were at the connection vertical heights. No horizontal breaking of volumes was performed in the initial nodalization plan.

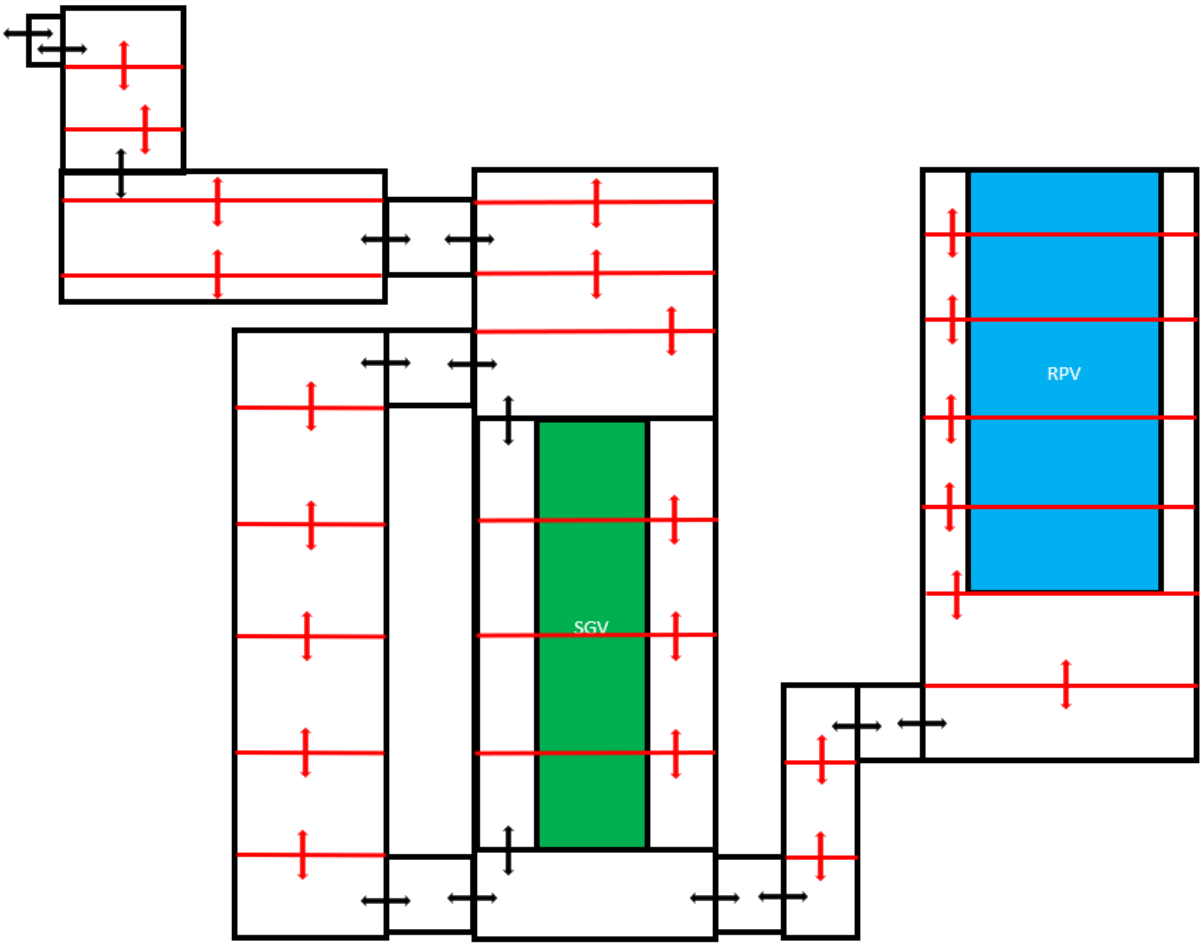

Fig. 4.5. Initial Model Nodalization.

Following the initial nodalization, planning information was provided by the project head from Purdue University on the location of planned oxygen sensors in the test assembly. Considering the locations of the oxygen sensors, volumes needed to be divided into many smaller regions to get localized gas concentrations instead of the overall averaged concentrations being provided by the initial models. A 2" band in the 1/28th-scale model was given around each oxygen sensor location to divide the volumes into subregions to gather better information in the nodalized regions, as shown in Fig. 4.6. Following the creation of a nodalization figure, the spreadsheet of dimension and connection information was updated for the nodalized regions to compute the MELCOR input information for input deck updating and construction.

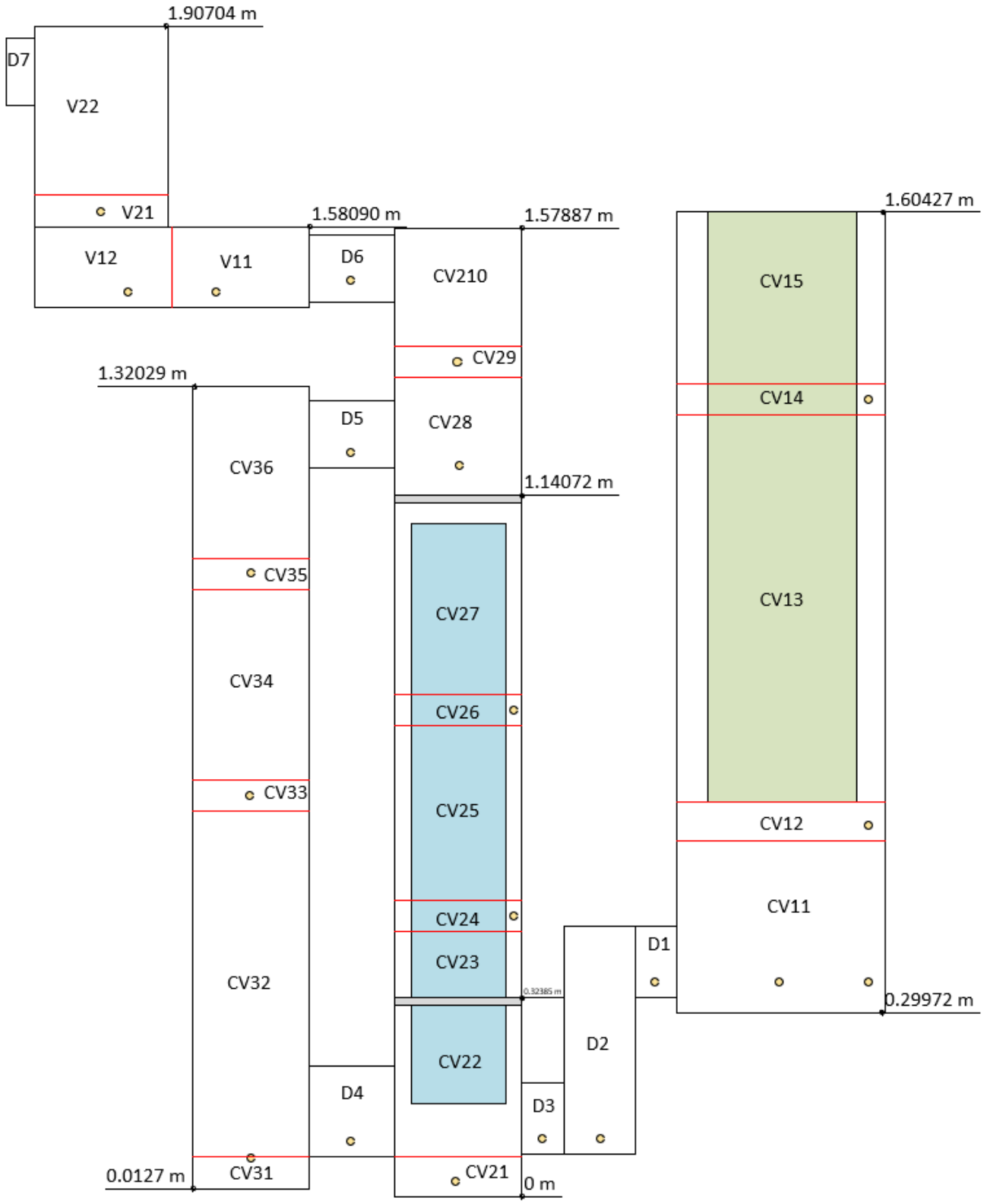

Fig. 4.6. Nodalization of Experimental Input Deck in Correctly Scaled Model.

4.3 Input Deck Creation

Input development can then begin on the actual MELCOR input deck. Beginning first, it is wise to declare and define the input deck with a logical naming scheme, as many input decks may be created and could be confused without a proper naming. When starting the input writing, it is best to define within the first few lines of the top of the code what is being simulated and under what conditions, this helps to define the input deck when others view it or for later reference. Following the beginning definition of the input deck, the next section is to define output and operation filenames. When naming these files, it is important to give them distinct names that identify their purpose, what file they are, and distinguish between iterations of the file. A short section starts the MELGEN portion of the input that declares the non-compressible gasses that the simulation will use, in this case N_2, O_2, Ar, CO_2, and He, and sets them to use the default values in the simulation.

The next major section of the input deck defines the volumes to be simulated by MELCOR, in the case being simulated it would consist of the individual volumes declared in the nodalized model. These start with being named (CV11, CV12, etc.) to distinguish the volumes apart in the program and results, as well as being given a "type" related to their overall physical volume (CV1, CV2, etc.). Each individual volume is then defined by their elevations by defining major elevations and their associated physical volumes to define their proportions. Thermodynamic cards must then be input to define their interior contents to MELCOR, including temperature, pressure, humidity, and the type of atmospheric content (liquid pool, gas only, mix). Finally, the elemental contents of the volume are input by using material cards with mass percentages to be used in the input simulation.

Due to the main concern of the simulation being the study the reactor building, the primary coolant system is simplified into a single volume that contains the helium coolant at operating temperature and pressure. This simplified volume will be moved between the primary coolant boundary break locations, due to the nonphysical placement of MELCOR volumes, and contains a volume of roughly 25% larger than the RPV as an approximation of the total primary coolant system volume, as recommended by the Purdue University project lead . This simplified volume does not contain the depth of volumetric flow information that a fully modelled system would, but it will still allow the tracking of oxygen and atmospheric influx into the system on a mass quantified level for comparison of its potential effects.

The next major section of the input deck is the flow path definition and set up. Much like the control volume set up, the implementation of a flow path begins with giving the flow path a name and a designated number indicator. Following the initial definition, the flow path is defined by giving the two control volumes that it is connecting. This is further defined by giving the central altitude junction of the connection of the path. The geometry of the flow path then needs to be described by entering the area of the path, the length (which in the case of the inputs here is an arbitrary 1 cm), and the fraction that the flow path is open. Also, the flow path junction heights are added in the case that a flow path is vertical to allow a physical difference in the flow path for MELCOR calculations.

Flow paths are then defined as being horizontal or vertical and any bubble models are disabled as gaseous flow is the only thing being modelled. The final component to each flow paths definition is the piping segment information of the connection. Information declared here includes the area of flow, the length of the segment, the hydraulic diameter, a roughness of the segment surface, a laminar flow toggle, and a laminar flow coefficient. These components must be defined

for each flow path, which in the case of the input decks being created for this project are individual larger overall flow paths that have been split into two equal halves to allow bi-directional flow under a single MELCOR timestep. A final input to be declared in this section is valve control, which are individual flow paths that are controlled via control functions. For these inputs the blowout panel is declared as two individual valves operating on a single control function and the blowdown pathway, which operates on a time delay from the simulation start.

The next major input section is for the control functions utilized in the simulation. Messaging functions are created to declare when the blowdown occurs and when the blowout panel initiates. The blowout panel is operated through the previously declared valve function, with two control functions defined in this section. First is a function which takes the pressure difference across the blowout panel to determine the pressure difference between the connection ducts and the steam generator cavity. The second function is the valve control function for the blowout panel that compares the pressure difference, which when exceeding 1 psid opens the valve, and with it the flow path, completely from being closed in the initial input. The final created function opens the blowdown flow path valve between the helium volume and connected control volume.

The final section of the MELGEN portion of the input is the executive package input. It is here that a title is given to the simulation officially and an initial timestep is given for the simulation. Next, the MELCOR portion of the input deck, which solely consists of executive package input, is written. Here again, the simulation is given a title along with a set of central processing unit (CPU) processing limitations to prevent runover. An end time for the simulation is declared here along with an input table giving timestep values for the simulation to use, including maximum/minimal timesteps, plotting rate, editing rate, restart rate, and CPU restart rate. With this input, the MELCOR section is closed and the input is ready to be ran.

5. TESTING METHODOLOGY FOR NEW EVALUATION TECHNIQUE

For examination of the reactor building models, a testing suite was created to add variation to simulation runs. This test suite aids in the examination of the reactor building response to varying conditions. The main condition tested in simulation runs was the location of primary coolant boundary break in the reactor building layout. Two locations were tested as break initiation points, the top of the SGV and the physical top of the RPV. An original break location was chosen for testing located at the top of the physical RPV. This is analog to a control rod drive penetration in the RPV undergoing a weld failure and is believed to lead to a blowdown through all the reactor building cavities, dimensions implemented for this break are defined for both scales in Table 5.1 (General Atomics,R6-4-2,1986). The SGV location was chosen as it is the PORV location of the primary coolant system. This location is the most likely point of entry into the reactor building volumes for the primary coolant due to safety measures and a short path to the atmosphere, dimensions implemented for this break are defined for both scales in Table 5.2. This location was also of interest as it was a design basis event (DBE) primary coolant break (DBE 10) location that was tested by General Atomics for the reactor design.

Table 5.1.
RPV Break Parameters.

	Full-Scale	$1/28^{th}$-Scale
Break Elevation (m)	40.22948	1.43677
Break Size (m^2)	6.5E-4	8.29081E-7

Table 5.2.
SGV Break Parameters.

	Full-Scale	$1/28^{th}$-Scale
Break Elevation (m)	30.72390	1.09728
Break Size (m^2)	0.00819	1.04509E-5

For both break scenario types, the entire primary coolant inventory is assumed to be able to transfer to the reactor building volumes. For a reactor coolant inventory, a volume of 25% larger than the RPV was chosen to be used in the experiment setup designed by Purdue which was replicated in the MELCOR input deck and placed into the appropriate vessel for each break location. Virtually, the coolant volume does not exist in the space of the reactor building model so not to interfere with simulation comparison to real world results. The coolant volume was set to a pressure of 6.4 MPa to give the appropriate pressure differential between the reactor building and the primary coolant system, to replicate blowdown conditions that would be experienced in an operational reactor, under a worst-case scenario from full operation with no intervention.

Fig. 5.1 inscribes the break locations into a diagram of the overall model. The RPV break is illustrated by the pink triangle in RC and the SGV break is illustrated by the green triangle in SGC, both with lower points illustrating the break point and the expanding cone to represent the flow direction. It will be noted again that break locations can intersect vessels in the model diagram as MELCOR models are two-dimensional representations of three-dimensional space, with no delineation in horizontal placement. In addition to the two break locations, two layout changes will be tested to examine the layout effects on blowdown and refill of the MHTGR reactor building. The first alternate layout will close the equipment shaft, forcing all atmosphere flow up through the steam generator cavity. This is performed by closing the flow paths at their connection to the SGC, illustrated in Fig. 5.1 by the red lines separating the EQS from the SGC at their duct connection. This will be of interest as the cavity currently has very restricted flow paths that simulate the experimental steam generator vessel passing through the plate dividers. The second alternate layout will remove the vertical flow paths from the bottom plate of the steam generator cavity, blocking flow through the center of the cavity, illustrated by the lower orange dividing bar

of the SGC in Fig. 5.1. This will force the flow of the blowdown from the reactor cavity up and through the equipment shaft alone, instead of allowing it to rise through the steam generator cavity as well, and limit downwards expansion from the SGV break.

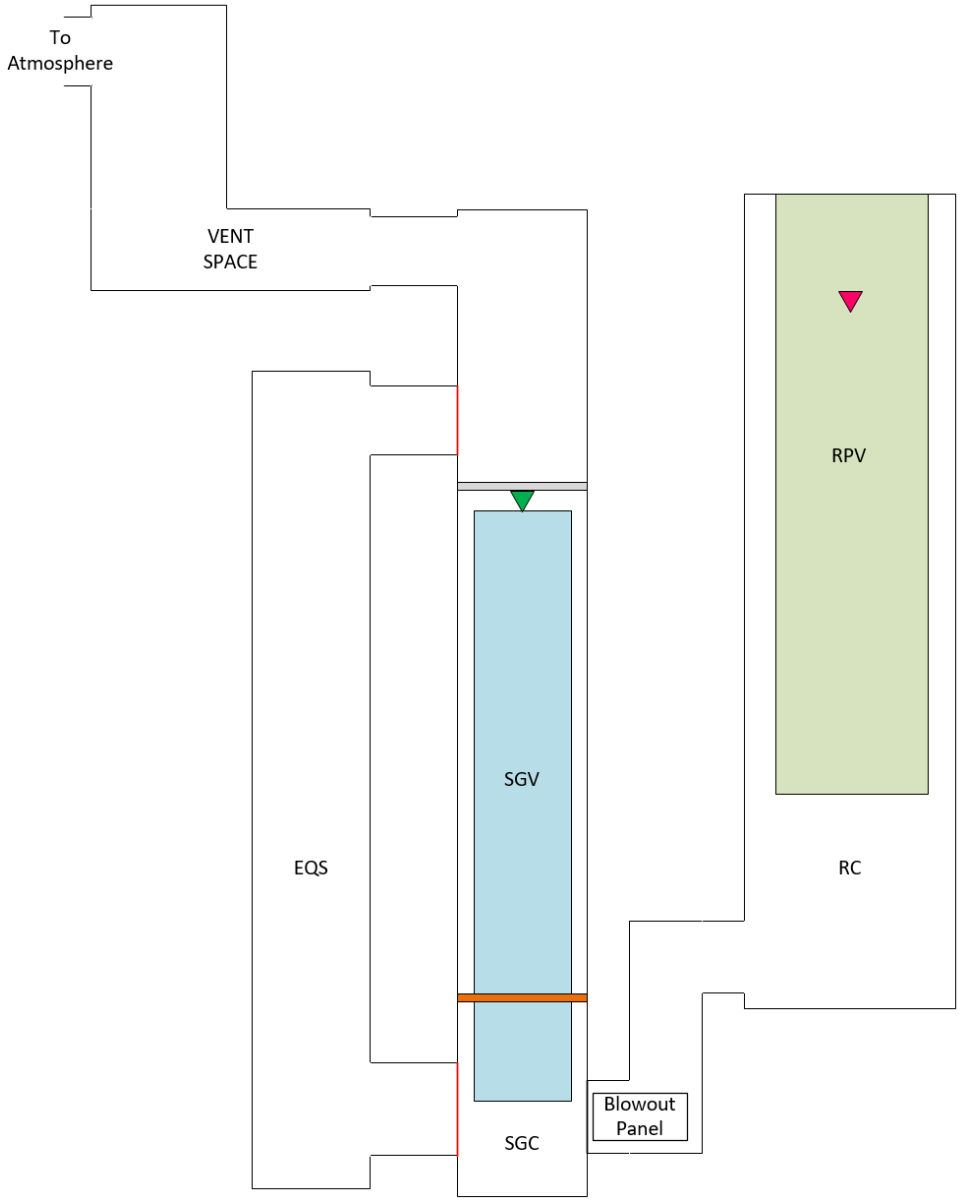

Fig. 5.1. Diagram of Testing Regime Changes.

Table 5.3 illustrates the scenarios that will be testing the model under the previously described break locations and layout changes. Each of the scenarios in the table will be used to test the models of both scales for comparison. Scenario 0 is a baseline run of the models with no break

in the primary coolant boundary to get baseline information of the reactor building for comparison to the tested scenarios. Scenario 1 is an RPV break with no change of the overall layout of the reactor building which allows the largest volume for blowdown progression and no blocked passageways. Scenario 2 is an SGV break with no change of the overall layout of the reactor building or pathways. Scenario 3 is an RPV break with the equipment shaft closed off at the connecting ducts from the steam generator cavity. This prevents flow to the shaft, forcing the RPV break through the constricted steam generator cavity flow paths around the SGV. Scenario 4 is an SGV break with the equipment shaft closed preventing possible backflow deeper into the reactor building from the nearby EQS connection from the SGV break. Scenario 5 is an RPV break with the steam generator cavity closed to upwards flow at the bottom dividing plate, forcing all flow up through the equipment shaft around the center steam generator cavity. Scenario 6 is an SGV break with the center steam generator cavity closed to upward flow by closing the bottom plate off. In total, there are 14 different simulation scenarios that will be run for comparison.

Table 5.3.
Scenarios Overview.

Scenario	RPV Break	SGV Break	EQS Closed	SGV Cavity Divided
0	Baseline			
1	☑			
2		☑		
3	☑		☑	
4		☑	☑	
5	☑			☑
6		☑		☑

From each simulation scenario, a number of critical data sets are being looked at to show the progression of the accident. Of main concern is the oxygen concentration, movement, and dispersion throughout the reactor building. It is critical to know the location of oxygen concentration and movement throughout the reactor building to identify concentration points that could increase the risk of fire. Tracking of the helium coolant throughout the reactor building will also be of interest to find its collection points through the various cavities and volumes much like oxygen.

With the current state of the model, no forced flow of gases is simulated other than that of the blowdown release of helium coolant from the reactor with the primary coolant boundary break. With no forced flow other than the blowdown, all atmosphere redistribution will follow the natural movement process of atmospheric redistribution. These will be worst-case scenarios with no human intervention in a post-break reactor building environment to show the natural response of the reactor building to a proposed primary coolant boundary break. Each scenario will be run with a 1-day time period of simulation with the primary coolant boundary break occurring 20 seconds after simulation start. It is expected that this amount of time after blowdown initiation can help to determine the natural backfill timeline of the reactor building following a primary coolant blowdown. With no heat structures implemented in the current model, no heat transfer is to be performed simulating heat transfer to the walls of the reactor building. This will limit heat transfer to that which is occurring between gaseous species of the reactor building atmosphere, giving the worst-case for each of the proposed scenarios as heat will not be able to be absorbed by the concrete mass of the walls.

6. RESULTS AND DISCUSSION

6.1 1/28th-Scale Simulation Results

This first section of results is compiled to present and explain the simulation results of the 1/28th-scale model, made to examine the response to the experimental setup of the MHTGR. This model was tested with the scenario regime exhibited in Table 5.3. Results of the simulations were exported to Excel using the PTFRead extension developed by SNL for better ease of access of the results from the binary output files. The results were then imported into MATLAB where more efficient plotting of the desired results with user-specified figure formatting could be performed from the gathered simulation data.

When plotting the results, only parameters from the control volumes that make up the larger reactor building spaces will be plotted. Due to the large number of individual volumes being plotted, a focus on plotting just the larger volumes was chosen due to the scale of testing. Ducts will not be plotted as being connections between the various volumes lead them to exhibit the same behaviors as the volumes they are connecting. Leaving them in the plotted results leads to a cluttered view of the larger volume results as well as difficulty in parsing the connections between volumes that follow similar patterns. Also removed are the results for the external atmosphere volume that surrounds the reactor building. This atmosphere volume simulates an exterior expansion volume. In many of the plotted results, the volume's parameter of interest was represented by simply a constant line across the plot due to the comparably large size of the volume. This large size led to the volume being relatively unperturbed. Some plots have been simplified to major trends for results presented in this section but plots containing all individual data sets plotted are included in Appendix D.

6.1.1 1/28th-Scale Scenario 0 Results

Scenario 0, the baseline scenario, was run without any blowdown progression to get base readings of the 1/28th-scale model. The scenario also was used to ensure stability of the model across the full 24 hours of test time outside of accident progression scenarios. The results, while not much more than constant values, set the baseline for the overall model in steady state conditions and demonstrate the model's calculational stability.

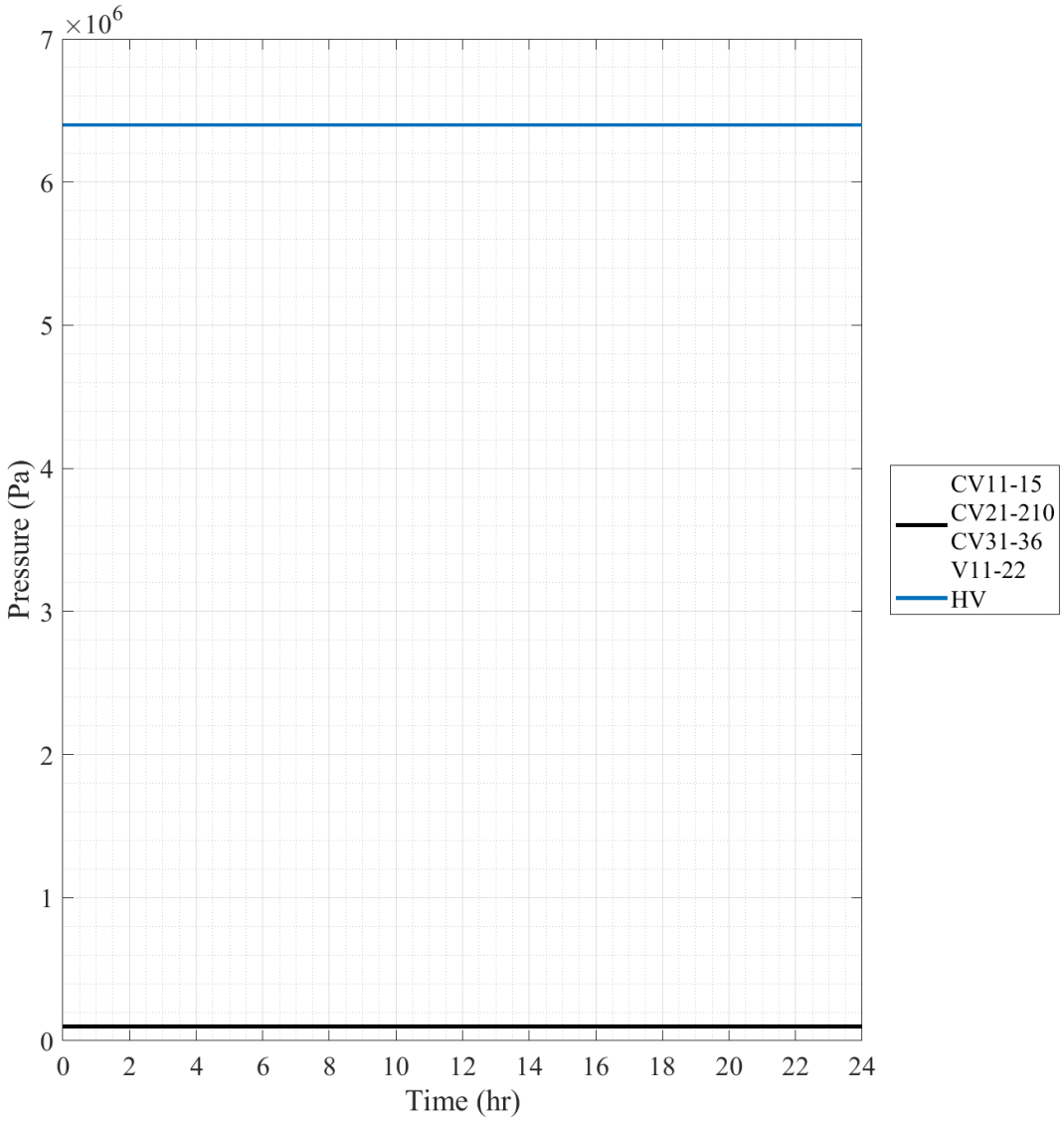

Fig. 6.1. 1/28th-Scale Scenario 0 Pressure.

The pressure plot of Scenario 0, as expected, stays constant through the entire simulation timeframe, as seen in Fig. 6.1. Across the simulation duration, the helium volume, HV, remained constant at 6.4 MPa as designed, while all other volumes remained at roughly 100 kPa. At the beginning of the simulation the 100 kPa volumes undergo a slight redistribution of pressure where they settle within a range of 100.0005 to 99.97 kPa, which is negligable variance in terms of a distribution.

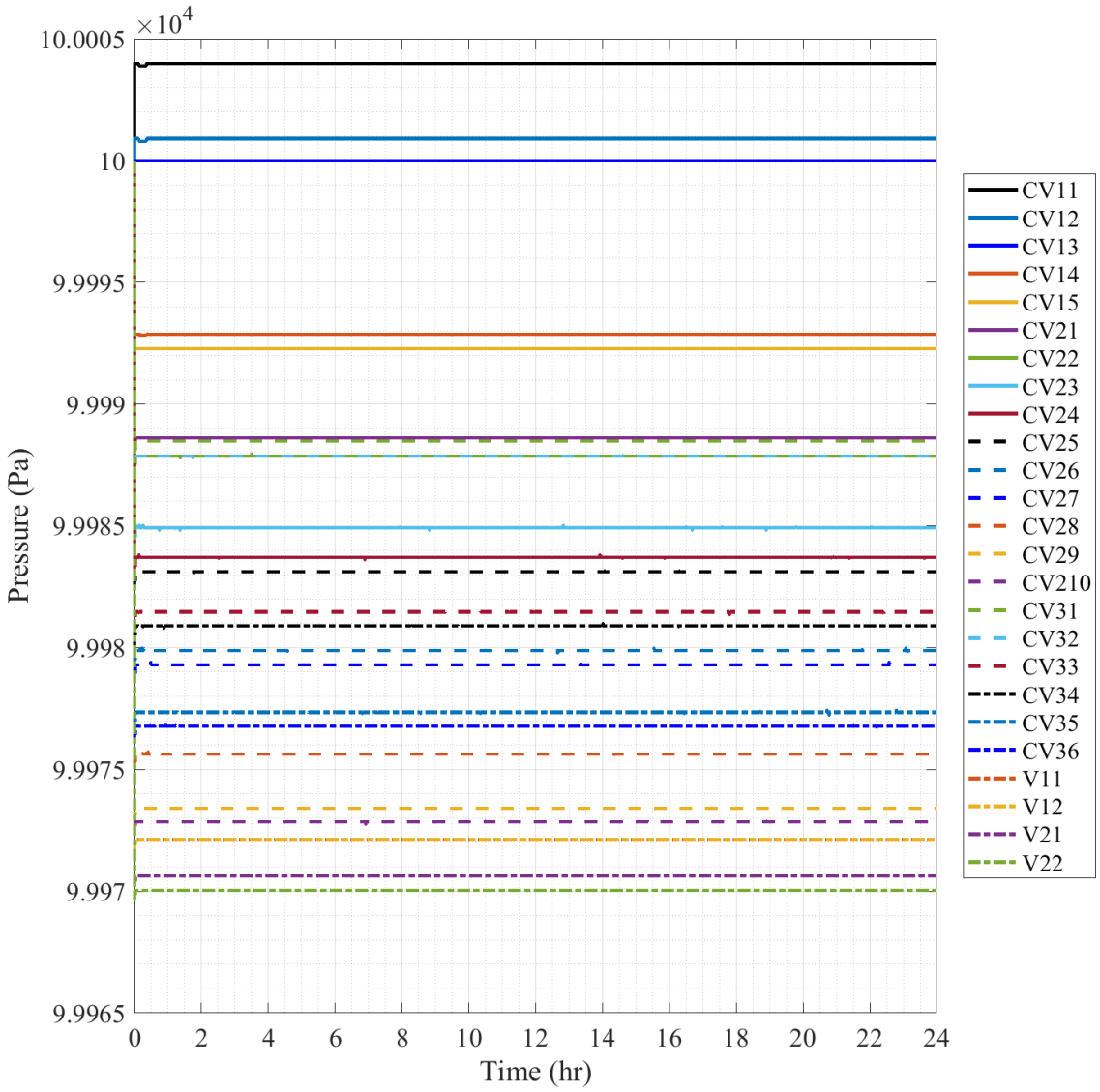

Fig. 6.2. Natural Pressure Redistribution at 1/28th-Scale.

Fig. 6.2 shows the pressure redistribution naturally created in the model at the beginning of simulation runs. From the figure it can be seen that a natural pressure difference of ~34 Pa develops within the model as it is run. This pressure difference is not within a contiguous open volume space though as the upper volume of the results is behind the perpetually closed blowout panel in this scenario. A better indication of pressure differential can be taken from CV21 to V22 to indicate an open and connected volume space from the top to the bottom of the model. A pressure differential, taken from the figure from CV21 to V22, is seen to be ~19 Pa. A basic height pressure variation calculation shows that at the 1.90704 m height of the model, 1.225 $\frac{kg}{m^3}$ air density, and 9.80665 $\frac{m}{s^2}$ gravitational acceleration, a pressure difference of ~22.9 Pa is to be expected. The observed simulation pressure is a ~48% increase over the expected pressure variance value when accounting for the full results, but only ~21% lower when accounting for true model contiguous volumes, possibly due to the complex geometry of the model on such small-scale volumes.

The plot of the helium mass fraction results in as expected constant values which is seen in Fig. 6.3. The helium containing volume, HV, maintained a 100% value as expected as no break scenario was implemented. All other volumes remained at 0% as helium is not part of the natural atmosphere mixture and no primary coolant boundary breach occurs.

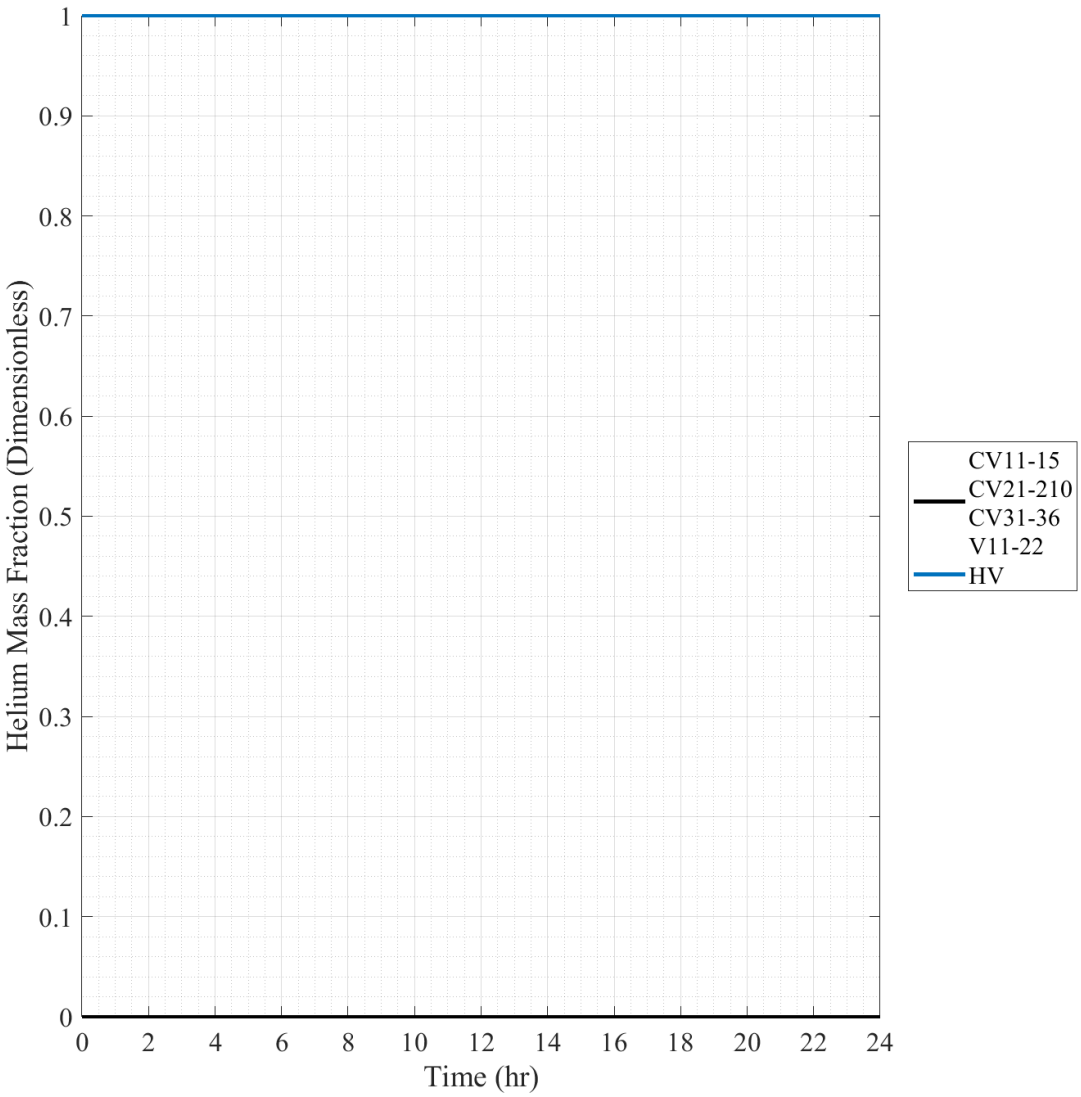

Fig. 6.3. 1/28th-Scale Scenario 0 Helium Mass Fraction.

Oxygen mass fractions stayed constant across the testing timeframe as expected which is seen in Fig. 6.4. The helium volume, HV, maintains at 0% as no oxygen was present in the initial volume definition and no atmosphere ingress could occur into the volume. All other volumes maintain a constant oxygen mass fraction of 23.14%, the mass fraction of oxygen in normal atmospheric air.

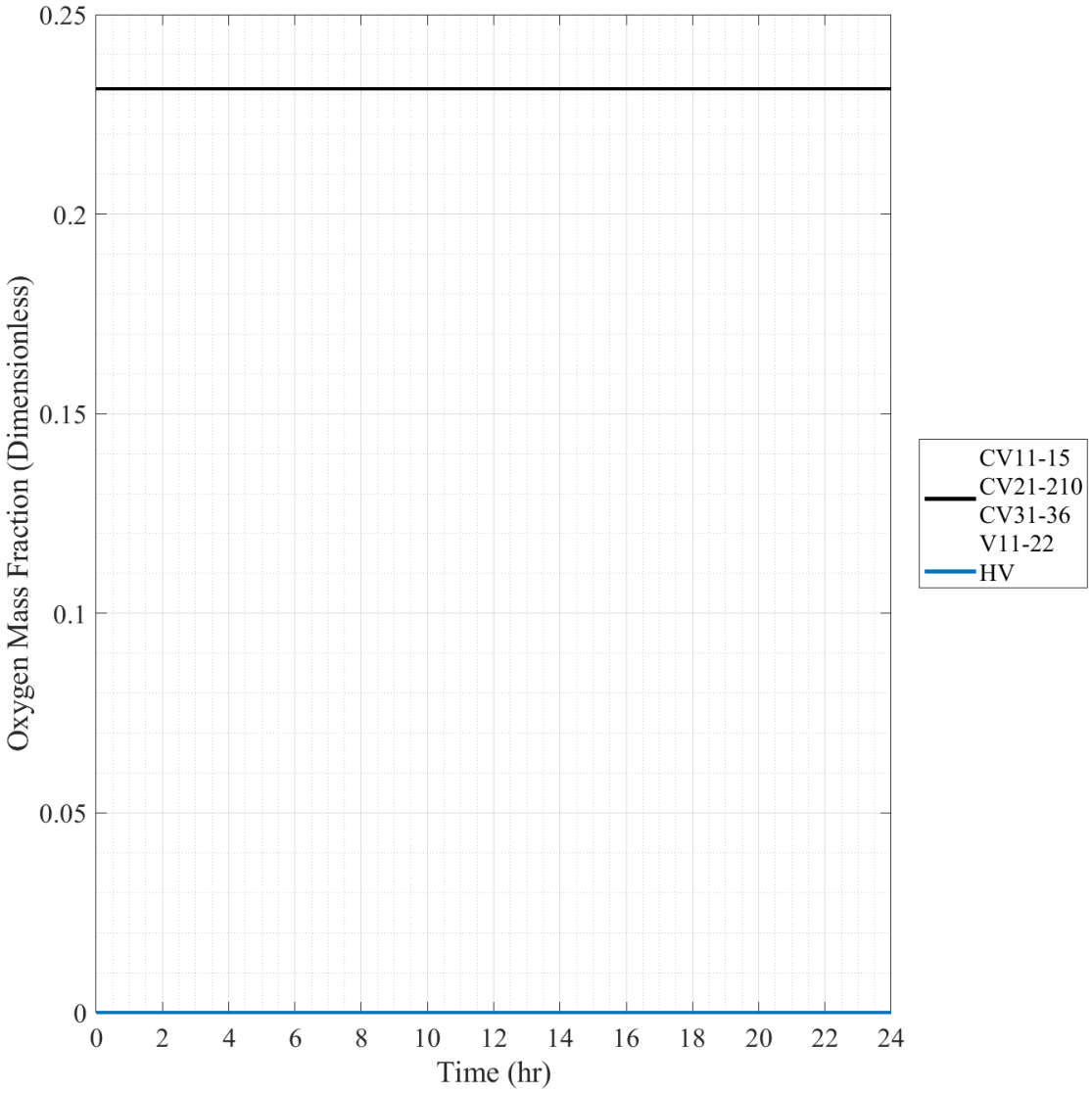

Fig. 6.4. 1/28th-Scale Scenario 0 Oxygen Mass Fraction.

Nitrogen mass fractions also stayed constant across the testing timeframe as expected which is seen in Fig. 6.5. The helium volume, HV, maintains at 0% as no nitrogen was present in the initial volume definition and no atmosphere ingress could occur into the volume. All other volumes maintain a constant nitrogen mass fraction of 75.51%, the expected mass fraction of nitrogen in normal atmospheric air.

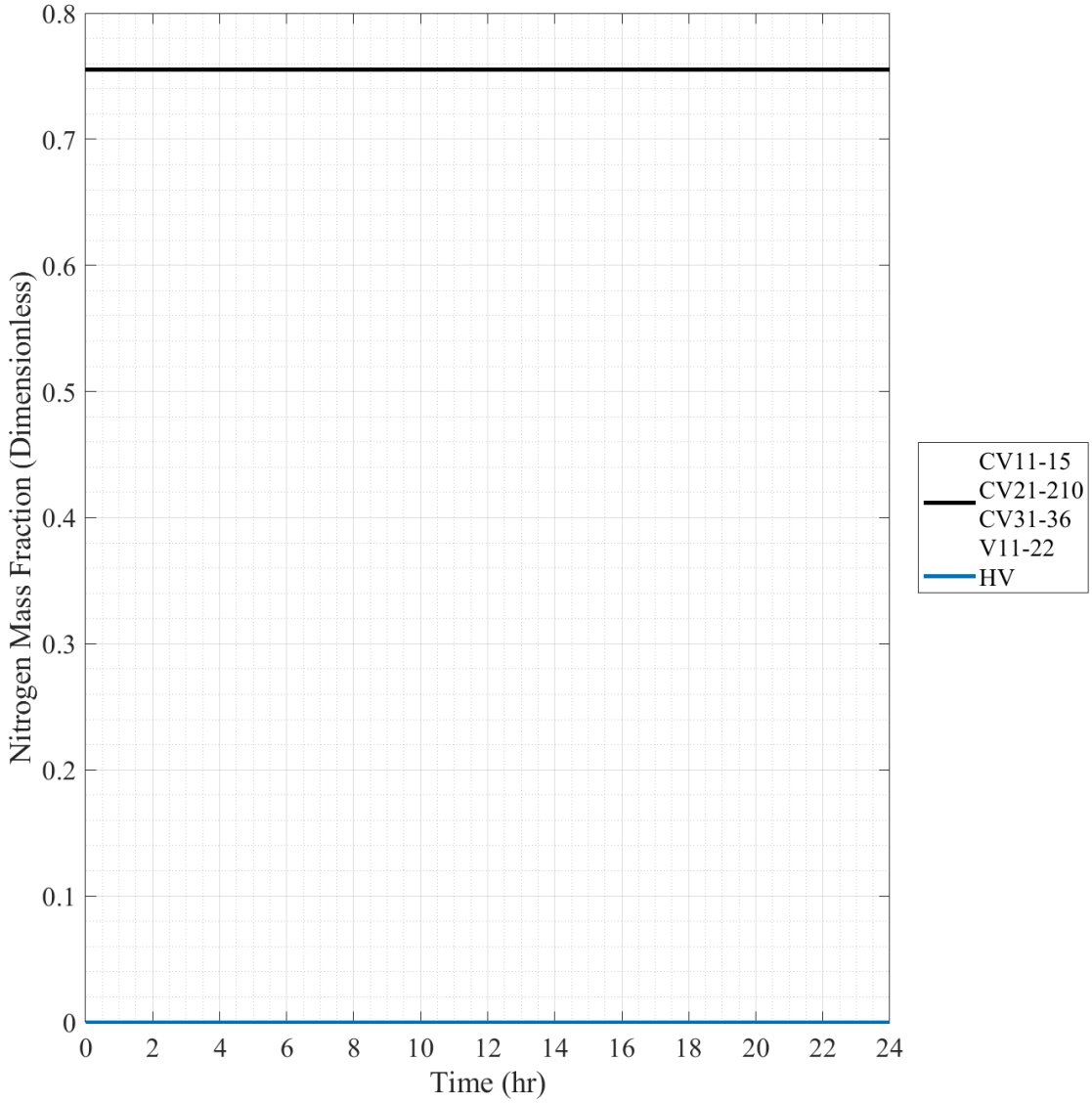

Fig. 6.5. 1/28th-Scale Scenario 0 Nitrogen Mass Fraction.

To better interpret atmospheric mass fraction results in an environment undergoing mixing interactions the results of the mass fraction from the nitrogen and oxygen were combined into a "Combination" mass fraction that represents the sum of their fractions. This should give a relative high estimation of the movement and concentration of the standard atmosphere than by singular mass fraction results. As seen in Fig. 6.6, a constant value for combination mass fraction was obtained as expected with all volumes, other than the helium volume which remains at 0%, maintaining a 98.66% mass fraction.

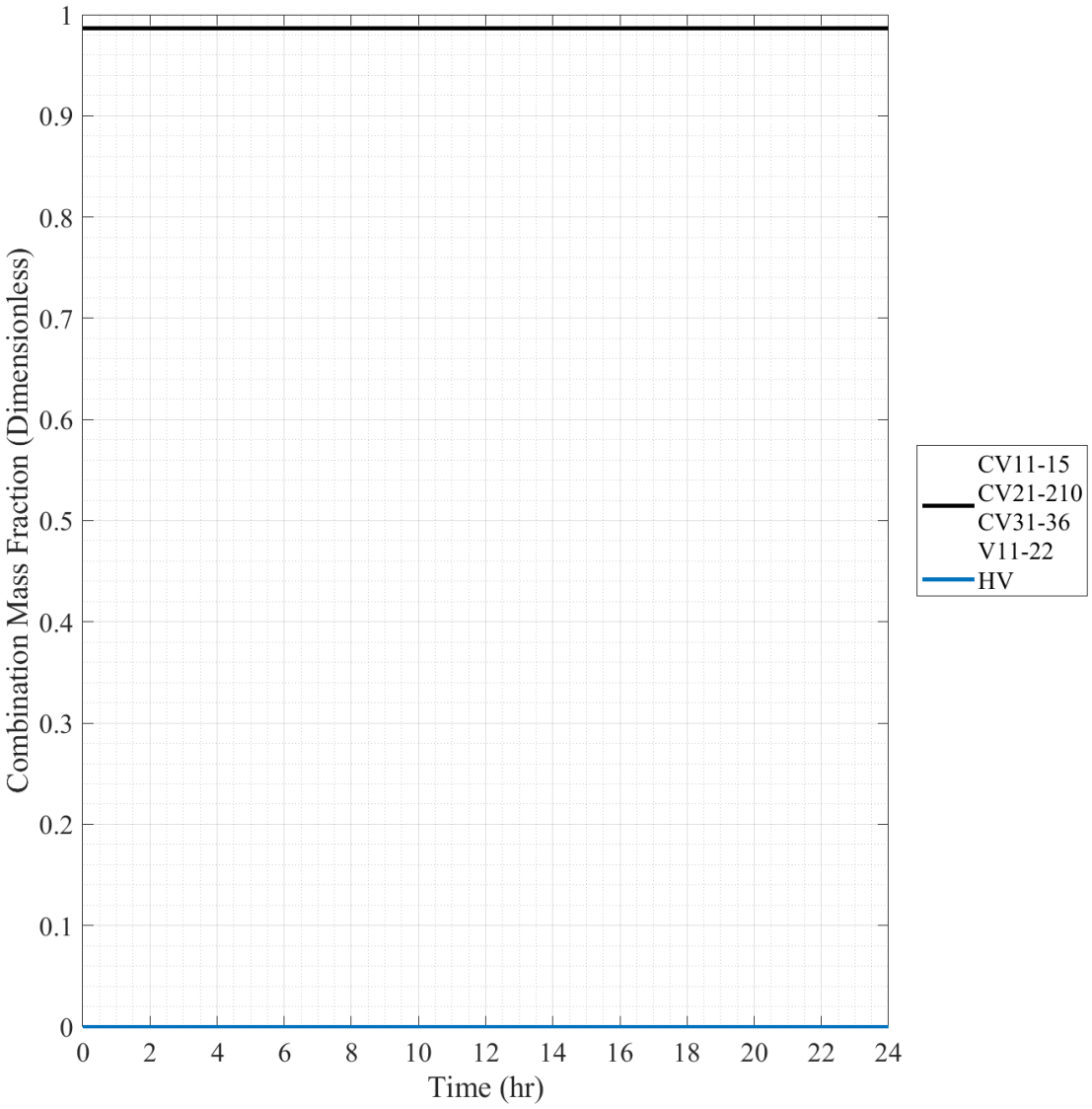

Fig. 6.6. 1/28th-Scale Scenario 0 Combination Mass Fraction.

6.1.2 1/28th-Scale Scenario 1 Results

Scenario 1 is the base RPV break scenario, with no changes to the basic layout of the 1/28th-scale reactor building model. This model is the baseline for comparing to Scenarios 3 and 5 which change the standard layout in their scenario parameters. In this model, flow from the blowdown progresses through all volumes of the model due to the break occurring at one of the furthest points from the vent to the exterior volume. Fig. 6.7 gives a visual example of this scenario's estimated progression, utilizing a figure of the basic regions of the model.

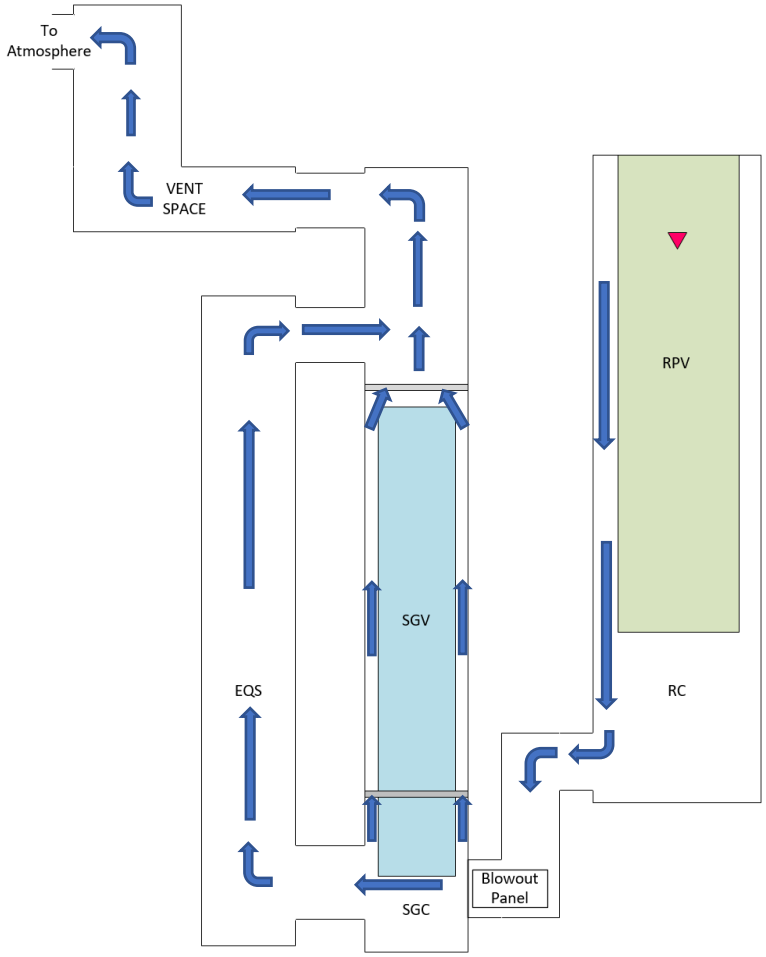

Fig. 6.7. Scenario 1 Estimated Blowdown Progression.

The first plot of results for scenario 1, Fig. 6.8, shows the pressure results of the scenario across the full timeframe of the simulation. Due to the scale of the pressure of the helium volume,

HV, which peaks at the set overal 6.4 MPa, the overall scale of the pressure plot makes it difficult to determine post blowdown pressures of the reactor building volumes. The timescale of the plot is too extended to determine a blowdown timeframe from the break and needs to be cut down to a shorter period of time in order to determine a time to pressure equalization.

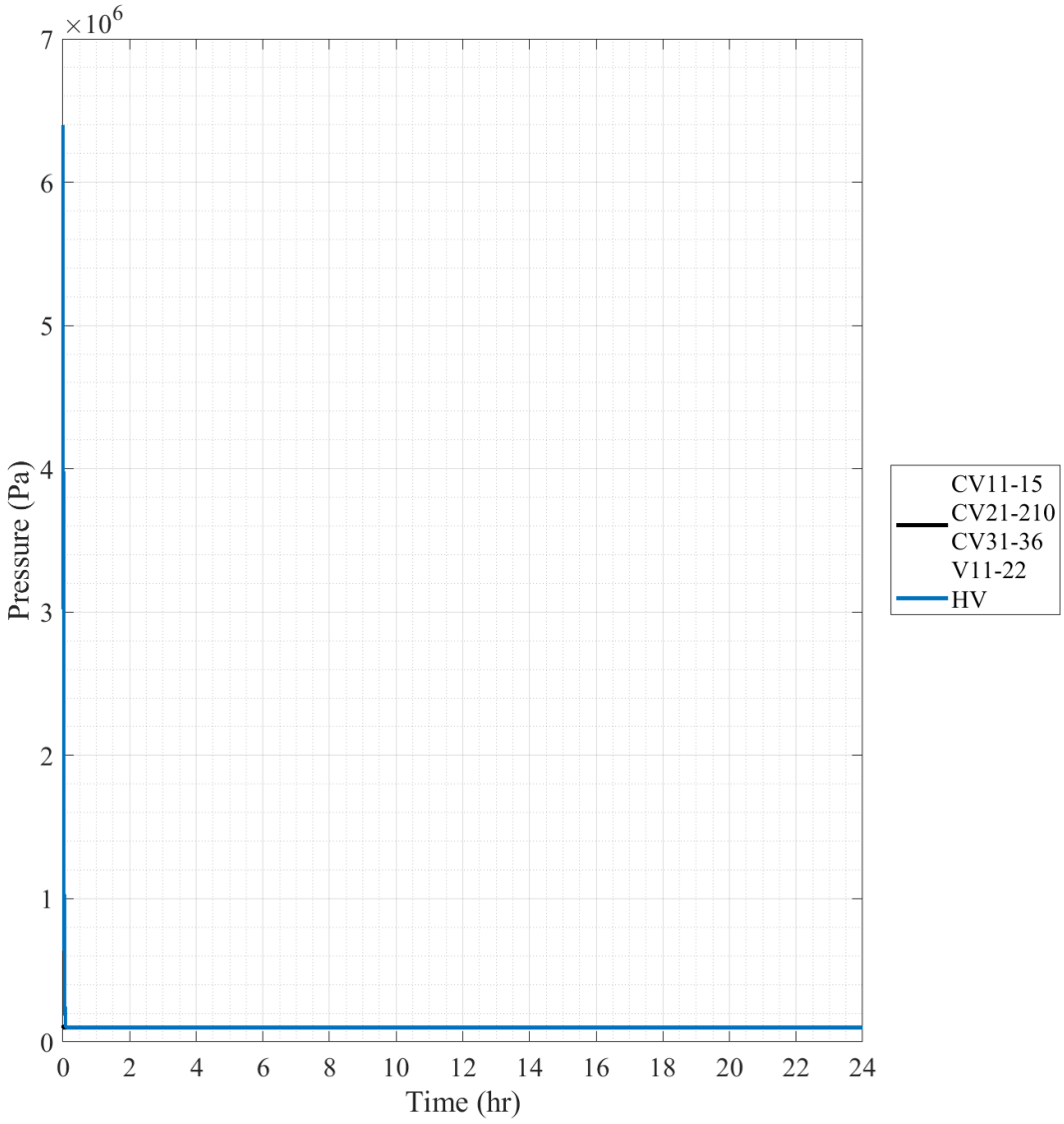

Fig. 6.8. 1/28th-Scale Scenario 1 Pressure.

Reducing the timescale of the pressure plot to 500 seconds, Fig. 6.9 gives a good overview of the progression of the RPV break on a pressure scale. The initial pressure of 6.4 MPa can be seen well at the initial time, then at 20 seconds the pressure begins to fall at an exponential rate as

the boundary break flow path is opened and helium expands out and into the RC volumes. The HV reaches an equalized pressure of ~100 kPa at ~293 seconds following the blowdown initiation, ~313 seconds post simulation initiation.

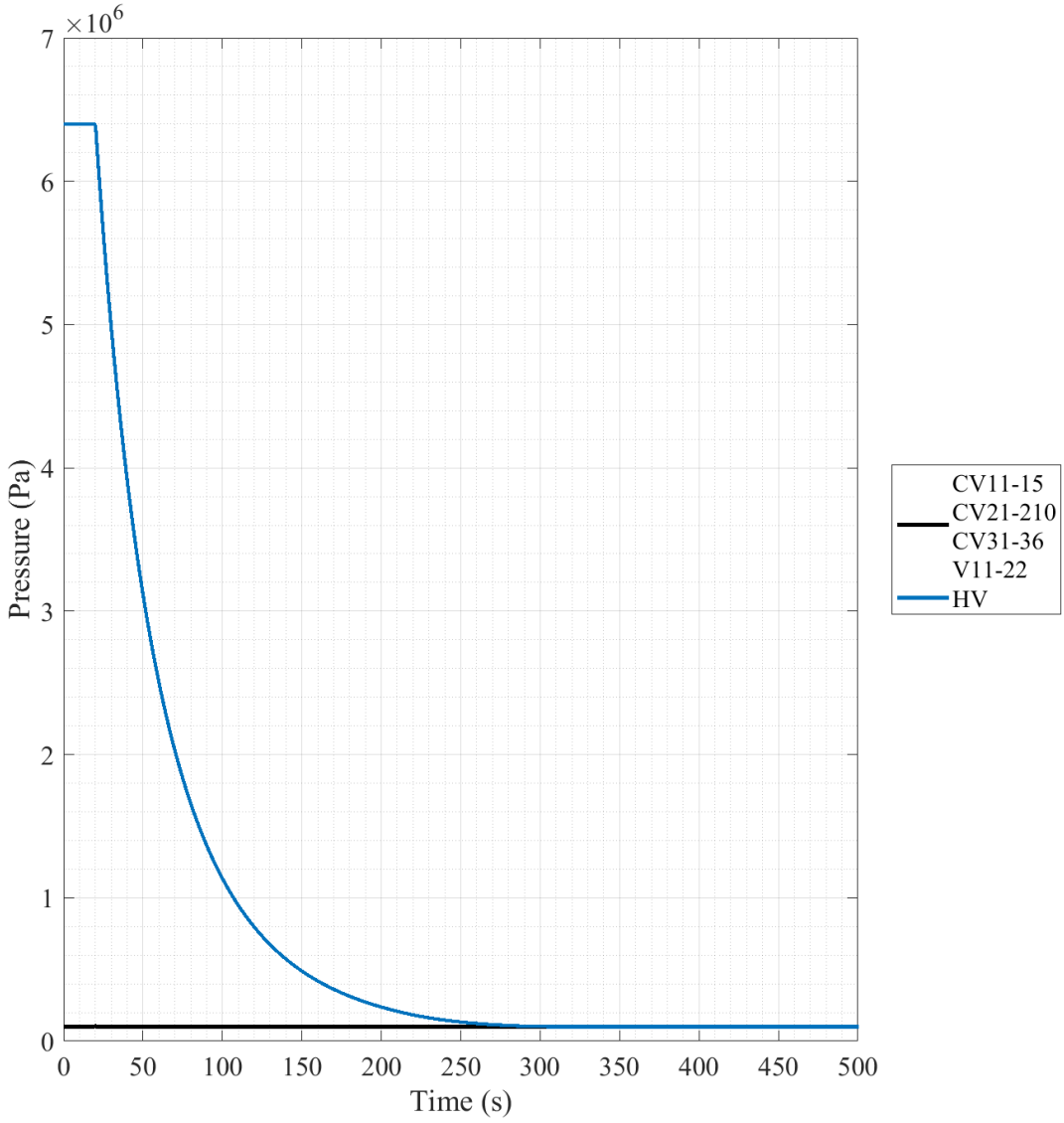

Fig. 6.9. 1/28th-Scale Scenario 1 Pressure, 500 second Timescale.

To bring the view into the true models' response to the helium blowdown, the helium volume is removed from plotting and the timescale is dropped to the 5 seconds following the break initiation. The full breadth of the reactor building model response can then be viewed as the helium volume is not expanding the vertical scale. The full response of the reactor building volumes to

the pressure release is contained to this short timeframe following the helium release. Fig. 6.10 illustrates the building volumes response to the break, with the largest spike occurring in the volumes of CV11-15 (RC) as they are the initial volumes that the helium releases into, with a spike in pressure up to 1.0935×10^5 Pa (9.35 kPa increase).

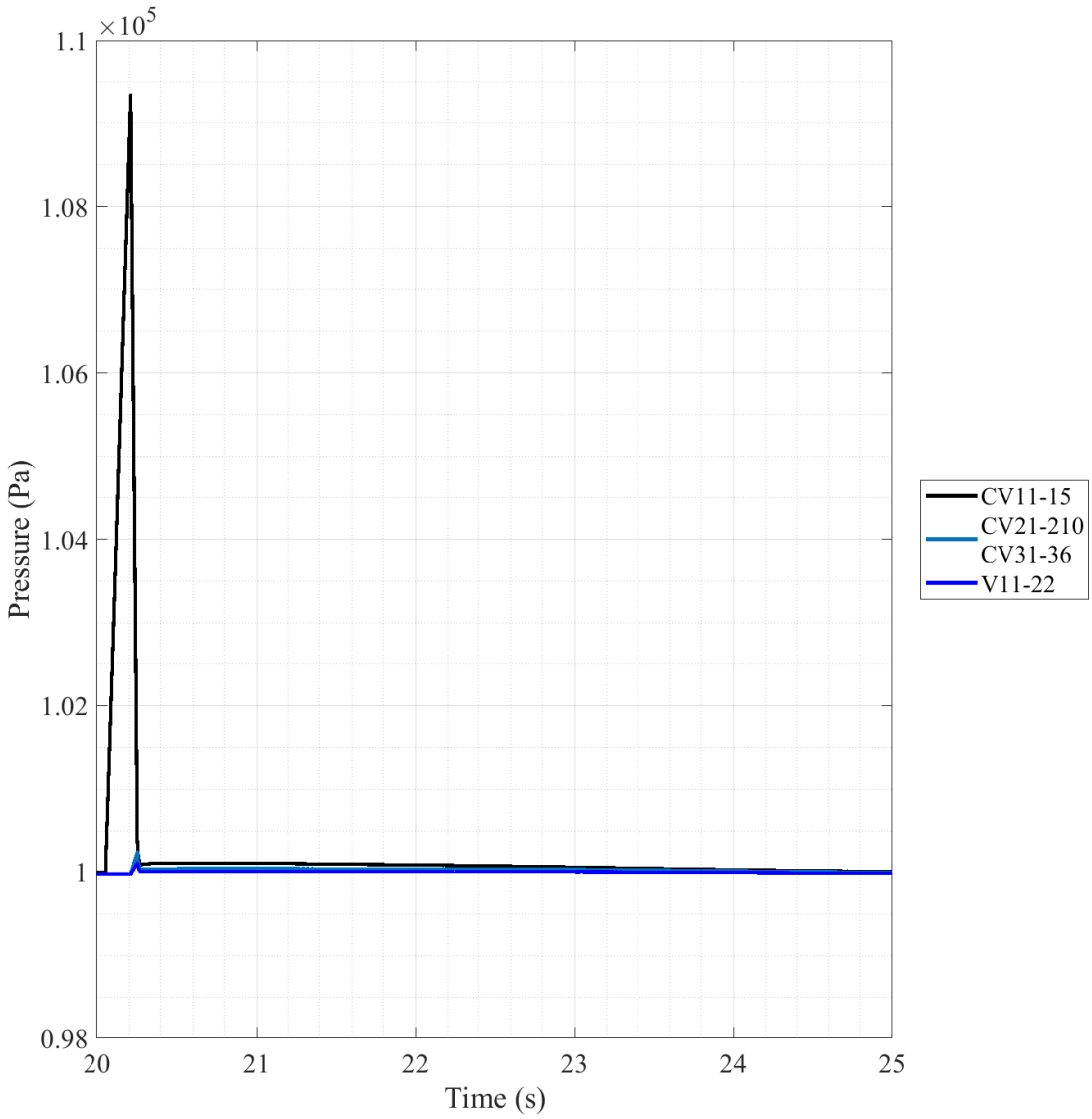

Fig. 6.10. 1/28th-Scale Scenario 1 Pressure, 20-25 second Timescale.

The spiking rise in pressure is linear in response as the helium expands into the RC volumes, compressing the atmosphere into the duct connection and against the blowout panel. The actuation and opening of the panel can be seen as the pressure drops extremely quickly and the

other volumes rise to equalize and fall with the CV11-15 spike, though in much less magnitude. To get a better view of the spikes Fig. 6.11 reduces in the timescale to much closer to the break to gather the minutiae of the reactor building cavity response to the primary coolant boundary break.

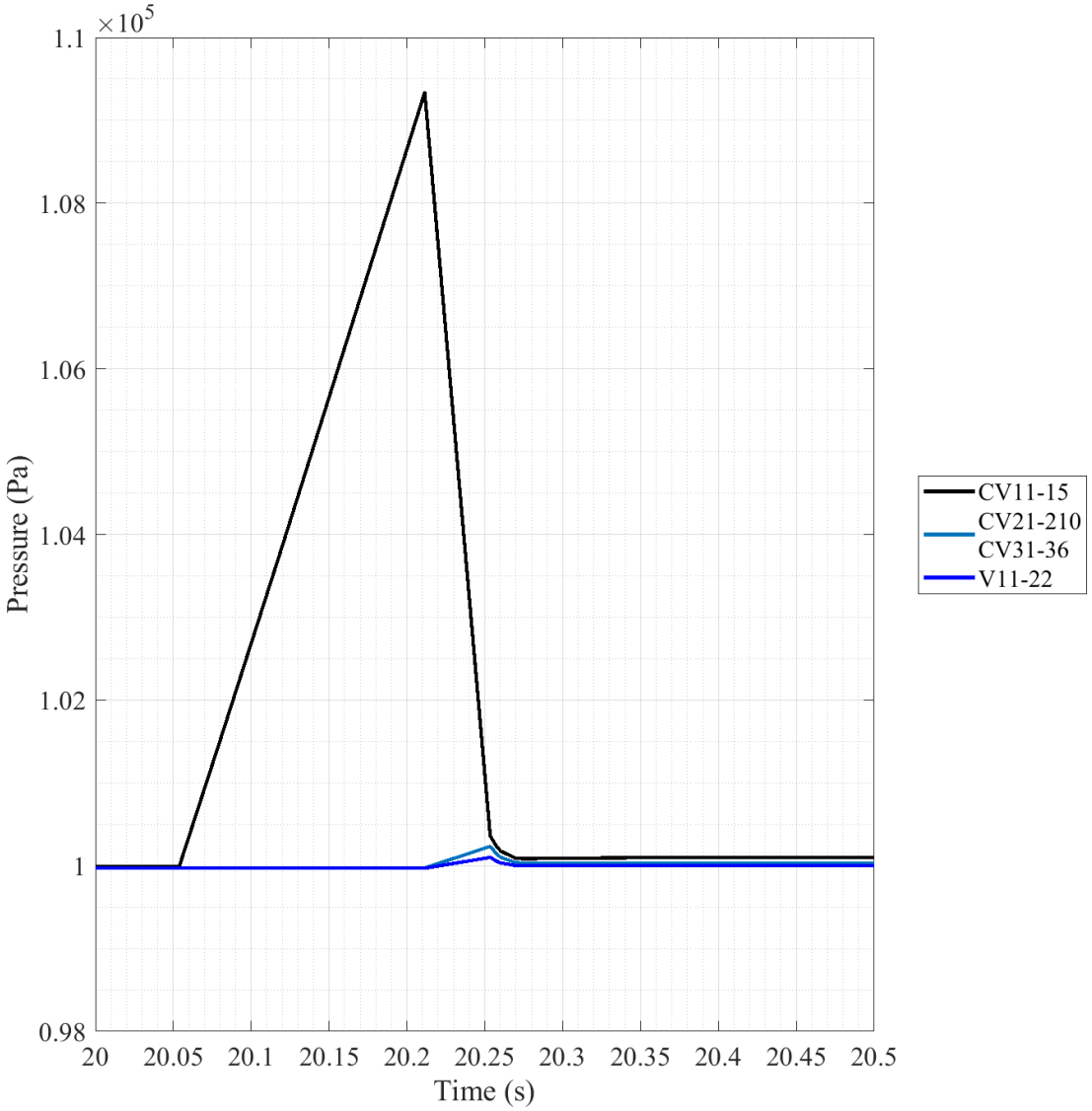

Fig. 6.11. 1/28th-Scale Scenario 1 Pressure, 20-20.5 second Timescale.

Due to the way MELCOR handles timesteps, the break does not occur until ~20.05 seconds in the simulation event, though set to initiate at 20 seconds exactly. Progression of the blowdown in CV11-15 (RC) is confirmed to be linear until the 20.21 second mark, when the blowout panel initiates, and the pressure begins to fall. This decrease is joined with the rise in the lower volumes

pressures as they experience the displaced atmosphere and helium moving through their volumes. They rise to the point of roughly equalizing with the CV11-15 spike as it falls, and they jointly fall to a range around ~100 kPa as they settle in this short timeframe.

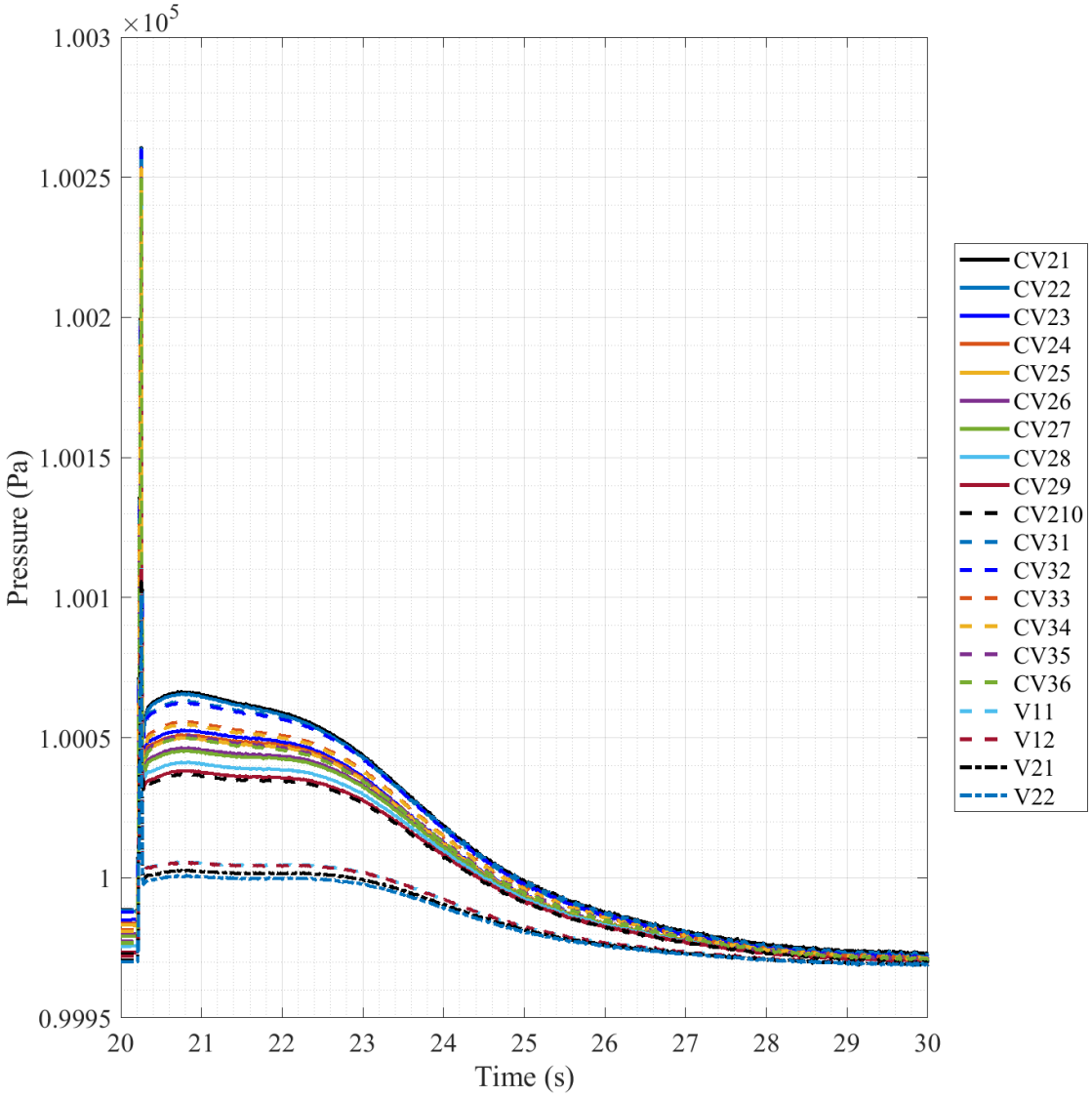

Fig. 6.12. 1/28th-Scale Scenario 1 Pressure, 20-30 second Timescale, No CV11-15.

To get a better view of the volumes other than CV11-15, it is then removed from plotting and the timescale is pulled back to the 10 seconds following the break initiation. Fig. 6.12 shows the results of this plotting, with an overall spike much lower in scale but difficult to discern the groups undergoing the rise. What can be seen though is that there are two distinct groups of

volumes that respond to the blowdown of the helium, an upper and lower group. Both groups undergo a spike that results in higher pressures in the following time, though both decay over the ~10 seconds following the spike to rejoin in a new equilibrium that they didn't have before the blowdown was initiated, which can be seen by comparing the left and right sides of the plot.

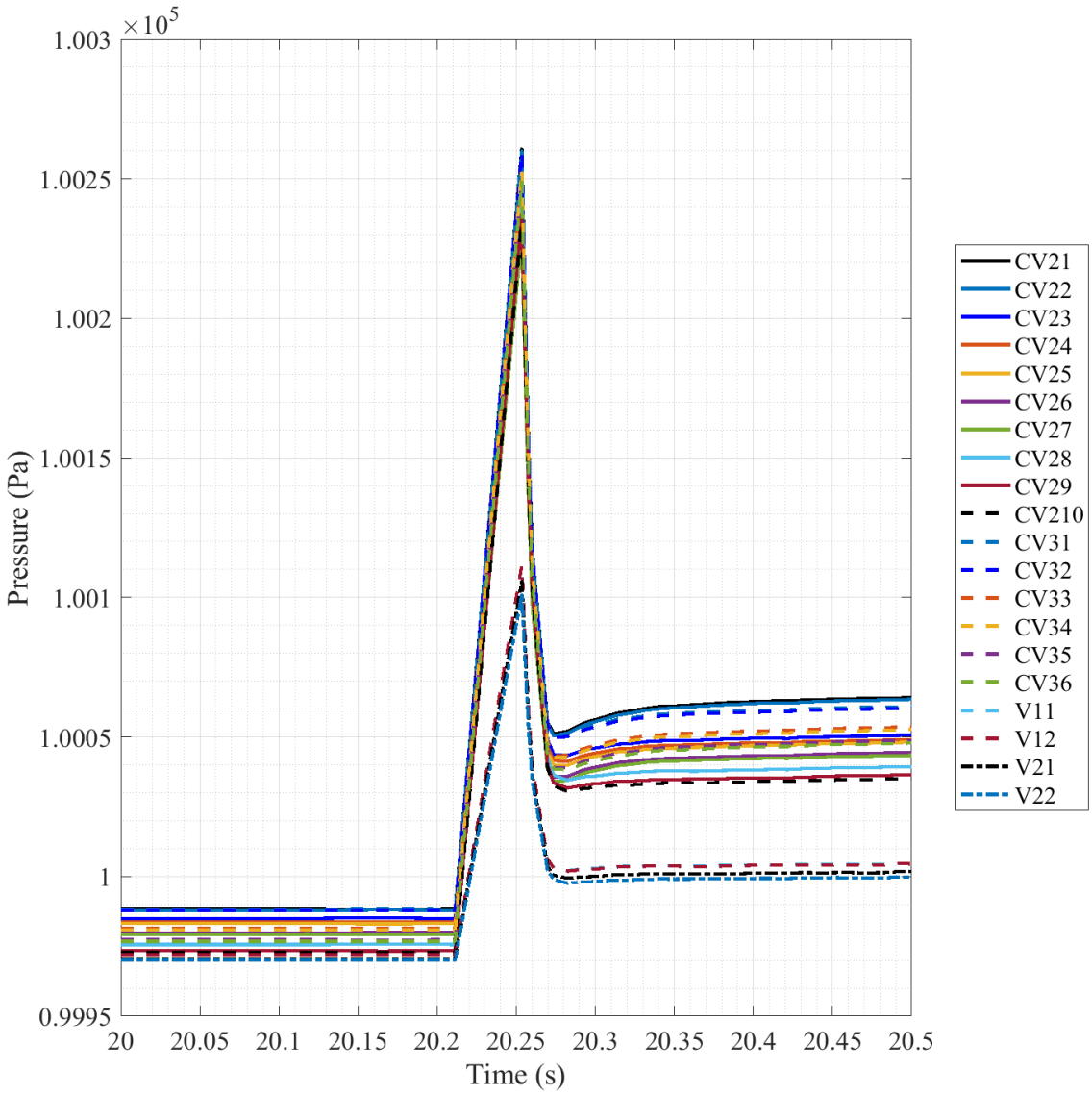

Fig. 6.13. 1/28th-Scale Scenario 1 Pressure, 20-20.5 second Timescale, No CV11-15.

Cutting the timescale back down to the 20-20.5 second range, Fig. 6.13 allows a better view of the plotted volumes response. The distinction can be made between the two groups as they rise at different rates following the blowout panel initiation, their primary difference being their

location overall in the model. The upper group is composed of CV21-210 (SGC) and CV31-36 (EQS) as they spike to a max pressure of ~1.0026×10^5 Pa (~260 Pa increase), then fall into a group of distributed pressures around the 1.0005×10^5 Pa range which eventually recombines as discussed previously. The bottom spike is composed of the vent space volumes of V11-22 (Vent Space) and only spike to a maximum of ~1.0011×10^5 Pa (~110 Pa increase), likewise falling to a ~100 kPa range before the recombination period roughly 10 seconds following.

The next portion of plots examine the mass fractions of several major gases being tracked in the volumes across the simulation. Three of these gases, helium, oxygen, and nitrogen, were chosen to be plotted based on their importance in tracking the blowdown progression through the volumes being simulated. Nitrogen and oxygen were also chosen to be plotted as they make up the vast majority of the mass of the standard atmospheric air and therefore should give a good indication of the displacement of atmosphere and potential refill.

The first gas mass fraction to be plotted is that of helium, which can be seen in Fig 6.14. CV11-15, CV22-29, and CV32-36 are filled completely or near max with helium in the figure. All volumes start at initial concentrations of 0% and then spike to near completely filled fractions as the blowdown occurs and the atmosphere is displaced. On the opposite end of the scale, V22 experiences a spike in helium concentration as the blowdown occurs and the blowdown advances through the volumes, but it quickly falls back to near 0% as it is very close to the exterior volume allowing a quick refill. CV21 and CV31 experience little change along the progression of the scenario, with very slight increases in helium content in the range of E-3 mass fraction addition to their normal air composition.

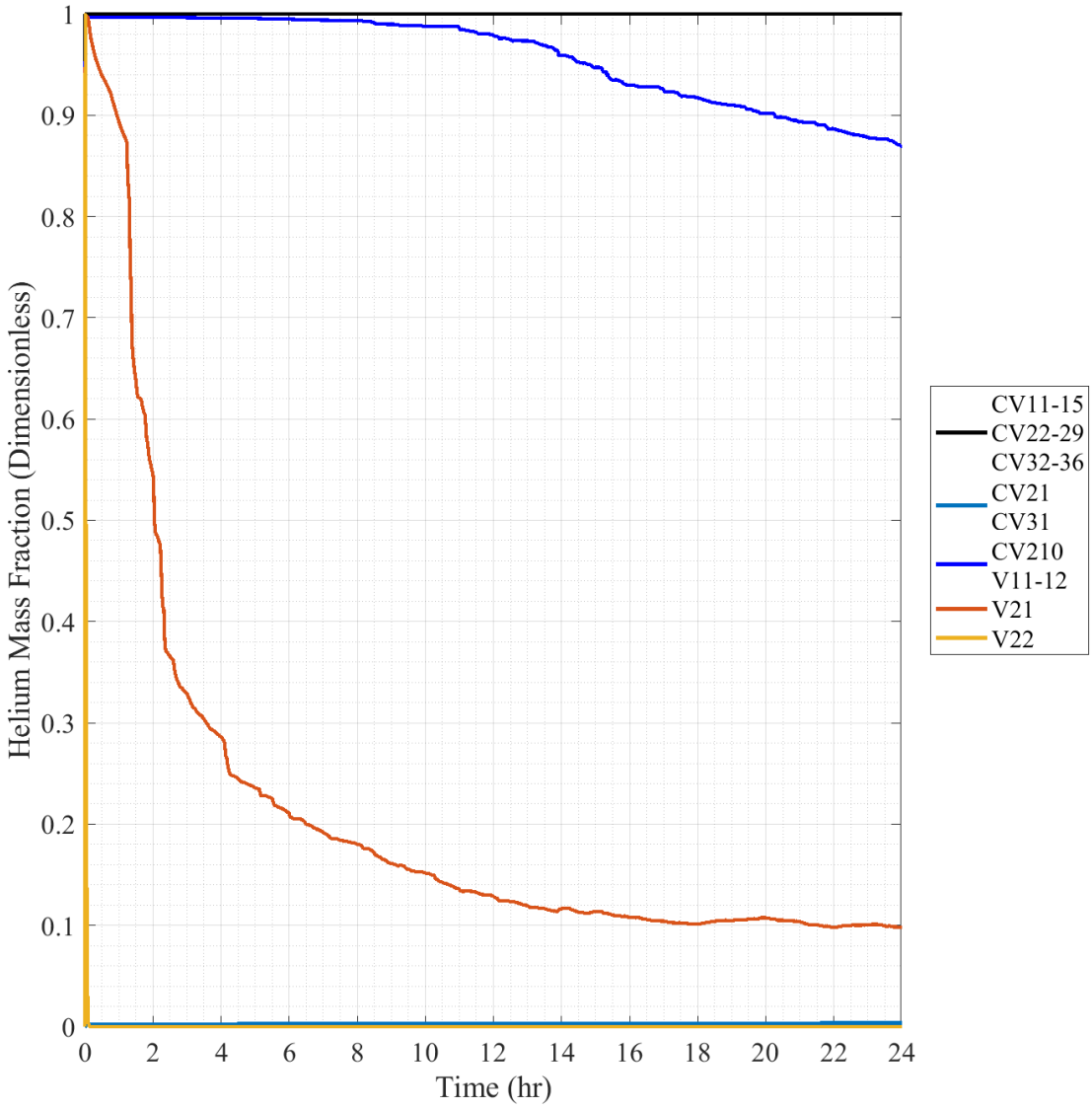

Fig. 6.14. 1/28th-Scale Scenario 1 Helium Mass Fraction.

V21 experiences the long trailing lower transient of the figure, as it slowly refills with atmosphere following V22 undergoing a quick refill. As V21's concentration drops to ~30% the upper transient of V11-12 and CV210 begin a decrease in helium concentration as air begins to refill into those volumes. Across the entire time of the scenario progression V21 falls to ~10% where it seems to plateau to the end of the simulation while the volumes below it begin to slowly refill, maybe showing an indication of helium being redistributed up and out of the reactor building

as refill was occurring. Getting a better look at the initial distribution changes will require a shrinking of the timescale which will be performed in a later plot.

Fig. 6.15 presents the mass fraction data for oxygen throughout the reactor building volumes. As was seen in the scenario 0 data, the maximum concentration of oxygen in the model at any one time is 23.14% which is replicated in this figure's data. Comparing the trends of this figure to what was seen in Fig. 6.14 it can be seen the trends are simply inverses of each other, where instead of downward trends as refill occurs, upward trends occur.

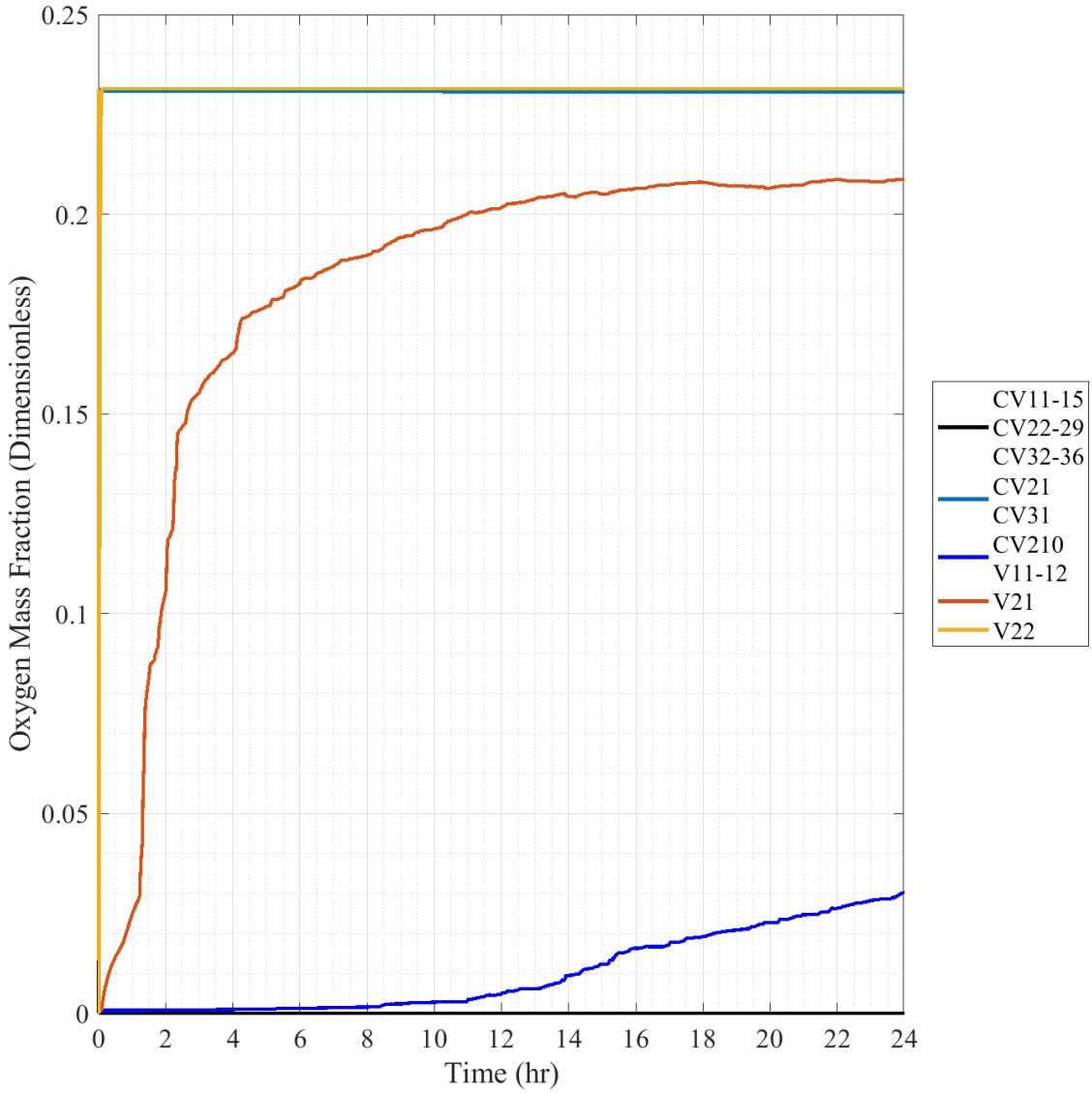

Fig. 6.15. 1/28th-Scale Scenario 1 Oxygen Mass Fraction.

Fig. 6.16 presents the mass fraction data for nitrogen throughout the scenario, and much like the previous figure of oxygen mass fraction, shows the same inverse trends in comparison to what was seen of the helium data. The major difference with this figure is the changed scale of the results, with a maximum nitrogen fraction of 75.51%. Fig. 6.15 and 6.16 have both shown that atmospheric standard air returns and is displaced in equal portions and do not suffer from disassociation between its gaseous components.

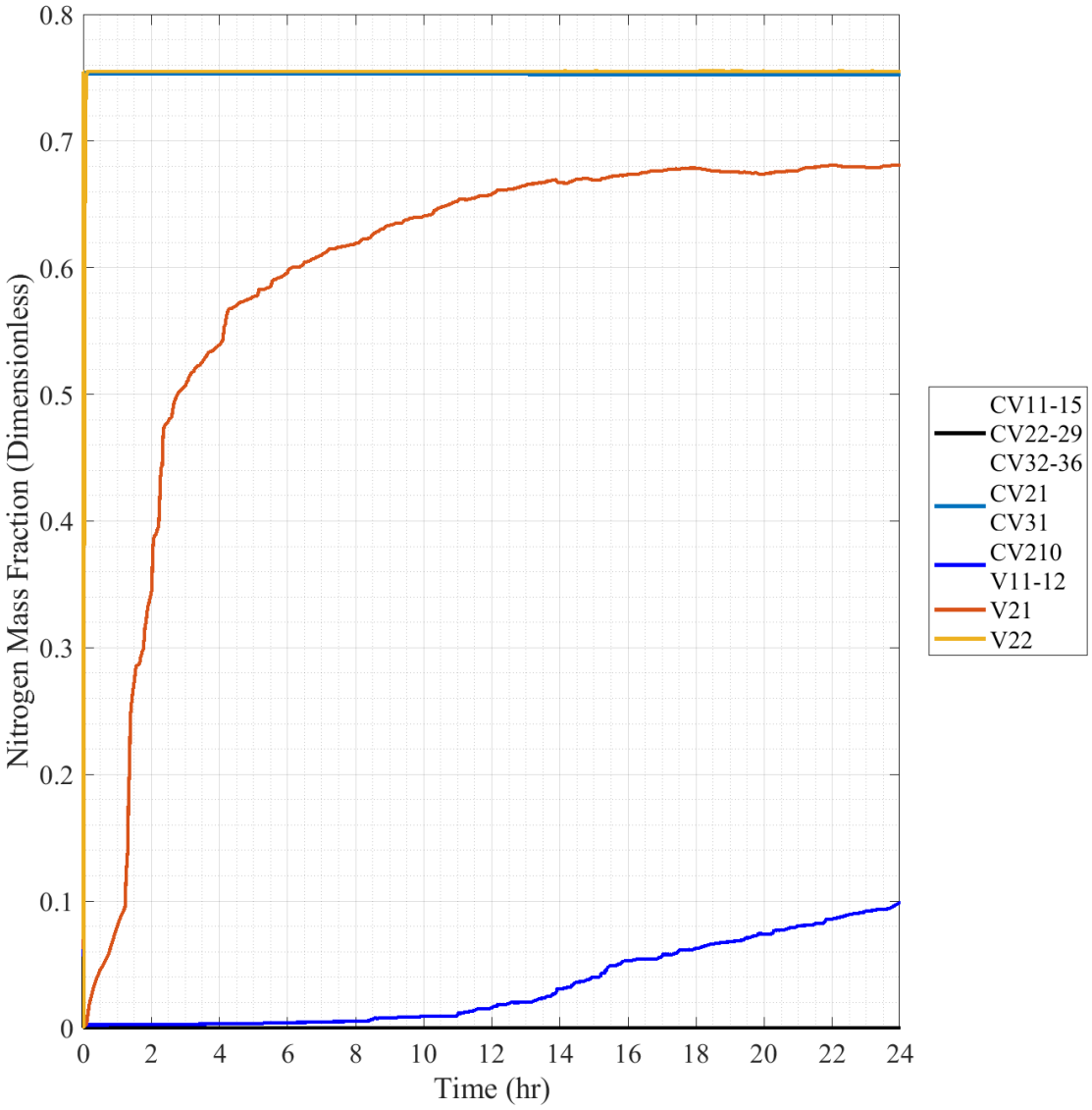

Fig. 6.16. 1/28th-Scale Scenario 1 Nitrogen Mass Fraction.

Due to this lack of dissociation, a decision was made to combine the mass fractions of nitrogen and oxygen to give an approximation of total atmosphere displacement done by helium. Results sections past scenario 2 will not include nitrogen and oxygen mass fractions plots as there are no fractional differences between them and they can be relegated to a consolidated combination mass fraction to show results. Their plots will be included in Appendix D for further reference.

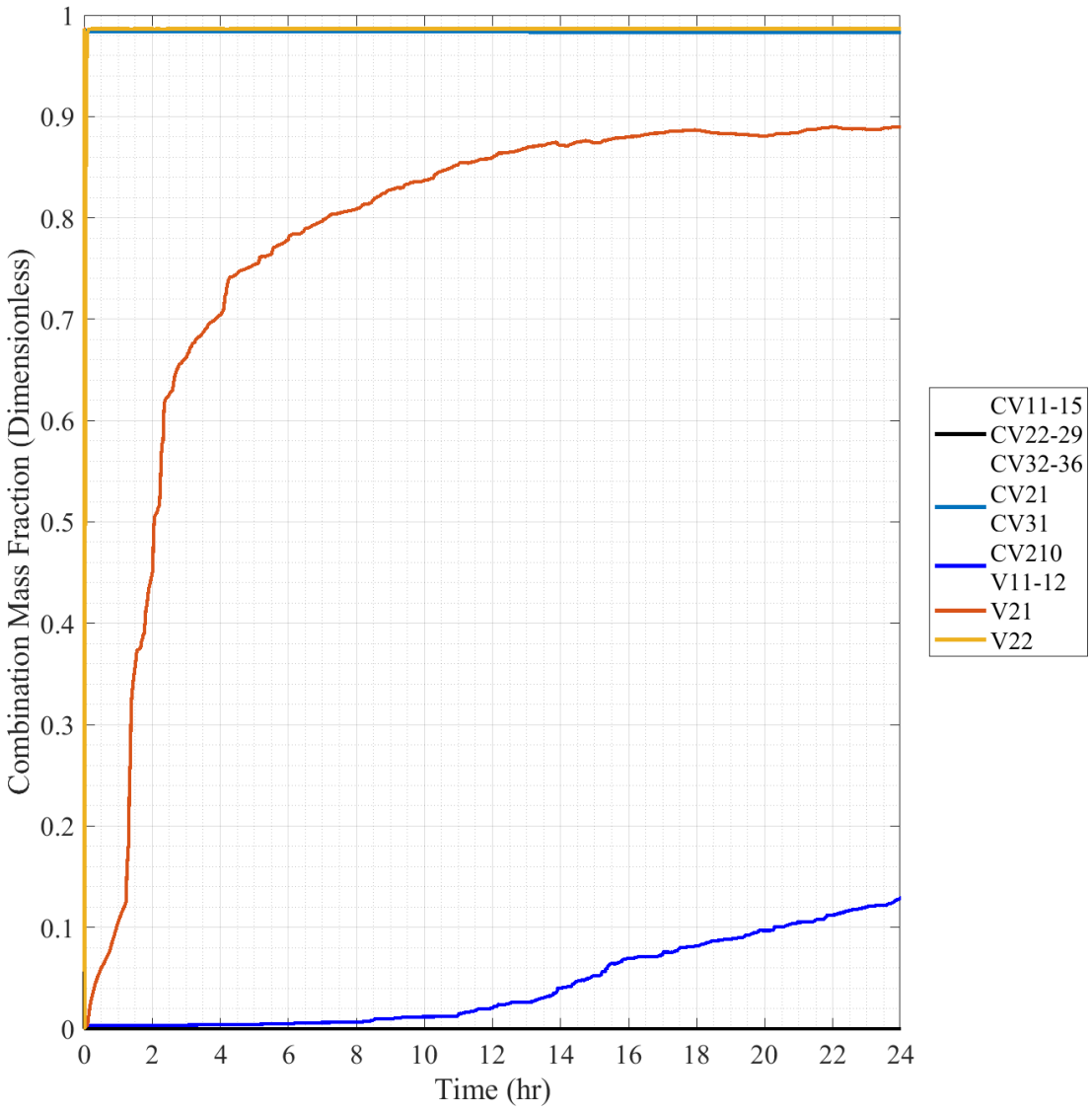

Fig. 6.17. 1/28th-Scale Scenario 1 Combination Mass Fraction.

Fig. 6.17 sums the oxygen and nitrogen mass fractions together as previously discussed to an "Combination" mass fraction composed of the combination of the two individual mass

fractions. The combination of these two gases make up 98.66% of the total mass fraction of standard air and should be a good comparison to the helium mass fraction for comparisons. Finally, by comparison with 6.17, and what has been previously discussed with the individual oxygen and nitrogen mass fraction figures, it can be seen that the figure is simply an inverse of the helium trends. Due to the linked relationship of the results, this set of data will be used to examine the initial details of the blowdown from a mass fraction perspective as was done with the pressure.

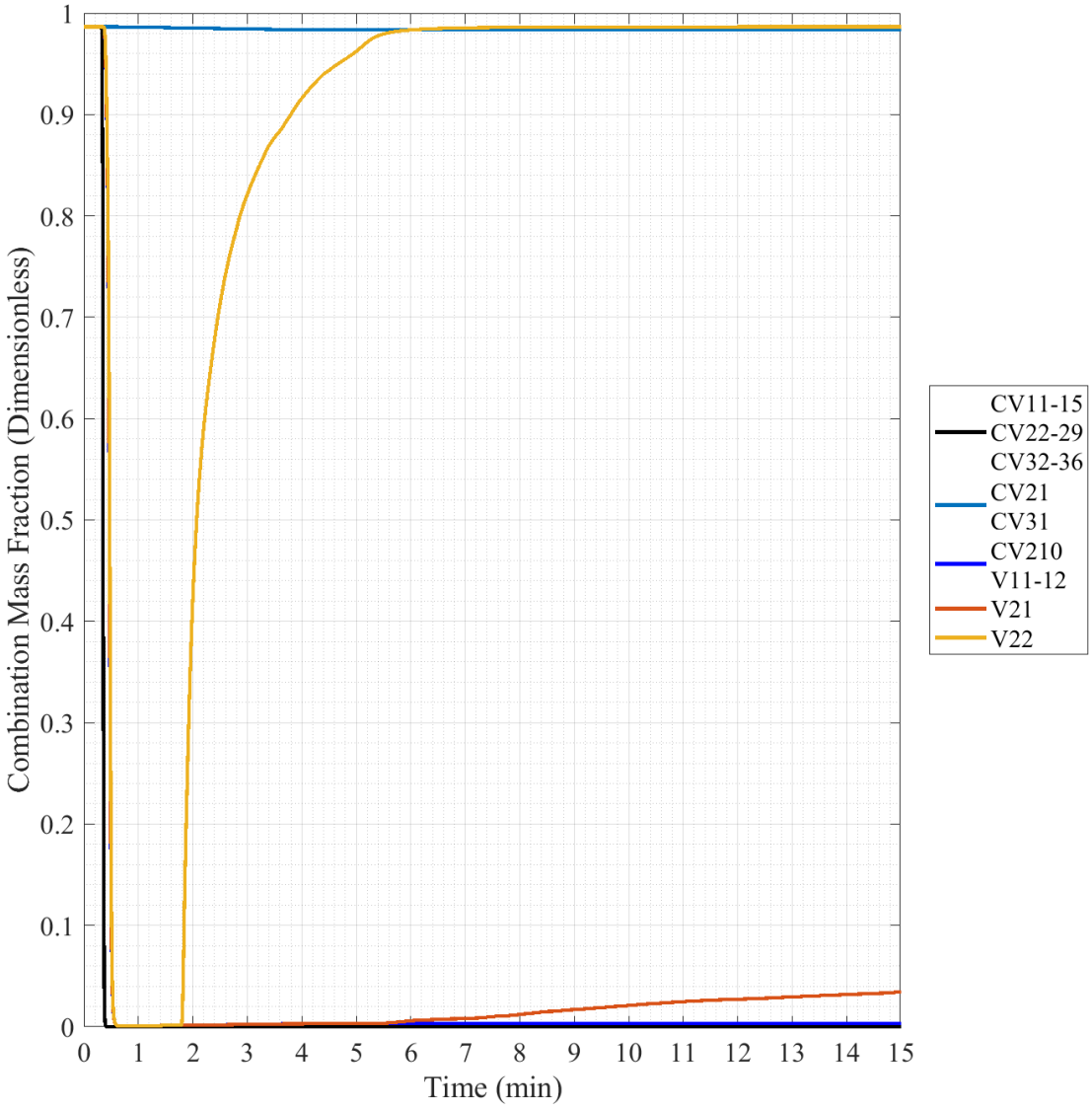

Fig. 6.18. 1/28th-Scale Scenario 1 Combination Mass Fraction, 15 minute Timescale.

Fig. 6.18 reduces in the timescale of the combination mass fraction to get details of the initial post-break building response to the spreading helium. In V22, the combination mass fraction is seen to drop from the start time of the break, then at ~1.8 minutes the volume begins to refill, taking only ~4 minutes to do so, during which there is slight unrest in the volumes that are filled with helium. When V22 reaches a completely refilled with air state, V21 begins to refill which can be seen from ~6 minutes onward. To obtain more blowdown knowledge, the data must be shown on a further expanded timescale.

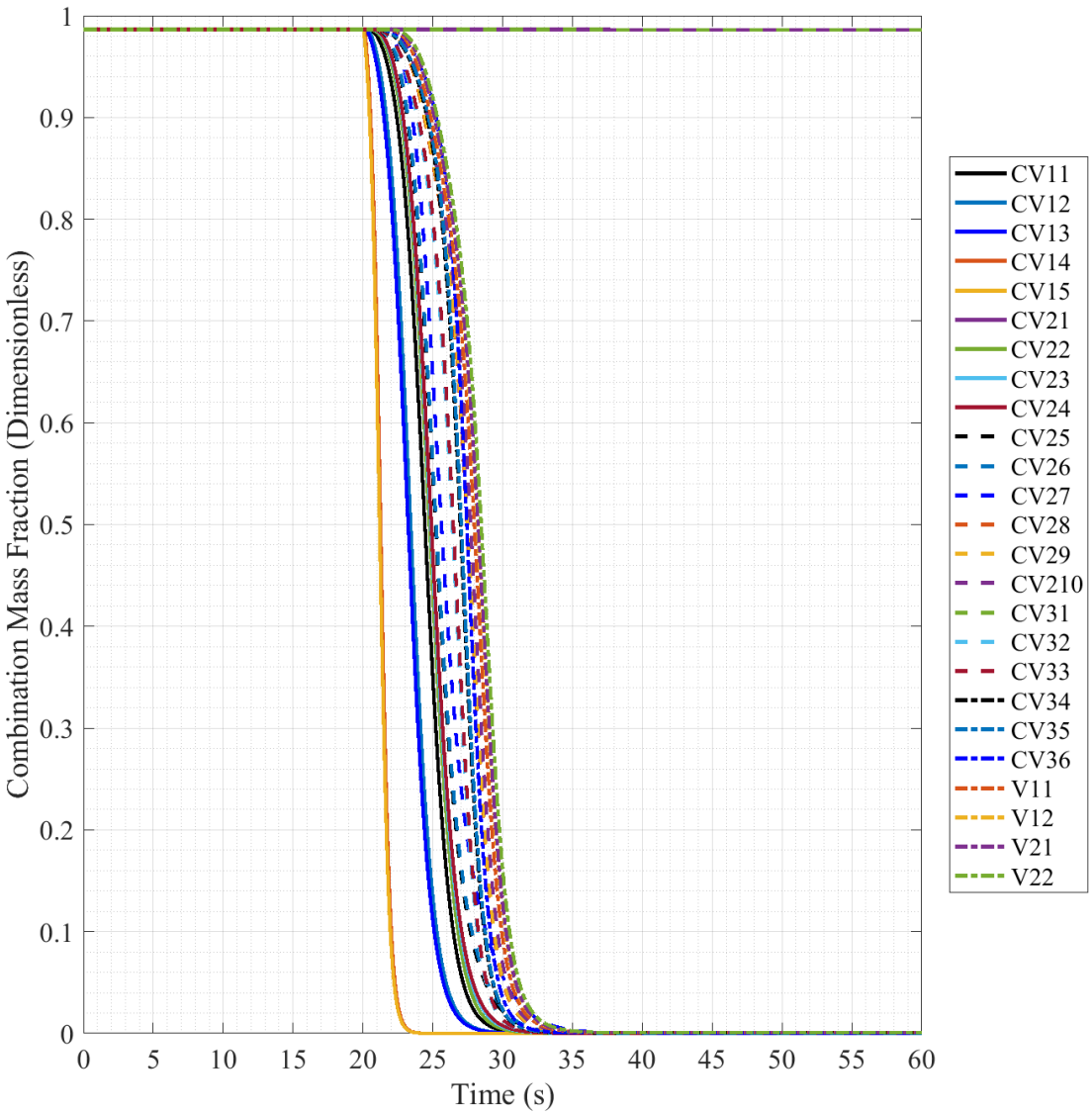

Fig. 6.19. 1/28th-Scale Scenario 1 Combination Mass Fraction, 60 second Timescale.

Fig. 6.19 shows the combination mass fraction during the first 60 seconds of the scenario, where the progression of loss of air content in various CV's is apparent. Post-break initiation, about 15 seconds is needed for all volumes to be voided of their air content, barring CV21 and CV31 which undergo very little helium influx. Going from left to right on the plot the general flow path of helium through the volumes can be seen, with the left most volumes being in the RC, and moving right moves into the SGC and EQS, ending with the vent spaces on the far right being voided last as expected.

6.1.3 1/28th-Scale Scenario 2 Results

Scenario 2 is the base SGV break scenario, with no changes to the basic layout of the 1/28th-scale reactor building model. This model is the baseline for comparing to Scenarios 4 and 6 which change the standard layout in their scenario parameters. In this model, flow from the blowdown progresses through a majority of the volumes of the model, excluding the RC (CV11-15) and the ducts that connect them to the SGC as the blowout panel does not activate. Fig. 6.20 gives a visual example of this scenario's estimated progression, utilizing a figure of the basic regions of the model.

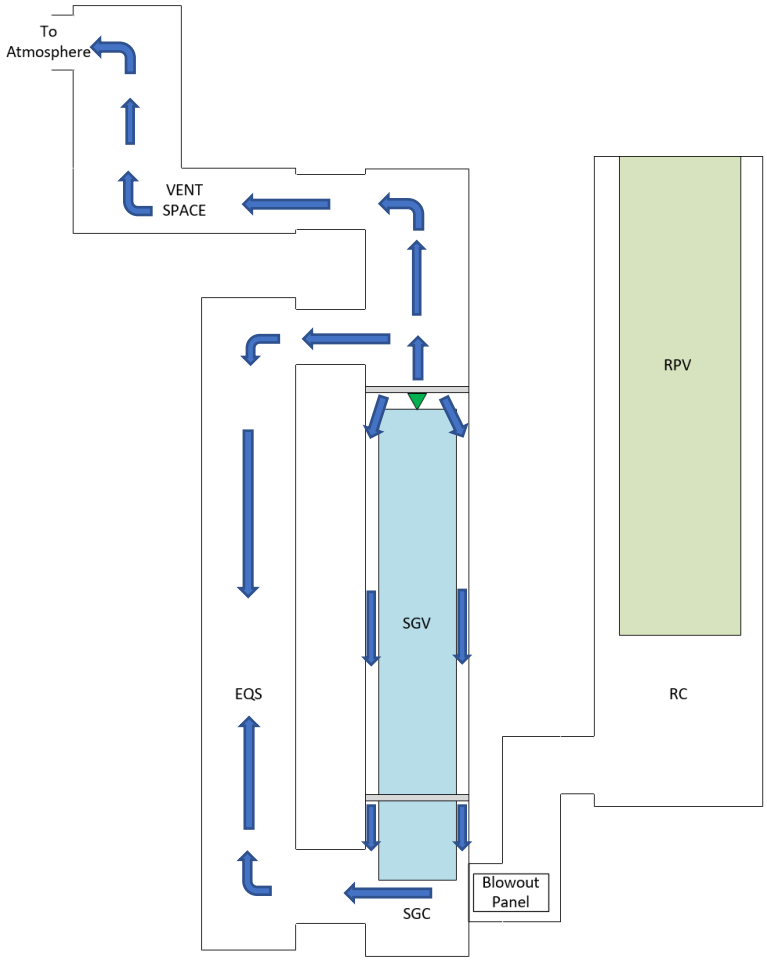

Fig. 6.20. Scenario 2 Estimated Blowdown Progression.

The first plot of results for scenario 2, Fig. 6.21, shows the pressure results of the scenario across the full timeframe of the simulation. Much like the plot in scenario 1, due to the scale of the pressure of the helium volume, HV, peaking at the 6.4 MPa, the overall scale of the pressure plot makes it difficult to determine post blowdown progression of the reactor building volumes and the blowdown time. The timescale of the plot is too extended to determine a blowdown timeframe from the break and needs to be cut down to a shorter period of time in order to determine a time to pressure equalization.

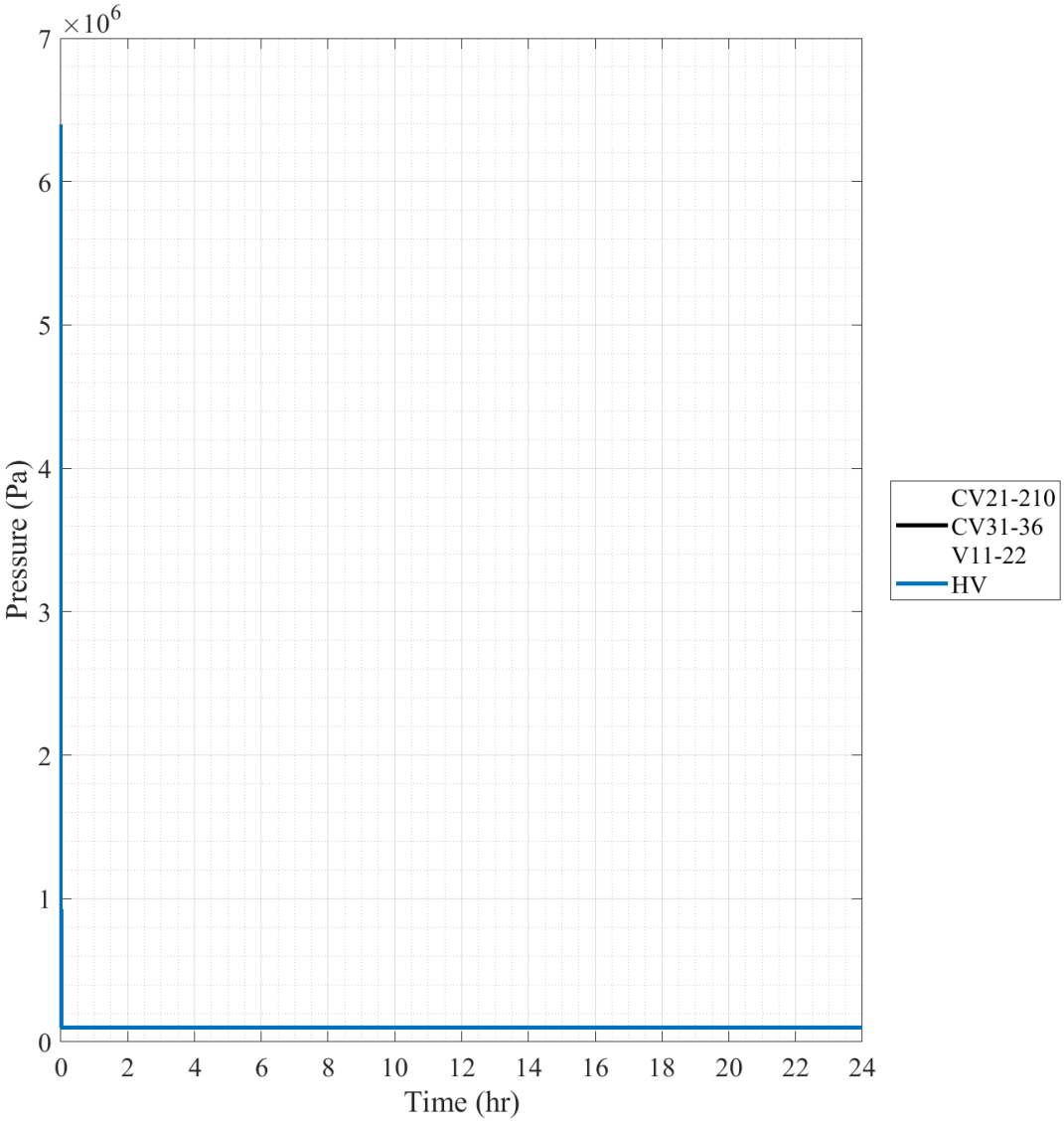

Fig. 6.21. 1/28th-Scale Scenario 2 Pressure.

Reducing the timescale of the pressure plot to 50 seconds, Fig. 6.22 gives a overview of the progression of the SGV break on a pressure scale. The initial pressure of 6.4 MPa can be seen extremely well at the initial time, then at 20 seconds the pressure begins to fall at an exponential rate as the break flow path is opened and helium expands out and into the SGC volumes. The HV reaches an equalized pressure of ~100 kPa at ~22.1 seconds following the blowdown initiation, ~41.1 seconds post simulation initiation.

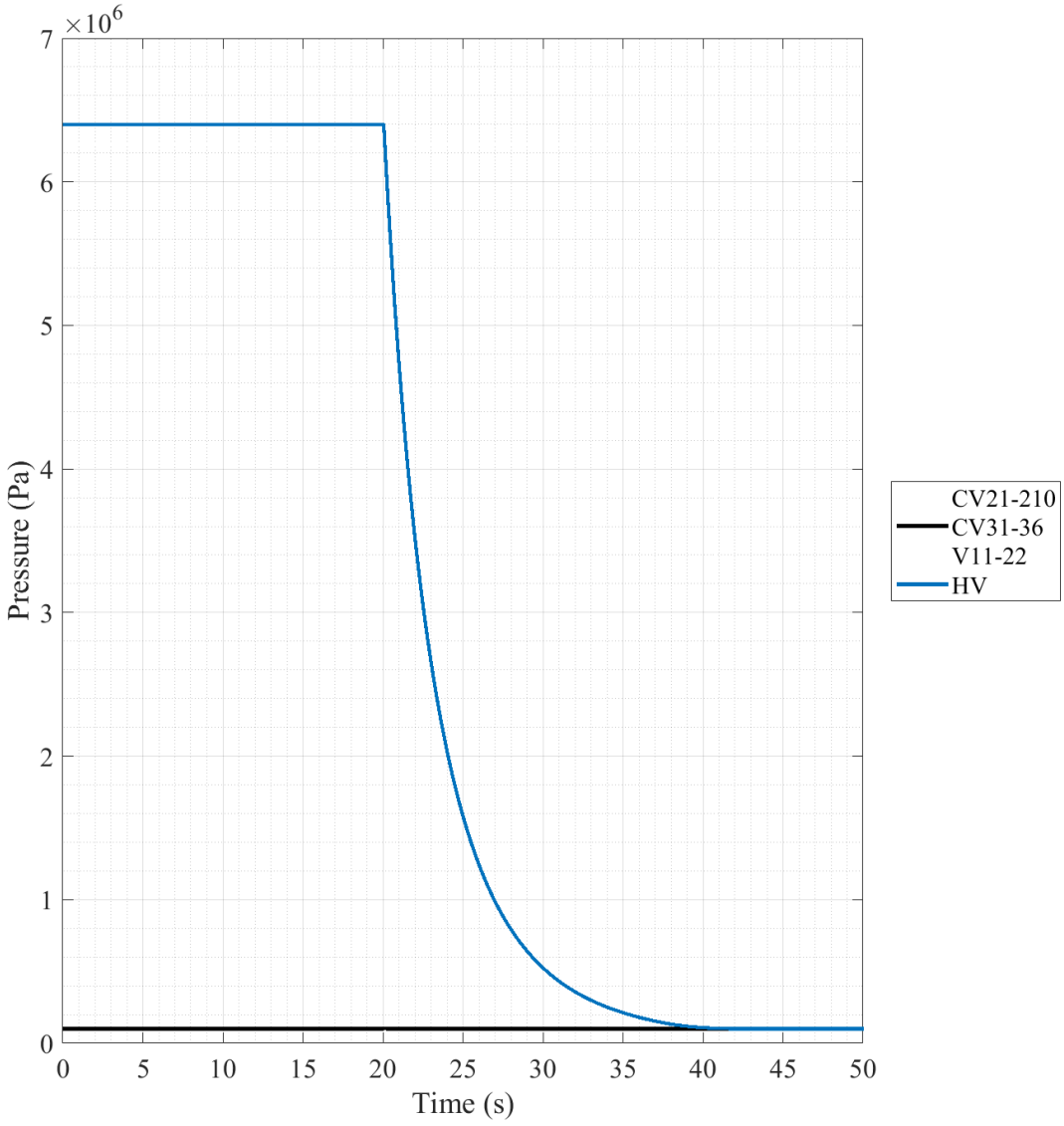

Fig. 6.22. 1/28th-Scale Scenario 2 Pressure, 50 second Timescale.

Removing the helium volume from the plot allows a better view of the reactor building response to the helium release, which can be seen in Fig. 6.23. It can be seen, though roughly at this timescale that there are two separate groups of volumes undergoing different pressure transients following the break. These transients though come back together in the following 5 seconds of post-break initiation to achieve equilibrium at ~100 kPa. To get a better view of the spikes, the timeframe needs to be reduced.

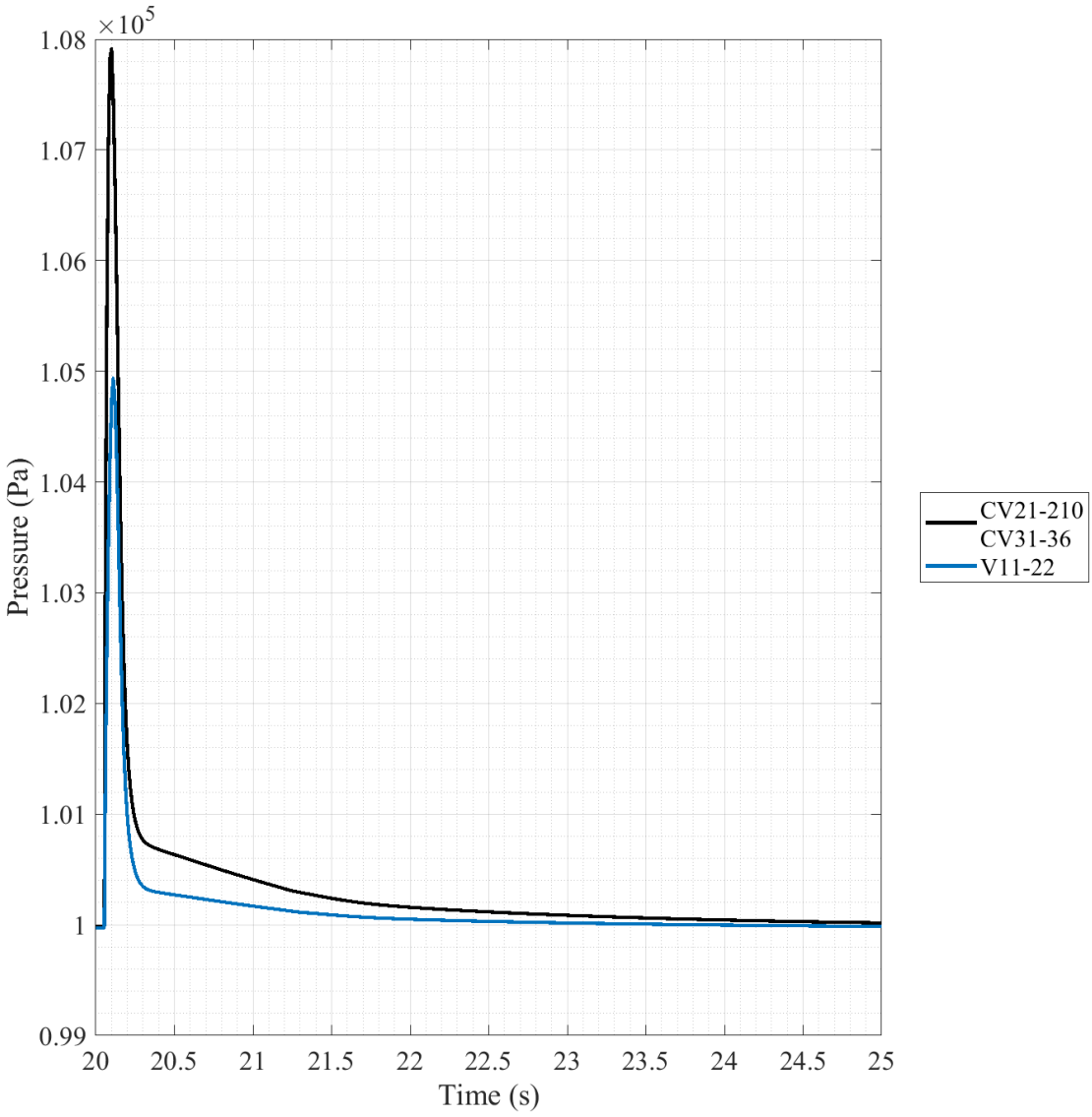

Fig. 6.23. 1/28th-Scale Scenario 2 Pressure, 20-25 second Timescale.

Fig. 6.24. reduces the timescale down to the half second following the break initiation. As described in scenario 1, the break is not initiated in the model until ~20.05 seconds even though set to initiate at exactly 20 seconds due to the way MELCOR handles timesteps. Following the break initiation, the pressure changes instantly throughout all the volumes of the model as atmosphere is displaced by the expanding helium. As the blowout panel is not affected in this scenario there is no pressure buildup before activation and all pressure increase is almost normally distributed as pressure rises through the volumes.

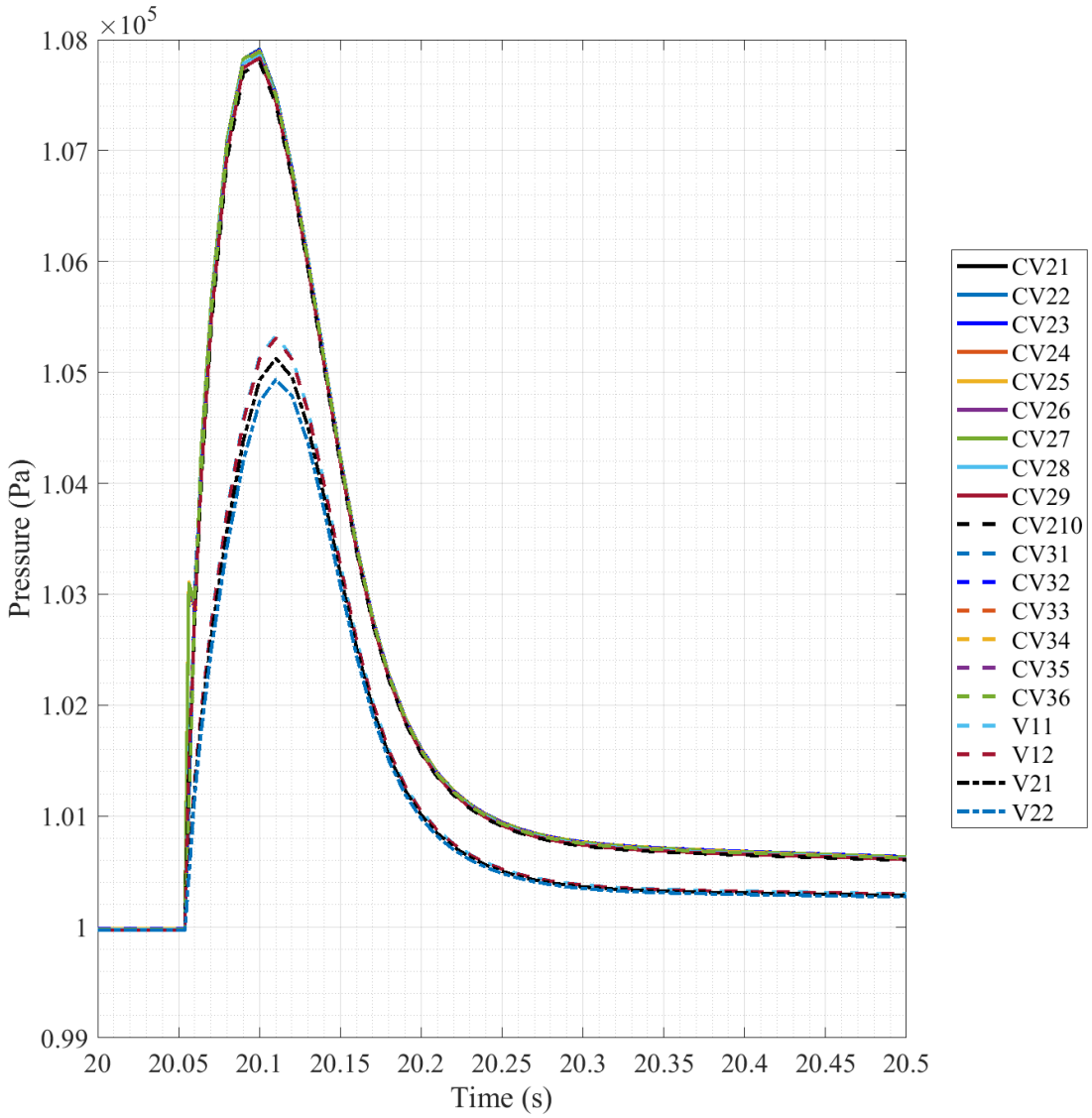

Fig. 6.24. 1/28th-Scale Scenario 2 Pressure, 20-20.5 second Timescale.

From Fig. 6.24 it can be seen that CV21-210 (SGC) and CV31-36 (EQS) increase to a maximum pressure of 1.0791×10^5 Pa (7.91 kPa increase) before falling back to near normal pressure. The smaller peak is endured by V11-22 (Vent Space) and increases to a maximum in the range of ~1.05×10^5 Pa (5 kPa increase) before falling. A note of interest should be made of the initial rise of the upper peak which has a smaller peak post initial rise that then continues into the normally distributed rise.

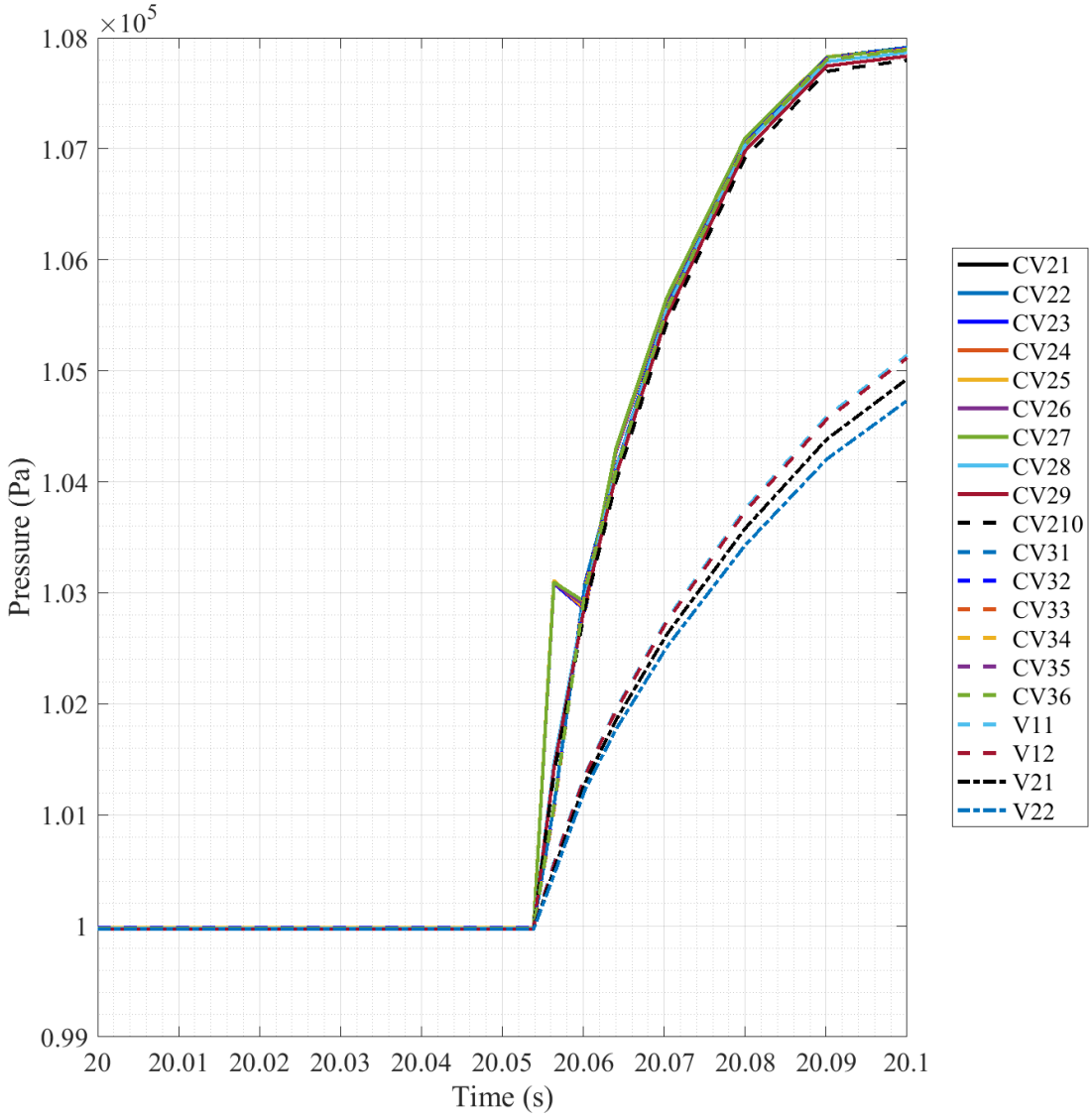

Fig. 6.25. 1/28th-Scale Scenario 2 Pressure, 20-20.1 second Timescale.

Fig. 6.25 reduces the timescale down even further to the first $1/10^{th}$ of a second post set break initiation in order to better view the initial spike. CV23-27 undergo this disturbance from the normal rise of the pressure, a departure from what all the other reactor building volumes experience. This disturbance lasts for only 0.005 seconds but seems to be an indication of the initial pressure disturbance being trapped within the central SGC volume that is separated by the dividing plates. These plates may be trapping some of the initial pressure wave from the helium release before flow is established through the plate cutouts to the other volumes. Another possibility is conflicting distribution waves conflicting as helium pushes the atmosphere deeper into the containment in the EQS shaft but also pushing downwards from within the SGC itself creating a pressure "bubble" within the central SGC cavity.

The next portion of plots examine the mass fractions of several major gases being tracked in the volumes across the simulation. Three of these gases, helium, oxygen, and nitrogen, were chosen to be plotted based on their importance in tracking the blowdown progression through the volumes being simulated. Nitrogen and oxygen were also chosen to be plotted as they make up the vast majority of the mass of the standard atmospheric air and therefore should give a good indication of the displacement of atmosphere and potential refill.

The first gas mass fraction to be plotted is that of helium, which can be seen in Fig. 6.26. All volumes in this scenario maintain a relatively large amount of normal air in their volumes in comparison to scenario 1. Also, much like the previous scenario, CV21 and CV31 experience little change along the progression of the scenario, with a very slight increase in helium content on in the range of E-3 mass fraction addition to their normal air composition. And finally, V22 experiences a spike in helium concentration much like scenario 1 as the break occurs but as the blowdown advances through the volumes it quickly falls back to near 0% as it is very close to the

exterior volume allowing a quick refill. This is where the similarities in the two scenarios end though as this scenario has a much different flow path from that scenario.

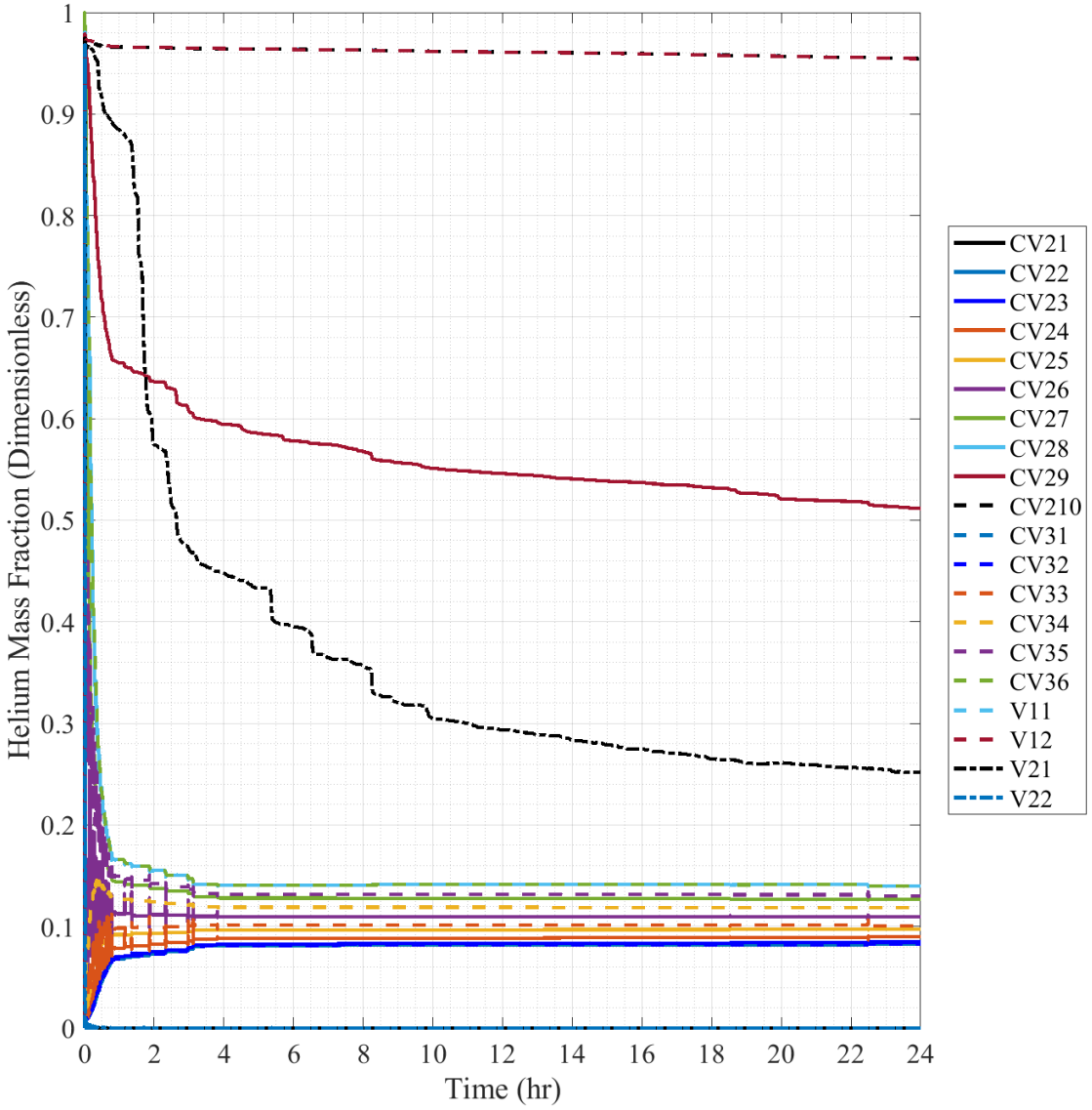

Fig. 6.26. 1/28th-Scale Scenario 2 Helium Mass Fraction.

Beginning with the upper transient, CV210 and V11-12 spike to ~98% and then steadily decay to 96% over the full scenario timescale. Moving down to the next transient, V21 experiences a long trailing transient much like in scenario 1 but it doesn't fall to the extent of that scenario, only to ~25% instead of ~10%. In the initial 2 hours V21 drops ~40% from its peak spike fraction then it trails off the final ~35% over the final 22 hours. The other central transient is that of CV29,

which also experiences a spike initial but then falls ~30% over the first 2 hours then falling ~15% over the remaining 22 hours.

For the main interesting portion of these results is the banding result of helium mixture throughout all the remaining reactor building volumes, CV22-28 and CV32-36, which is seen at the bottom of the figure. A majority of the volumes in this bottom banding structure experience spikes of helium content around the break initiation, some to almost a full 100% and others experiencing no spike at all, but then they all fall to this ~6% band of mass fractions where they plateau. When the volumes fall into the banding structure, they keep their elevation ranking in their concentrations, with higher elevations experiencing higher mass fractions and lower volumes experiencing lower fractions. This is most likely due to the helium being less dense than air and wanting to relocate to higher altitudes but a good amount of mixing in the gases appears to take place due to the striation and steadiness of the mass fraction as the scenario progresses. A note must be made of the initial busy region following the blowdown leading to striated banding, as a large amount of oscillation is taking distorting the results in this region. This will be approached in later plots as they will get a better look at the initial distribution changes which requires a shrinking of the timescale.

Fig. 6.27 presents the mass fraction data for oxygen throughout the reactor building volumes. As was seen in the scenario 0 data, the maximum concentration of oxygen in the model at any one time is 23.14% which is replicated in this figures data. Comparing the trends of this figure to what was seen in Fig. 6.26 it can be seen the trends a simply inverses of each other, where instead of downward trends as refill occurs, upward trends occur.

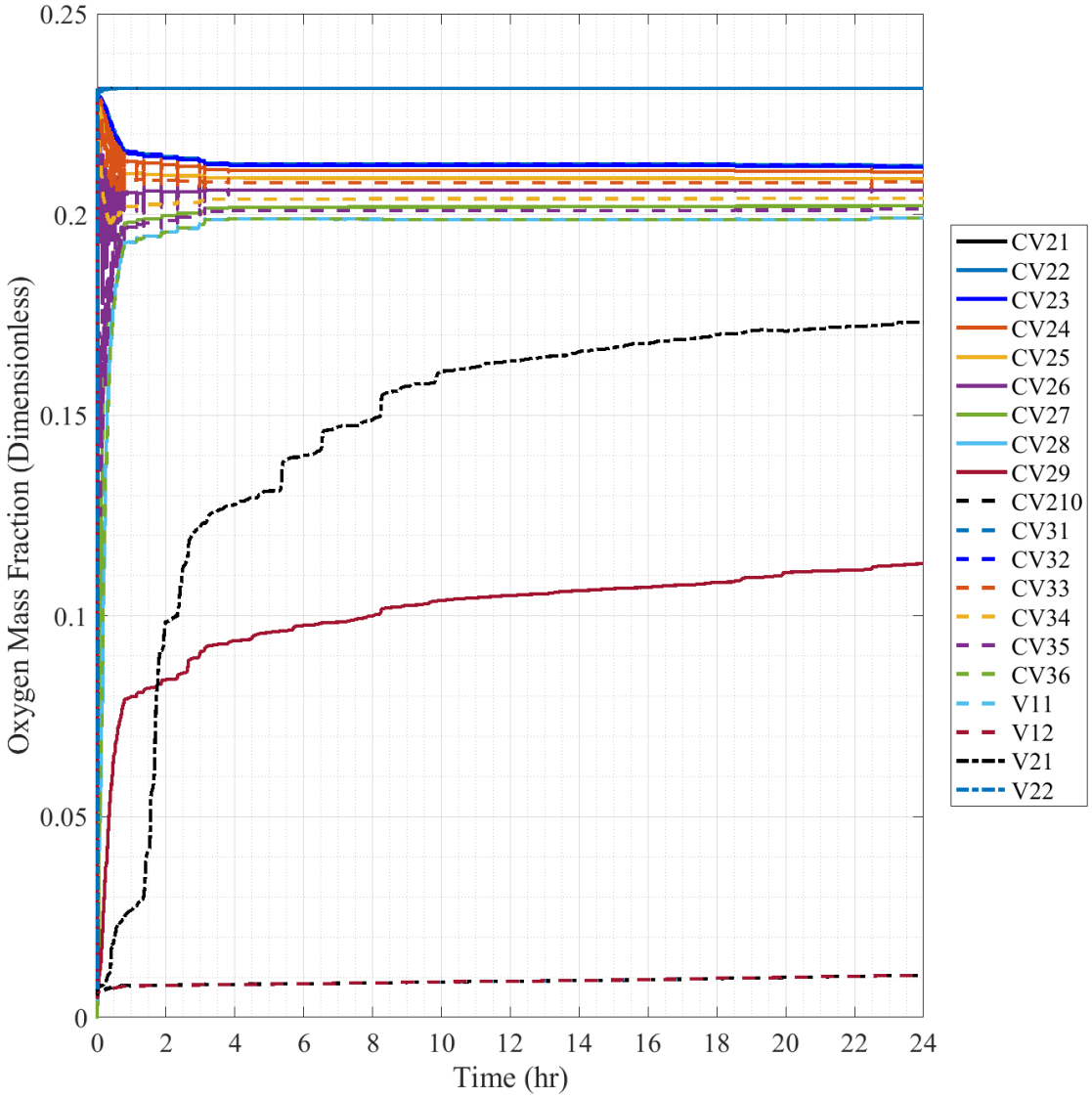

Fig. 6.27. 1/28th-Scale Scenario 2 Oxygen Mass Fraction.

Fig. 6.28 presents the mass fraction data for nitrogen throughout the scenario, and much like the previous figure of oxygen mass fraction, shows the same inverse trends in comparison to what was seen of the helium data. The major difference with this figure is the changed scale of the results, with a maximum nitrogen fraction of 75.51%. Fig. 6.27 and 6.28 have both shown that atmospheric standard air returns and is displaced in equal portions and do not suffer from disassociation between its gaseous components. Due to this, a decision was made to combine the mass fractions of nitrogen and oxygen to give a good approximation of total atmosphere

displacement done by helium. Results sections past scenario 2 will not include nitrogen and oxygen mass fractions plots as there are no fractional differences between them and the can be relegated to a consolodated combination mass fraction to show results, but their plots will be included in the Appendix D for further reference.

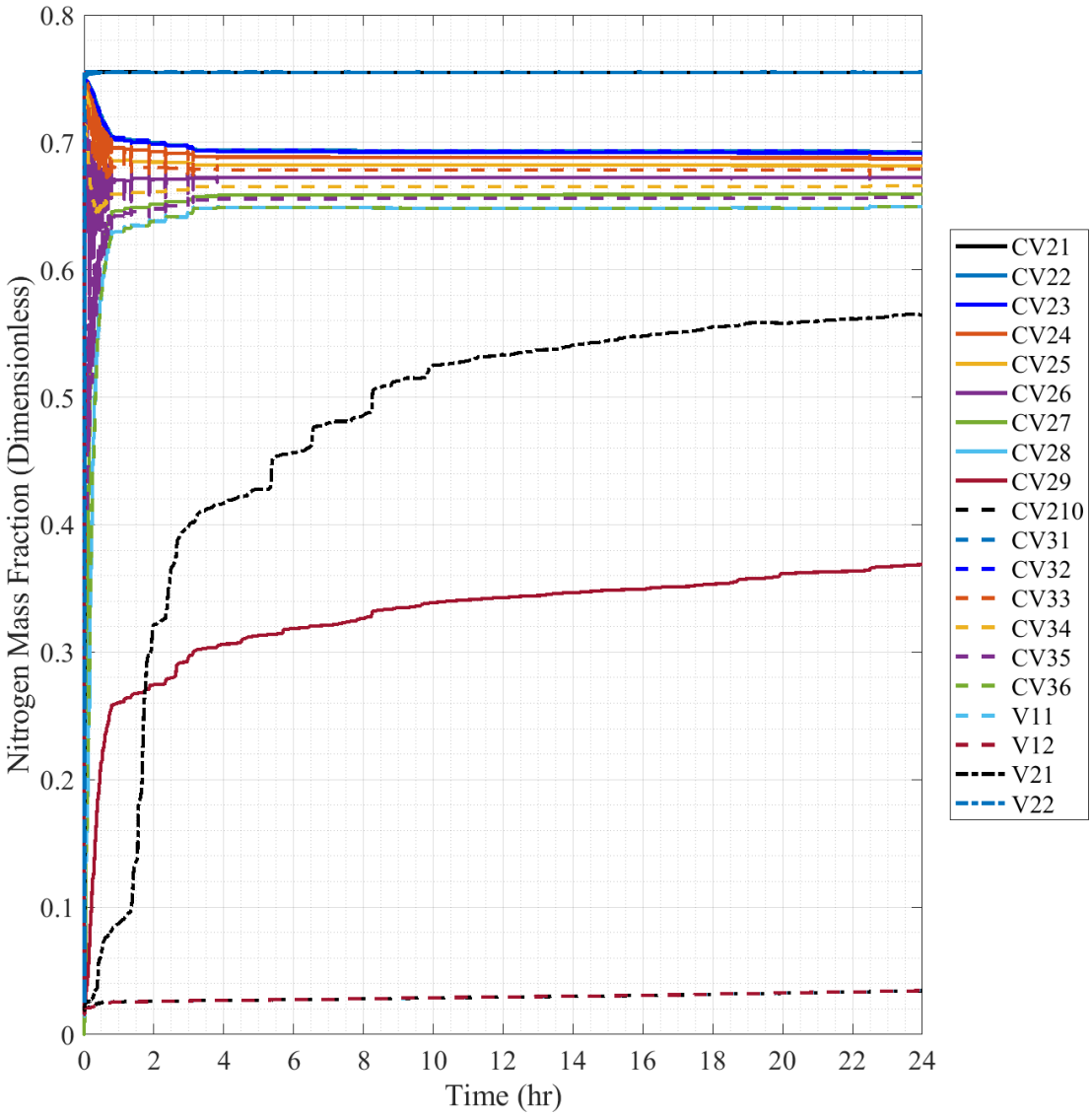

Fig. 6.28. 1/28th-Scale Scenario 2 Nitrogen Mass Fraction.

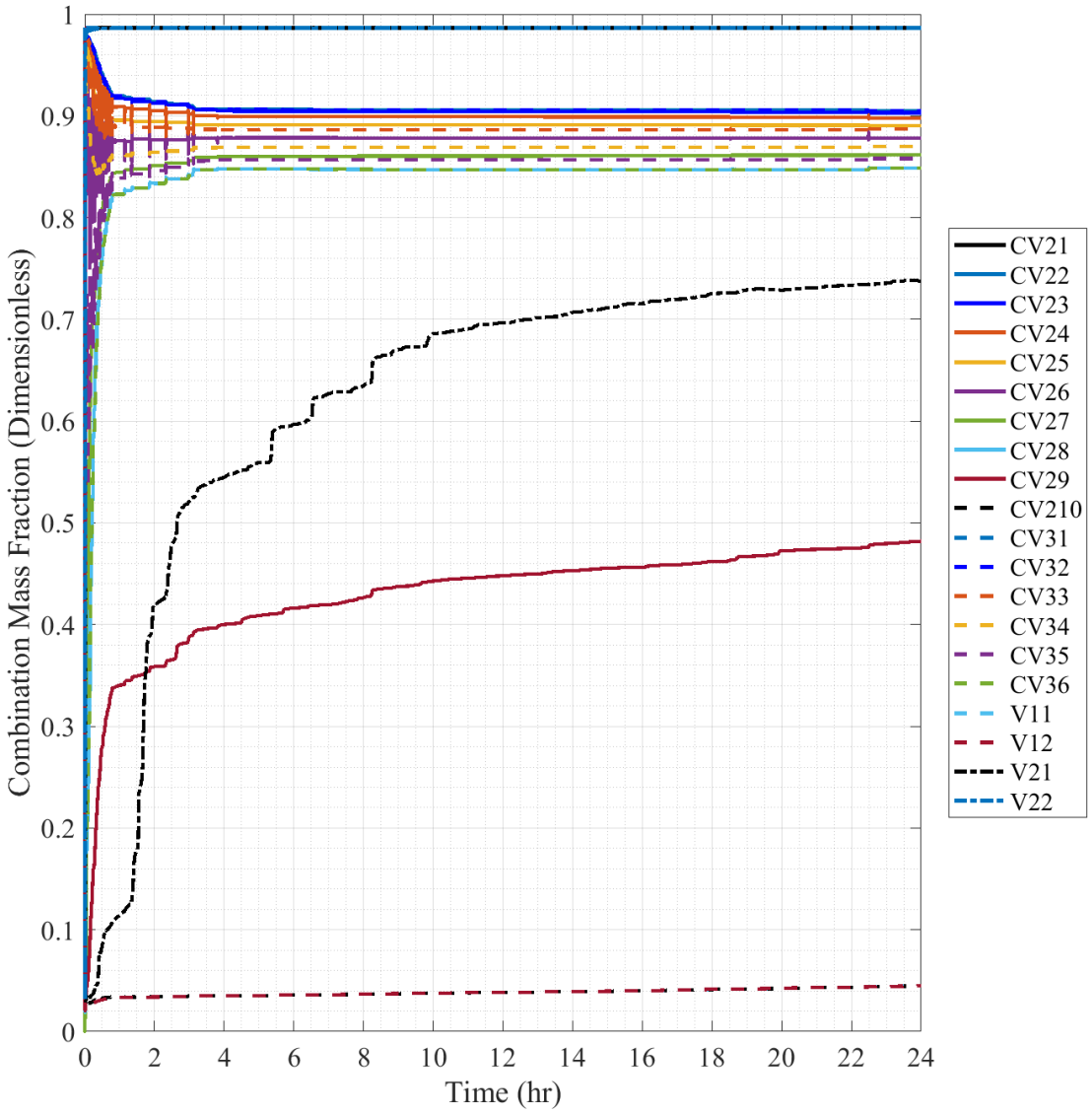

Fig. 6.29. 1/28th-Scale Scenario 2 Combination Mass Fraction.

Fig. 6.29 sums the oxygen and nitrogen mass fractions together as previously discussed to a "Combination" mass fraction composed of the combination of the two individual mass fractions. The combination of these two gases make up 98.66% of the total mass fraction of standard air and should be a good comparison to the helium mass fraction for comparisons. Finally, by comparison with Fig. 6.26 and what has been previously discussed with the individual oxygen and nitrogen mass fraction figures, it can be seen that the figure is simply an inverse of the helium trends. Due

to the linked relationship of the results, this set of data will be used to examine the initial details of the blowdown from a mass fraction perspective as was done with the pressure.

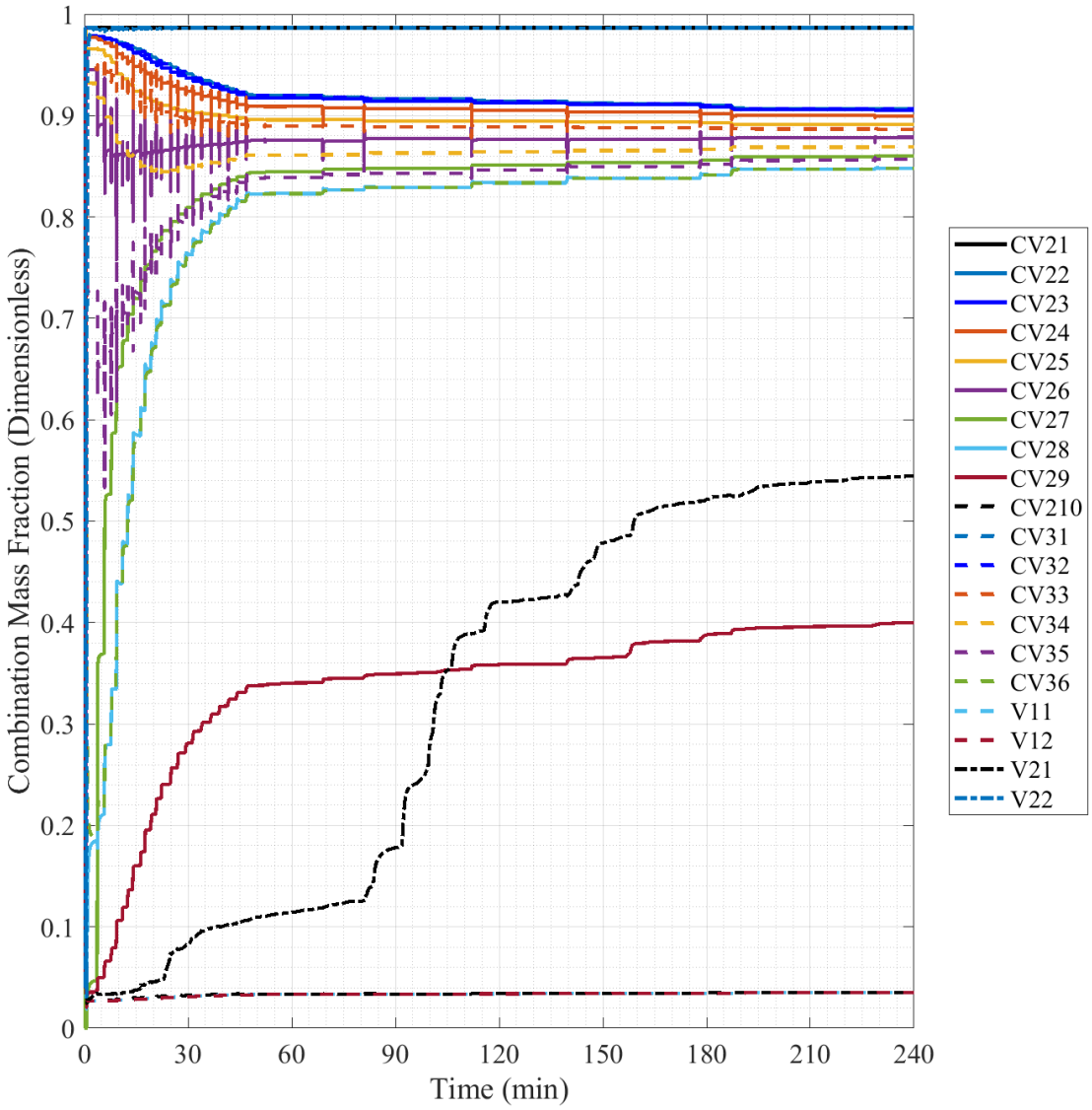

Fig. 6.30. 1/28th-Scale Scenario 2 Combination Mass Fraction, 240 minute Timescale.

Fig. 6.30 reduces the timescale down to the first 240 minutes of the scenario to get a better look at the major oscillations in the volumes entering into the striated banding region of ~88%. At this scale, the oscillations in a major volumes come into view as occuring with CV24, CV26, CV33, and CV35 being the main constituents with oscillations of potentially up to ~10% at points. Outside of these volumes though a number of associated volumes also experience unexpected

results as they undergo severe “stair stepping” of their results which can be seen with CV23, CV27-29, CV32, and CV36 where they experience a step either up or down in their resulting conecntrations in conjuntion with the oscillation times seen in the volumes talked of previously. V21, CV34, CV25, and CV22 do not seem to undergo these stepping in results though even as they are located in path with the affect volumes. Upon further reference back to Fig. 4.6, the volumes undergoing major oscillations are those that are small band volumes made to give centralized results around oxygen sensors to be placed in the experimental model.

Fig. 6.31 reduces the timescale in even further to the first 60 minutes of the scenario to look at the primary region where the oscillation of volumes was occurring. At this scale, the magnitude of the oscillations comes into view, with some approaching a delta of ~18% air concentration but in most cases being a delta of less than 10%. As time progresses through the scenario the oscillations decrease and become less frequent, ending roughly before 240 minutes post-break simulation initiation which is confirmed by Fig. 6.30.

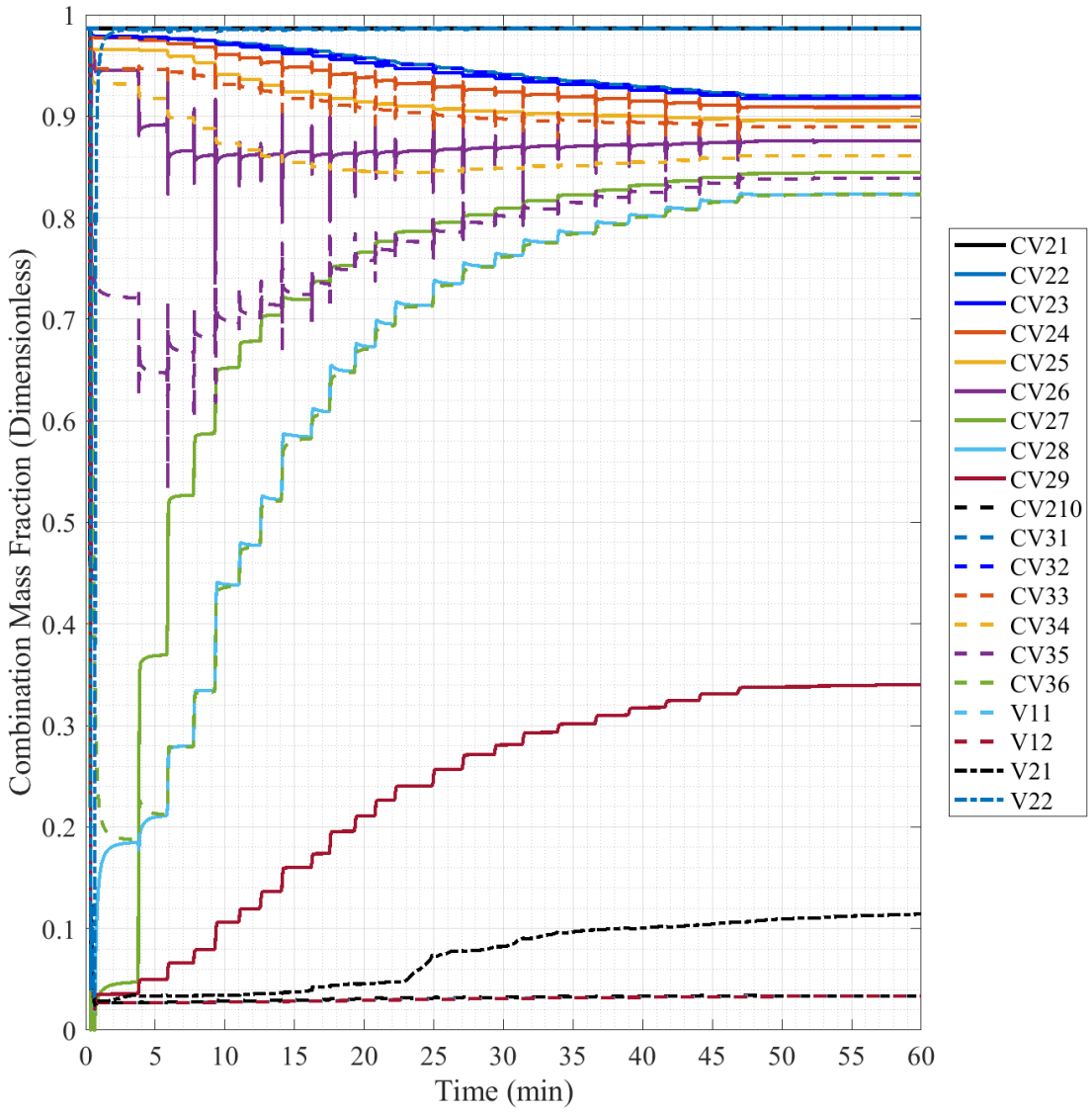

Fig. 6.31. 1/28th-Scale Scenario 2 Combination Mass Fraction, 60 minute Timescale.

Fig. 6.32 reduces the timescale down to the first 300 seconds of the scenario, where the initial oscillation of the affected volumes can be seen as well as some initial voiding of volumes. Initial details of the blowdown are difficult to determine at this timesscale but V22 can be seen to decrease with the blowdown, then following some initial spiking rises individually to be refilled with air. CV28 rises following V22 to meet CV36 that has been on a steady decline since the break started. CV35 decreases along with CV36 following the break but only to ~72% where it peaks and steadys into a plataeu.

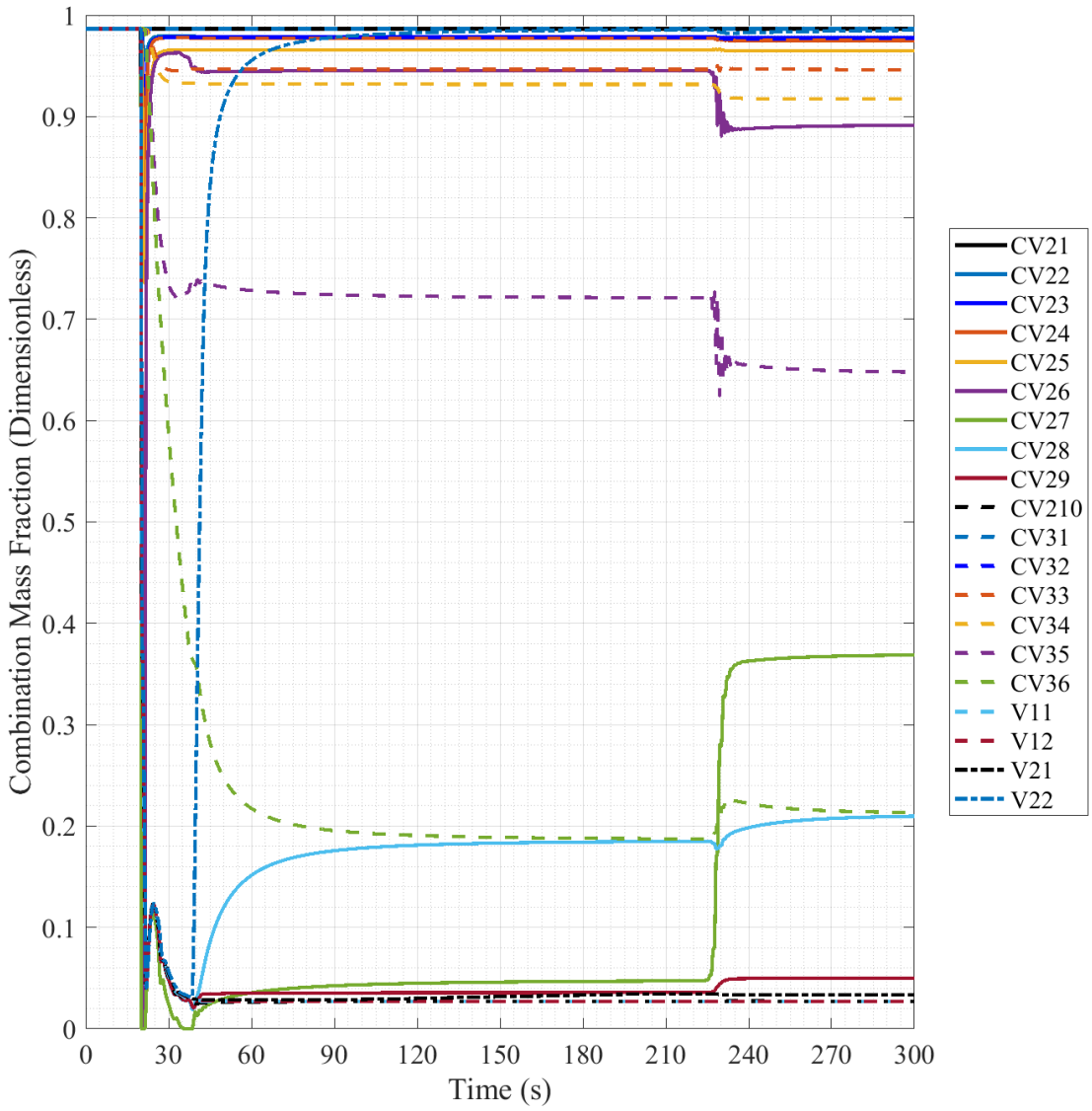

Fig. 6.32. 1/28th-Scale Scenario 2 Combination Mass Fraction, 300 second Timescale.

The oscillation of the scenario occurs at ~225 seconds and causes a number of notable effects on transients. CV26 which was steady following some initial voiding and refill but at the initial oscillation falling ~6% following the oscillation. CV35 was also steady following the initial blowdown progression but at the oscillation period it drops ~7% following oscillating. Meanwhile at the bottom of the plot CV27 undergoes a large spike from ~4% to ~36% while the oscillations occur. CV28 and CV36, which were in equilibrium before the oscillation, diverge with CV36 spiking in air content and CV28 initially dropping but then rising to form a new equilibrium with

CV36 ~4% higher than pre-oscillation. CV29 experiences an increase at the time of the oscillation, rising ~1% in oxygen concentration.

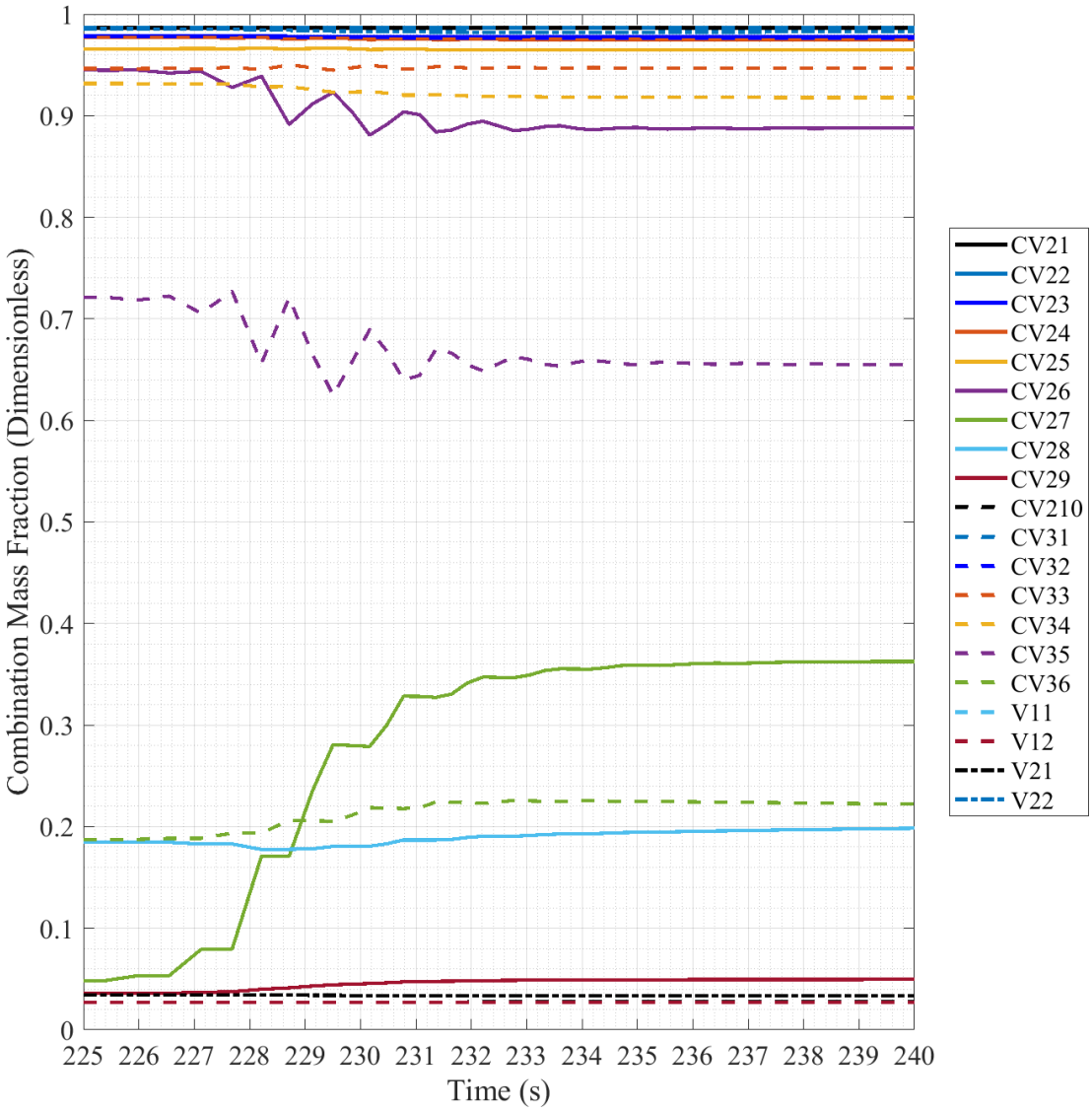

Fig. 6.33. 1/28th-Scale Scenario 2 Combination Mass Fraction, 225-240 second Timescale.

Fig. 6.33 gives a dedicated look at the initial oscillation from a 15 second time period surrounding it. This oscillation seems to occur for ~10 seconds before the volumes become stable again. CV26 and CV35 appear to undergo opposite reactions, while one rises the other falls in their oscillation. CV27 only undergoes a rise across the oscillation which appears to be tied to the

oscillation of CV35. As CV27 experiences a spike in concentration, CV35 decreases and as CV35 increases, CV27 is stable at its concentration.

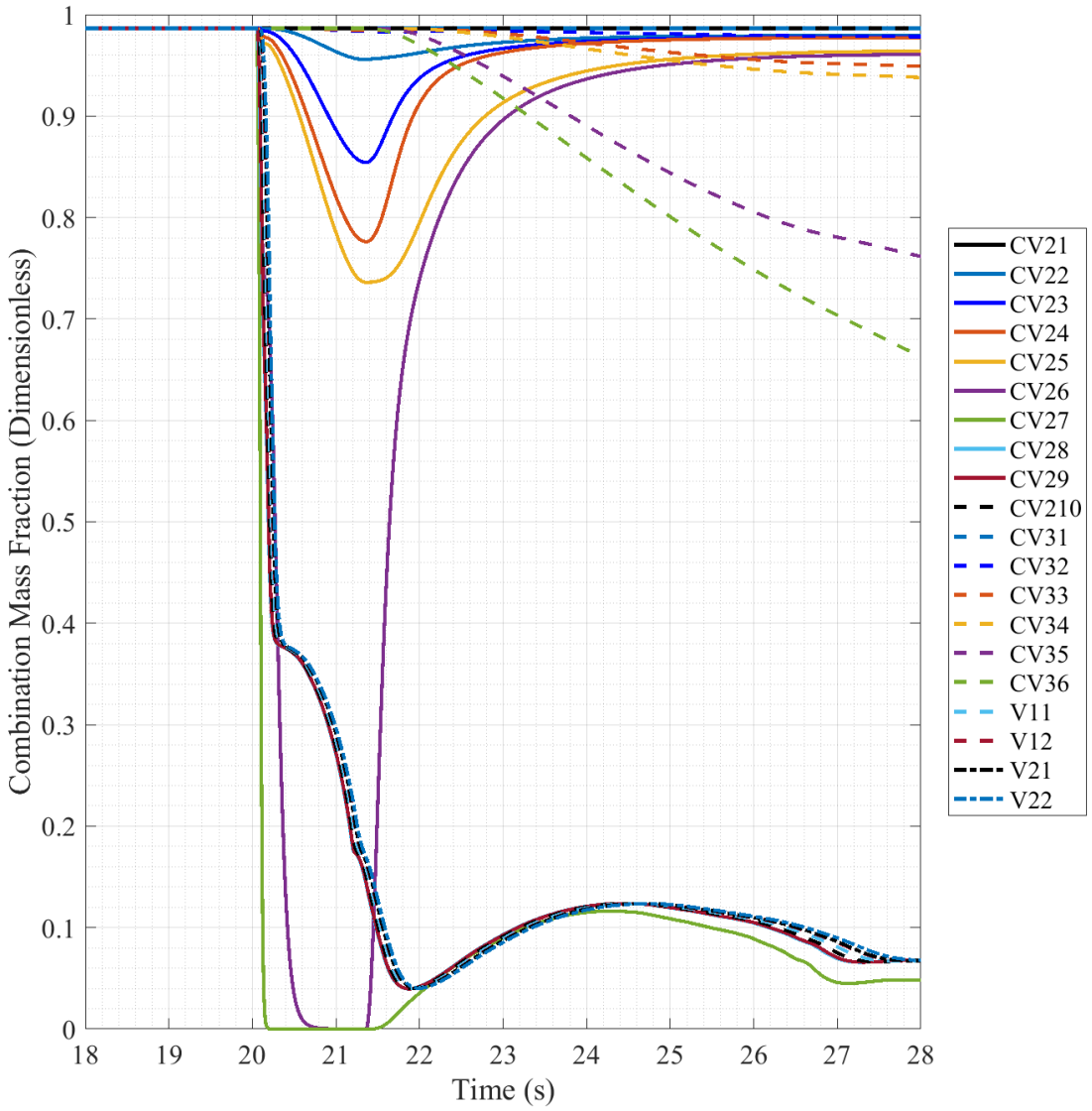

Fig. 6.34. 1/28th-Scale Scenario 2 Combination Mass Fraction, 18-28 second Timescale.

Fig. 6.34 reduces the timescale in much further to get fine details of the initial voiding in this scenario. At this timescale it can be seen that CV26-27 are the only two volumes to fall completely to ~0%, though they both quickly are returned to a small level of air concentration in under two seconds. CV26 rebounds to almost being completely filled with air again within six seconds, while CV27 rises following CV26 to join with some other voiding volumes as they

rebound for the time period of 22-27 seconds. CV22-25 all experience a momentary decrease in air content post-break, but then rise following a peak decrease ~1.5 seconds post-break to greater than 95% air content on this short timescale. CV28-210 and V11-22 void with the blowdown but only to ~38% where their rate of voiding changes until they reach a low at ~22 seconds before a period of rising and falling to ~6% at the end of the timescale. CV33-36 undergo a decrease following the break, splitting inth two separate groups of CV33-34 and CV35-36, the the later which decreases to lower levels of air and the former which stays relativly stable, which can be seen in Fig. 6.31.

Finally, Fig. 6.35 reduces the timescale to the single second following the break initiation. Post-break initiation volumes located above the break in elevation, CV27-210 and V11-22, begin to be voided quickly of the air in their volumes. CV26, while located below the break location, drops with the blowdown progression before returning back to near full air content which was seen in Fig. 6.34. CV27 fully falls to ~0% as all other volumes undergo a severe change in voiding rate ~0.3 seconds following the break, and as seen in the previous figure they do not reach a fully voided state.

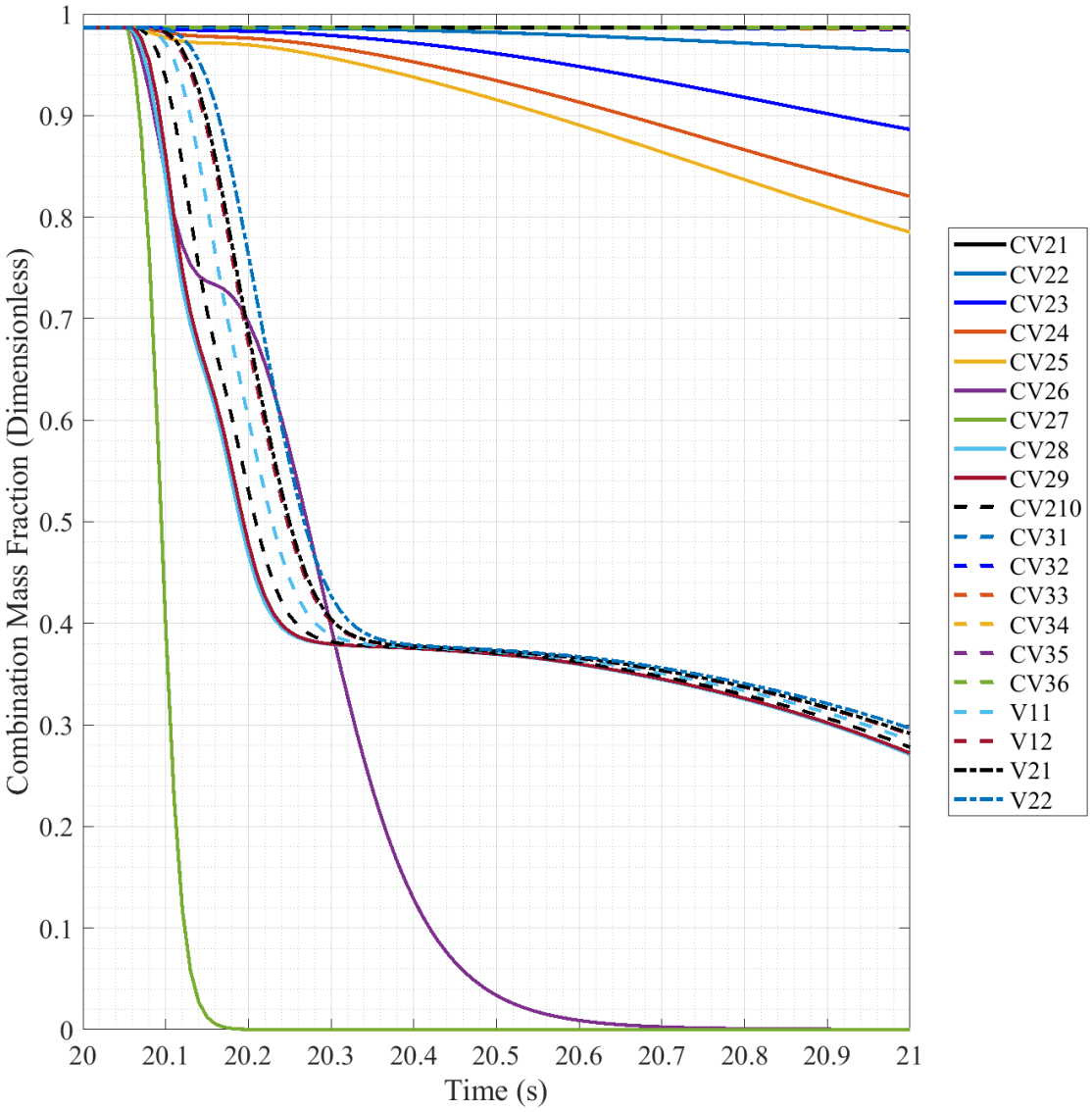

Fig. 6.35. 1/28th-Scale Scenario 2 Combination Mass Fraction, 20-21 second Timescale.

6.1.4 1/28th-Scale Scenario 3 Results

Scenario 3 is a RPV break scenario with the EQS closed to blowdown flow by closing the duct connections at their flow paths from the SGC. This forces the blowdown gases and atmosphere to rise through the center of the SGC, around the SGV and through the flow restrictive divider plates. For this scenario, any volumes from the EQS (CV31-36) will be omitted from plotted results as they undergo no changes during the scenario. Fig. 6.36 gives a visual example of this scenario's estimated progression, utilizing a figure of the basic regions of the model.

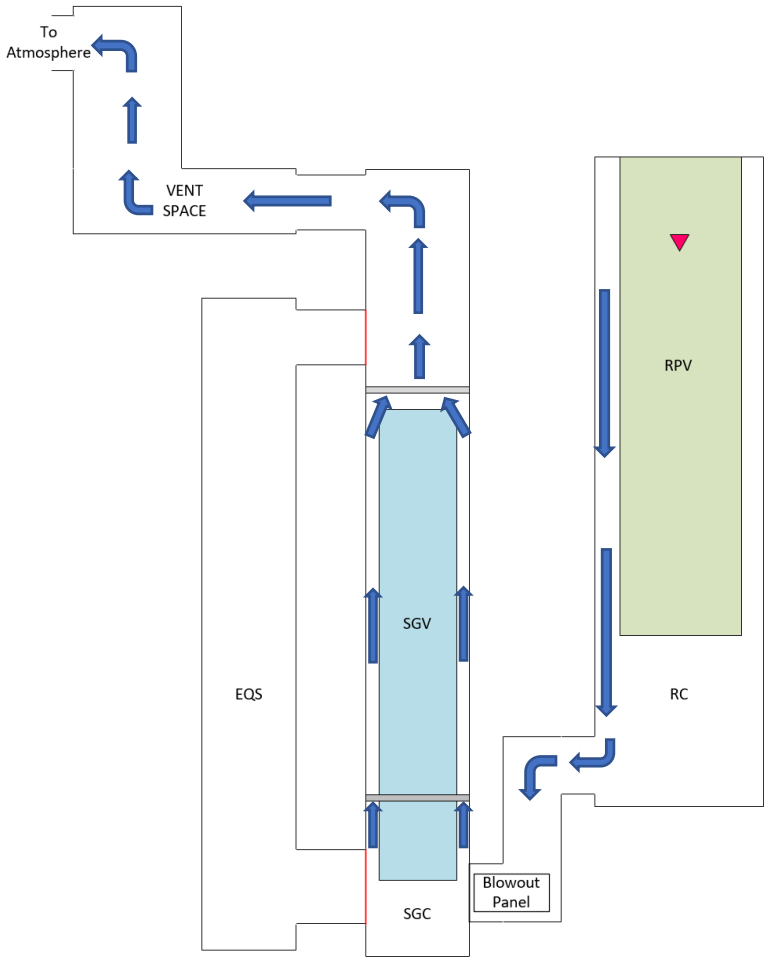

Fig. 6.36. Scenario 3 Estimated Blowdown Progression.

The initial pressure plot of scenario 3, with the pressure plotted across the full timescale, has been omitted as it simply shows the same information as the initial scenario 1 plot, with the

initial 6.4 MPa pressure of the helium volume resulting in vertical scale of the plot blownout due to its comparibly large size. Nowhere along the full timescale of the pressure for this scenario's results were any new transients observed. The full timescale plot has been included in Appendix D for reference to the actual data plot, but Fig. 6.8 can be used as a quick reference as it shows a similar plot, excluding the removed volumes from this scenario.

After reducing the timescale of the pressure plot to 500 seconds, like in scenario 1, the resulting plot was extremely similar to the plot made for that scenario. The initial helium pressure of 6.4 MPa can be seen well at the initial time, then at 20 seconds the pressure begins to fall at an exponential rate as the break flow path is opened and helium expands out and into the RC volumes. The HV reaches an equalized pressure of ~100 kPa at ~293 seconds following the blowdown initiation, ~313 seconds post simulation initiation. Overall, the progression of the pressure blowdown from the helium volumes seems to have not been affected by the change in the model layout. The pressure plot of this frame of time for this scenario has been included in Appendix D for further reference, or Fig. 6.9 can be used as a quick reference to the progression of the helium volume blowdown, excluding the removed volumes from this scenario.

Reducing the timescale down to 5 seconds following the break initiation helps get a better picture of the pressure transients. Fig. 6.37 illustrates the building volumes response to the blowdown, with the largest spike occurring the volumes of CV11-15 (RC) as they are the primary volumes that the helium releases into directly, with a spike in pressure up to 1.0935×10^5 Pa (9.35 kPa), much like with scenario 1. The primary difference in the case of this scenario is the increased pressures following the blowout panel operation, which are hard to determine in this plot.

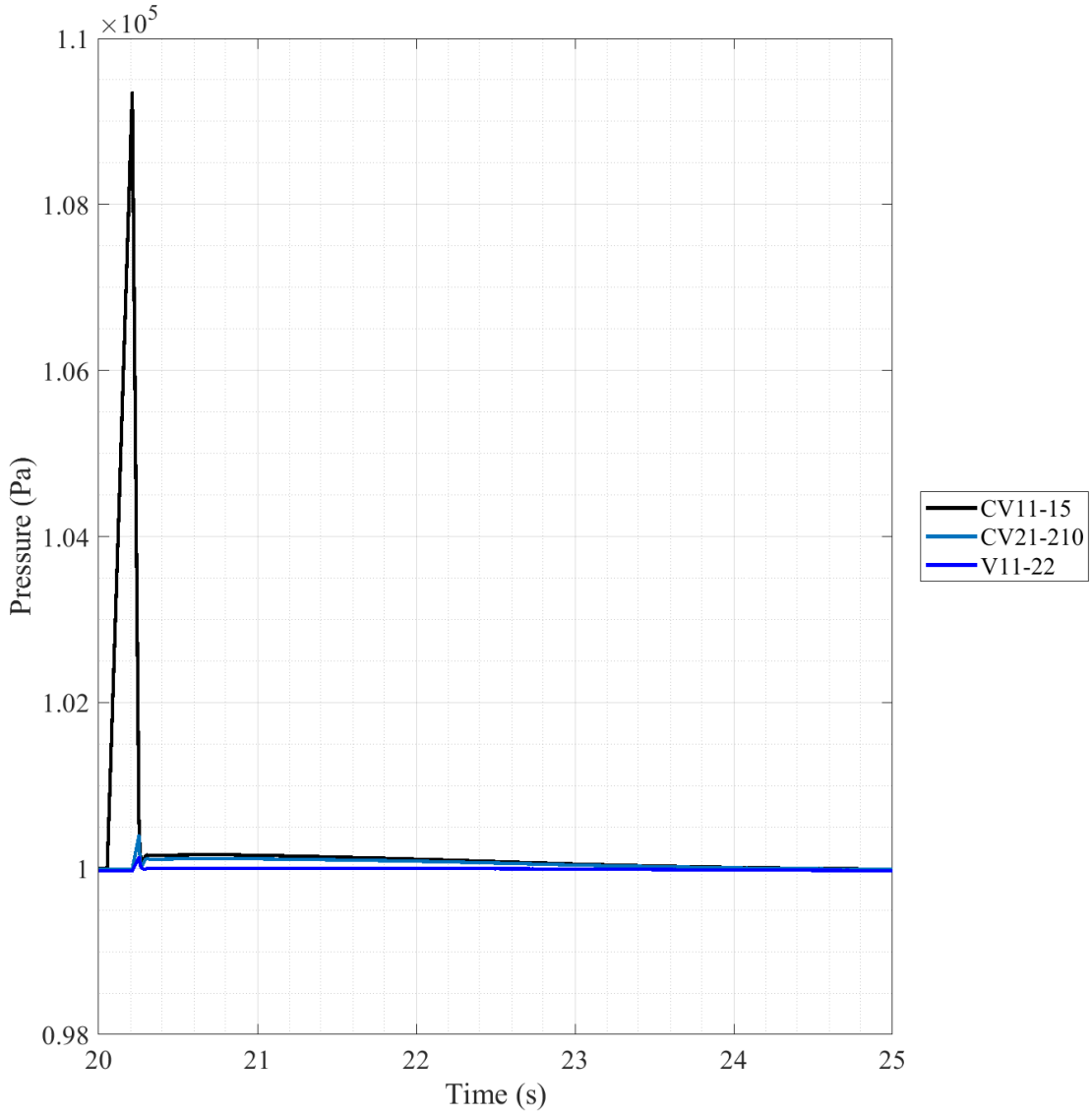

Fig. 6.37. 1/28th-Scale Scenario 3 Pressure, 20-25 second Timescale.

Dropping the timescale further, Fig. 6.38 reduces the timescale to the half second following the break giving a good view of the linear spike caused by the helium expanding into the RC volumes and causing compression of the atmosphere in the duct connection against the blowout panel. As in scenario 1, the actuation and opening of the panel can be seen as the pressure drops extremely quickly and the other volumes rise to equalize and fall with the CV11-15 spike, though in much less magnitude.

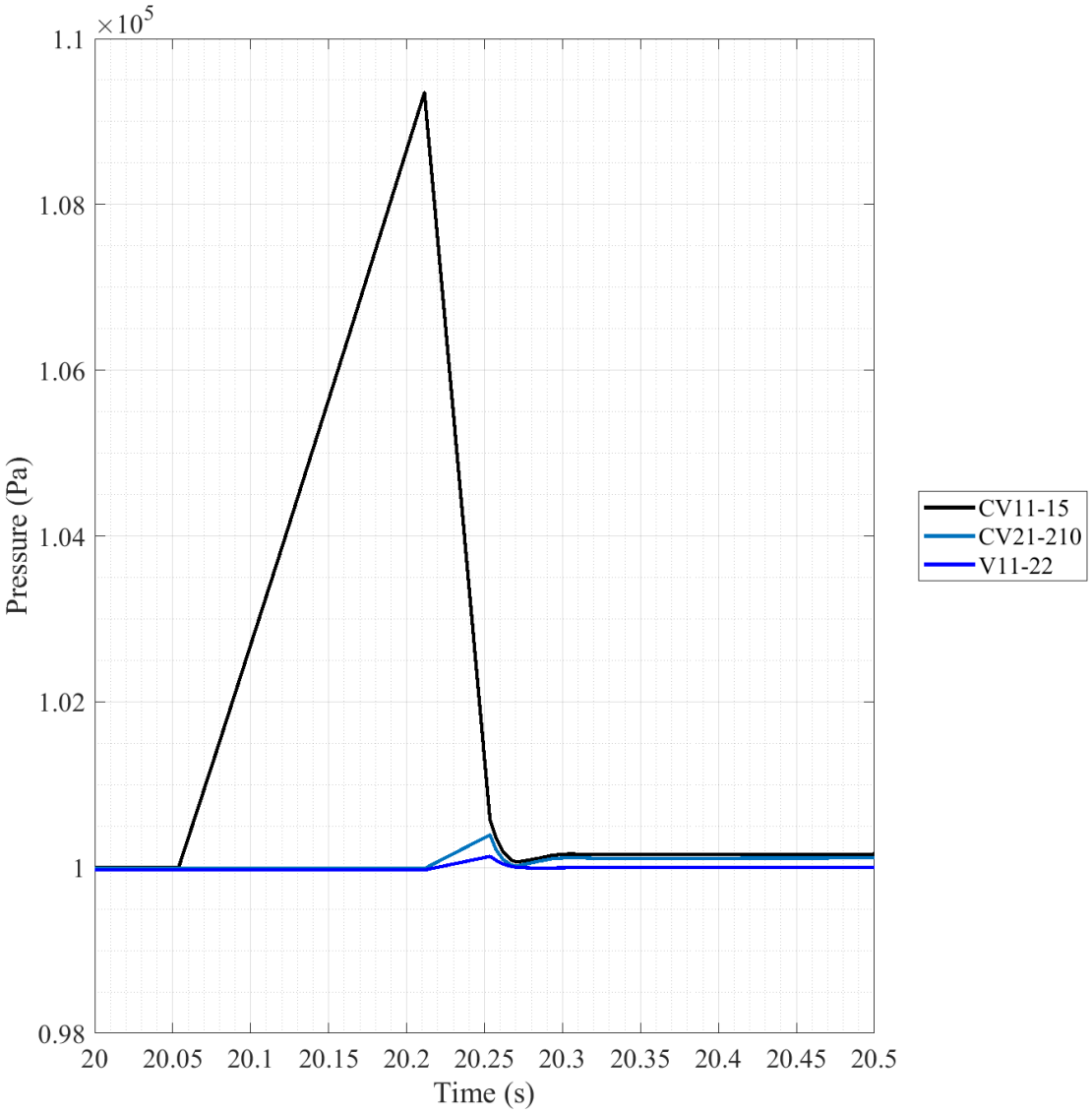

Fig. 6.38. 1/28th-Scale Scenario 3 Pressure, 20-20.5 second Timescale.

As in scenario 1, the break is delayed due to the way MELCOR handles timesteps and the break does not occur until 20.05 seconds in the simulation, even though set to initiate at 20 seconds exactly. The blowout panel initiates at the 20.21 second mark, like scenario 1, and the pressure begins to fall in CV11-15. This decrease joins with the rise in the lower volumes pressures as they experience the displaced atmosphere and helium moving through their volumes. Lower transients rise to the point of roughly equalizing with the CV11-15 spike as it falls, and jointly they fall to a

range around ~100 kPa. In this scenario, volumes experience a wider distribution of pressure following plateauing of pressures.

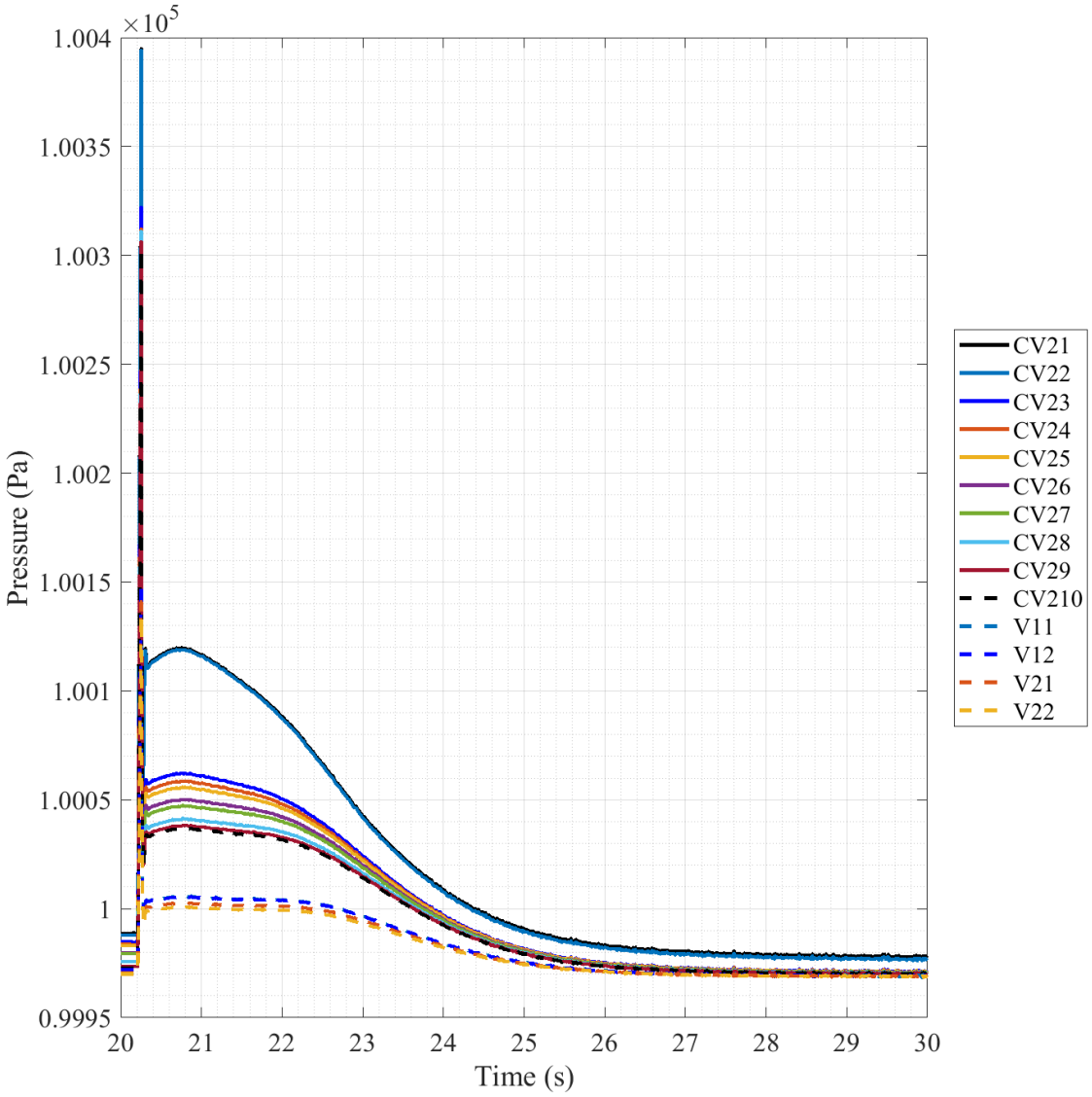

Fig. 6.39. 1/28th-Scale Scenario 3 Pressure, 20-30 second Timescale, No CV11-15.

To get a better view of the volumes other than CV11-15 (RC) it is removed from plot and the timescale is pulled back to the 10 seconds following the break initiation. Fig. 6.39 shows the results of this plotting, with an overall spike much lower in scale but difficult to discern the groups undergoing individual spikes. What can be determined from this plot is that there are three distinct groups of volumes that respond to the blowdown of the helium, an upper, middle, and lower group.

All groups undergo a spike that results in higher pressures in the following time period, though all decay over the ~10 seconds following the spike. They are split into two separate equilibrium groups as they settle, with the top transient staying by individual, but the lower two transients rejoining to a joint pressure range. Both equilibrium pressure groups fall within the range of pressures established before the break initiation, which can be seen by comparing the left and right sides of the plot.

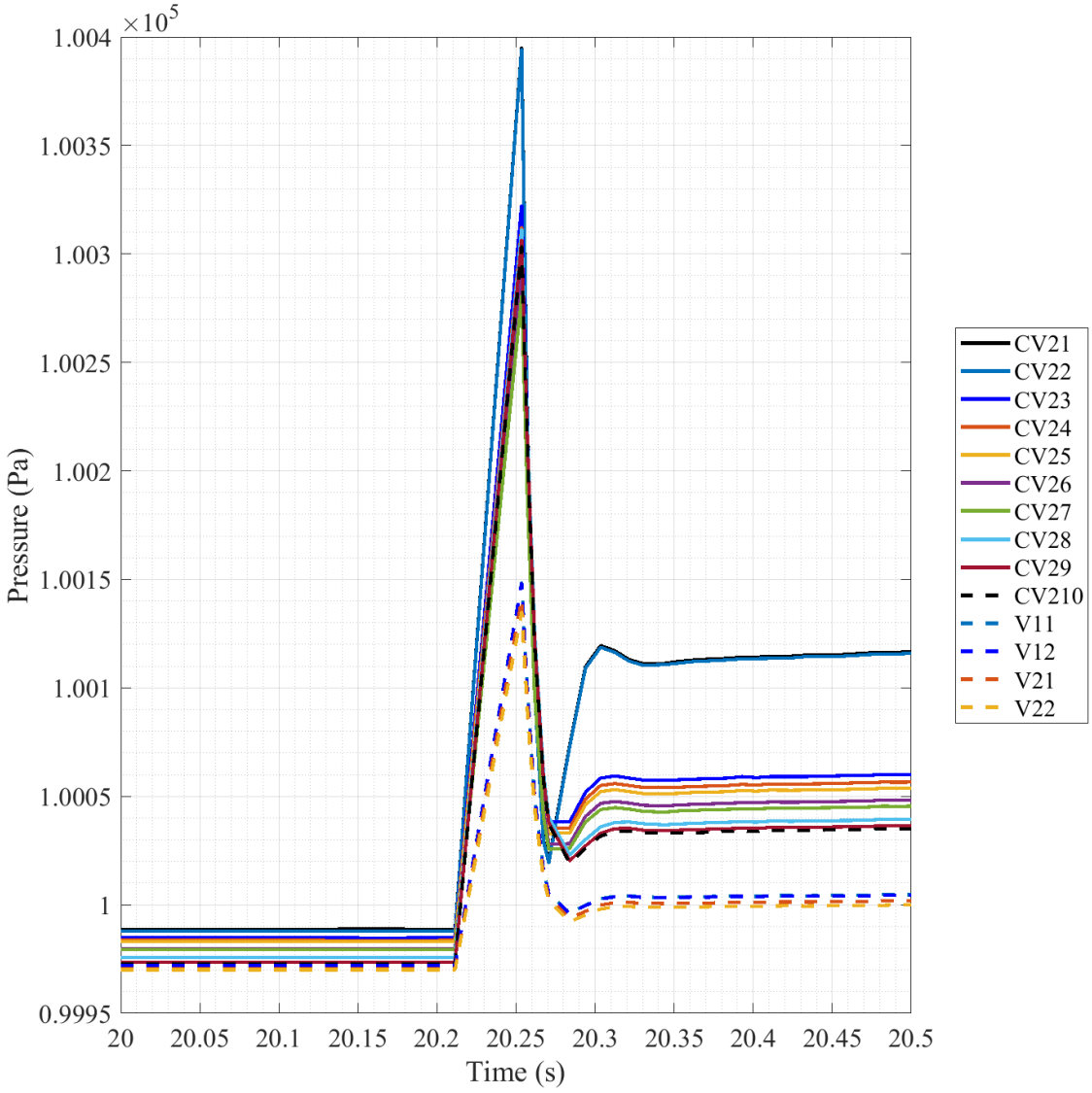

Fig. 6.40. 1/28th-Scale Scenario 3 Pressure, 20-20.5 second Timescale, No CV11-15.

Cutting the timescale back down to the 20-20.5 second range, like done in scenario 1, Fig. 6.40 allows a better view of the plotted volumes response. The distinction can be made between the three groups as they rise at different rates following the blowout panel initiation. The upper group is composed of CV21-22 as they spike to a max pressure of ~$1.0039x10^5$ Pa (~390 Pa increase), then falling into a group of distributed pressures around the $1.0005x10^5$ Pa range but spiking again back to a $1.0012x10^5$ Pa range as the volumes equalizes. The middle spike is composed of CV23-210 which spike to a maximum pressure of ~$1.0032x10^5$ Pa (~320 Pa increase) before falling and slightly rising back up to a $1.0005x10^5$ Pa range to then recombine with the lower group outside of the range of this plot. The bottom spike is composed of the vent space volumes of V11-22 and only spike to a maximum of ~$1.0015x10^5$ Pa (~150 Pa increase), likewise falling to a ~100 kPa range before the recombination period roughly 10 seconds following.

Mass fraction data of scenario 3 starts off with the presentation of the helium mass fraction plot, presented in Fig. 6.41. The singular transient of this scenario is composed of V21 by itself, spiking with the blowdown but then falling over the progression of the scenario to ~31%. All other volumes in this scenario go to the extremes of the mass fraction scale. V22, much like in all other scenarios, spikes very quickly at the break but falls almost instantly back to 0% in the scale visible on the plot. CV21 also experiences a very similar reaction as in scenario 1, with a very slight increase in helium content in the range of E-3 mass fraction addition to their normal air composition across the scenario time period. All other volumes of the model, CV11-15, CV22-210, and V11-12 maintain a very close or completely filled atmosphere of helium for the duration of the scenario post-break initiation spike. Getting a better look at early timescales will require a smaller timescale that will be explored in later plotted results.

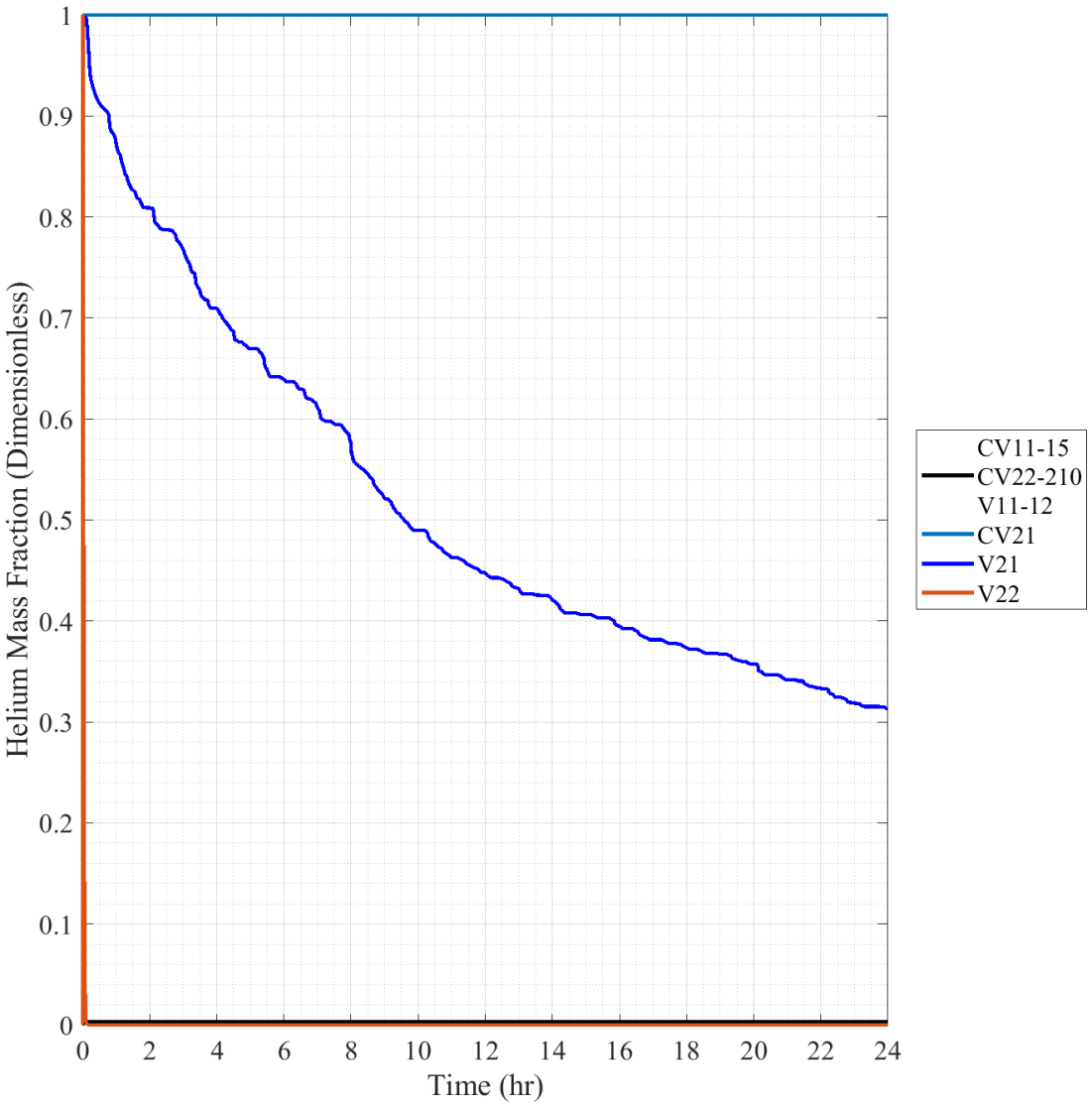

Fig. 6.41. 1/28th-Scale Scenario 3 Helium Mass Fraction.

In order to maintain a concise description of scenarios, the plots of oxygen and nitrogen mass fraction are not presented in this scenario as their results are reaffirmed best by a combination of their results to approximate a near full mass fraction of standard air. As was seen in scenario 1, oxygen and nitrogen mass fractions showed inverse results of the helium mass fraction and were simply differentiated by the resulting scale differences in the gas mass fractions. Plotted results for both the oxygen and nitrogen mass fraction can be found in Appendix D for further reference but are left out of this scenario to be concise.

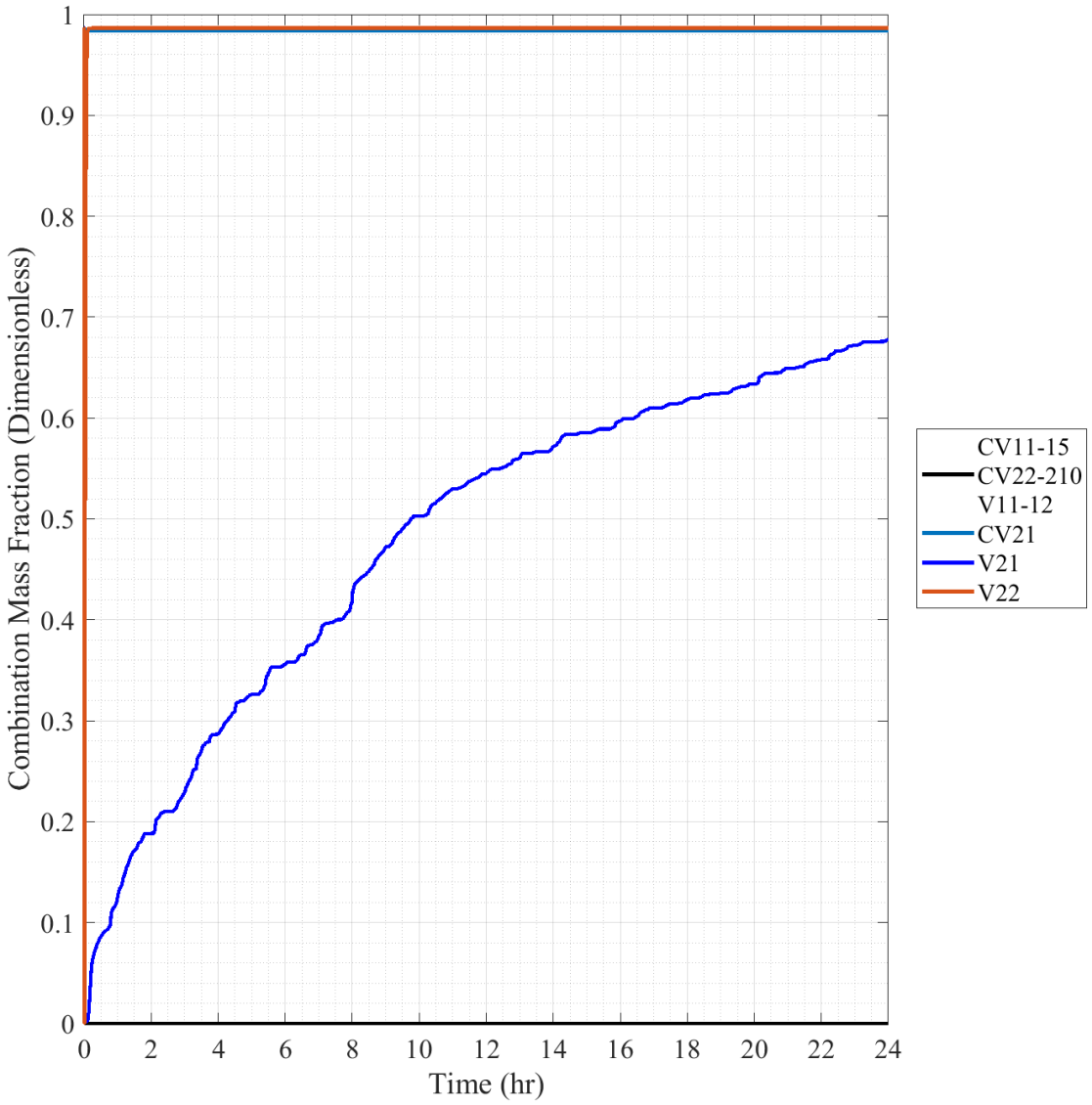

Fig. 6.42. 1/28th-Scale Scenario 3 Combination Mass Fraction.

Fig. 6.42 sums the oxygen and nitrogen mass fractions together as previously discussed to a "Combination" mass fraction composed of the combination of the two individual mass fractions. The combination of these two gases make up 98.66% of the total mass fraction of standard air and should be a good comparison to the helium mass fraction for comparisons. Finally, by comparison with 6.41, it can be seen that the figure is simply an inverse of the helium trends. Due to the linked relationship of the results, this set of data will be used to examine the initial details of the blowdown from a mass fraction perspective as was done with the pressure.

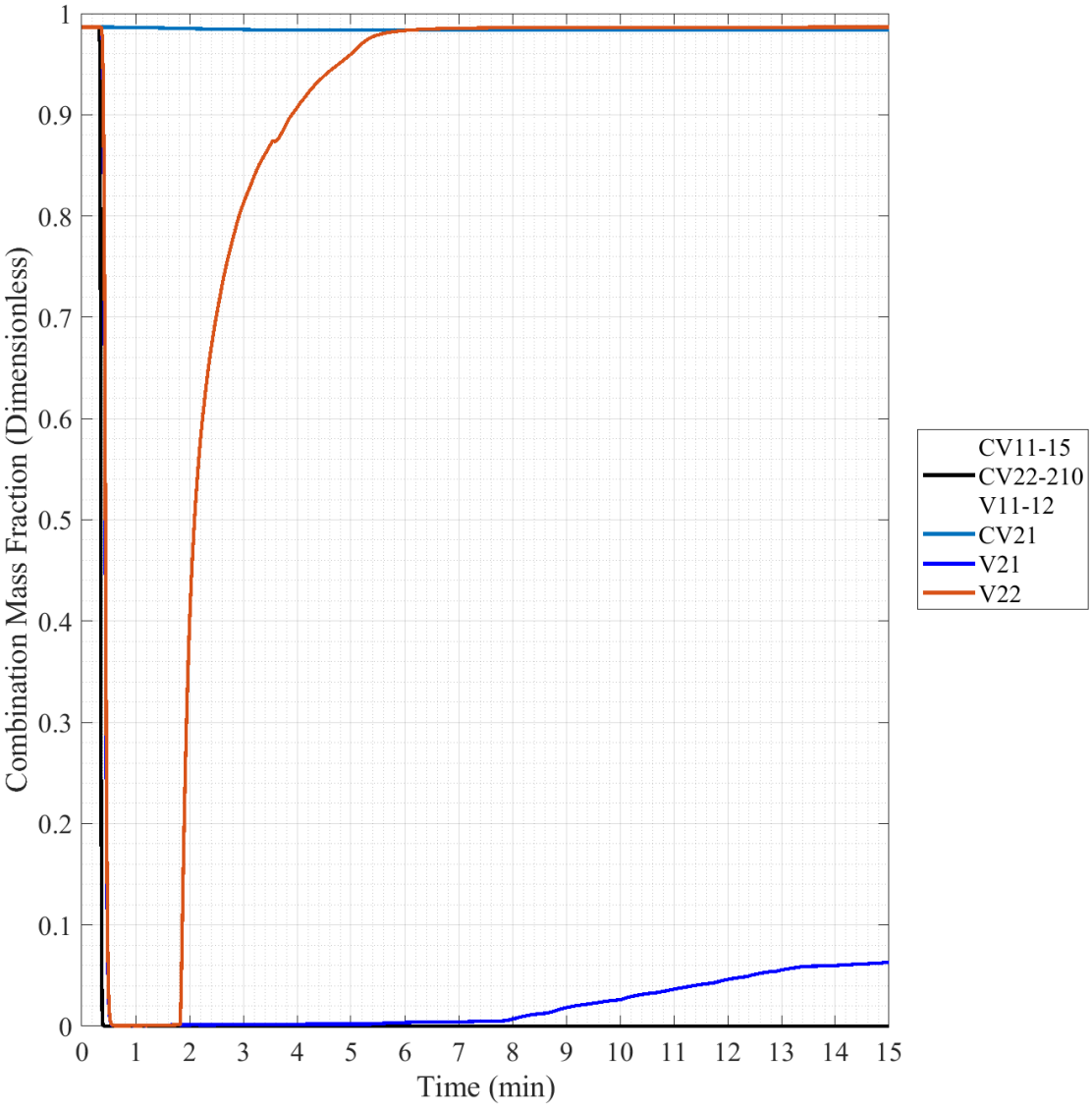

Fig. 6.43. 1/28th-Scale Scenario 3 Combination Mass Fraction, 15 minute Timescale.

Fig. 6.43 reduces in the timescale of the combination mass fraction to get details of the initial post-break building response to the spreading helium. V22 is seen to drop with the blowdown, then at ~1.8 minutes is when the volume begins to refill and only takes ~4 minutes to do so, like in scenario 1. During this period there is little unrest in the volumes that are filled with helium, unlike seen in scenario 1, and when V22 reaches a completely refilled with air state, V21 begins to refill which can be seen from ~6 minutes onward. To obtain more blowdown knowledge the timescale must be reduced further.

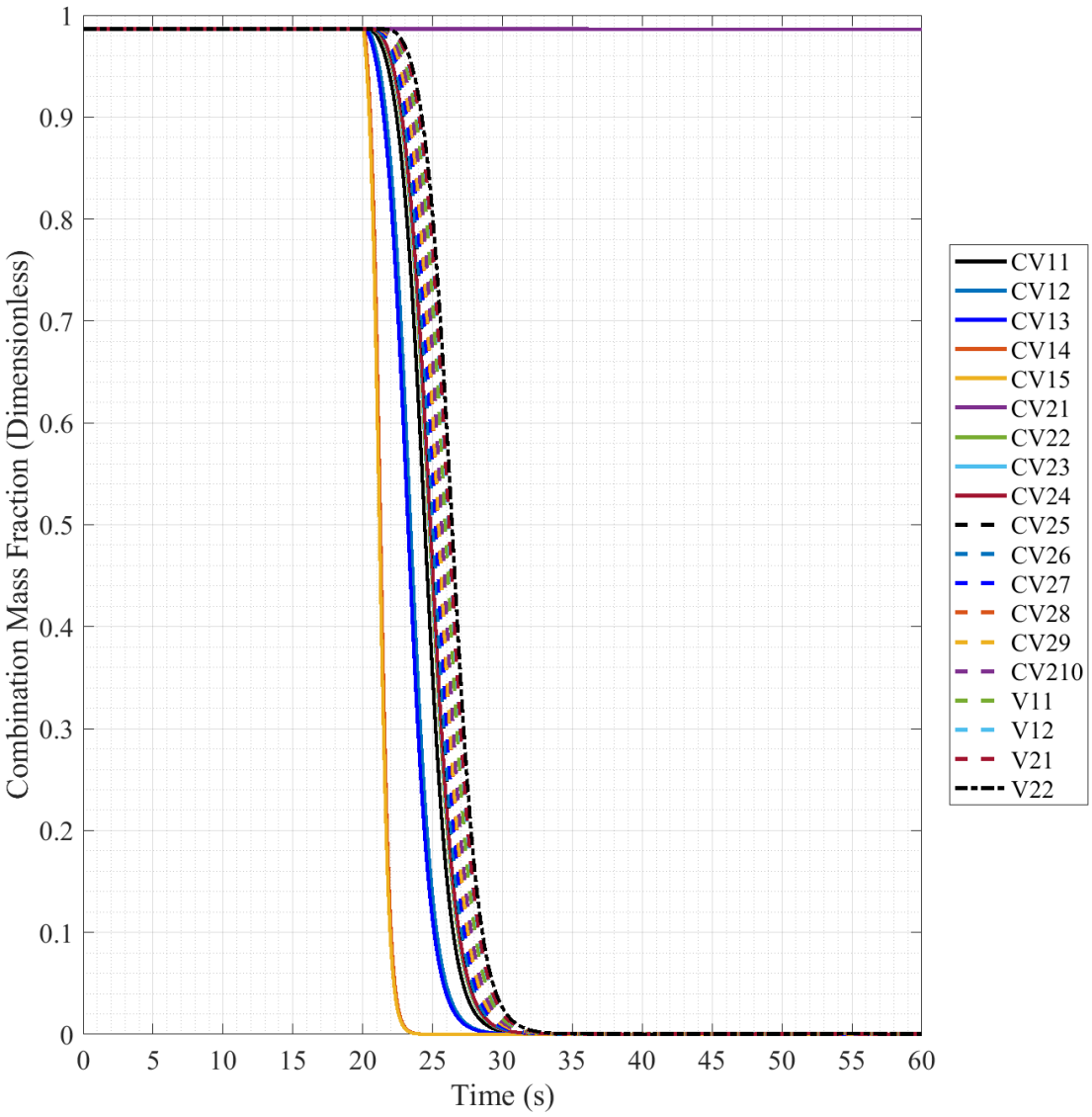

Fig. 6.44. 1/28th-Scale Scenario 3 Combination Mass Fraction, 60 second Timescale.

Fig. 6.44 reduces the timescale to the first 60 seconds of the scenario, where the progression of volumes voiding can be seen. Post-break initiation it takes ~13 seconds for all volumes to be voided, baring CV21 and CV31 which undergo very little helium influx. A shorter blowdown period is to be expected in this scenario due to the decreased volume to be displaced, resulting in a quicker blowdown. Going from left to right on the plot the general flow path of helium through the volumes can be seen, with the left most volumes being in the RC, and moving right moves into the SGC and finally the vent spaces, being on the far right and voided last.

6.1.5 1/28th-Scale Scenario 4 Results

Scenario 4 is a SGV break scenario with the EQS closed to flow from the blowdown from entering by closing the duct connections at their flow paths from the SGC. This will force blowdown gases either directly to the vent space or down deeper into the SGC. For this scenario any volumes from the EQS (CV31-36) and the RC (CV1-15) will be omitted from plotted results as they undergo no changes during the scenario. Fig. 6.45 gives a visual example of this scenario's estimated progression, utilizing a figure of the basic regions of the model.

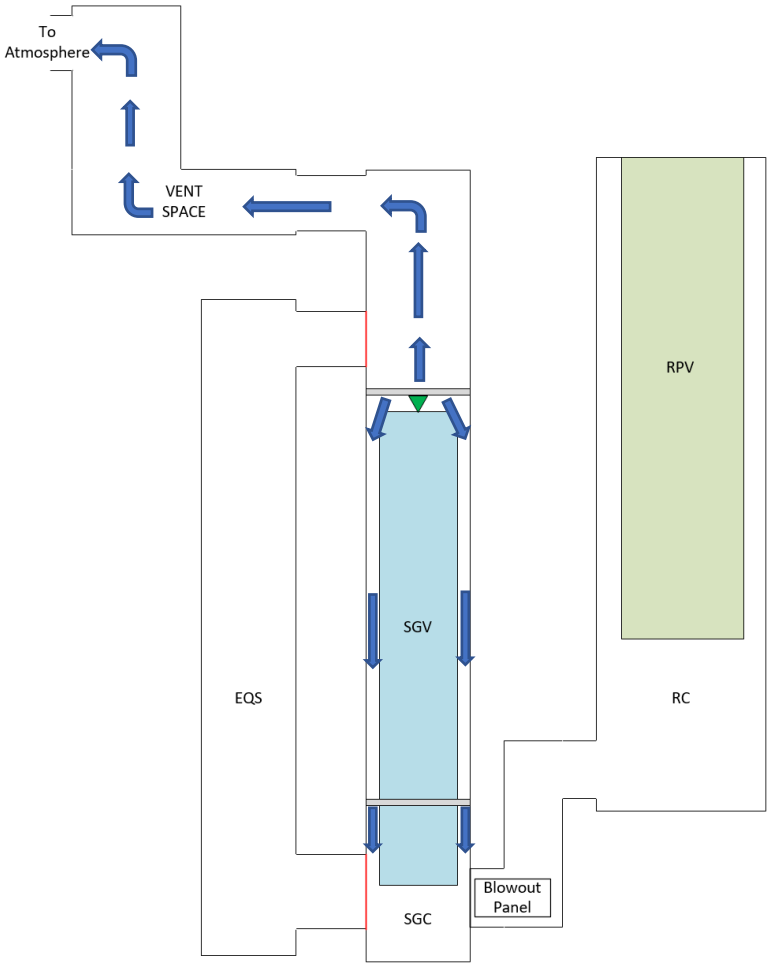

Fig. 6.45. Scenario 4 Estimated Blowdown Progression.

The initial pressure plot of scenario 4, with the pressure plotted across the full timescale, has been omitted as it simply shows the same information as the initial scenario 2 plot, with the

initial 6.4 MPa pressure of the helium volume resulting in vertical scale of the plot blownout due to its comparibly large size. Nowhere along the full timescale of the pressure for this scenario's results were any new transients observed. The full timescale plot has been included in Appendix D for reference to the actual data plot, but Fig. 6.21 can be used as a quick reference as it shows a similar plot, excluding the removed volumes from this scenario.

After reducing the timescale of the pressure plot to 50 seconds, like in scenario 2, the resulting plot was extremely similar to the plot made for that scenario. The initial helium pressure of 6.4 MPa can be seen extremely well at the initial time, then at 20 seconds the pressure begins to fall at an exponential rate as the break flow path is opened and helium expands out and into the SGC volumes. The HV reaches an equalized pressure of ~100 kPa at ~22.1 seconds following the blowdown initiation, ~41.1 seconds post simulation initiation. Overall, the progression of the pressure blowdown from the helium volumes seems to have not been affected by the change in the model layout. The pressure plot of this frame of time for this scenario has been included in Appendix D for further reference, or Fig. 6.22 can be used as a quick reference to the progression of the helium volume blowdown, excluding the removed volumes from this scenario.

Removing the helium volume from the plot allows a better view of the reactor building response to the helium release, which can be seen in Fig 6.46. As previously discussed, at this timescale that there are two separate groups of volumes undergoing different pressure transients following the break. These transients come back together in the 5 seconds following break initiation to an equilibrium at ~100 kPa. Reducing the timeframe further will allow a better view of the transient peaks.

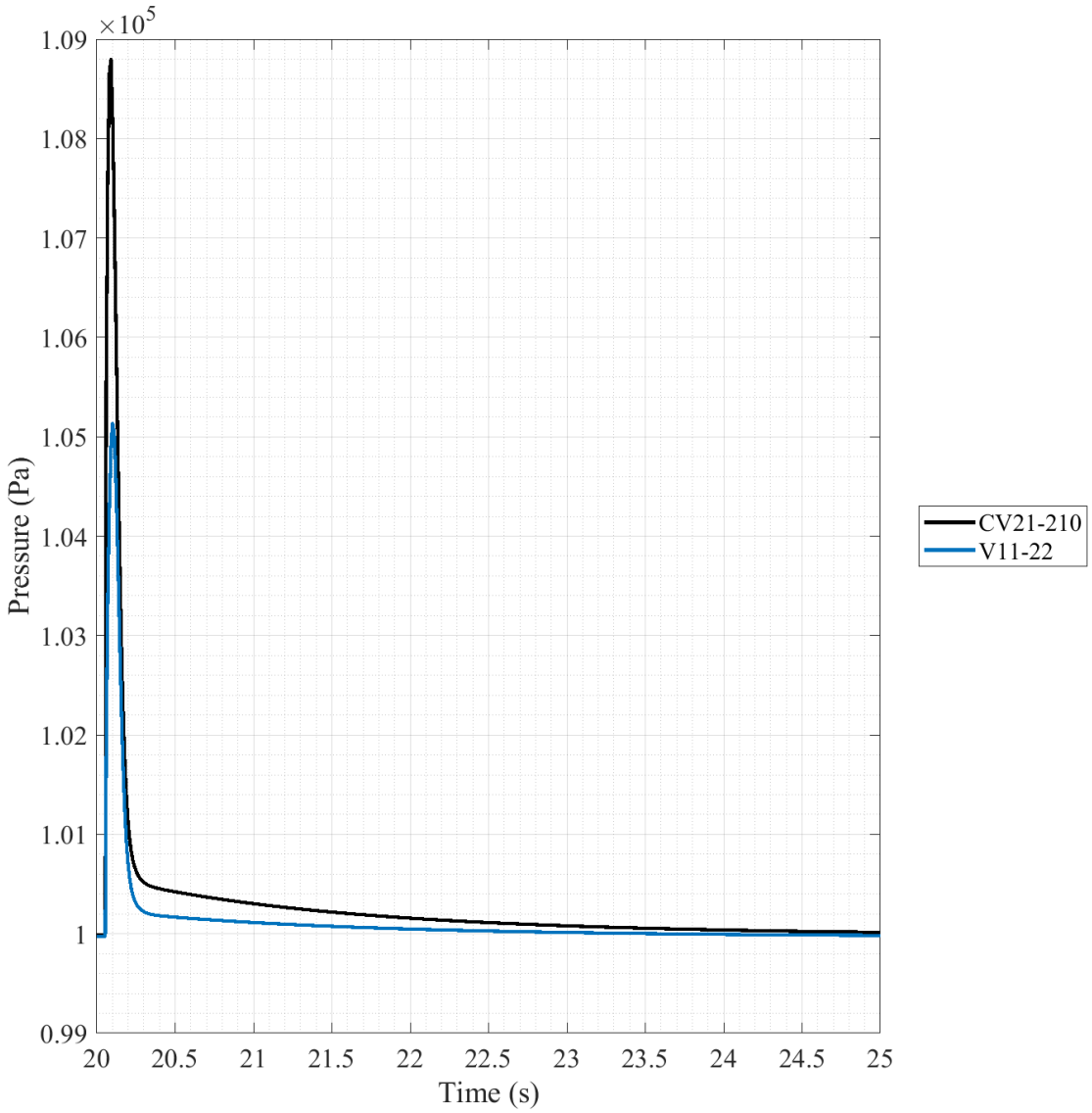

Fig. 6.46. 1/28th-Scale Scenario 4 Pressure, 20-25 second Timescale.

Fig. 6.47 reduces the timescale down to the half second following the break initiation. As described in scenario 1, the break is not initiated in the model until ~20.05 seconds even though set to initiate at exactly 20 seconds due to the way MELCOR handles timesteps. Following the break initiation, the pressure changes instantly throughout all the volumes of the model as atmosphere is displaced by the expanding helium.

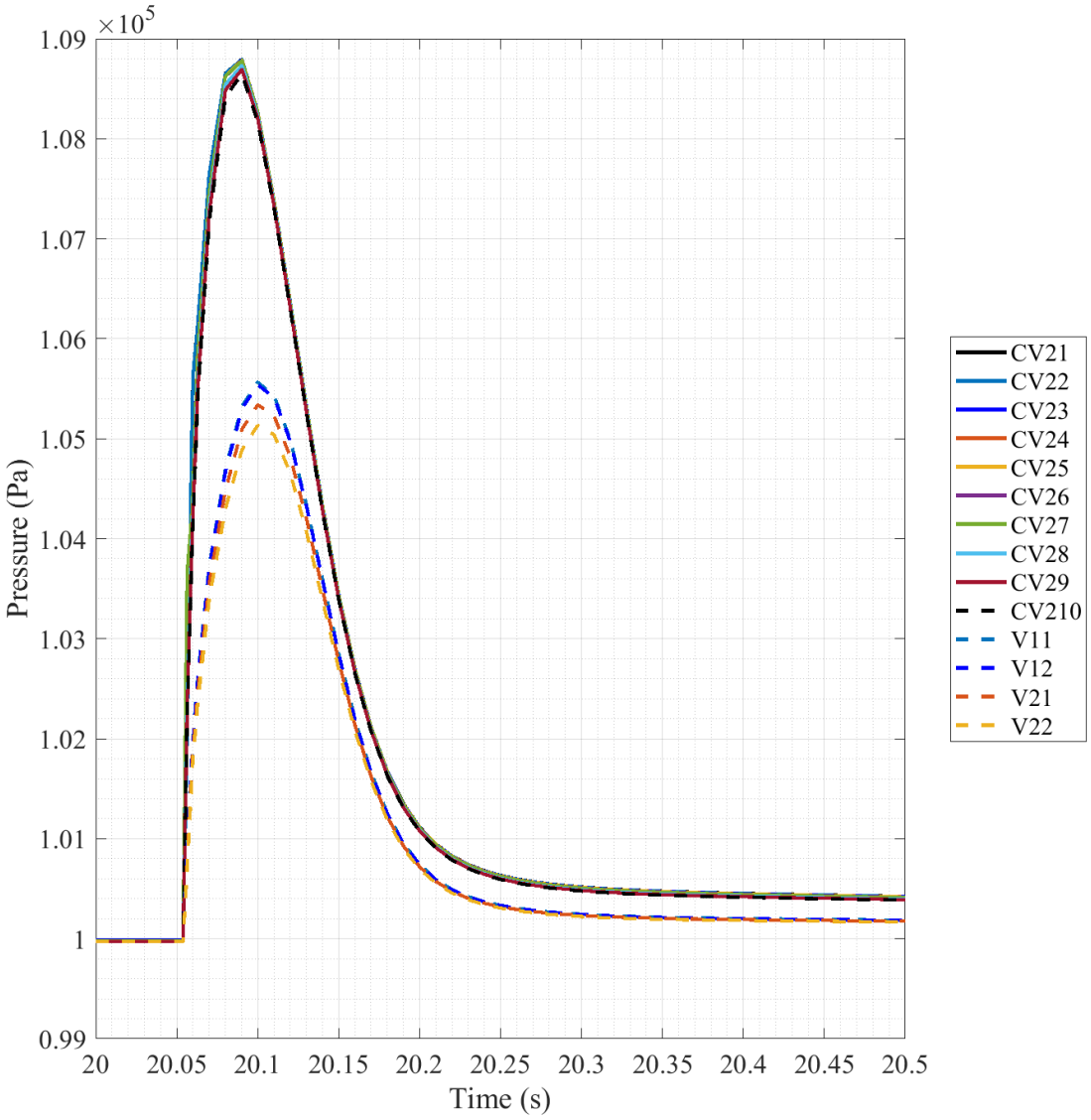

Fig. 6.47. 1/28th-Scale Scenario 4 Pressure, 20-20.5 second Timescale.

From Fig. 6.47 it can be seen that CV21-210 (SGC) increases to a maximum pressure of 1.0879x10^5 Pa (8.79 kPa increase) before falling back to near normal pressure. The smaller peak is endured by V11-22 and increases to a maximum in the range of ~1.05x10^5 Pa (5 kPa increase) before falling. In contrast to scenario 2, it appears that no peak occurs on the rising side of the CV21-210 transient, though this will be examined with a closer look at the short timescale again.

Fig. 6.48 reduces the timescale down to the first 1/10th of a second post set break initiation to determine if there is an early transient disturbance. CV23-27 do undergo a slight disturbance

from the rise, but not to the extent of scenario 2. Overall, the upper transient is less uniform on the rising side with CV21-22 gaining pressure faster than the other volumes of the transient. This is most likely do the constricted flow path choices in this scenario as the EQS is closed off. This means and flow oriented downwards will build faster as it has nowhere to expand to until flow is established, which in the scenario happens relatively quickly, ~0.5 second later.

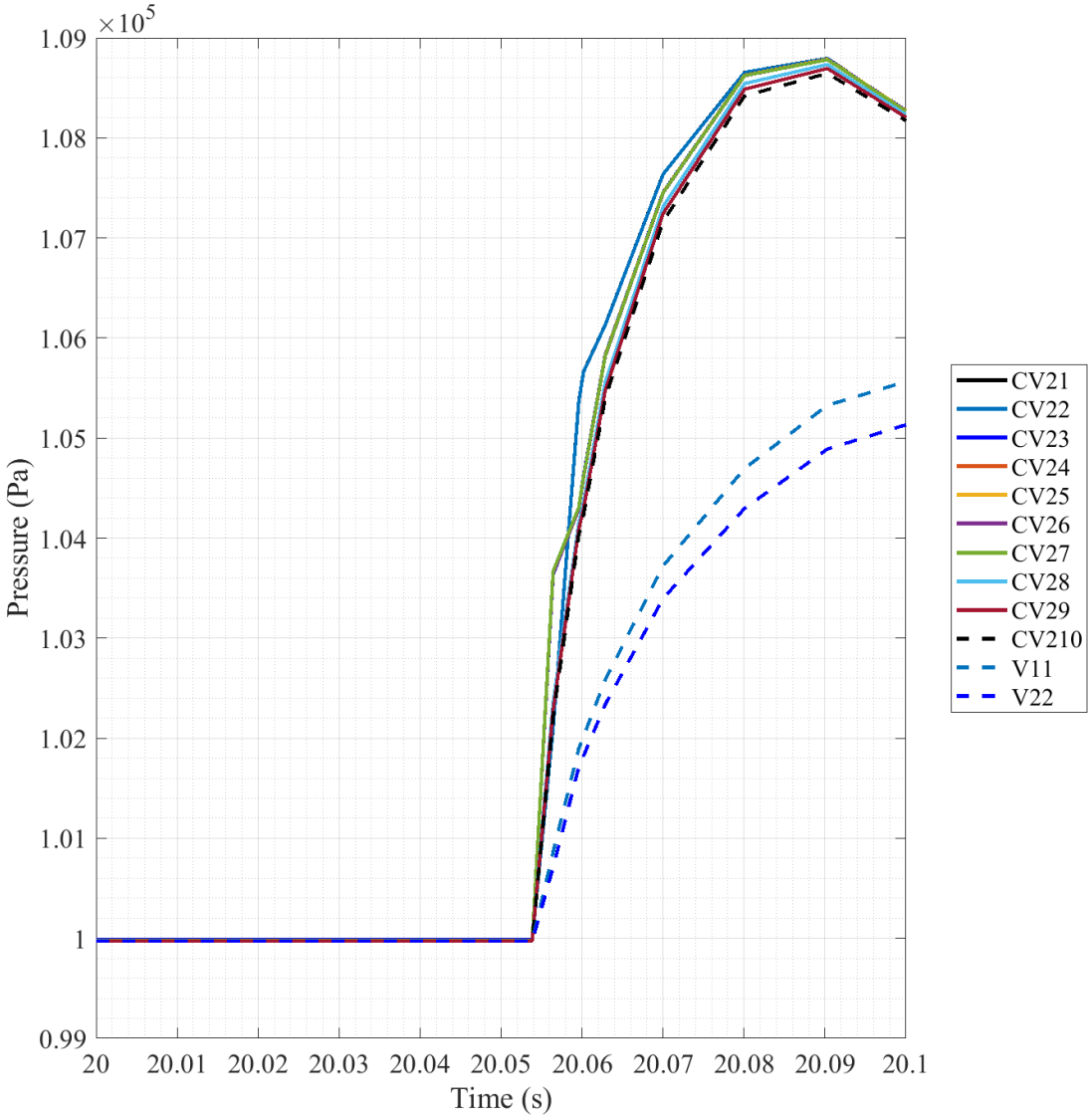

Fig. 6.48. 1/28th-Scale Scenario 4 Pressure, 20-20.1 second Timescale.

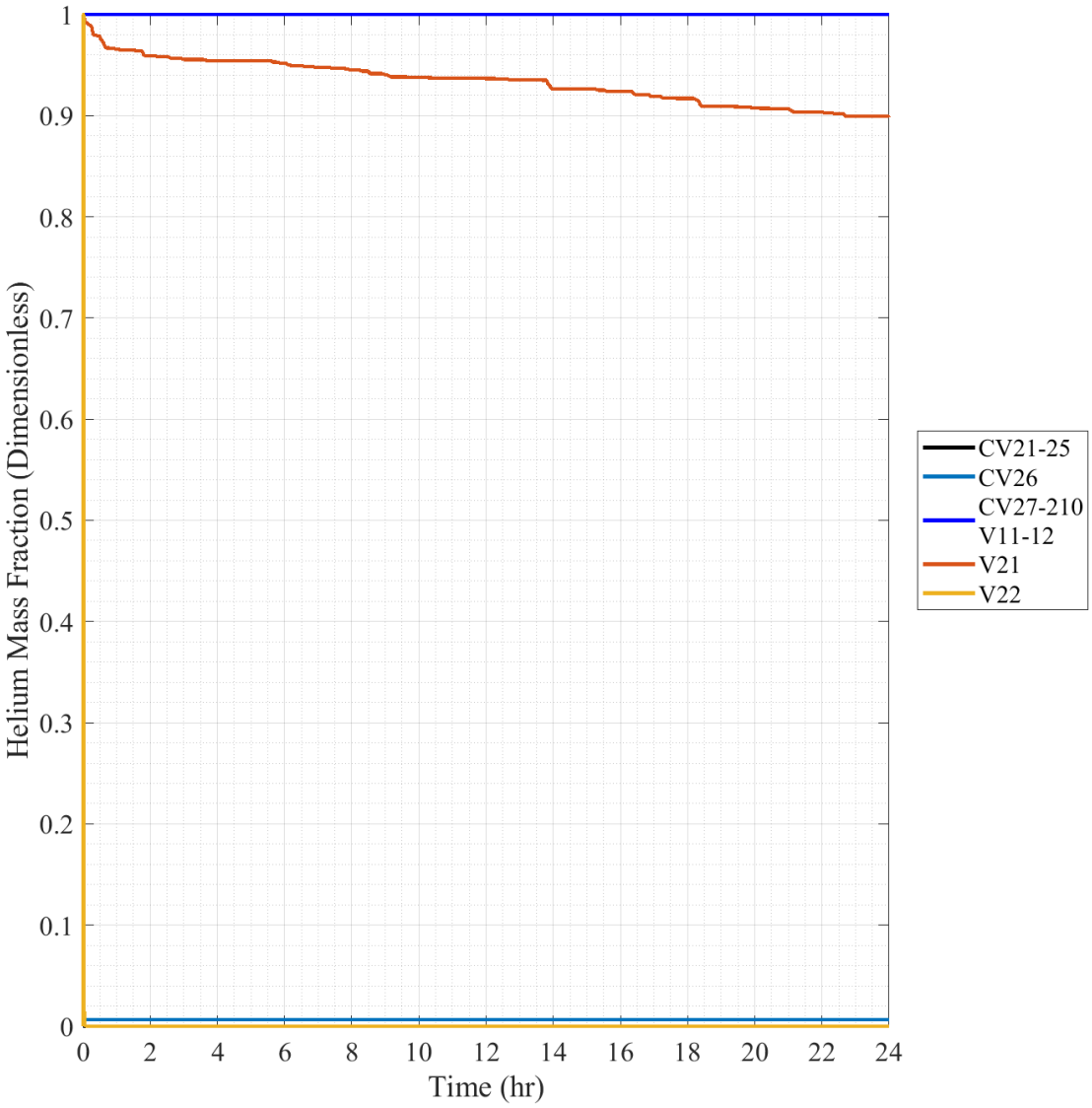

Fig. 6.49. 1/28th-Scale Scenario 4 Helium Mass Fraction.

Mass fraction data of scenario 4 starts off with the presentation of the helium mass fraction plot, presented in Fig. 6.49. The singular transient of this scenario is composed of V21 by itself, spiking with the blowdown but then falling over the progression of the scenario to ~90%. This is a stark contrast to scenario 2 where there was much more differentiation to be made between the volumes following the break, and more reminiscent of the previous scenario. All other volumes in this scenario go to the extremes of the mass fraction scale. V22, much like in all other scenarios, spikes very quickly at the break but falls almost instantly back to 0% in the scale visible on the

plot. CV21-25 experiences a reaction similar to what was seen with CV21 in previous scenarios, with a very slight increase in helium content over the period of the scenario but that is almost imperceptibly small. CV26 undergoes a very slight spike but rests at ~0.6%, as it is right below the actual break location of the scenario. Finally, CV27-210 and V11-12 all maintain a very close or completely filled atmosphere of helium for the duration of the scenario post-break initiation spike due to the very short path to the exterior of this scenario. Getting a better look at early timescales will require a smaller timescale that will be explored in later plotted results.

In order to maintain a concise description of scenarios, the plots of oxygen and nitrogen mass fraction are not presented in this scenario as their results are reaffirmed best by a combination of their results to approximate a near full mass fraction of standard air. As was seen in scenario 2, oxygen and nitrogen mass fractions showed inverse results of the helium mass fraction and were simply differentiated by the resulting scale differences in the gas mass fractions. Plotted results for both the oxygen and nitrogen mass fraction can be found in Appendix D for further reference but are left out of this scenario to be concise.

Fig. 6.50 sums the oxygen and nitrogen mass fractions together as previously discussed to a “Combination” mass fraction composed of the combination of the two individual mass fractions. The combination of these two gases make up 98.66% of the total mass fraction of standard air and should be a good comparison to the helium mass fraction for comparisons. Finally, by comparison with Fig. 6.49, it can be seen that the figure is simply an inverse of the helium trends. Due to the linked relationship of the results, this set of data will be used to examine the initial details of the blowdown from a mass fraction perspective as was done with the pressure.

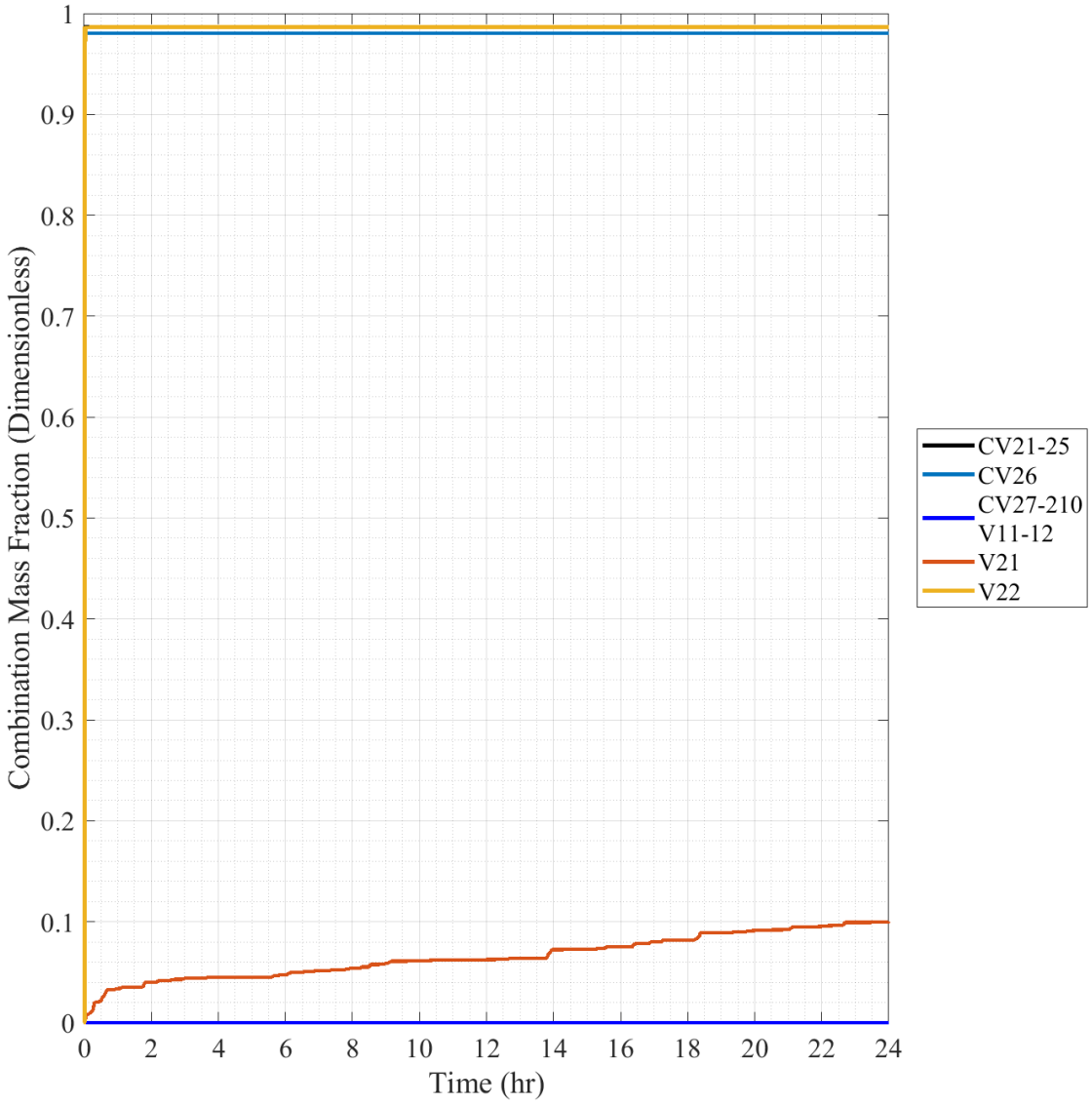

Fig. 6.50. 1/28th-Scale Scenario 4 Combination Mass Fraction.

Fig. 6.51 reduces in the timescale of the combination mass fraction to get details of the initial post-break building response to the spreading helium. V22 can be seen to be voided with the blowdown, but then ~18 seconds post-break it begins to refill. V21 also begins to refill slightly at this timescale, as it slowly pulls away from ~0%, but within this period it refills little even though V22 is near completely refilled. CV26 can be seen with the small amount of helium mixture at the top of the plot. The initial break at this scale is still a relatively linear and will need to be explored at a smaller timescale.

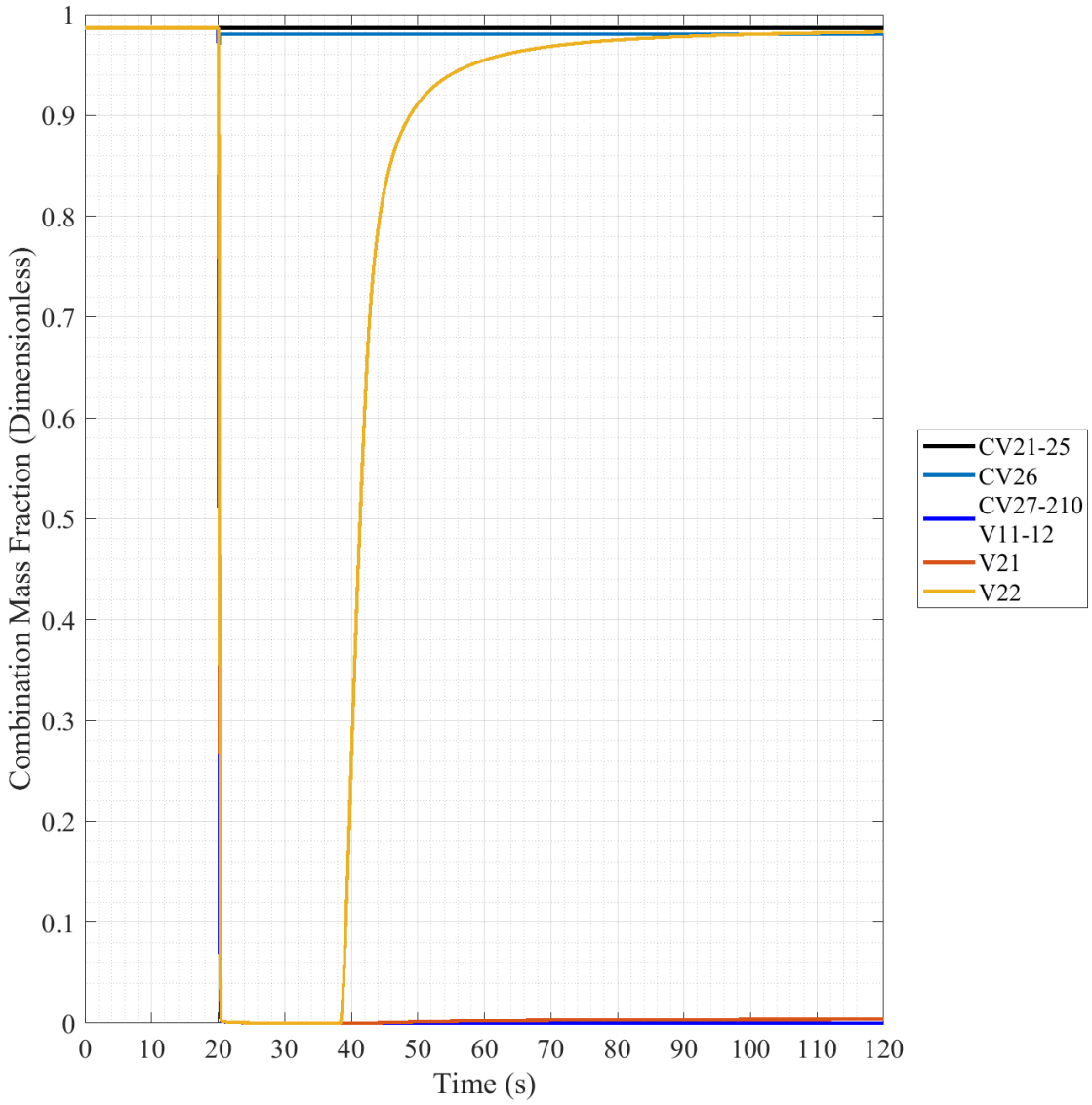

Fig. 6.51. 1/28th-Scale Scenario 4 Combination Mass Fraction, 120 second Timescale.

Fig. 6.52 shows the initial voiding produced by the helium introduction to the reactor building volumes. Overall, all affected volumes are voided of the air content within ~0.5 second of the break initiation. CV26's initial deviation to its stable level can be seen on this scale as it decreases but rises to plateau. CV27 has the largest deviation of voiding volumes, changing slope significantly before dropping again at ~20.14 seconds leading to slight compression of the overall voiding transient band. This band of voiding volumes is arranged from left to right by their general position in the flow path to the exterior of the model from the break location, with

volumes like CV27-210 being on the left and moving to the right shows the progression through the vent space volumes.

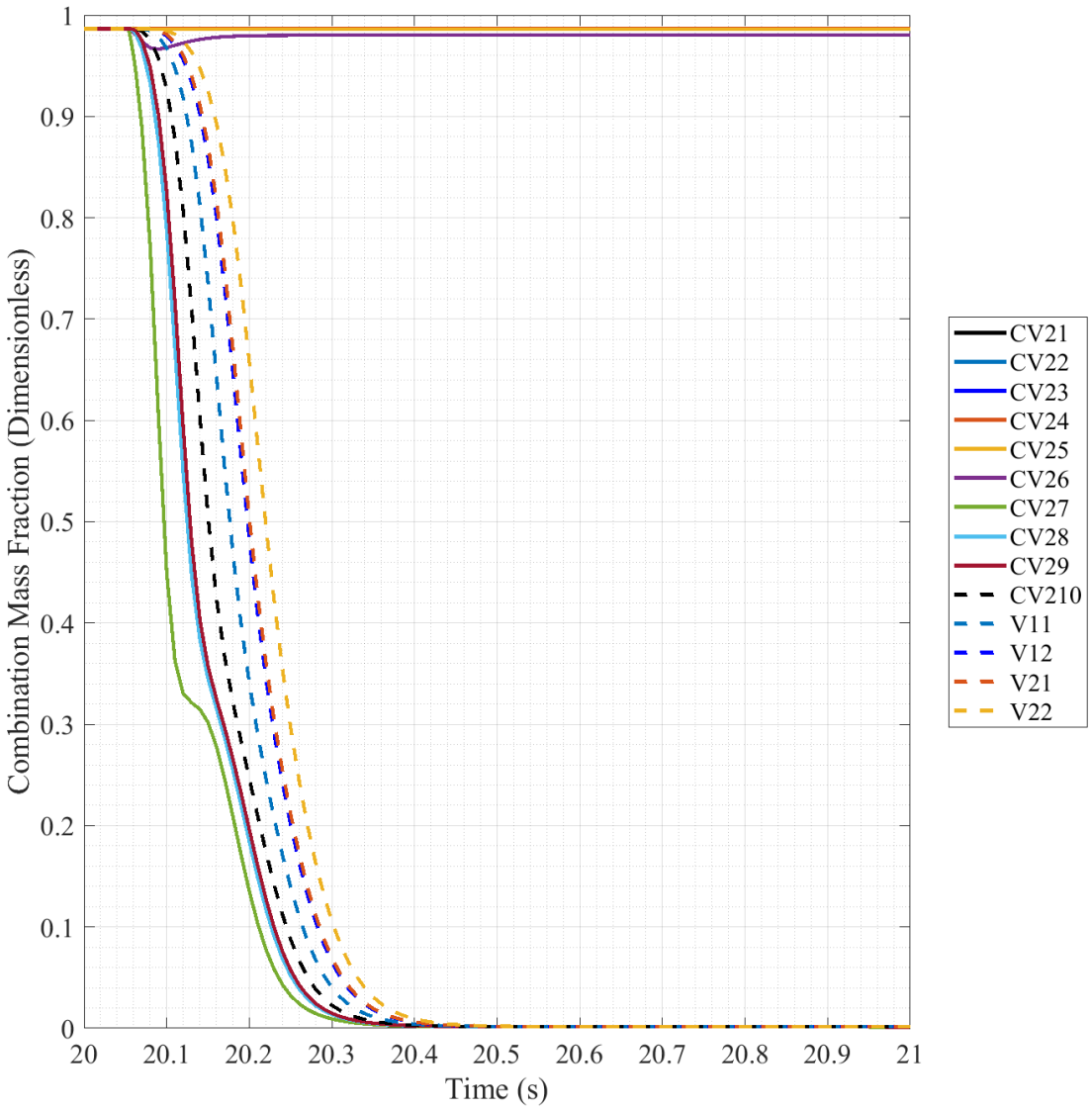

Fig. 6.52. 1/28th-Scale Scenario 4 Combination Mass Fraction, 20-21 second Timescale.

6.1.6 1/28th-Scale Scenario 5 Results

Scenario 5 is a RPV break scenario with the lower SGC dividing plate closed to upward flow at its flow path. This forces the blowdown gases and atmosphere to rise through the EQS, giving the blowdown a longer required flow distance through the reactor building before reacting the exterior volume. No volumes are discarded from plotted results as they all may be interacted with by the blowdown progression. Fig. 6.53 gives a visual example of this scenario's estimated progression, utilizing a figure of the basic regions of the model.

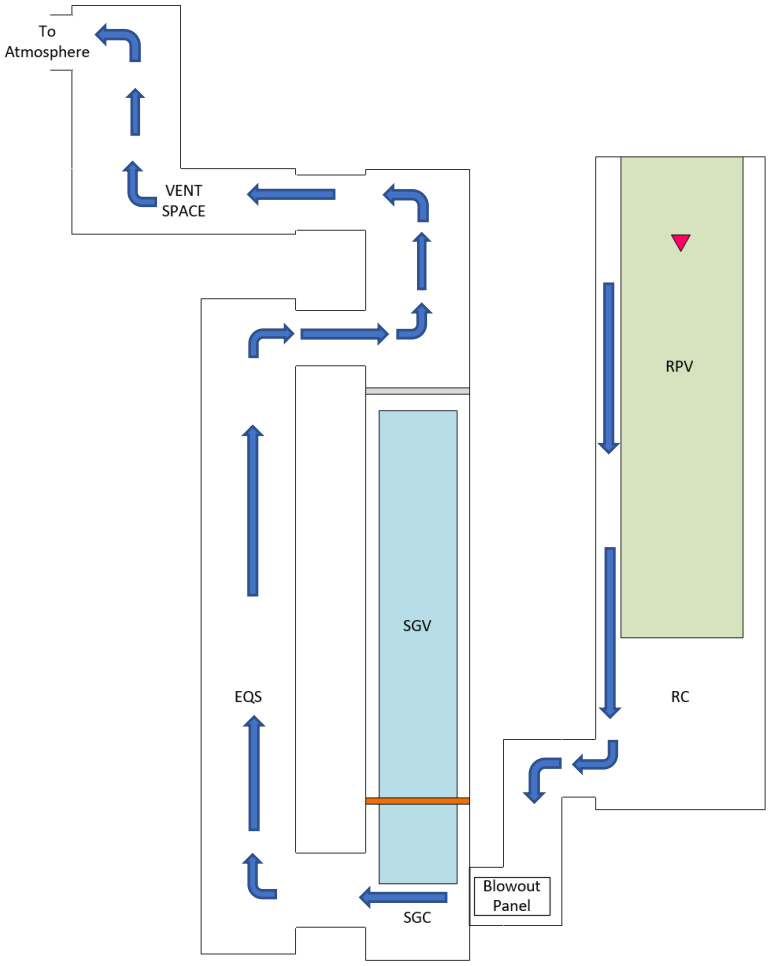

Fig. 6.53. Scenario 5 Estimated Blowdown Progression.

The initial pressure plot of scenario 5, with the pressure plotted across the full timescale, has been omitted as it simply shows the same information as the initial scenario 1 plot, with the

initial 6.4 MPa pressure of the helium volume resulting in vertical scale of the plot blownout due to its comparibly large size. Nowhere along the full timescale of the pressure for this scenario's results were any new transients observed. The full timescale plot has been included in Appendix D for reference to the actual data plot, but Fig. 6.8 can be used as a quick reference as it shows a similar plot.

After reducing the timescale of the pressure plot to 500 seconds, like in scenario 1, the resulting plot was extremely similar to the plot made for that scenario. The initial helium pressure of 6.4 MPa can be seen well at the initial time, then at 20 seconds the pressure begins to fall at an exponential rate as the break flow path is opened and helium expands out and into the RC volumes. The HV reaches an equalized pressure of ~100 kPa at ~293 seconds following the blowdown initiation, ~313 seconds post simulation initiation. Overall, the progression of the pressure blowdown from the helium volumes seems to have not been affected by the change in the model layout. The pressure plot of this frame of time for this scenario has been included in Appendix D for further reference, or Fig. 6.9 can be used as a quick reference to the progression of the helium volume blowdown.

Reducing the timescale down to 5 seconds following the break initiation helps get a better picture of the pressure transients. Fig. 6.54. illustrates the building volumes response to the blowdown, with the largest spike occurring the volumes of CV11-15 as they are the primary volumes that the helium releases into directly, with a spike in pressure up to 1.0935×10^5 Pa (9.35 kPa increase), much like with scenario 1. This scenario looks very similar to scenario 1 but with an increased lower spike pressure as in scenario 3, without the increased post-spike pressure.

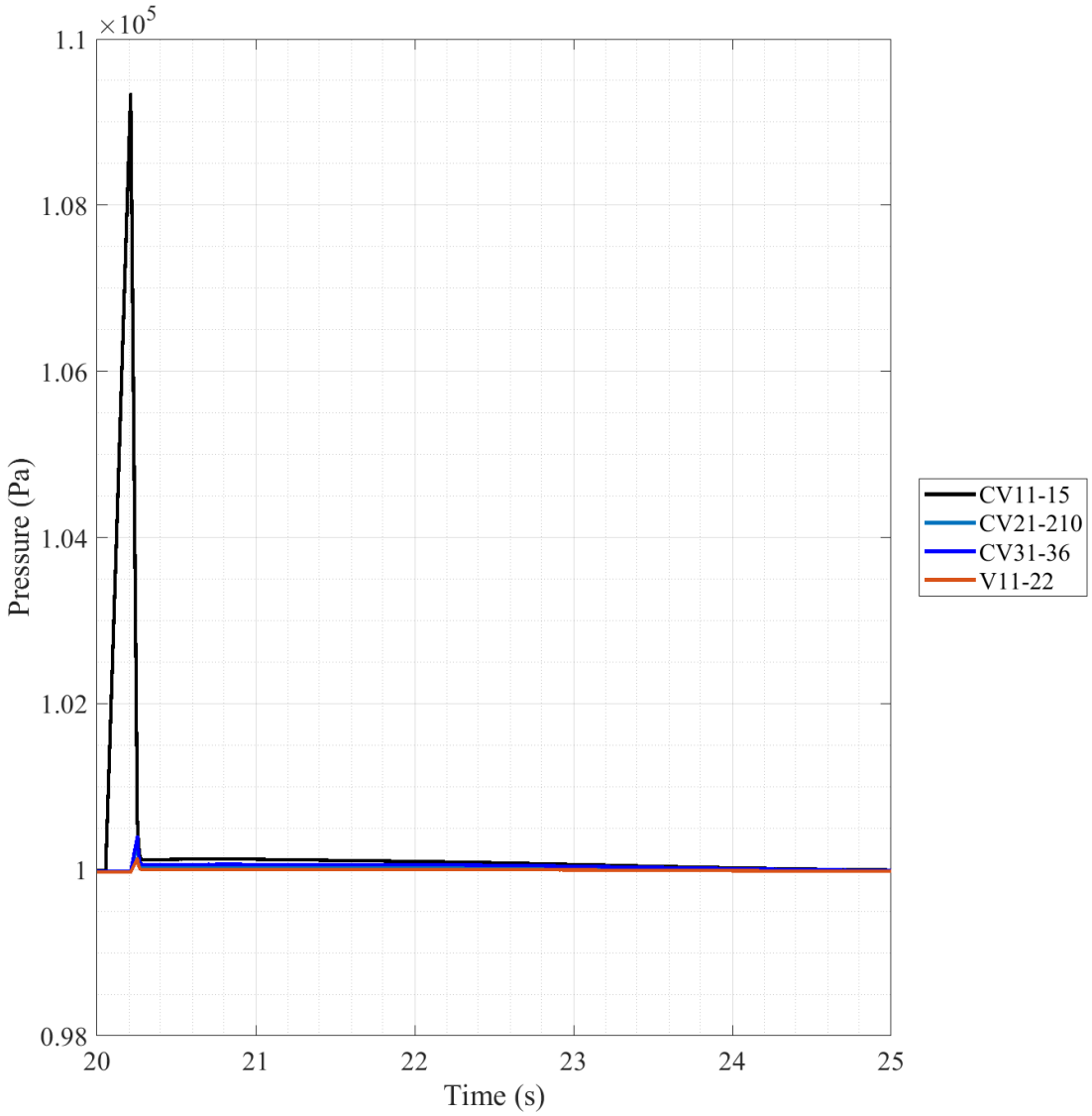

Fig. 6.54. 1/28th-Scale Scenario 5 Pressure, 20-25 second Timescale.

Dropping the timescale further, Fig. 6.55 reduces the timescale to the half second following the break, giving a good view of the linear spike caused by the helium expanding into the RC volumes and causing compression of the atmosphere in the duct connection against the blowout panel. As in scenario 1, the actuation and opening of the panel can be seen as the pressure drops extremely quickly and the other volumes rise to equalize and fall with the CV11-15 spike, though in much less magnitude.

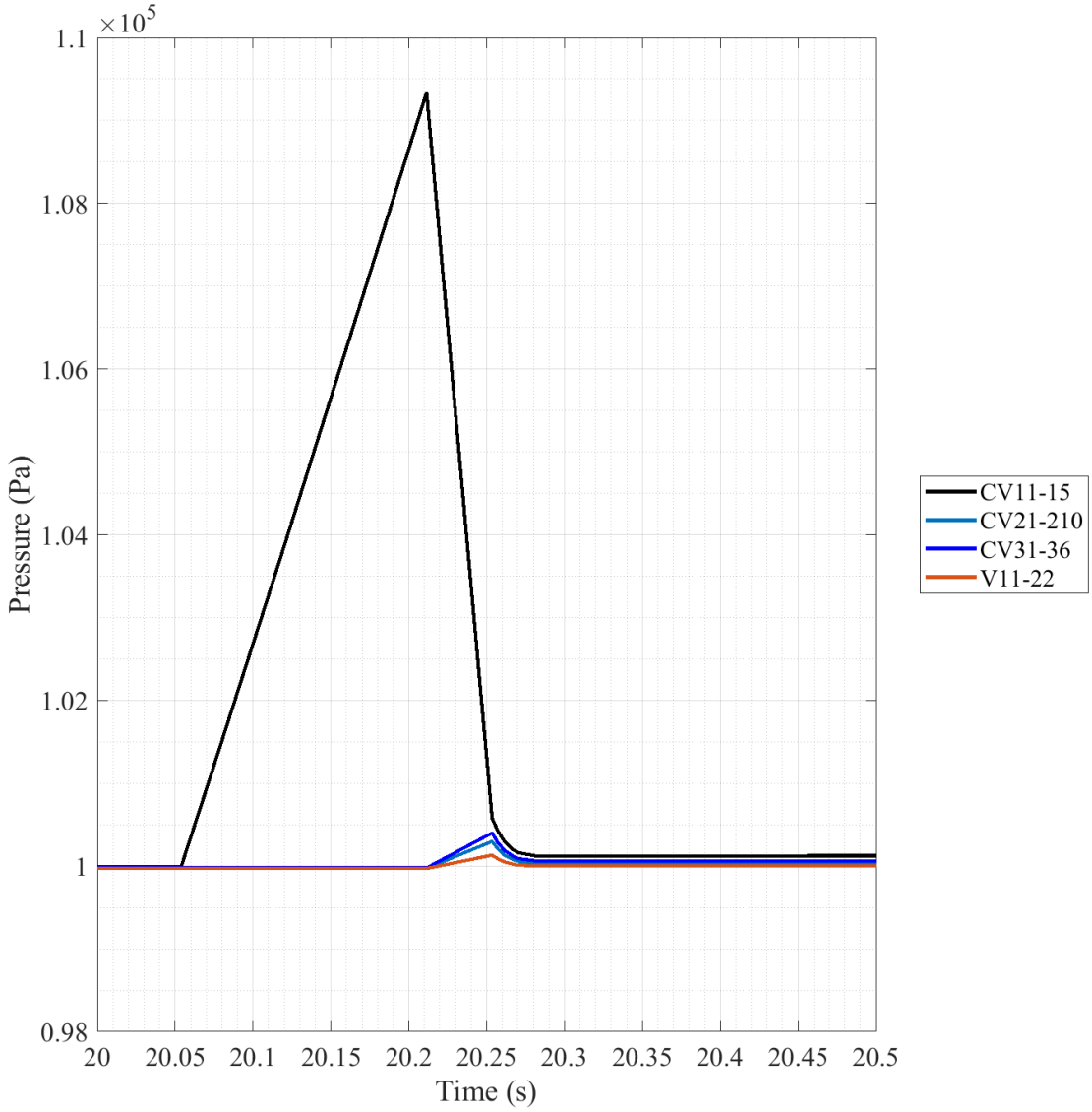

Fig. 6.55. 1/28th-Scale Scenario 5 Pressure, 20-20.5 second Timescale.

As in scenario 1, the break is delayed due to the way MELCOR handles timesteps and the break does not occur until 20.05 seconds in the simulation, even though set to initiate at 20 seconds exactly. The blowout panel initiates at the 20.21 second mark, like scenario 1, and the pressure begins to fall in CV11-15. This decrease joins with the rise in the other volume pressures as they experience the displaced atmosphere and helium moving through their volumes. The lower spikes rise to the point of roughly equalizing with the CV11-15 spike as it falls, and together they fall to

a range around ~100 kPa. Unlike scenario 3, scenario 5 follows a similar pattern to scenario 1 with an overall regrouping of pressures following the spikes.

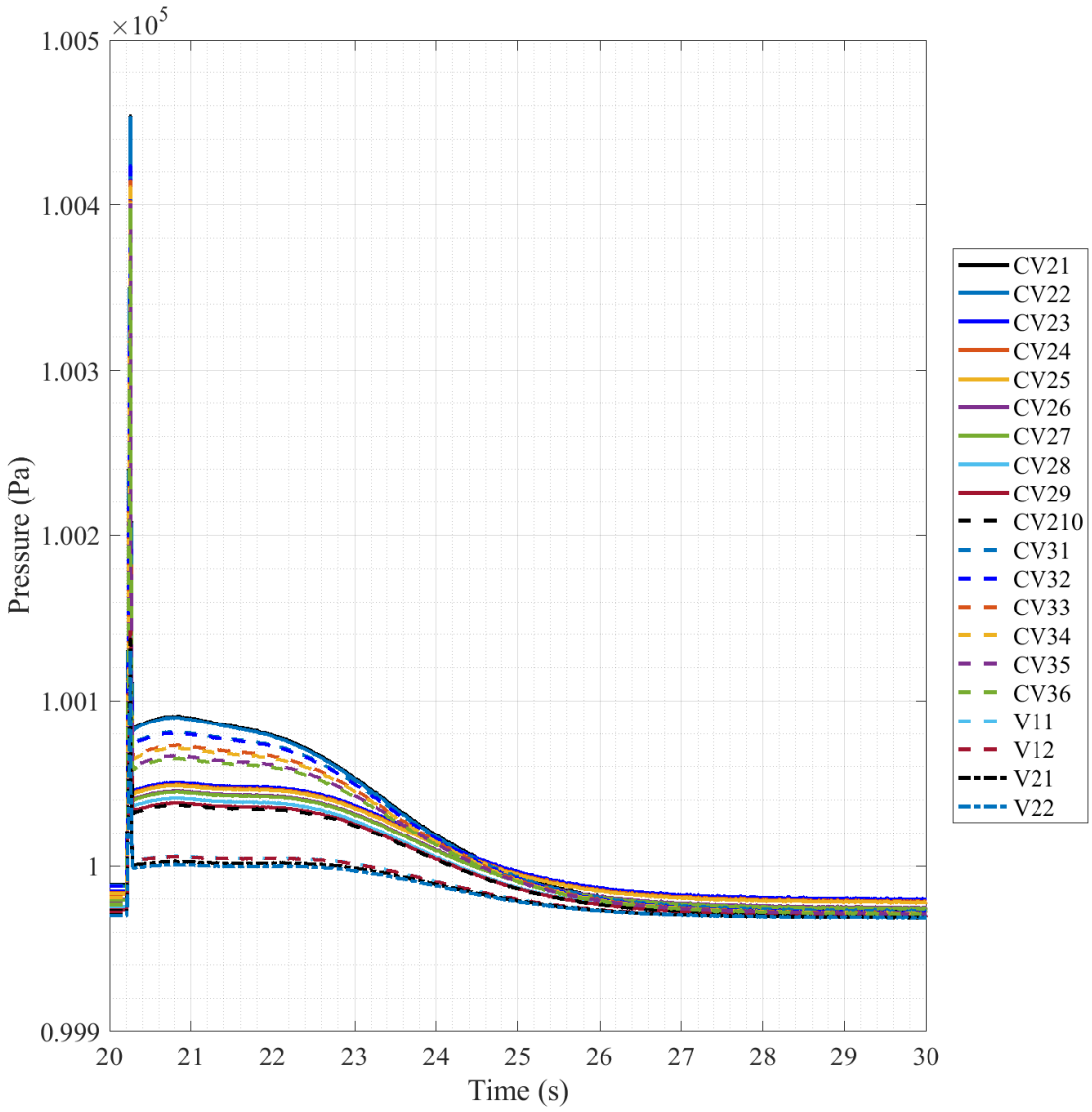

Fig. 6.56. 1/28th-Scale Scenario 5 Pressure, 20-30 second Timescale, No CV11-15.

To get a better view of the volumes other than CV11-15 it is removed from plotting and the timescale is pulled back to the 10 seconds following the break initiation. Fig. 6.56 shows the results of this plotting, with an overall spike much lower in scale but difficult to discern individual transient groups. What can be determined though is that there are roughly three groups of volumes that respond to the blowdown of the helium, an upper, middle, and lower group. All groups

undergo a spike that results in higher pressures following the break, though all decay over the ~10 seconds following the spike to rejoin in a closer equilibrium that they didn't have before the break was initiated, which can be seen by comparing the left and right sides of the plot. This is contrary to scenario 3 which established two separate equilibrium groups and is more reminiscent of scenario 1's post blowdown response.

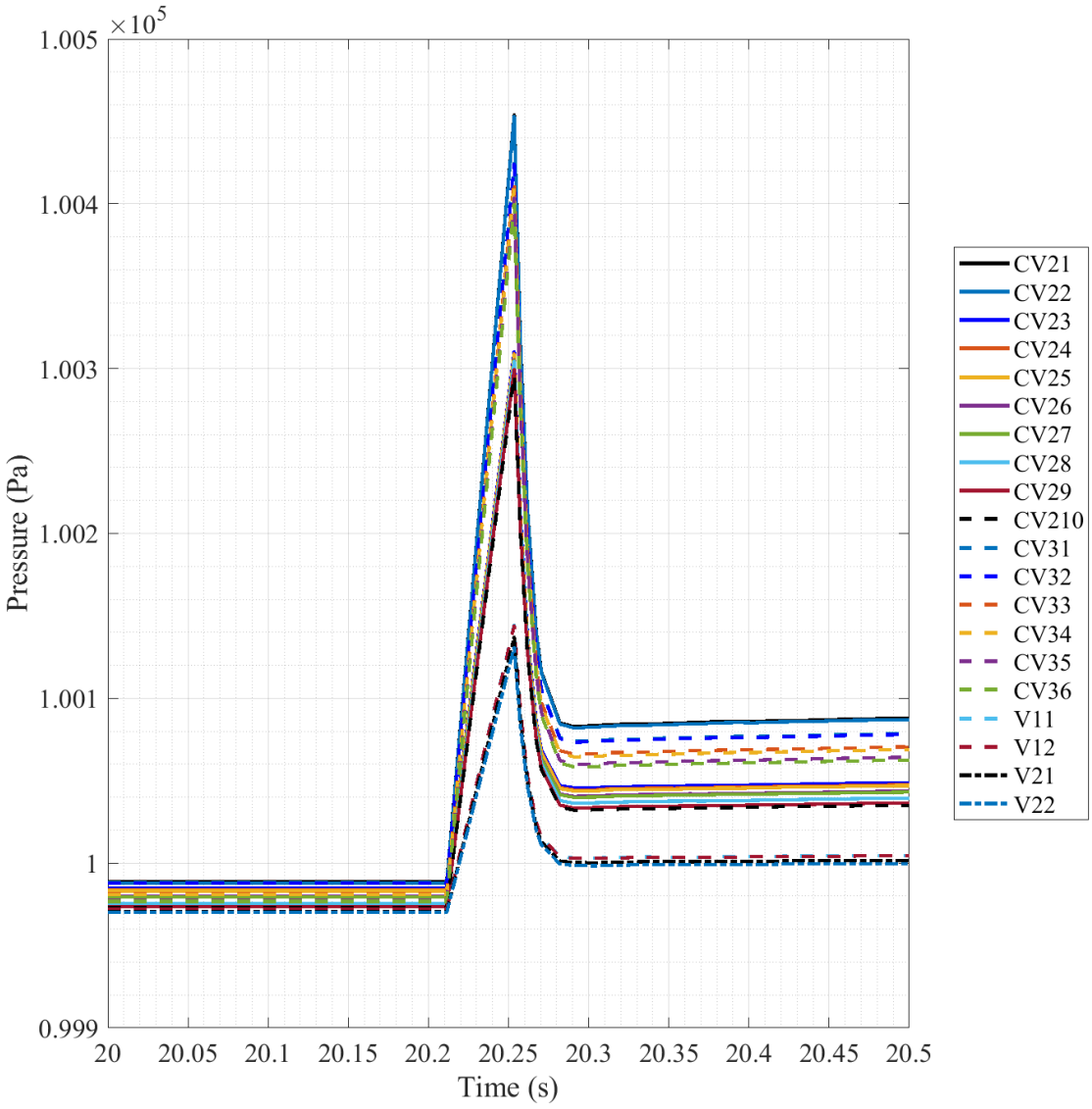

Fig. 6.57. 1/28th-Scale Scenario 5 Pressure, 20-20.5 second Timescale, No CV11-15.

Cutting the timescale down to the 20-20.5 second range, like done in scenario 1, Fig. 6.57 allows a better view of the plotted volumes response. With this plot the distinction can be made

between the three groups as they rise at different rates following the blowout panel initiation. The upper group is composed of CV21-22 and CV31-36 as they spike to a max pressure of ~$1.0045x10^5$ Pa (~450 Pa increase) then they fall into a group of distributed pressures around the $1.0008x10^5$ Pa range. The middle spike is composed of CV23-210 which spike to a maximum pressure of ~$1.0032x10^5$ Pa (~320 Pa increase) before falling to a $1.0004x10^5$ Pa range. The bottom spike is composed of the vent space volumes of V11-22 and only spike to a maximum of ~$1.0014x10^5$ Pa (~150 Pa increase), likewise falling to a ~100 kPa range before the recombination period roughly 10 seconds following. All of these groups then recombine in the ~10 seconds following blowdown to a new equilibrium around their initial pressures, which can be seen in Fig. 6.56.

Mass fraction data of scenario 5 starts off with the presentation of the helium mass fraction plot, presented in Fig. 6.58. The singular transient of this scenario, as with the other changed layout scenarios, is composed of V21 by itself, spiking with the blowdown but then falling over the progression of the scenario to ~31%. All other volumes in this scenario go to the extremes of the mass fraction scale. V22, much like in all other scenarios, spikes very quickly during the blowdown but falls almost instantly back to 0% in the timescale of the plot. CV21 and CV31 experiences a very similar reaction as in scenario 1 and 3, with a very slight increase in helium content in the range of E-3 mass fraction addition to their normal air composition across the scenario time period. Similar to what occurred in scenario 4, CV23-26 experience no introduction of helium to their volumes over the course of this scenario, due most likely to the complex flow path to reach that location of the cavity. Also similar to the previous scenario, CV27 experiences a very slight introduction of helium to the volume in the scenario, due in most part to it being the upper most central SGC volume next to the flow path that helium would be passing through.

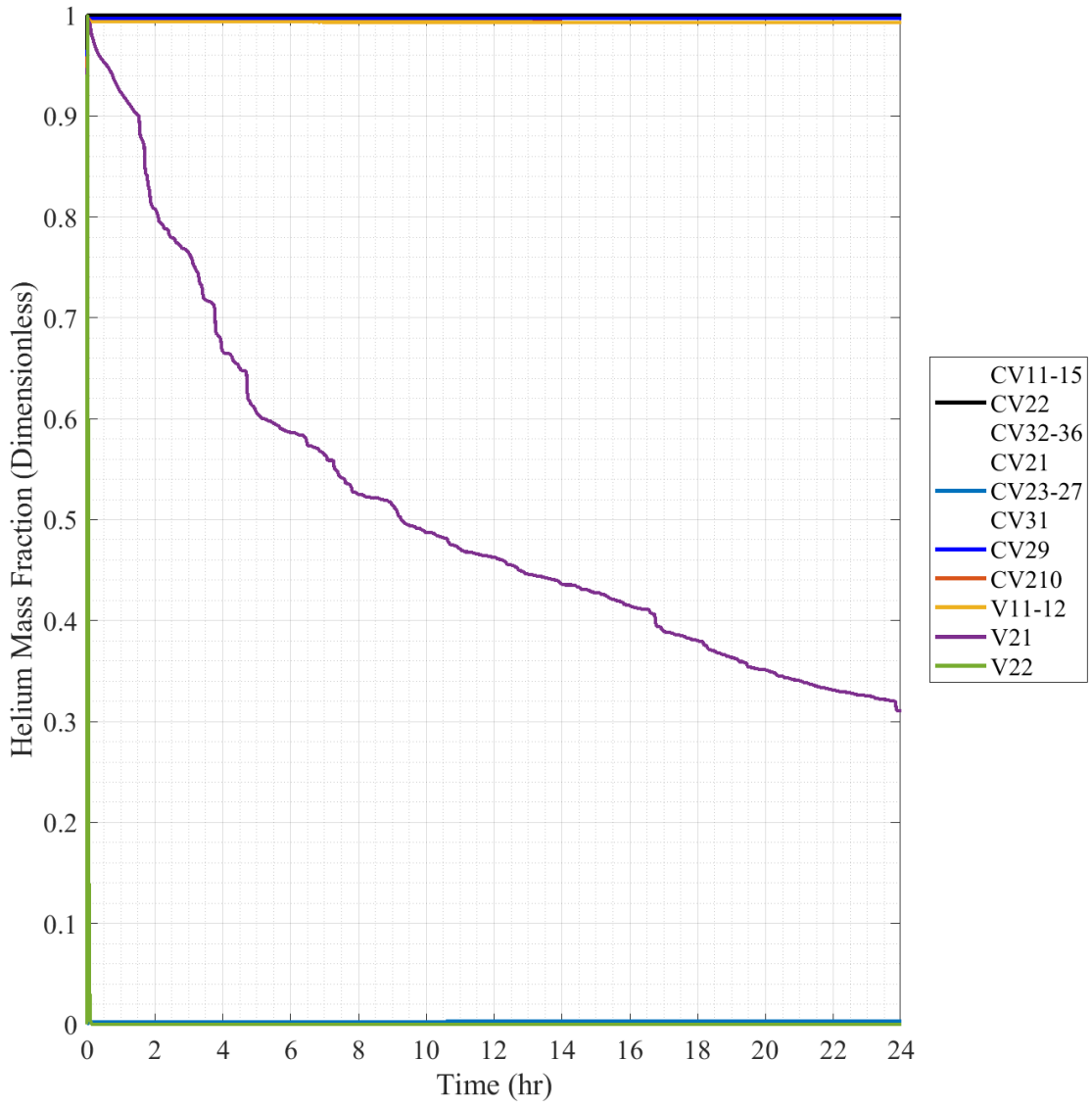

Fig. 6.58. 1/28th-Scale Scenario 5 Helium Mass Fraction.

All other volumes of the model, CV11-15, CV22, CV28-210, CV32-36, and V11-12 experience an almost complete fill of their volume by helium in this scenario. CV28 and CV36 undergo a very slight transient over the period of the scenario, falling to 98% by the end of the time period. CV210 and V11-12 also a very slight transient over the time period, ending at ~99% with CV29 ending at a slightly higher percentage. CV11-15, CV22, and CV32-36 all plateau at an essential completely helium filled concentration for the period of time following the break

initiation. A better look at an earlier progression will require a smaller timescale to be explored in later plotted results.

In order to maintain a concise description of scenarios, the plots of oxygen and nitrogen mass fraction are not presented in this scenario as their results are reaffirmed best by a combination of their results to approximate a near full mass fraction of standard air. As was seen in scenario 1, oxygen and nitrogen mass fractions showed inverse results of the helium mass fraction and were simply differentiated by the resulting scale differences in the gas mass fractions. Plotted results for both the oxygen and nitrogen mass fraction can be found in Appendix D for further reference but are left out of this scenario to be concise.

Fig. 6.59 sums the oxygen and nitrogen mass fractions together as previously discussed to a “Combination” mass fraction composed of the combination of the two individual mass fractions. The combination of these two gases make up 98.66% of the total mass fraction of standard air and should be a good comparison to the helium mass fraction for comparisons. Finally, by comparison with Fig. 6.58, it can be seen that the figure is simply an inverse of the helium trends. Due to the linked relationship of the results, this set of data will be used to examine the initial details of the break from a mass fraction perspective as was done with the pressure.

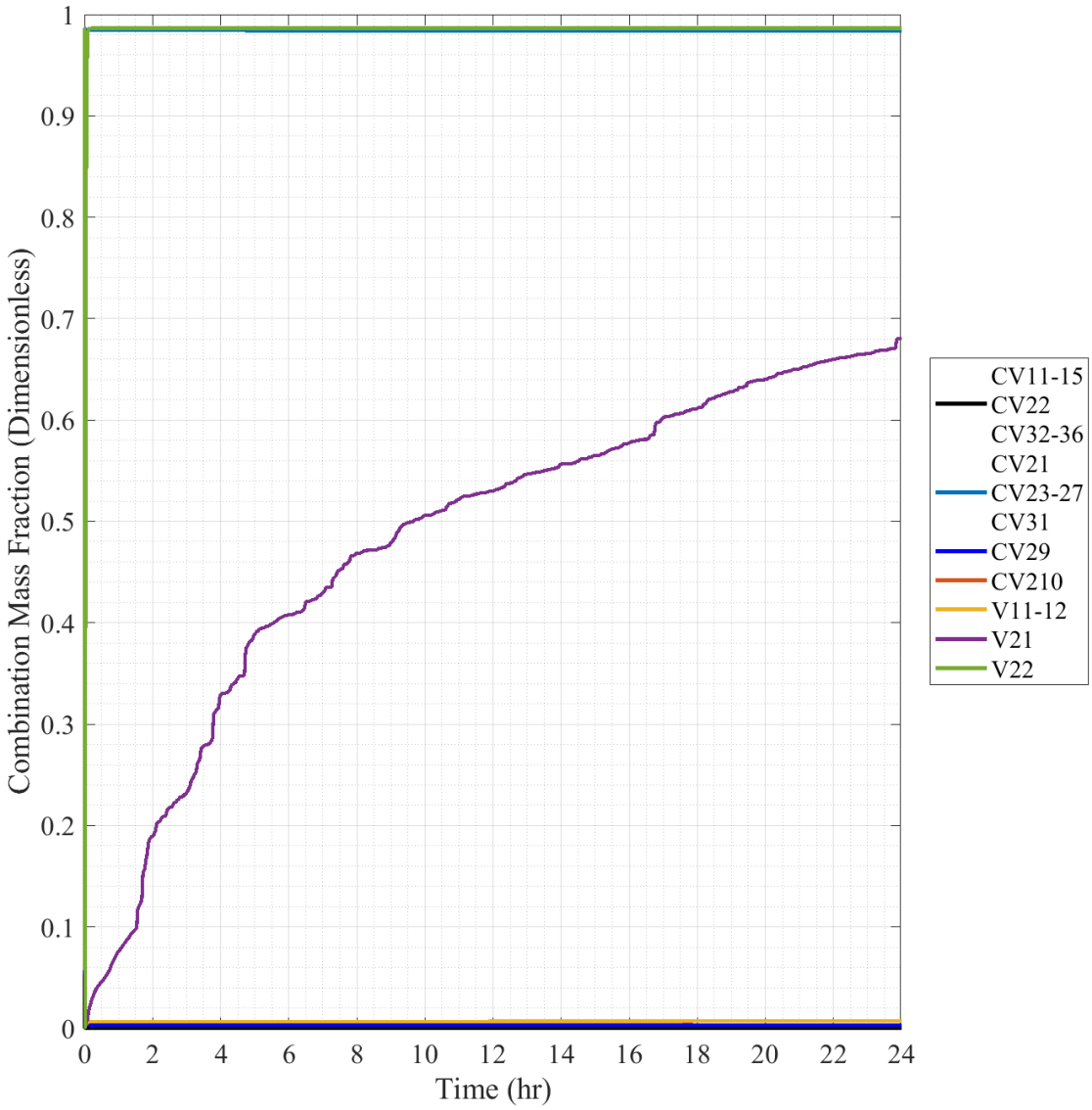

Fig. 6.59. 1/28th-Scale Scenario 5 Combination Mass Fraction.

Fig. 6.60 reduces in the timescale of the combination mass fraction to get details of the initial post-break building response to the spreading helium. V22 is seen to drop with the blowdown, then at ~1.8 minutes is when the volume begins to refill and only takes ~4 minutes to do so, like in scenario 1. During this period there is unrest in the volumes that are filled with helium, like seen in scenario 1 resulting in a rise in air content in some volumes, and when V22 reaches a completely refilled with air state, V21 begins to refill which can be seen from ~6 minutes onward. To obtain more blowdown knowledge the timescale must be reduced further.

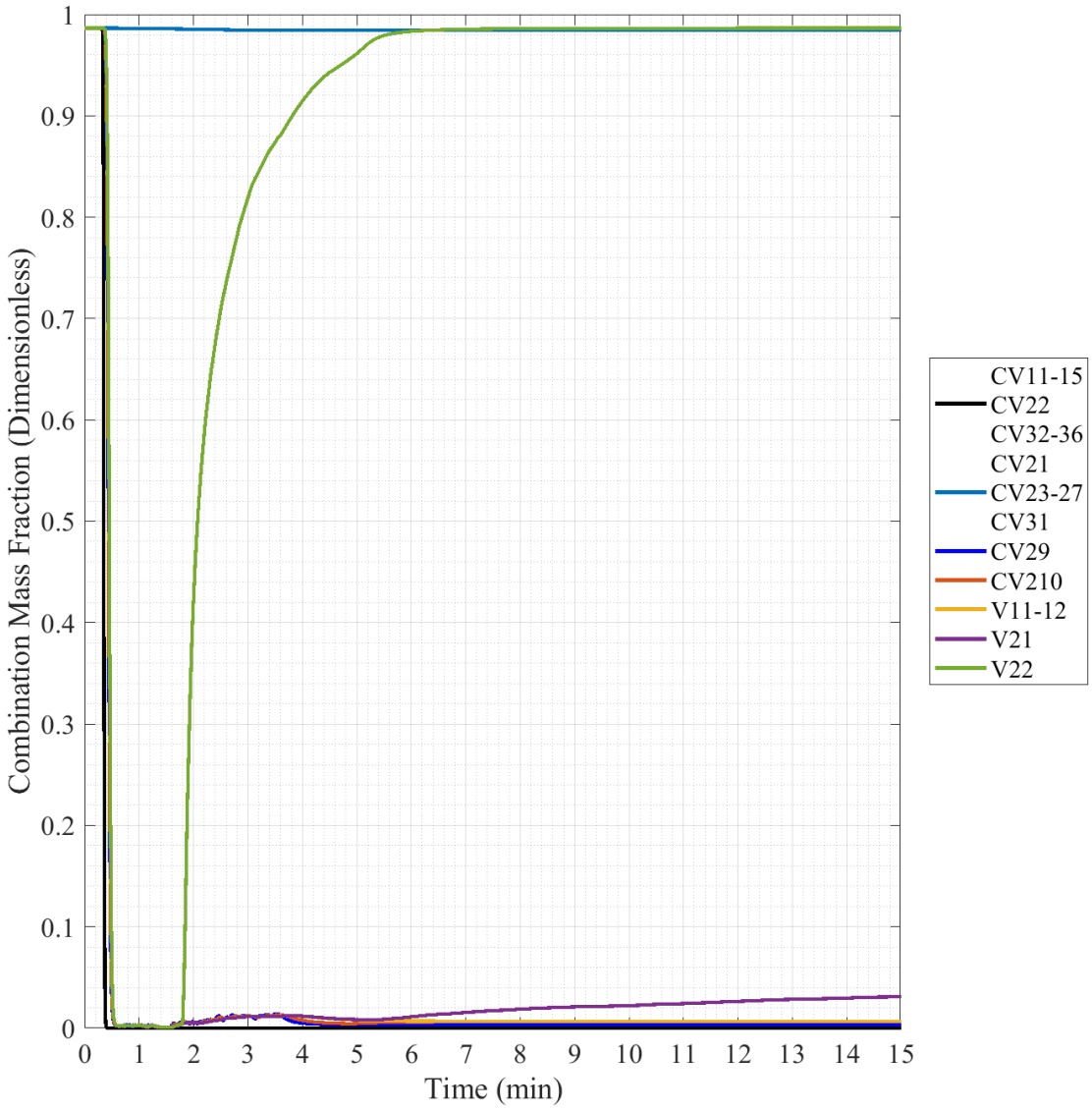

Fig. 6.60. 1/28th-Scale Scenario 5 Combination Mass Fraction, 15 minute Timescale.

Fig. 6.61 reduces the timescale in to the first 60 seconds of the scenario, where the progression of volumes losing their air content can be seen. Post-break initiation it takes ~14 seconds for all volumes to be voided of their air content, baring CV21 and CV31 which undergo very little helium influx. This scenario stands at a midground between scenarios 1 and 3, ~15 and ~13 seconds to completely void respectively, which most likely is due to an extended flow path for the helium but also it being dedicated on a set path to the exterior instead of multiple paths to

exterior resulting in conflicting gas movement. Going from left to right on the plot the general flow path of helium through the volumes can be seen, with the left most volumes being in the RC, and moving right moves into the lower SGC, up the EQS, back into the upper SGC, and finally into the vent spaces, the far right and voided last.

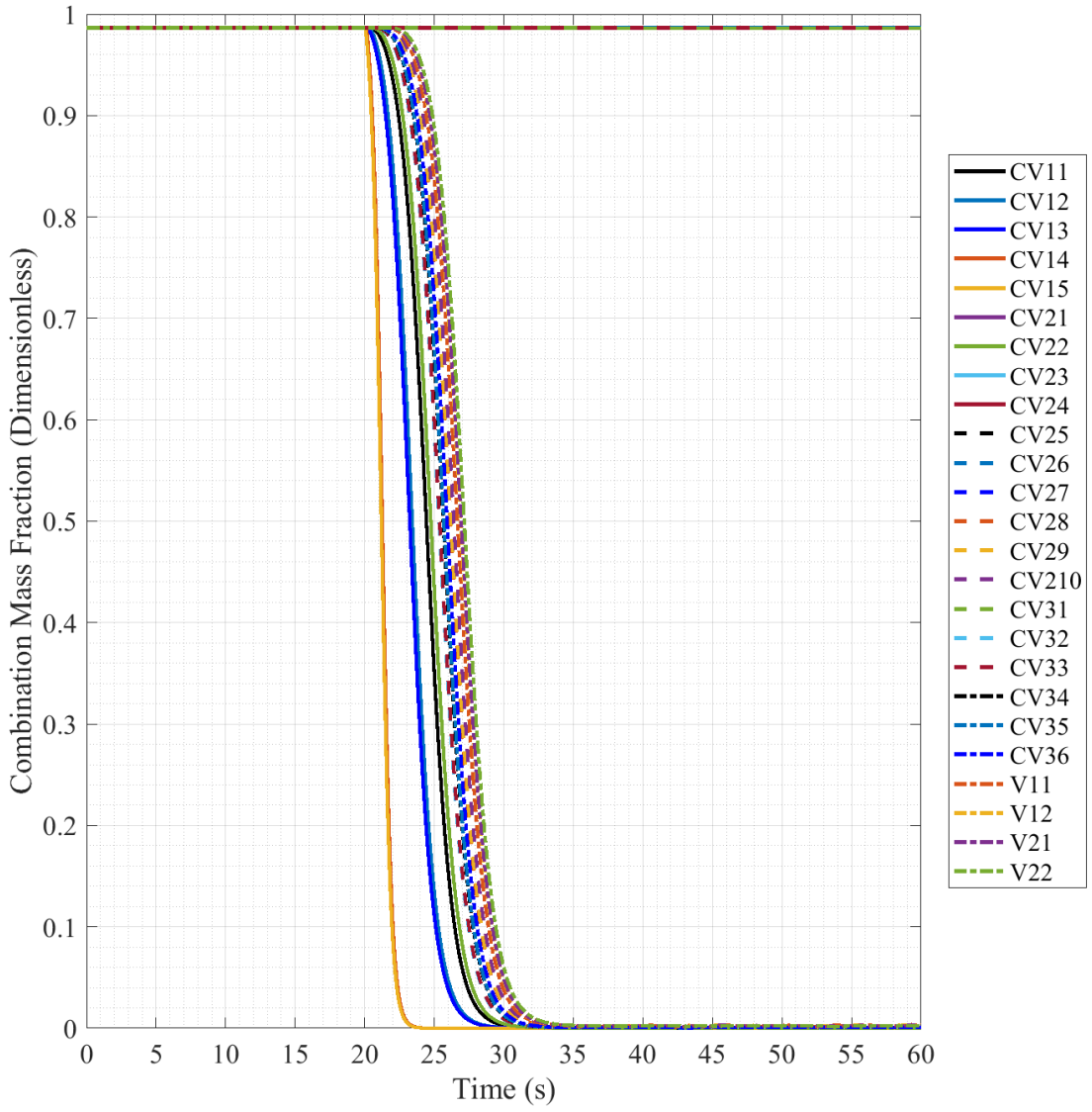

Fig. 6.61. 1/28th-Scale Scenario 5 Combination Mass Fraction, 60 second Timescale.

6.1.7 1/28th-Scale Scenario 6 Results

Scenario 6 is a SGV break scenario with the lower SGC dividing plate closed to upward flow at its flow path. This will allow gases to progress not only directly to the vent space but also into the EQS and deeper into the reactor building with no expansion path for the compressed building atmosphere due to the closed SGC bottom plate. For this scenario any volumes from RC (CV1-15) will be omitted from plotted results as they undergo no changes during the scenario. Fig. 6.62 gives a visual example of this scenario's estimated progression, utilizing a figure of the basic regions of the model.

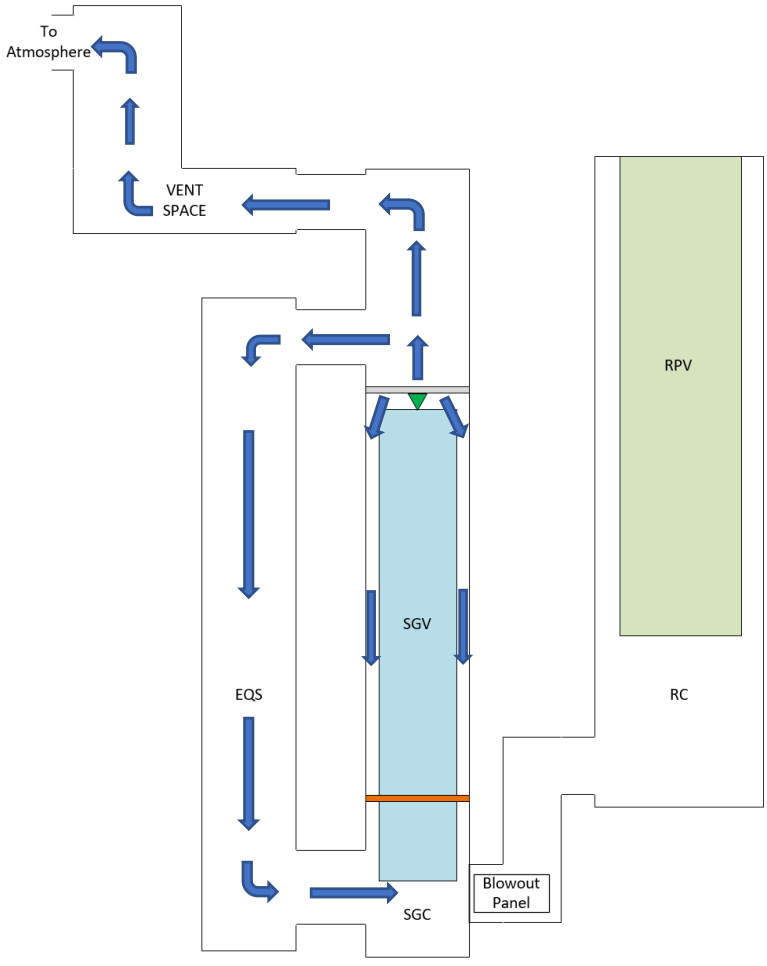

Fig. 6.62. Scenario 6 Estimated Blowdown Progression.

The initial pressure plot of scenario 6, with the pressure plotted across the full timescale, has been omitted as it simply shows the same information as the initial scenario 2 plot, with the initial 6.4 MPa pressure of the helium volume resulting in vertical scale of the plot blownout due to its comparibly large size. Nowhere along the full timescale of the pressure for this scenario's results were any new transients observed. The full timescale plot has been included in Appendix D for reference to the actual data plot, but Fig. 6.21 can be used as a quick reference as it shows a similar plot.

After reducing the timescale of the pressure plot to 50 seconds, like in scenario 2, the resulting plot was extremely similar to the plot made for that scenario. The initial helium pressure of 6.4 MPa can be seen extremely well at the initial time, then at 20 seconds the pressure begins to fall at an exponential rate as the break flow path is opened and helium expands out and into the SGC volumes. The HV reaches an equalized pressure of ~100 kPa at ~22.1 seconds following the blowdown initiation, ~41.1 seconds post simulation initiation. Overall, the progression of the pressure blowdown from the helium volumes seems to have not been affected by the change in the model layout. The pressure plot of this frame of time for this scenario has been included in Appendix D for further reference, or Fig. 6.22 can be used as a quick reference to the progression of the helium volume blowdown.

Removing the helium volume from the plot allows a better view of the reactor building response to the helium release, which can be seen in Fig. 6.63. As previously discussed, at this timescale that there are two separate groups of volumes undergoing different pressure transients following the break. These transients come back together in the following 5 seconds of post-break initiation to come back to equilibrium at ~100 kPa. Reducing the timeframe further will allow a better view of the transient peaks.

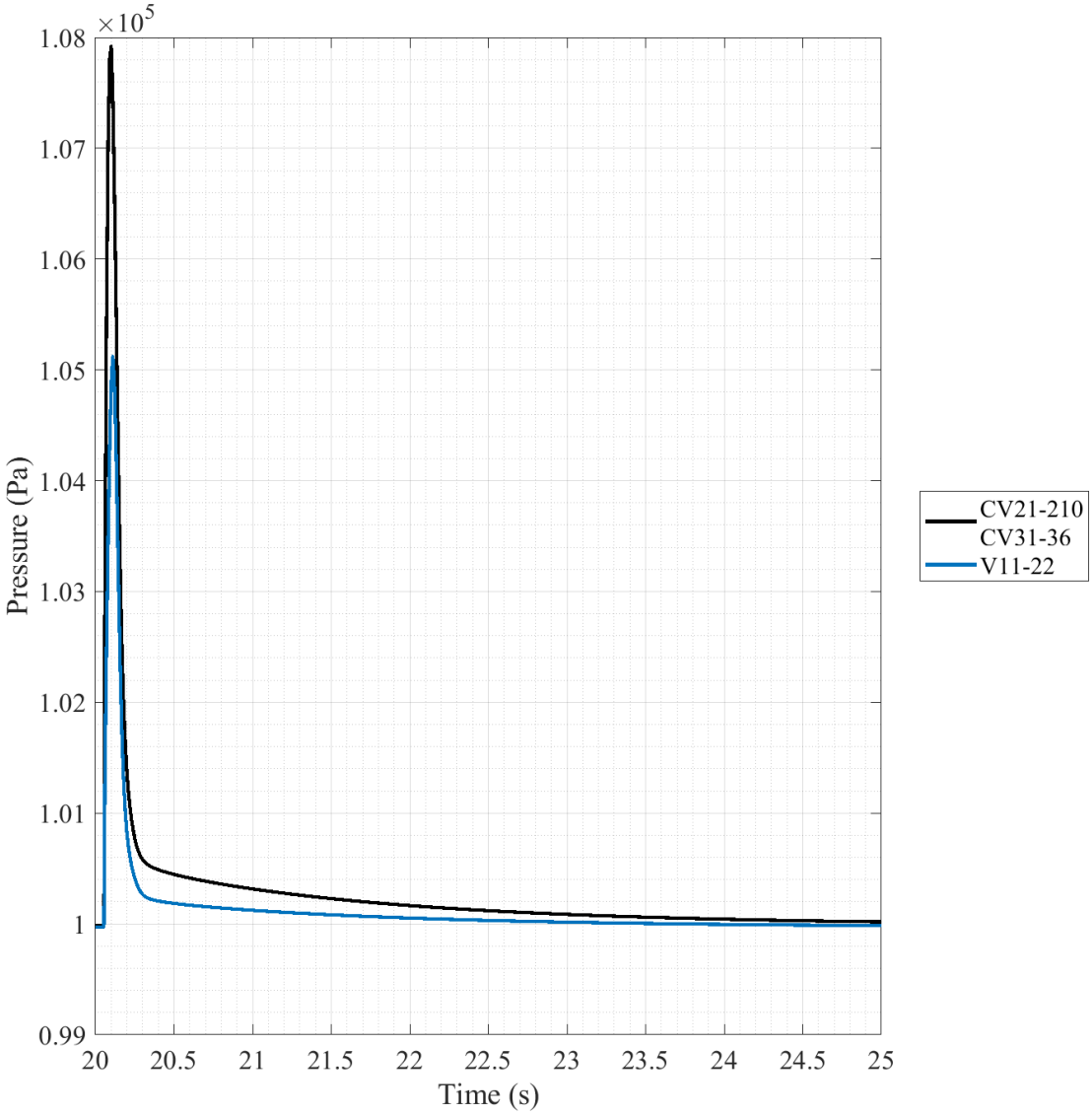

Fig. 6.63. 1/28th-Scale Scenario 6 Pressure, 20-25 second Timescale.

Fig. 6.64 reduces the timescale down to the half second following the break initiation. As described in scenario 1, the break is not initiated in the model until ~20.05 seconds, even though set to initiate at exactly 20 seconds due to the way MELCOR handles timesteps. Following the break initiation, the pressure changes instantly throughout all the volumes of the model as atmosphere is displaced by the expanding helium.

From Fig. 6.64 it can be seen that CV21-210 and CV31-36 increase to a maximum pressure of 1.0794×10^5 Pa (7.94 kPa increase) before falling back to near normal pressure. The smaller peak

is endured by V11-22 and increases to a maximum in the range of ~1.05x10^5 Pa (5 kPa increase) before falling. In contrast to scenario 4, the peak reappears on the rising side of the upper transient and will be examined in the following plot.

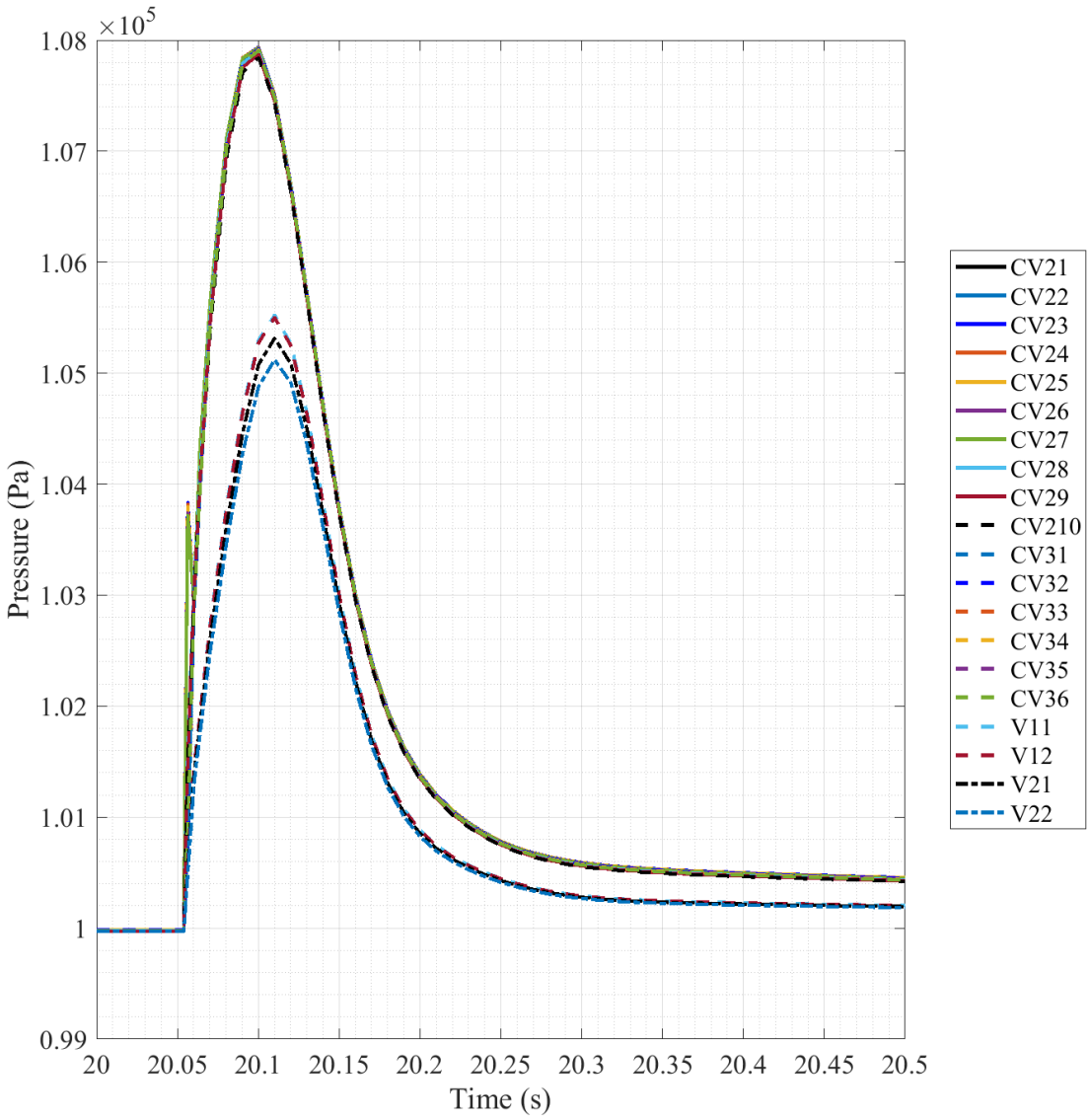

Fig. 6.64. 1/28th-Scale Scenario 6 Pressure, 20-20.5 second Timescale.

Fig. 6.65 reduces the timescale down to the first 1/10th of a second post-break initiation in order to better view the initial spike. CV23-27 undergoes a larger pressure increase in the disturbance in comparison to scenario 2. This disturbance still lasts for only 0.005 seconds but again seems to be an indication of the initial pressure disturbance being trapped within the central

SGC volume that is separated by the dividing plates. Since the bottom plate is closed completely in this scenario the theory of the initial pressure wave being trapped in the central SGC cavity may be valid.

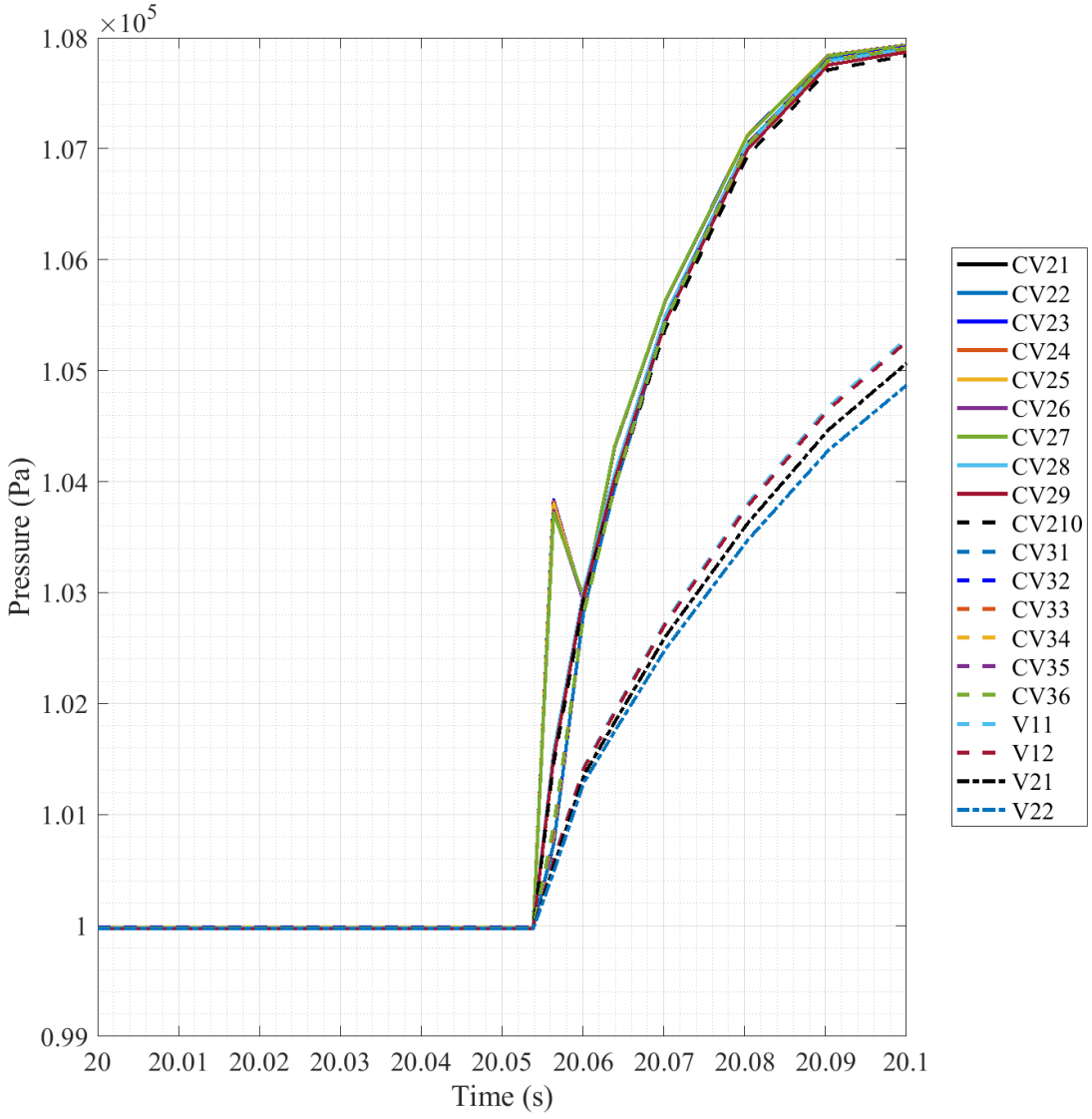

Fig. 6.65. 1/28th-Scale Scenario 6 Pressure, 20-20.1 second Timescale.

Mass fraction data of scenario 6 starts off with the presentation of the helium mass fraction data, presented in Fig. 6.66. This scenario is the busiest of the alternate layout scenarios, as it doesn't initiate a singular transient. The singular descending transient of this scenario is composed of V21 by itself, spiking with the blowdown but then falling over the progression of the scenario

to ~50%. This is a stark contrast to scenario 3-5 where there was little in the way of atmosphere movement or redistribution. A similarity seen to previous scenarios, V22 spikes with the blowdown but quickly falls to 0%. CV31 experiences an imperceptible addition of helium to its mixture, similar to what was seen in CV21 in scenario 4. CV21-22 experience very little change as they are the most distance away volumes from the break in this model due to the bottom plate flow path being closed. CV23-25 and CV32-34 also remain at ~0% similar to CV31, due in most part to being the lowest volumes in their constituent cavities and being below the break elevation.

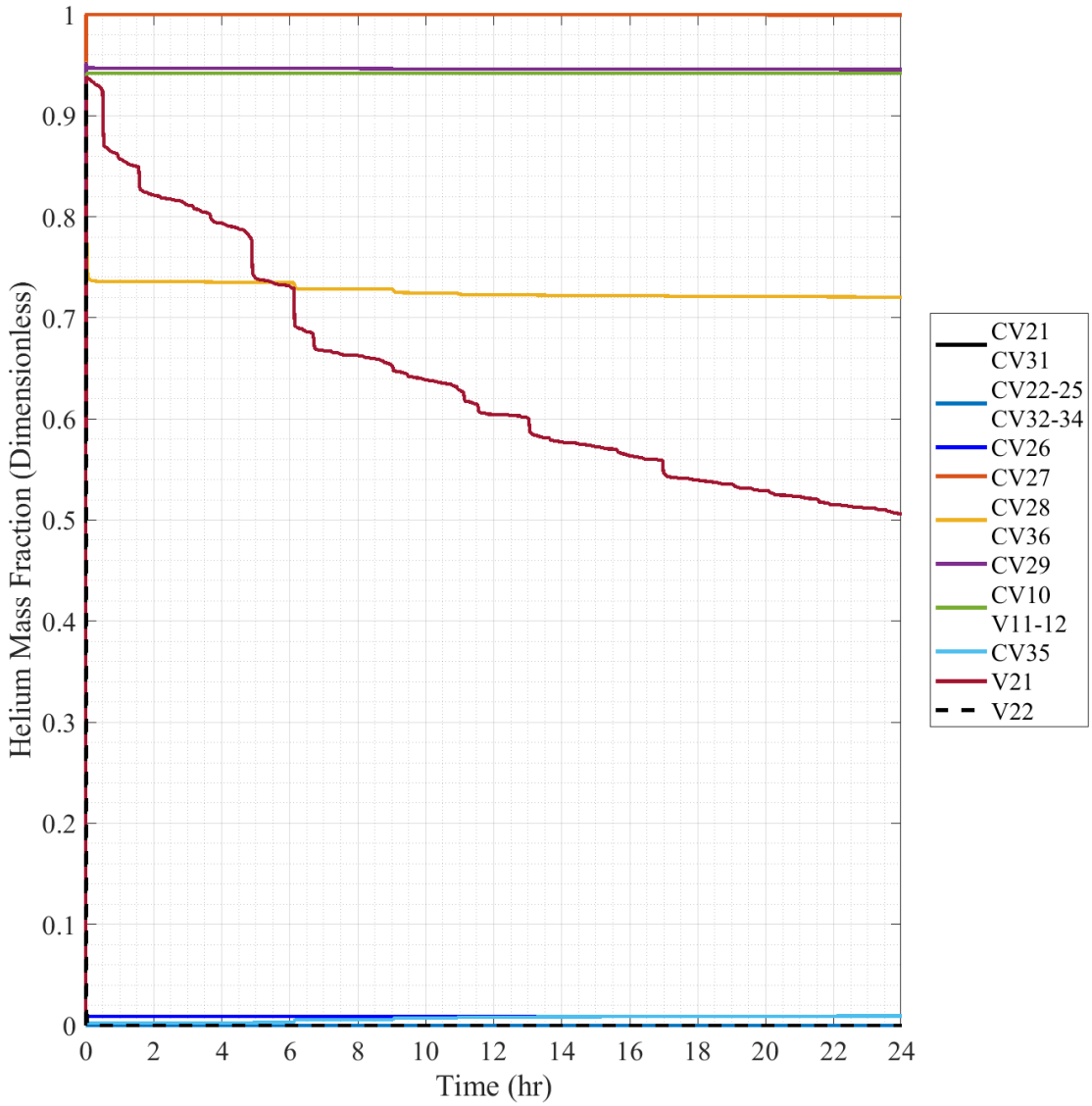

Fig. 6.66. 1/28th-Scale Scenario 6 Helium Mass Fraction.

Similar to scenario 4, CV26 undergoes a very slight spike but rests at ~0.6%, due to its proximity of the break location in this scenario. CV35 experiences a slight influx of helium over the scenario rising to the level of CV26 as the helium distributes over the whole scenario time period. Moving to the horizontal transients of the scenario, CV28 and CV36 transient from ~74% to 72% over the scenario time period, an equal transient for the two directly linked volumes. Moving up to the upper transients, CV210 and V11-12 spike with the blowdown but do not fall greatly in the following time period and remain at ~94% helium mass fraction. CV29, similarly acts as the previous discussed at ~94.5%. The final volume of discussion is that of CV27 which spikes to ~100% where it maintains across the entire scenario. Getting a better look at early time periods will require a smaller timescale that will be explored in later plotted results.

In order to maintain a concise description of scenarios, the plots of oxygen and nitrogen mass fraction are not presented in this scenario as their results are reaffirmed best by a combination of their results to approximate a near full mass fraction of standard air. As was seen in scenario 2, oxygen and nitrogen mass fractions showed inverse results of the helium mass fraction and were simply differentiated by the resulting scale differences in the gas mass fractions. Plotted results for both the oxygen and nitrogen mass fraction can be found in Appendix D for further reference but are left out of this scenario to be concise.

Fig. 6.67 sums the oxygen and nitrogen mass fractions together as previously discussed to a “Combination” mass fraction composed of the combination of the two individual mass fractions. The combination of these two gases make up 98.66% of the total mass fraction of standard air and should be a good comparison to the helium mass fraction for comparisons. Finally, by comparison with Fig. 6.66, it can be seen that the figure is simply an inverse of the helium trends. Due to the

linked relationship of the results, this set of data will be used to examine the initial details of the blowdown from a mass fraction perspective as was done with the pressure.

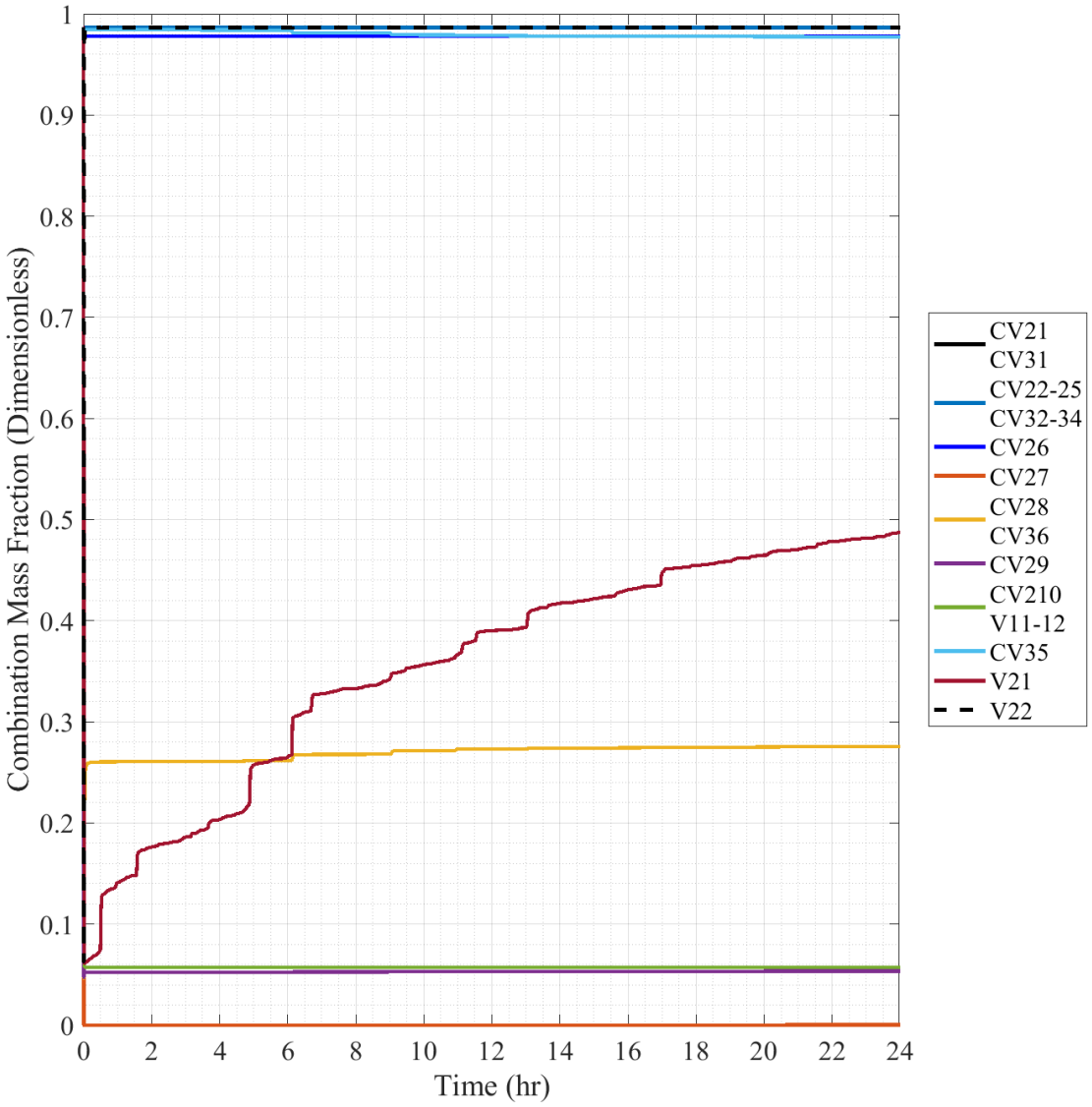

Fig. 6.67. 1/28th-Scale Scenario 6 Combination Mass Fraction.

Fig. 6.68 reduces in the timescale of the combination mass fraction to get details of the initial post-break building response to the spreading helium. CV27 is seen to be the only volume to completely void in this scenario, falling to ~0% with the break. All other volumes in this scenario that begin voiding stop and plateau at ~6% which is similar to what was seen in scenario 2 but at a higher remaining air content. V22 can be seen to be void with the blowdown to the plateau

followed by a refill beginning ~18 seconds post-break. V21 during this time period seems to remain relatively stable and does not begin any level of refill which is also similar to what was seen in scenario 2, though at later time periods it does refill in greater amounts which can be seen in Fig. 6.66.

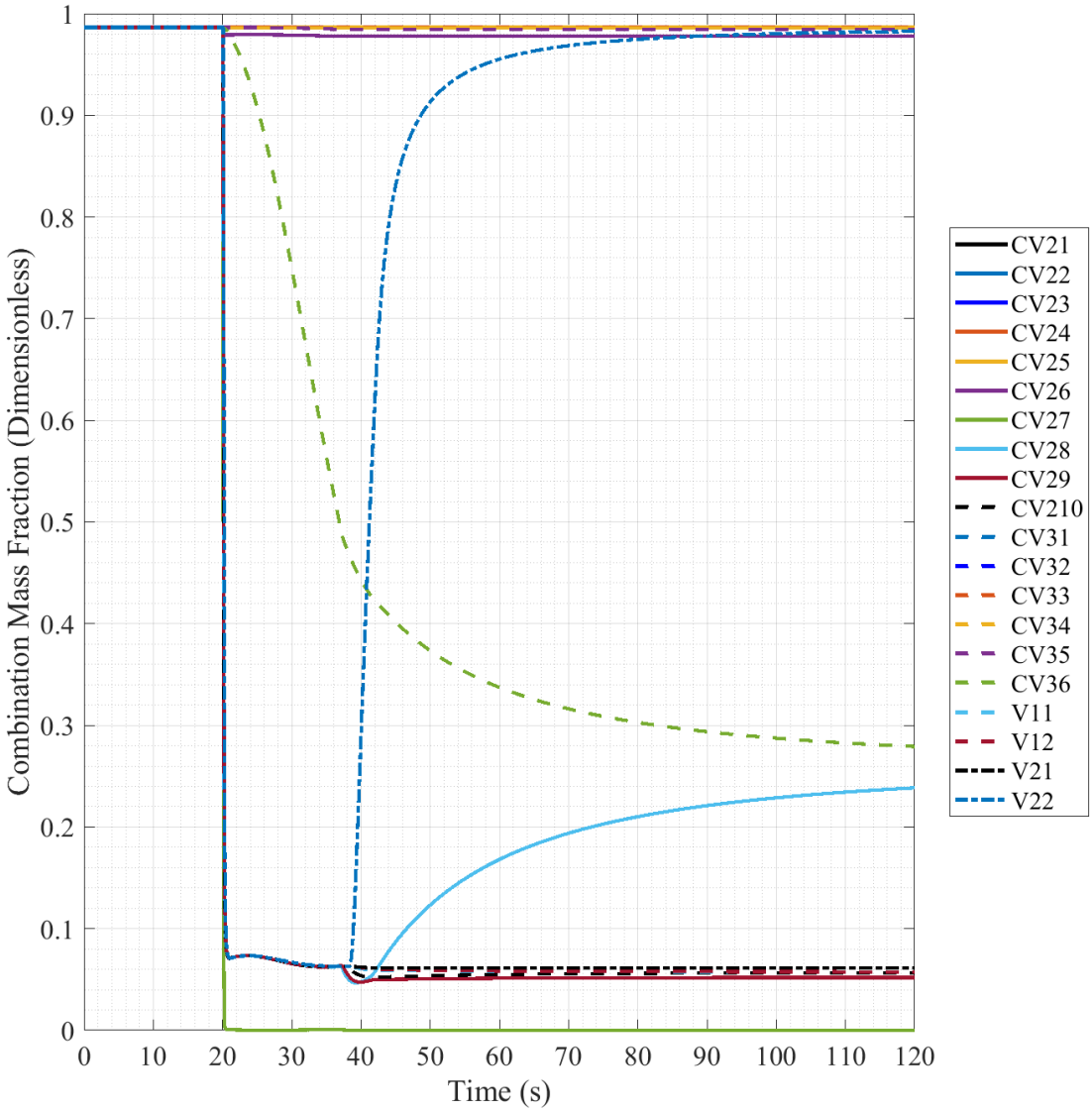

Fig. 6.68. 1/28th-Scale Scenario 6 Combination Mass Fraction, 120 second Timescale.

CV28 and CV36 undergo what appears to be a mixing of their gases in the period, with CV36 falling and CV28 rising from its low oxygen concentration to a begin to head into an equilibrium which can be seen in Fig. 6.66. The initial spike of CV28 appears to take CV29 as

well but it is left at a decreased air content along with the lower vent spaces of V11-12. CV26 can be seen with the small amount of helium mixture at the top of the plot. The initial blowdown at this scale is still a relatively linear and will need to be explored at a smaller scale.

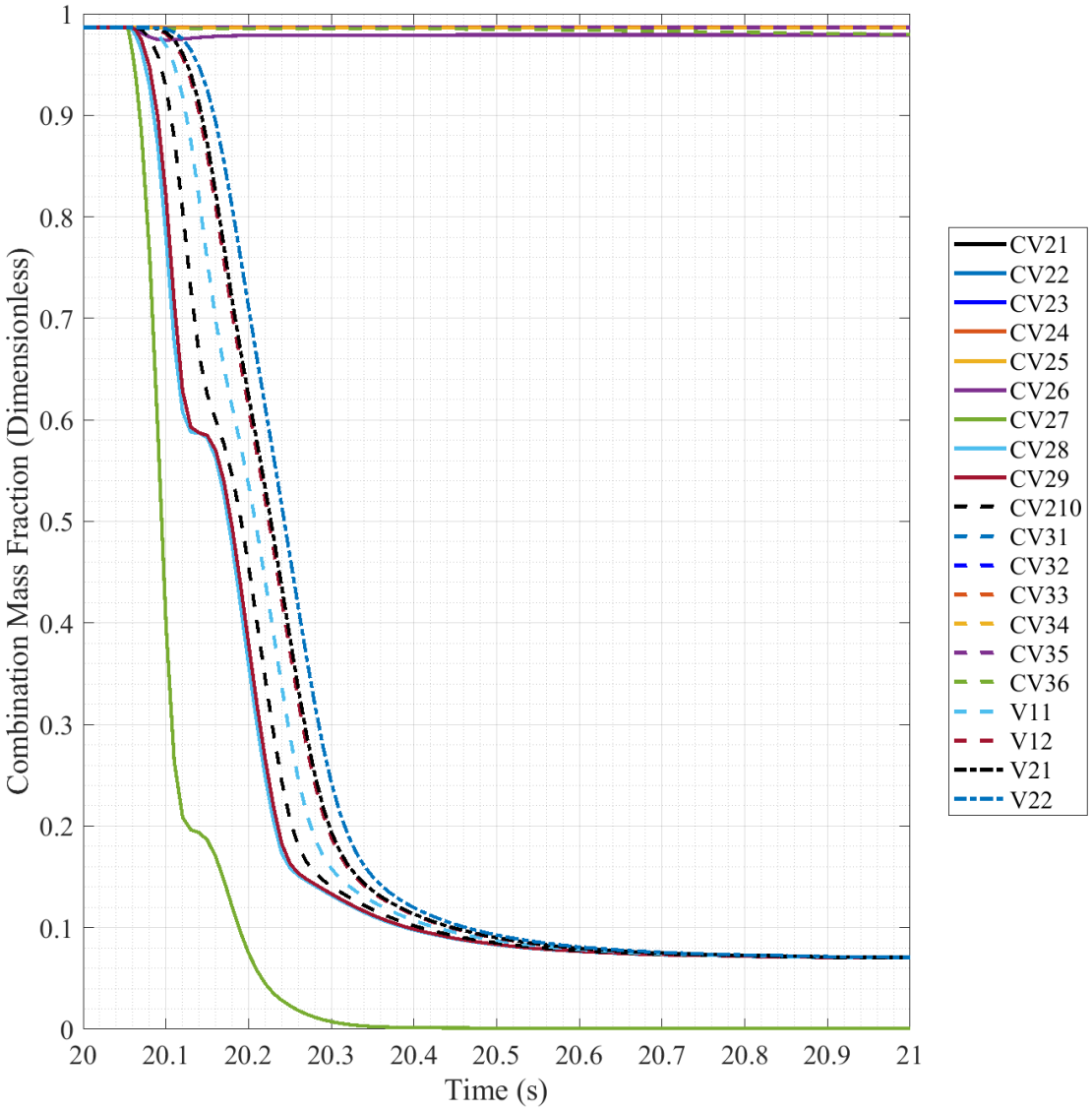

Fig. 6.69. 1/28th-Scale Scenario 6 Combination Mass Fraction, 20-21 second Timescale.

Fig. 6.69 shows the initial voiding produced by the helium introduction to the reactor building volumes. Overall, all affected volumes are voided of the air content within ~0.5 second of the break initiation. CV26's initial deviation to its stable level can be seen at this timescale, decreasing but rising back to a plateau relatively quickly. CV27 undergoes the largest deviation,

changing slope significantly before dropping again at ~20.14 seconds. This then also has an effect on CV28-29 which undergo a similar disturbance, leading to a compression of the voiding volume distribution. CV27 is the only volume in this scenario to be completely voided, taking ~0.35 second to fall to ~0%, while all other voiding volumes undergo a severe change in voiding rate and plateau at ~8% during this time period. This band of voiding volumes is arranged from left to right by their general position in the flow path to the exterior of the model from the break location, with volumes like CV27-210 being on the left and moving to the right shows the progression through the vent space volumes.

6.2 Full-Scale Simulation Results

This second section of results is compiled to present and explain the results of the full-scale model made for comparison of the experimental setup of the MHTGR to full-scale of the true reactor. It was tested with the same testing scenario regime exhibited in Table 5.3 as the $1/28^{th}$-scale model for comparison. Data was exported in the same manner as the previous results section using PTFRead, Excel, and MATLAB for compilation and presentation. Much like explained in the $1/28^{th}$-scale results, the duct and atmosphere volume results have not been plotted in the following plots. This is due to them simply being connecting volumes between the larger overall volumes and the atmospheric volume being the overflow volume from the reactor building volumes. Plots have been simplified to major trends for results presented in this section but plots containing all individual data sets plotted are included in Appendix E.

A note needs to be made about the atmosphere volume in the full-scale simulations as due to the scaling up of the model some adverse effects were seen. The atmosphere volumes' physical volume was not scaled up in conjunction with the model, resulting in an increase in the pressure of the atmosphere volume. As the blown down atmosphere expanded from the reactor building there was sufficient volume to result in a pressure increase in the exterior volume. This can be seen in Fig. 6.70 which is a pressure plot of Scenario 1, including the atmosphere volume in the plotted results specifically.

It can be seen that the internal volumes still return to their initial ~100 kPa pressure following the blowdown initiation, but as a result of the atmosphere physical volume pushed to the exterior volume the pressure of the exterior volume became perturbed and increased, which did not occur in the $1/28^{th}$-scale model. It rose in conjunction and follows the same trend as the model volume results but then settles in at ~1.006×10^5 Pa (~600 Pa increase). This rise, while

unfortunate for the oversight on the model creation, should not overall hamper the results of the model simulation. In the future it would be wise to scale up the volume of the overflow external atmosphere to be able to handle the blown-out reactor building gas volume in a better manner by giving more expansion volume, or by setting the atmosphere volumes to be a time independent sink to handle any potential expansion.

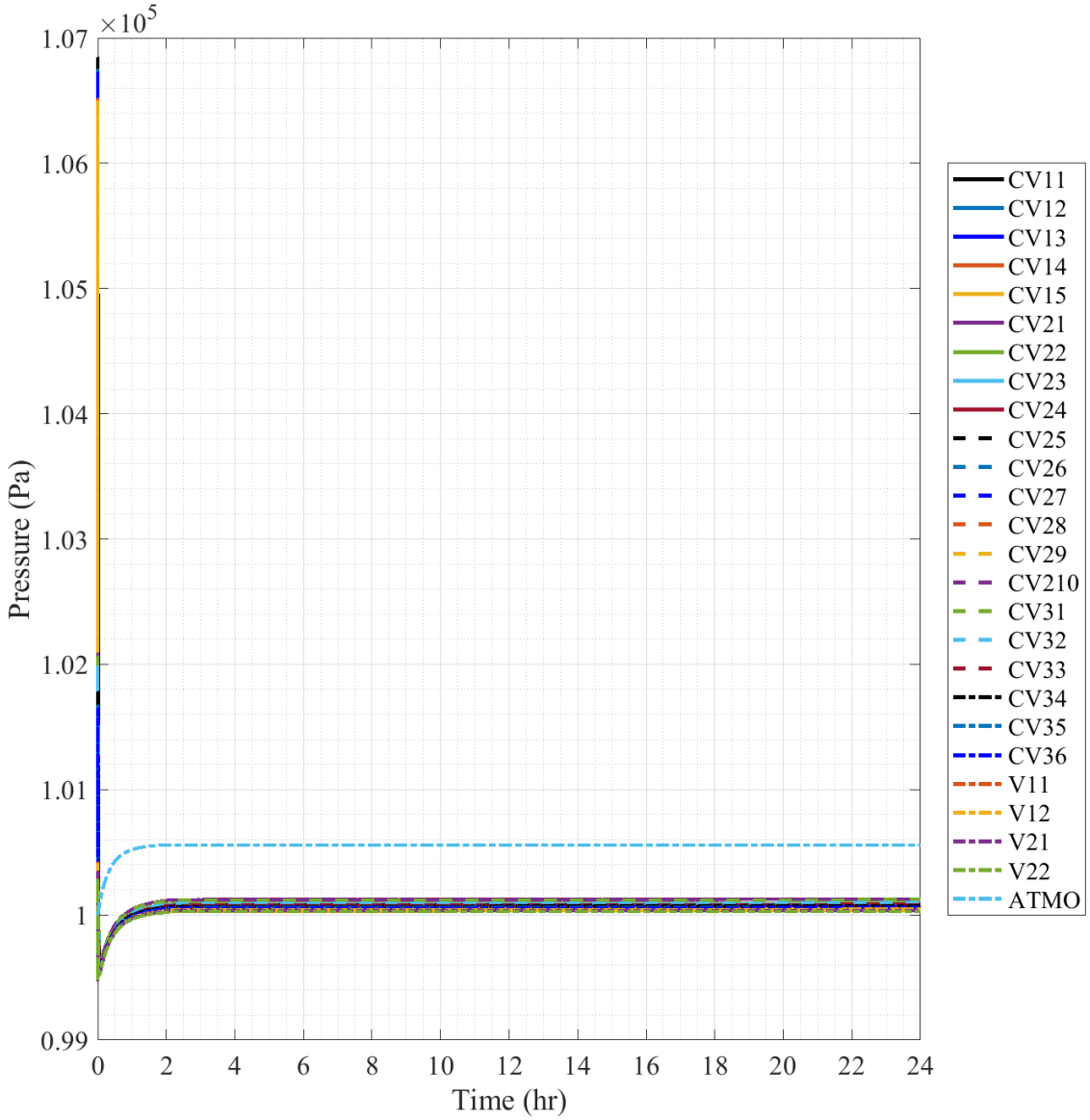

Fig. 6.70. Full-Scale Scenario 1 Pressure with Atmosphere Volume.

6.2.1 Full-Scale Scenario 0 Results

Scenario 0, the baseline scenario, was run without any blowdown progression to get base readings of the full-scale model. The scenario also was used to ensure stability of the model across the full 24 hours of test time outside of accident progression scenarios. The results, while not much more than constant values, set the baseline for the overall model in steady state conditions and demonstrate the model's calculational stability.

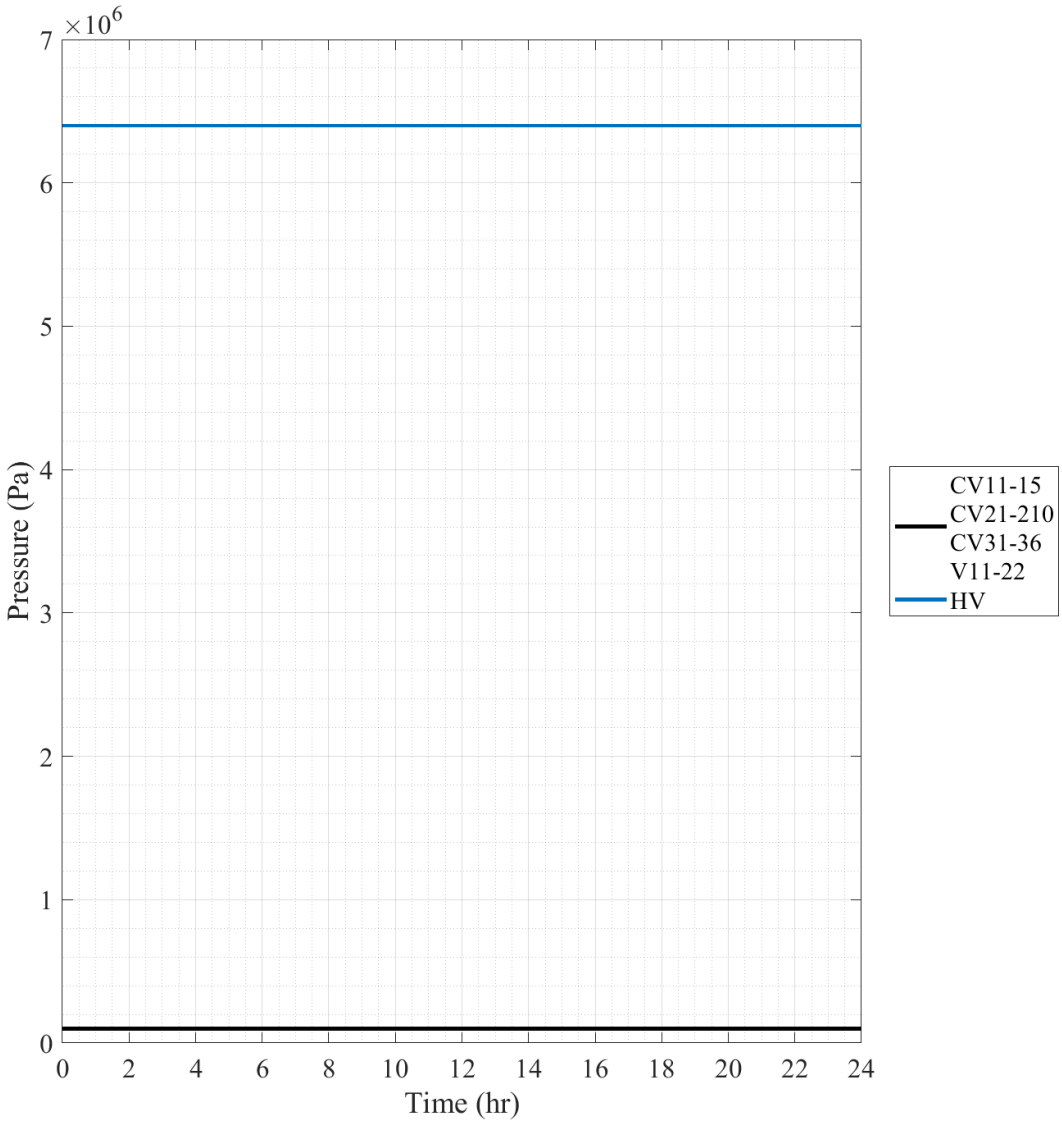

Fig. 6.71. Full-Scale Scenario 0 Pressure.

The pressure plot of Scenario 0, as expected, stays constant through the entire simulation timeframe, which can be seen in Fig. 6.71. Across the simulation duration, the helium volume, HV, remained constant at 6.4 MPa as designed, while all other volumes remained at roughly 100 kPa. At the beginning of the simulation the 100 kPa volumes undergo a slight redistribution of pressure where they settle within a range of 100.011 to 99.946 kPa, which is negligable variance in terms of a distribution..

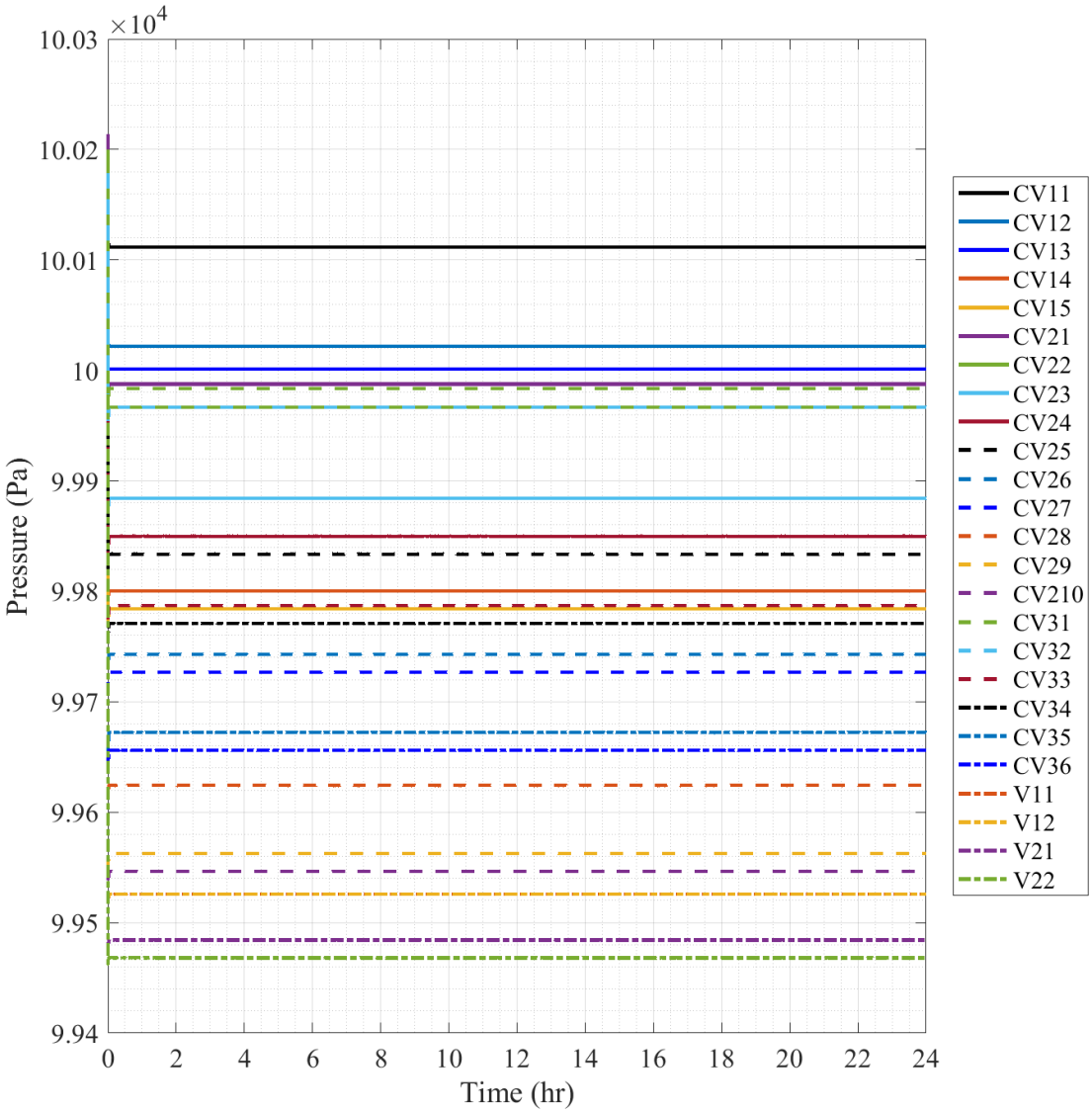

Fig. 6.72. Natural Pressure Redistribution at Full-Scale.

Fig. 6.72 reduces the pressure redistribution naturally created in the model at the beginning of simulation runs. From the figure it can be seen that a natural pressure difference of ~650 Pa develops within the model as it is run. This pressure difference is not within a contiguous open volume space though as the upper volume of the results is behind the perpetually closed blowout panel in this scenario. A better indication of pressure differential can be taken from CV21 to V22 to indicate an open and connected volume space from the top to the bottom of the model. A pressure differential, taken from the figure from CV21 to V22, is seen to be ~520 Pa.

A basic pressure variation calculation shows that at the 53.397 m height of the model, 1.225 $\frac{kg}{m^3}$ air density, and 9.80665 $\frac{m}{s^2}$ gravitational acceleration, a pressure difference of ~641.5 Pa is to be expected. The observed simulation pressure is ~1% increase over the expected pressure variance value when accounting for the full results, but only ~23% lower when accounting for true model contiguous volumes. Compared to what was seen at 1/28th-scale, the full-scale results were very close to the calculated value when covering all volumes, but this is not a very accurate comparison. Comparing the CV21 to V22 results though shows that the relative percent difference in the models was very close, 21-23% off the calculated value, showing a very close response overall between the model scales on pressure redistribution.

The plot of the helium mass fraction results in as expected constant values which is seen in Fig. 6.73. The helium containing volume, HV, maintained a 100% value as expected as no break scenario was implemented. All other volumes remained at 0% as helium is not part of the natural atmosphere mixture and no blowdown occurs.

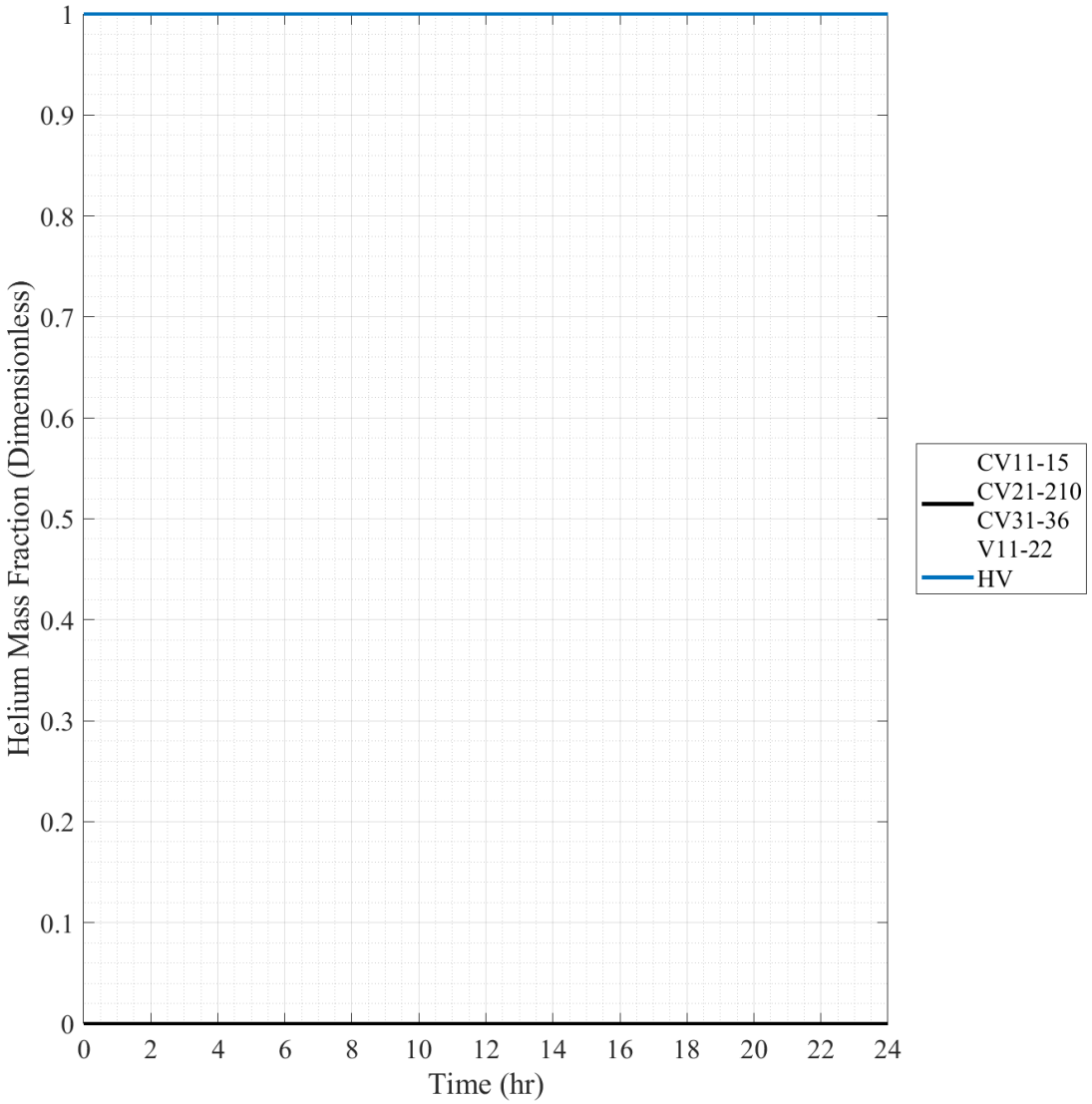

Fig. 6.73. Full-Scale Scenario 0 Helium Mass Fraction.

Oxygen mass fractions stayed constant across the testing timeframe as expected which is seen in Fig. 6.74. The helium volume, HV, maintains at 0% as no oxygen was present in the initial volume definition and no atmosphere ingress could occur into the volume. All other volumes maintain a constant oxygen mass fraction of 23.14%, the mass fraction of oxygen in normal atmospheric air.

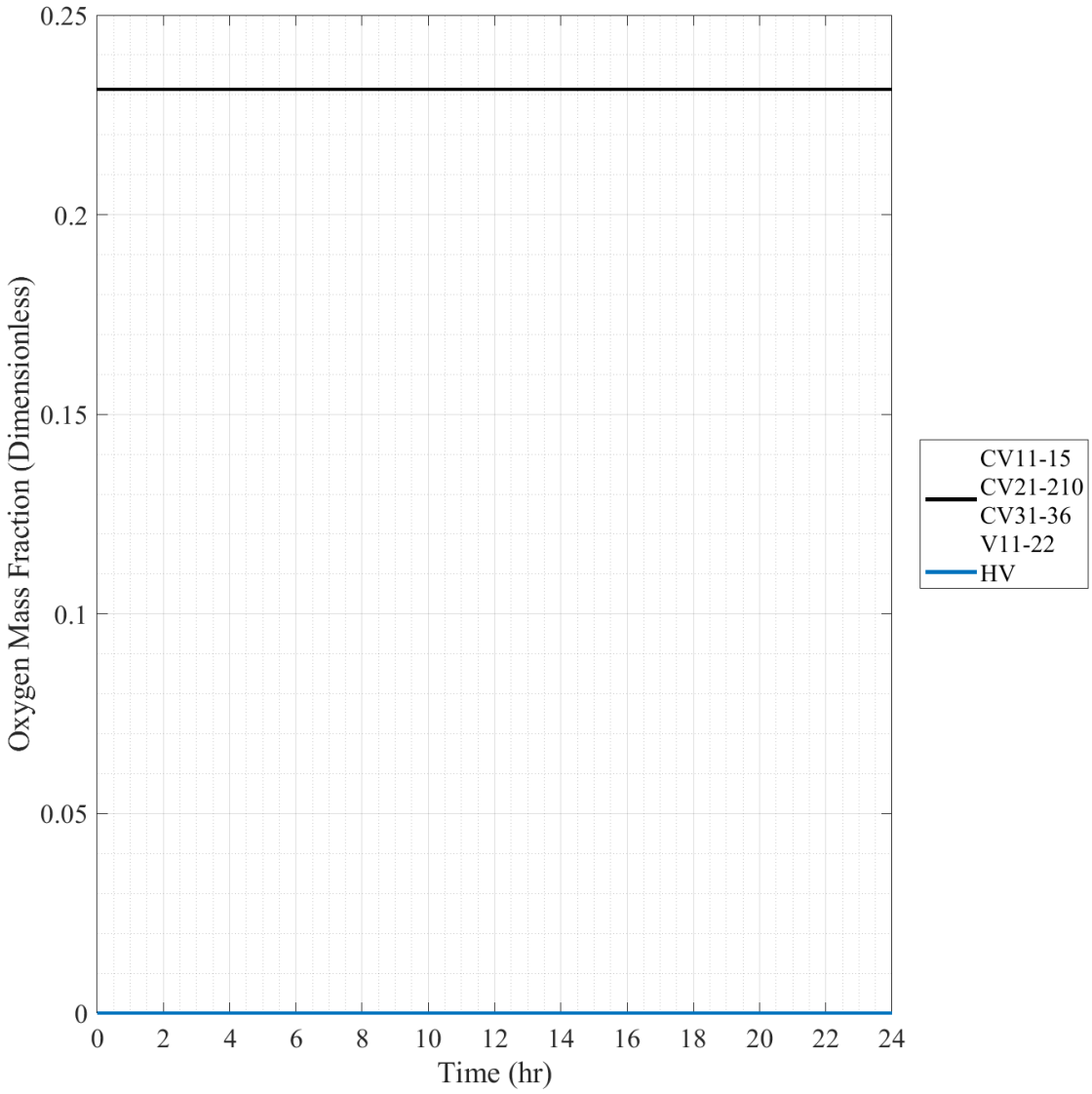

Fig. 6.74. Full-Scale Scenario 0 Oxygen Mass Fraction.

Nitrogen mass fractions also stayed constant across the testing timeframe as expected which is seen in Fig. 6.75. The helium volume, HV, maintains at 0% as no nitrogen was present in the initial volume definition and no atmosphere ingress could occur into the volume. All other volumes maintain a constant nitrogen mass fraction of 75.51%, the mass fraction of nitrogen in normal atmospheric air.

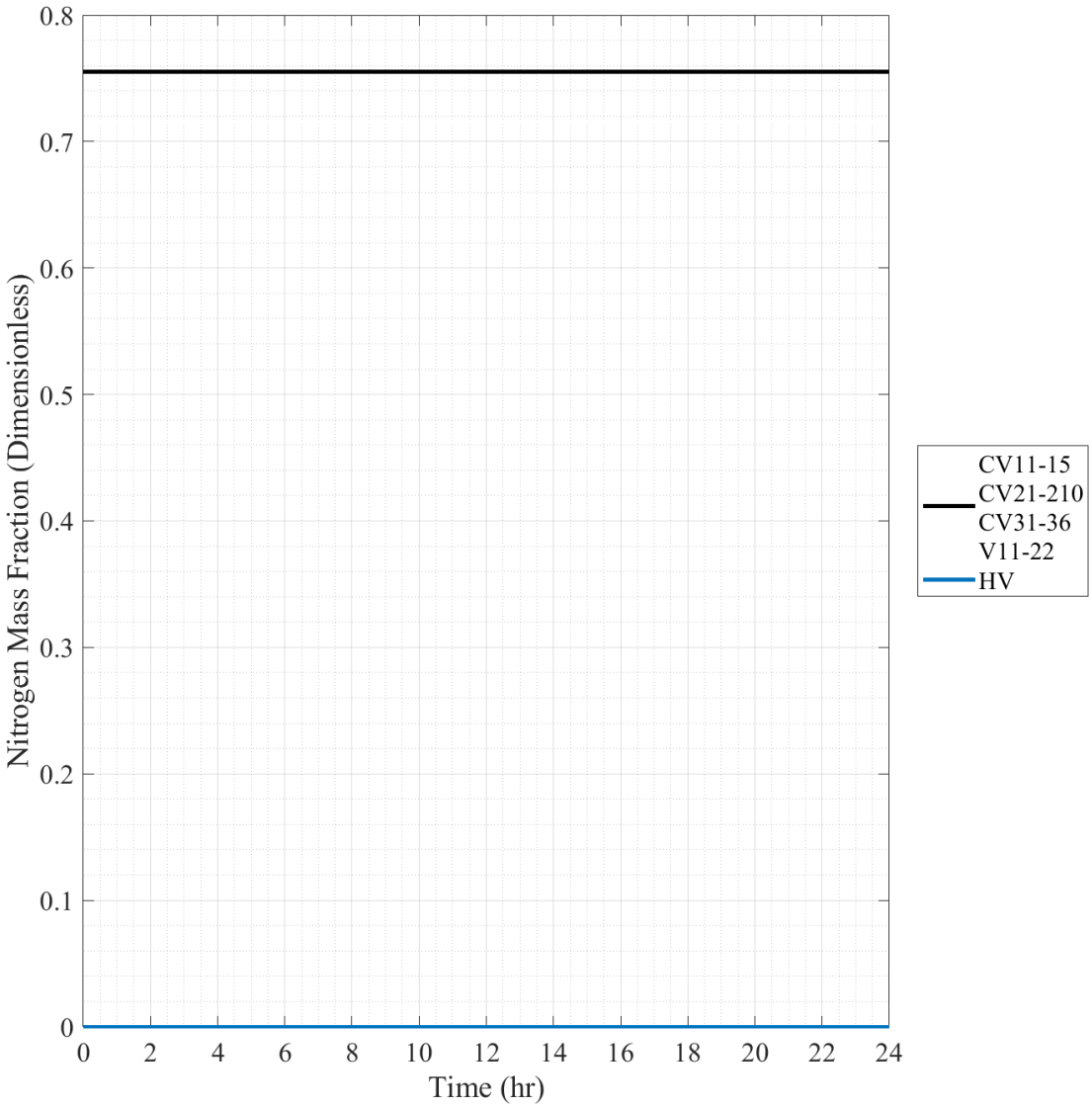

Fig. 6.75. Full-Scale Scenario 0 Nitrogen Mass Fraction.

To better interpret atmospheric mass fraction results in an environment undergoing mixing interactions the results of the mass fraction from the nitrogen and oxygen were combined into a “Combination” mass fraction that represents the sum of their fraction. This should give a relative high estimation of the movement and concentration of the standard atmosphere than by singular mass fraction results. As seen in Fig. 6.76, a constant value for combination mass fraction was obtained as expected with all volumes, other than the helium volume which remains at 0%, maintaining a 98.66% mass fraction.

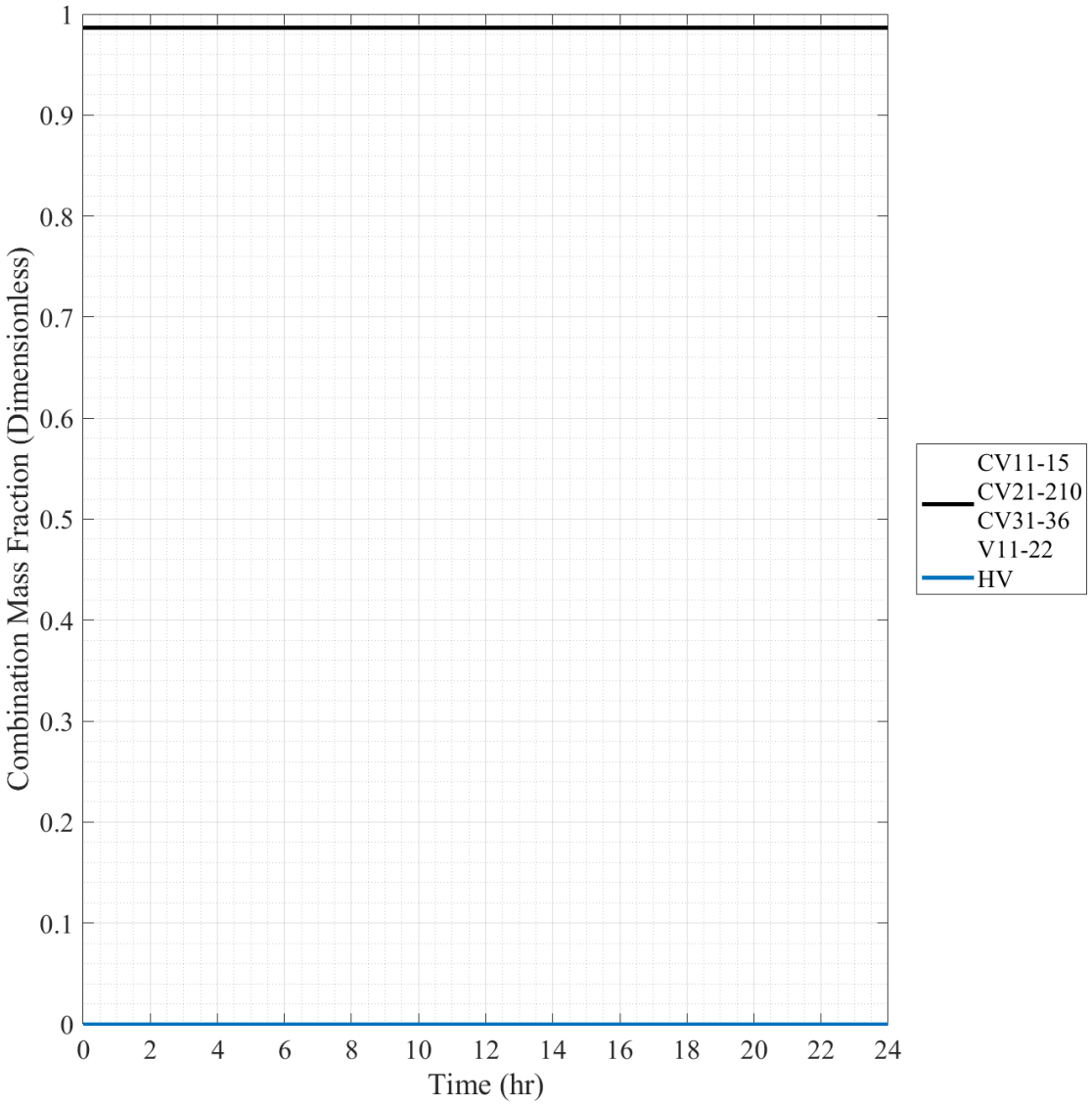

Fig. 6.76. Full-Scale Scenario 0 Combination Mass Fraction.

6.2.2 Full-Scale Scenario 1 Results

Scenario 1 is the base RPV break scenario, with no changes to the basic layout of the full-scale reactor building model. This model is the baseline for comparing to scenarios 3 and 5 which change the standard layout in their scenario parameters. In this model, flow from the blowdown progresses through all volumes of the model due to the break occurring at one of the furthest points from the vent to the exterior volume. A visual example of this scenario's estimated progression can be seen in the 1/28th-scale results section of this scenario, Fig. 6.7.

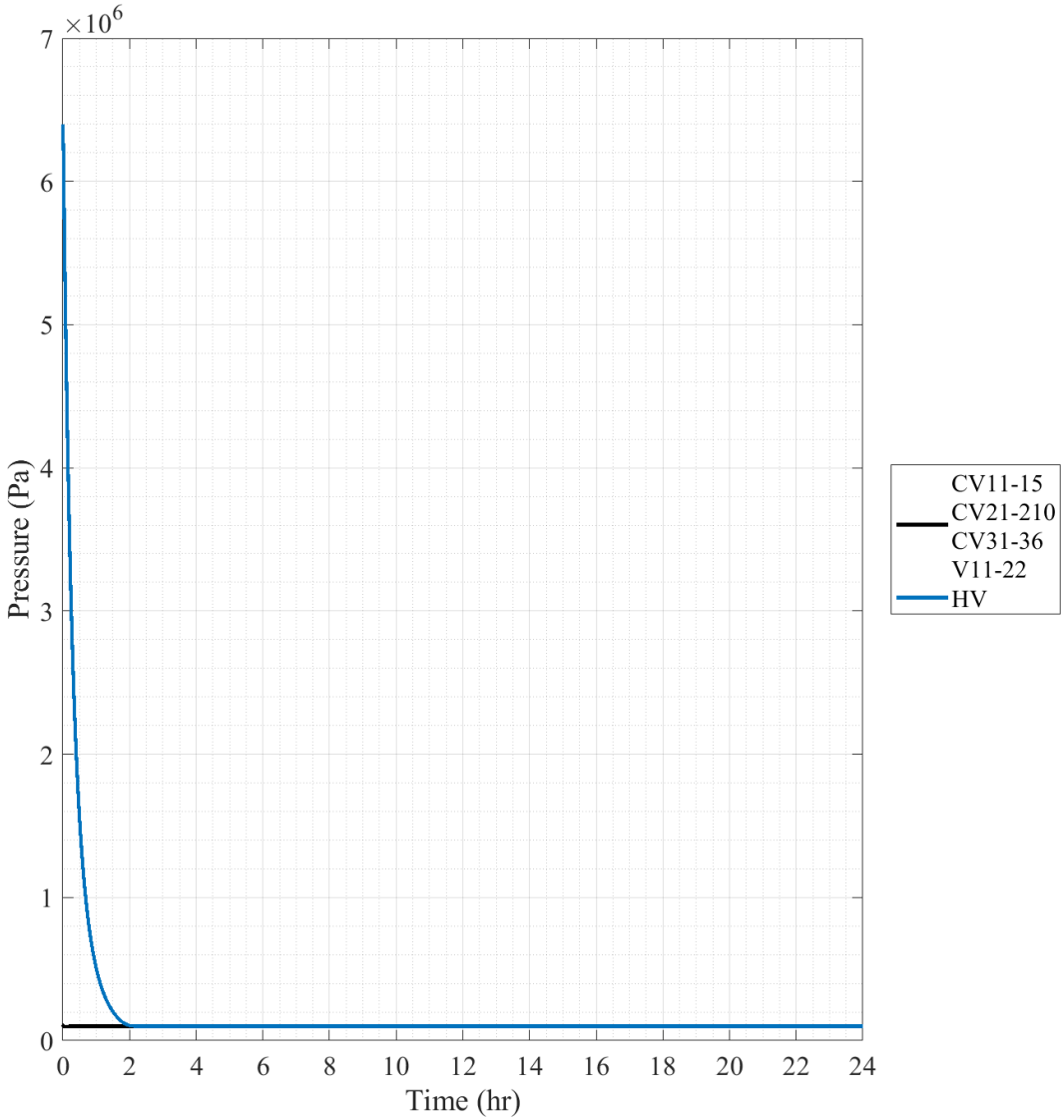

Fig. 6.77. Full-Scale Scenario 1 Pressure.

The first plot of results for scenario 1, Fig. 6.77, shows the pressure results of the scenario across the full timeframe of the simulation. Due to the scale of the pressure of the helium volume, HV, which peaks at the set overal 6.4 MPa, the overall scale of the pressure plot makes it difficult to determine post blowdown pressures of the reactor building volumes. The timeframe of the plot is also too extended to determine a blowdown timeframe from the break and needs to be reduced to a shorter period of time in order to determine a time to pressure equalization.

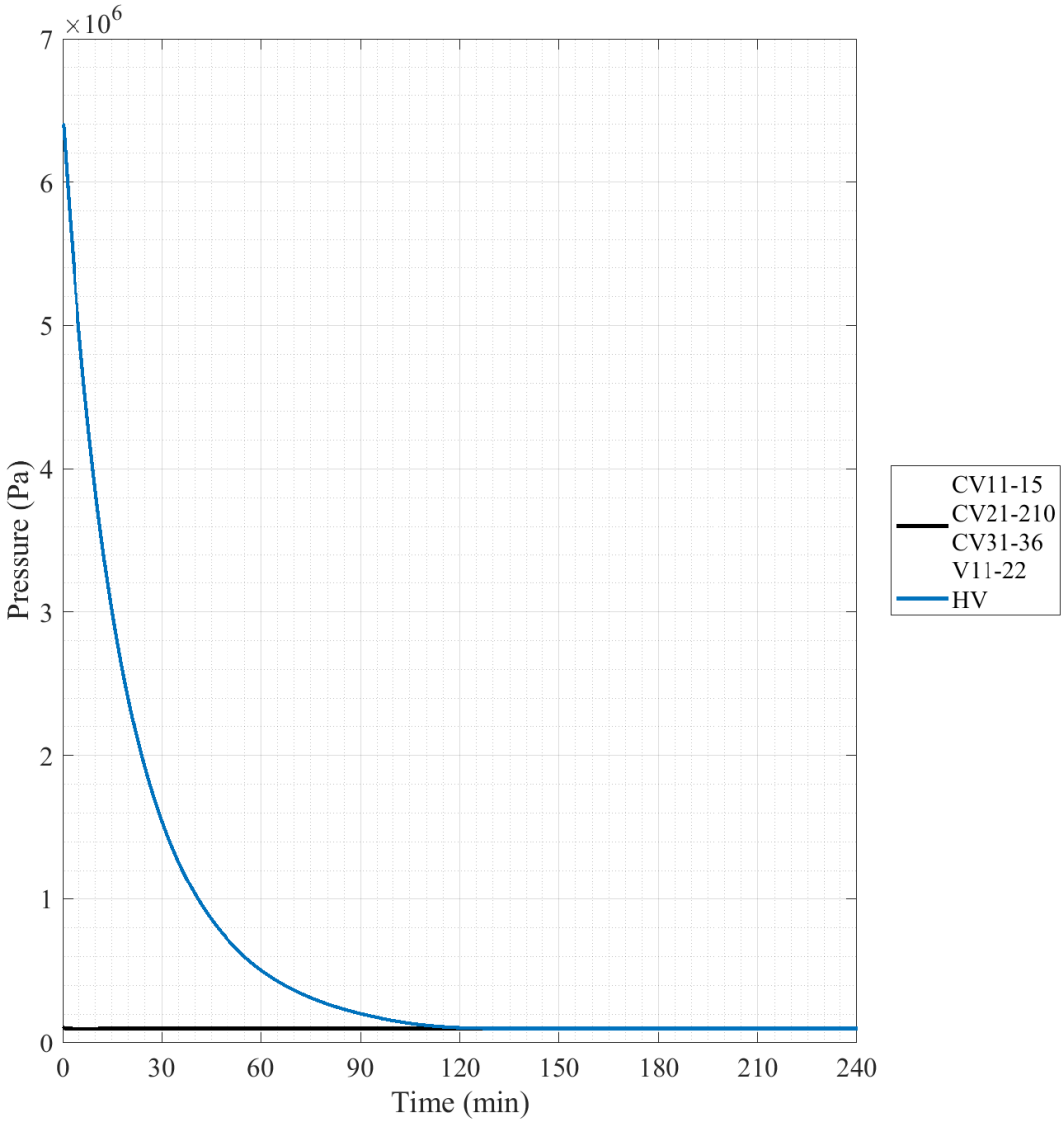

Fig. 6.78. Full-Scale Scenario 1 Pressure, 240 minute Timescale.

Reducing the timescale of the pressure plot to 240 minutes, Fig. 6.78 gives an overview of the progression of the RPV break on a pressure scale. The initial pressure of 6.4 MPa can be seen at the initial time, then at 20 seconds the pressure begins to fall at an exponential rate as the break flow path is opened and helium expands out and into the RC volumes. The HV reaches an equalized pressure of ~100 kPa at ~129.4 minutes following the blowdown initiation.

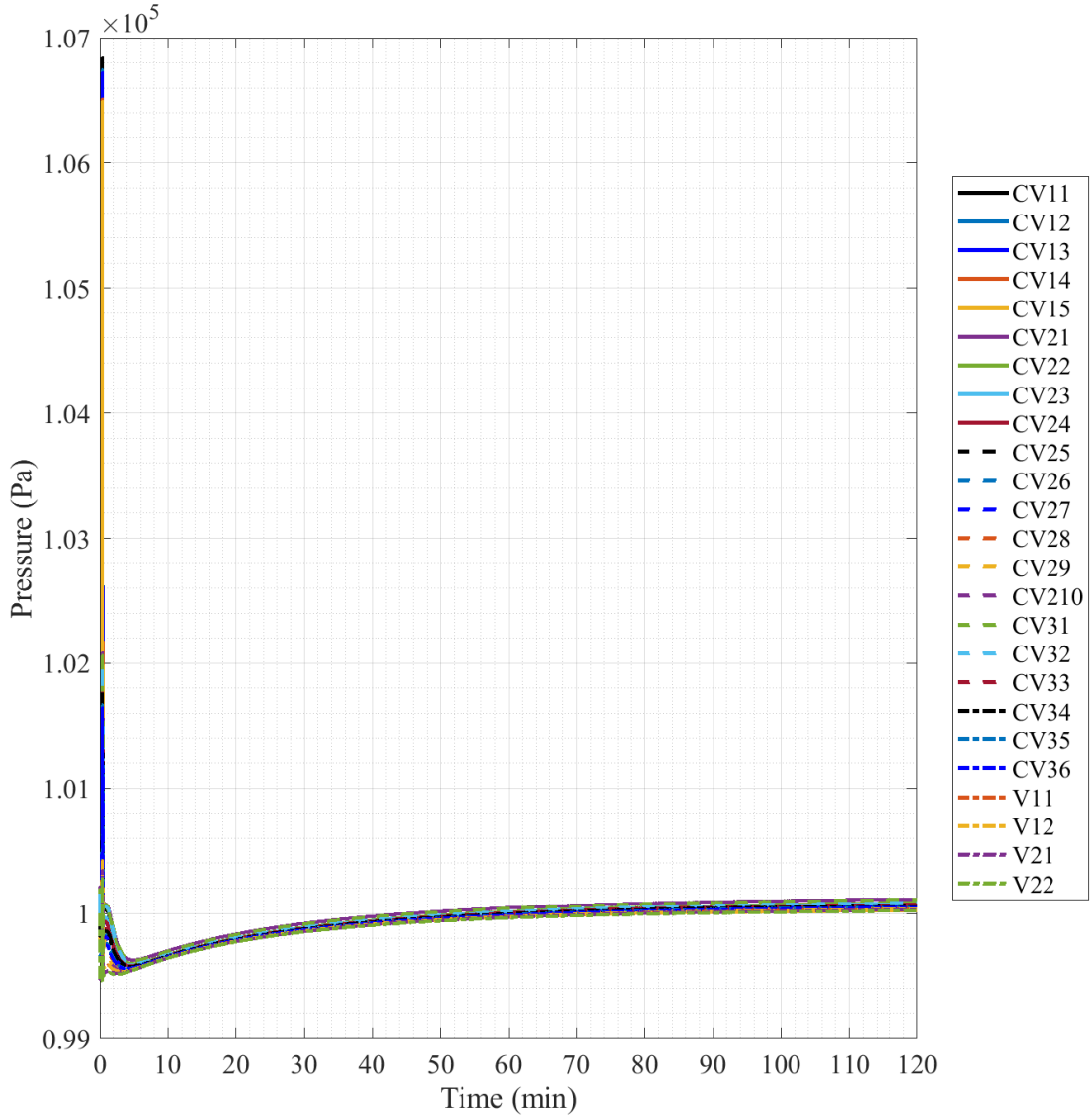

Fig. 6.79. Full-Scale Scenario 1 Pressure, 120 minute Timescale.

Fig. 6.79 gives a first look at the reactor building volume response to the helium release into its volumes. Much like the initial pressure plot, the timescale makes the pressure spike difficult

to gather information from. What can be seen in this figure is that post pressure spike the volumes enter a decreased pressure state that slowly returns back to ~100 kPa in roughly the timeframe of an hour where the pressures plateau.

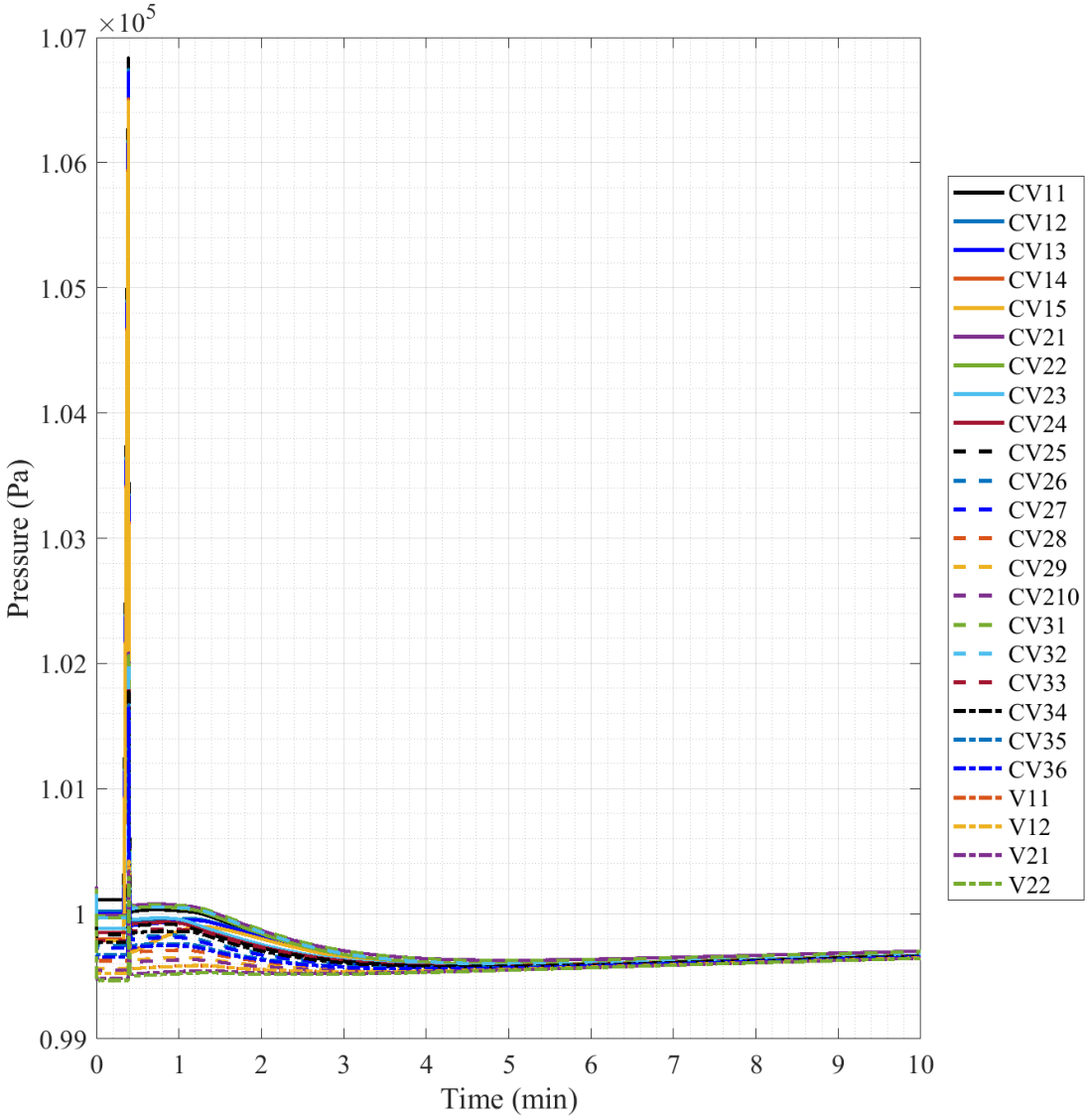

Fig. 6.80. Full-Scale Scenario 1 Pressure, 10 minute Timeframe.

Reducing in the timeframe to the 10 minutes, Fig. 6.80 shows the initial pressure separation of the volumes as they naturally redistribute at the beginning of the simulation, which can be seen by the initial vertical movement at time zero, coming to rest at steady state initial pressures. The spike occurs in the break initiation period, but it is still too difficult to describe

accurately at this timeframe. Post-break the volumes undergo a pressure spike where they come back to a separated range of pressures, but as the model progresses the range of pressure values begin to collapse into a band of much more closely related pressures that will eventually rise back to the ~100 kPa discussed in Fig. 6.79.

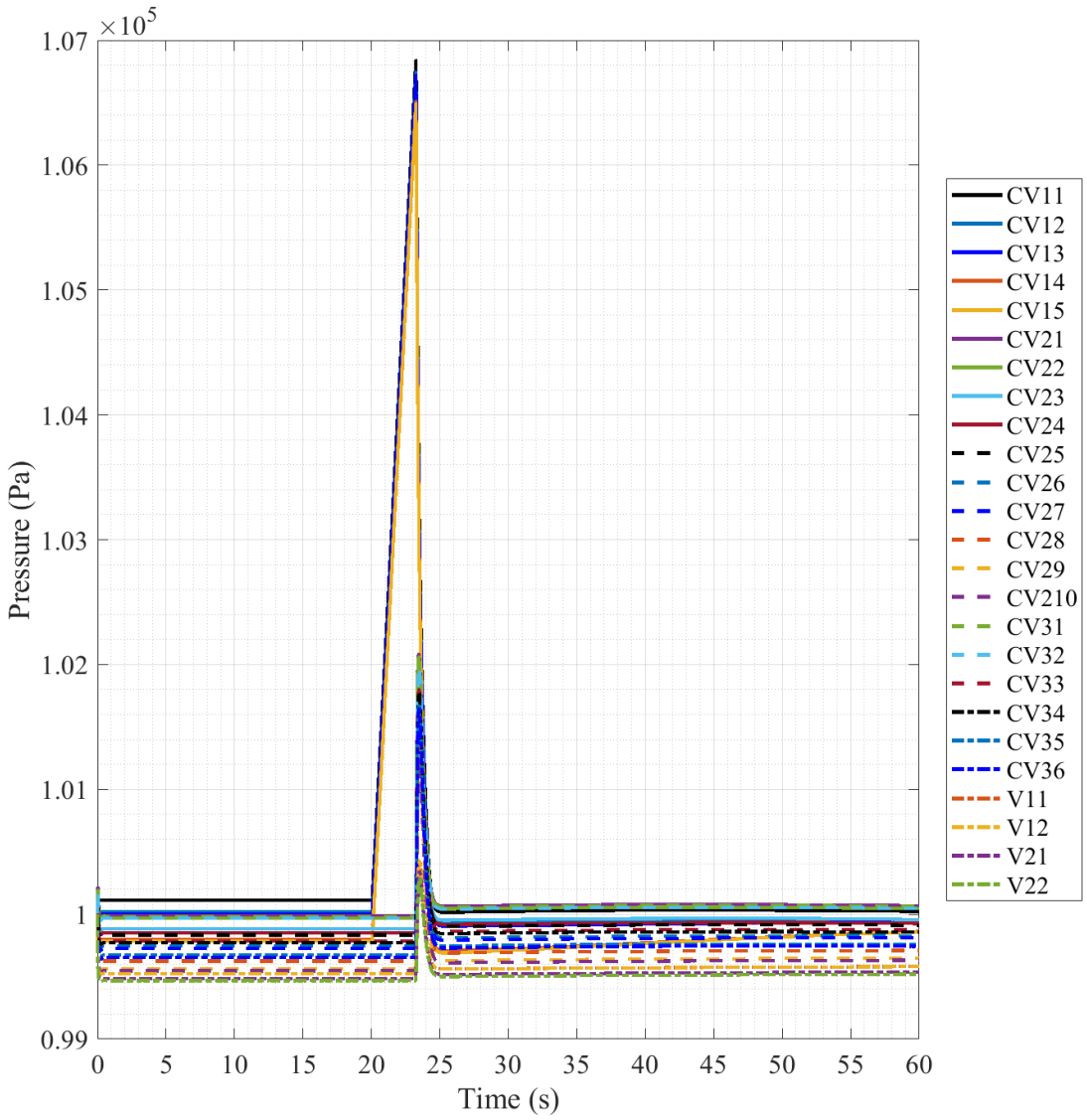

Fig. 6.81. Full-Scale Scenario 1 Pressure, 60 second Timescale.

Reducing the timescale down further to the 60 seconds post simulation start, Fig. 6.81 gives good information about the initial scenario timeframe. At the onset, the initial pressure banding movement can be seen where volumes naturally move from their initial positions to their steady

state positions. The pressure spike comes into better view with the initial spike occurring at the set 20 seconds, with a pressure following spike culminating in the blowout panel actuating ~3 seconds later. Most volumes appear to keep their relative location in the post-spike pressure banding.

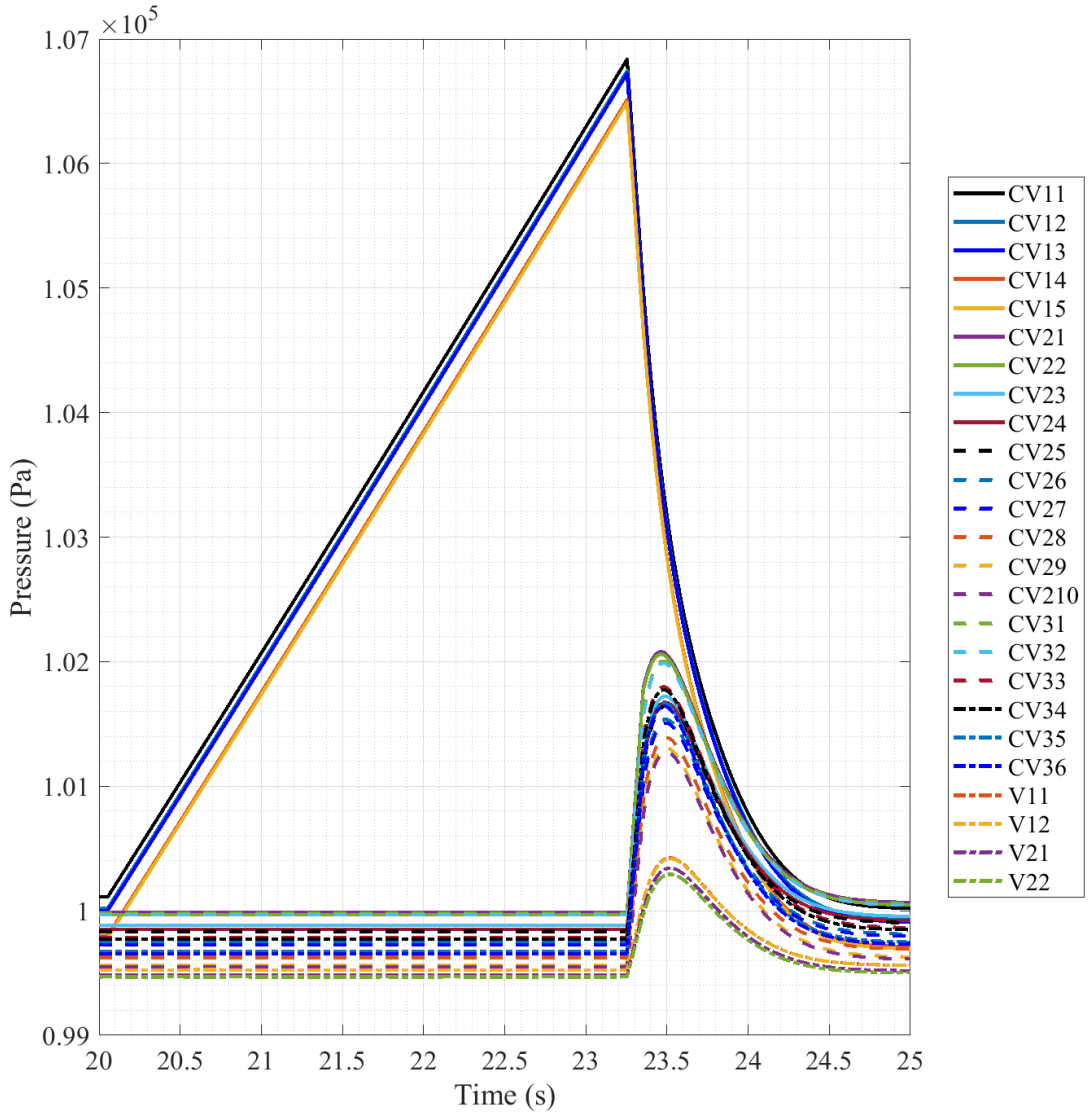

Fig. 6.82. Full-Scale Scenario 1 Pressure, 5 second Timeframe, Post Break.

Reducing the timeframe even more, Fig. 6.82 shows the 5 seconds post-break initiation of the model. With this, the linear rise of the CV11-15 (RC) volumes can be seen as pressure builds up behind the blowout panel, reaching a maximum of 1.0684×10^5 Pa (6.84 kPa increase). Pressure is built up for ~3.25 seconds before the blowout panel actuates, resulting in the pressure in the RC

volumes to fall quickly causing a rise in the other volumes of the reactor building in two distinct groups. The central transient of volumes consists of CV21-210 (SGC) and CV31-36 (EQS) which spike to a pressure range centralized around ~1.016×10^5 Pa (~1.6 kPa increase) with a maximum of ~1.021×10^5 Pa (~2.1 kPa increase). The bottom transient group consists of the vent space volumes of V11-22 which spike to a pressure of only ~1.004×10^5 Pa (~0.4 kPa increase) before falling back to the banded pressures. Both transient groups rise to their maximum pressure but then fall back into the pressure banding they roughly experienced before.

The next portion of plots examine the mass fractions of several major gases being tracked in the volumes across the simulation. Three of these gases, helium, oxygen, and nitrogen, were chosen to be plotted based on their importance in tracking the blowdown progression through the volumes being simulated. Nitrogen and oxygen were also chosen to be plotted as they make up the vast majority of the mass of the standard atmospheric air and therefore should give a good indication of the displacement of atmosphere and potential refill.

The first gas mass fraction to be plotted is that of helium, which can be seen in Fig. 6.83. CV11-15, CV22-210, CV32-36, and V11-22 are filled completely or near max with helium in the figure. All volumes start at initial concentrations of 0%, then spike to near completely filled fractions as the break occurs and the atmosphere is displaced. These joint volumes then proceed with time to fall in their concentrations leading to a “scattering” of volume fractions, with lower elevations volumes dropping concentration quicker than those that are higher. This leads to the lower elevation volumes being lower on the scattering portion of the plot with higher volumes remaining much closer or at 100%.

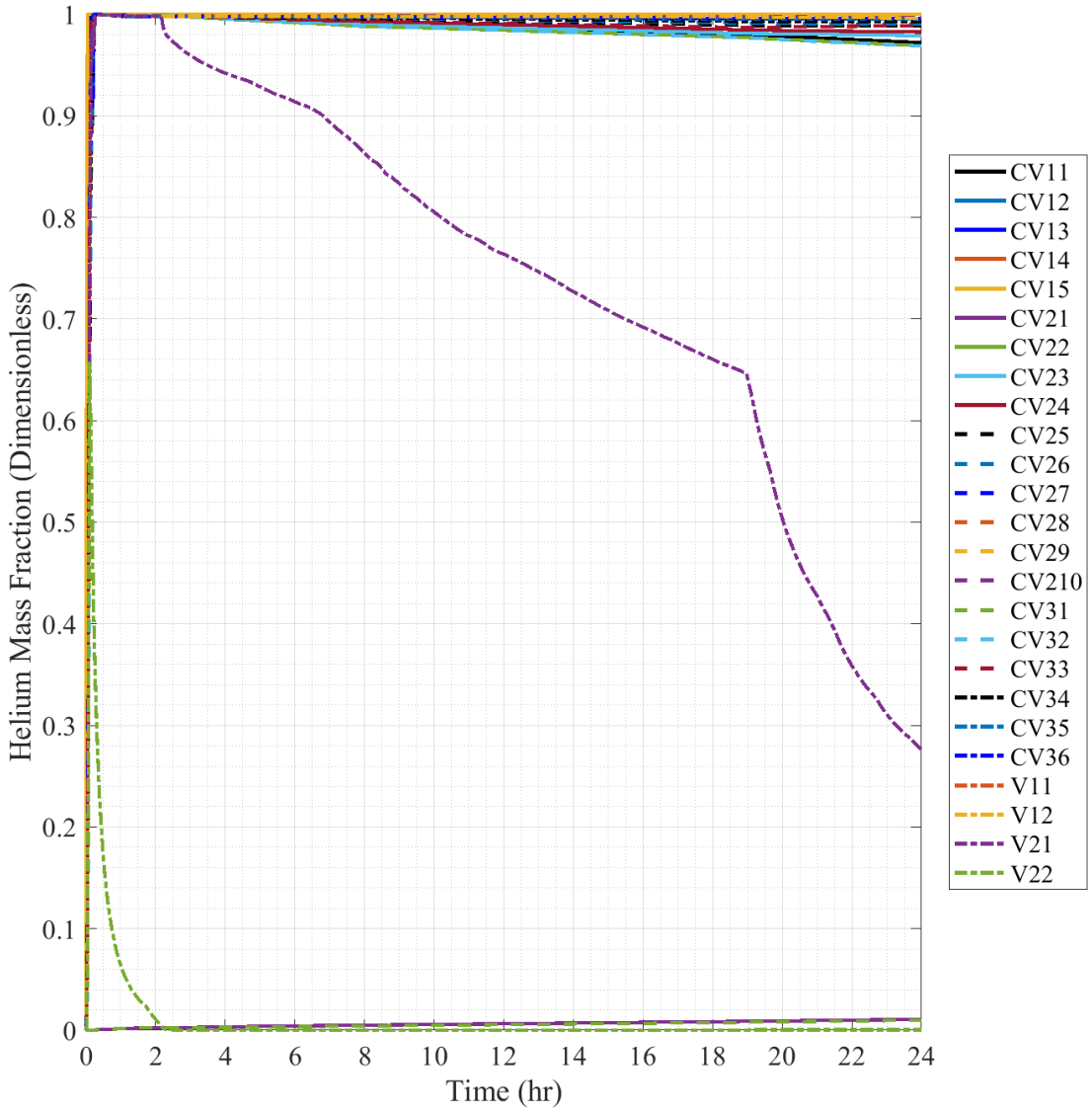

Fig. 6.83. Full-Scale Scenario 1 Helium Mass Fraction.

On the opposite end of the scale, CV21 and CV31 stay relatively close to 0% for a majority of the scenario with an increase of ~1% over the time period. The interesting portion of this scenario once again comes from the pair of V21 and V22 which through the previous scale results showed a pairing. In this full scale result the spike in V22 helium mass fraction can be seen even at this full-time scale, with a spike to ~65% and then a fall to 0% over the period of ~2 hours. This better shows the link then with V21 which then begins its downward transient at this time showing the preliminary refill of air into the volumes at a much larger timescale. V21 experiences generally

a very smooth transient, until it reaches ~19 hours where its slope increases greatly before ending the scenario period at 28% helium mass fraction. Even at this increased scale to get a better look at the initial distribution changes will require a reducing of the timescale which will be performed in a later plot.

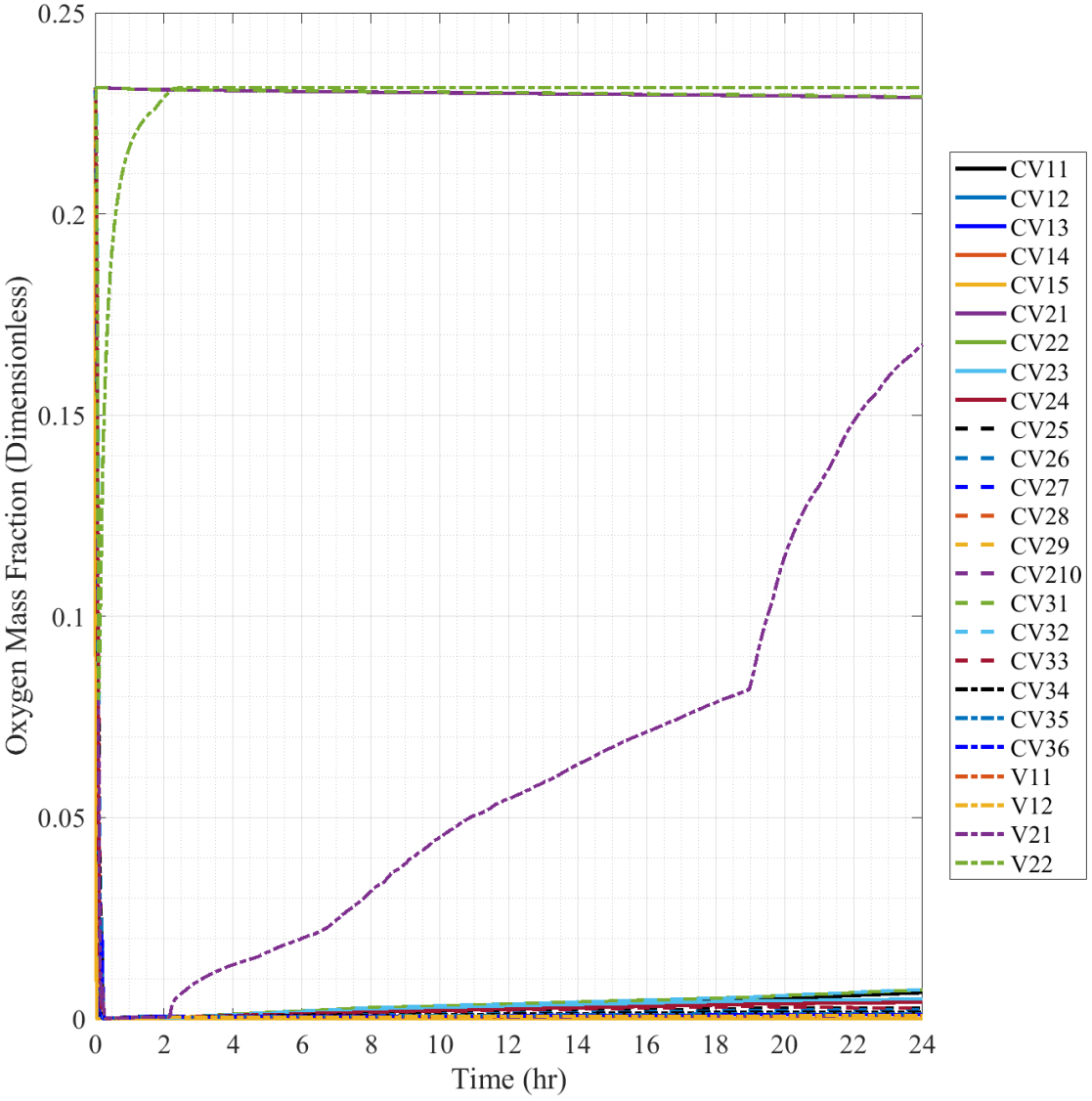

Fig. 6.84. Full-Scale Scenario 1 Oxygen Mass Fraction.

Fig. 6.84 presents the mass fraction data for oxygen throughout the reactor building volumes. As was seen in the scenario 0 data, the maximum concentration of oxygen in the model at any one time is 23.14% which is replicated in this figures data. Comparing the trends of this

figure to what was seen in Fig. 6.83 it can be seen the trends a simply inverses of each other, where instead of downward trends as refill occurs, upward trends occur.

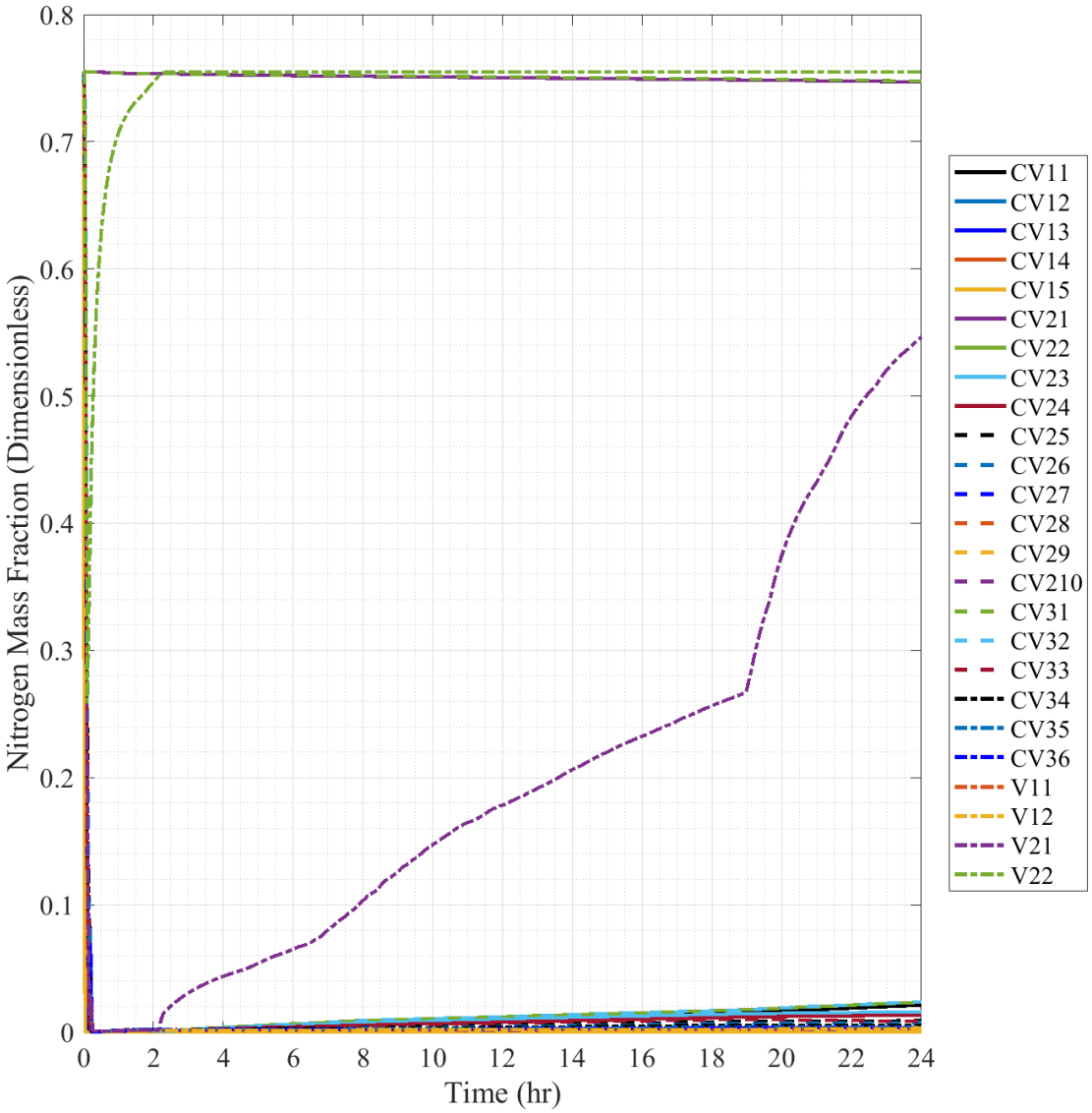

Fig. 6.85. Full-Scale Scenario 1 Nitrogen Mass Fraction.

Fig. 6.85 presents the mass fraction data for nitrogen throughout the scenario, and much like the previous figure of oxygen mass fraction, shows the same inverse trends in comparison to what was seen of the helium data. The major difference with this figure is the changed scale of the results, with a maximum nitrogen fraction of 75.51%. Fig. 6.83 and 6.84 have both shown that atmospheric standard air returns and is displaced in equal portions and do not suffer from

disassociation between its gaseous components. Due to this, a decision was made to combine the mass fractions of nitrogen and oxygen to give a good approximation of total atmosphere displacement done by helium. Results sections past scenario 2 will not include nitrogen and oxygen mass fractions plots as there are no fractional differences between them and the can be relegated to a consolodated combination mass fraction to show results, but their plots will be included in Appendix E for further reference.

Fig. 6.86 sums the oxygen and nitrogen mass fractions together as previously discussed to a “Combination” mass fraction composed of the combination of the two individual mass fractions. The combination of these two gases make up 98.66% of the total mass fraction of standard air and should be a good comparison to the helium mass fraction for comparisons. Finally, by comparison with 6.83 and what has been previously discussed with the individual oxygen and nitrogen mass fraction figures, it can be seen that the figure is simply an inverse of the helium trends. Due to the linked relationship of the results, this set of data will be used to examine the initial details of the blowdown from a mass fraction perspective as was done with the pressure.

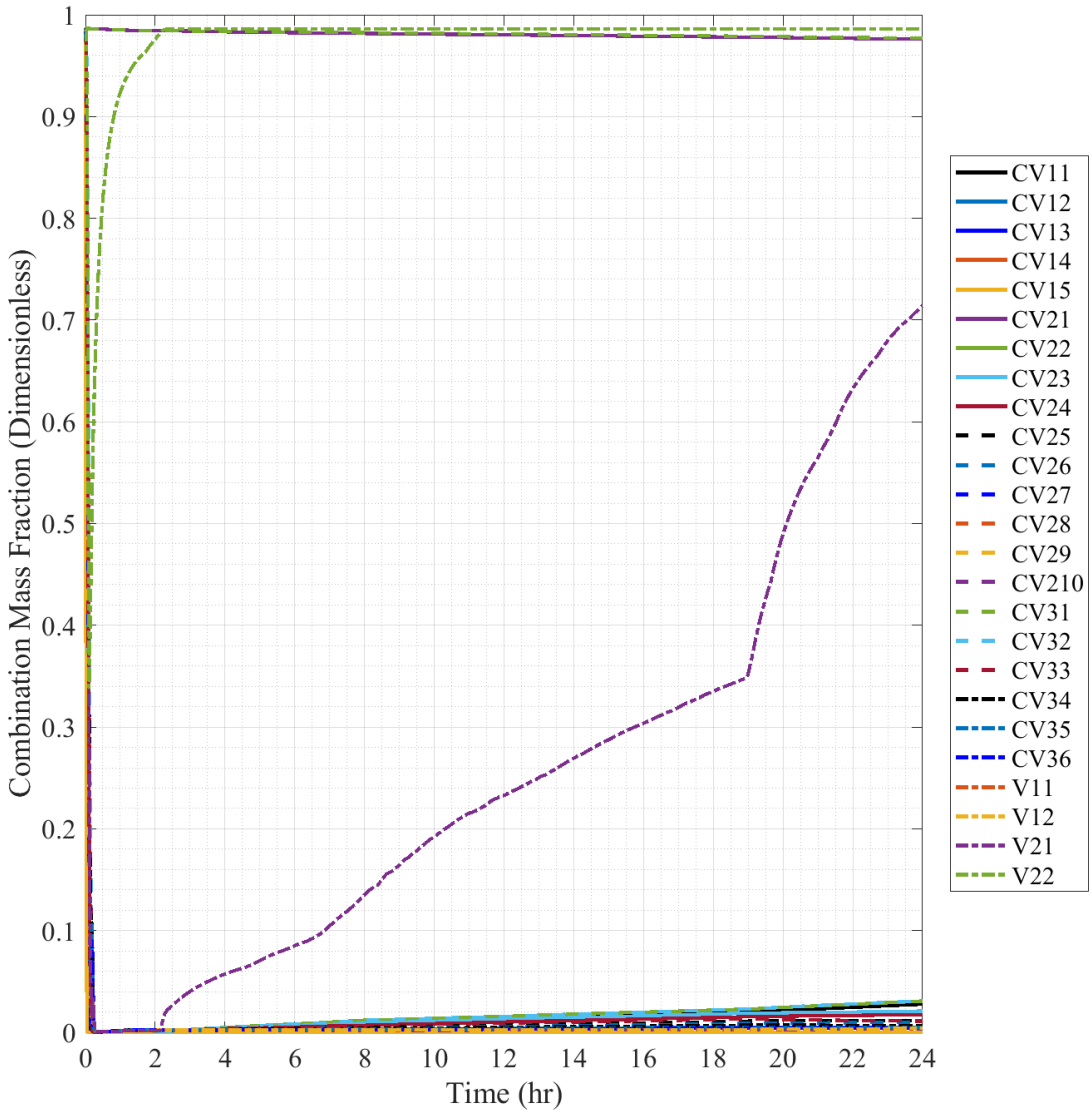

Fig. 6.86. Full-Scale Scenario 1 Combination Mass Fraction.

Fig. 6.87 reduces in the timescale of the combination mass fraction to get details of the initial post-break building response to the spreading helium. Much of the displacement happens within the first 15 minutes of the scenario. V22 can be seen to fall to only ~34% air content before refill begins and over the following ~2 hours it fills back to ~100% normal air. At that point, V21 can be seen to refill as has been seen previously. Some interesting behavior as the volumes get near voiding before 15 minutes will be explored at a smaller timescale.

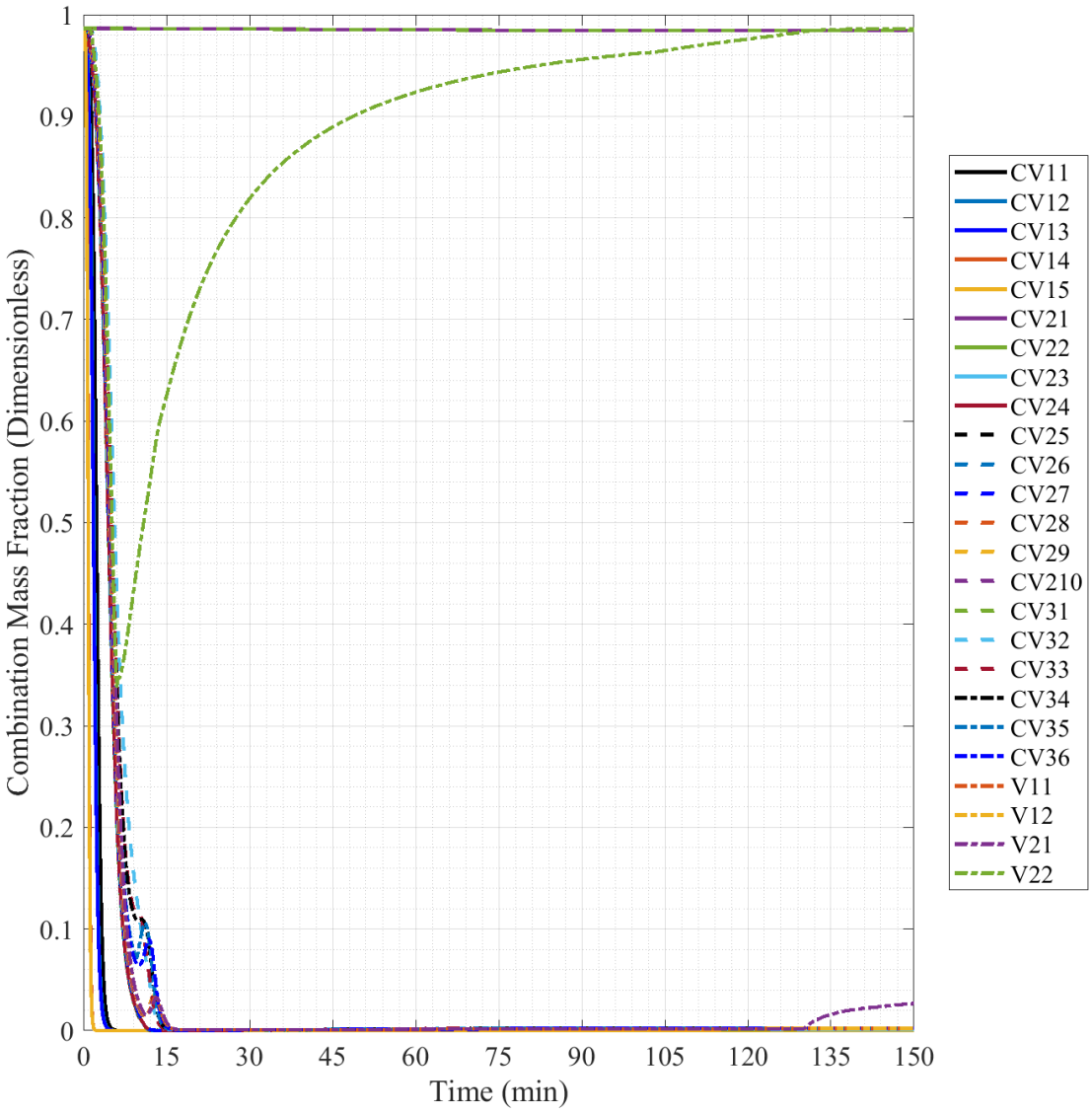

Fig. 6.87. Full-Scale Scenario 1 Combination Mass Fraction, 150 minute Timescale.

Fig. 6.88 reduces the timescale down to the first 30 minutes of the scenario to get the finer details of the volume voiding. As seen in the previous figure, V22 drops to ~34% at ~6 minutes before beginning to rise in air concentration. Volumes mostly progress from left to right in order of their path in the blowdown progression with RC volumes on the left and SGC, EQS, and vent space volumes heading towards the right.

A decrease in the rate of air displacement begins at ~8 minutes with volumes experiencing spikes in air concentration before continuing to be voided. These volumes consist of CV28-210,

CV33-36, and V11-21 and their orientations seem to be related to their volume elevations, with lower volume undergoing the spike earlier and later volumes experiencing it later. These spikes most visibly affect the EQS volumes of CV23-26, and CV22 to a lesser extent as it is pushed into a more delayed decline, and those of the upper SGC volumes of CV28-210 which may indicate fighting in flow as the EQS flow of gases conflicts with rejoining the gases flowing up the SGC volumes leading to a "bubble" of air being pushed through the volumes and showing up at various stages of the blowdown across multiple volumes.

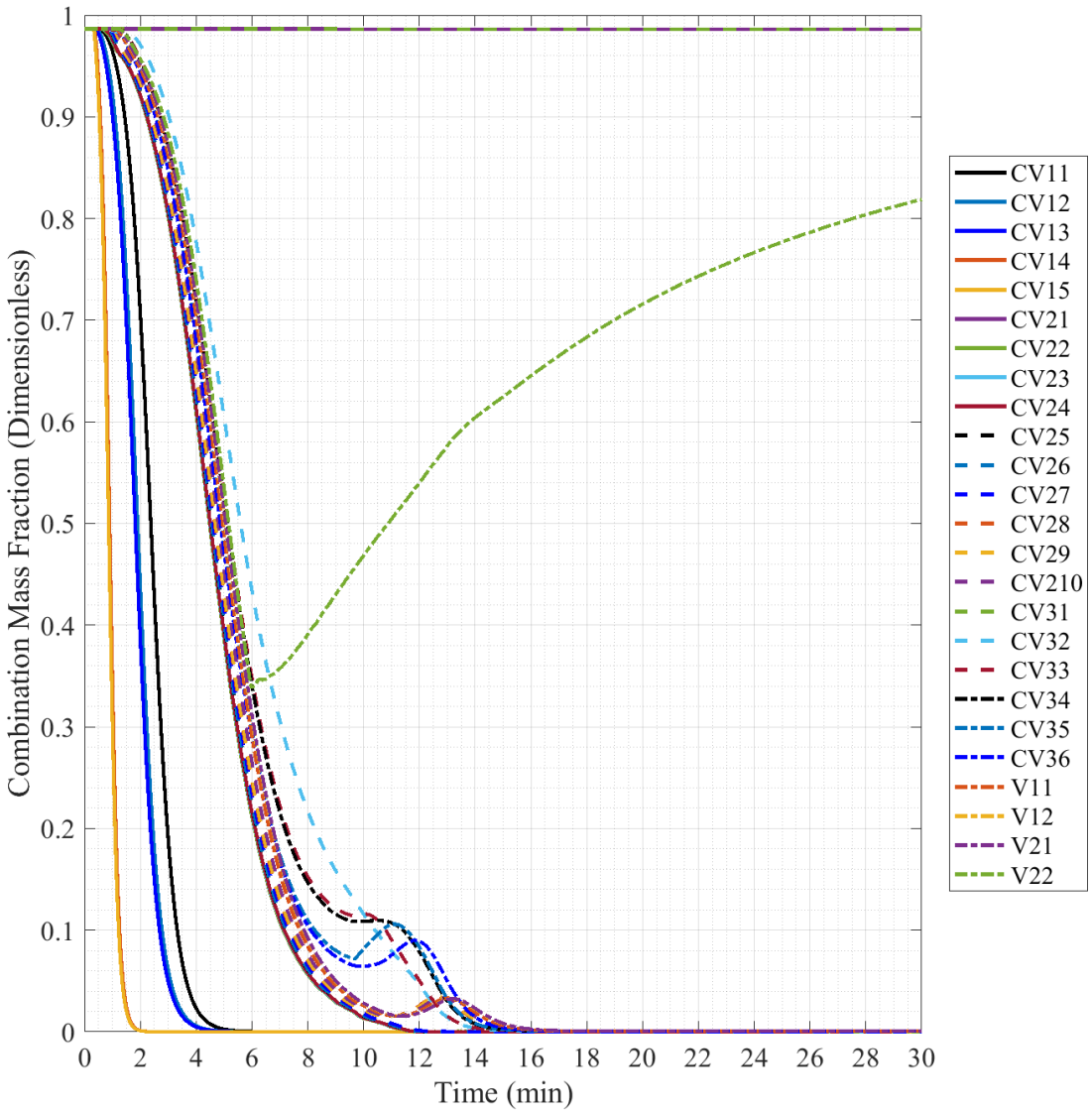

Fig. 6.88. Full-Scale Scenario 1 Combination Mass Fraction, 30 minute Timescale.

6.2.3 Full-Scale Scenario 2 Results

Scenario 2 is the base SGV break scenario, with no changes to the basic layout of the full-scale reactor building model. This model is the baseline for comparing to Scenarios 4 and 6 which change the standard layout in their scenario parameters. In this model, flow from the blowdown progresses through a majority of the volumes of the model, excluding the RC (CV11-15) and the ducts that connect them to the SGC. A visual example of this scenario's estimated progression can be seen in the 1/28th-scale results section of this scenario, Fig. 6.20.

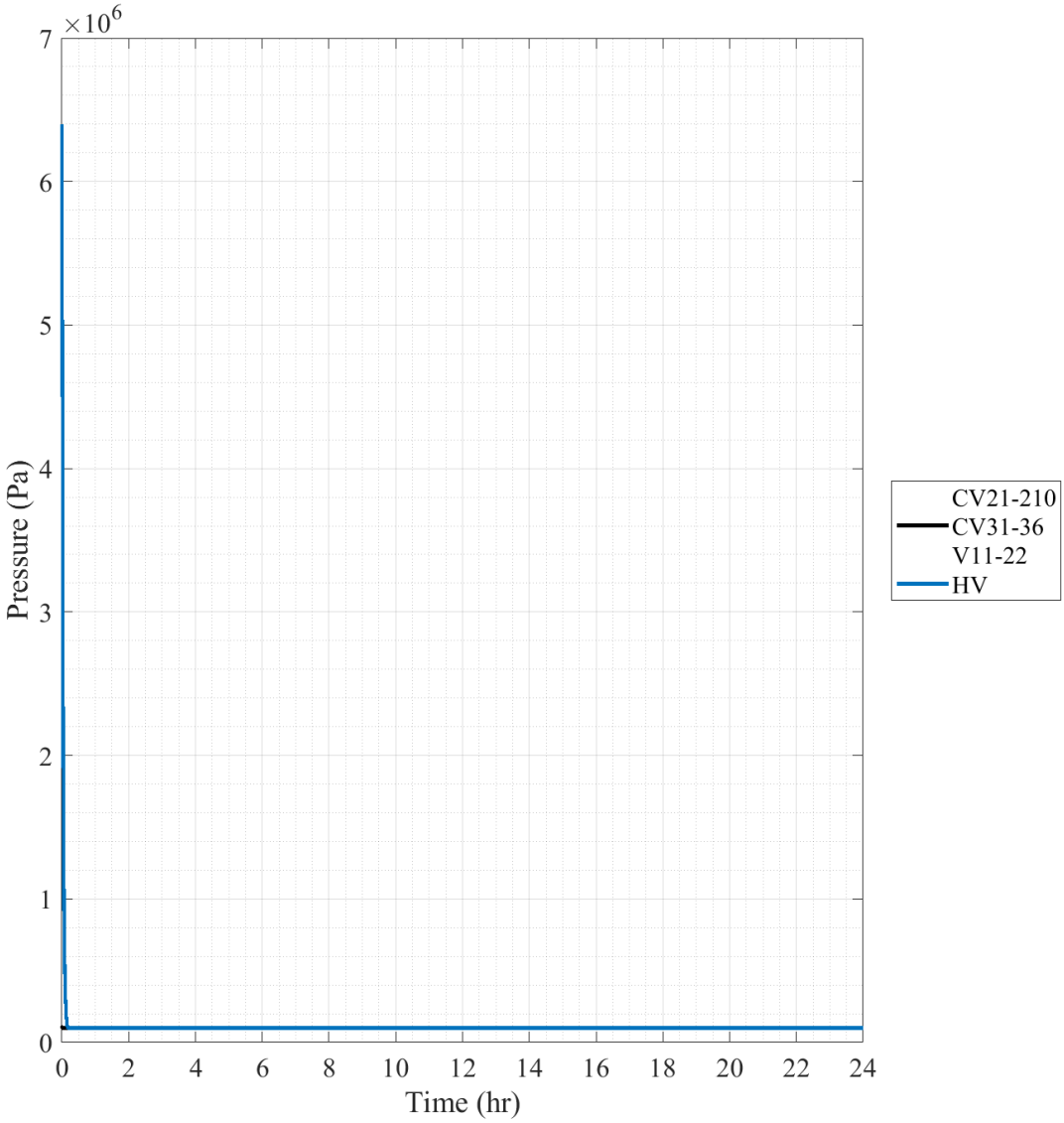

Fig. 6.89. Full-Scale Scenario 2 Pressure.

The first plot of results for scenario 2, Fig. 6.89, shows the pressure results of the scenario across the full timeframe of the simulation. Much like the plot in scenario 1, due to the scale of the pressure of the helium volume, HV, peaking at 6.4 MPa, the overall scale of the pressure plot makes it difficult to determine post blowdown progression of the reactor building volumes and the blowdown time. The plotted timeframe must be reduced in order to gather discernable details for further pressure results.

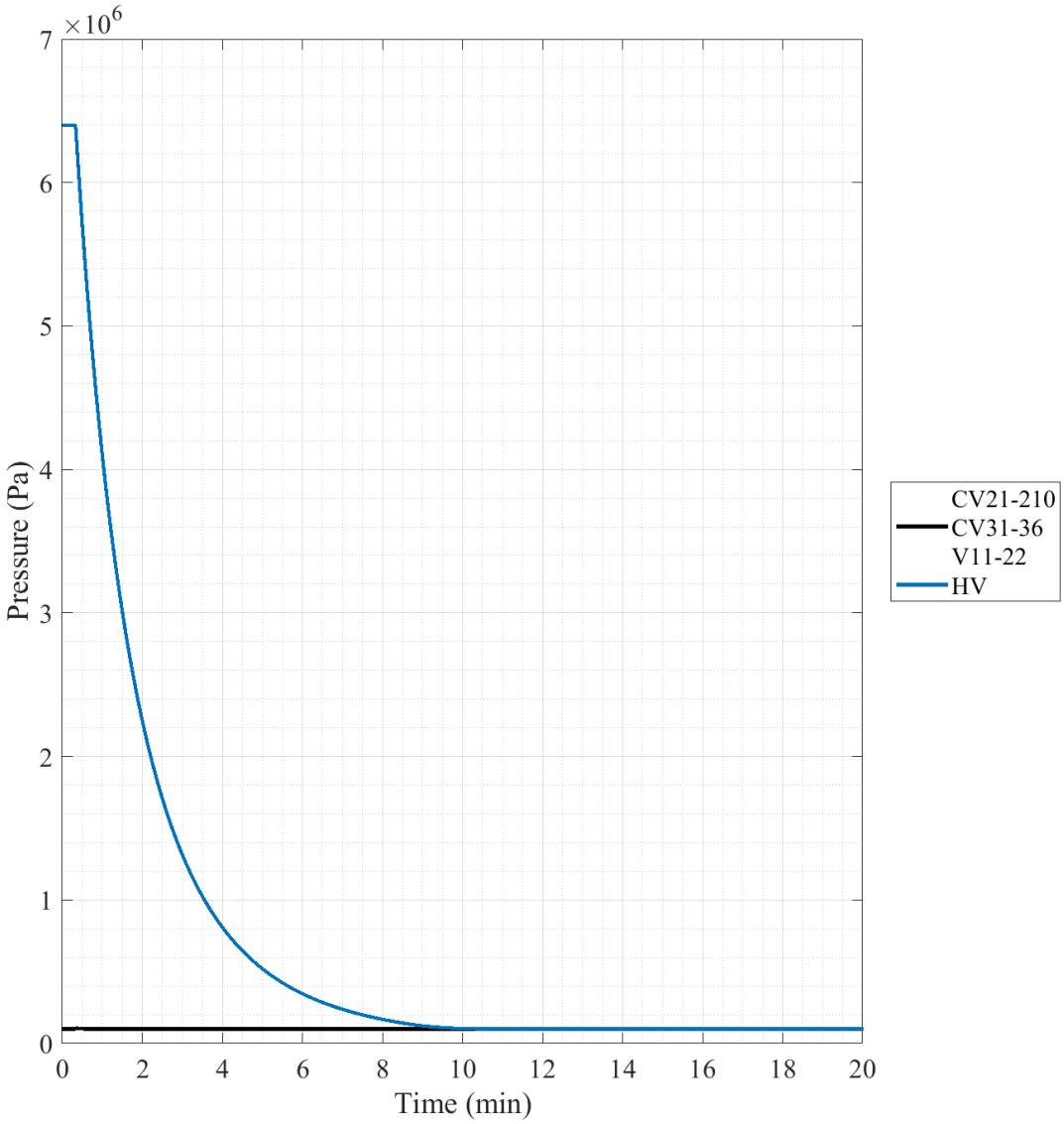

Fig. 6.90. Full-Scale Scenario 2 Pressure, 20 minute Timescale.

Reducing the timescale of the pressure plot to 20 minutes, Fig. 6.90 gives a overview of the progression of the SGV break on a pressure scale. The initial pressure of 6.4 MPa can be seen well at the initial time, then at 20 seconds the pressure begins to fall at an exponential rate as the break flow path is opened and helium expands out and into the SGC volumes. The HV reaches an equalized pressure of ~100 kPa at ~10.21 minutes following the blowdown initiation, ~10.5 minutes post simulation initiation.

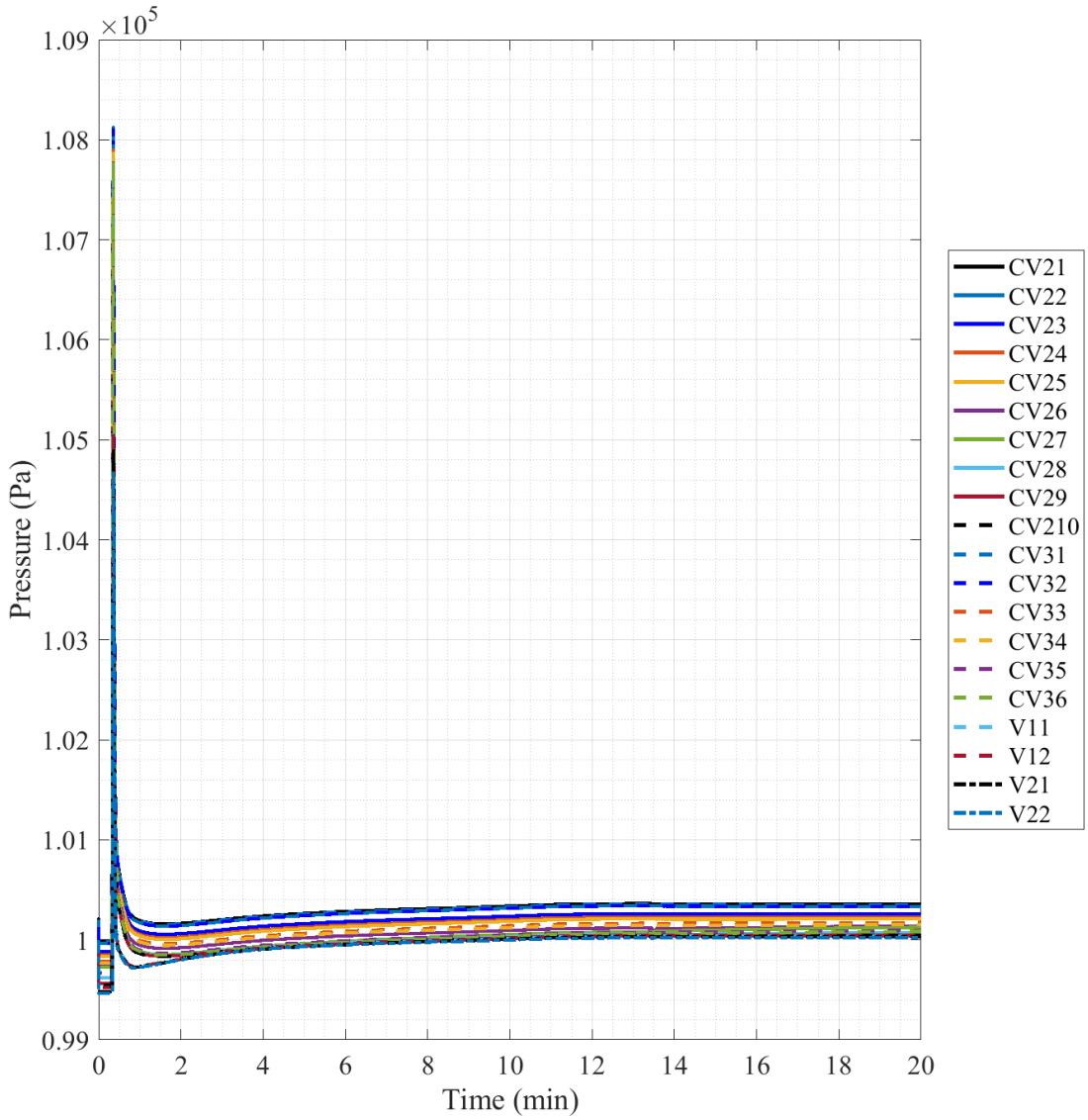

Fig. 6.91. Full-Scale Scenario 2 Pressure, 20 minute Timescale.

Fig. 6.91 gives a first look at the reactor building volume response to the helium release into its volumes. Much like the initial pressure plot, the timescale makes the pressure spike difficult to gather information. What can be determined from this figure is that post pressure spike the volumes enter an increased pressure band state that slowly plateaus to ~100.2 kPa in roughly the timeframe of ~12 minutes.

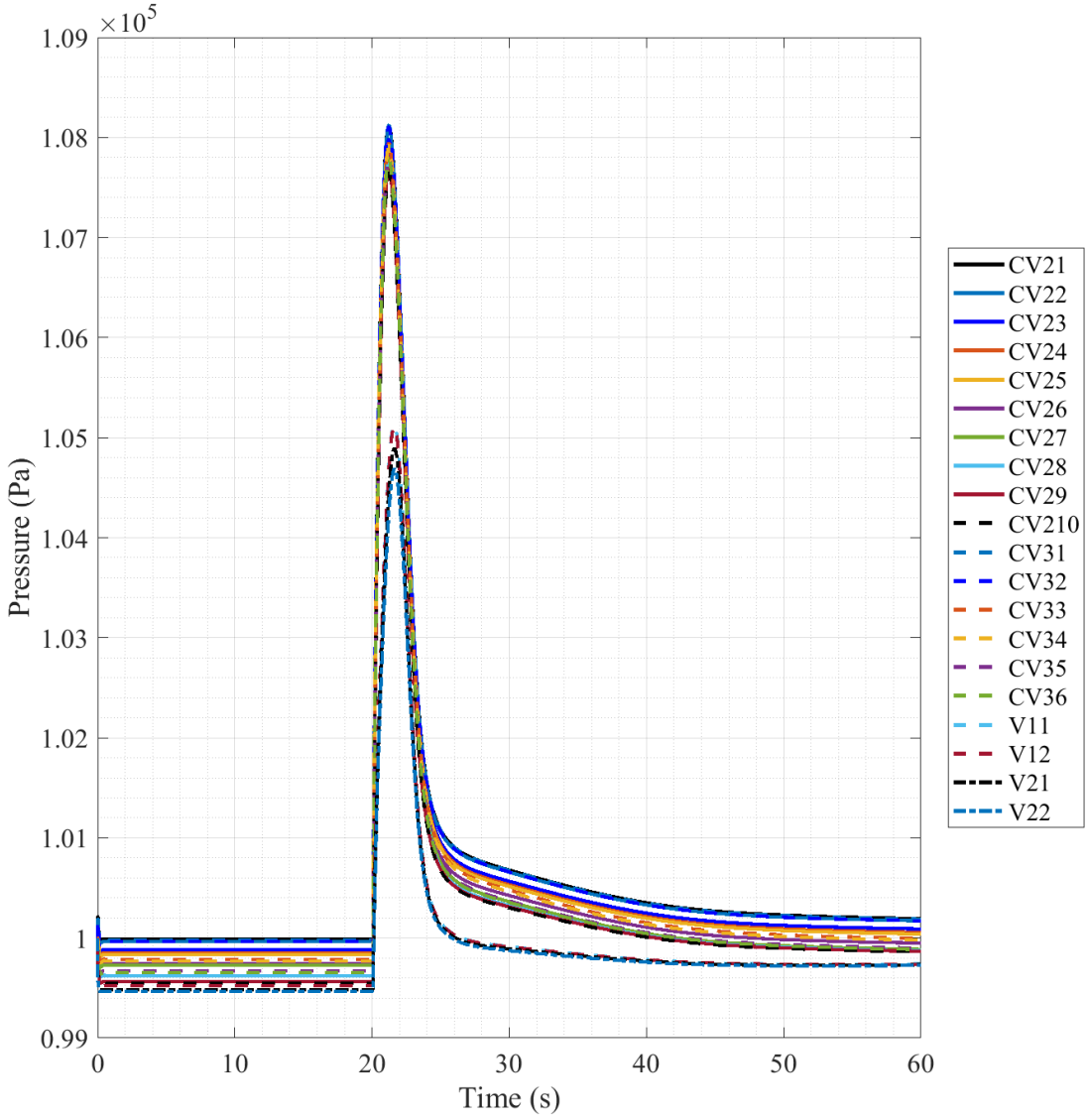

Fig. 6.92. Full-Scale Scenario 2 Pressurel, 60 second Timescale.

Reducing the timescale down to the 60 seconds post simulation start, Fig. 6.92 gives information about the initial scenario timeframe. At the onset of the simulation the initial pressure

banding movement can be seen, where volumes naturally move from their initial positions to the steady state positions. Since there is no blowout panel actuation in this scenario the pressure rise at the break initiation is analogous to being normally distributed. Following the pressure spike, volumes settle back pressure bands but at a raised pressure from what they settled at post simulation start which can be seen in both Fig. 6.91 and 6.92.

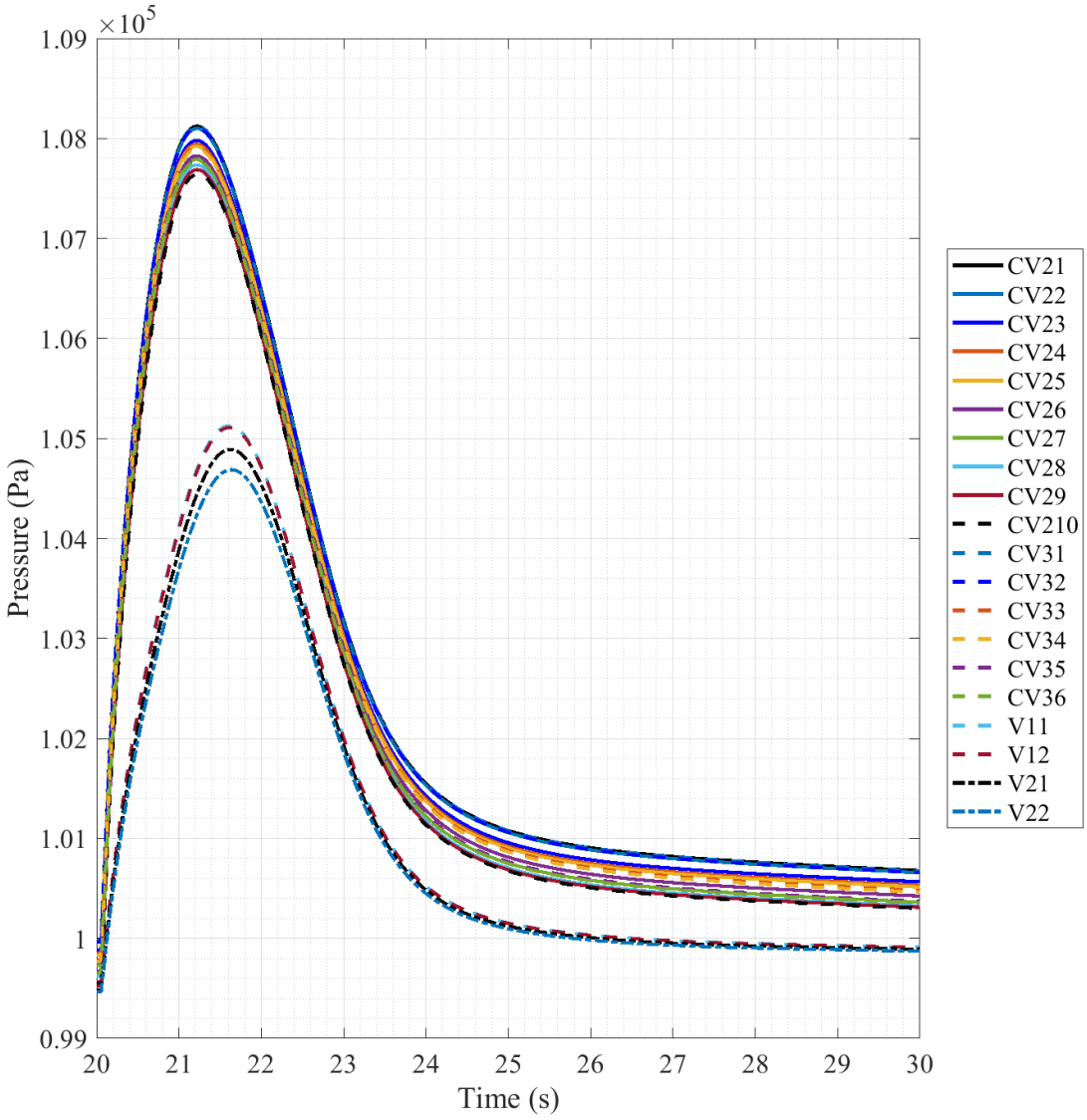

Fig. 6.93. Full-Scale Scenario 2 Pressure, 20-30 second Timeframe.

Reducing the timeframe in even more, Fig. 6.93 shows the 10 seconds post-break initiation of the model. The upper transient of volumes consists of CV21-210 and CV31-36 and spike to a

pressure range centralized around ~1.078x10^5 Pa (~7.8 kPa increase) and a max of 1.0812x10^5 Pa (8.12 kPa increase). The bottom transient group consists of the vent space volumes of V11-22 which spike to a pressure range of only ~1.048x10^5 Pa (~4.8 kPa increase), with a max of 1.0513 x10^5 Pa (5.13 kPa increase), before falling back to the banded pressures that come to join back together in the minute following the pressure spike.

The next portion of plots examine the mass fractions of several major gases being tracked in the volumes across the simulation. Three of these gases, helium, oxygen, and nitrogen, were chosen to be plotted based on their importance in tracking the blowdown progression through the volumes being simulated. Nitrogen and oxygen were also chosen to be plotted as they make up the vast majority of the mass of the standard atmospheric air and therefore should give a good indication of the displacement of atmosphere and potential refill.

The first gas mass fraction to be plotted is that of helium, which can be seen in Fig. 6.94. Similar to scenario 2 of the 1/28th-scale, this scenario undergoes interesting transients in comparison to other scenarios. Beginning at the top of the plot, volumes undergo spikes to ~100% but quickly fall away. V22, like seen in all results, undergoes a spike with the blowdown to ~100% but then quickly falling away ~0%. CV21 and CV31 experience only a very slight introduction of helium to their volumes, on the scale of E-5, a contribution of their low elevations.

The upper transient consists of CV210 and V11-12, which experience spikes up to ~100%, but then fall to ~90% where the begin a downward transient ending the scenario period at ~85%. The next down transient consists of V21, which after spiking to ~100% falls to ~89% where it is constant for ~1.5 hours before beginning a downward transient and ending at 20%. It is interesting as in this scenario it doesn't appear that V21 is directly tied to V22 as it was in scenario 1, as V22 falls to 0% far before V21 begins its downwards transient. The last transient is that of CV29, which

spikes to 100% and then falls to ~56% in ~30 minutes before changing slope and dropping to ~36% in ~15.5 hours when it becomes almost stable and falling ~1% over the final 8 hours.

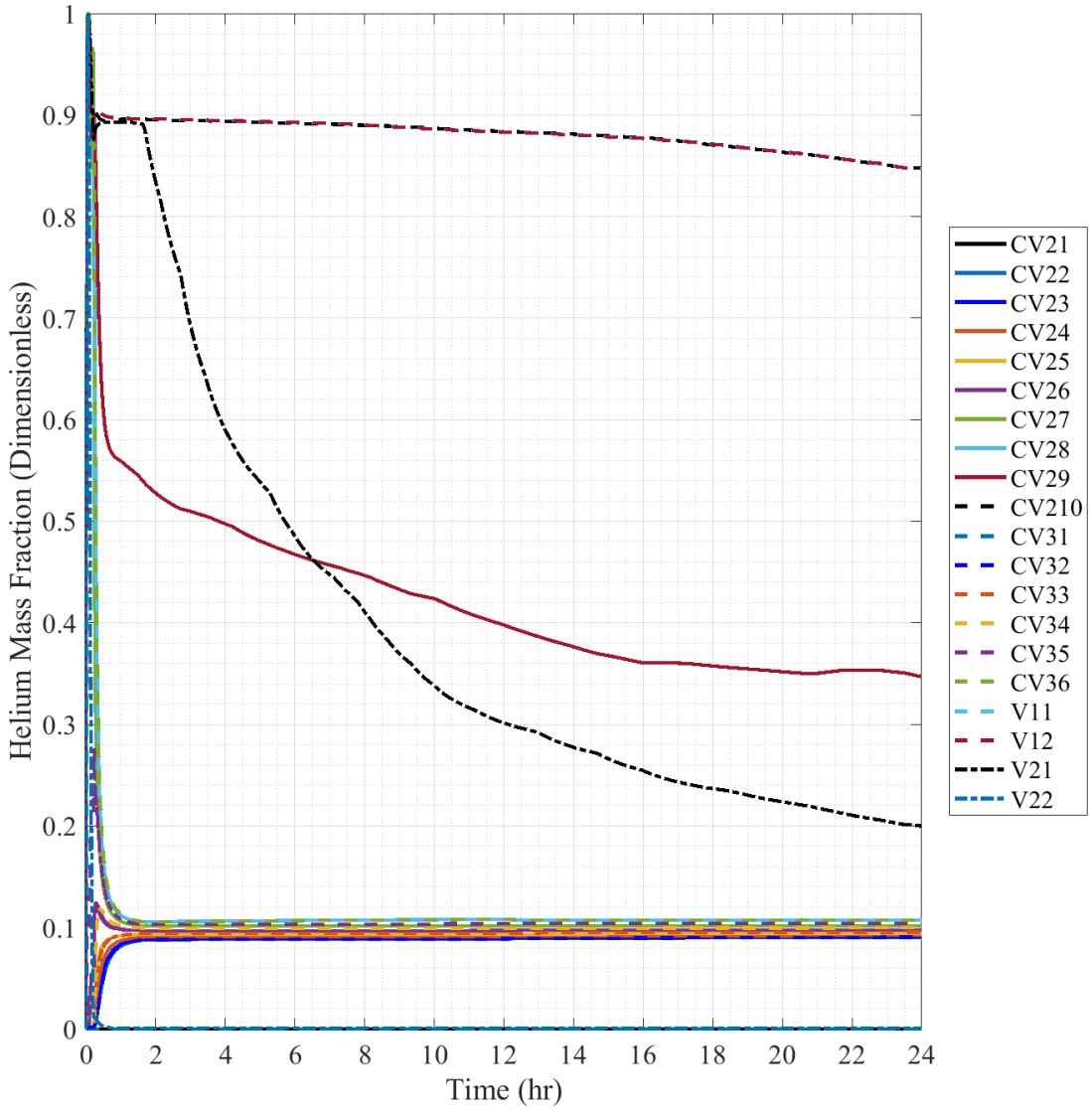

Fig. 6.94. Full-Scale Scenario 2 Helium Mass Fraction.

All remaining volumes, CV22-28 and CV32-36, fall into the striated banding that was previously seen in scenario 2 of the 1/28th-scale results. With the results of this scale, the initial region of the banding is much clearer to the 1/28th-scale as the oscillations do not appear at this scale. With this it can be seen that only CV27-28 and CV36 undergo major pressure spikes to 100% for this group, and all experience much smaller peaks or simply rising to the plateau banding.

As was also shown in then smaller scale, the banding is organized by the elevation of the participating volumes, with volumes at lower elevations being lower on the band and those higher being at the top. With this scale of results, it is also shown that the pressure spike is mainly limited to those higher volumes which are almost directly within the line of helium expansion flow path. Even though results at this increased scale are visible, a better look at the initial distribution changes will require a shrinking of the timescale which will be performed in a later plot.

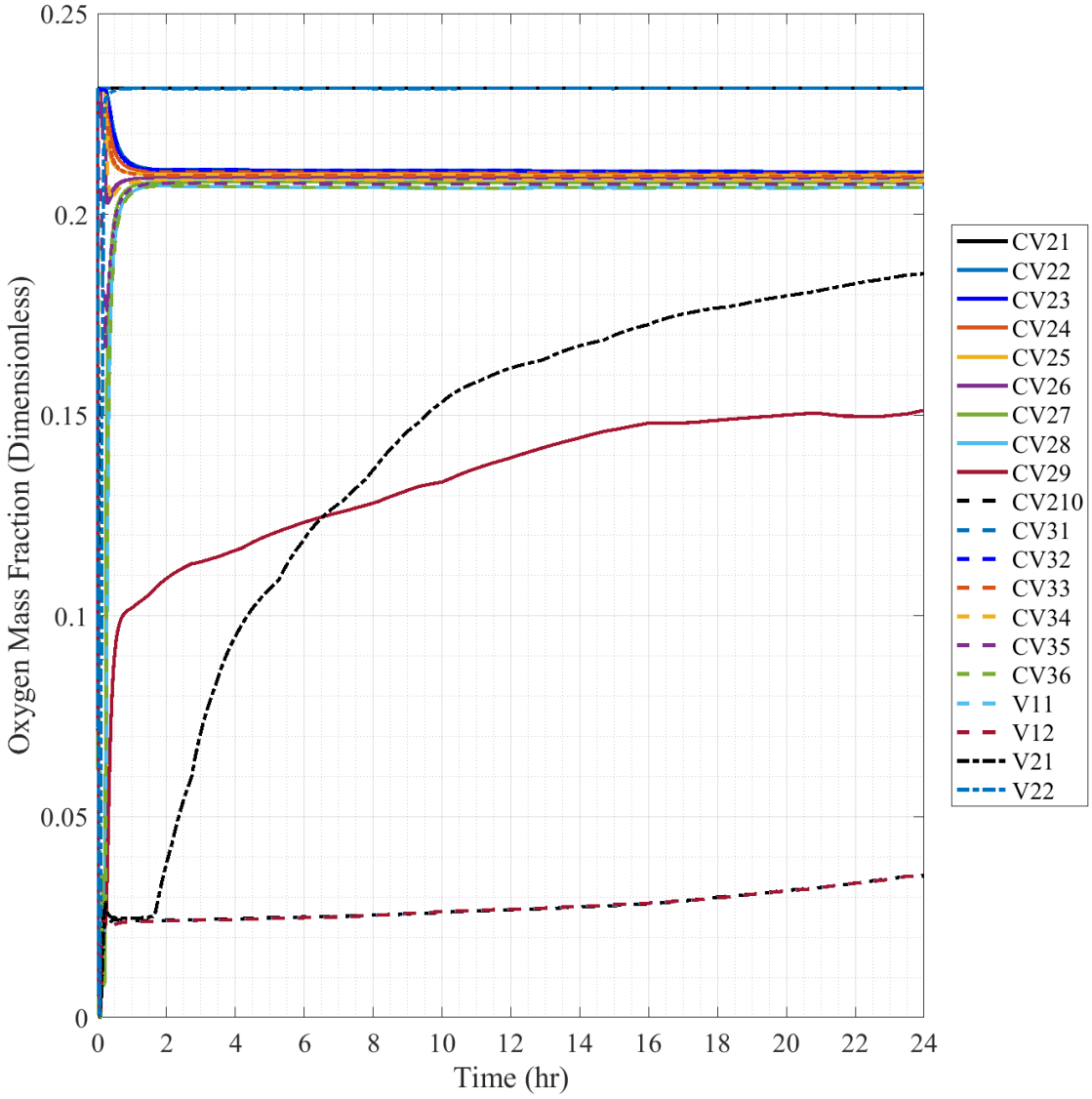

Fig. 6.95. Full-Scale Scenario 2 Oxygen Mass Fraction.

Fig. 6.95 presents the mass fraction data for oxygen throughout the reactor building volumes. As was seen in the scenario 0 data, the maximum concentration of oxygen in the model at any one time is 23.14% which is replicated in this figure's data. Comparing the trends of this figure to what was seen in Fig. 6.94 it can be seen the trends a simply inverses of each other, where instead of downward trends as refill occurs, upward trends occur.

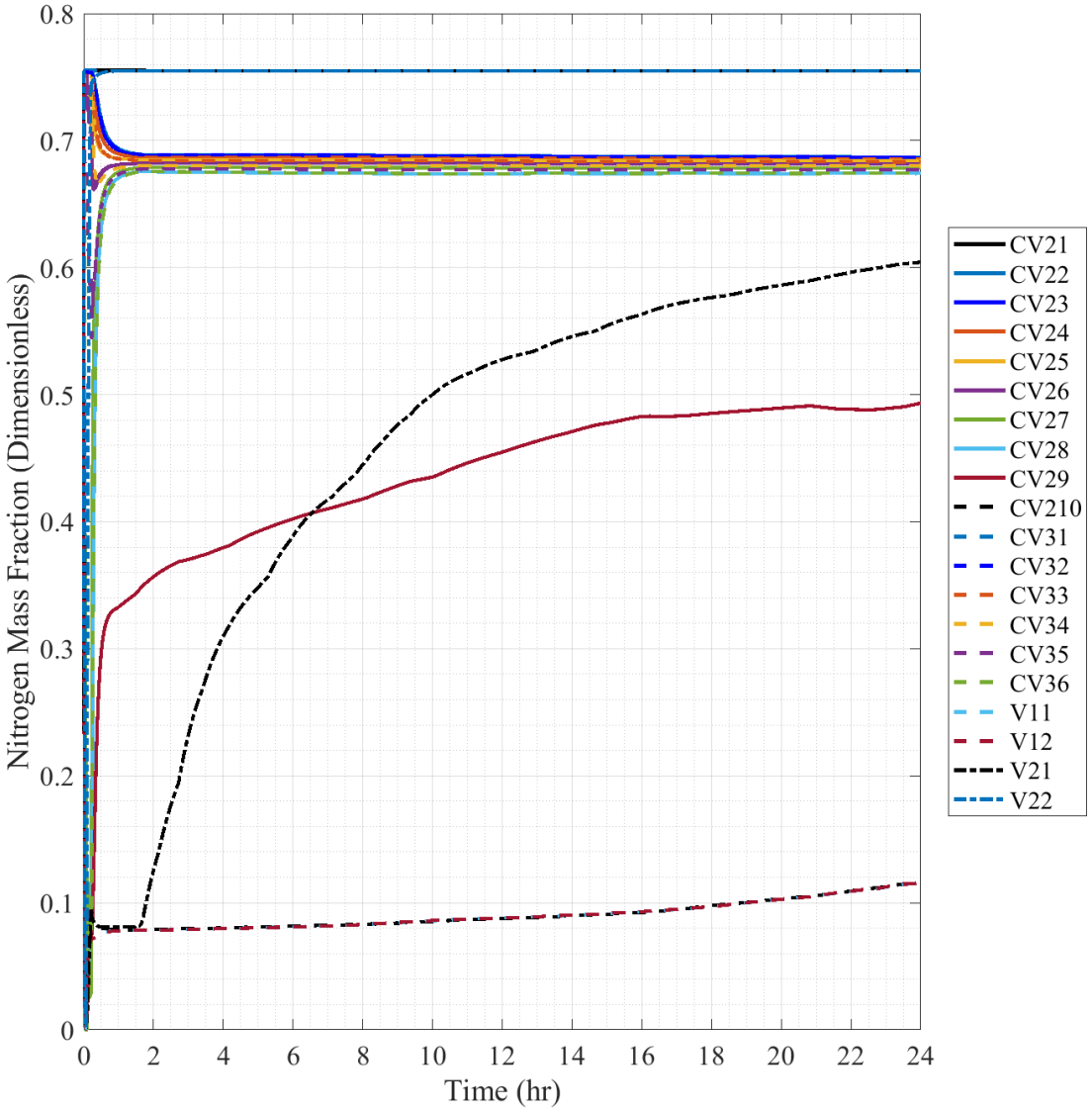

Fig. 6.96. Full-Scale Scenario 2 Nitrogen Mass Fraction.

Fig. 6.96 presents the mass fraction data for nitrogen throughout the scenario, and much like the previous figure of oxygen mass fraction, shows the same inverse trends in comparison to

what was seen of the helium data. The major difference with this figure is the changed scale of the results, with a maximum nitrogen fraction of 75.51%. Fig. 6.95 and 6.96 have both shown that atmospheric standard air returns and is displaced in equal portions and do not suffer from disassociation between its gaseous components. Due to this, a decision was made to combine the mass fractions of nitrogen and oxygen to give a good approximation of total atmosphere displacement done by helium. Results sections past scenario 2 will not include nitrogen and oxygen mass fractions plots as there are no fractional differences between them and the can be relegated to a consolodated combination mass fraction to show results, but their plots will be included in Appendix E for further reference.

Fig. 6.97 sums the oxygen and nitrogen mass fractions together as previously discussed to a “Combination” mass fraction composed of the combination of the two individual mass fractions. The combination of these two gases make up 98.66% of the total mass fraction of standard air and should be a good comparison to the helium mass fraction for comparisons. Finally, by comparison with Fig. 6.94, and what has been previously discussed with the individual oxygen and nitrogen mass fraction figures, it can be seen that the figure is simply an inverse of the helium trends. Due to the linked relationship of the results, this set of data will be used to examine the initial details of the blowdown from a mass fraction perspective as was done with the pressure.

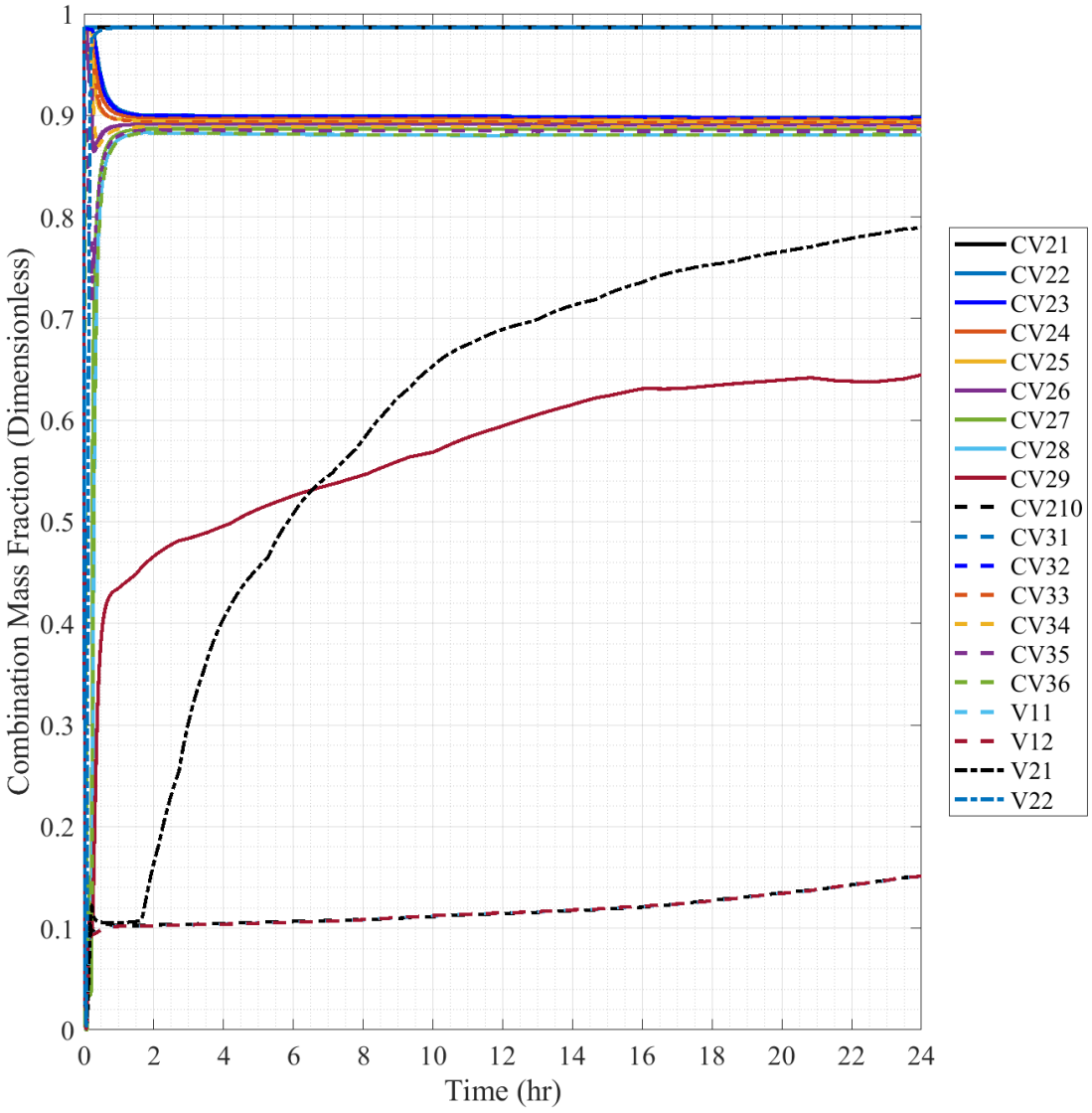

Fig. 6.97. Full-Scale Scenario 2 Combination Mass Fraction.

Fig. 6.98 reduces in the timescale of the combination mass fraction to get details of the initial post-break building response to the spreading helium. This scenario, much like what was seen with the 1/28th-scale results, produces unique movement throughout the volumes of the model. As discussed in helium results, a majority of volumes collapse and move into the striated banding structure at ~90%. To get a better look at the initial details of the blowdown the timescale needs to be dropped as there are a number of interesting transients underway in that period.

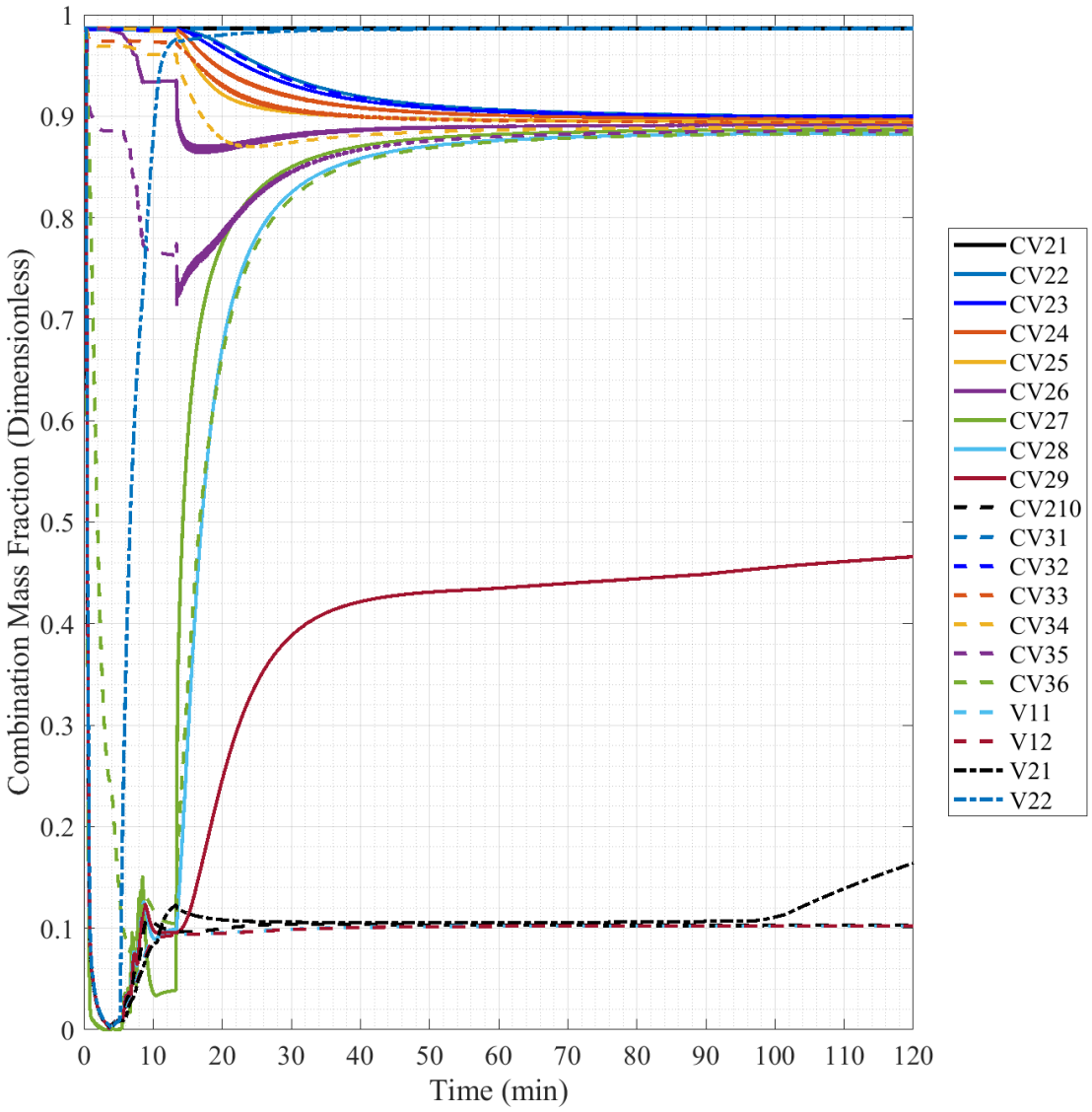

Fig. 6.98. Full-Scale Scenario 2 Combination Mass Fraction, 120 minute Timescale.

Reducing the timescale down to the first 20 minutes of the scenario, Fig. 6.99 allows us to see a number of interesting mechanisms as this layout begins to refill. Volumes situated above the break, CV27-210 and V11-22, spike down with the blowdown as they are voided of air but other volumes stay relatively filled as they are not in direct flowpaths. V22 begins its spike back up as air begins to refill it at ~5 minutes, refilling over the next ~10 minutes. As V22 refills, many of the volumes that were voided experience similar rises in air content in spikes over the following ~5 minutes, and settle in a ~10% range of air content.

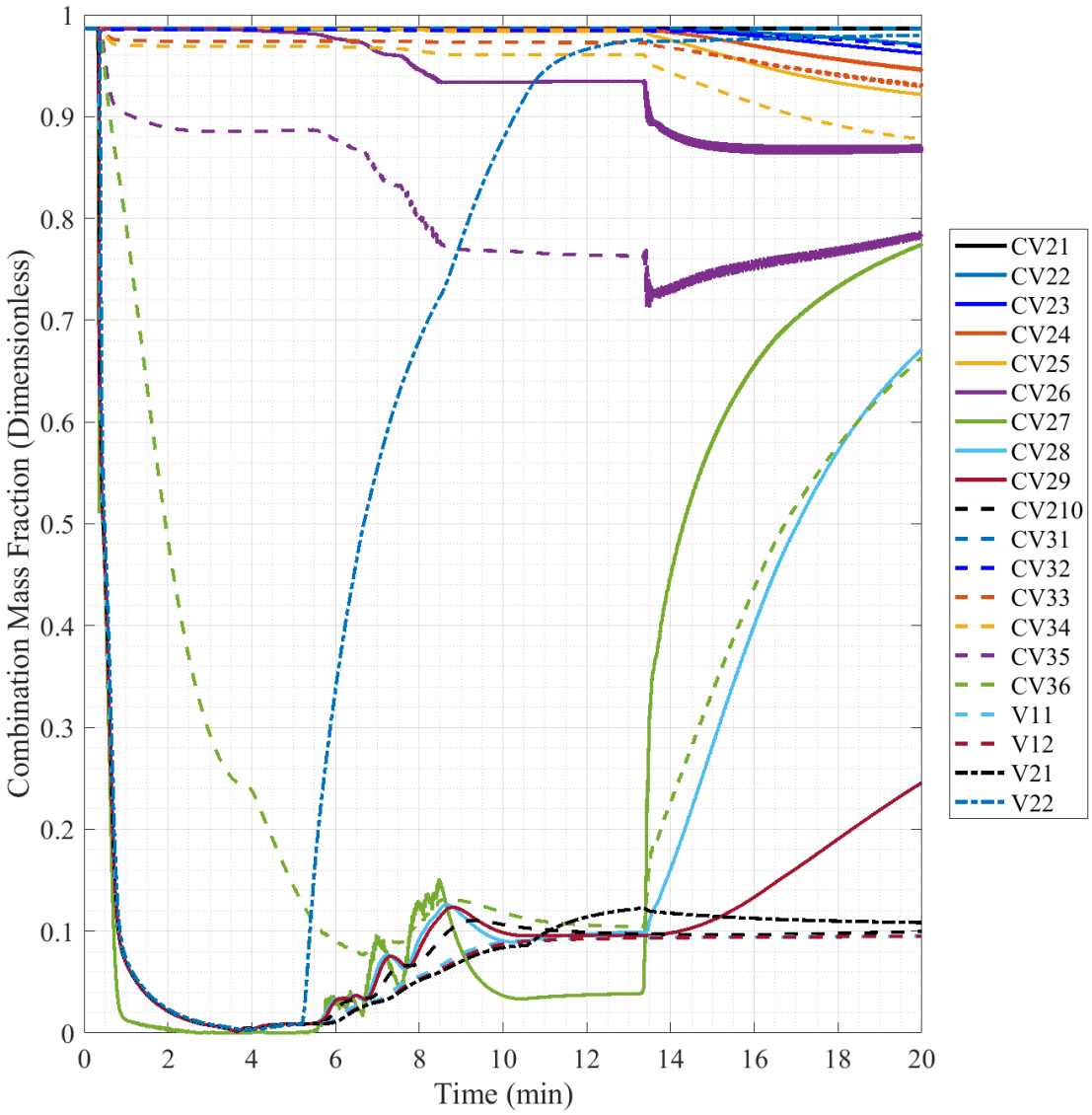

Fig. 6.99. Full-Scale Scenario 2 Combination Mass Fraction, 20 minute Timescale.

The final major detail that can be determined by this plot is that at ~13.5 minutes the air concentration of CV27 spikes severely, rising ~70% in under 5 minutes. This coincides with similar severe changes in CV26 and CV35, which undergo severe oscillations as seen in the smaller scale but then continue oscillations as they rise into the striated bandings, which can also be seen in Fig. 6.98. This event seems to occur at the rough approximation of the period of pressure equalization of the model following the initial pressure decrease and subsequent rise which can be

seen in Fig. 6.91. This possibily could be attributed due to the smaller volumes being in close proximity to larger one undergoing redistribution.

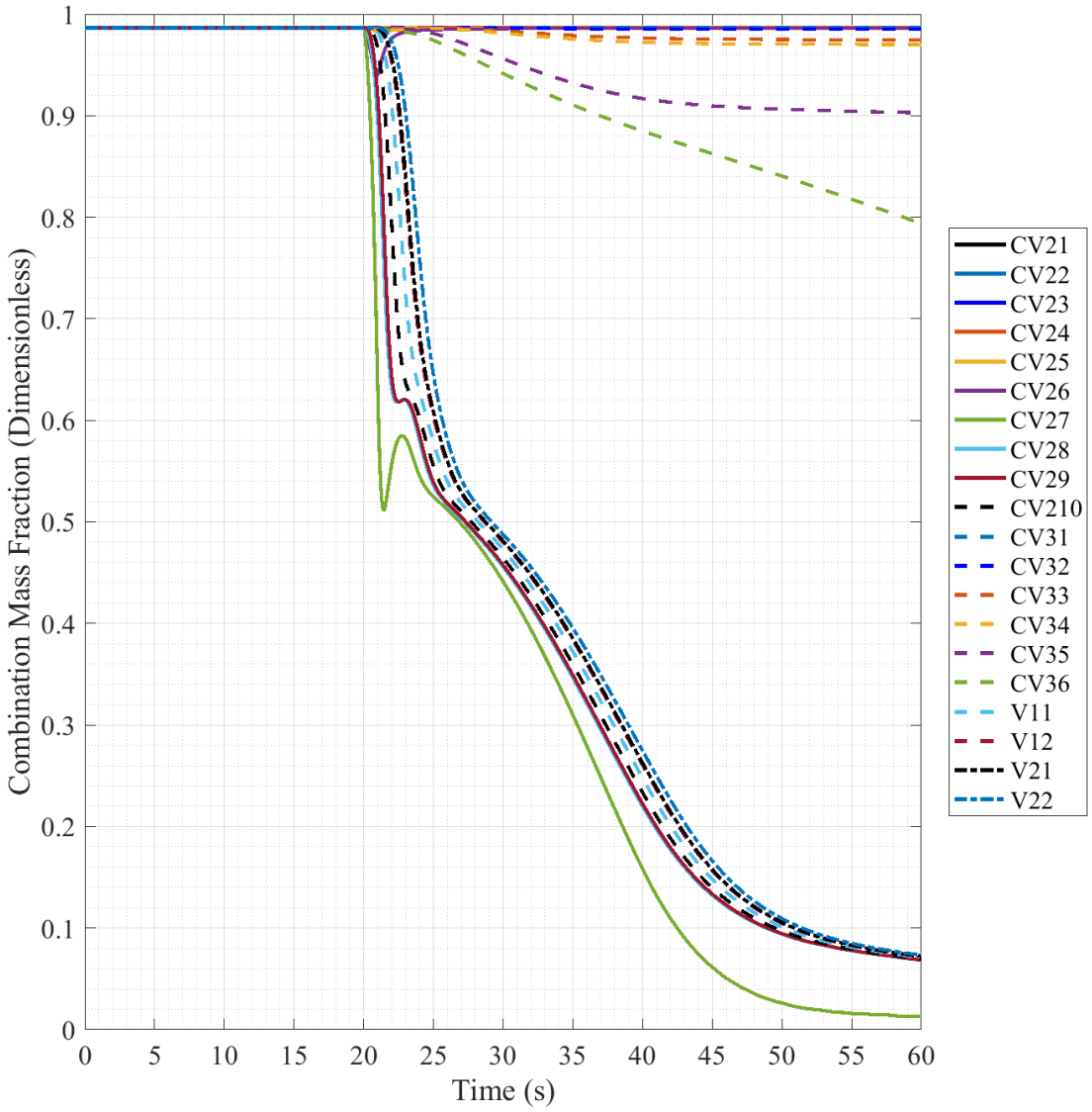

Fig. 6.100. Full-Scale Scenario 2 Combination Mass Fraction, 60 second Timescale.

Fig. 6.100 reduces the timescale even further to the first 60 seconds of the scenario to get the fine details of the initial voiding of the model. For the first second of the blowdown, the displacement of volume air is steady, but at ~21 seconds CV27 experiences a spike in air content that changes the subsequent rate of voiding in the period following it. This spike in air content can be seen to a lesser extent in CV28-29, which undergoes a lesser, but coordinated spike with CV27

before falling. CV27 then seems to dictate the minimum air mass fraction before all the voiding volumes continue to be voided over the remaining time of this scale. Following this period of time these volumes continue decreasing, reaching a near completely voided state at ~3.5 minutes, which can best be seen in Fig. 6.99.

6.2.4 Full-Scale Scenario 3 Results

Scenario 3 is a RPV break scenario with the EQS closed to flow from the blowdown from entering by closing the duct connections at their flow paths from the SGC. This forces the blowdown gases and atmosphere to rise through the center of the SGC, around the SGV and through the flow restrictive divider plates. For this scenario any volumes from the EQS (CV31-36) will be omitted from plotted results as they undergo no changes during the scenario. A visual example of this scenario's estimated progression can be seen in the $1/28^{th}$-scale results section of this scenario, Fig. 6.36.

The initial pressure plot of scenario 3, with the pressure plotted across the full timescale, has been omitted as it simply is a shows the same information as the initial scenario 1 plot, with the initial 6.4 MPa pressure of the helium volume and the resulting vertical scale of the plot blownout because of it. Nowhere along the full timescale of the pressure results were any new transients observed. The full timescale plot has been included in Appendix E for reference to the actual data plot, but Fig. 6.77 can be used as a quick reference as it shows a similar plot, excluding the removed volumes from this scenario.

After reducing the timescale of the pressure plot to 240 minutes, like in scenario 1, the resulting plot was extremely similar to the plot made for that scenario. The initial helium pressure of 6.4 MPa can be seen at the initial time, then at 20 seconds the pressure begins to fall at an exponential rate as the break flow path is opened and helium expands out and into the RC volumes. The HV reaches an equalized pressure of ~100 kPa at ~129.4 minutes following the blowdown initiation, ~129.7 minutes post simulation initiation. Overall, the progression of the pressure blowdown from the helium volumes seems to have not been affected by the change in the model layout. The plot of this pressure timescale for this scenario has been included in Appendix E for

further reference, or Fig. 6.78 can be used as a quick reference to the progression of the helium volume blowdown, excluding the removed volumes from this scenario.

Fig. 6.101. gives a first look at the reactor building volume response to the helium release into its volumes for scenario 3. Much like what was seen in scenario 1, post pressure spike the reactor volumes enter a decreased pressure state that slowly returns back to ~100 kPa in roughly the timeframe of an hour, where the pressures plateau. At this current timescale information about the pressure spike is hard to determine so the timescale must be reduced further.

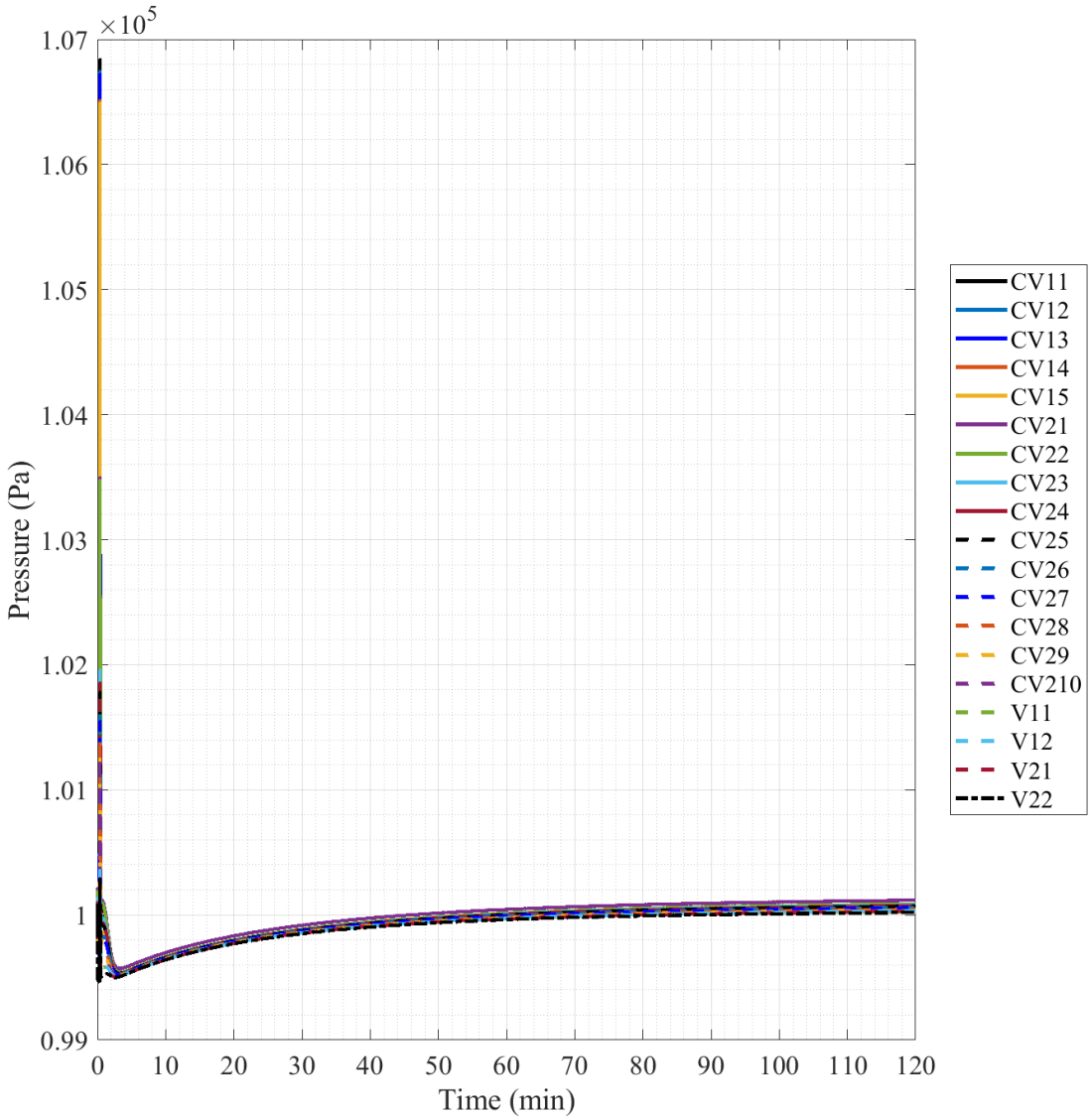

Fig. 6.101. Full-Scale Scenario 3 Pressure, 120 minute Timescale.

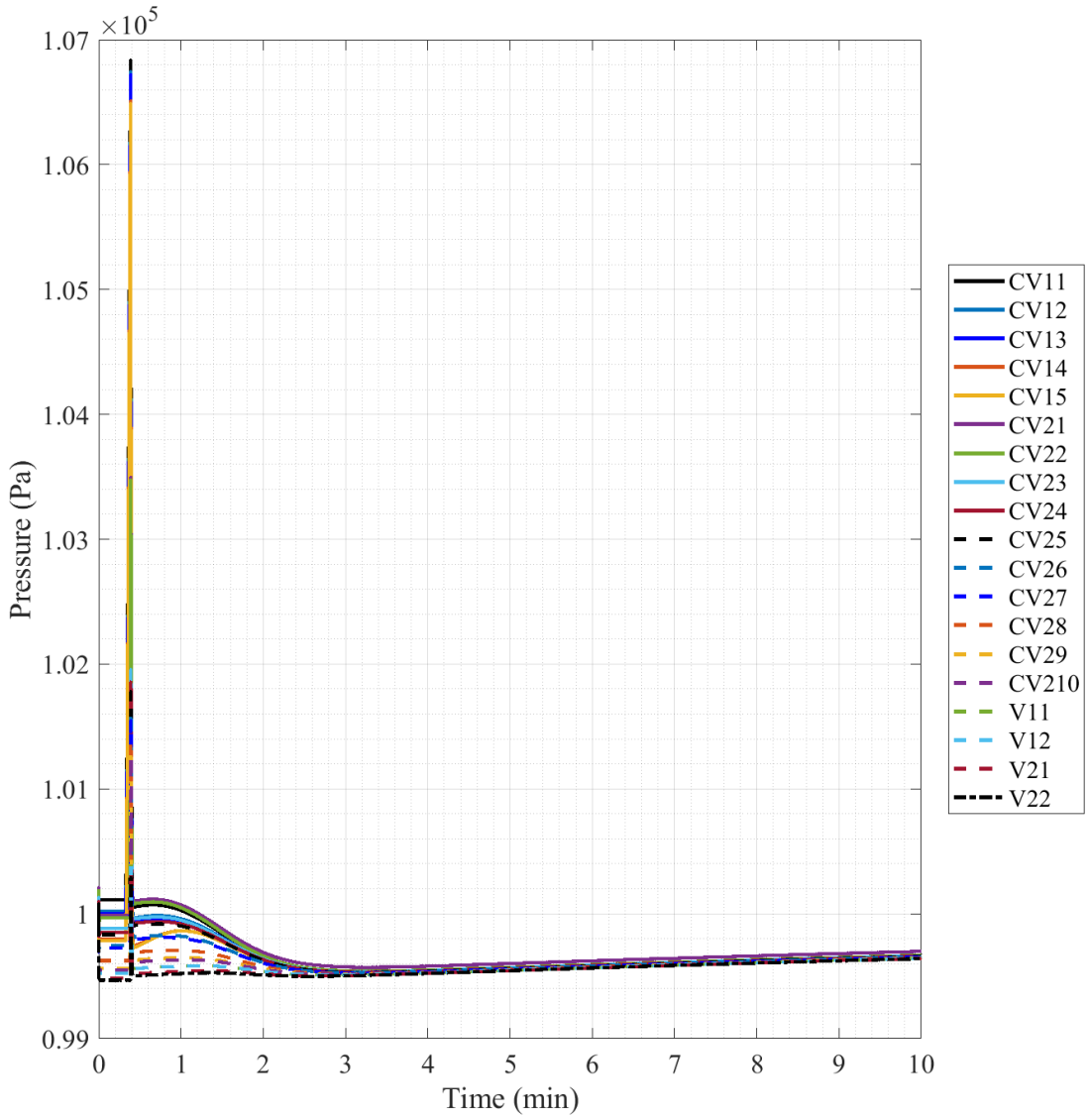

Fig. 6.102. Full-Scale Scenario 3 Pressure, 10 minute Timeframe.

Reducing the timeframe to the initial 10 minutes, Fig. 6.102. shows the initial pressure separation of the volumes as they naturally redistribute at the beginning of the simulation, which can be seen by the initial vertical movement at time zero, which come to rest at steady state pressures. The spike in this scenario is difficult to determine at this timescale. Post pressure spike, volumes come back to a separated range of pressures as they were before as seen in scenario 1, but as the model progresses more minutes the range of pressure values begin to collapse into pressure banding seen previously in Fig. 6.101 that comes back to roughly atmospheric pressure. The

primary difference in this scenario and scenario 1 is that the post-spike wide pressure banding that was similar to pre-break pressure banding collapses much faster into the tight pressure banding, in the matter of roughly 3 minutes in comparison to 5 minutes, which can be seen in Fig. 6.80.

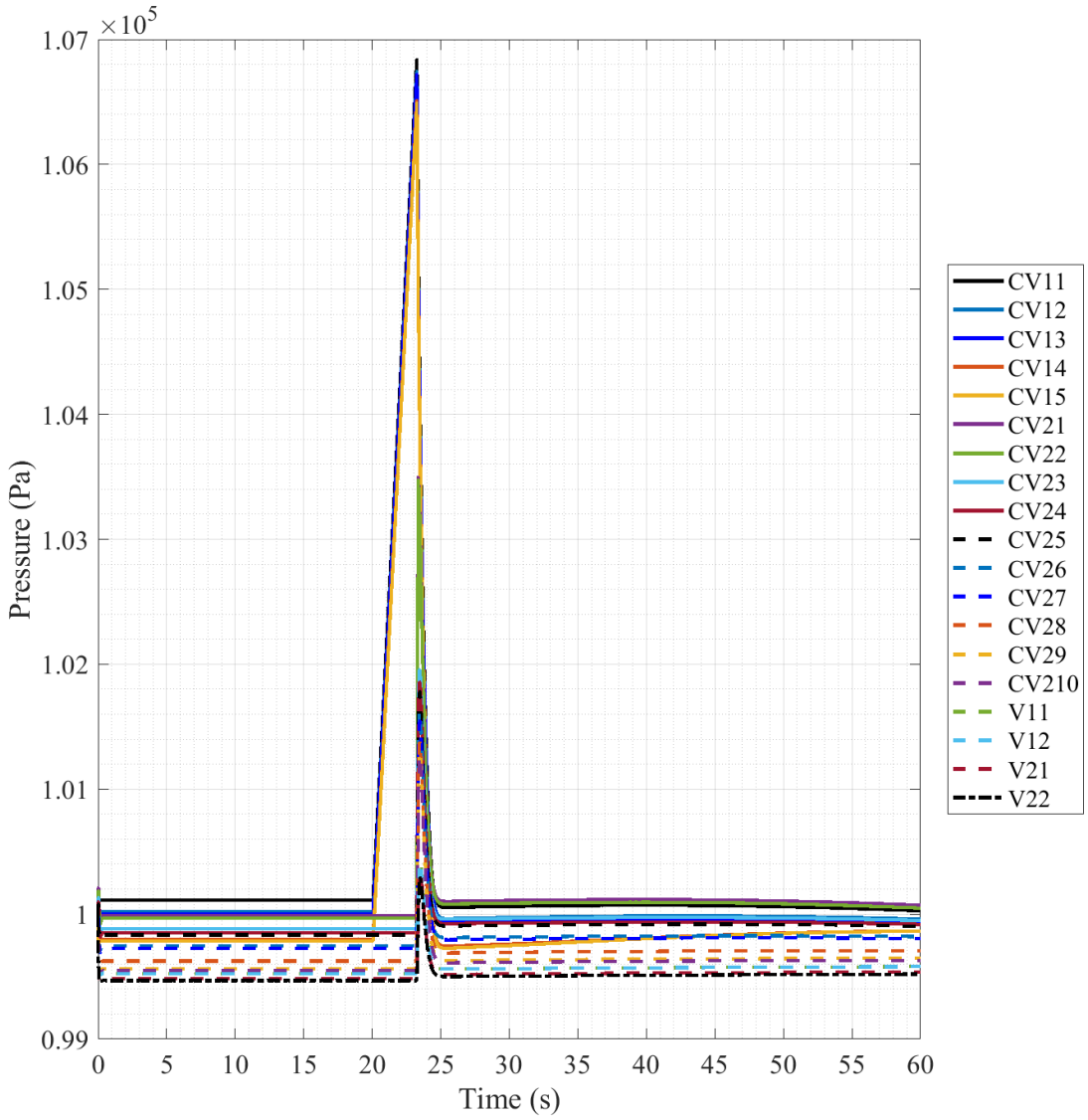

Fig. 6.103. Full-Scale Scenario 3 Pressure, 60 second Timescale.

Reducing the timescale further to the 60 seconds post simulation start, Fig. 6.103 gives information about the initial scenario timeframe. At the onset, the initial pressure banding movement can be seen where they naturally move from their initial positions to the steady state positions as discussed previously. The pressure spike comes into better view, with the initial spike

occurring at the set 20 seconds and the following spike as the blowout panel actuates ~3 seconds later. Most volumes seem to keep their relative location in the post spike pressure banding.

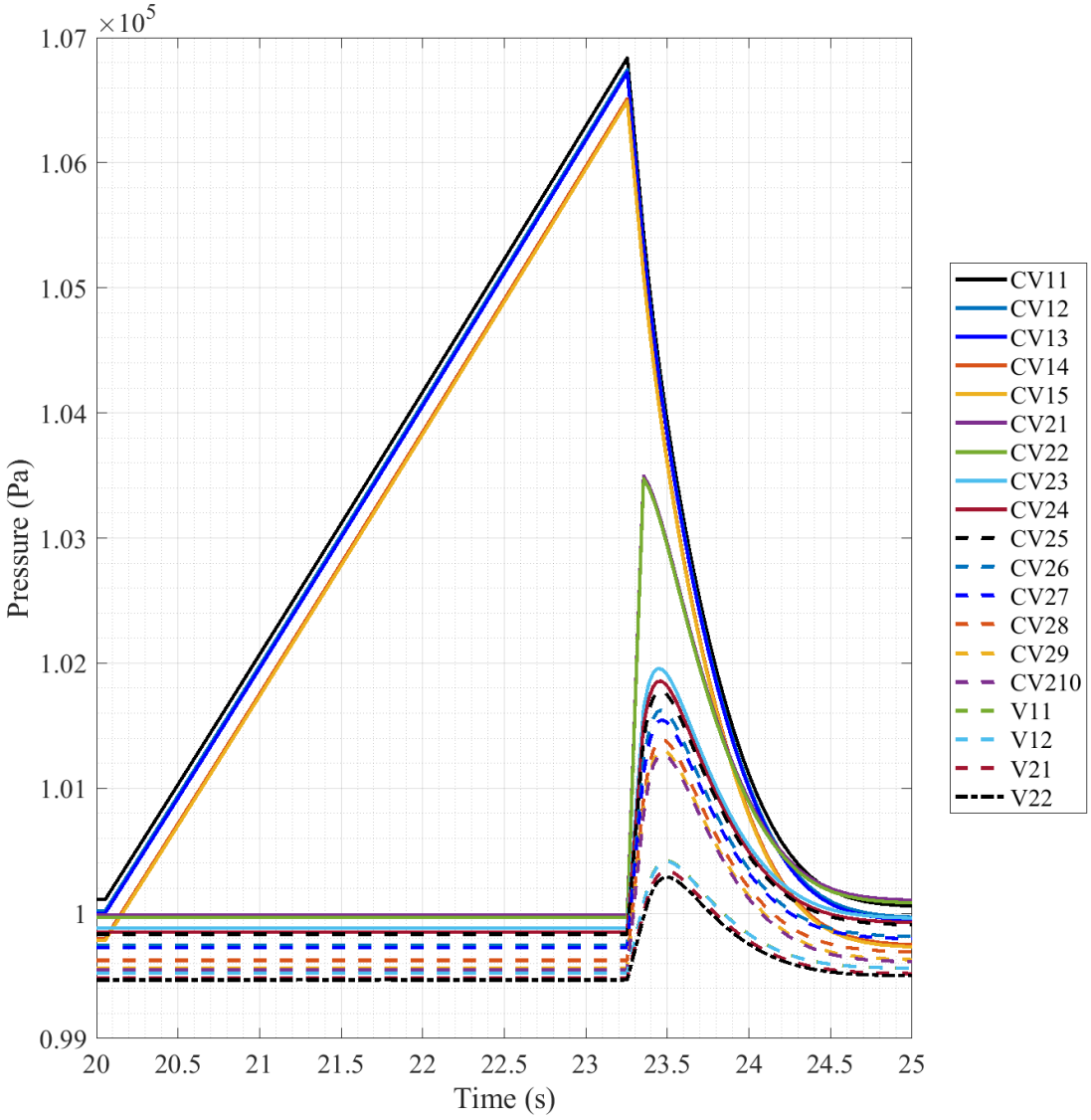

Fig. 6.104. Full-Scale Scenario 3 Pressure, 5 second Timescale, Post Break.

Reducing the timeframe in even more, Fig. 6.104 shows the 5 seconds post-break initiation of the model. With this, the linear rise of the CV11-15 (RC) volumes can be seen as pressure builds up behind the blowout panel, reaching a maximum of 1.0684×10^5 Pa (6.84 kPa increase) as it did in scenario 1. Pressure is built up for ~3.25 seconds before the blowout panel actuates and the pressure in the RC volumes falls quickly, causing a rise in the other volumes of the reactor building

in three distinct groups. The upper central transient of volumes consists of CV21-22 and spikes to a pressure around ~$1.035x10^5$ Pa (~3.5 kPa increase). The lower central transient of volumes consists of CV23-210 and spikes to a pressure range around ~$1.016x10^5$ Pa (~1.6 kPa increase) with a maximum of $1.02x10^5$ Pa (~2.0 kPa increase). The bottom transient group consists of the vent space volumes of V11-22 (Vent Space) which spike to a pressure of only $1.004x10^5$ Pa (~400 Pa increase) before falling back to the banded pressures. All transient groups rise to their maximum pressure but then fall back into the pressure banding they roughly experienced before. Of interest is that CV11-15, CV23-210, and V11-22 maintain the same pressure spike maximums, but the lower SGC volumes, CV21-22, undergo a raised pressure maximum, most likely due to the removal of the EQS shaft from the expansion pathway and a resulting buildup of pressure in the lower SGC cavity before it begins to move up through the central SGC cavity as the lower plate divider is limited in area.

Mass fraction data of scenario 3 starts off with the presentation of the helium mass fraction plot, presented in Fig. 6.105. The singular major transient group of this scenario is composed of V21 and V22, showing their joint relationship that was seen in scenario 1. V22 initially spikes with the break to ~88% but then falls to ~0% in ~2 hours where V21 begins its transient. V21s transient curves to an almost plateau until at ~6 hours, where it steeply drops for the rest of the scenario period to ~28%. On the opposite end of the scale, CV21 stays relatively close to 0% for a majority of the scenario with an increase of ~1% over the time period like in scenario 1. All other volumes, CV11-15, CV22-210, and V11-12, spike to near 100% with the blowdown, but CV11 and CV22 fall by 2% over the time period. All other volumes remaining at ~100% over the full period of the scenario. Getting a better look at the early time period will require a smaller timescale that will be explored in later plotted results.

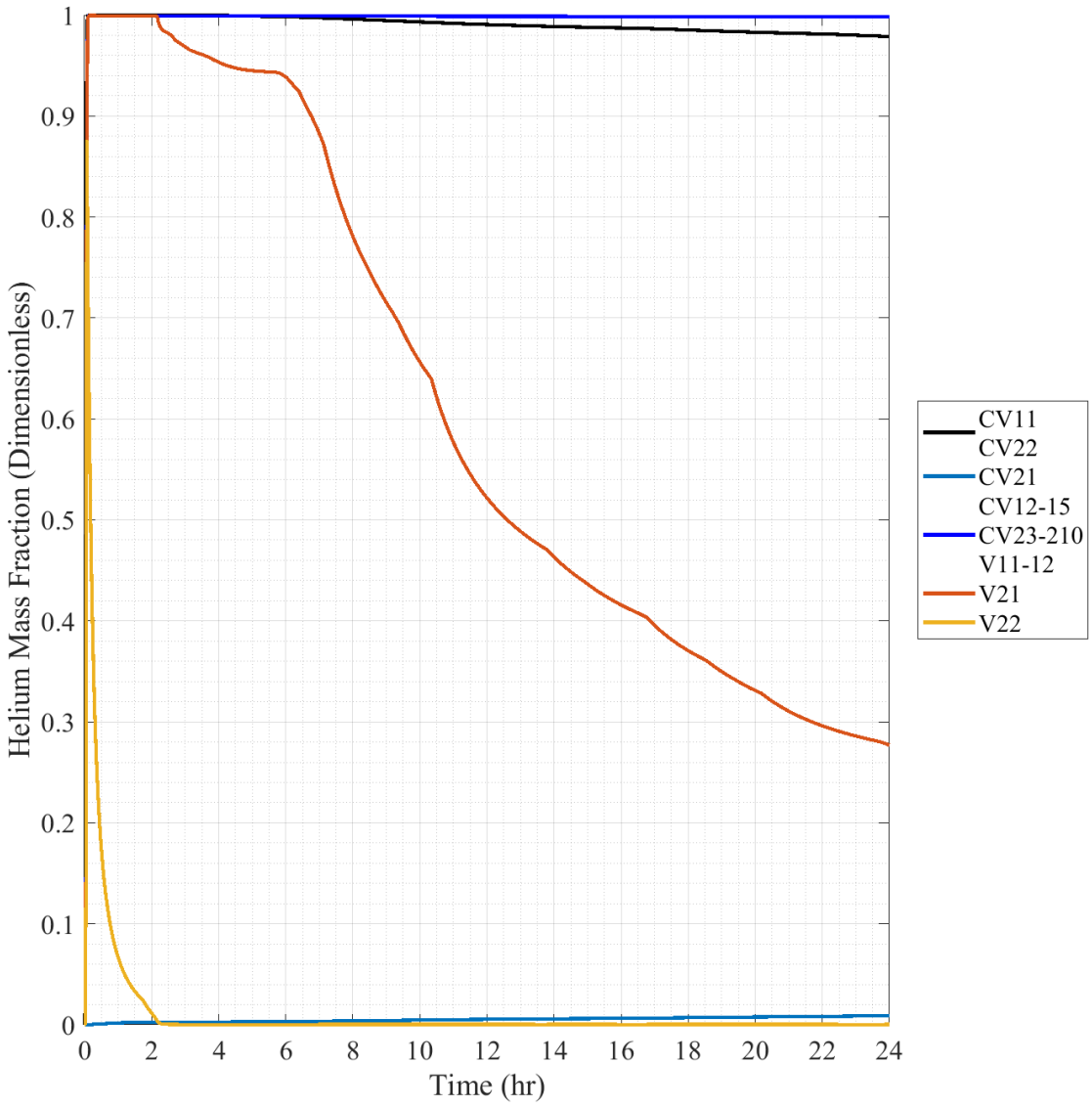

Fig. 6.105. Full-Scale Scenario 3 Helium Mass Fraction.

In order to maintain a concise description of scenarios, the plots of oxygen and nitrogen mass fraction are not presented in this scenario as their results are reaffirmed best by a combination of their results to approximate a near full mass fraction of standard air. As was seen in scenario 1, oxygen and nitrogen mass fractions showed inverse results of the helium mass fraction and were simply differentiated by the resulting scale differences in the gas mass fractions. Plotted results for both the oxygen and nitrogen mass fraction can be found in Appendix E for further reference but are left out of this scenario to be concise.

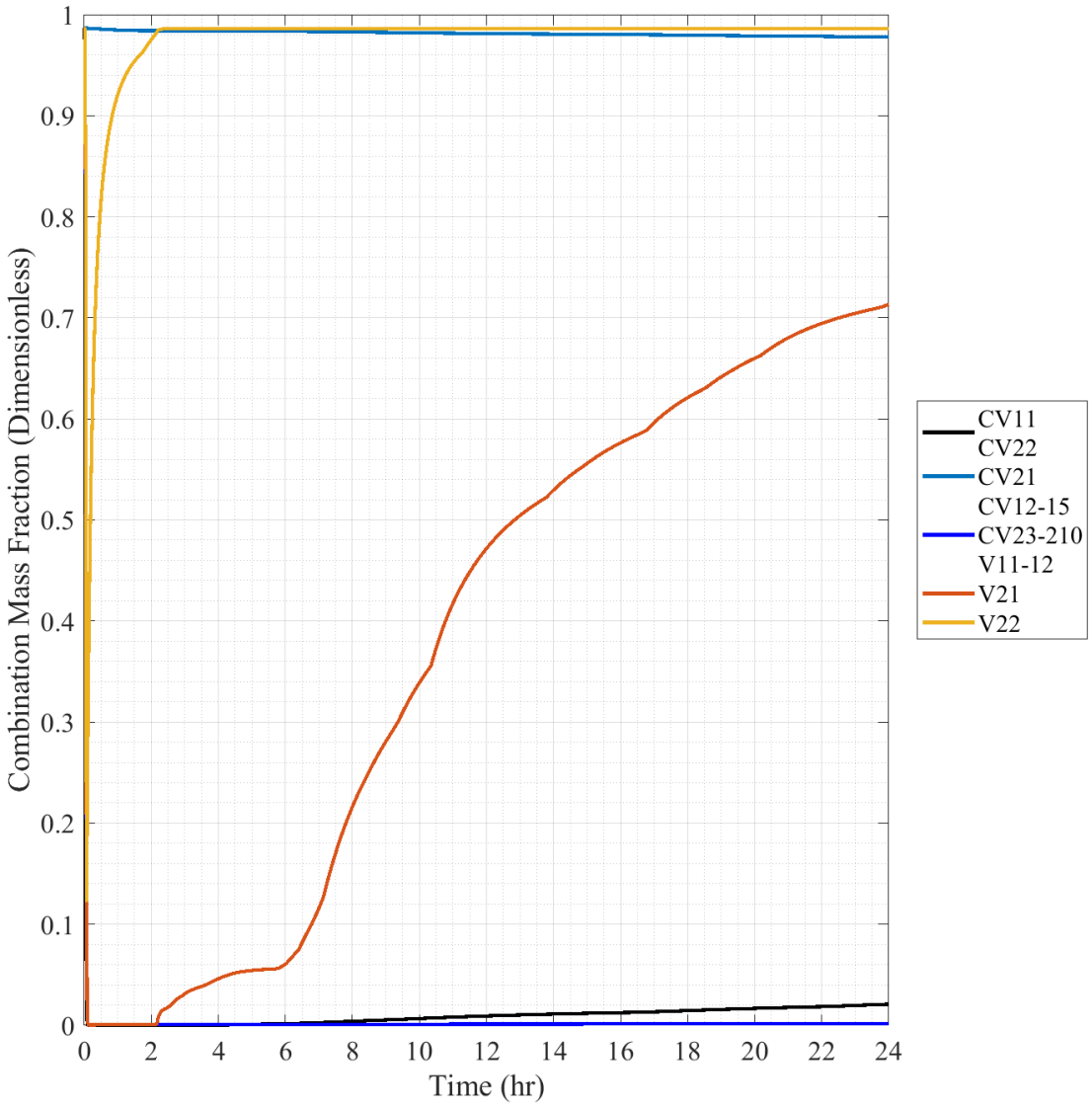

Fig. 6.106. Full-Scale Scenario 3 Combination Mass Fraction.

Fig. 6.106 sums the oxygen and nitrogen mass fractions together as previously discussed to a "Combination" mass fraction composed of the combination of the two individual mass fractions. The combination of these two gases make up 98.66% of the total mass fraction of standard air and should be a good comparison to the helium mass fraction for comparisons. Finally, by comparison with Fig. 6.105, it can be seen that the figure is simply an inverse of the helium trends. Due to the linked relationship of the results, this set of data will be used to examine the initial details of the blowdown from a mass fraction perspective as was done with the pressure.

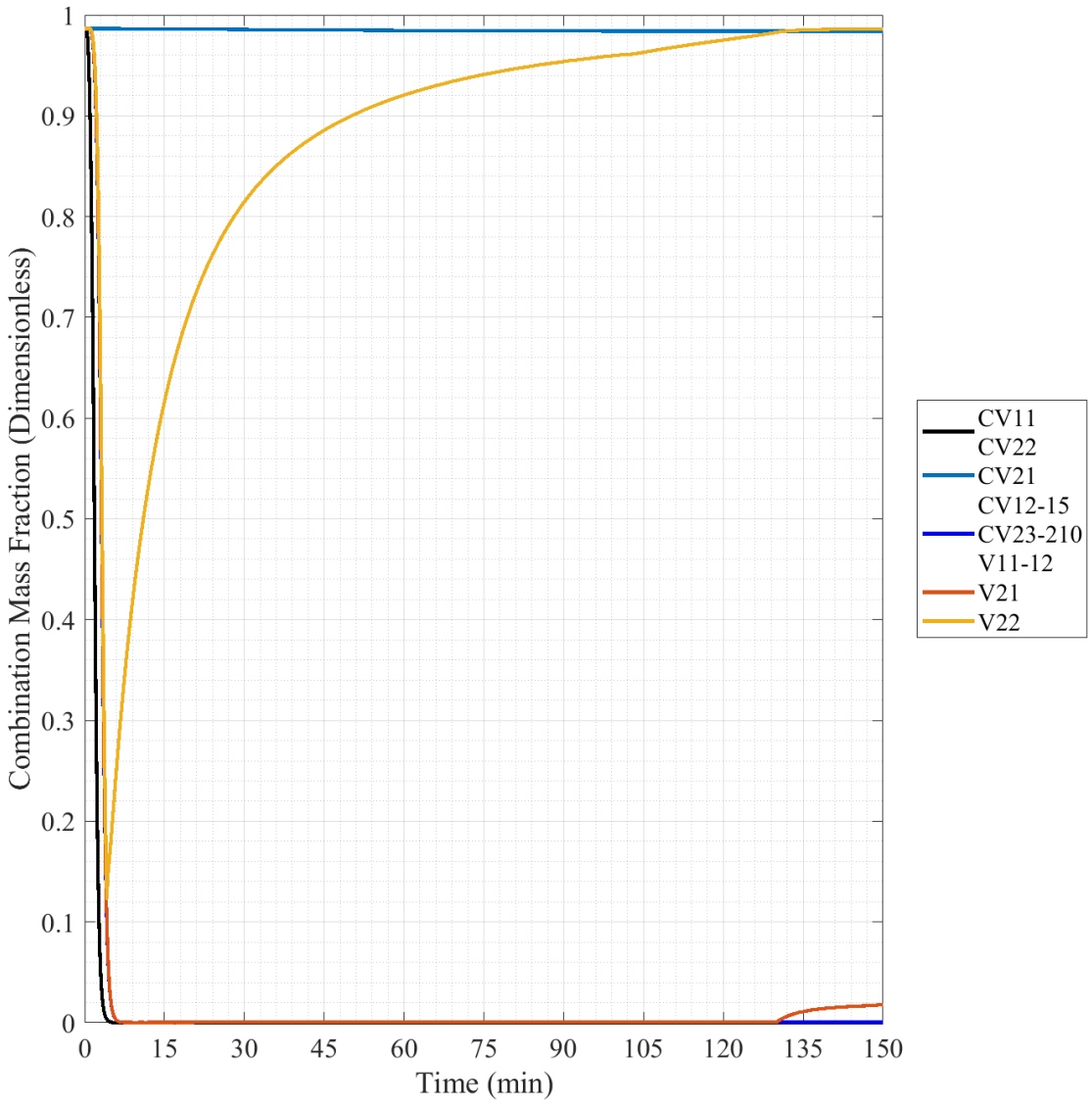

Fig. 6.107. Full-Scale Scenario 3 Combination Mass Fraction, 150 minute Timescale.

Fig. 6.107 reduces the timescale of the combination mass fraction to get details of the initial post-break building response to the spreading helium. Much of the displacement happens within the first ~5 minutes of the scenario. V22 can be seen to fall to only ~12% air content before refill begins and over the following 2 hours it fills back to ~100% normal air. At that point, V21 can be seen to refill as has been seen previously in scenarios. In comparison to scenario 1, no interruptions appear to take place in the voiding of volumes, but the smaller timescale will still be examined.

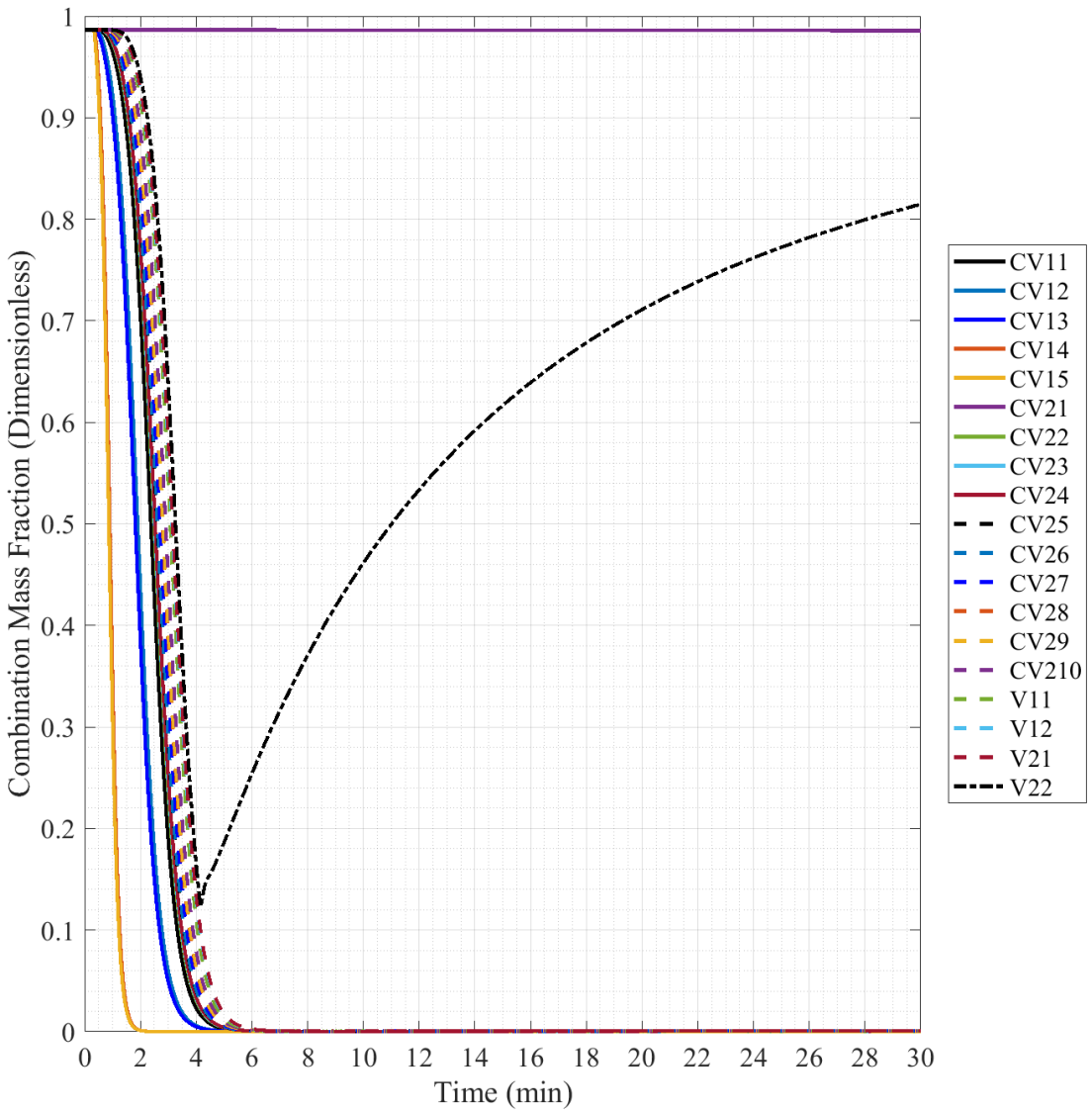

Fig. 6.108. Full-Scale Scenario 3 Combination Mass Fraction, 30 minute Timescale.

Fig. 6.108 reduces the timescale down to the first 30 minutes of the scenario to get the finer details of the volume voiding. As seen previously, V22 drops to ~34% at ~4 minutes, before rising in air concentration again. Volumes mostly progress from left to right in order of their path in the blowdown progression, with RC volumes on the left and vent space volumes on the right. In comparison to scenario 1, this scenario is much more stable in progression, as volumes cleanly void of their oxygen content. This may be a further indication of conflicting flow in scenario 1, as this scenario only has a singular path of progression through the volumes.

6.2.5 Full-Scale Scenario 4 Results

Scenario 4 is a SGV break scenario with the EQS closed to flow from the blowdown from entering by closing the duct connections at their flow paths from the SGC. This will force blowdown gases either directly to the vent space or down deeper into the SGC. For this scenario any volumes from the EQS (CV31-36) and the RC (CV1-15) will be omitted from plotted results as they undergo no changes during the scenario. A visual example of this scenario's estimated progression can be seen in the 1/28th-scale results section of this scenario, Fig. 6.45.

The initial pressure plot of scenario 4, with the pressure plotted across the full timescale, has been omitted as it simply is a shows the same information as the initial scenario 2 plot, with the initial 6.4 MPa pressure of the helium volume and the resulting vertical scale of the plot blownout because of it. Nowhere along the full timescale of the pressure results were any new transients observed. The full timescale plot has been included in Appendix E for reference to the actual data plot, but Fig. 6.89 can be used as a quick reference as it shows a similar plot, excluding the removed volumes from this scenario.

After reducing the timescale of the pressure plot to 20 minutes, like in scenario 2, the resulting plot was extremely similar to the plot made for that scenario. The initial helium pressure of 6.4 MPa can be seen well at the initial time, then at 20 seconds the pressure begins to fall at an exponential rate as the break flow path is opened and helium expands out and into the SGC volumes. The HV reaches an equalized pressure of ~100 kPa at ~10.21 minutes following the blowdown initiation, ~10.5 minutes post simulation initiation. Overall, the progression of the pressure blowdown from the helium volumes seems to have not been affected by the change in the model layout. The plot of this pressure timescale for this scenario has been included in Appendix

E for further reference, or Fig. 6.90 can be used as a quick reference to the progression of the helium volume blowdown, excluding the removed volumes from this scenario.

Fig. 6.109 gives a first look at the reactor building volume response to the helium release into its volumes for scenario 4. The timescale at this scale is still not enough to determine pressure spike information accurately. What can be determined from this figure is that post pressure spike the volumes enter an increased pressure band state that slowly plateaus to ~100.2 kPa in roughly the timeframe of ~12 minutes as was seen in scenario 2.

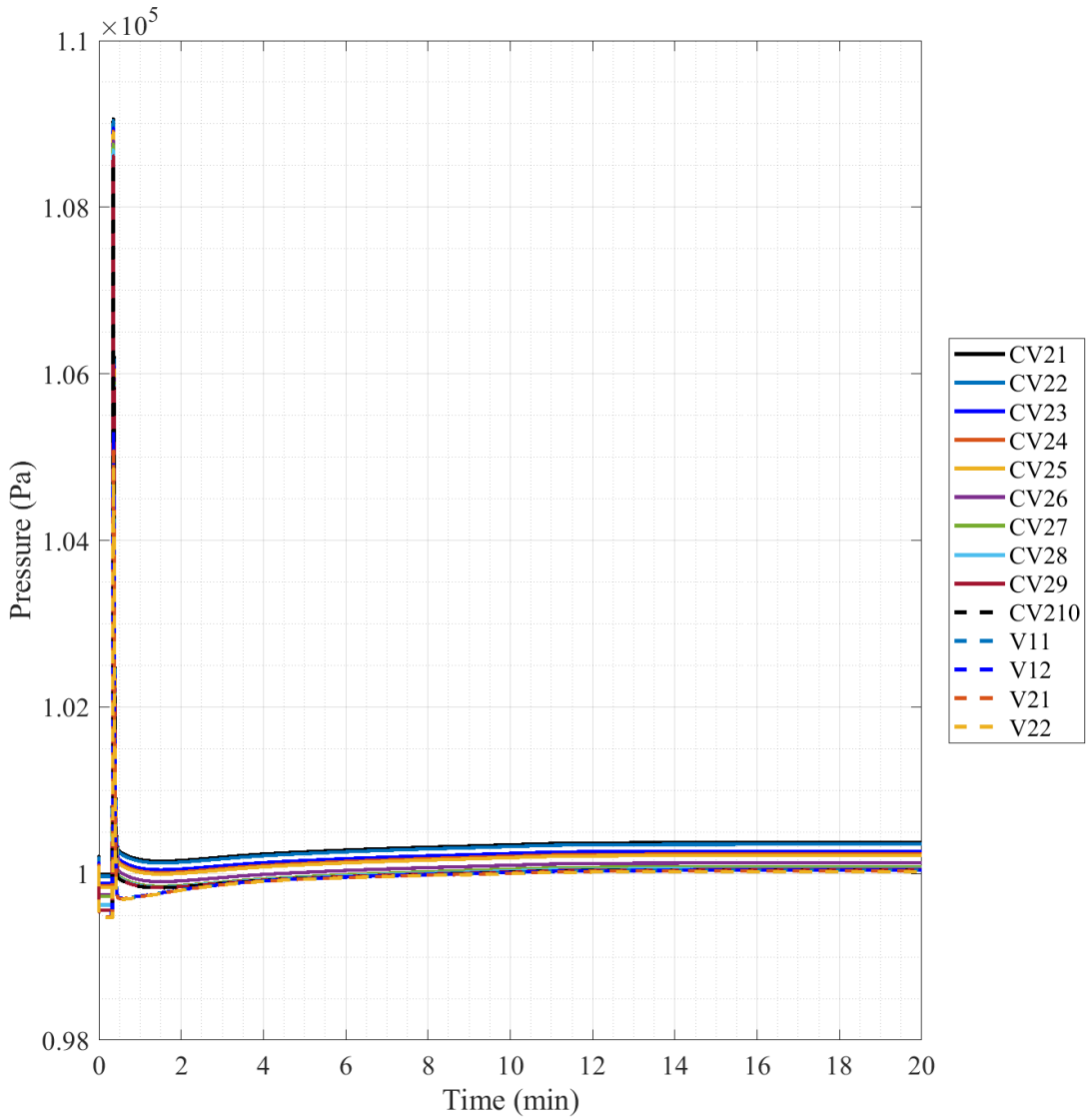

Fig. 6.109. Full-Scale Scenario 4 Pressure, 20 minute Timescale.

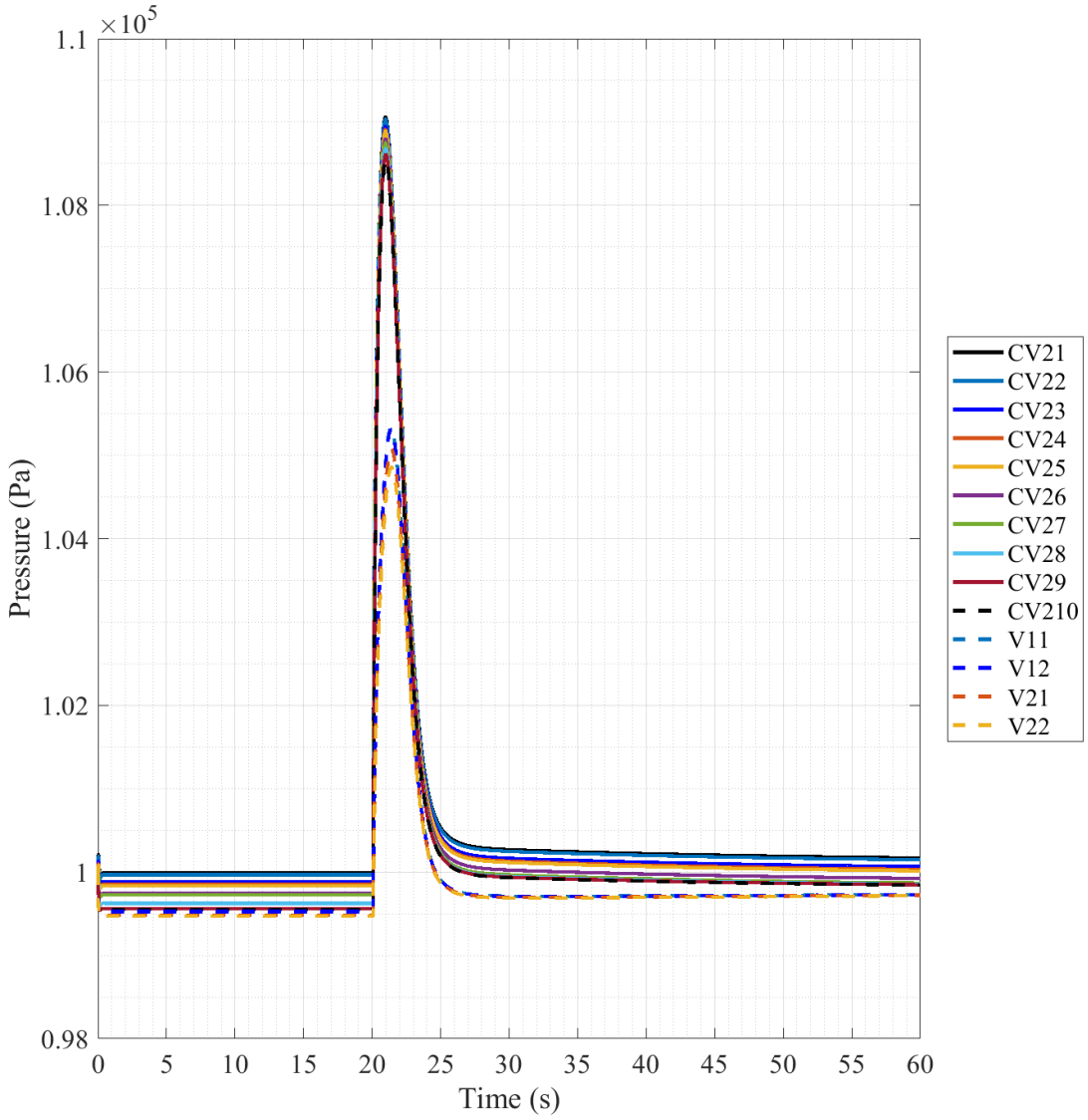

Fig. 6.110. Full-Scale Scenario 4 Pressure, 60 second Timescale.

Reducing the timescale to the 60 seconds post simulation start, Fig. 6.110 gives information about the initial scenario timeframe of scenario 4. At the onset, the initial pressure banding movement can be seen where volumes naturally move from their initial positions to the steady state positions as discussed previously. Since there is no blowout panel actuation in this scenario the pressure rise at the break initiation is analogous to being normally distributed. Following the pressure spike, the volumes settle back into a pressure band, but at a raised pressure from what they settled at pre-break, which can be seen in both Fig. 6.109 and 6.110.

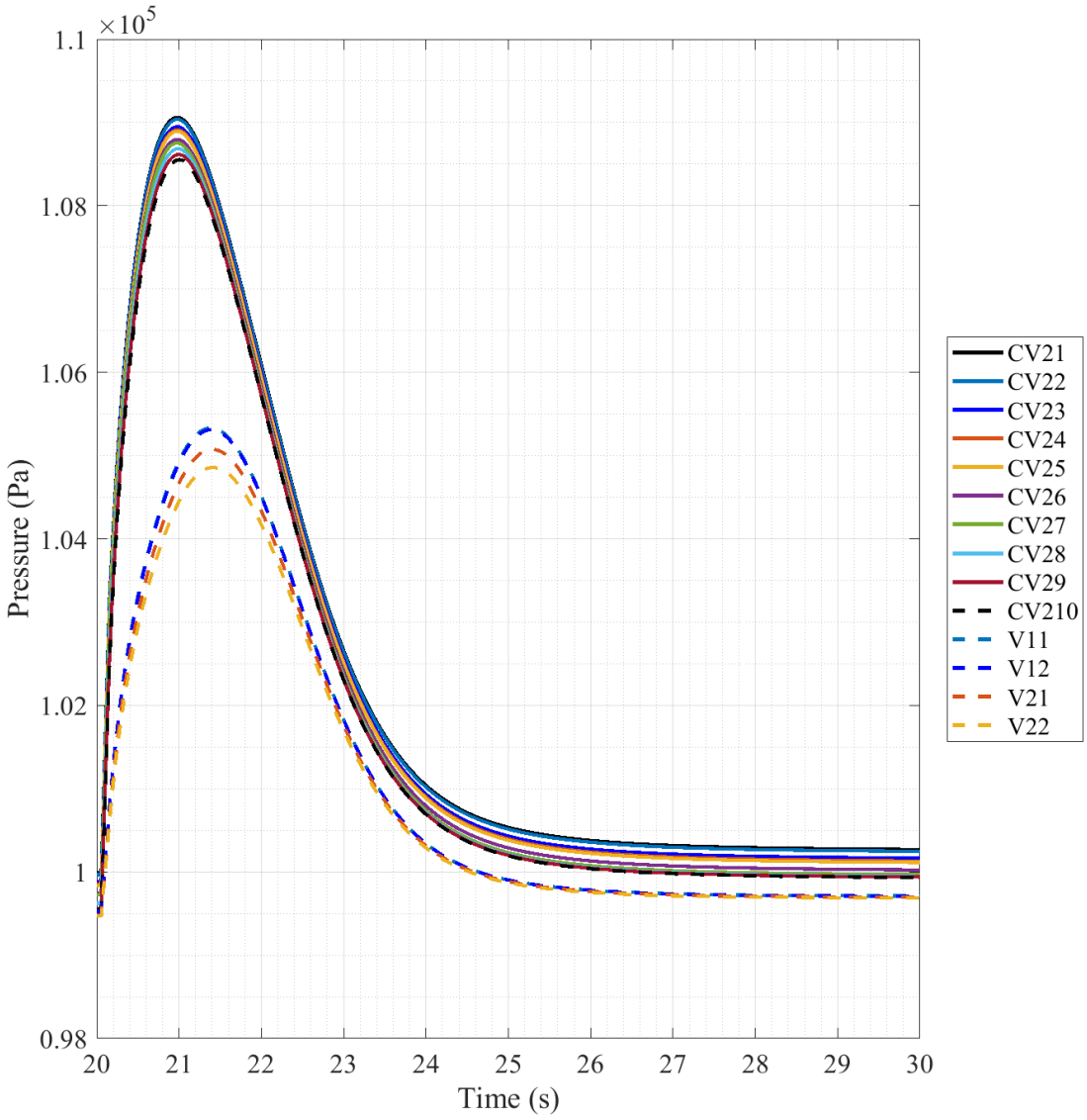

Fig. 6.111. Full-Scale Scenario 4 Pressure, 20-30 second Timescale.

Reducing the timeframe in even more, Fig. 6.111 shows the 10 seconds post-break initiation of the model. The upper transient of volumes consists of CV21-210 (SGC) where they spike to a pressure range centralized around ~1.089x10^5 Pa (~8.9 kPa increase) and a max of 1.091x10^5 Pa (9.1 kPa increase). The bottom transient group consists of the vent space volumes of V11-22 which spike to a pressure range of ~1.05x10^5 Pa (~5 kPa increase) with a max of ~1.053 x10^5 Pa (~5.3 kPa increase), before falling back to the banded pressures that come to join back together in the minute following the pressure spike. Overall, the response in this scenario is very

similar to scenario 1, but at a slightly higher-pressure response which is to be expected as the EQS is lost to pressure expansion and most of the blowdown progression goes straight to the vent space.

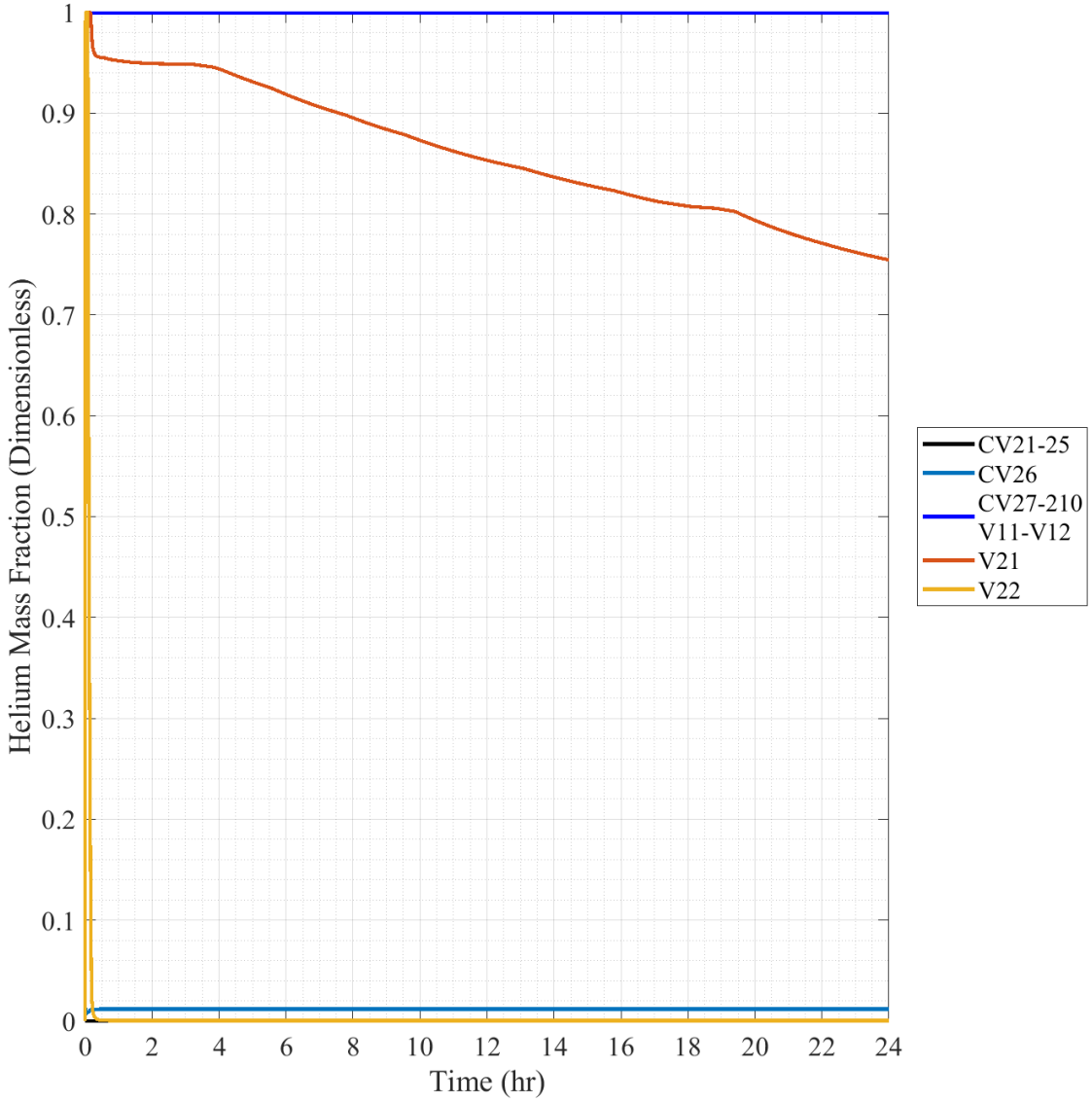

Fig. 6.112. Full-Scale Scenario 4 Helium Mass Fraction.

Mass fraction data of scenario 4 starts off with the presentation of the helium mass fraction plot, presented in Fig. 6.112. The singular major transient group of this scenario again is composed of V21 and V22, showing a different relationship than was seen in scenario 2. V22 initially spikes with the blowdown to ~100% but then falls to ~0% in ~15 minutes, where V21 begins its transient. V21's transient curves to an almost plateau until at ~4 hours where its slope changes and drops

quicker for the rest of the scenario period to ~76%. On the opposite end of the scale, CV21-25 experience a very slight increase introduction of helium on the scale of E-4 or less, mainly due to their location being lower than the break location. CV26 experiences a very slight increase to ~1% with the blowdown but it stays constant over the remaining scenario time period. All other volumes, CV27-210 and V11-12, spike to near 100% with the blowdown where they remain at ~100% over the full period of the scenario. Getting a better look at earlier time periods will require a smaller timescale that will be explored in later plotted results.

In order to maintain a concise description of scenarios, the plots of oxygen and nitrogen mass fraction are not presented in this scenario as their results are reaffirmed best by a combination of their results to approximate a near full mass fraction of standard air. As was seen in scenario 2, oxygen and nitrogen mass fractions showed inverse results of the helium mass fraction and were simply differentiated by the resulting scale differences in the gas mass fractions. Plotted results for both the oxygen and nitrogen mass fraction can be found in Appendix E for further reference but are left out of this scenario to be concise.

Fig. 6.113 sums the oxygen and nitrogen mass fractions together as previously discussed to a “Combination” mass fraction composed of the combination of the two individual mass fractions. The combination of these two gases make up 98.66% of the total mass fraction of standard air and should be a good comparison to the helium mass fraction for comparisons. Finally, by comparison with Fig. 6.112, it can be seen that the figure is simply an inverse of the helium trends. Due to the linked relationship of the results, this set of data will be used to examine the initial details of the blowdown from a mass fraction perspective as was done with the pressure.

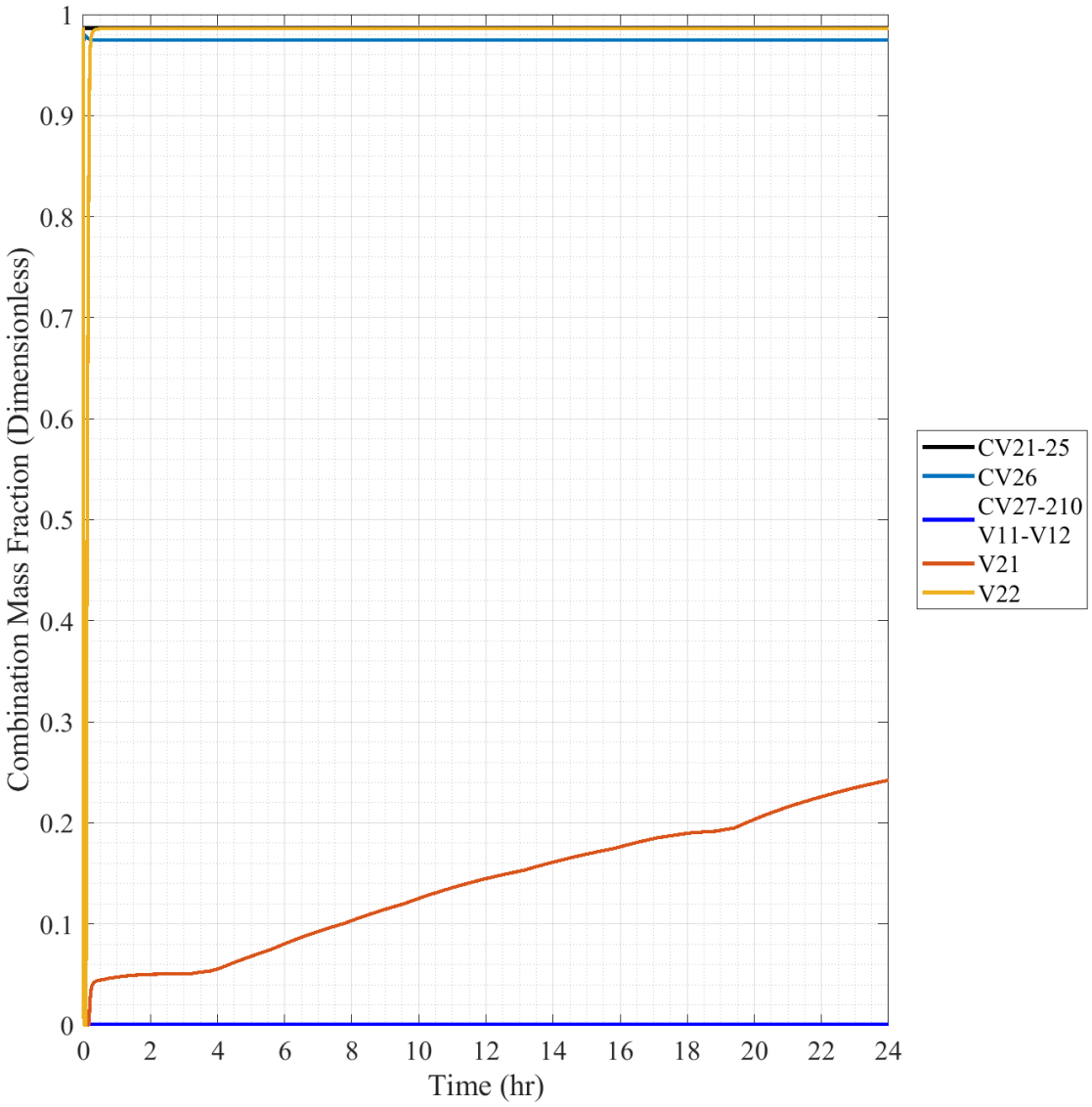

Fig. 6.113. Full-Scale Scenario 4 Combination Mass Fraction.

Fig. 6.114 reduces the timescale of the combination mass fraction to get details of the initial post-break building response to the spreading helium. At this timescale, not a great deal of information can be gathered as this scenario is much more stable than what was seen in scenario 2. It can be seen though that the connection between V22 and V21 seems to persist as has been seen in other scenario results, once V22 is near filled with normal air V21 begins to rise.

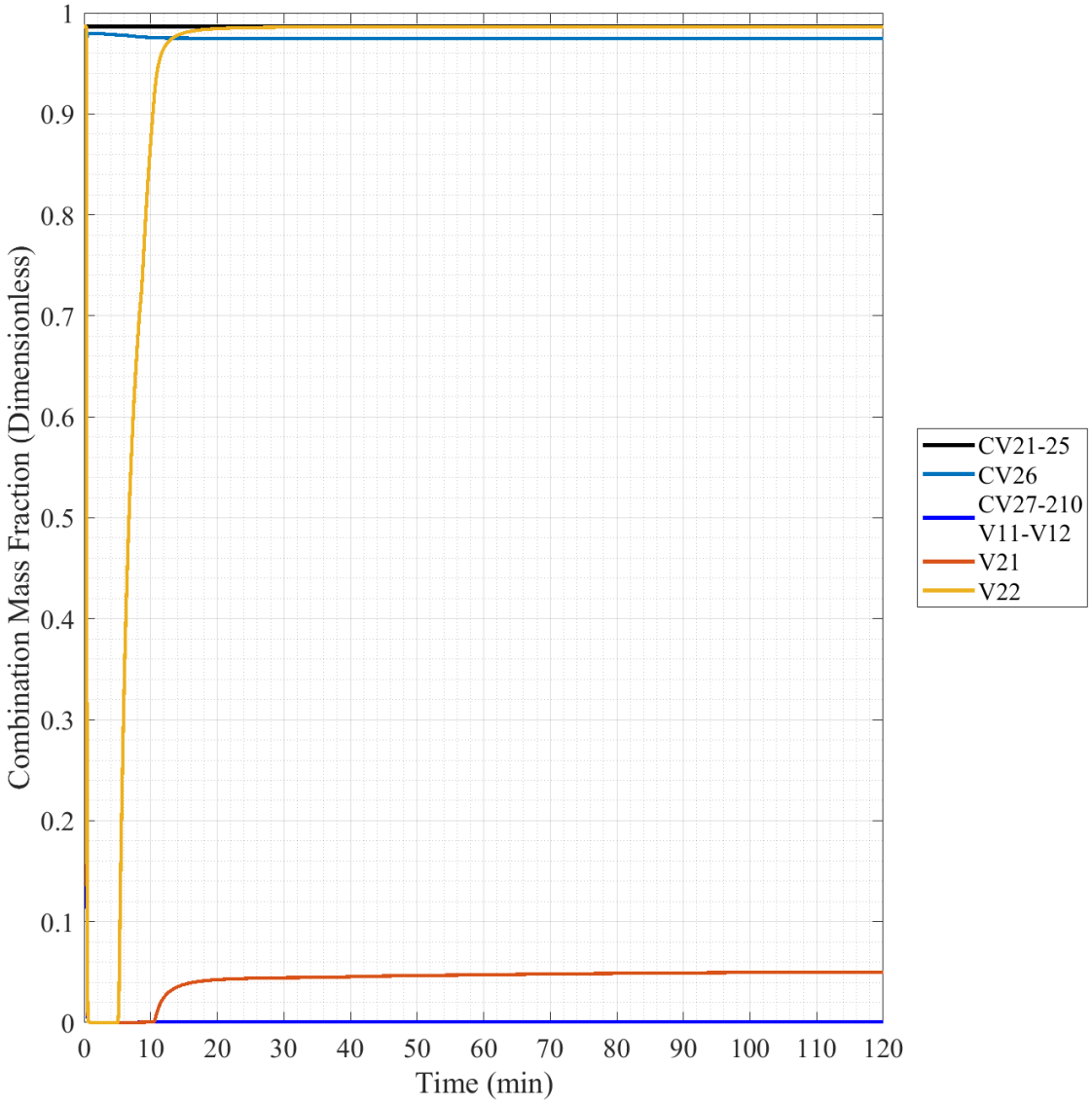

Fig. 6.114. Full-Scale Scenario 4 Combination Mass Fraction, 120 minute Timescale.

Fig. 6.115 reduces the timescale even further to the first 20 minutes of the scenario in an effort to gather more information on the initial blowdown. Much like the previous figure, V22 and V21 are the only changing transients of this figure, though CV26 can be seen with its slight mixture of helium near the top. V22 spikes down with the blowdown, then at ~5 minutes begins to rise coming to a near completely air-filled state ~10 minutes later. V21 begins its upward trend early in this model, rising at ~11 minutes and coming to a plateau relatively quickly at this timescale, which will persist through the first ~4 hours of the scenario, as seen in Fig. 6.113.

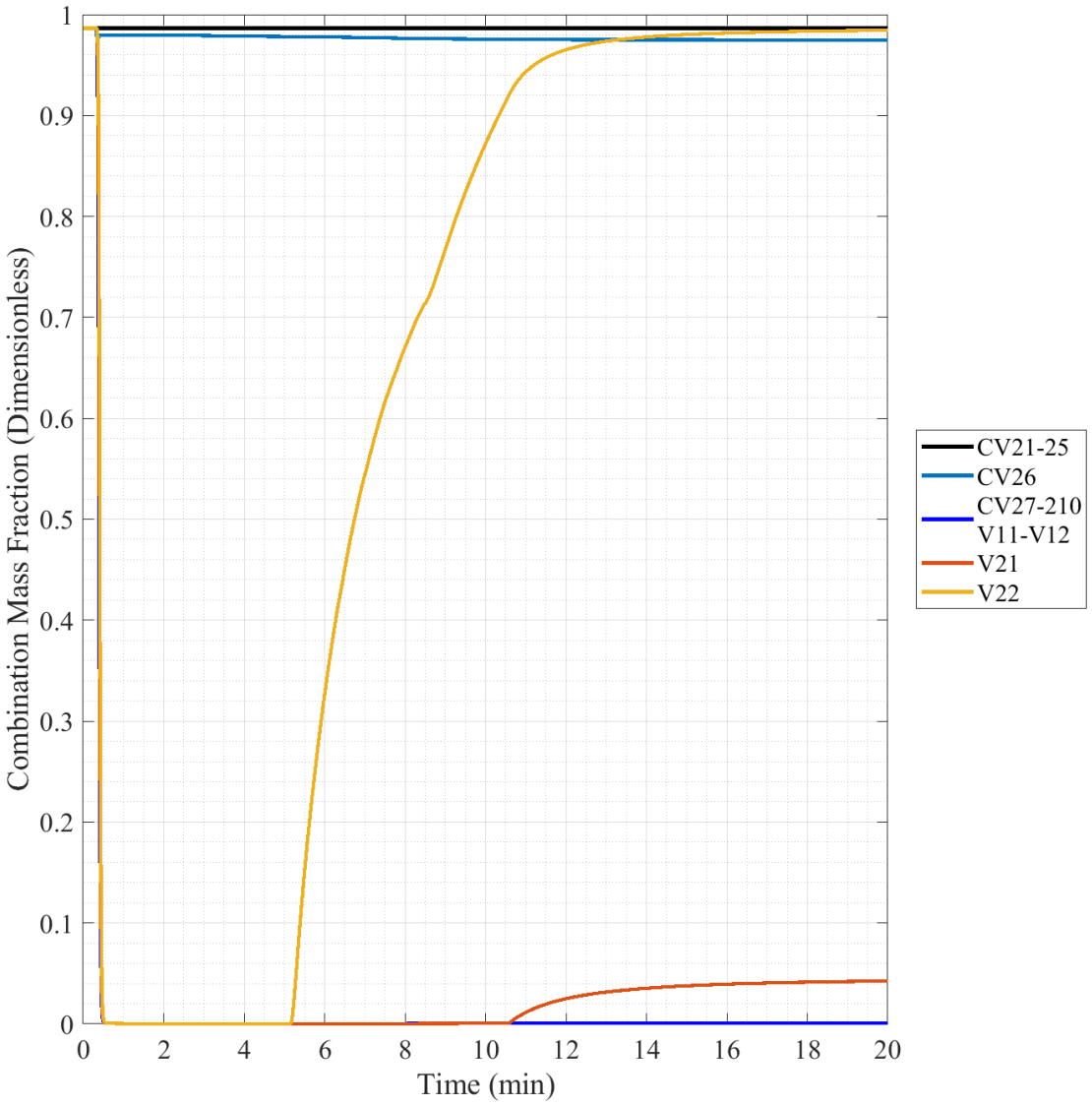

Fig. 6.115. Full-Scale Scenario 4 Combination Mass Fraction, 20 minute Timescale.

Fig. 6.116 reduces the timescale even further to the first 60 seconds of the scenario to gather information on the initial voiding of the volumes. In comparison to scenario 2, the voiding of this scenario is nearly uninterrupted. CV27 still undergoes a slight deviation off its initial decrease, but it does not change the overall voiding, which was seen in scenario 2. All other voiding volumes, CV28-210 and V11-22, continue on their stable voiding rate and they void in the period of ~10 seconds following the break initiation.

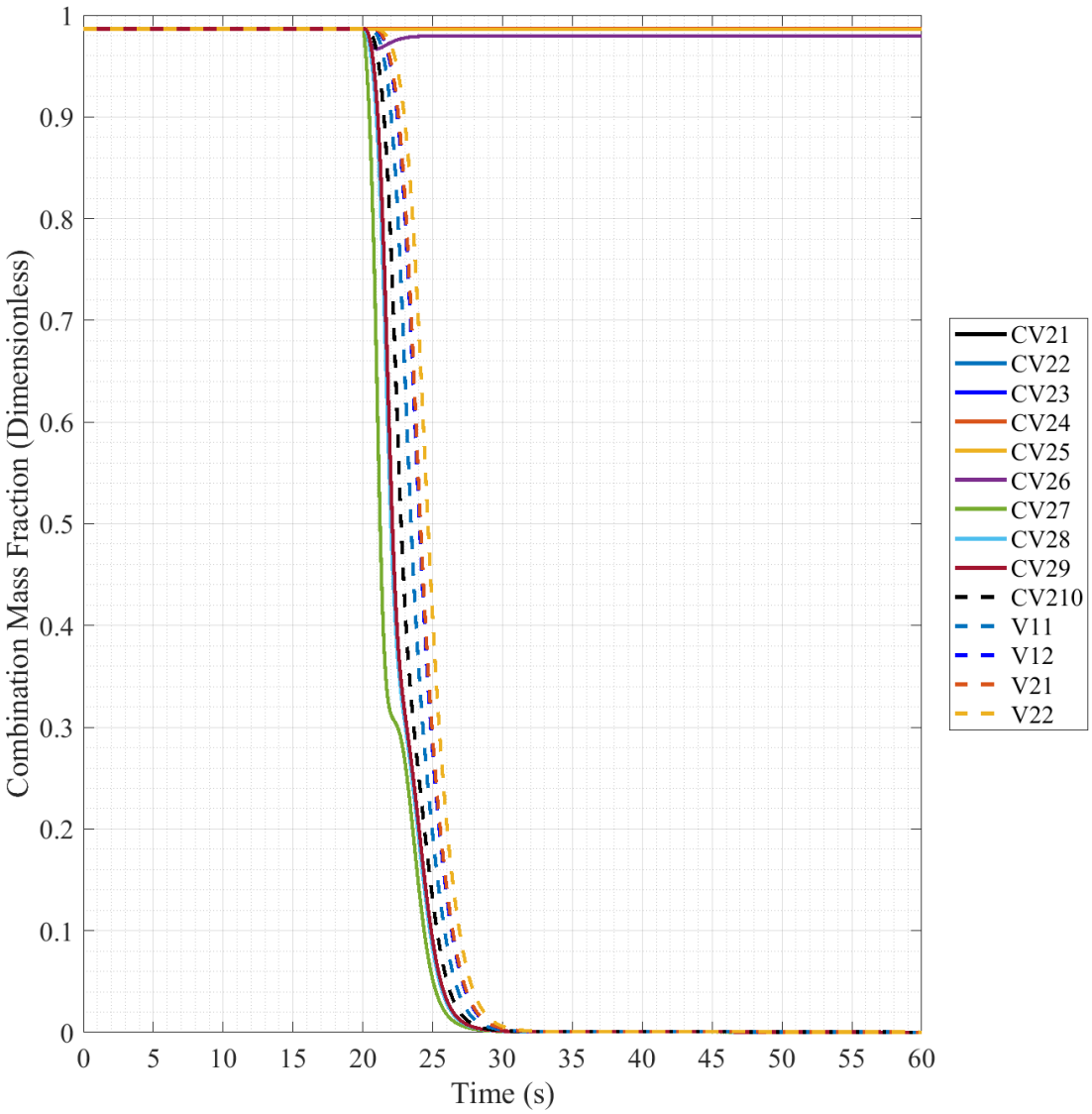

Fig. 6.116. Full-Scale Scenario 4 Combination Mass Fraction, 60 second Timescale.

6.2.6 Full-Scale Scenario 5 Results

Scenario 5 is a RPV break scenario with the lower SGC dividing plate closed to upward flow at its flow path. This forces the blowdown gases and atmosphere to rise through the EQS and giving the blowdown a longer required flow distance through the reactor building before reacting the exterior volume. No volumes are discarded from plotted results as they all may be interacted with by the blowdown progression. A visual example of this scenario's estimated progression can be seen in the 1/28th-scale results section of this scenario, Fig. 6.53.

The initial pressure plot of scenario 5, with the pressure plotted across the full timescale, has been omitted as it simply is a shows the same information as the initial scenario 1 plot, with the initial 6.4 MPa pressure of the helium volume and the resulting vertical scale of the plot blownout because of it. Nowhere along the full timescale of the pressure results were any new transients observed. The full timescale plot has been included in Appendix E for reference to the actual data, but Fig. 6.77 can be used as a quick reference as it shows a similar plot,

After reducing the timescale of the pressure plot to 240 minutes, like in scenario 1, the resulting plot was extremely similar to the plot made for that scenario. The initial helium pressure of 6.4 MPa can be seen at the initial time, then at 20 seconds the pressure begins to fall at an exponential rate as the break flow path is opened and helium expands out and into the RC volumes. The HV reaches an equalized pressure of ~100 kPa at ~129.4 minutes following the blowdown initiation, ~129.7 minutes post simulation initiation. Overall, the progression of the pressure blowdown from the helium volumes seems to have not been affected by the change in the model layout. The plot of this pressure timescale for this scenario has been included in Appendix E for further reference, or Fig. 6.78 can be used as a quick reference to the progression of the helium volume blowdown.

Fig. 6.117. gives a first look at the reactor building volume response to the helium release into its volumes for scenario 5. Much like what was seen in scenario 1, post pressure spike the reactor volumes enter a decreased pressure state that slowly returns back to ~100 kPa in roughly the timeframe of an hour where the pressures plateau. A difference can be seen though as the the volumes post spike maintain a much wider pressure band as they rise to plateau in comparison to scenario 1 and 3. Pressure spike information is difficult to determine at this timescale.

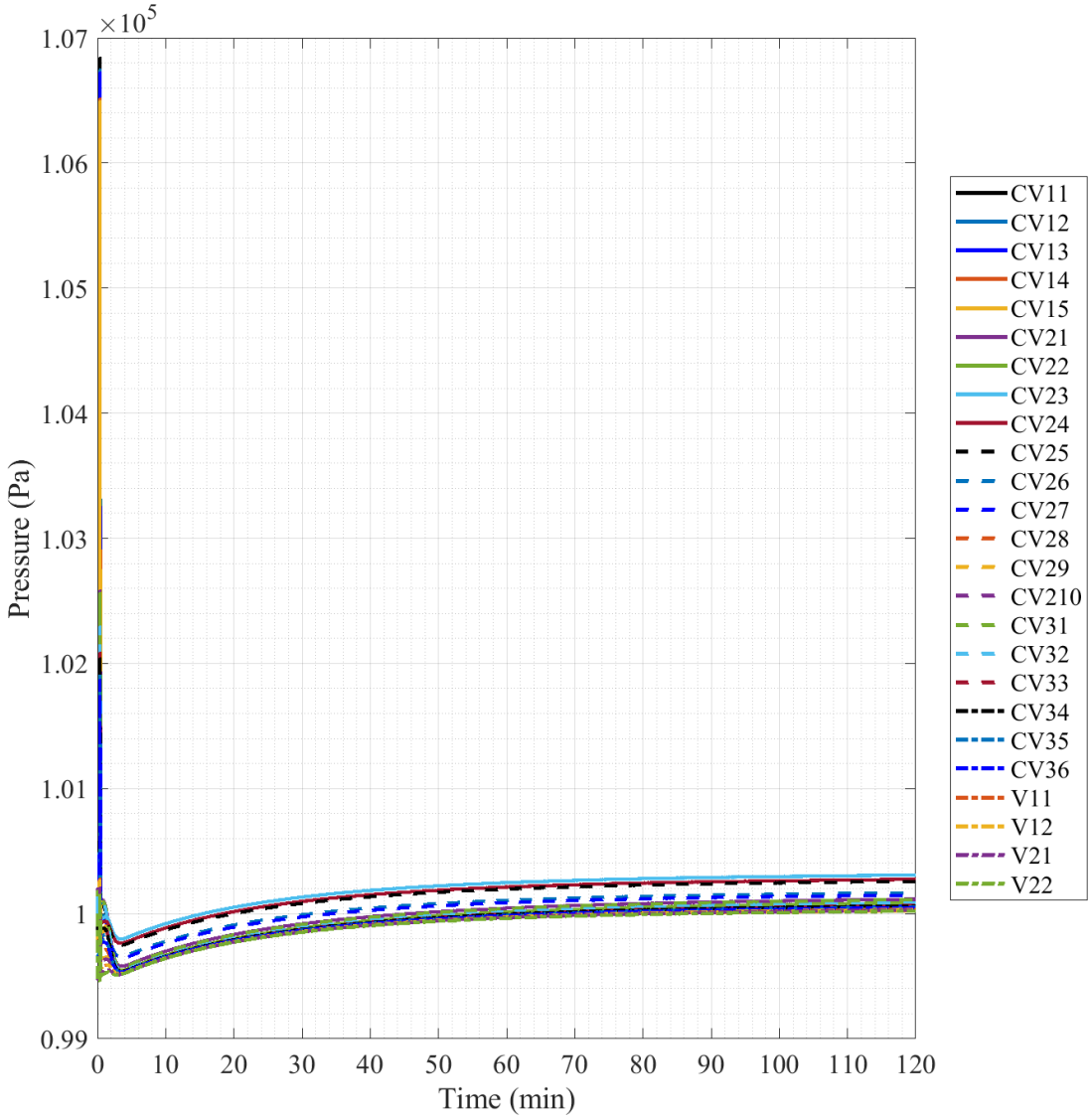

Fig. 6.117. Full-Scale Scenario 5 Pressure, 120 minute Timescale.

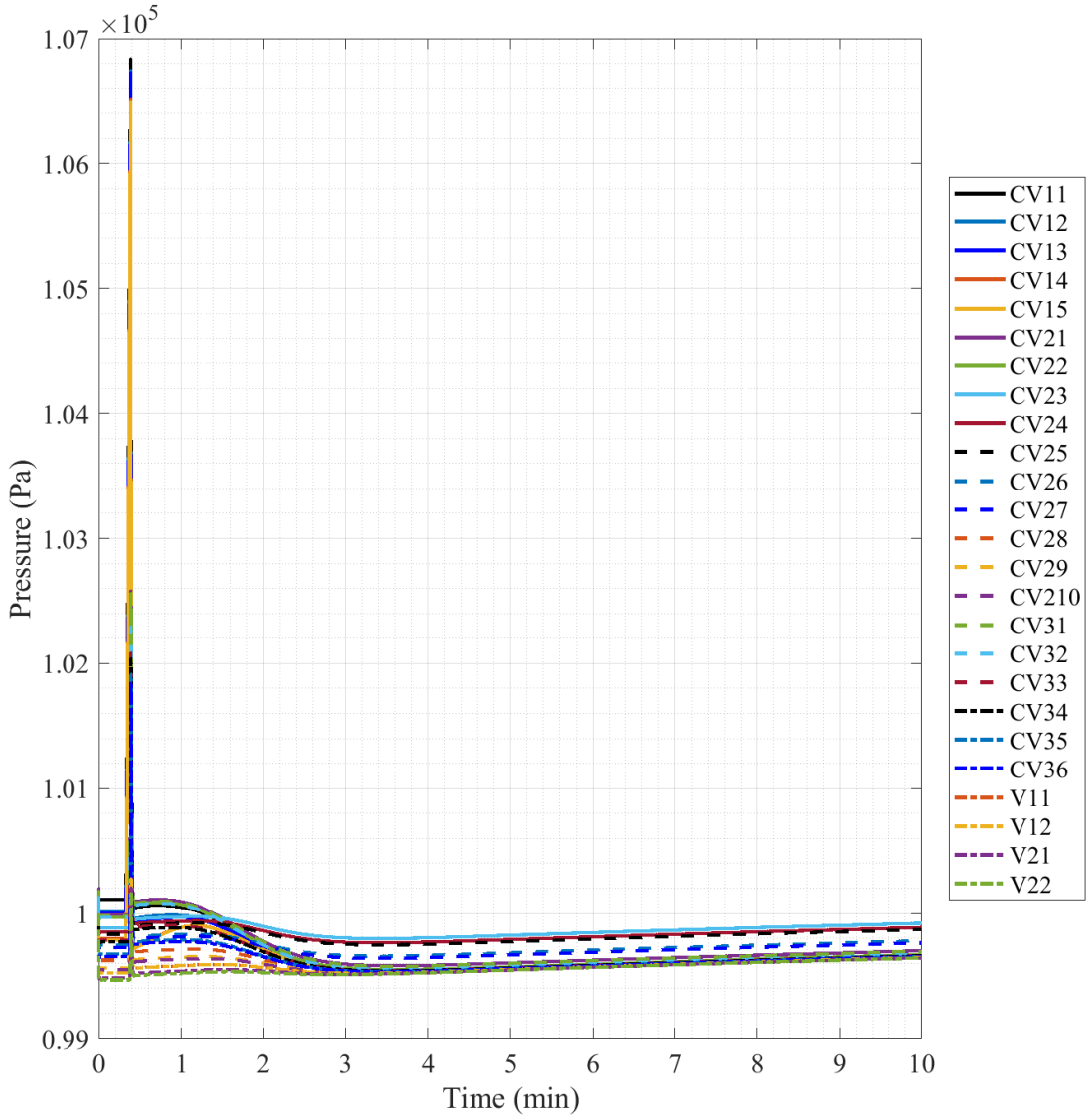

Fig. 6.118. Full-Scale Scenario 5 Pressure, 10 minute Timescale.

Reducing the timeframe to the initial 10 minutes, Fig. 6.118 shows the initial pressure separation of the volumes as they naturally redistribute at the beginning of the simulation, which can be seen by the initial vertical movement at time zero, which come to rest at steady state pressures. The spike in this scenario is still too difficult to determine at this timescale. Post pressure spike, volumes come back to a separated range of pressures as they were before as seen in scenario 1, but as the model progresses a majority of the volumes collapse into a tight band of pressures like in scenario 3. The major difference occurs in that the volumes in the central SGC cavity,

CV23-27, do not fall into the tight pressure band and remain at a higher pressure as the pressures rise and plateau. This is mostly like due to the singular entry into that region as the bottom dividing plate is closed in this scenario limiting the flow into and out of this region as it is not in an active region with flow through it.

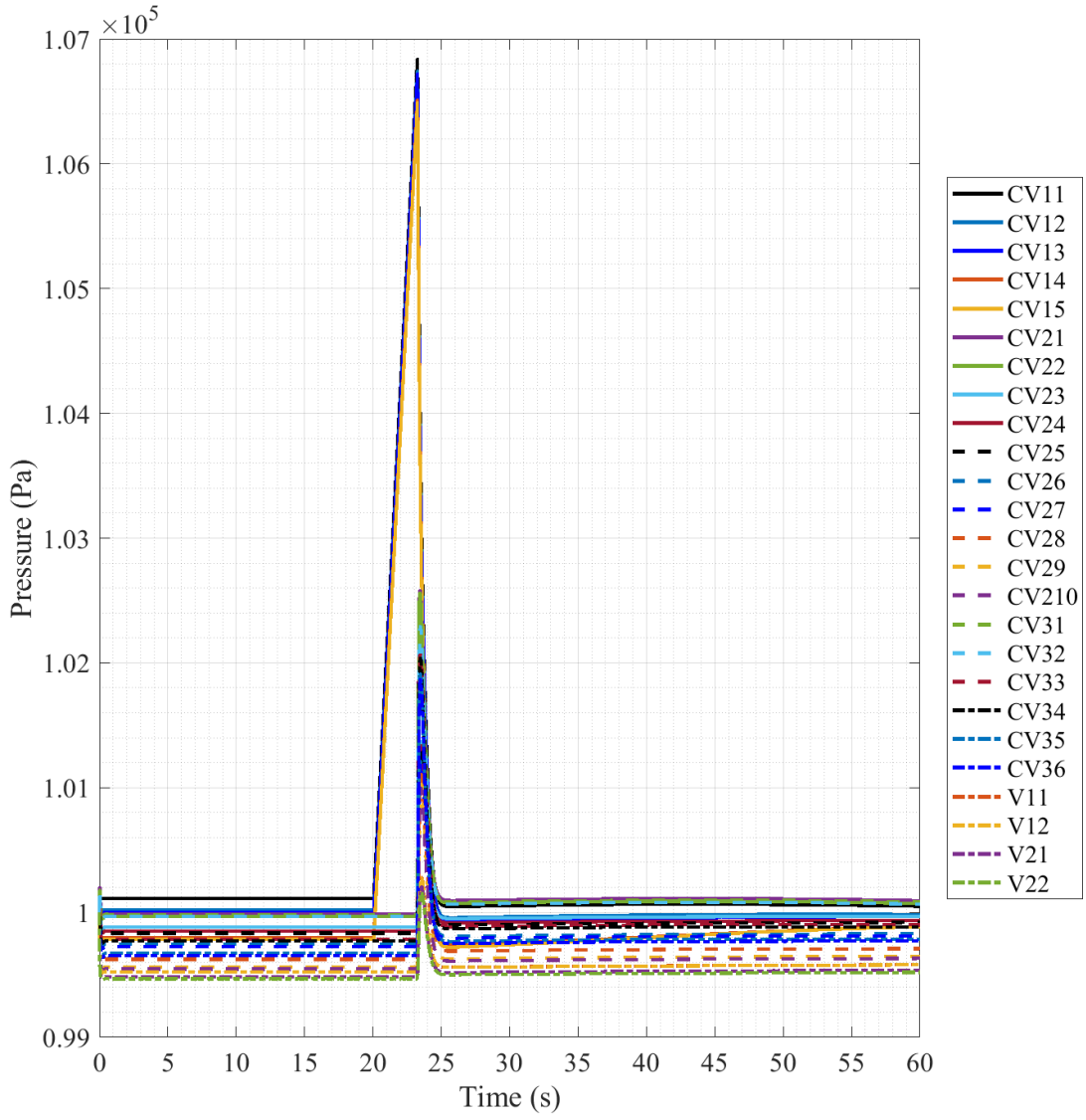

Fig. 6.119. Full-Scale Scenario 5 Pressure, 60 second Timescale.

Reducing the timescale further to the 60 seconds post simulation start, Fig. 6.119 gives information about the initial scenario timeframe. At the onset the initial pressure banding movement can be seen where they naturally move from their initial positions to the steady state

positions as discussed previously. The pressure spike comes into better view with the initial spike occurring at the set 20 seconds, and the following spike as the blowout panel actuates ~3 seconds later, leading to all volumes falling back into a similar pressure banding.

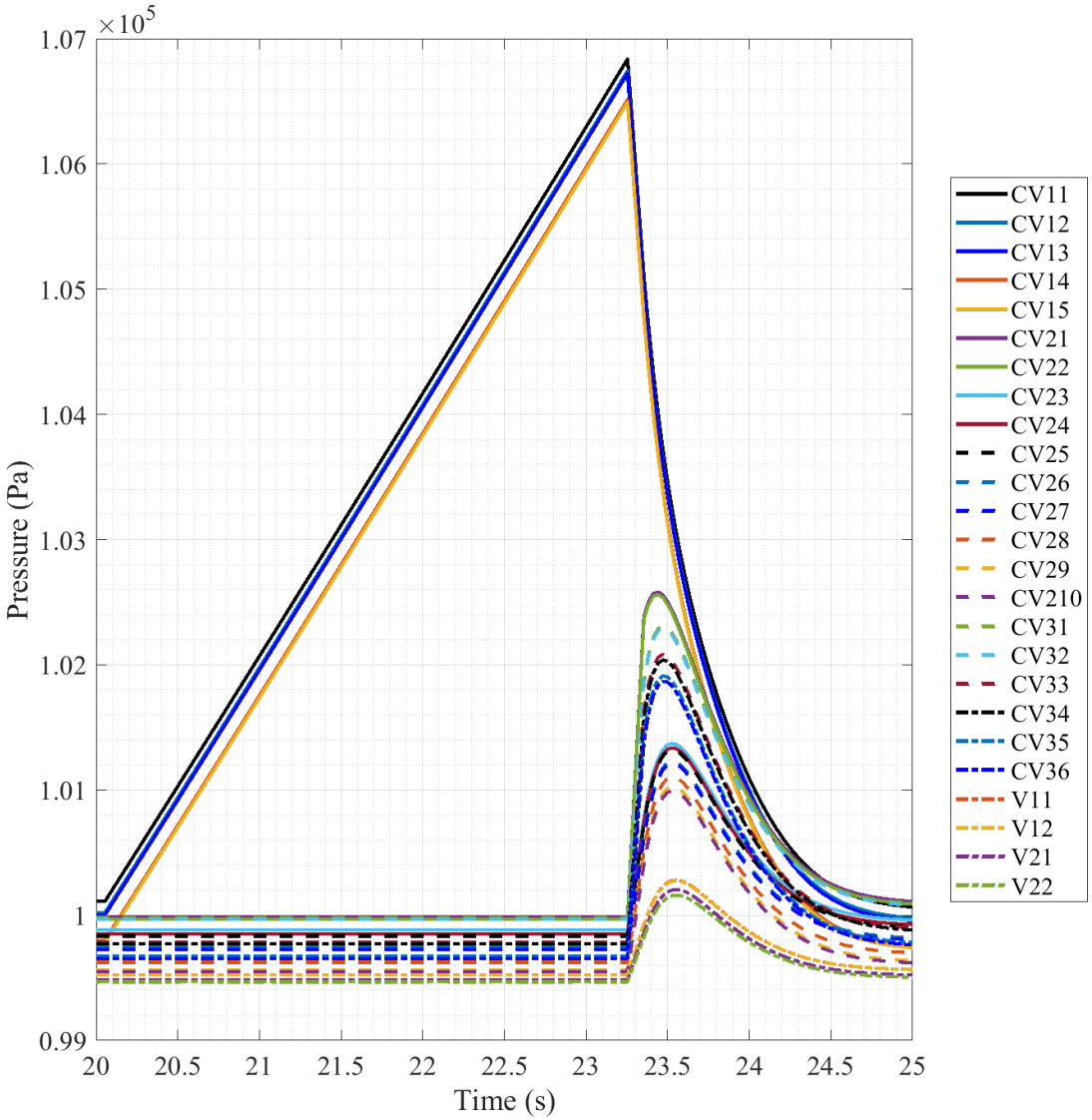

Fig. 6.120. Full-Scale Scenario 5 Pressure, 5 second Timescale, Post Break.

Reducing the timeframe in even more, Fig. 6.120 shows the 5 seconds post-break initiation of the model. With this, the linear rise of the CV11-15 (RC) volumes can be seen as pressure builds up behind the blowout panel, reaching a maximum of 1.0684×10^5 Pa (6.84 kPa increase) as it did in scenario 1 and 3. Pressure is built up for ~3.25 seconds before the blowout panel actuates and

the pressure in the RC volumes falls quickly, causing a rise in the other volumes of the reactor building in three distinct groups. The upper central transient of volumes consists of CV21-22 and CV31-36 which spike to a pressure around ~$1.022x10^5$ Pa (~2.2 kPa increase), with a maximum of $1.026x10^5$ Pa (~2.6 kPa increase) in CV21-22. The lower central transient of volumes consists of CV23-210 and spikes to a pressure range around ~$1.012x10^5$ Pa (~1.2 kPa increase), with a maximum of $1.014x10^5$ Pa (~1.4 kPa increase). The bottom transient group consists of the vent space volumes of V11-22 which spike to a pressure of only $1.002x10^5$ Pa (200 Pa increase) before falling back to the banded pressures. All transient groups rise to their maximum pressure but then fall back into the pressure banding they roughly experienced before.

CV11-15 maintains the same pressure spike maximums as seen in scenario 1 and 3 but the other volumes experience a lower pressure rise in comparison, such at V11-22. CV21-22 still experience the greatest pressure rise, as they did in scenario 2, but due to the larger and less obstructed flow path to the EQS they suffer a much less severe and more controlled pressure transient. Also, the plot shows the pressure increase in the central SGC cavity volumes as being a transient of its own due to the isolated nature of the cavity, as previously discussed, which later leaves the volumes to expand the reformed pressure banding which is not seen in scenario 1 or 3.

Mass fraction data of scenario 5 starts off with the presentation of the helium mass fraction plot, presented in Fig. 6.121. Of all the mass fraction results, this scenario is the busiest with many resulting transients, which did not occur with the smaller scale simulation of this scenario. Starting off with the most commonly seen transients, V22 undergoes a spike with the blowdown to ~84% before falling in ~2 hours as previously seen in other scenarios. CV23-26 gain only a meager amount of helium over the course of the scenario, on the scale of E-4. CV12-15 and CV33-34 spike with the blowdown to ~100% where they consistently stay for the entire scenario period.

CV21 and CV31 are not greatly affected by the blowdown but progressively rise in concentration, with an increase in gain at ~16 hours, over the scenario, with CV21 ending at ~3% and CV31 ending at ~4%. CV27 rises across the entire scenario period as well ending at ~4% with CV31, though its rise is much more constant, with no great change in the slope which has been seen consistently in previous scenarios.

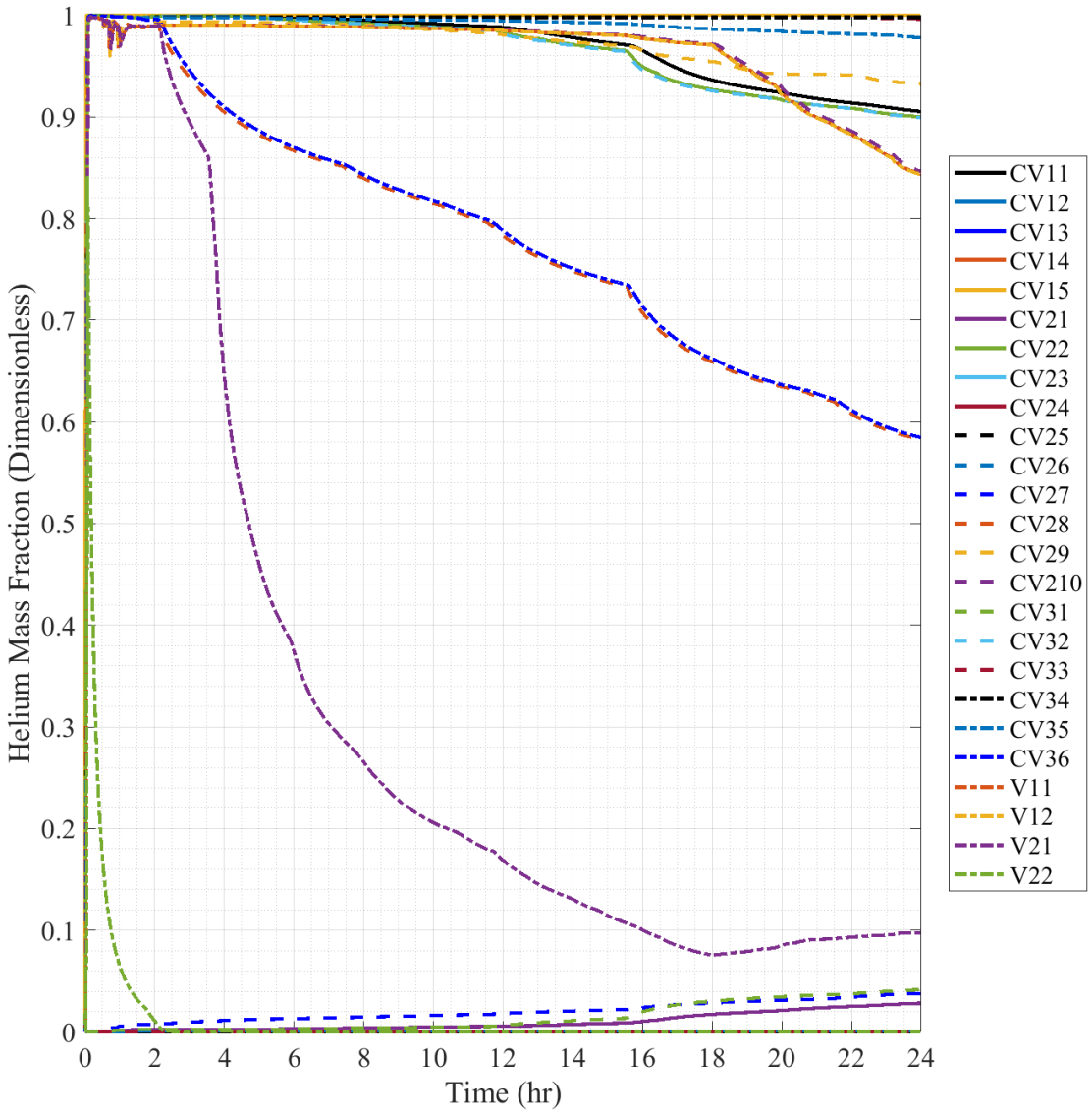

Fig. 6.121. Full-Scale Scenario 5 Helium Mass Fraction.

Moving to the top of the figure all remaining volumes, CV11, CV22, CV28-210, CV32, CV35-36, and CV11-21, spike with the blowdown to ~100% helium concentration. CV35 is the

upper most transient, slowly falling over the period of the scenario to ~98%. CV22 and CV32 remain constant at ~100% for ~4 hours, then it beginning to decrease and fall to ~96% at ~16 hours, before steeply dropping and continuing to fall to ~90%. CV11 undergoes a similar transient, consistent for ~4 hours at 100%, then falling to ~97% before a quick change of slope at ~16 hours, before ending at ~90.5%. The final normal transient is that of CV36, which is stable at ~100% for the first ~2 hours but begins to drop, as V22 hits 0%, ending at ~58%. An interesting note is to be made of this transient as it peaks roughly 4 times before changing slope and decreasing further.

The final volumes, CV28-210 and V11-21, go through a period of an hour from 30 minutes onwards where there is oscillation in the helium content. This will be looked at in further plots so their later transients will be discussed now. Beginning with the uppermost transient of these volumes, CV210 and V11-12 are on a slight sloping decrease following the oscillation period until ~18 hours, when at ~97%, the concentration begins decreasing much quicker, ending with a concentration of ~84% at the end of the scenario period. CV29 continues from the oscillation and stays on a relatively constant decrease ending at ~93%. CV28 is tied with the CV36 post oscillation falling with the 4 peak transient and ending at ~58%. The final transient is that of V21 which begins to drop at V22 drops to 0% as was seen in previous scenarios where it decreases to ~18 hours, where it then begins to rise again ending at ~10%. Another interesting note of this scenario is that the oscillation period occurs during the decrease of V21 and generally stops occurring once V22 reaches 0%. Getting a better look at early time period will require a smaller timescale that will be explored in later plotted results.

In order to maintain a concise description of scenarios, the plots of oxygen and nitrogen mass fraction are not presented in this scenario as their results are reaffirmed best by a combination of their results to approximate a near full mass fraction of standard air. As was seen in scenario 1,

oxygen and nitrogen mass fractions showed inverse results of the helium mass fraction and were simply differentiated by the resulting scale differences in the gas mass fractions. Plotted results for both the oxygen and nitrogen mass fraction can be found in Appendix E for further reference but are left out of this scenario to be concise.

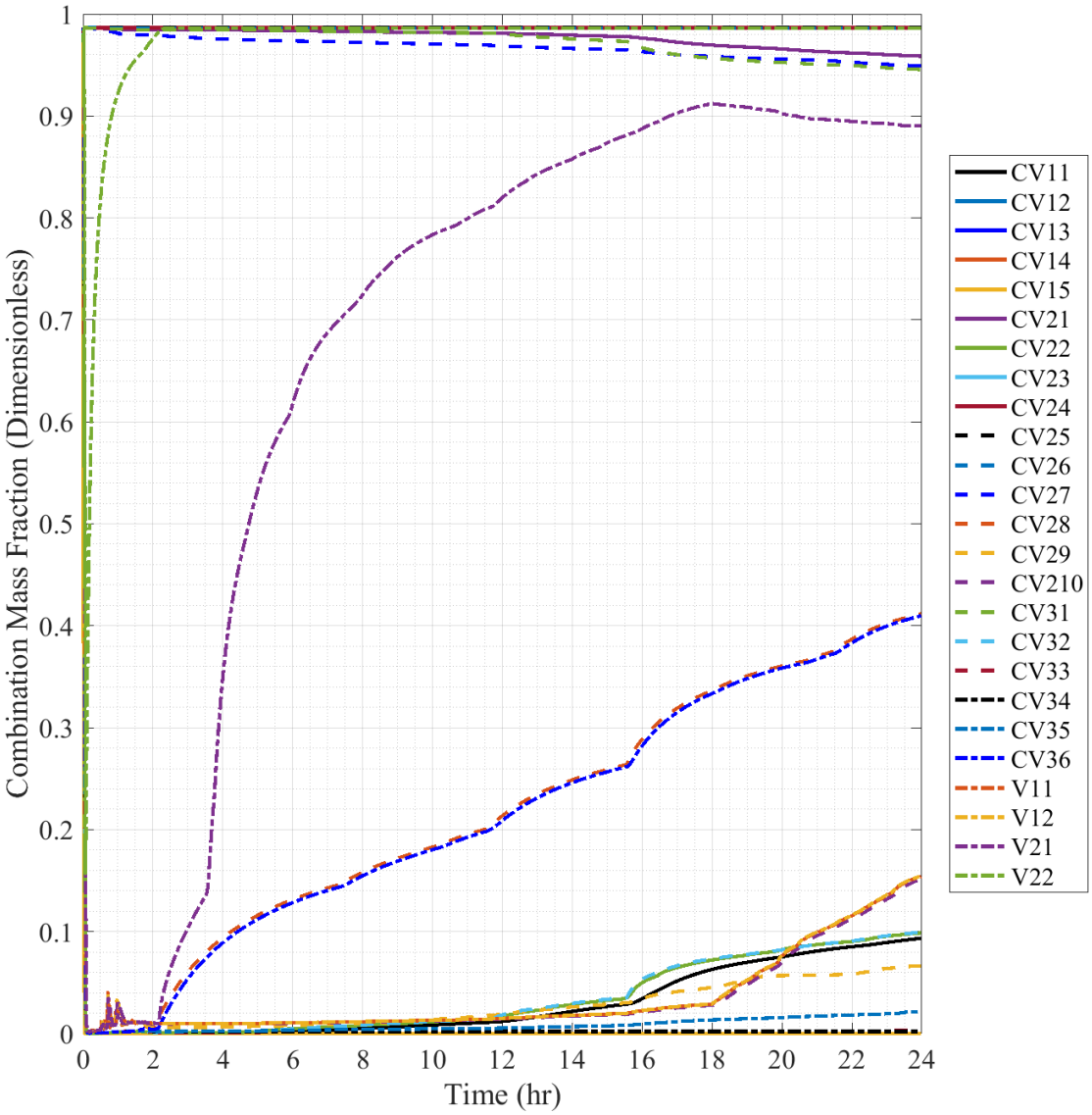

Fig. 6.122. Full-Scale Scenario 5 Combination Mass Fraction.

Fig. 6.122 sumss the oxygen and nitrogen mass fractions together as previously discussed to a “Combination” mass fraction composed of the combination of the two individual mass fractions. The combination of these two gases make up 98.66% of the total mass fraction of

standard air and should be a good comparison to the helium mass fraction for comparisons. Finally, by comparison with Fig. 6.121, it can be seen that the figure is simply an inverse of the helium trends. Due to the linked relationship of the results, this set of data will be used to examine the initial details of the blowdown from a mass fraction perspective as was done with the pressure.

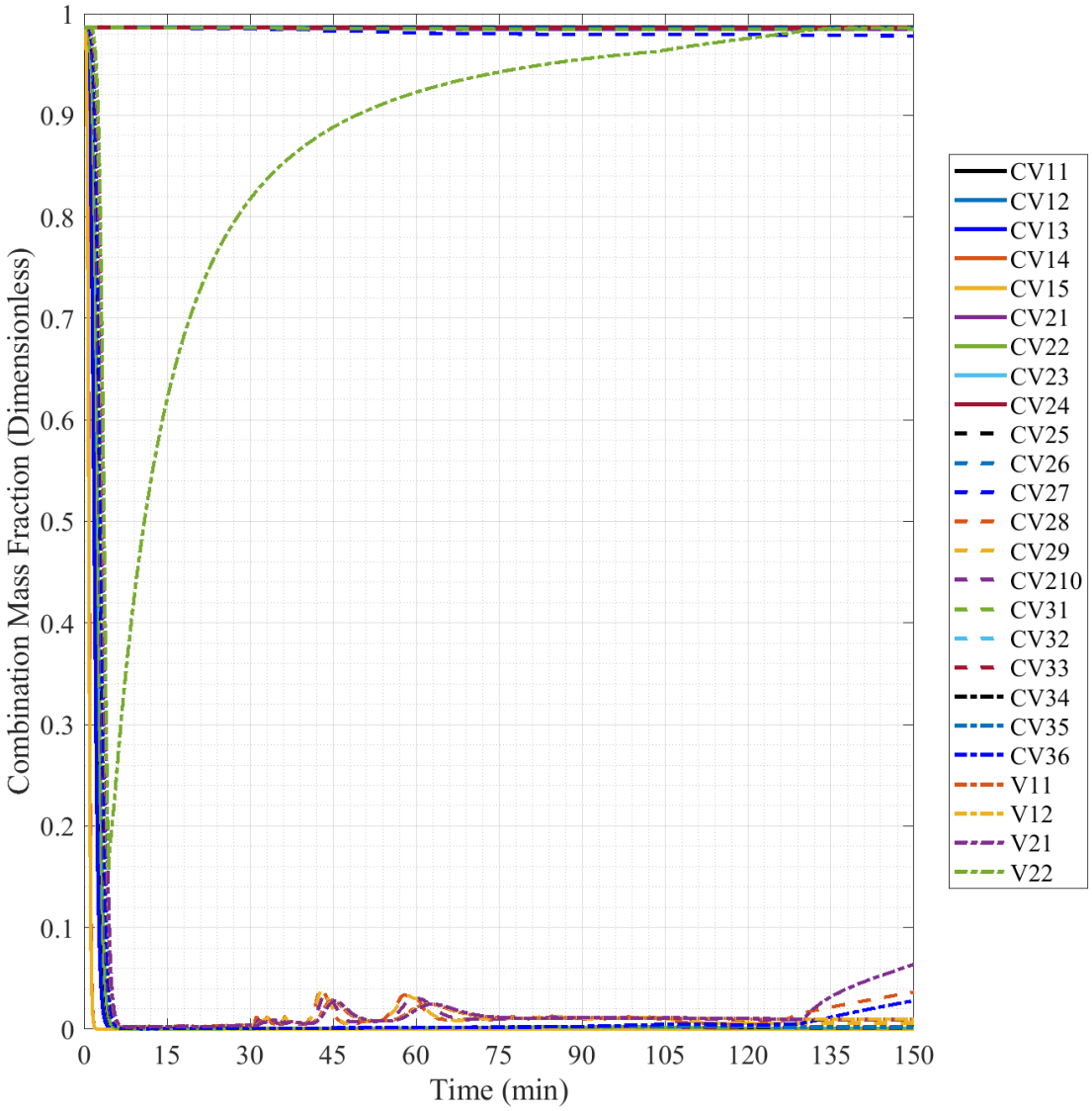

Fig. 6.123. Full-Scale Scenario 5 Combination Mass Fraction, 150 minute Timescale.

Fig. 6.123 reduces in the timescale of the combination mass fraction to get details of the initial post-break building response to the spreading helium. Much of the displacement happens within the first ~5 minutes of the scenario. V22 can be seen to fall to only ~16% air content before

refill begins, and over the following 2 hours it fills back to ~100% normal air. At that point, V21 can be seen to refill as has been seen previously. In comparison to scenario 1 and 3, no interruptions appear to take place in the voiding of volumes, but as V22 refills disturbances occur in CV28-210 and V11-21. These disturbances are introductions of air back into voided volumes which may be able to be attributed to air coming from the offshoot central SGC volumes entering the helium filled volumes. The spike progression shown by the plot initially appears in the CV28-210 volume followed by the spike in the V11-21 volumes.

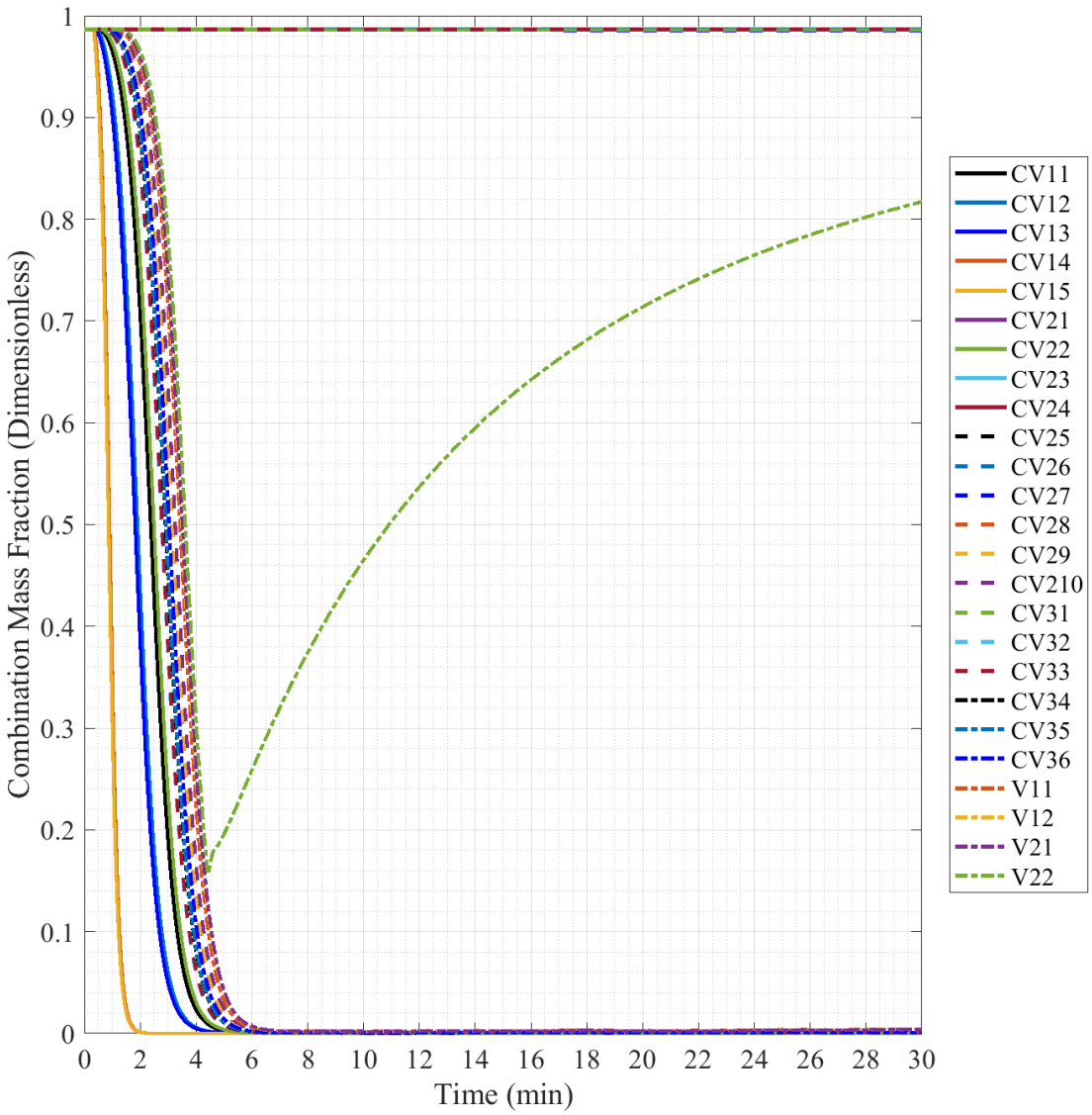

Fig. 6.124. Full-Scale Scenario 5 Combination Mass Fraction, 30 minute Timescale.

Fig. 6.124 reduces the timescale to the first 30 minutes of the scenario to get the finer details of the volume voiding. As seen in the previous figure, V22 drops to ~16% at ~4 minutes before it begins rising in air concentration again. Volumes mostly progress from left to right in order of their path in the blowdown progression with RC volumes on the left and SGC, EQS, and vent space volumes heading towards the right. In comparison to what was seen in scenario 1, this scenario is much more stable in its initial progression, as volumes cleanly empty of their oxygen content. This may be an additional indicator of the presence of conflicting flow in scenario 1 as in this scenario the flow only has a singular path of progression through the volumes, with no place for flow to intersect, which corroborates what was seen with scenario 3.

6.2.7 Full-Scale Scenario 6 Results

Scenario 6 is a SGV break scenario with the lower SGC dividing plate closed to upward flow at its flow path. This will allow gases to progress not only directly to the vent space but also into the EQS deeper into the reactor building with no expansion path for the compressed building atmosphere due to the closed upward SGC bottom plate. For this scenario any volumes from RC (CV1-15) will be omitted from plotted results as they undergo no changes during the scenario. A visual example of this scenario's estimated progression can be seen in the 1/28th-scale results section of this scenario, Fig. 6.62.

The initial pressure plot of scenario 6, with the pressure plotted across the full timescale, has been omitted as it simply is a shows the same information as the initial scenario 2 plot, with the initial 6.4 MPa pressure of the helium volume and the resulting vertical scale of the plot blownout because of it. Nowhere along the full timescale of the pressure results were any new transients observed. The full timescale plot has been included in Appendix E for reference to the actual data plot, but Fig. 6.89 can be used as a quick reference as it shows a similar plot.

After reducing the timescale of the pressure plot to 20 minutes, like in scenario 2, the resulting plot was extremely similar to the plot made for that scenario. The initial helium pressure of 6.4 MPa can be seen well at the initial time, then at 20 seconds the pressure begins to fall at an exponential rate as the break flow path is opened and helium expands out and into the SGC volumes. The HV reaches an equalized pressure of ~100 kPa at ~10.21 minutes following the blowdown initiation, ~10.5 minutes post simulation initiation. Overall, the progression of the pressure blowdown from the helium volumes seems to have not been affected by the change in the model layout. The plot of this pressure timescale for this scenario has been included in Appendix

E for further reference, or Fig. 6.90 can be used as a quick reference to the progression of the helium volume blowdown.

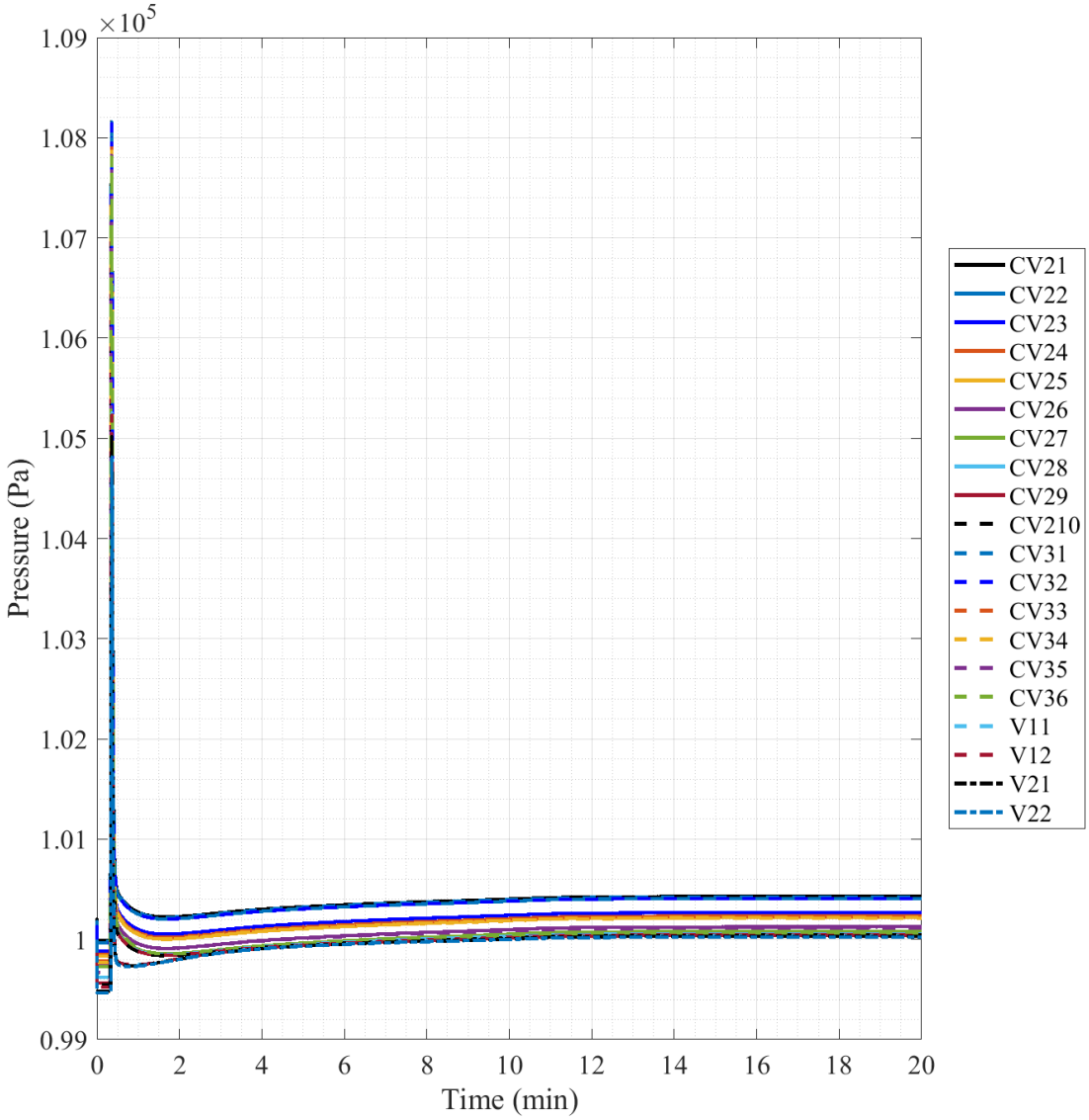

Fig. 6.125. Full-Scale Scenario 6 Pressure, 20 minute Timescale.

Fig. 6.125 gives a first look at the reactor building volume response to the helium release into its volumes for scenario 6. The timescale at this small scale is still not enough to determine pressure spike information accurately. What can be determined from this figure is that post pressure spike the volumes enter an increased pressure band state that slowly plateaus to ~100.2 kPa in roughly the timeframe of ~12 minutes as was seen in scenario 2 and 4 as well. For this

scenario though, the resulting pressure banding is much wider in its pressure values than what was seen in the previous scenarios.

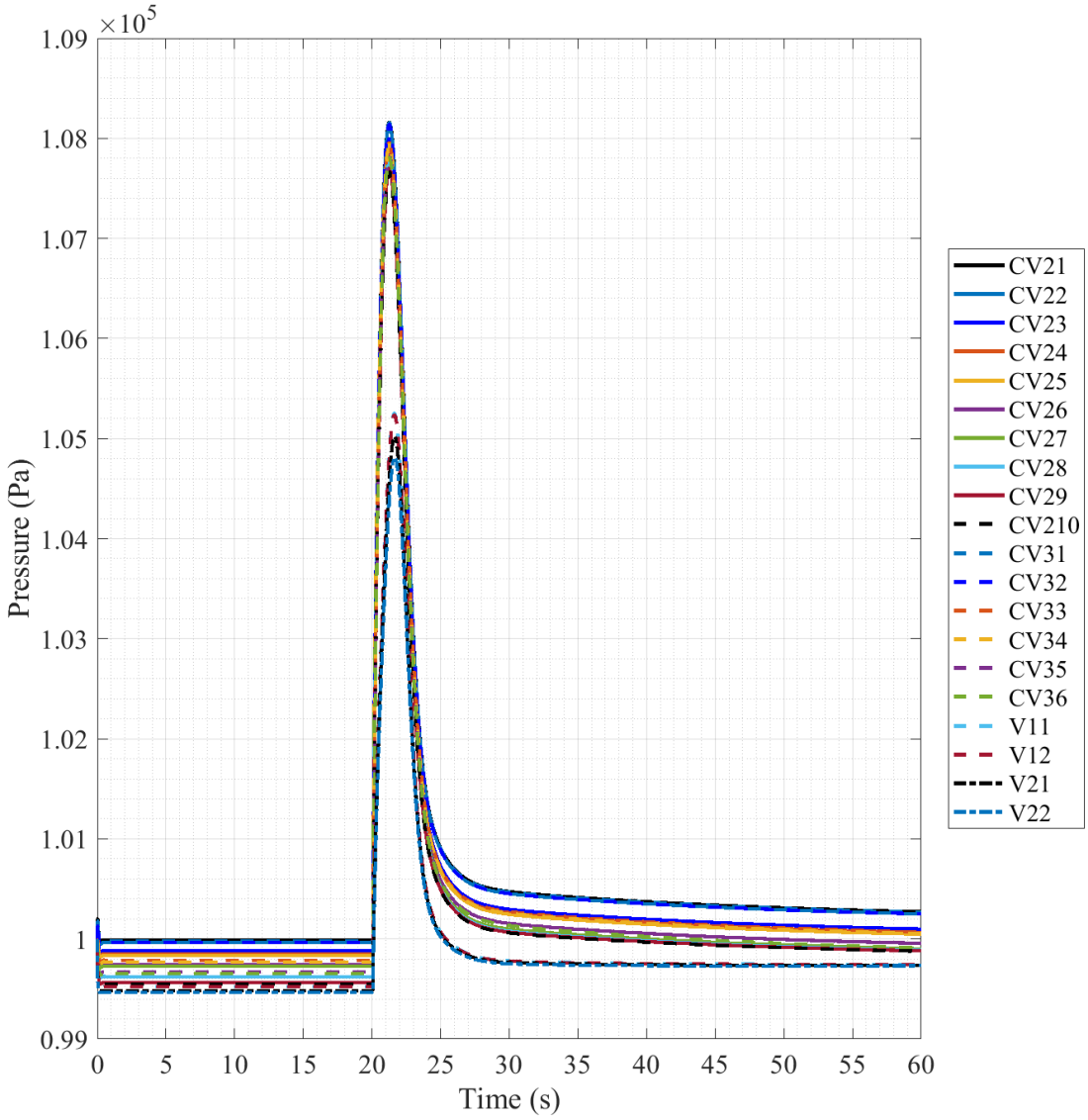

Fig. 6.126. Full-Scale Scenario 6 Pressure, 60 second Timescale.

Reducing the timescale to the 60 seconds post simulation start, Fig. 6.126 gives information about the initial scenario timeframe of scenario 6. At the onset, the initial pressure banding movement can be seen where volumes naturally move from their initial positions to the steady state positions as discussed previously. Since there is no blowout panel actuation in this scenario the pressure rise at the break initiation is analogous to being normally distributed. Following the

pressure spike, volumes settle back pressure bands but at a raised pressure from what they settled at post simulation start which can be seen in both Fig. 6.125 and 6.126.

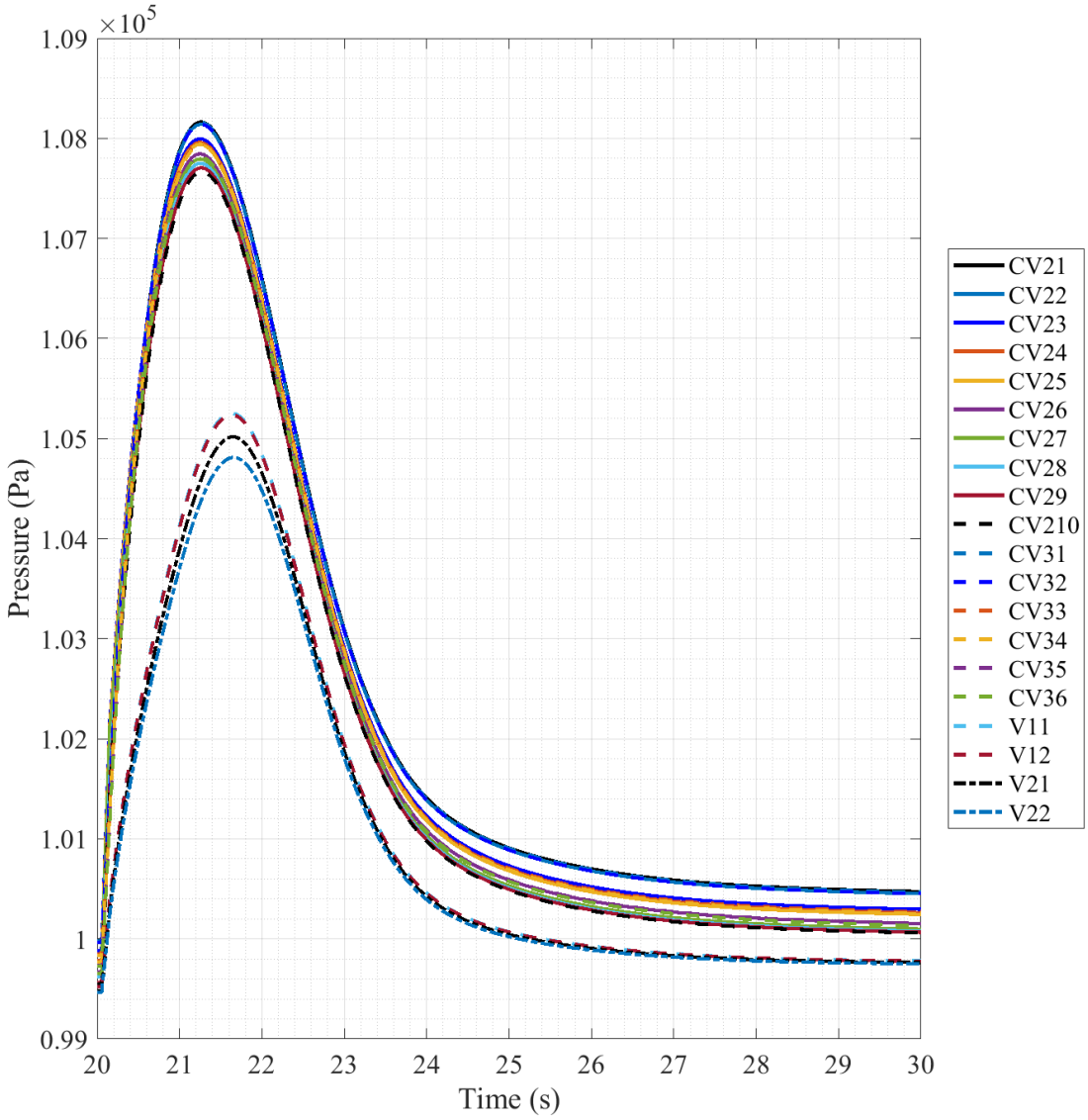

Fig. 6.127. Full-Scale Scenario 6 Pressure, 20-30 second Timescale.

Reducing the timeframe in even more, Fig. 6.127 shows the 10 seconds post-break initiation of the model. The upper transient of volumes consists of CV21-210 and CV31-36 where they spike to a pressure range centralized around ~1.078x10^5 Pa (~7.8 kPa increase) and a max of 1.0816x10^5 Pa (8.16 kPa increase). The bottom transient group consists of the vent space volumes of V11-22 which spike to a pressure range of ~1.05x10^5 Pa (5.0 kPa increase), with a max of

1.0525 x10^5 Pa (5.25 kPa increase), before falling back to the banded pressures that come to join back together in the minute following the pressure spike. Overall, the response in this scenario is very similar to scenario 1, as the pressures do not vary greatly from that scenario, but they are slightly increased in the maximum that that they peak to following the break initiation.

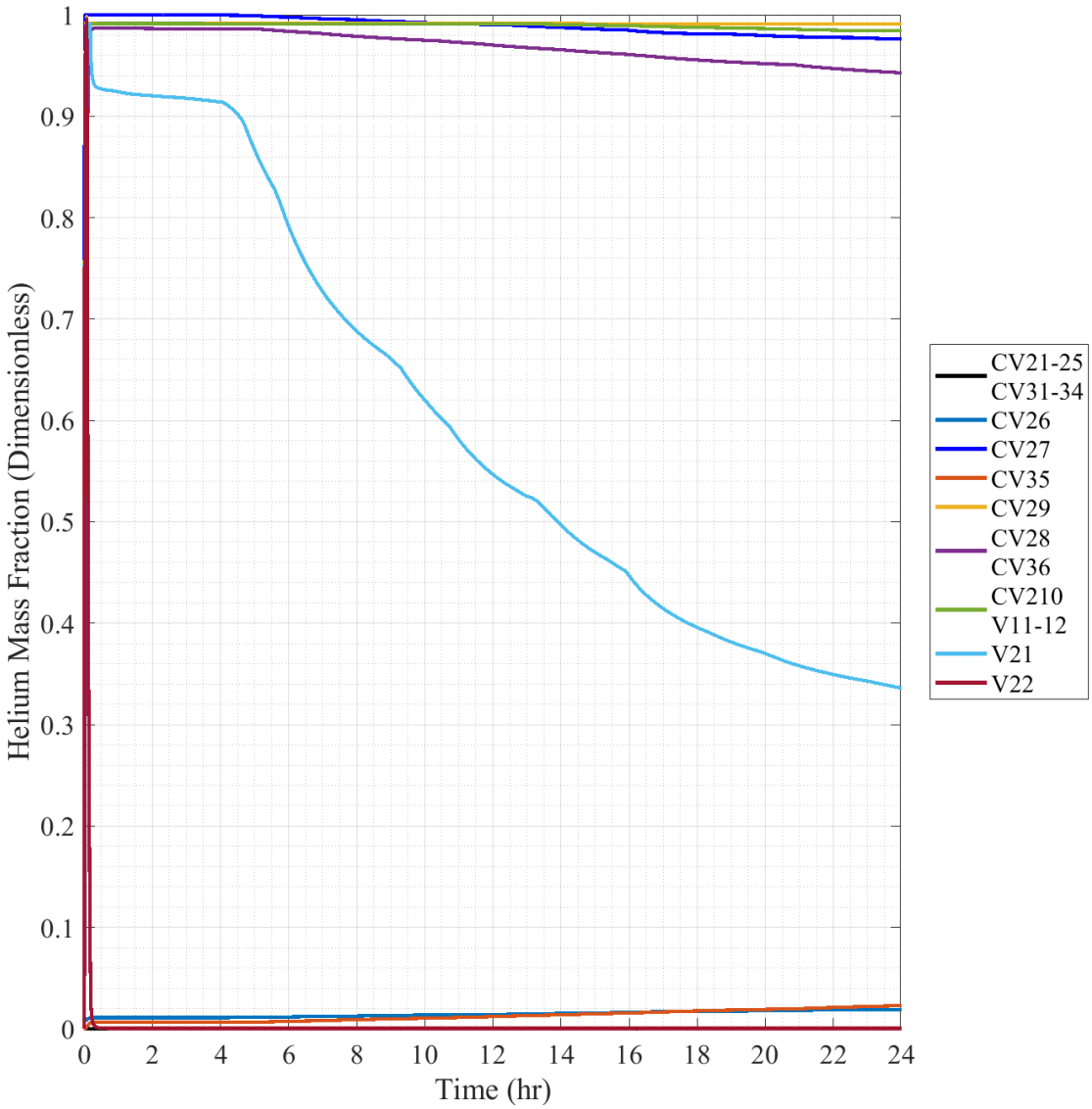

Fig. 6.128. Full-Scale Scenario 6 Helium Mass Fraction.

Mass fraction data of scenario 6 starts off with the presentation of the helium mass fraction plot, presented in Fig. 6.128. The singular major transient group of this scenario again is composed of V21 and V22, showing a different relationship than was seen in scenario 2. V22 initially spikes

with the blowdown to ~100% but then falls to ~0% in ~15 minutes, where V21 begins its transient. V21s transient curves to an almost plateau until at ~4 hours, where its slope changes and drops quicker for the rest of the scenario period to ~34%. On the opposite end of the scale, CV21-25 and CV31-34 experience a very slight increase introduction of helium on the scale of E-4 or less, mainly due to their location being lower than the break location. CV26 experiences a very slight increase to ~1% with the blowdown but stays constant over the remaining scenario time period. The final bottom transient is that of CV35, which slightly spikes with the blowdown but then slowly rises in helium content over the scenario period to ~2%.

All other volumes, CV27-210, CV36, and V11-12, spike with the blowdown to near 100%. CV27 spikes up to 100% with the blowdown, but then at ~4 hours it begins a steady decline to right below 98% by the end of the scenario. CV210 and V11-12 fill to roughly ~99% with the blowdown where they stay relatively stable, falling slightly to ~98% across the scenario. Similarly, CV29 fills with the blowdown to ~99%, but it remains relatively stable at this concentration across the period. The final upper transient consists of CV28 and CV36, which spikes with the blowdown to ~100% but then falling to ~98.5% where it remains for ~6 hours, then falling steadily over the remaining scenario period to ~94%. Getting a better look at early timescales will require a smaller timescale that will be explored in later plotted results.

In order to maintain a concise description of scenarios, the plots of oxygen and nitrogen mass fraction are not presented in this scenario as their results are reaffirmed best by a combination of their results to approximate a near full mass fraction of standard air. As was seen in scenario 1, oxygen and nitrogen mass fractions showed inverse results of the helium mass fraction and were simply differentiated by the resulting scale differences in the gas mass fractions. Plotted results for

both the oxygen and nitrogen mass fraction can be found in Appendix E for further reference but are left out of this scenario to be concise.

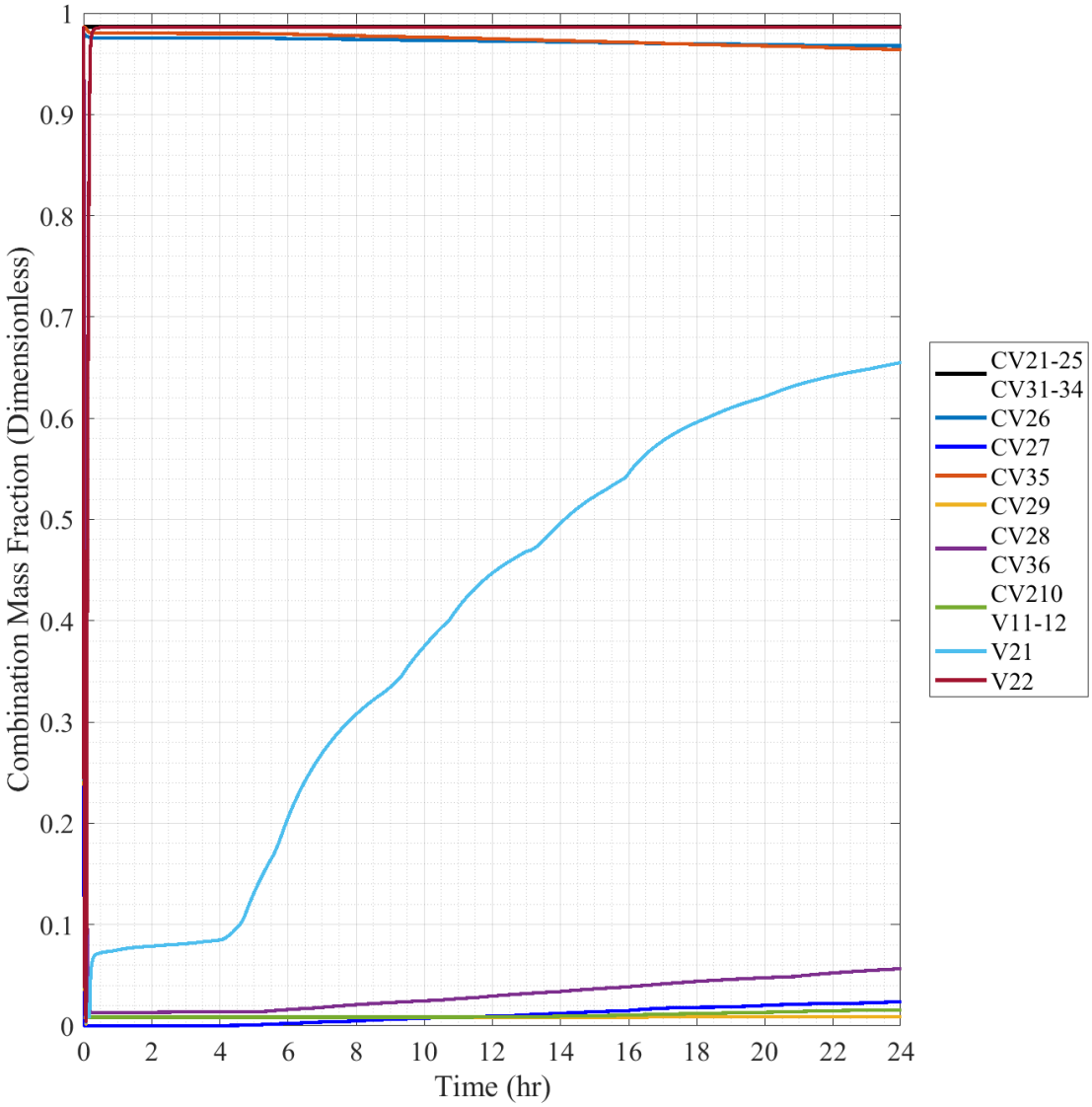

Fig. 6.129. Full-Scale Scenario 6 Combination Mass Fraction.

Fig. 6.129 sums the oxygen and nitrogen mass fractions together as previously discussed to a "Combination" mass fraction composed of the combination of the two individual mass fractions. The combination of these two gases make up 98.66% of the total mass fraction of standard air and should be a good comparison to the helium mass fraction for comparisons. Finally, by comparison with Fig. 6.127, it can be seen that the figure is simply an inverse of the helium

trends and as such discussion of it will not be performed. Due to the linked relationship of the results, this set of data will be used to examine the initial details of the blowdown from a mass fraction perspective as was done with the pressure.

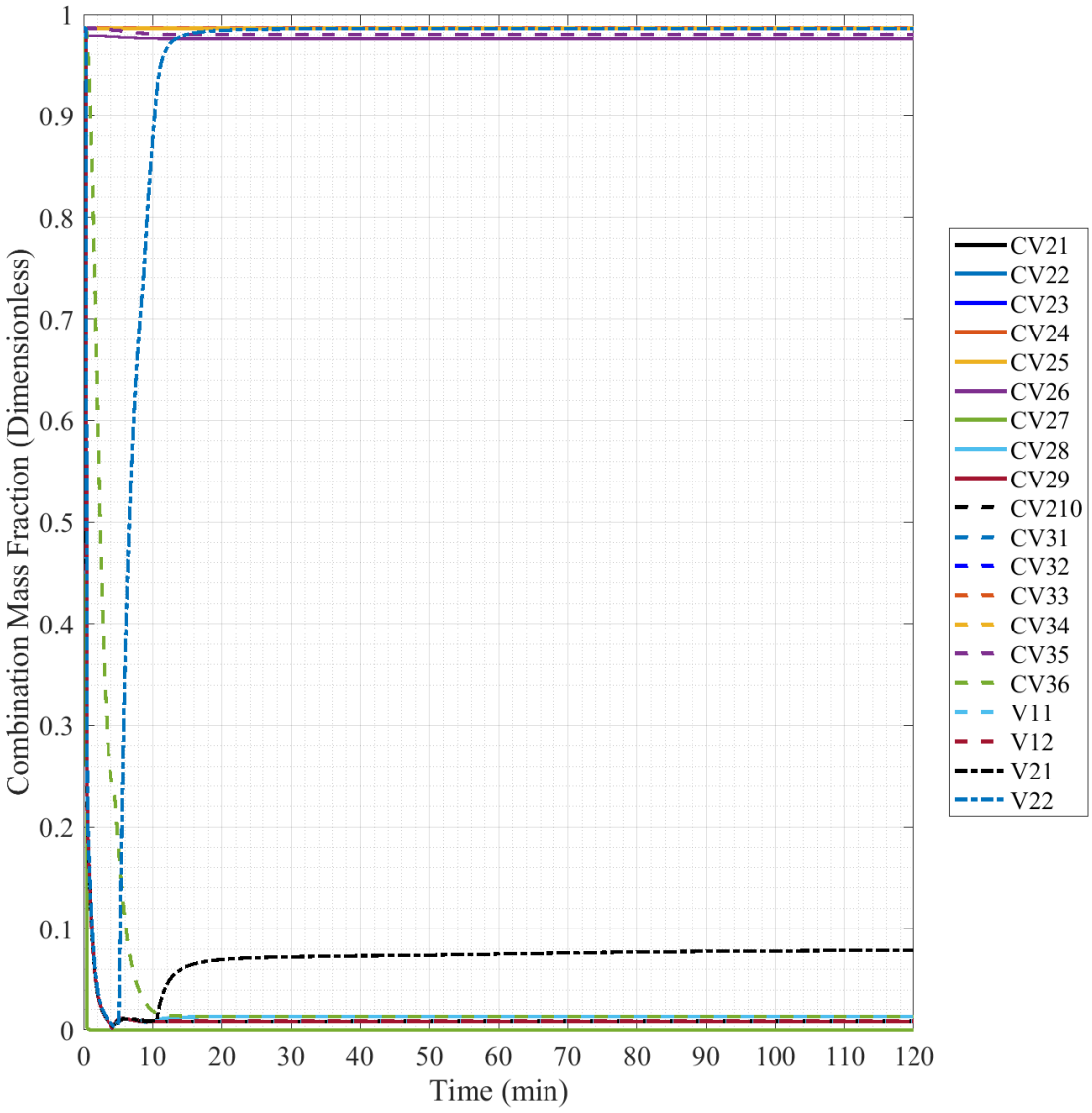

Fig. 6.130. Full-Scale Scenario 6 Combination Mass Fraction, 120 minute Timescale.

Fig. 6.130 reduces the timescale of the combination mass fraction to get details of the initial post-break building response to the spreading helium. At this timescale, not a great deal of information can be gathered as this scenario is much more stable than that which was seen in scenario 2. It can be seen though that the connection between V22 and V21 seems to persist as has

been seen in other scenario results, once V22 is near filled with normal air V21 begins to rise. CV36 also appears in this scenario to have its own transient decrease, which would occur as it slowly has helium added due to its close positioning to the break, but not on the direct flow path.

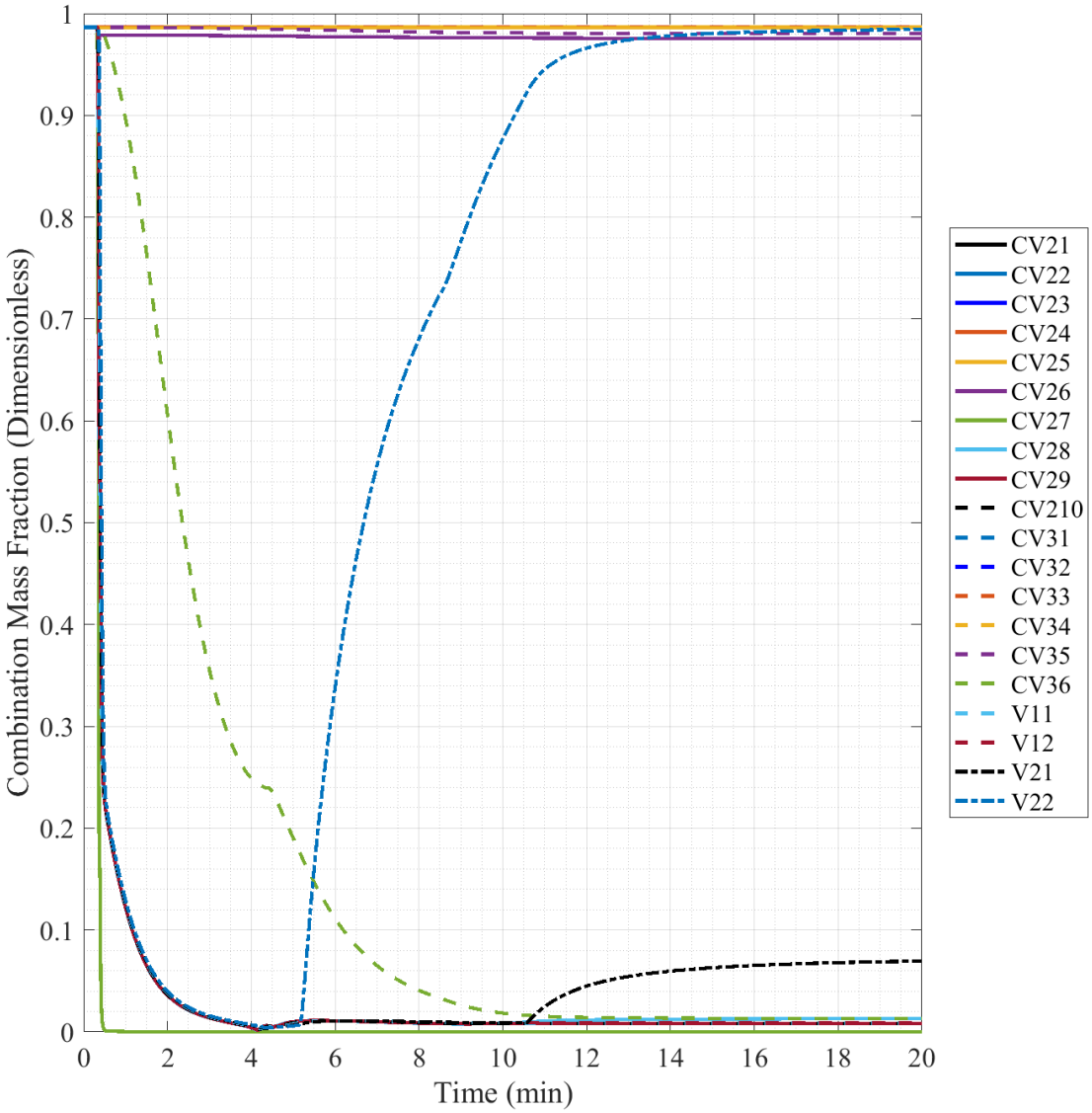

Fig. 6.131. Full-Scale Scenario 6 Combination Mass Fraction, 20 minute Timescale.

Fig. 6.131 reduces the timescale even further to the first 20 minutes of the scenario in an effort to gather more information. Much like the previous figure, V22 and V21 are the only changing transients of this figure, though CV26 can be seen with its slight mixture of helium near the top. V22 spikes down with the blowdown, then at ~5 minutes begins to rise coming to a near

completely air-filled state ~10 minutes later. V21 begins its upward trend early in this model, rising at ~11 minutes and coming to a plateau relatively quickly at this timescale, which will persist through the first ~4 hours of the scenario, as seen in Fig. 6.129. Discussed when looking at the previous figure, CV36 is voided over a long period of time in comparison to those in the direct break flow path. Its voiding is relatively constant until the point where V22 begins to refill where a slight plateau occurs before the voiding continues.

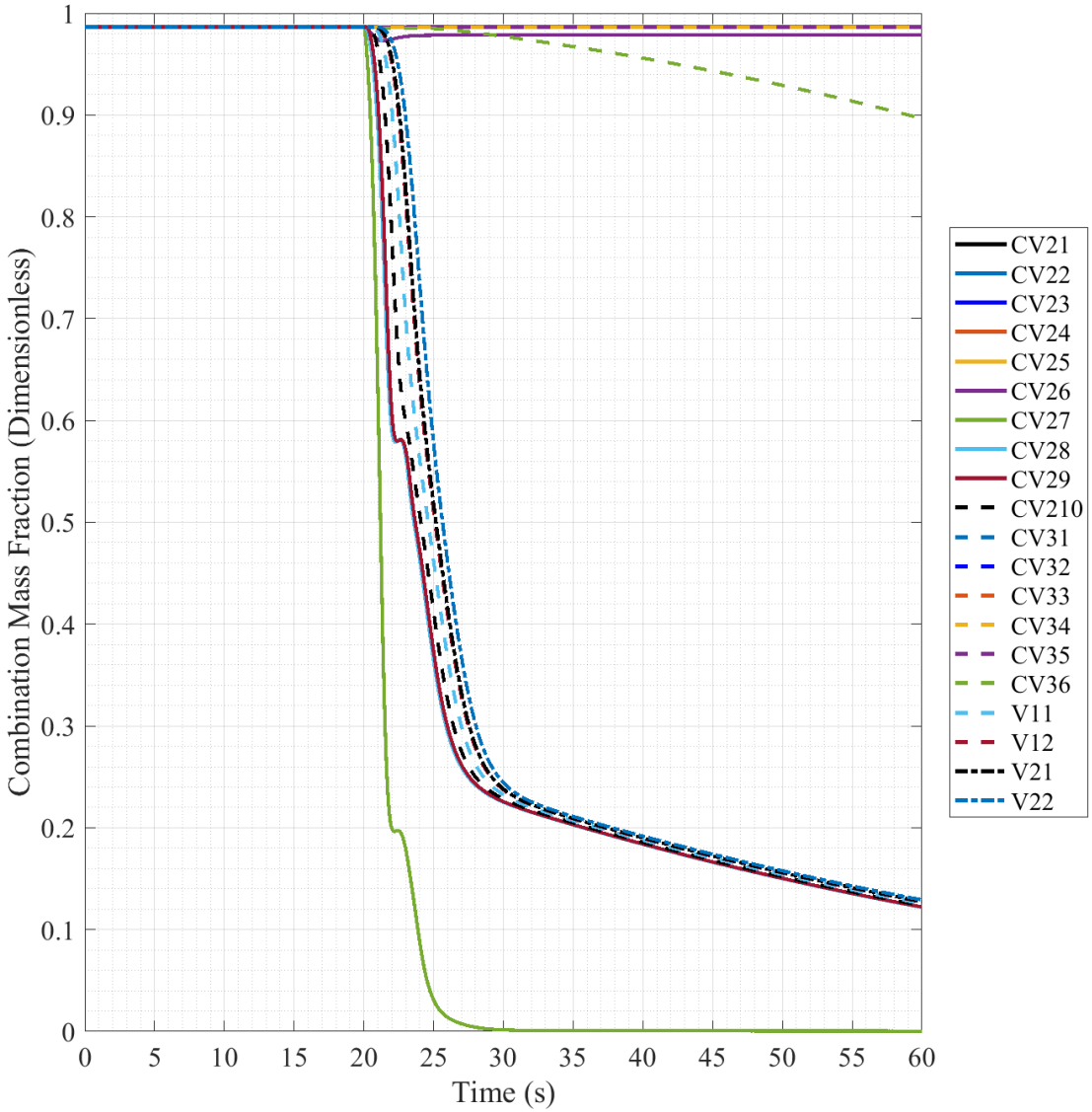

Fig. 6.132. Full-Scale Scenario 6 Combination Mass Fraction, 60 second Timescale.

Fig. 6.132 reduces the timescale even further to the first 60 seconds of the scenario to gather information on the initial voiding of the volumes. In comparison to scenario 2, the voiding of this scenario undergoes a similar, but less severe spike. CV27 undergoes a slight spike ~2 seconds following break start that again shows in CV28-29 as in scenario 2. This later leads to a divergence of voiding at ~27.5 seconds and the overall rate of decrease is significantly lessened. CV27 is the only volume completely voided in this period, ~10 seconds like in scenario 4. Following this period of time these volumes continue decreasing, reaching a near completely voided state at ~3.5 minutes, which can best be seen in Fig. 6.131.

6.3 Discussion

Examining the pressure plots of the scenarios lead to interesting similarities being discovered between individual scenarios and the scale of the models themselves. By examining the resulting blowdown progressions seen across the 14 scenarios, trends showed that the scenarios can be differentiated mainly by their break location and the model scale. Overall, the models showed no discernable differences between scenarios of the same break location on the general progression of events, each resulting in a blowdown to an equilibrium pressure with the other volumes of the model in the same amount of time. Table 6.1 collates the different blowdown times to equilibrium pressure with the surrounding volumes along with a multiplicative time difference between the full and 1/28th-scale model results.

Table 6.1.
Approximate Blowdown Times.

Break Location	Scale		Multiplicative Time Difference
	1/28th	Full	
RPV	293	7764	26.50x
SGV	22.1	613	27.74x

As presented in the table, time differences in the model were similar to the physical dimension scale differentiation between the individual models. The RPV situated break progressed at a rate less than the dimensionally scaled difference by -1.5x, while the SGV break faired much closed to the dimension scale at -0.26x difference. Overall, the models appear to follow a relatively close progression scaling to their dimensional scaling, resulting in a much quicker progression at the smaller scale even though break flow areas and overall blowdown amounts are scaled with the dimensional change.

This would seem to be corroborated by the stable voiding curves seen in the combination mass fraction results of scenario 4 between the two scales, Fig. 6.52 and Fig. 6.116, for the 1/28th-

scale and full-scales respectively. Of the voiding results between scales, this scenario is the singular result undergoing similar transients that are close enough to closely compare. At 1/28th scale, voiding of the affected volumes occurs in ~0.4 seconds, while at the full-scale voiding occurs within ~11 seconds. This aligns with a 28x scale difference between the same scenario between the different model scales, corroborating what was seen with the blowdown pressure progression results.

Post-break initiation, volumes having their atmospheres voided undergo an initial pressure spike, a feature of the rapidly expanding helium coolant as it is released into the surrounding volumes. This initial pressure spike does not occur over a long period of time, 0.5 seconds for the 1/28th-scale and 4 seconds in the full-scale, before falling to near standard pressure. Table 6.2 brings together all of the maximum pressures experienced in each scenario test for both scales. For RPV scenarios, the maximum pressures were always experienced in the RC volumes of CV11-15, due to buildup behind the blowout panel, while in the SGV scenarios the maximum pressures occurred relatively evenly over all volumes of the reactor building post-break.

Table 6.2.
Maximum Pressure Response of Volumes, Excluding HV.

Scenario	Maximum Pressure Difference kPa (psid)	
	1/28th	Full
1	9.35 (1.36)	6.84 (0.99)
2	7.91 (1.15)	8.12 (1.18)
3	9.35 (1.36)	6.84 (0.99)
4	8.79 (1.27)	9.06 (1.31)
5	9.35 (1.36)	6.84 (0.99)
6	7.94 (1.15)	8.16 (1.18)

Observance of these values shows a number of trends with the largest being that RPV scenarios always experienced the same maximum, in individual scales, due to the reliance on the blowout panel. SGV scenarios obtained different maximum values for each scenario, with scenario

4 being the highest pressure result of the scenarios as it overall had the smallest expansion volume for the blowdown. Scenario 6 was next highest, and the base scenario 2 being lowest, with both of these scenarios having the same expansion volume but differing flow paths for the expanding helium. The 1/28th-scale model overall experienced higher-pressure response than that of the full-scale model. As a base reference point, the PSID for the MHTGR references the maximum pressure response as being 0.8 psid in response to a 30 in^2 helium break in the RC (General Atomics,R 6-10-5,1986). For comparison, this would most likely be simulated by scenario 1 which experienced a 0.99 psid difference, a 23.75% increase over the expected value. This may be attributed to the lost volume at the top of the RC due to the shape of the RPV chosen to support the experimental testing, as in the actual RC the volume is relatively open except for the RPV protruding control rod drive mechanisms.

One oddity discovered with the pressure results was that in the 1/28th-scale SGV break, an initial pressure spike would occur with the break initiation that would drive CV23-27 into a sharp spike before falling back into normal rise with the other reactor building volumes. The spike primarily occurs in scenario 2 and 6, and to a lesser extent in scenario 4. Discussed in a limited form throughout the affected results, this effect was thought to be caused by the creation of a pressure “bubble” in the central cavity which led to a quick burst of pressure that quickly bled away as flow is established in and out of the central cavity of the SGC. This oddity did not occur with the full-scale model, so it may be an issue with the smaller size of the volumes and MELCOR’s ability to handle the transfer between them.

Moving to the mass fraction results, a majority of the scenarios undergo a small amount of refill over the period of the scenario, with a majority of the refill occurring only in the upper most vent spaces of V21-22. In the 1/28th-scale only, Scenario 2 undergoes a major amount of mass

fraction change post-break. The full-scale model experiences a good amount of change across its scenarios though, with scenario 4 being the only scenario to not undergo refill outside of V21-22. Overall, the refilling of volumes was very minimal, driven mainly by natural flow between the volumes, and due to the shorter time period of simulation, did not drive a large amount of movement, though the full-scale does start to refill a number of the volumes over the shorter time period.

Scenario 2 is relatively unique in its mass fraction response, so it will be saved to talk about for a later period. Looking at scenarios 1, 3, and 6 of the full-scale results, the main refill occurring is still that of V21-22, but refill begins occurring in some of the volumes completely voided by the blowdown over the scenario period, a rise of less than 10%, but still a start to a return to a fill of normal air. Scenario 5 of the full-scale results stands as an outlier as it was the only scenario to undergo a large amount refill and atmospheric movement, with CV28 and CV36 exceeding air mass fractions of over 40% by the end of the 24 hour-simulation time, as well as the greatest refills amounts seen of all 14 tested scenarios. This is most likely due to a combination of factors as the full-scale model experienced much more refill overall and the extended flow path leads to extended pressure drop and atmosphere relocation.

Scenario 2, of all the scenarios, brings the most eventful results from its combination mass fraction results, as it is the only scenario to develop a unique banding structure of volume air mass fractions. Both scales undergo very similar results, which is not the point of discussion, but the oscillations that occur and were explored in the results sections of those scenarios. The $1/28^{th}$-scale results have a large number of these singular oscillations across the first 4 hours of the results, while the full-scale underwent only a single major oscillation followed by a lower constant oscillation until settling as the volumes entered the banding region. The volumes undergoing

oscillations were identified to be the small band volumes created by the nodalization to give more precise information on the elevations immediately surrounding oxygen sensors that were to be placed in the experimental setup.

Upon consulting the MELCOR group and conversing with them about these results, a set cause could not be determined that could potentially be causing the oscillations. A few potential causes were discussed which potentially could be related to the coupling method which is used in the code to link volumes or potentially the timestep. Timestep was described as potentially being an issue if it decreases to small enough, which had been seen in previous results that they had experienced. These oscillations could potentially be an overprediction/underprediction issue as the code handles the changes between the timesteps at such a small scale, results would be less consistent as if they were handled by a larger timestep and averaged over the period. From the differences seen between the two models, it would appear that the code has more difficulties handling the smaller timescale with the smaller volumes as the oscillations would swing across a larger range of values than they would in the full-scale. The full-scale by comparison undergoes much smaller, but constant, oscillations as it moved into a region of stabilization.

7. CONCLUSIONS AND RECOMMENDATIONS

7.1 Summary

MELCOR input decks of a 1/28th-scale and a full-scale MHTGR reactor building were constructed from a scaling study by Purdue University for the use in building an experimental test facility. Additional information was gathered from preliminary design documentation of the MHTGR to fill information gaps in knowledge to determine key features of models. Modeling focused on the major volumes and their flow paths between them to study the displacement of atmosphere from the experimental test facility and a full-scale facsimile. This would allow the determination of differences that scale would have on the response of the reactor building and how comparable experimental data would be to an actual constructed reactor building. Experimental data, while initially to be used for comparison in this paper, was delayed due to COVID-19 as the experimental facility construction was delayed.

Knowledge gathered from the construction of the input decks was documented to aid in future development of input decks and models of reactor buildings. The techniques developed during the creation of these models will aid in the future development of MELCOR models to study the spatial and temporal gas concentrations in gas-cooled reactor buildings. This is important as this use case extends beyond the standard use case of the code and helps to produce a more nodalized and localized dataset of volumes showing the wide response of specific volumes across an individual model that an overarching, simplified model would not be able to show. MELCOR models were successfully created using the new modeling techniques, a first-of-its-kind simulation using MELCOR in the study of gas concentrations through a HTGR reactor building. To allow for comparable data to be produced, a testing regime was produced to test the model under two

primary coolant boundary break locations and three changes to its layout to determine the reactor building response to changing circumstances.

7.2 Conclusions

The full testing regime was completed for the reactor models, both 1/28th-scale and full-scale, for a baseline and two break location and 3 layout changes, 14 scenarios total. Both breaks led to predicted results for most cases, with general progression through blowdown and beginning of refill as predicted. A singular scenario, 2, produced unique results that were not expected due to its complex blowdown and progression geometry, leading to a result of a relatively quick return to a high air content in many volumes.

Overall, the scale was seen to align closely between time and dimension changes with comparable results showing a close to 28x scale between the two models on the pressure and atmosphere mass fraction results. Maximum pressures recorded in the scenarios of RPV breaks was shown to be increased over expected values listed in the preliminary documentation of the MHTGR due in part to the simplified geometry of the vessels under consideration, leading to a decreased expansion volume in the reactor cavity.

Oscillations appeared in both combination mass fraction results for scenario 2. The manner of coupling for inter-volume transfer is potentially leading to the creation of the oscillation of gathered data. This issue only appears to occur between volumes specifically created to gather nodalized data in a small band around planned oxygen sensor locations in the Purdue experimental facility. This issue would most likely be alleviated in models that would divide cavities into more equal-sized volumes. The results of this testing will be of use in the further construction and testing of the Purdue facility and the models created herein are able to be extended to any future warranted testing needed for the facility testing.

7.3 Recommendations

During the progression of this research a few continuations and furthering methods for this research were discussed for the future of this section of research. Of highest importance would be better integration and modelling of the actual design of the reactor building of the MHTGR. Current models are based on the scaling study performed by Purdue University for the experimental setup, with all the limitations integrated of having a physical experimental setup. The full-scale model is a simple translation of the $1/28^{th}$-scale model to full size but retaining the limitations in an effort to show better comparison to the two scales. In the future, it would be prudent to make models based on the true layout of the reactor, with proper division of the steam generator cavities, HVAC systems, and full louver system function.

Longer term testing of the models would produce better results about refill patterns of the models. Currently with the time period of 24 hours, a large amount of collected data is limited to the initial volumes near the exterior volume, as without any forced circulation refill rates and movement of gases is very limited. A longer period of simulation would allow for more natural movement of gases to see how the reactor building would respond on its own to a longer-term displacement scenario. The introduction of methods to blow out the reactor building volumes from their helium filled state would be a potentially viable research path in the future.

The next concern would be full heat structure modelling of the reactor building walls and structures, to allow heat transfer and deposition into the physical structure of the building. With the models used in this testing, all volumes were surrounded with adiabatic surfaces, trapping all heat within the atmosphere of the volumes, with no transfer into the mass of the structure. By modelling the walls as proper structures with mass and the ability to absorb heat, characteristics of the accident progression could potentially change as energy is removed from the atmosphere of

the volumes and deposited into the walls and structures. This has the potential to change flow characteristics as temperature stratification could be decreased, leading to less natural flow being produced within volumes.

With the modelling of heat structures, it would be prudent to model the actual functioning reactor system as well as proper safety systems for coolant and reactor systems. In the case of primary coolant breaks, coolant is set to be pumped out of the primary system into holding tanks preventing larger scale transfer to the reactor building on the scale tested in these models. As well, since the reactor operates with an uninsulated vessel, under operation conditions the reactor cavity operates at a much higher temperature than modelled in this research. In a true MHTGR, waste heat is transferred in the reactor cavity which is then cooled off the operation of the RCCS wall cooling system, which would also help contribute to a natural circulation in the reactor cavity.

A full modelling of the reactor core and cooling system would give a more proper representation of a reactor primary coolant boundary break then the currently implemented volume method. The current model's single coolant volume is a relative gross simplification of the reactor coolant inventory volume. With proper modelling of the reactor volumes, connections, and connected equipment, coolant redistribution and atmospheric ingress into the reactor would be possible. This would serve a large number of possible research purposes in post-accident progression, not limited to the study of core graphite oxidation, radiation transfer out of the reactor core, and transfer of radiation out of the reactor building.

REFERENCES

Beeny, B., Vierow, K., 2015. Gas-Cooled Reactor Thermal Hydraulic Analyses with MELCOR. Progress in Nuclear Energy 85, 404–414. https://doi.org/10.1016/j.pnucene.2015.06.002

Brey, H.L., 1991. Fort St. Vrain Operations and Future. Energy 16, 47–58. https://doi.org/10.1016/0360-5442(91)90086-2

General Atomics, 1986. Preliminary Safety Information Document for the Standard MHTGR. https://www.nrc.gov/docs/ML0935/ML093560560.pdf

Ham, T.K., Arcilesi, D.J., Kim, I.H., Sun, X., Christensen, R.N., Oh, C.H., 2013. On the Effects of Containment Design to GT-MHR Air-ingress Accidents. Transactions of the American Nuclear Society 109, 316–319.

Haynes, M., Moreno, E., Owens, M., 2017. Evaluation and Testing of HTGR Reactor Building Response to Depressurization Accidents: FINAL PROJECT REPORT. Prepared for U.S. Department of Energy under DE-NE-0008324. https://www.osti.gov/servlets/purl/1398376

Humphries, L.L., Beeny, B.A., Faucett, C., Gelbard, F., Haskin, T., Louie, D.L., Phillips, J., Esmaili, H., 2017a. MELCOR Computer Code Manuals Vol. 2: Reference Manual. https://www.nrc.gov/docs/ML1704/ML17040A420.pdf

Humphries, L.L., Beeny, B.A., Gelbard, F., Louie, D.L., Phillips, J., Esmaili, H., 2017b. MELCOR Computer Code Manuals Vol. 1: Primer and Users' Guide. https://www.nrc.gov/docs/ML1704/ML17040A429.pdf

Jeon, J., Kim, Y.S., Choi, W., Kim, S.J., 2019. Identification of Hydrogen Flammability in Steam Generator Compartment of OPR1000 using MELCOR and CFX Codes. Nuclear Engineering and Technology 51, 1939–1950. https://doi.org/10.1016/J.NET.2019.06.024

Kang, J.C., Jeong, J.S., Lee, D.H., George, T.L., Lane, J.W., Thomasson, S.G., 2021. Coupling Gothic and RELAP5 for Passive Containment Cooling Modeling. Nuclear Technology. https://doi.org/10.1080/00295450.2020.1858628

Paladino, D., Zboray, R., Benz, P., Andreani, M., 2010. Three-Gas Mixture Plume Inducing Mixing and Stratification in a Multi-Compartment Containment. Nuclear Engineering and Design 240, 210–220. https://doi.org/10.1016/J.NUCENGDES.2008.07.014

Revankar, S., 2020. MHTGR Experimental Scaling Study. Personal Communication.

Safarzadeh, O., Noori-kalkhoran, O., Gei, M., Morini, L., Ahangari, R., 2021. Full Scope Simulation of VVER-1000 Blowdown Source and Containment Pressurization in a LBLOCA by Parallel Coupling of TRACE and CONTAIN. Progress in Nuclear Energy 140, 103897. https://doi.org/10.1016/J.PNUCENE.2021.103897

Skolik, K., Allison, C., Hohorst, J., Malicki, M., Perez-Ferragut, M., Pieńkowski, L., Trivedi, A., 2021. Analysis of Loss of Coolant Accident Without ECCS and DHRS in an Integral Pressurized Water Reactor Using RELAP/SCDAPSIM. Progress in Nuclear Energy 134, 103648. https://doi.org/10.1016/J.PNUCENE.2021.103648

Stempniewicz, M.M., 2000. Analysis of PANDA Passive Containment Cooling Steady-State Tests with the SPECTRA Code. Nuclear Technology 131, 82–101. https://doi.org/10.13182/NT00-A3106

Vierow, K., Hogan, K., Metzroth, K., Aldemir, T., 2014. Application of Dynamic Probabilistic Risk Assessment Techniques for Uncertainty Quantification in Generation IV Reactors. Progress in Nuclear Energy 77, 320–328. https://doi.org/10.1016/j.pnucene.2014.04.012

Williams, P.M., Silady, F.A., Dunn, T.D., Noren, R.C., McEachern, D.W., Dilling, D.A., Berkoe, J.M., Homan, F.J., Mears, L.D., Penfield, S.R., Lidsky, L.M., Yan, X.L., Reid, C.L., 1994. MHTGR Development in the United States. Progress in Nuclear Energy 28, 265–346. https://doi.org/10.1016/0149-1970(94)90002-7

Yang, S.R., Kappes, E., Nguyen, T., Vaghetto, R., Hassan, Y., 2018. Experimental Study on 1/28 Scaled NGNP HTGR Reactor Building Test Facility Response to Depressurization Event. Annals of Nuclear Energy 114, 154–164. https://doi.org/10.1016/J.ANUCENE.2017.12.023

Yildiz, M.A., Yang, S.R., Vaghetto, R., Hassan, Y.A., 2018. Numerical Analysis of 1/28 Scaled NGNP HTGR Reactor Building Test Facility Response to Depressurization Event Using GOTHIC. Annals of Nuclear Energy 119, 46–65. https://doi.org/10.1016/J.ANUCENE.2018.04.030

APPENDIX A: 1/28th-SCALE MHTGR INPUT NOTEBOOK

Appendix A gives package-by- package breakdown of an input deck for the 1/28th-scale model. Input cards used are given as well as variable names for correlation to the MELCOR user guide. The given example numbers are given from the Scenario 1. Further scenario variable numbers are given in Appendix C.

Table A.1: Global Data Block

Card	Variable	Value
MEG_DIAGFILE	DIAGFILE	'MHTGRSSg-1.dia'
MEL_DIAGFILE	DIAGFILE	'MHTGRSS-1.dia'
MEG_OUTPUTFILE	OUTPUTFILE	'MHTGRSSg-1.out'
MEL_OUTPUTFILE	OUTPUTFILE	'MHTGRSS-1.out'
MEG_RESTARTFILE	RESTARTFILE	'MHTGRSSg-1.rst'
MEL_RESTARTFILE	RESTARTFILE	'MHTGRSS-1.rst'
	NCYCLE	NCYCLE
	NREST	-1
MEG_HTML	HTMLFILE	'MHTGRSSg-1.html'
MEL_HTML	HTMLFILE	'MHTGRSS-1.html'
PLOTFILE	PLOTFILE	'MHTGRSSplot-1.ptf'
NOTEPAD++	-	ON
defaultdirectory	DefDIR	'Results'

Table A.2: MELGEN Initiation and NCG block

Card	Variable	Value
ALLOWREPLACE	-	-
NCG_INPUT	-	-
NCG_ID	MNAME	'N2'
NCG_ID	MNAME	'O2'
NCG_ID	MNAME	'AR'
NCG_ID	MNAME	'CO2'
NCG_ID	MNAME	'HE'

Table A.3: MELGEN CVH Block

Card	Variable	Value
CVH_INPUT	-	-
CV_ID	CVNAME	Table A.4
	ICVNUM	
CV_TYP	ICVTYP	
CV_VAT	ICVVZP	Table A.5
	NCVZ	
	CVZ	
	CVVOL	
CV_THR	ICVTHR	NONEQUIL
	IPFSW	FOG
	ICVACT	ACTIVE
CV_PAS	ITYPTH	SEPARATE
	IPORA	ONLYATM
	VAPORSTATE	SUPERHEATED
CV_PTD	PTDID	PVOL
	PVOL	Table A.4
CV_AAD	ATMID	TATM
	TATM	Table A.4
CV_NCG	NMMAT	Table A.6
	NCGID	
	RHUM	
	NUM	
	NAMGAS	
	MLFR	

Table A.4: CV_PTD, CV_AAD

CV_ID		CV_TYP	CV_PTD	CV_AAD	Description
CVNAME	**ICVNUM**	**ICVTYP**	**PVOL**	**TATM**	
CV11	101	‘CV1’	100000.000	300.00	Standardized Atmosphere Parameters
CV12	102				
CV13	103				
CV14	104				
CV15	105				
CV21	201	‘CV2’			
CV22	202				
CV23	203				
CV24	204				
CV25	205				
CV26	206				
CV27	207				
CV28	208				
CV29	209				
CV210	210				
CV31	301	‘CV3’			
CV32	302				
CV33	303				
CV34	304				
CV35	305				
CV36	306				
V11	411	‘V1’			
V12	412				
V21	421	‘V2’			
V22	422				
D1	510	‘D1’			
D2	520	‘D2’			
D3	530	‘D3’			
D4	540	‘D4’			
D5	550	‘D5’			
D6	560	‘D6’			
D7	570	‘D7’			
ATMO	900	‘HV’			
HV	800	‘ATMO’	6400000.000	960.000	Operating MHTGR Parameters

Table A.5: CV_VAT

CV_ID		CV_VAT				Description
CVNAME	**ICVNUM**	**ICVVZP**	**NCVZ**	**CVZ**	**CVVOL**	
CV11	101	2	1	0.29972	0.000000	Bottom of RC Cavity
			2	0.57912	0.031694	
CV12	102	2	1	0.57192	0.000000	
			2	0.64415	0.008193	
CV13	103	2	1	0.64415	0.000000	
			2	1.27406	0.042038	
CV14	104	2	1	1.27406	0.000000	
			2	1.32486	0.003390	
CV15	105	2	1	1.32486	0.000000	
			2	1.60427	0.018647	Top of RC Cavity
CV21	201	2	1	0.00000	0.000000	Bottom of Lower SGC Cavity
			2	0.06566	0.002862	
CV22	202	3	1	0.06566	0.000000	
			2	0.15240	0.003781	
			3	0.31115	0.008934	Top of Lower SGC Cavity
CV23	203	2	1	0.32385	0.000000	Bottom of Central SGC Cavity
			2	0.43180	0.002657	
CV24	204	2	1	0.43180	0.000000	
			2	0.48260	0.001250	
CV25	205	2	1	0.48260	0.000000	
			2	0.76708	0.007002	
CV26	206	2	1	0.76708	0.000000	
			2	0.81788	0.001250	
CV27	207	2	1	0.81788	0.000000	
			2	1.12802	0.008216	Top of Central SGC Cavity
CV28	208	2	1	1.14072	0.000000	Bottom of Top SGC Cavity
			2	1.33439	0.008442	
CV29	209	2	1	1.33439	0.000000	
			2	1.38519	0.002214	

CV210	210	2	1	1.38519	0.000000	
			2	1.57887	0.008443	Top of Top SGC Cavity
CV31	301	2	1	0.01270	0.000000	Bottom of EQS Cavity
			2	0.06566	0.001891	
CV32	302	2	1	0.06566	0.000000	
			2	0.62840	0.020097	
CV33	303	2	1	0.62840	0.000000	
			2	0.67920	0.001814	
CV34	304	2	1	0.67920	0.000000	
			2	0.99009	0.011103	
CV35	305	2	1	0.99009	0.000000	
			2	1.04089	0.001814	
CV36	306	2	1	1.04089	0.000000	
			2	1.32029	0.009978	Top of EQS Cavity
V11	411	2	1	1.44983	0.000000	Bottom of Lower Vent Space
			2	1.58090	0.009555	
V12	412	2	1	1.44983	0.000000	
			2	1.58090	0.009555	Top of Lower Vent Space
V21	421	2	1	1.58090	0.000000	Bottom of Upper Vent Space
			2	1.63170	0.001675	
V22	422	2	1	1.63170	0.000000	
			2	1.90704	0.009081	Top of Upper Vent Space
D1	510	2	1	0.32614	0.000000	
			2	0.44196	0.000730	
D2	520	2	1	0.06909	0.000000	
			2	0.44196	0.003920	
D3	530	2	1	0.06909	0.000000	
			2	0.18491	0.000730	
D4	540	2	1	0.06566	0.000000	
			2	0.21374	0.002410	
D5	550	2	1	1.18694	0.000000	
			2	1.29718	0.001330	
D6	560	2	1	1.45822	0.000000	
			2	1.56795	0.001320	

D7	570	2	1	1.77826	0.000000	
			2	1.88799	0.000430	
ATMO	900	2	1	-1.00000	0.000000	
			2	55.00000	1000000	
HV	800	2	1	0.64415	0.000000	
			2	1.43677	0.056050	

Table A.6: CV_NCG

CV_ID		CV_NCG					
CVNAME	**ICVNUM**	**NMMAT**	**NCGID**	**RHUM**	**NUM**	**NAMGAS**	**MLFR**
CV11	101	4	RHUM	0.000	1	‘N2’	0.78084
CV12	102						
CV13	103						
CV14	104						
CV15	105						
CV21	201						
CV22	202						
CV23	203						
CV24	204						
CV25	205				2	‘O2’	0.20946
CV26	206						
CV27	207						
CV28	208						
CV29	209						
CV210	210						
CV31	301						
CV32	302						
CV33	303				3	‘AR’	0.00934
CV34	304						
CV35	305						
CV36	306						
V11	411						
V12	412						
V21	421						
V22	422						
D1	510				4	‘CO2’	0.00036
D2	520						
D3	530						
D4	540						
D5	550						
D6	560						
D7	570						
ATMO	900						
HV	800	1			1	‘HE’	1.00000

Table A.7: MELGEN FL Block

Card	Variable	Value
FL_INPUT	-	-
FL_ID	FPNAME	Table A.8
	IFPNUM	
FL_FT	KCVFM	
	KCVTO	
	ZFM	
	ZTO	
FL_JSW	KFLGFL	
	IBUBF	NoBubbleRise
	IBUBT	NoBubbleRise
FL_GEO	FLARA	Table A.9
	FLLEN	
	FLOPO	
	FLHGTF	
	FLHGTT	
FL_JLF	ZBJFM	
	ZTJFM	
FL_JLT	ZBJTO	
	ZTJTO	
FL_SEG	IPNSG	1
	NSEG	1
	SAREA	Table A.10
	SLEN	
	SHYD	
	SRGH	5.0E-05
	LAMFG	CONST
	SLAM	0.0
FL_VLV	NVALVE	Table A.11
	NV	
	VLVNAME	
	FLNAME	
	KEYTRIP	
	NVFONF	

Table A.8: FL_ID, FL_FT, FL_JSW

FL_ID		FL_FT				FL_JSW
FPNAME	**IFPNUM**	**KCVFM**	**KCVTO**	**ZFM**	**ZTO**	**KFLGFL**
‘CV1-12’	101	‘CV11’	‘CV12’	0.57912	0.57912	0
‘CV1-21’	102	‘CV12’	‘CV11’			
‘CV1-23’	103	‘CV12’	‘CV13’	0.64415	0.64415	0
‘CV1-32’	104	‘CV13’	‘CV12’			
‘CV1-34’	105	‘CV13’	‘CV14’	1.27406	1.27406	0
‘CV1-43’	106	‘CV14’	‘CV13’			
‘CV1-45’	107	‘CV14’	‘CV15’	1.32486	1.32486	0
‘CV1-54’	108	‘CV15’	‘CV14’			
‘CV2-12’	201	‘CV21’	‘CV22’	0.06566	0.06566	0
‘CV2-21’	202	‘CV22’	‘CV21’			
‘CV2-23’	203	‘CV22’	‘CV23’	0.31115	0.32385	0
‘CV2-32’	204	‘CV23’	‘CV22’	0.32385	0.31115	
‘CV2-34’	205	‘CV23’	‘CV24’	0.43180	0.43180	0
‘CV2-43’	206	‘CV24’	‘CV23’			
‘CV2-45’	207	‘CV24’	‘CV25’	0.48260	0.48260	0
‘CV2-54’	208	‘CV25’	‘CV24’			
‘CV2-56’	209	‘CV25’	‘CV26’	0.76708	0.76708	0
‘CV2-65’	210	‘CV26’	‘CV25’			
‘CV2-67’	211	‘CV26’	‘CV27’	0.81788	0.81788	0
‘CV2-76’	212	‘CV27’	‘CV26’			
‘CV2-78’	213	‘CV27’	‘CV28’	1.12802	1.14072	0
‘CV2-87’	214	‘CV28’	‘CV27’	1.14072	1.12802	
‘CV2-89’	215	‘CV28’	‘CV29’	1.33439	1.33439	0
‘CV2-98’	216	‘CV29’	‘CV28’			
‘CV2-910’	217	‘CV29’	‘CV210’	1.38519	1.38519	0
‘CV2-109’	218	‘CV210’	‘CV29’			
‘CV3-12’	301	‘CV31’	‘CV32’	0.06566	0.06566	0
‘CV3-21’	302	‘CV32’	‘CV31’			
‘CV3-23’	303	‘CV32’	‘CV33’	0.62840	0.62840	0
‘CV3-32’	304	‘CV33’	‘CV32’			
‘CV3-34’	305	‘CV33’	‘CV34’	0.67920	0.67920	0
‘CV3-43’	306	‘CV34’	‘CV33’			
‘CV3-45’	307	‘CV34’	‘CV35’	0.99009	0.99009	0
‘CV3-54’	308	‘CV35’	‘CV34’			
‘CV3-56’	309	‘CV35’	‘CV36’	1.04089	1.04089	0
‘CV3-65’	310	‘CV36’	‘CV35’			
‘V1-12’	401	‘V11’	‘V12’	1.54813	1.54813	3
‘V1-21’	402	‘V12’	‘V11’	1.48260	1.48260	
‘V12V21’	403	‘V12’	‘V21’	1.58090	1.58090	0
‘V21V12’	404	‘V21’	‘V12’			

‘V2-12’	405	‘V21’	‘V22’	1.63170	1.63170	0
‘V2-21’	406	‘V22’	‘V21’			
‘CV11D1’	501	‘CV11’	‘D1’	0.41300	0.41300	3
‘D1CV11’	502	‘D1’	‘CV11’	0.35509	0.35509	
‘D1D2’	503	‘D1’	‘D2’	0.41300	0.41300	3
‘D2D1’	504	‘D2’	‘D1’	0.35484	0.35484	
‘D2D3’	505	‘D2’	‘D3’	0.15596	0.15596	3
‘D3D2’	506	‘D3’	‘D2’	0.09804	0.09804	
‘D3CV22’	507	‘D3’	‘CV22’	0.15596	0.15596	3
‘CV22D3’	508	‘CV22’	‘D3’	0.09804	0.09804	
‘CV22D4’	509	‘CV22’	‘D4’	0.17672	0.17672	3
‘D4CV22’	510	‘D4’	‘CV22’	0.10268	0.10268	
‘D4CV32’	511	‘D4’	‘CV32’	0.17672	0.17672	3
‘CV32D4’	512	‘CV32’	‘D4’	0.10268	0.10268	
‘CV36D5’	513	‘CV36’	‘D5’	1.26962	1.26962	3
‘D5CV36’	514	‘D5’	‘CV36’	1.21450	1.21450	
‘D5CV28’	515	‘D5’	‘CV28’	1.26962	1.26962	3
‘CV28D5’	516	‘CV28’	‘D5’	1.21450	1.21450	
‘CV210D6’	517	‘CV210’	‘D6’	1.54051	1.54051	3
‘D6CV210’	518	‘D6’	‘CV210’	1.48565	1.48565	
‘D6V11’	519	‘D6’	‘V11’	1.54051	1.54051	3
‘V11D6’	520	‘V11’	‘D6’	1.48565	1.48565	
‘V22D7’	521	‘V22’	‘D7’	1.86055	1.86055	3
‘D7V22’	522	‘D7’	‘V22’	1.80569	1.80569	
‘D7ATMO’	524	‘D7’	‘ATMO’	1.86055	1.86055	3
‘ATMOD7’	525	‘ATMO’	‘D7’	1.80569	1.80569	
‘TL’	600	‘HV’	‘CV15’	1.43677	1.43677	0

Table A.9: FL_GEO, FL_JLF, FL_JLT

FL_ID	FL_GEO					FL_JLF		FL_JLT	
FPNAME	FLARA	FLLEN	FLOPO	FLHGTF	FLHGTT	ZBJFM	ZTJFM	ZBJTO	ZTJTO
'CV1-12'	0.05672	0.01000	1.0	0.58912	0.57912	-	-	-	-
'CV1-21'				0.57912	0.58912	-	-	-	-
'CV1-23'	0.03337	0.01000	1.0	0.65415	0.64415	-	-	-	-
'CV1-32'				0.64415	0.65415	-	-	-	-
'CV1-34'	0.03337	0.0100	1.0	1.28406	1.27406	-	-	-	-
'CV1-43'				1.27406	1.28406	-	-	-	-
'CV1-45'	0.03337	0.01000	1.0	1.33486	1.32486	-	-	-	-
'CV1-54'				1.32486	1.33486	-	-	-	-
'CV2-12'	0.021795	0.01000	1.0	0.07566	0.06566	-	-	-	-
'CV2-21'				0.06566	0.07566	-	-	-	-
'CV2-23'	0.002925	0.21270	1.0	-	-	-	-	-	-
'CV2-32'				-	-	-	-	-	-
'CV2-34'	0.012305	0.01000	1.0	0.44180	0.43180	-	-	-	-
'CV2-43'				0.43180	0.44180	-	-	-	-
'CV2-45'	0.012305	0.01000	1.0	0.49260	0.48260	-	-	-	-
'CV2-54'				0.48260	0.49260	-	-	-	-
'CV2-56'	0.012305	0.01000	1.0	0.77708	0.76708	-	-	-	-
'CV2-65'				0.76708	0.77708	-	-	-	-
'CV2-67'	0.012305	0.01000	1.0	0.82788	0.81788	-	-	-	-
'CV2-76'				0.81788	0.82788	-	-	-	-
'CV2-78'	0.0124145	0.21270	1.0	-	-	-	-	-	-
'CV2-87'				-	-	-	-	-	-
'CV2-89'	0.021795	0.01000	1.0	1.34439	1.33439	-	-	-	-
'CV2-98'				1.33439	1.34439	-	-	-	-
'CV2-910'	0.021795	0.01000	1.0	1.39519	1.38519	-	-	-	-
'CV2-109'				1.38519	1.39519	-	-	-	-
'CV3-12'	0.017855	0.01000	1.0	0.07566	0.06566	-	-	-	-
'CV3-21'				0.06566	0.07566	-	-	-	-

‘CV3-23’	0.017855	0.01000	1.0	0.63840	0.62840	-	-	-	-
‘CV3-32’				0.62840	0.63840	-	-	-	-
‘CV3-34’	0.017855	0.01000	1.0	0.68920	0.67920	-	-	-	-
‘CV3-43’				0.67920	0.68920	-	-	-	-
‘CV3-45’	0.017855	0.01000	1.0	1.00001	0.99009	-	-	-	-
‘CV3-54’				0.99009	1.00009	-	-	-	-
‘CV3-56’	0.017855	0.01000	1.0	1.05089	1.04089	-	-	-	-
‘CV3-65’				1.04089	1.05089	-	-	-	-
‘V1-12’	0.04275	0.01000	1.0	-	-	1.51537	1.58090	1.51537	1.58090
‘V1-21’				-	-	1.44983	1.51537	1.44983	1.51537
‘V12V21’	0.01649	0.01000	1.0	1.59090	1.58090	-	-	-	-
‘V21V12’				1.58090	1.59090	-	-	-	-
‘V2-12’	0.01649	0.01000	1.0	1.64170	1.63170	-	-	-	-
‘V2-21’				1.63170	1.64170	-	-	-	-
‘CV11D1’	0.00527	0.01000	1.0	-	-	0.38405	0.44196	0.38405	0.44196
‘D1CV11’				-	-	0.32614	0.38405	0.32614	0.38405
‘D1D2’	0.00527	0.01000	1.0	-	-	0.38405	0.44196	0.38405	0.44196
‘D2D1’				-	-	0.32614	0.38405	0.32614	0.38405
‘D2D3’	0.00527	0.01000	1.0	-	-	0.12700	0.18491	0.12700	0.18491
‘D3D2’				-	-	0.06909	0.12700	0.6909	0.12700
‘D3CV22’	0.00527	0.01000	0.0	-	-	0.12700	0.18491	0.12700	0.18491
‘CV22D3’				-	-	0.06909	0.12700	0.6909	0.12700
‘CV22D4’	0.00861	0.01000	1.0	-	-	0.13970	0.21374	0.13970	0.21374
‘D4CV22’				-	-	0.06566	0.13970	0.06566	0.13970
‘D4CV32’	0.00861	0.01000	1.0	-	-	0.13970	0.21374	0.13970	0.21374
‘CV32D4’				-	-	0.06566	0.13970	0.06566	0.13970
‘CV36D5’	0.00477	0.01000	1.0	-	-	1.24206	1.29718	1.24206	1.29718
‘D5CV36’				-	-	1.18694	1.24206	1.18694	1.24206
‘D5CV28’	0.00477	0.01000	1.0	-	-	1.24206	1.29718	1.24206	1.29718
‘CV28D5’				-	-	1.18694	1.24206	1.18694	1.24206
‘CV210D6’	0.00482	0.01000	1.0	-	-	1.51308	1.56795	1.51308	1.56795
‘D6CV210’				-	-	1.45822	1.51308	1.45822	1.51308

‘D6V11’	0.00482	0.01000	1.0	-	-	1.51308	1.56795	1.51308	1.56795
‘V11D6’				-	-	1.45822	1.51308	1.45822	1.51308
‘V22D7’	0.00482	0.01000	1.0	-	-	1.83312	1.88799	1.83312	1.88799
‘D7V22’				-	-	1.77826	1.83312	1.77826	1.83312
‘D7ATMO’	0.00482	0.01000	1.0	-	-	1.83312	1.88799	1.83312	1.88799
‘ATMOD7’				-	-	1.77826	1.83312	1.77826	1.83312
‘TL’	8.29080E-7	0.01000	1.0	-	-	-	-	-	-

Table A.10: FL_SEG

FL_ID	FL_SEG		
FPNAME	**SAREA**	**SLEN**	**SHYD**
‘CV1-12’	0.05672	0.01000	0.33680
‘CV1-21’			
‘CV1-23’	0.03337	0.01000	0.12632
‘CV1-32’			
‘CV1-34’	0.03337	0.01000	0.12632
‘CV1-43’			
‘CV1-45’	0.03337	0.01000	0.12632
‘CV1-54’			
‘CV2-12’	0.021795	0.01000	0.20878
‘CV2-21’			
‘CV2-23’	0.002925	0.21270	0.02235
‘CV2-32’			
‘CV2-34’	0.012305	0.01000	0.07438
‘CV2-43’			
‘CV2-45’	0.012305	0.01000	0.07438
‘CV2-54’			
‘CV2-56’	0.012305	0.01000	0.07438
‘CV2-65’			
‘CV2-67’	0.012305	0.01000	0.07438
‘CV2-76’			
‘CV2-78’	0.0124145	0.21270	0.17780
‘CV2-87’			
‘CV2-89’	0.021795	0.01000	0.20878
‘CV2-98’			
‘CV2-910’	0.021795	0.01000	0.20878
‘CV2-109’			
‘CV3-12’	0.017855	0.01000	0.18898
‘CV3-21’			
‘CV3-23’	0.017855	0.01000	0.18898
‘CV3-32’			
‘CV3-34’	0.017855	0.01000	0.18898
‘CV3-43’			
‘CV3-45’	0.017855	0.01000	0.18898
‘CV3-54’			
‘CV3-56’	0.017855	0.01000	0.18898
‘CV3-65’			
‘V1-12’	0.04275	0.01000	0.18699
‘V1-21’			
‘V12V21’	0.01649	0.01000	0.17885
‘V21V12’			

‘V2-12’	0.01649	0.01000	0.17885
‘V2-21’			
‘CV11D1’	0.00527	0.01000	0.11582
‘D1CV11’			
‘D1D2’	0.00527	0.01000	0.11582
‘D2D1’			
‘D2D3’	0.00527	0.01000	0.11582
‘D3D2’			
‘D3CV22’	0.00527	0.01000	0.11582
‘CV22D3’			
‘CV22D4’	0.00861	0.01000	0.14808
‘D4CV22’			
‘D4CV32’	0.00861	0.01000	0.14808
‘CV32D4’			
‘CV36D5’	0.00477	0.01000	0.11024
‘D5CV36’			
‘D5CV28’	0.00861	0.01000	0.14808
‘CV28D5’			
‘CV210D6’	0.00482	0.01000	0.10973
‘D6CV210’			
‘D6V11’	0.00482	0.01000	0.10973
‘V11D6’			
‘V22D7’	0.00482	0.01000	0.10973
‘D7V22’			
‘D7ATMO’	0.00482	0.01000	0.10973
‘ATMOD7’			
‘TL’	8.29082E-7	0.01000	0.10973

Table A.11: FL_VLV

FL_VLV					
NVALVE	**NV**	**VLVNAME**	**FLNAME**	**KEYTRIP**	**NVFONF**
3	1	BO1	‘D3CV22’	NoTRIP	CF_BO
	2	BO2	‘CV22D3’	NoTRIP	CF_BO
	3	LV	‘TL’	NoTRIP	CF_L

Table A.12: MELGEN CF Block

Card	Variable	Value
CF_INPUT	-	-
CF_ID	CFNAME	Table A.13
	ICFNUM	
	CFTYPE	
CF_SAI	CFSCAL	
	CFADCN	
	CFVALR	
CF_ARG	NCFARG	Table A.14
	NARG	
	CHARG	
	ARSCAL	
	ARADCN	
CF_FORMULA	NCFARG	Table A.15
	FTEXT	
	NARG	
	SHORTNAME	
	CHARG	
CF_LIV	LCFVAL	Table A.16
CF_MSG	MSGFIL	
	SWTMSG	
CF_CLS	CLASS	

Table A.13: CF_ID, CF_SAI

CF_ID			CF_SAI		
CFNAME	**ICFNUM**	**CFTYPE**	**CFSCAL**	**CFADCN**	**CFVALR**
DIFF-P	100	ADD	1.0	0.0	0.0
CF_BO	200	FORMULA	1.0	0.0	0.0
CF_L	210	FORMULA	1.0	0.0	0.0
OVER-PRES	300	L-GT	-	-	-
LEAK	310	L-GT	-	-	-

Table A.14: CF_ARG

CF_ID	CF_ARG				
CFNAME	**NCFARG**	**NARG**	**CHARG**	**ARSCAL**	**ARADCN**
DIFF-P	2	1	CVH-P(D3)	1.0	0.0
		2	CVH-P(CV22)	-1.0	0.0
CF_BO	-	-	-	-	-
CF_L	-	-	-	-	-
OVER-PRES	2	1	CF-VALU(CF_BO)	1.0	0.0
		2	EXEC-TIME	0.0	0.0
LEAK	2	1	CF-VALU(CF_L)	1.0	0.0
		2	EXEC-TIME	0.0	0.0

Table A.15: CF_FORMULA

CF_ID	**CF_FORMULA**				
CFNAME	**NCFARG**	**FTEXT**	**NARG**	**SHORTNAME**	**CHARG**
DIFF-P	-	-	-	-	-
CF_BO	5	L-A-IFTE(P1-P2>dP,ONE,SELF)	1	P1	CVH-P(D3)
			2	P2	CVH-P(CV22)
			3	DP	6894.85
			4	ONE	1.0
			5	SELF	CF-VALU('CF_BO')
CF_L	4	L-A-IFTE (T>TSTART,ONE,ZERO)	1	T	EXEC-TIME
			2	TSTART	20.0
			3	ONE	1.0
			4	ZERO	0.0
OVER-PRES	-	-	-	-	-
LEAK	-	-	-	-	-

Table A.16: CF_LIV, CF_MSG, CF_CLS

CF_ID	**CF_LIV**	**CF_MSG**		**CF_CLS**
CFNAME	LCFVAL	MSGFIL	SWTMSG	CLASS
DIFF-P	-	-	-	-
CF_BO	-	-	-	-
CF_L	-	-	-	-
OVER-PRES	FALSE	FULL-OUTPUT	'Blowout Panel Blown Out'	LATCH
LEAK	FALSE	FULL-OUTPUT	'Leak Initiated'	LATCH

Table A.17: MELGEN EXEC Block

Card	Variable	Value
EXEC_INPUT	-	-
EXEC_TITLE	Title	‘'MHTGR 1/28 SCALE SCENARIO 1'
EXEC_DTTIME	DT	1.0E-04

Table A.18: MELCOR EXEC Block

Card	Variable	Value
EXEC_INPUT	-	-
EXEC_TITLE	Title	‘'MHTGR 1/28 SCALE SCENARIO 1'
EXEC_CPULEFT	CPULEF	200.0
EXEC_CPULIM	CPULIM	25000.0
EXEC_TEND	TEND	86400
EXEC_TIME	NTMINV	3
	N	Table A.19
	TIME	
	DTMAX	
	DTMIN	
	DTEDIT	
	DTPLOT	
	DTREST	
	DCREST	
EXEC_DTTIME	DT	1.0E-02
EXEC_SOFTDTMIN	UNDERRUN_FRACTION	1.0E-06

Table A.19: EXEC_TIME

EXEC_TIME							
N	**TIME**	**DTMAX**	**DTMIN**	**DTEDIT**	**DTPLOT**	**DTREST**	**DCREST**
1	0.00E+00	1.00E-01	1.00E-06	0.10E+01	0.01E+00	0.10E+04	0.10E+11
2	2.00E+02	1.00E+00	1.00E-06	0.10E+02	0.10E+00	0.10E+04	0.10E+11
3	1.00E+03	1.00E+01	1.00E-06	0.10E+03	1.00E+00	0.10E+04	0.10E+11

APPENDIX B: FULL-SCALE MHTGR INPUT NOTEBOOK

Appendix A gives package-by- package breakdown of an input deck for the full-scale model. Input cards used are given as well as variable names for correlation to the MELCOR user guide. The given example numbers are given from the Scenario 1. Further scenario variable numbers are given in Appendix C.

Table B.1: Global Data Block

Card	Variable	Value
MEG_DIAGFILE	DIAGFILE	'MHTGRFSg-1.dia'
MEL_DIAGFILE	DIAGFILE	'MHTGRFS-1.dia'
MEG_OUTPUTFILE	OUTPUTFILE	'MHTGRFSg-1.out'
MEL_OUTPUTFILE	OUTPUTFILE	'MHTGRFS-1.out'
MEG_RESTARTFILE	RESTARTFILE	'MHTGRFSg-1.rst'
MEL_RESTARTFILE	RESTARTFILE	'MHTGRFS-1.rst'
	NCYCLE	NCYCLE
	NREST	-1
MEG_HTML	HTMLFILE	'MHTGRFSg-1.html'
MEL_HTML	HTMLFILE	'MHTGRFS-1.html'
PLOTFILE	PLOTFILE	'MHTGRFSplot-1.ptf'
NOTEPAD++	-	ON
defaultdirectory	DefDIR	'Results'

Table B.2: MELGEN Initiation and NCG block

Card	Variable	Value
ALLOWREPLACE	-	-
NCG_INPUT	-	-
NCG_ID	MNAME	'N2'
NCG_ID	MNAME	'O2'
NCG_ID	MNAME	'AR'
NCG_ID	MNAME	'CO2'
NCG_ID	MNAME	'HE'

Table B.3: MELGEN CVH Block

Card	Variable	Value
CVH_INPUT	-	-
CV_ID	CVNAME	Table B.4
	ICVNUM	
CV_TYP	ICVTYP	
CV_VAT	ICVVZP	Table B.5
	NCVZ	
	CVZ	
	CVVOL	
CV_THR	ICVTHR	NONEQUIL
	IPFSW	FOG
	ICVACT	ACTIVE
CV_PAS	ITYPTH	SEPARATE
	IPORA	ONLYATM
	VAPORSTATE	SUPERHEATED
CV_PTD	PTDID	PVOL
	PVOL	Table B.4
CV_AAD	ATMID	TATM
	TATM	Table B.4
CV_NCG	NMMAT	Table B.6
	NCGID	
	RHUM	
	NUM	
	NAMGAS	
	MLFR	

Table B.4: CV_PTD, CV_AAD

CV_ID		CV_TYP	CV_PTD	CV_AAD	Description
CVNAME	**ICVNUM**	**ICVTYP**	**PVOL**	**TATM**	
CV11	101	‘CV1’	100000.000	300.00	Standardized Atmosphere Parameters
CV12	102				
CV13	103				
CV14	104				
CV15	105				
CV21	201	‘CV2’			
CV22	202				
CV23	203				
CV24	204				
CV25	205				
CV26	206				
CV27	207				
CV28	208				
CV29	209				
CV210	210				
CV31	301	‘CV3’			
CV32	302				
CV33	303				
CV34	304				
CV35	305				
CV36	306				
V11	411	‘V1’			
V12	412				
V21	421	‘V2’			
V22	422				
D1	510	‘D1’			
D2	520	‘D2’			
D3	530	‘D3’			
D4	540	‘D4’			
D5	550	‘D5’			
D6	560	‘D6’			
D7	570	‘D7’			
ATMO	900	‘HV’			
HV	800	‘ATMO’	6400000.000	960.000	Operating MHTGR Parameters

Table B.5: CV_VAT

CV_ID		CV_VAT				Description
CVNAME	**ICVNUM**	**ICVVZP**	**NCVZ**	**CVZ**	**CVVOL**	
CV11	101	2	1	08.39218	000.00000	Bottom of RC Cavity
			2	16.21536	695.73990	
CV12	102	2	1	16.21536	000.00000	
			2	18.03607	179.85010	
CV13	103	2	1	18.03607	000.00000	
			2	35.67368	922.82780	
CV14	104	2	1	35.67368	000.00000	
			2	37.09608	074.42222	
CV15	105	2	1	37.09608	000.00000	
			2	44.91948	409.33280	Top of RC Cavity
CV21	201	2	1	00.00000	000.00000	Bottom of Lower SGC Cavity
			2	01.83848	062.82965	
CV22	202	3	1	01.83846	000.00000	
			2	04.26721	083.00129	
			3	08.71222	134.90070	Top of Lower SGC Cavity
CV23	203	2	1	09.06782	000.00000	Bottom of Central SGC Cavity
			2	12.09040	058.32264	
CV24	204	2	1	12.09040	000.00000	
			2	13.51280	027.44611	
CV25	205	2	1	13.51280	000.00000	
			2	21.47824	153.69820	
CV26	206	2	1	21.47824	000.00000	
			2	22.90064	027.44611	
CV27	207	2	1	22.90064	000.00000	
			2	31.58446	180.36404	Top of Central SGC Cavity
CV28	208	2	1	31.94006	000.00000	Bottom of Top SGC Cavity
			2	37.36292	185.32519	
CV29	209	2	1	37.36292	000.00000	
			2	38.78532	048.61021	

CV210	210	2	1	38.78532	000.00000	
			2	44.20828	185.32848	Top of Top SGC Cavity
CV31	301	2	1	00.35560	000.00000	Bottom of EQS Cavity
			2	01.83848	041.51805	
CV32	302	2	1	01.83848	000.00000	
			2	17.59520	441.16081	
CV33	303	2	1	17.59520	000.00000	
			2	19.01760	039.82473	
CV34	304	2	1	19.01760	000.00000	
			2	27.72252	243.72265	
CV35	305	2	1	27.72252	000.00000	
			2	29.14492	039.82473	
CV36	306	2	1	29.14492	000.00000	
			2	36.96825	219.03966	Top of EQS Cavity
V11	411	2	1	40.59538	000.00000	Bottom of Lower Vent Space
			2	44.26518	209.73710	
V12	412	2	1	40.59538	000.00000	
			2	44.26518	209.73710	Top of Lower Vent Space
V21	421	2	1	44.26518	000.00000	Bottom of Upper Vent Space
			2	45.68760	036.77943	
V22	422	2	1	45.68760	000.00000	
			2	53.39700	199.34110	Top of Upper Vent Space
D1	510	2	1	09.13183	000.00000	
			2	12.37490	015.92087	
D2	520	2	1	01.93447	000.00000	
			2	12.37490	086.00793	
D3	530	2	1	01.93447	000.00000	
			2	05.17755	015.92087	
D4	540	2	1	01.83846	000.00000	
			2	05.98476	052.81625	
D5	550	2	1	33.23444	000.00000	
			2	36.32106	029.26913	
D6	560	2	1	40.83007	000.00000	
			2	43.90246	028.99999	

D7	570	2	1	49.79121	000.00000	
			2	52.86360	009.49091	
ATMO	900	2	1	-1.00000	000.00000	
			2	55.00000	10000000	
HV	800	2	1	18.03607	000.00000	
			2	40.22948	1230.30130	

Table B.6: CV_NCG

CV_ID		CV_NCG					
CVNAME	**ICVNUM**	**NMMAT**	**NCGID**	**RHUM**	**NUM**	**NAMGAS**	**MLFR**
CV11	101	4	RHUM	0.000	1	‘N2’	0.78084
CV12	102						
CV13	103						
CV14	104						
CV15	105						
CV21	201						
CV22	202						
CV23	203						
CV24	204						
CV25	205				2	‘O2’	0.20946
CV26	206						
CV27	207						
CV28	208						
CV29	209						
CV210	210						
CV31	301						
CV32	302						
CV33	303				3	‘AR’	0.00934
CV34	304						
CV35	305						
CV36	306						
V11	411						
V12	412						
V21	421						
V22	422						
D1	510				4	‘CO2’	0.00036
D2	520						
D3	530						
D4	540						
D5	550						
D6	560						
D7	570						
ATMO	900						
HV	800	1			1	‘HE’	1.00000

Table B.7: MELGEN FL Block

Card	Variable	Value
FL_INPUT	-	-
FL_ID	FPNAME	Table B.8
	IFPNUM	
FL_FT	KCVFM	
	KCVTO	
	ZFM	
	ZTO	
FL_JSW	KFLGFL	
	IBUBF	NoBubbleRise
	IBUBT	NoBubbleRise
FL_GEO	FLARA	Table B.9
	FLLEN	
	FLOPO	
	FLHGTF	
	FLHGTT	
FL_JLF	ZBJFM	
	ZTJFM	
FL_JLT	ZBJTO	
	ZTJTO	
FL_SEG	IPNSG	1
	NSEG	1
	SAREA	Table B.10
	SLEN	
	SHYD	
	SRGH	5.0E-05
	LAMFG	CONST
	SLAM	0.0
FL_VLV	NVALVE	Table B.11
	NV	
	VLVNAME	
	FLNAME	
	KEYTRIP	
	NVFONF	

Table B.8: FL_ID, FL_FT, FL_JSW

FL_ID		FL_FT				FL_JSW
FPNAME	**IFPNUM**	**KCVFM**	**KCVTO**	**ZFM**	**ZTO**	**KFLGFL**
‘CV1-12’	101	‘CV11’	‘CV12’	16.21536	16.21536	0
‘CV1-21’	102	‘CV12’	‘CV11’			
‘CV1-23’	103	‘CV12’	‘CV13’	18.03607	18.03607	0
‘CV1-32’	104	‘CV13’	‘CV12’			
‘CV1-34’	105	‘CV13’	‘CV14’	35.77368	35.67368	0
‘CV1-43’	106	‘CV14’	‘CV13’			
‘CV1-45’	107	‘CV14’	‘CV15’	37.09608	37.09608	0
‘CV1-54’	108	‘CV15’	‘CV14’			
‘CV2-12’	201	‘CV21’	‘CV22’	01.83848	0.183848	0
‘CV2-21’	202	‘CV22’	‘CV21’			
‘CV2-23’	203	‘CV22’	‘CV23’	08.71222	09.06782	0
‘CV2-32’	204	‘CV23’	‘CV22’	09.06782	08.71222	
‘CV2-34’	205	‘CV23’	‘CV24’	12.09040	12.09040	0
‘CV2-43’	206	‘CV24’	‘CV23’			
‘CV2-45’	207	‘CV24’	‘CV25’	13.51280	13.51280	0
‘CV2-54’	208	‘CV25’	‘CV24’			
‘CV2-56’	209	‘CV25’	‘CV26’	21.47824	21.47824	0
‘CV2-65’	210	‘CV26’	‘CV25’			
‘CV2-67’	211	‘CV26’	‘CV27’	22.90064	22.90064	0
‘CV2-76’	212	‘CV27’	‘CV26’			
‘CV2-78’	213	‘CV27’	‘CV28’	31.58446	31.94006	0
‘CV2-87’	214	‘CV28’	‘CV27’	31.94006	31.58446	
‘CV2-89’	215	‘CV28’	‘CV29’	37.36292	37.36292	0
‘CV2-98’	216	‘CV29’	‘CV28’			
‘CV2-910’	217	‘CV29’	‘CV210’	38.78532	38.78532	0
‘CV2-109’	218	‘CV210’	‘CV29’			
‘CV3-12’	301	‘CV31’	‘CV32’	01.83848	01.83848	0
‘CV3-21’	302	‘CV32’	‘CV31’			
‘CV3-23’	303	‘CV32’	‘CV33’	17.59520	17.59520	0
‘CV3-32’	304	‘CV33’	‘CV32’			
‘CV3-34’	305	‘CV33’	‘CV34’	19.01760	19.01760	0
‘CV3-43’	306	‘CV34’	‘CV33’			
‘CV3-45’	307	‘CV34’	‘CV35’	27.72252	27.72252	0
‘CV3-54’	308	‘CV35’	‘CV34’			
‘CV3-56’	309	‘CV35’	‘CV36’	29.14492	29.14492	0
‘CV3-65’	310	‘CV36’	‘CV35’			
‘V1-12’	401	‘V11’	‘V12’	43.34773	43.34773	3
‘V1-21’	402	‘V12’	‘V11’	41.51283	41.51283	
‘V12V21’	403	‘V12’	‘V21’	44.26518	44.26518	0
‘V21V12’	404	‘V21’	‘V12’			

‘V2-12’	405	‘V21’	‘V22’	45.68760	45.68760	0
‘V2-21’	406	‘V22’	‘V21’			
‘CV11D1’	501	‘CV11’	‘D1’	11.56414	11.56414	3
‘D1CV11’	502	‘D1’	‘CV11’	09.94260	09.94260	
‘D1D2’	503	‘D1’	‘D2’	11.56414	11.56414	3
‘D2D1’	504	‘D2’	‘D1’	09.94260	09.94260	
‘D2D3’	505	‘D2’	‘D3’	04.36678	04.36678	3
‘D3D2’	506	‘D3’	‘D2’	02.74524	02.74524	
‘D3CV22’	507	‘D3’	‘CV22’	04.36678	04.36678	3
‘CV22D3’	508	‘CV22’	‘D3’	02.74524	02.74524	
‘CV22D4’	509	‘CV22’	‘D4’	04.94818	04.94818	3
‘D4CV22’	510	‘D4’	‘CV22’	02.87506	02.87503	
‘D4CV32’	511	‘D4’	‘CV32’	04.94818	04.94818	3
‘CV32D4’	512	‘CV32’	‘D4’	02.87503	02.87503	
‘CV36D5’	513	‘CV36’	‘D5’	35.54940	35.54940	3
‘D5CV36’	514	‘D5’	‘CV36’	34.00610	34.00610	
‘D5CV28’	515	‘D5’	‘CV28’	35.54940	35.54940	3
‘CV28D5’	516	‘CV28’	‘D5’	34.00610	34.00610	
‘CV210D6’	517	‘CV210’	‘D6’	43.13437	43.13437	3
‘D6CV210’	518	‘D6’	‘CV210’	41.59817	43.59817	
‘D6V11’	519	‘D6’	‘V11’	43.13437	43.13437	3
‘V11D6’	520	‘V11’	‘D6’	41.59817	41.59817	
‘V22D7’	521	‘V22’	‘D7’	52.09550	52.09550	3
‘D7V22’	522	‘D7’	‘V22’	50.55931	50.55931	
‘D7ATMO’	524	‘D7’	‘ATMO’	52.09550	52.09550	3
‘ATMOD7’	525	‘ATMO’	‘D7’	50.55931	50.55931	
‘TL’	600	‘HV’	‘CV15’	40.22948	40.22948	0

Table B.9: FL_GEO, FL_JLF, FL_JLT

FL_ID	FL_GEO					FL_JLF		FL_JLT	
FPNAME	FLARA	FLLEN	FLOPO	FLHGTF	FLHGTT	ZBJFM	ZTJFM	ZBJTO	ZTJTO
‘CV1-12’	44.46655	0.10000	1.0	16.31536	16.21536	-	-	-	-
‘CV1-21’				16.21536	16.31536	-	-	-	-
‘CV1-23’	26.16080	0.10000	1.0	18.13607	18.03607	-	-	-	-
‘CV1-32’				18.03607	18.13607	-	-	-	-
‘CV1-34’	26.16080	0.10000	1.0	35.77368	35.67368	-	-	-	-
‘CV1-43’				35.67368	35.77368	-	-	-	-
‘CV1-45’	26.16080	0.10000	1.0	37.19608	37.09608	-	-	-	-
‘CV1-54’				37.09608	37.19608	-	-	-	-
‘CV2-12’	17.08739	0.10000	1.0	01.93848	01.83848	-	-	-	-
‘CV2-21’				01.83848	01.93848	-	-	-	-
‘CV2-23’	2.293304	0.55560	1.0	-	-	-	-	-	-
‘CV2-32’				-	-	-	-	-	-
‘CV2-34’	09.64782	0.10000	1.0	12.19040	12.09040	-	-	-	-
‘CV2-43’				12.09040	12.19040	-	-	-	-
‘CV2-45’	09.64782	0.10000	1.0	13.61280	13.51280	-	-	-	-
‘CV2-54’				13.51280	13.61280	-	-	-	-
‘CV2-56’	09.64782	0.10000	1.0	21.57824	21.47824	-	-	-	-
‘CV2-65’				21.47824	21.57824	-	-	-	-
‘CV2-67’	09.64782	0.10000	1.0	23.00064	22.90064	-	-	-	-
‘CV2-76’				22.90064	23.00064	-	-	-	-
‘CV2-78’	9.732875	0.55560	1.0	-	-	-	-	-	-
‘CV2-87’				-	-	-	-	-	-
‘CV2-89’	17.08739	0.10000	1.0	37.46292	37.36292	-	-	-	-
‘CV2-98’				37.36292	37.46292	-	-	-	-
‘CV2-910’	17.08739	0.10000	1.0	38.88532	38.78532	-	-	-	-
‘CV2-109’				38.78532	38.88532	-	-	-	-
‘CV3-12’	13.99913	0.10000	1.0	01.93848	01.83848	-	-	-	-
‘CV3-21’				01.83848	01.93848	-	-	-	-

‘CV3-23’	13.99913	0.10000	1.0	17.69520	17.59520	-	-	-	-
‘CV3-32’				17.59520	17.69520	-	-	-	-
‘CV3-34’	13.99913	0.10000	1.0	19.11760	19.01760	-	-	-	-
‘CV3-43’				19.01760	19.11760	-	-	-	-
‘CV3-45’	13.99913	0.10000	1.0	27.82252	27.72252	-	-	-	-
‘CV3-54’				27.72252	27.82252	-	-	-	-
‘CV3-56’	13.99913	0.10000	1.0	29.24492	29.14492	-	-	-	-
‘CV3-65’				29.14492	29.24492	-	-	-	-
‘V1-12’	33.51197	0.10000	1.0	-	-				
‘V1-21’				-	-				
‘V12V21’	12.92844	0.10000	1.0	44.36518	44.26518	-	-	-	-
‘V21V12’				44.26518	44.36518	-	-	-	-
‘V2-12’	12.92844	0.10000	1.0	45.78760	45.68760	-	-	-	-
‘V2-21’				45.68760	45.78760	-	-	-	-
‘CV11D1’	4.130235	0.10000	1.0	-	-	10.75337	12.37490	10.75337	12.37490
‘D1CV11’				-	-	09.13183	10.75337	09.13183	10.75337
‘D1D2’	4.130235	0.10000	1.0	-	-	10.75337	12.37490	10.75337	12.37490
‘D2D1’				-	-	09.13183	10.75337	09.13183	10.75337
‘D2D3’	4.130235	0.10000	1.0	-	-	03.55601	05.17755	03.55601	05.17755
‘D3D2’				-	-	01.93447	03.55601	01.93447	03.55601
‘D3CV22’	4.130235	0.10000	0.0	-	-	03.55601	05.17755	03.55601	05.17755
‘CV22D3’				-	-	01.93447	03.55601	01.93447	03.55601
‘CV22D4’	06.75122	0.10000	1.0	-	-	03.91161	05.98476	03.91161	05.98476
‘D4CV22’				-	-	01.83848	03.91161	01.83848	03.91161
‘D4CV32’	06.75122	0.10000	1.0	-	-	03.91161	05.98476	03.91161	05.98476
‘CV32D4’				-	-	01.83846	03.91161	01.83846	03.91161
‘CV36D5’	03.74132	0.10000	1.0	-	-	34.77775	36.32106	34.77775	36.32106
‘D5CV36’				-	-	33.23444	34.77775	33.23444	34.77775
‘D5CV28’	03.74132	0.10000	1.0	-	-	34.77775	36.32106	34.77775	36.32106
‘CV28D5’				-	-	33.23444	34.77775	33.23444	34.77775
‘CV210D6’	3.706915	0.10000	1.0	-	-	42.36627	43.90246	42.36627	43.90246
‘D6CV210’				-	-	40.83007	42.36627	40.83007	42.36627

‘D6V11’	3.706915	0.10000	1.0	-	-	42.36627	43.90246	42.36627	43.90246
‘V11D6’				-	-	40.83007	42.36627	40.83007	42.36627
‘V22D7’	3.706915	0.10000	1.0	-	-	51.32741	52.86360	51.32741	52.86360
‘D7V22’				-	-	49.79121	51.32741	49.79121	51.32741
‘D7ATMO’	3.706915	0.10000	1.0	-	-	51.32741	52.86360	51.32741	52.86360
‘ATMOD7’				-	-	49.79121	51.32741	49.79121	51.32741
‘TL’	6.5E-04	0.10000	1.0	-	-	-	-	-	-

Table B.10: FL_SEG

FL_ID	FL_SEG		
FPNAME	**SAREA**	**SLEN**	**SHYD**
‘CV1-12’	44.46655	0.10000	9.43034
‘CV1-21’			
‘CV1-23’	26.16080	0.10000	3.53695
‘CV1-32’			
‘CV1-34’	26.16080	0.10000	3.53695
‘CV1-43’			
‘CV1-45’	26.16080	0.10000	3.53695
‘CV1-54’			
‘CV2-12’	17.08739	0.10000	5.84576
‘CV2-21’			
‘CV2-23’	2.2933054	0.55560	0.62586
‘CV2-32’			
‘CV2-34’	9.64782	0.10000	2.08274
‘CV2-43’			
‘CV2-45’	9.64782	0.10000	2.08274
‘CV2-54’			
‘CV2-56’	9.64782	0.10000	2.08274
‘CV2-65’			
‘CV2-67’	9.64782	0.10000	2.08274
‘CV2-76’			
‘CV2-78’	9.732875	0.55560	4.97841
‘CV2-87’			
‘CV2-89’	17.08739	0.10000	5.84576
‘CV2-98’			
‘CV2-910’	17.08739	0.10000	5.84576
‘CV2-109’			
‘CV3-12’	13.99913	0.10000	5.29134
‘CV3-21’			
‘CV3-23’	13.99913	0.10000	5.29134
‘CV3-32’			
‘CV3-34’	13.99913	0.10000	5.29134
‘CV3-43’			
‘CV3-45’	13.99913	0.10000	5.29134
‘CV3-54’			
‘CV3-56’	13.99913	0.10000	5.29134
‘CV3-65’			
‘V1-12’	33.51197	0.10000	5.23558
‘V1-21’			
‘V12V21’	12.92844	0.10000	5.00780
‘V21V12’			

‘V2-12’	12.92844	0.10000	5.00780
‘V2-21’			
‘CV11D1’	4.130235	0.10000	3.24308
‘D1CV11’			
‘D1D2’	4.130235	0.10000	3.24308
‘D2D1’			
‘D2D3’	4.130235	0.10000	3.24308
‘D3D2’			
‘D3CV22’	4.130235	0.10000	3.24308
‘CV22D3’			
‘CV22D4’	6.75122	0.10000	4.14630
‘D4CV22’			
‘D4CV32’	6.75122	0.10000	4.14630
‘CV32D4’			
‘CV36D5’	3.74132	0.10000	3.08661
‘D5CV36’			
‘D5CV28’	3.74132	0.10000	3.08661
‘CV28D5’			
‘CV210D6’	3.706915	0.10000	3.07239
‘D6CV210’			
‘D6V11’	3.706915	0.10000	3.07239
‘V11D6’			
‘V22D7’	3.706915	0.10000	3.07239
‘D7V22’			
‘D7ATMO’	3.706915	0.10000	3.07239
‘ATMOD7’			
‘TL’	6.5E-04	0.10000	0.02877

Table B.11: FL_VLV

FL_VLV					
NVALVE	**NV**	**VLVNAME**	**FLNAME**	**KEYTRIP**	**NVFONF**
3	1	BO1	‘D3CV22’	NoTRIP	CF_BO
	2	BO2	‘CV22D3’	NoTRIP	CF_BO
	3	LV	‘TL’	NoTRIP	CF_L

Table B.12: MELGEN CF Block

Card	Variable	Value
CF_INPUT	-	-
CF_ID	CFNAME	Table B.13
	ICFNUM	
	CFTYPE	
CF_SAI	CFSCAL	
	CFADCN	
	CFVALR	
CF_ARG	NCFARG	Table B.14
	NARG	
	CHARG	
	ARSCAL	
	ARADCN	
CF_FORMULA	NCFARG	Table B.15
	FTEXT	
	NARG	
	SHORTNAME	
	CHARG	
CF_LIV	LCFVAL	Table B.16
CF_MSG	MSGFIL	
	SWTMSG	
CF_CLS	CLASS	

Table B.13: CF_ID, CF_SAI

CF_ID			CF_SAI		
CFNAME	**ICFNUM**	**CFTYPE**	**CFSCAL**	**CFADCN**	**CFVALR**
DIFF-P	100	ADD	1.0	0.0	0.0
CF_BO	200	FORMULA	1.0	0.0	0.0
CF_L	210	FORMULA	1.0	0.0	0.0
OVER-PRES	300	L-GT	-	-	-
LEAK	310	L-GT	-	-	-

Table B.14: CF_ARG

CF_ID	CF_ARG				
CFNAME	**NCFARG**	**NARG**	**CHARG**	**ARSCAL**	**ARADCN**
DIFF-P	2	1	CVH-P(D3)	1.0	0.0
		2	CVH-P(CV22)	-1.0	0.0
CF_BO	-	-	-	-	-
CF_L	-	-	-	-	-
OVER-PRES	2	1	CF-VALU(CF_BO)	1.0	0.0
		2	EXEC-TIME	0.0	0.0
LEAK	2	1	CF-VALU(CF_L)	1.0	0.0
		2	EXEC-TIME	0.0	0.0

Table B.15: CF_FORMULA

CF_ID	**CF_FORMULA**				
CFNAME	**NCFARG**	**FTEXT**	**NARG**	**SHORTNAME**	**CHARG**
DIFF-P	-	-	-	-	-
CF_BO	5	L-A-IFTE(P1-P2>dP,ONE,SELF)	1	P1	CVH-P(D3)
			2	P2	CVH-P(CV22)
			3	DP	6894.85
			4	ONE	1.0
			5	SELF	CF-VALU('CF_BO')
CF_L	4	L-A-IFTE (T>TSTART,ONE,ZERO)	1	T	EXEC-TIME
			2	TSTART	20.0
			3	ONE	1.0
			4	ZERO	0.0
OVER-PRES	-	-	-	-	-
LEAK	-	-	-	-	-

Table B.16: CF_LIV, CF_MSG, CF_CLS

CF_ID	**CF_LIV**	**CF_MSG**		**CF_CLS**
CFNAME	LCFVAL	MSGFIL	SWTMSG	CLASS
DIFF-P	-	-	-	-
CF_BO	-	-	-	-
CF_L	-	-	-	-
OVER-PRES	FALSE	FULL-OUTPUT	'Blowout Panel Blown Out'	LATCH
LEAK	FALSE	FULL-OUTPUT	'Leak Initiated'	LATCH

Table B.17: MELGEN EXEC Block

Card	Variable	Value
EXEC_INPUT	-	-
EXEC_TITLE	Title	‘'MHTGR FULL SCALE SCENARIO 1'
EXEC_DTTIME	DT	1.0E-04

Table B.18: MELCOR EXEC Block

Card	Variable	Value
EXEC_INPUT	-	-
EXEC_TITLE	Title	‘'MHTGR FULL SCALE SCENARIO 1'
EXEC_CPULEFT	CPULEF	200.0
EXEC_CPULIM	CPULIM	25000.0
EXEC_TEND	TEND	86400
EXEC_TIME	NTMINV	3
	N	Table B.19
	TIME	
	DTMAX	
	DTMIN	
	DTEDIT	
	DTPLOT	
	DTREST	
	DCREST	
EXEC_DTTIME	DT	1.0E-02
EXEC_SOFTDTMIN	UNDERRUN_FRACTION	1.0E-06

Table B.19: EXEC_TIME

EXEC_TIME							
N	**TIME**	**DTMAX**	**DTMIN**	**DTEDIT**	**DTPLOT**	**DTREST**	**DCREST**
1	0.00E+00	1.00E-01	1.00E-06	0.10E+01	0.01E+00	0.10E+04	0.10E+11
2	2.00E+02	1.00E+00	1.00E-06	0.10E+02	0.10E+00	0.10E+04	0.10E+11
3	1.00E+03	1.00E+01	1.00E-06	0.10E+03	1.00E+00	0.10E+04	0.10E+11

APPENDIX C: TESTING CRITERIA INPUT NOTEBOOK

Table C.1: 1/28th-Scale Steam Generator Break CV_VAT

CV_ID		CV_VAT			
CVNAME	**ICVNUM**	**ICVVZP**	**NCVZ**	**CVZ**	**CVVOL**
HV	570	2	1	0.15240	0.000000
			2	1.09728	0.05605

Table C.2: 1/28th-Scale Steam Generator Break FL_FT, FL_GEO

FL_ID	FL_FT				FL_GEO		
FPNAME	**KCVFM**	**KCVTO**	**ZFM**	**ZTO**	**FLARA**	**FLLEN**	**FLOPO**
'TL'	'HV'	'CV27'	1.09728	1.09728	1.04509E-05	0.01000	1.0

Table C.3: 1/28th-Scale Steam Generator Break FL_FT, FL_GEO

FL_ID	FL_SEG		
FPNAME	**SAREA**	**SLEN**	**SHYD**
'TL'	1.04509E-05	0.01000	0.00365

Table C.4: Full-Scale Steam Generator Break CV_VAT

CV_ID		CV_VAT			
CVNAME	**ICVNUM**	**ICVVZP**	**NCVZ**	**CVZ**	**CVVOL**
HV	570	2	1	04.26721	00.00000
			2	30.72390	1230.30130

Table C.5: Full-Scale Steam Generator Break FL_FT, FL_GEO

FL_ID	FL_FT				FL_GEO		
FPNAME	**KCVFM**	**KCVTO**	**ZFM**	**ZTO**	**FLARA**	**FLLEN**	**FLOPO**
'TL'	'HV'	'CV27'	30.72390	30.72390	0.00819	0.1000	1.0

Table C.6: Full-Scale Steam Generator Break FL_FT, FL_GEO

FL_ID	FL_SEG		
FPNAME	**SAREA**	**SLEN**	**SHYD**
'TL'	0.00819	0.1000	0.10212

Table C.7: Scenario FL_GEO variance, FLOPO set to 0.0 instead of 1.0

	Scenario						
	0	**1**	**2**	**3**	**4**	**5**	**6**
FPNAME	-	-	-	‘CV22D4’ ‘D4CV22’ ‘D5CV28’ ‘CV28D5’		‘CV2-23’ ‘CV2-32’	
IFPNUM	-	-	-	509 510 515 516		203 204	

APPENDIX D: 1/28th-SCALE RESULTS PLOTS

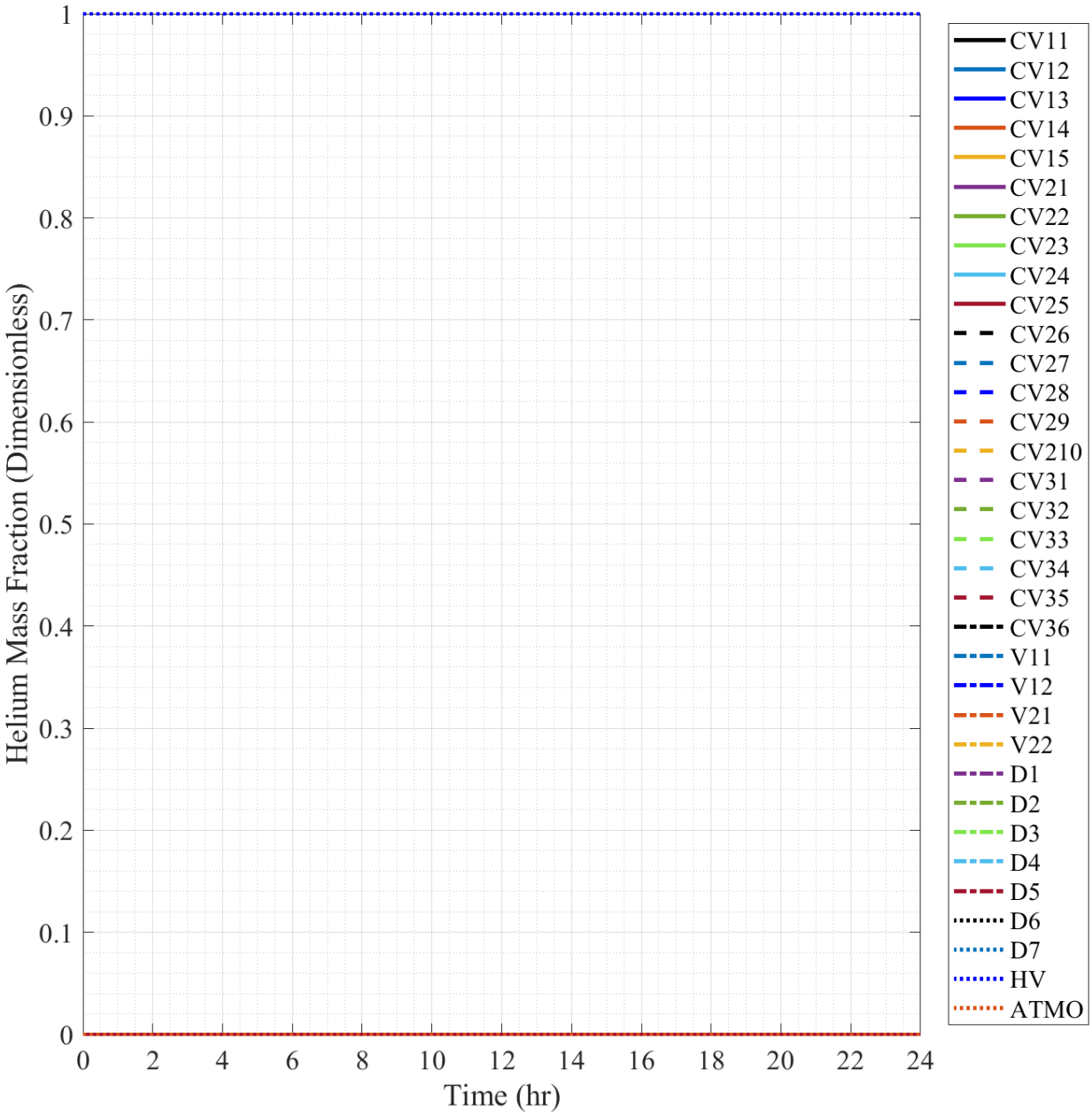

Fig. D.1. 1/28th-Scale Scenario 0 Pressure, Individual Data.

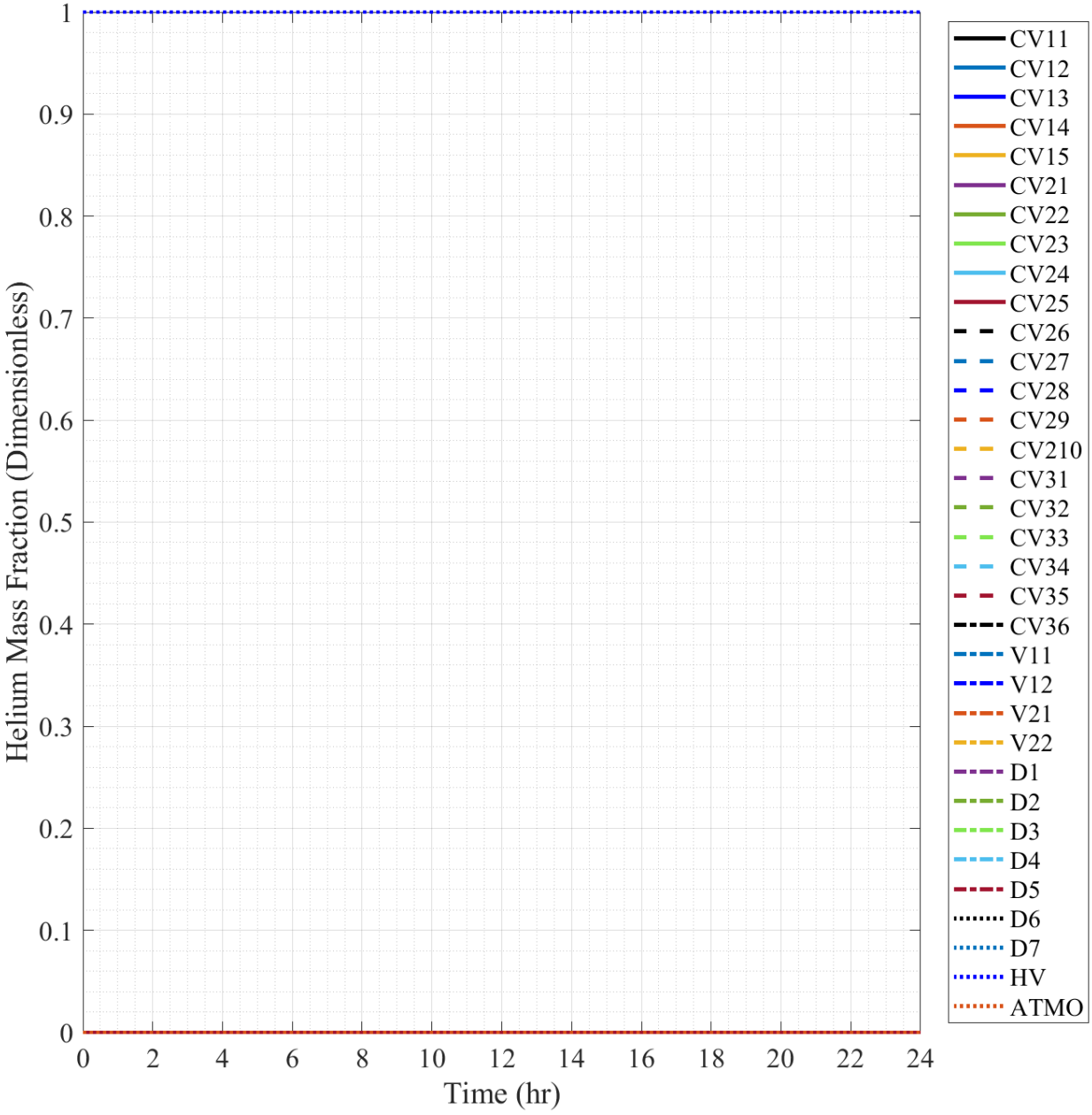

Fig. D.2. 1/28th-Scale Scenario 0 Helium Mass Fraction, Individual Data.

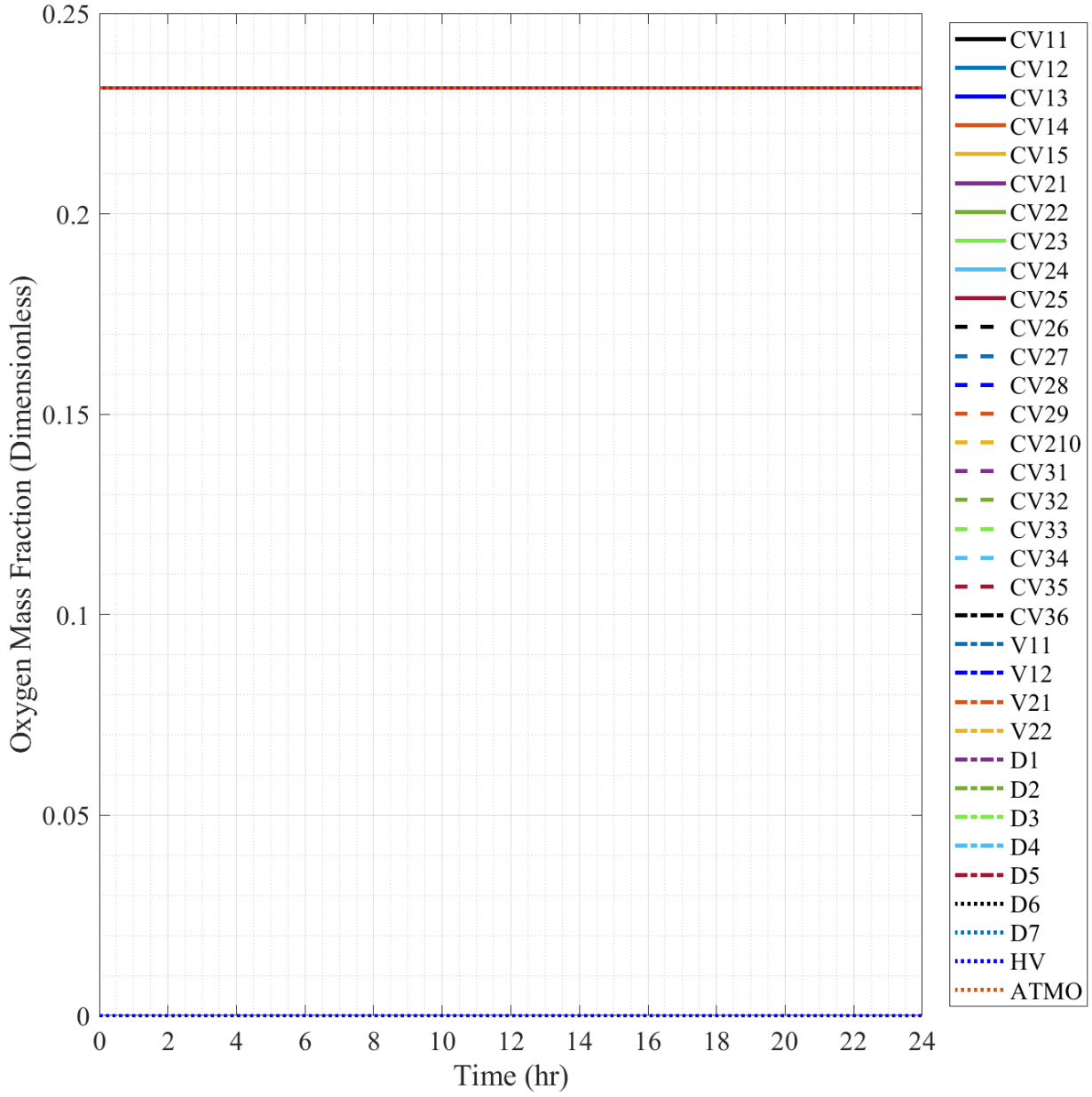

Fig. D.3. 1/28th-Scale Scenario 0 Oxygen Mass Fraction, Individual Data.

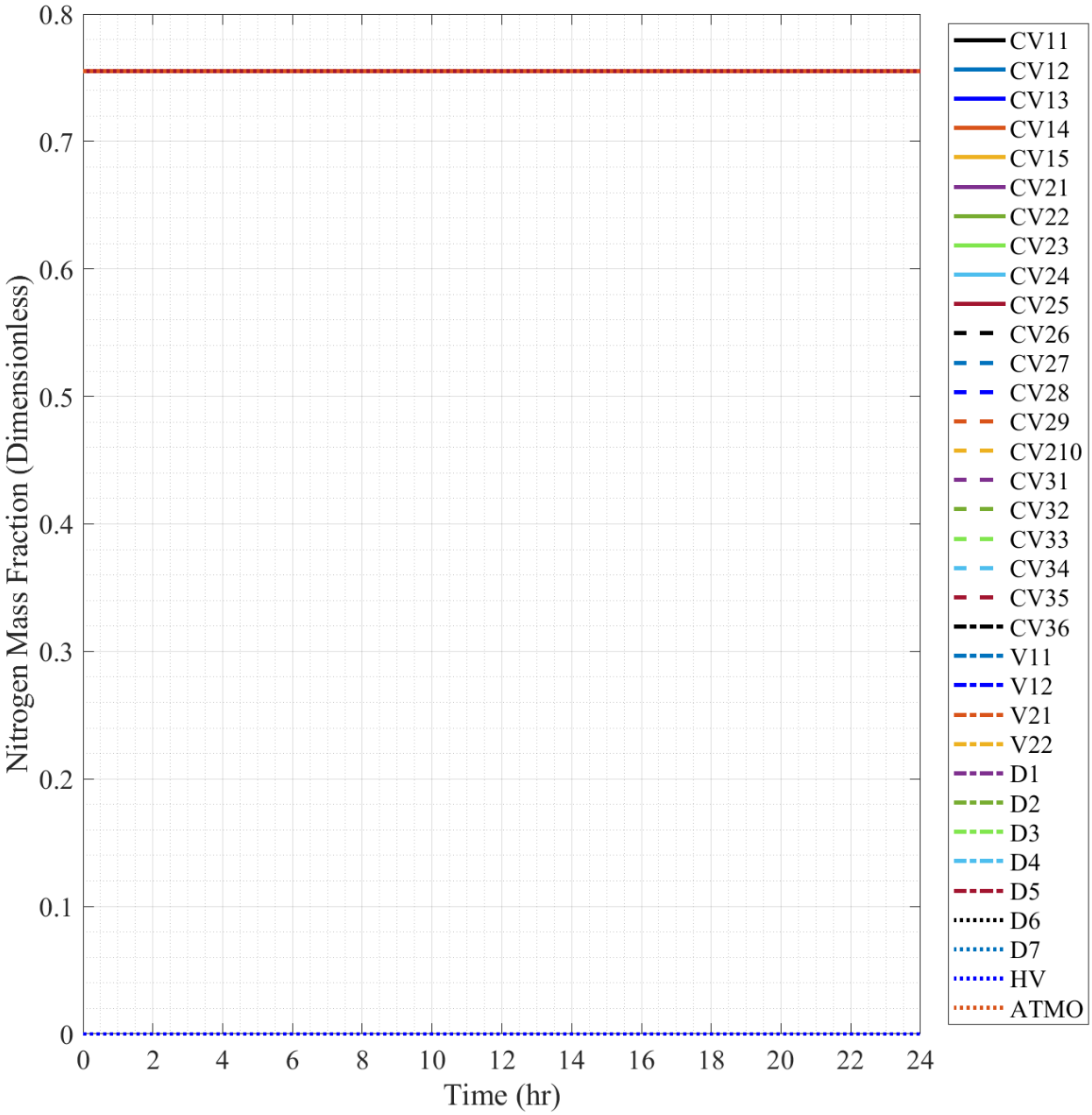

Fig. D.4. 1/28th-Scale Scenario 0 Nitrogen Mass Fraction,Individual Data.

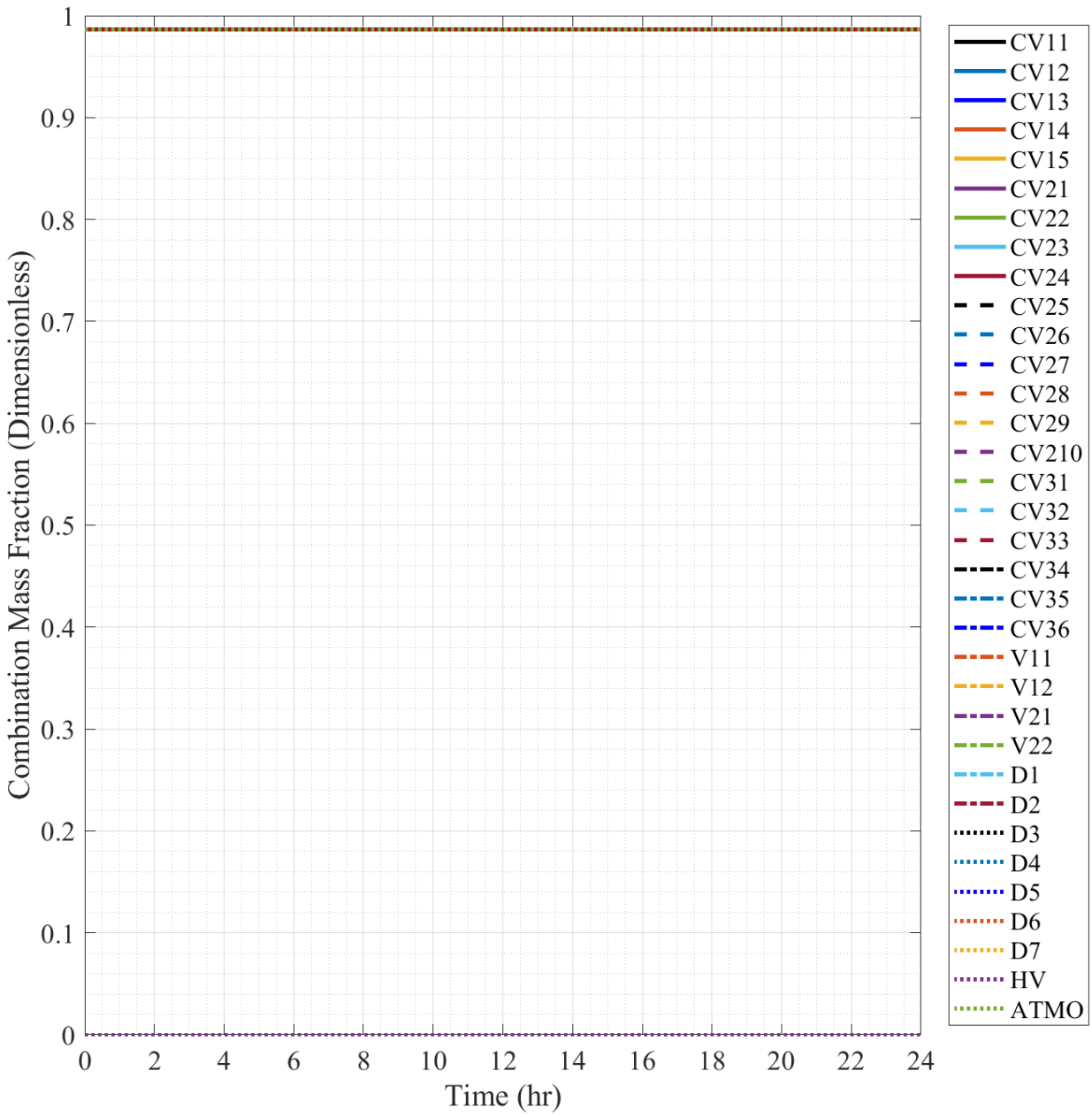

Fig. D.5. 1/28th-Scale Scenario 0 Combination Mass Fraction, Individual Data.

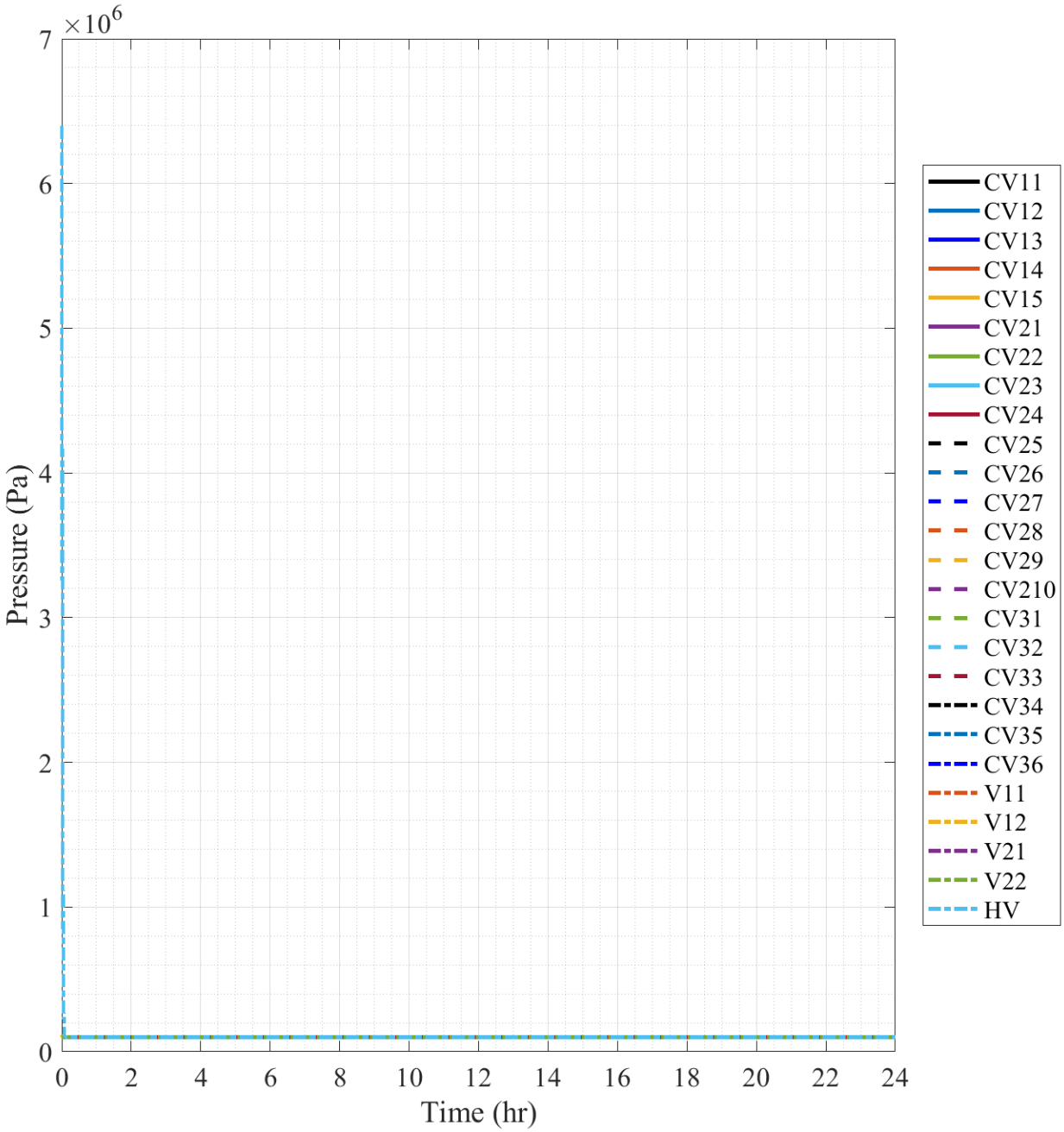

Fig. D.7. 1/28th-Scale Scenario 1 Pressure, Individual Data.

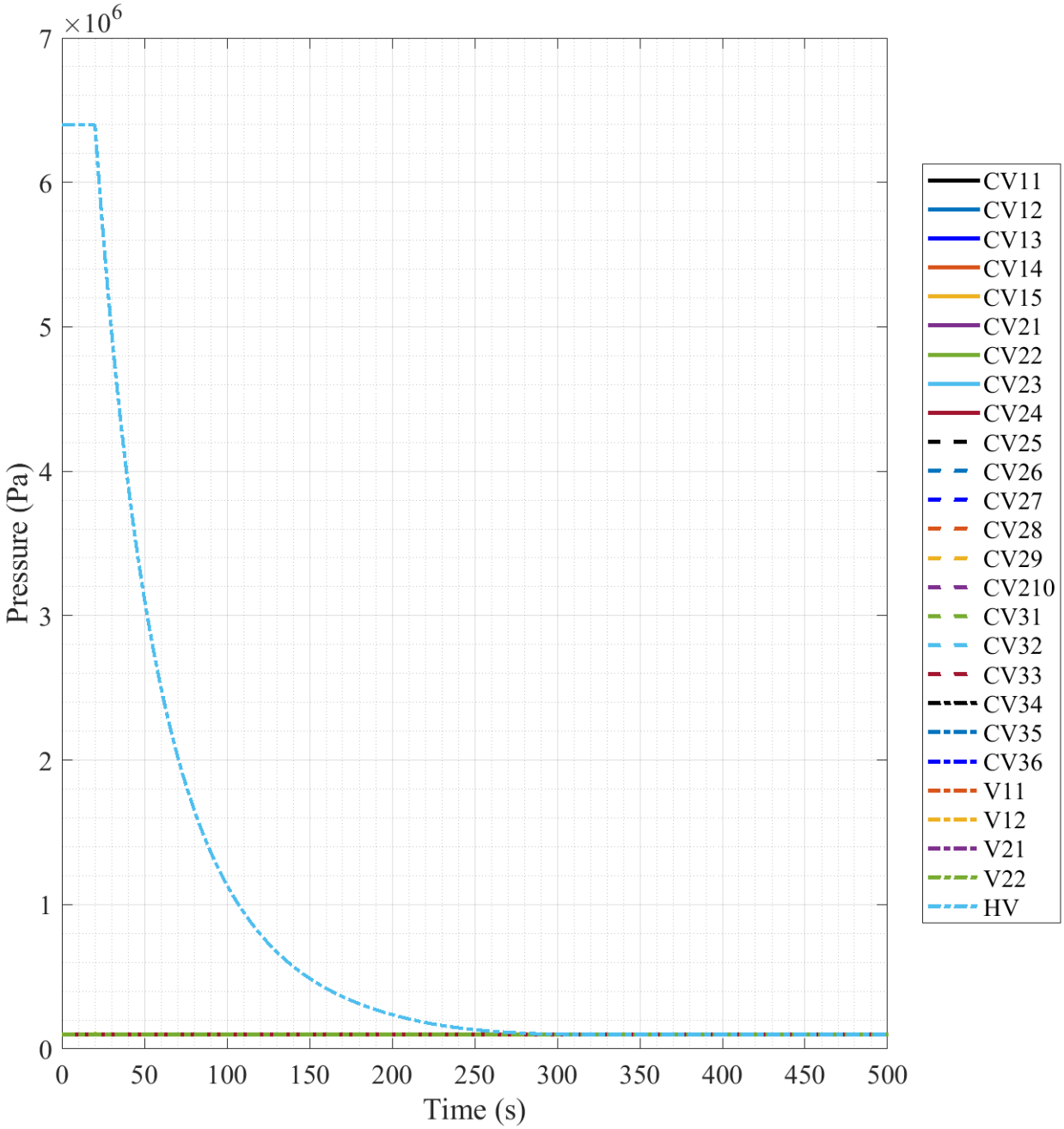

Fig. D.8. 1/28th-Scale Scenario 1 Pressure, 500 second Timescale, Individual Data.

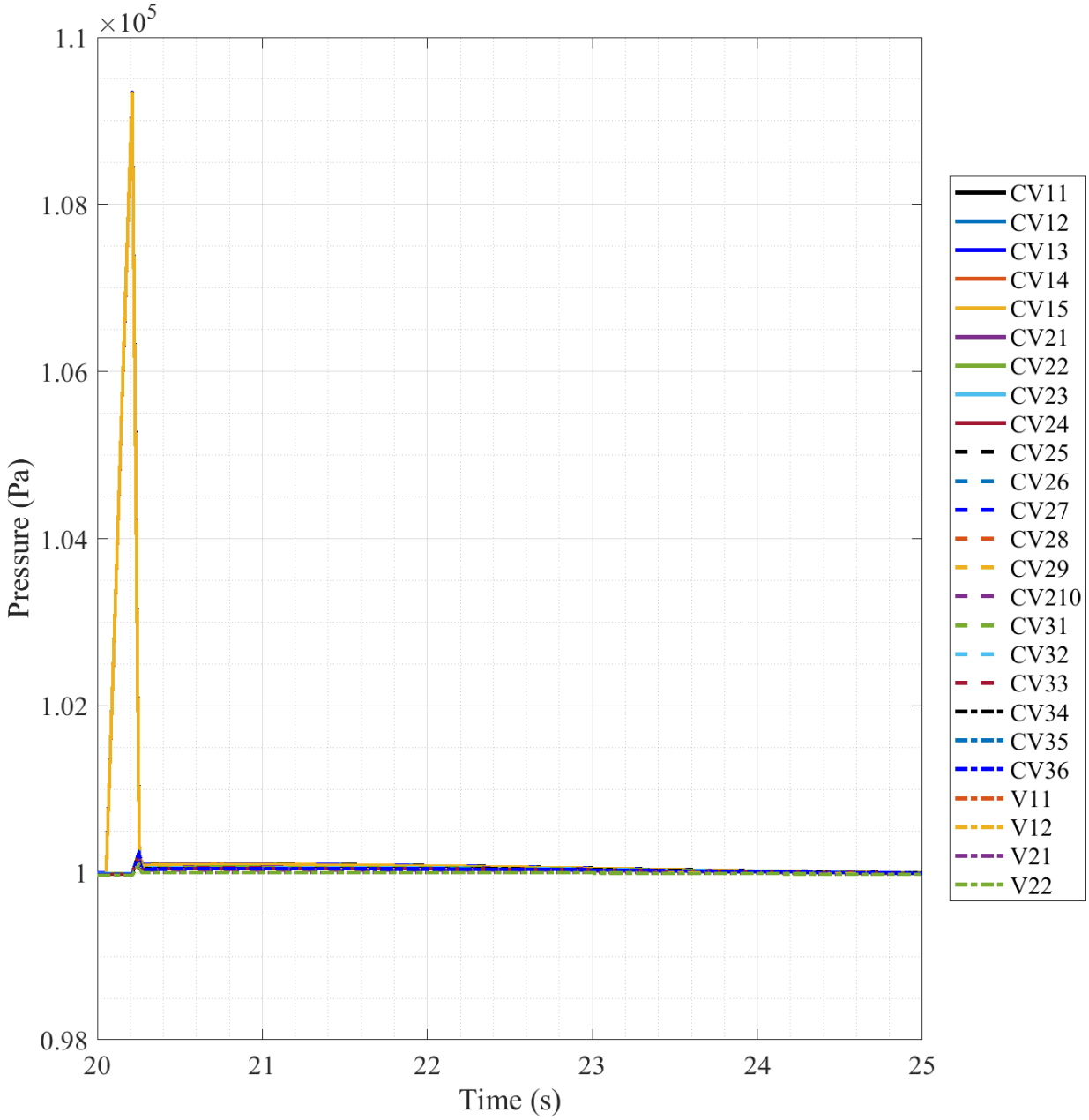

Fig. D.9. 1/28th-Scale Scenario 1 Pressure, 20-25 second Timescale, Individual Data.

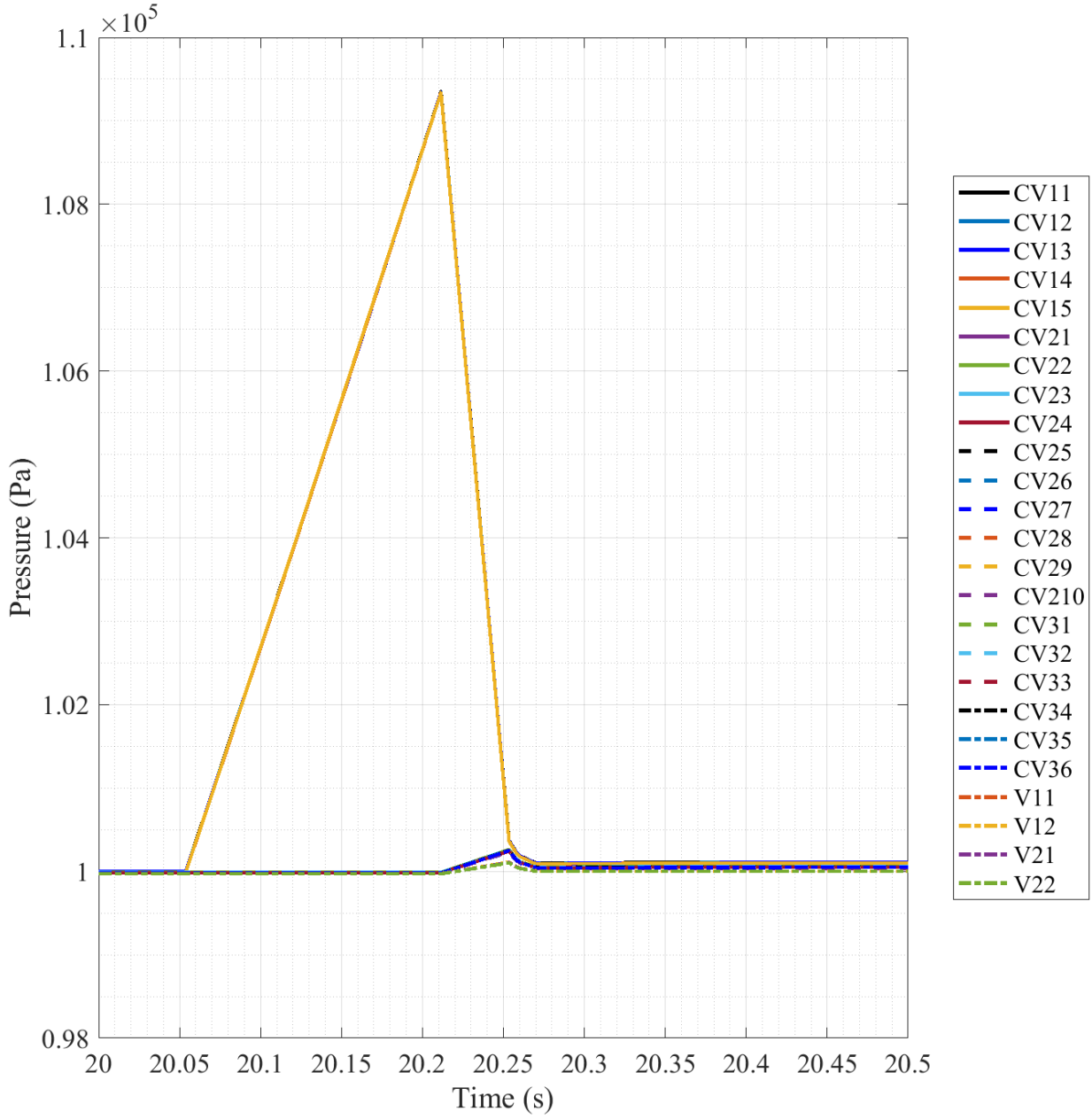

Fig. D.10. 1/28th-Scale Scenario 1 Pressure, 20-20.5 second Timescale.

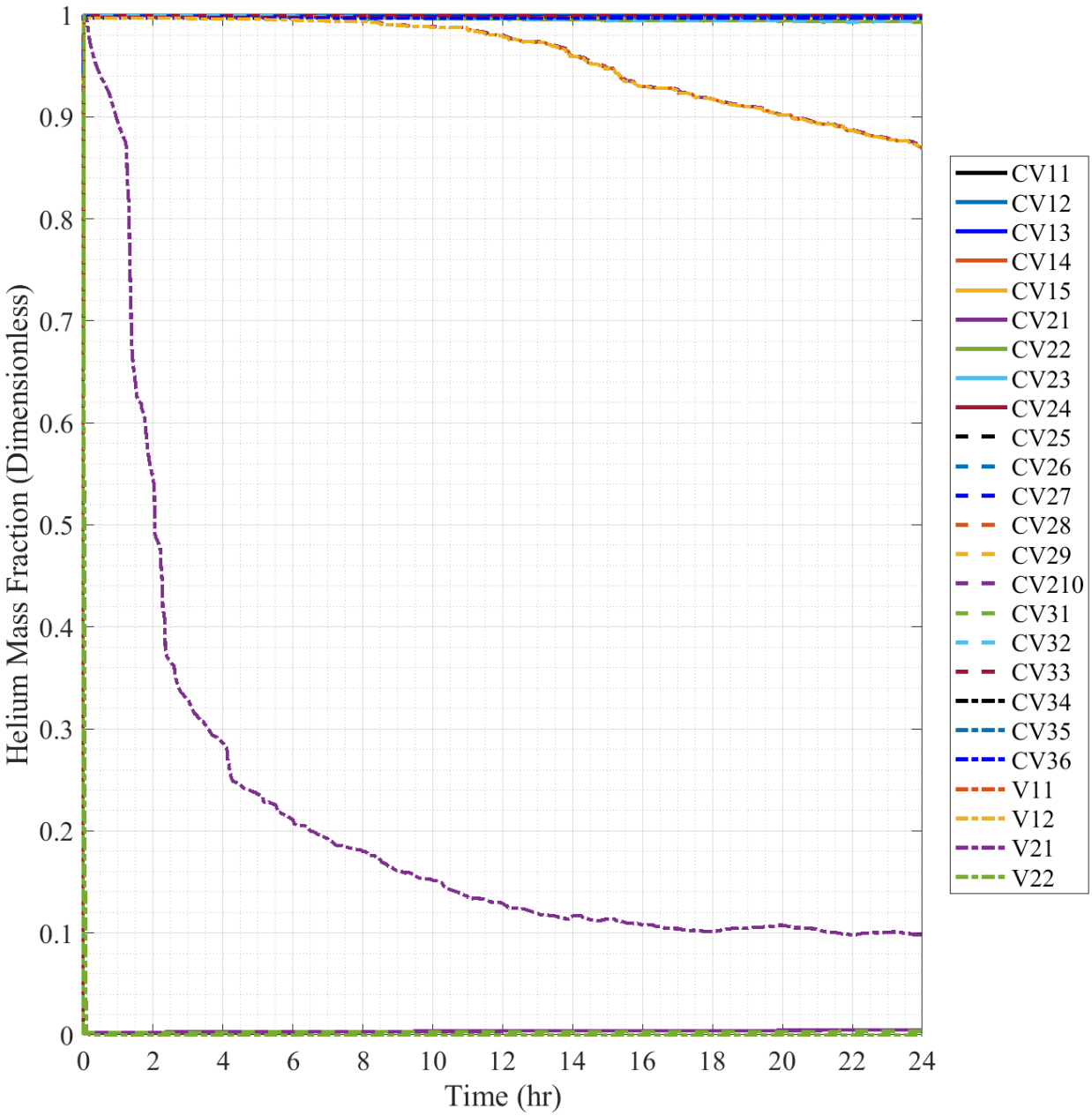

Fig. D.11. 1/28th-Scale Scenario 1 Helium Mass Fraction, Individual Data.

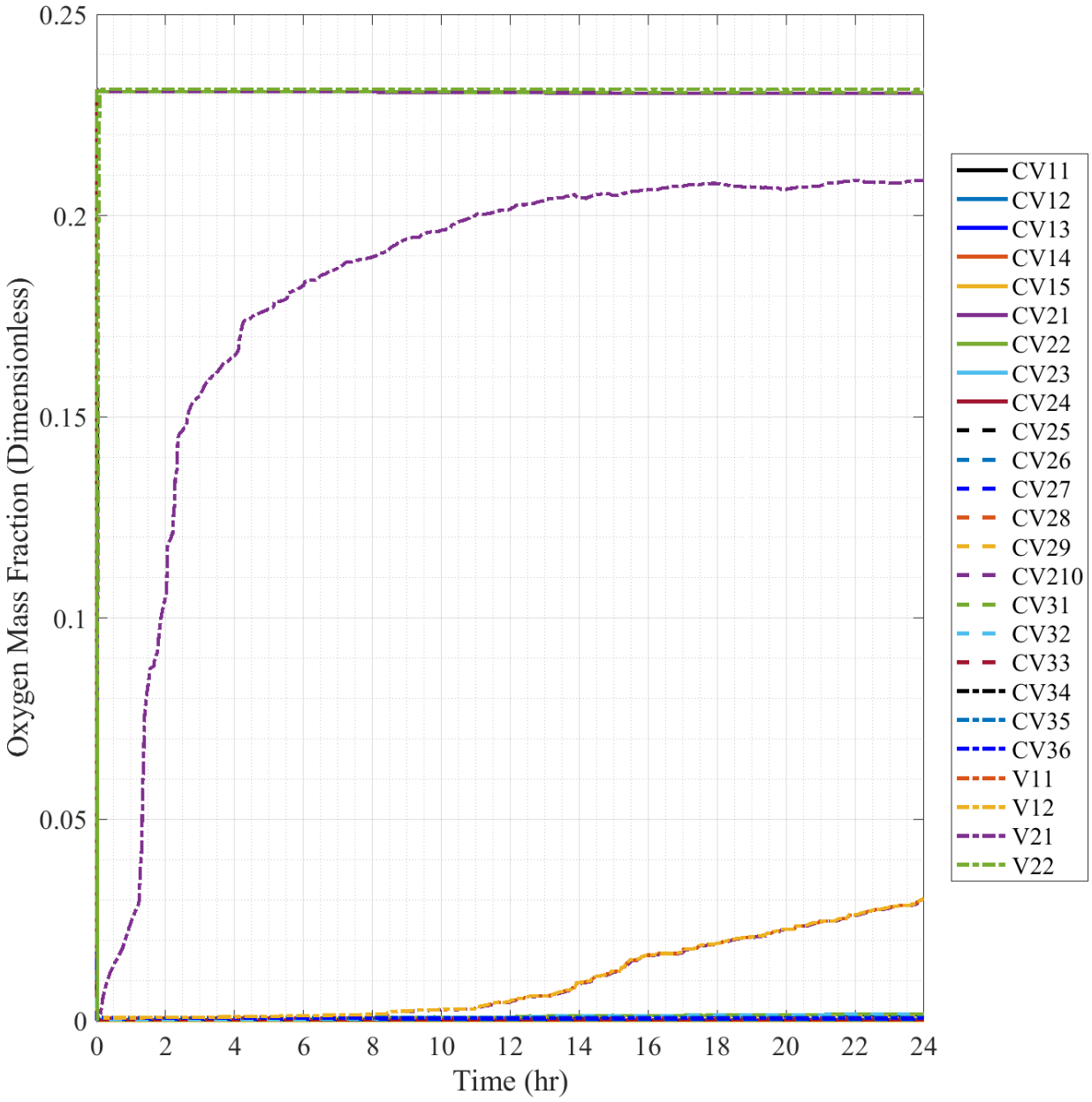

Fig. D.12. 1/28th-Scale Scenario 1 Oxygen Mass Fraction, Individual Data.

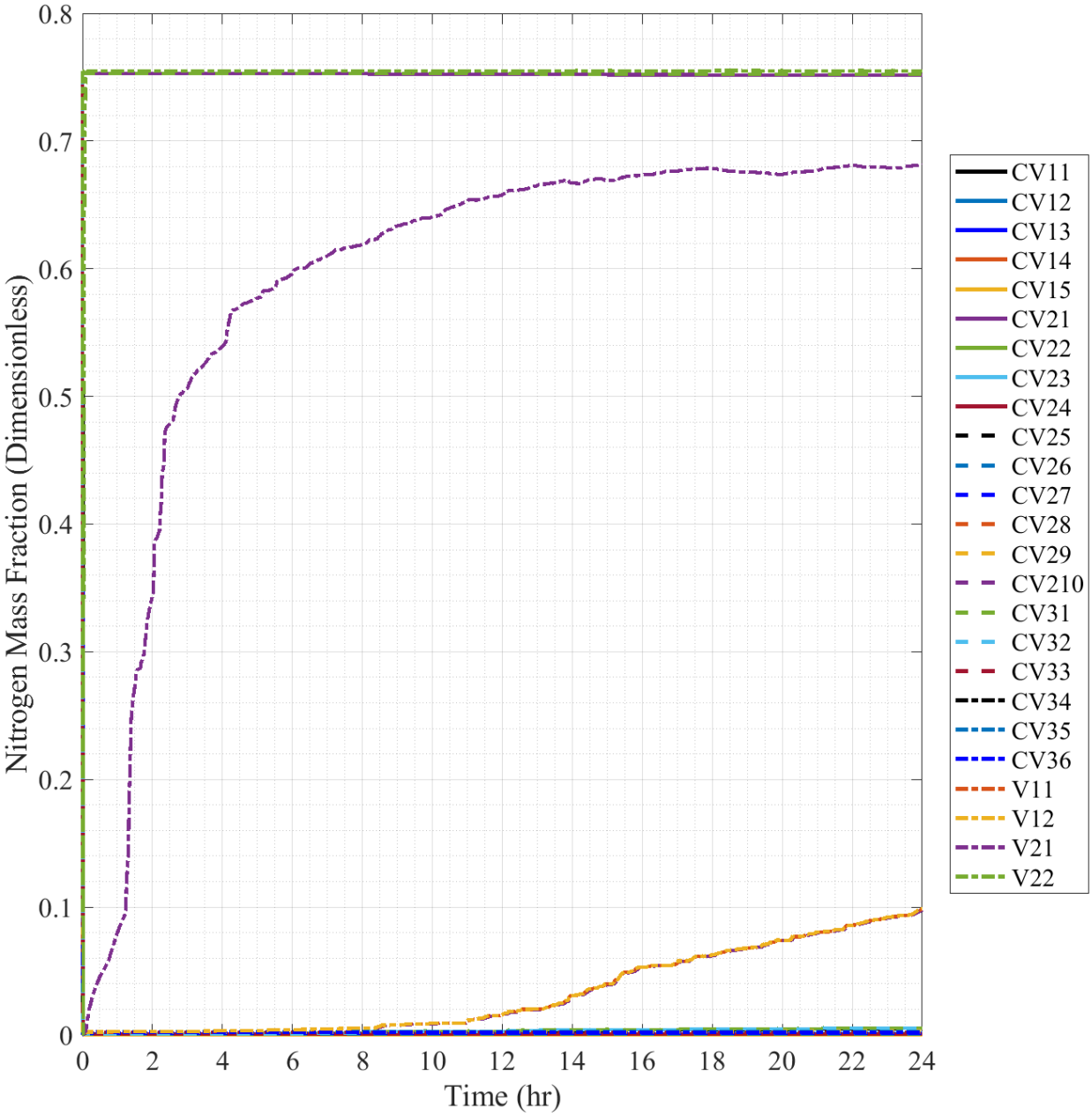

Fig. D.13. 1/28th-Scale Scenario 1 Nitrogen Mass Fraction, Individual Data.

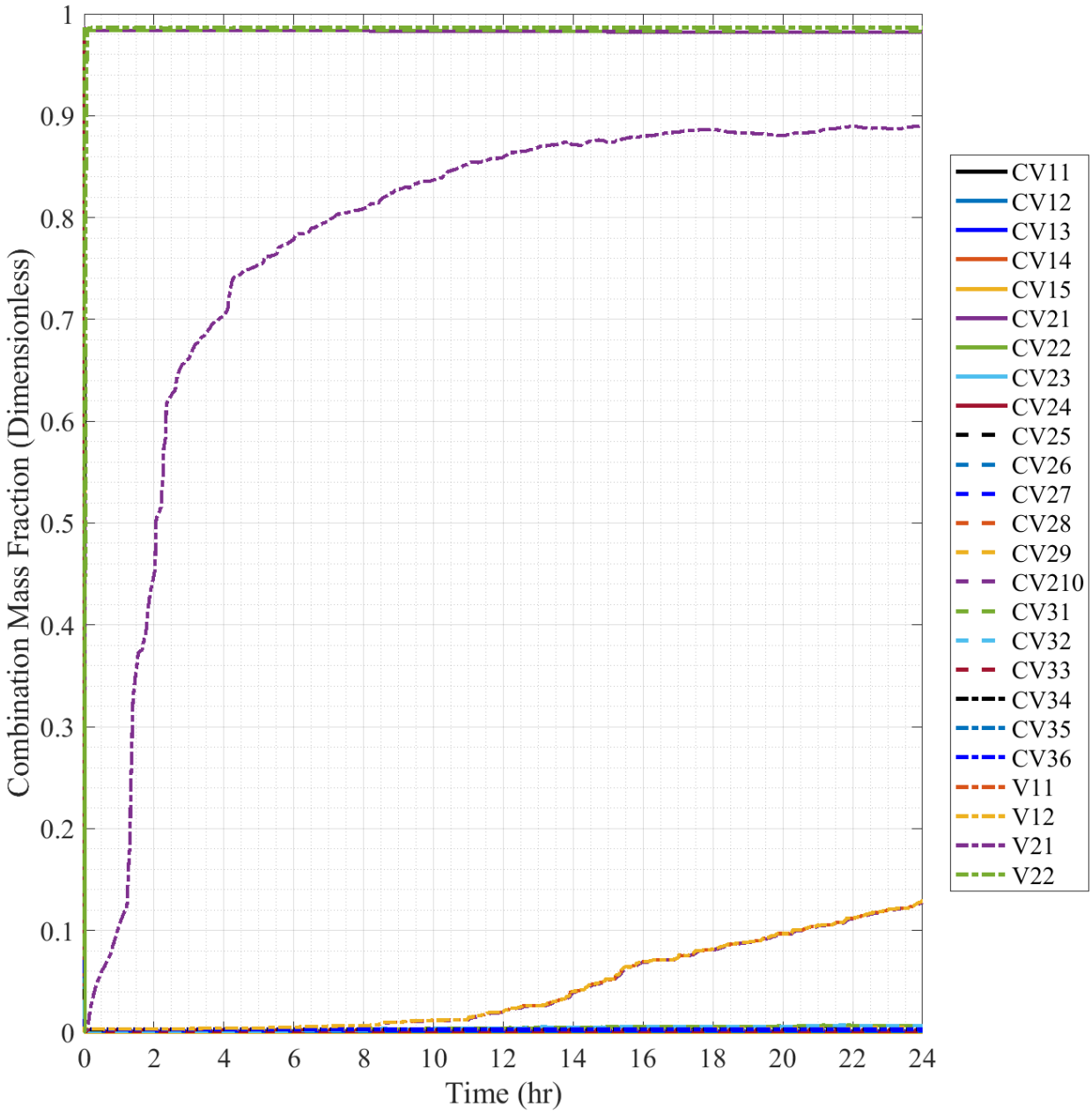

Fig. D.14. 1/28th-Scale Scenario 1 Combination Mass Fraction, Individual Data.

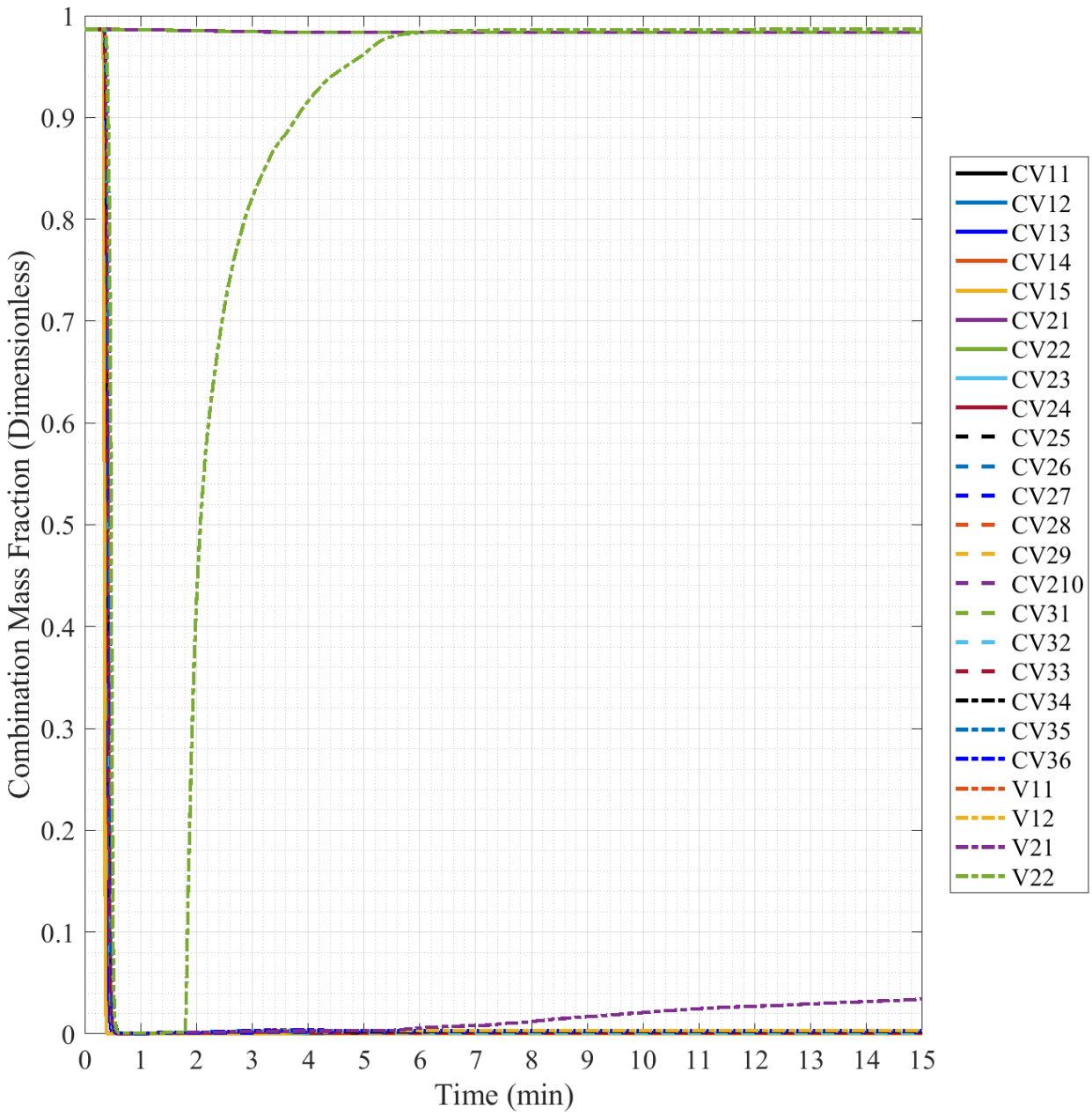

Fig. D.15. 1/28th-Scale Scenario 1 Combination Mass Fraction, 15 minute Timescale, Individual Data.

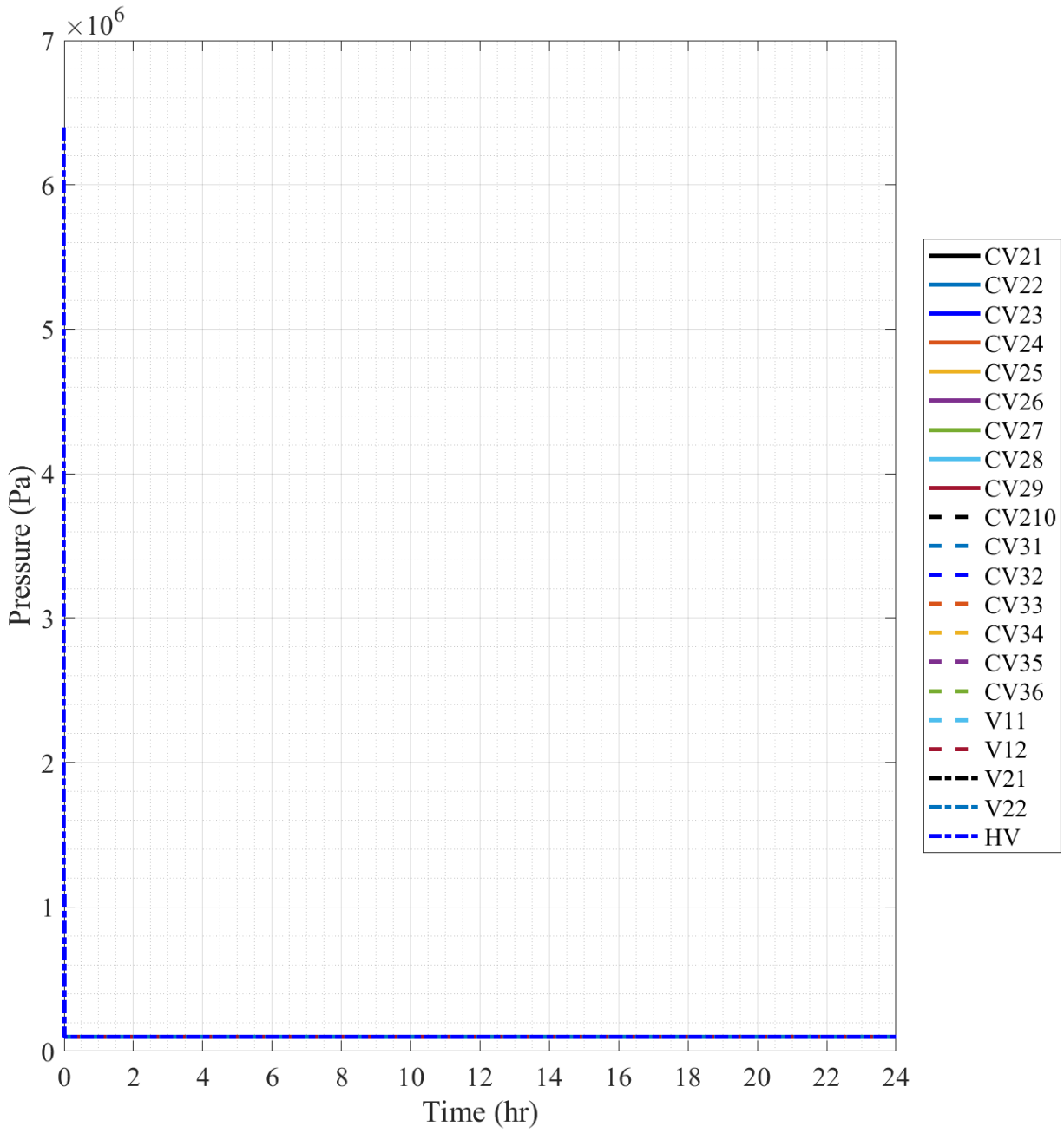

Fig. D.16. 1/28th-Scale Scenario 2 Pressure, Individual Data.

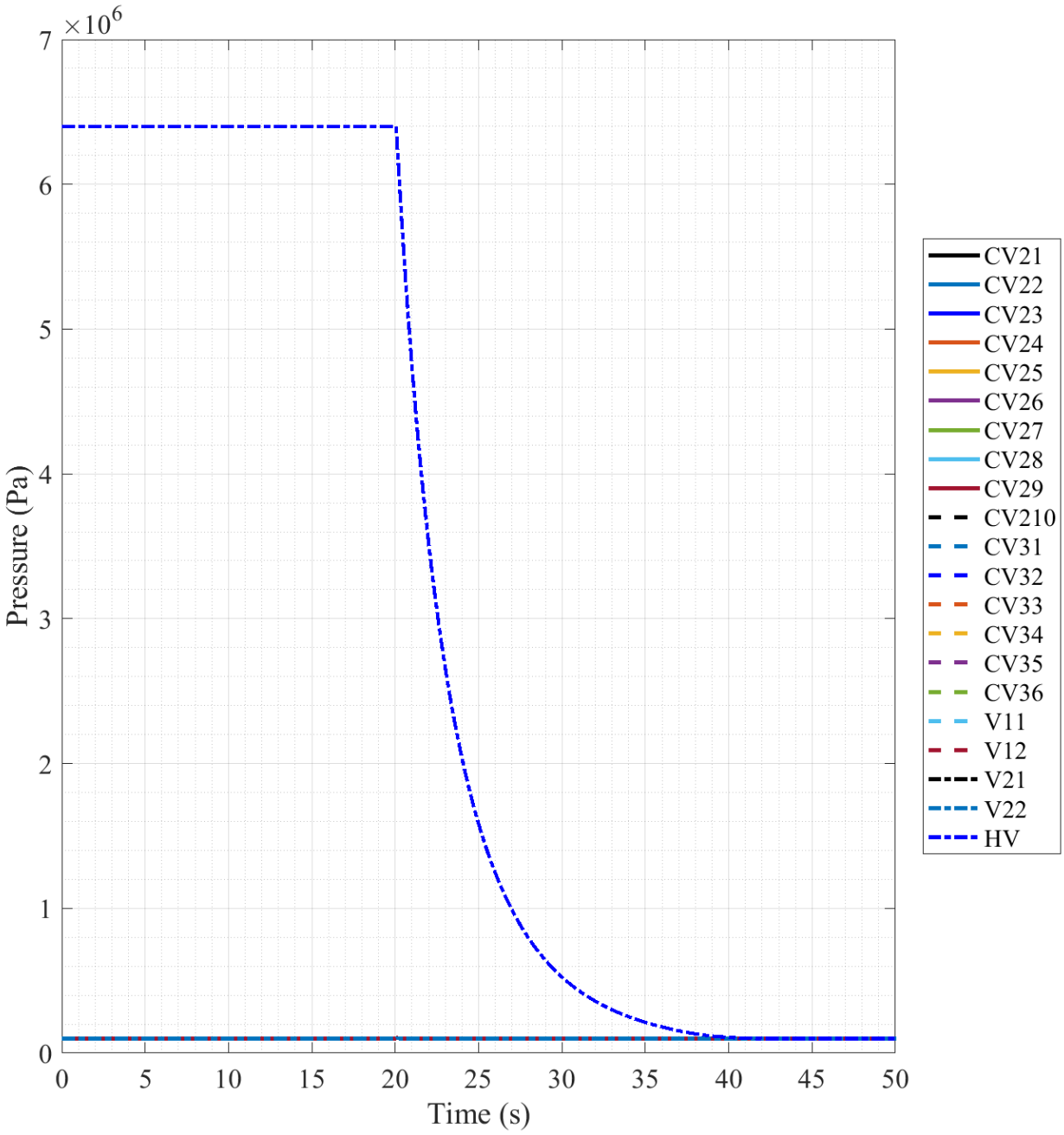

Fig. D.17. 1/28th-Scale Scenario 2 Pressure, 50 second Timescale, Individual Data.

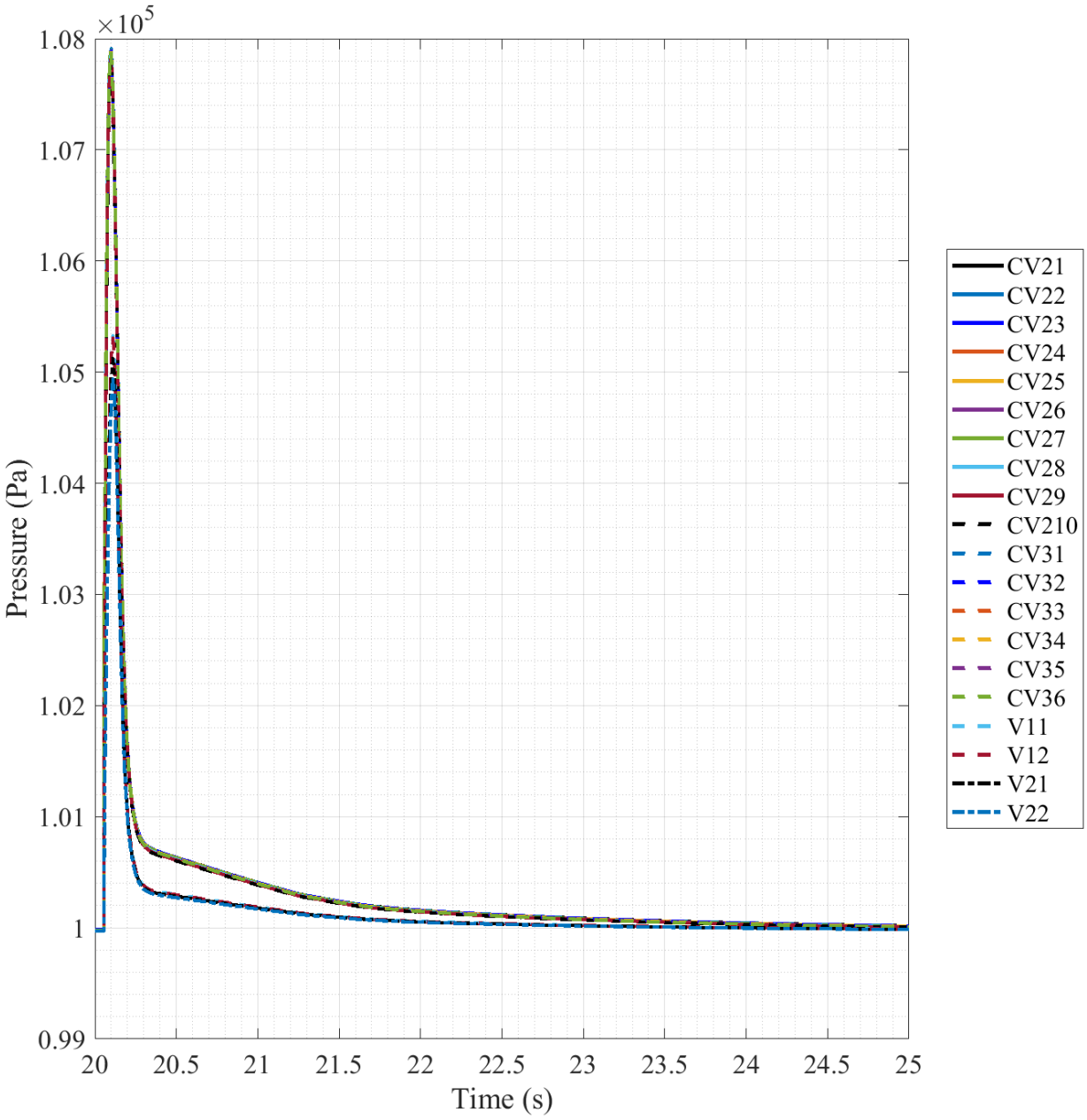

Fig. D.18. 1/28th-Scale Scenario 2 Pressure, 20-25 second Timescale, Individual Data.

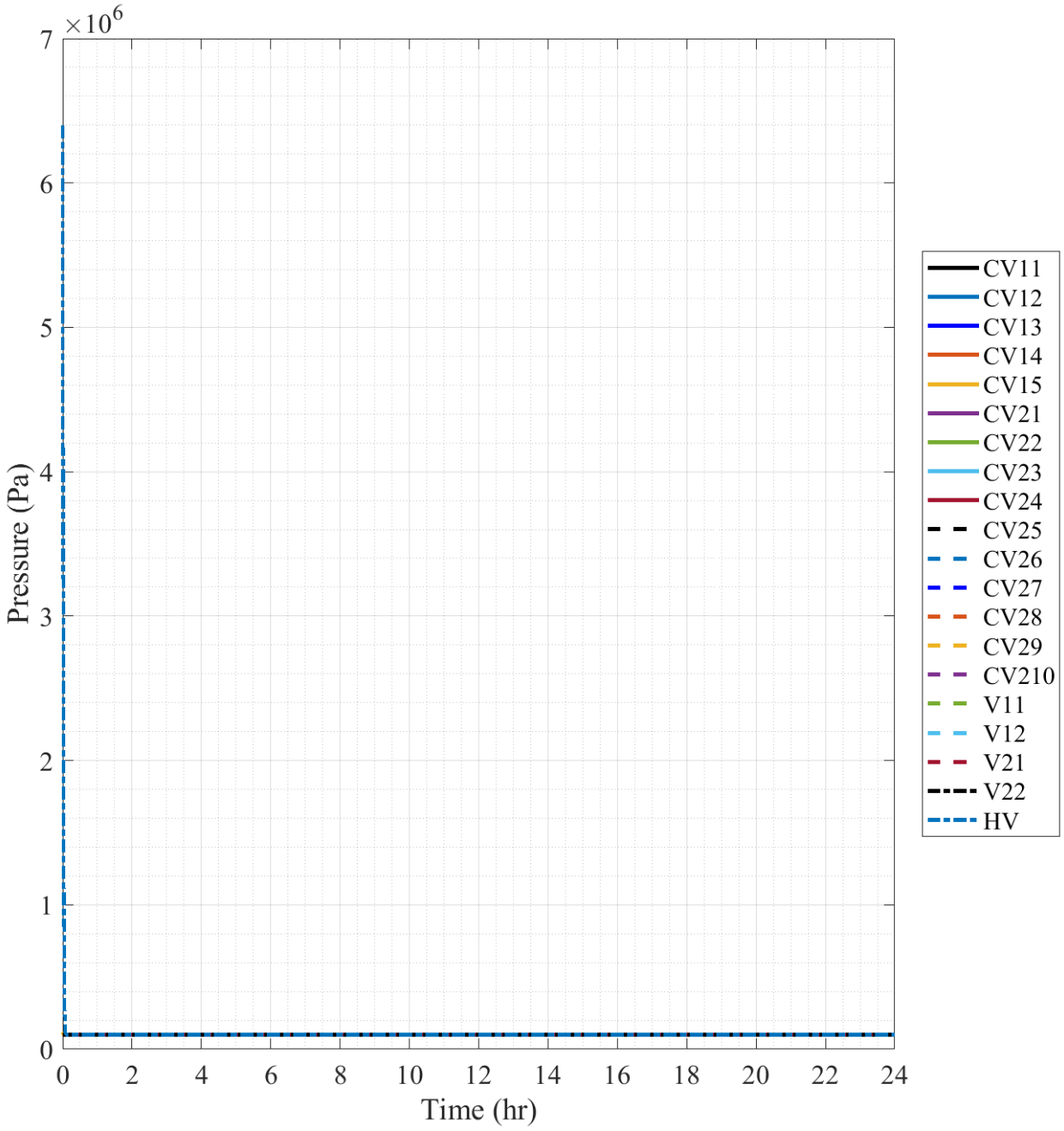

Fig. D.19. 1/28th-Scale Scenario 3 Pressure.

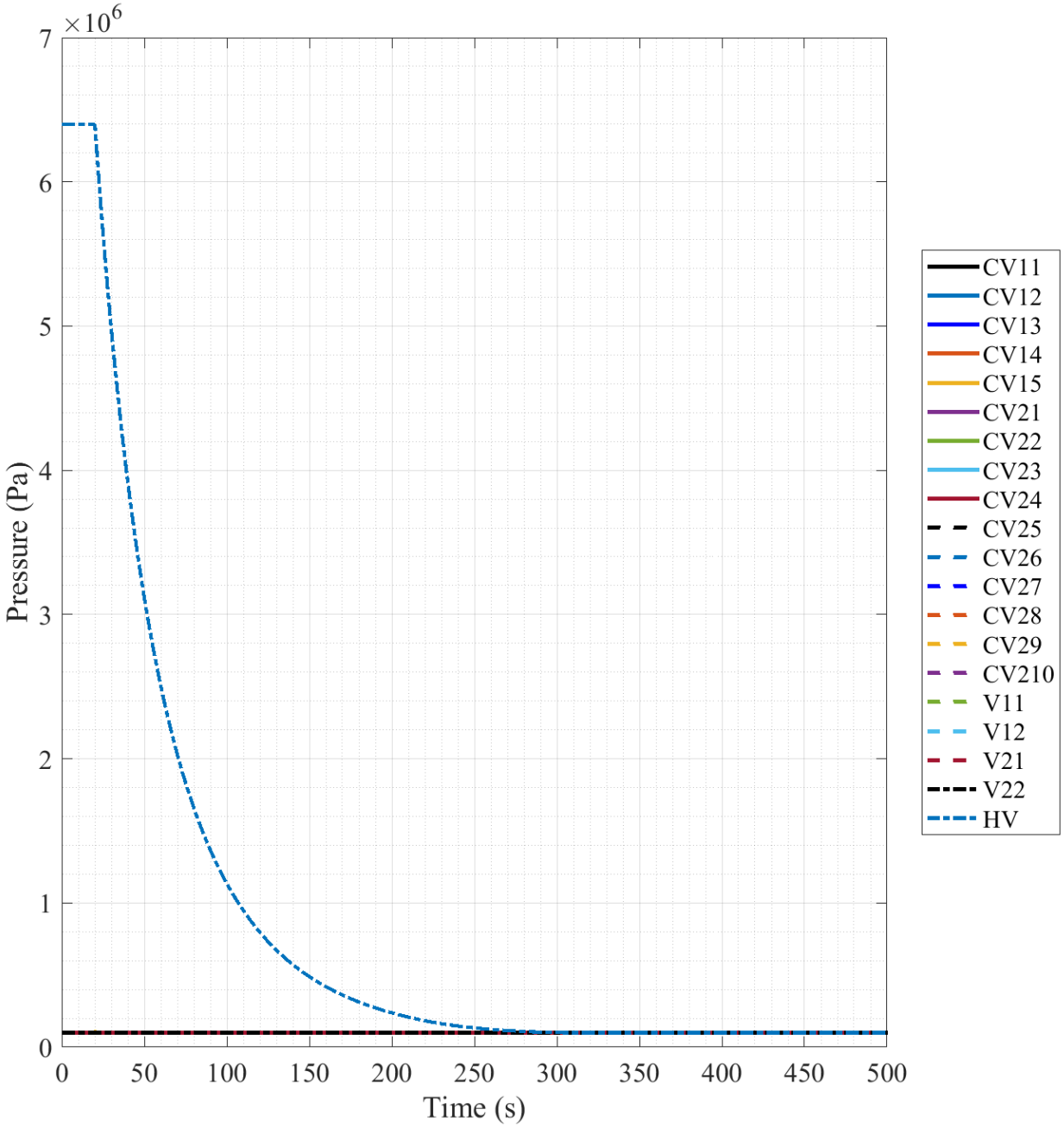

Fig. D.20. 1/28th-Scale Scenario 3 Pressure, 500 second Timescale.

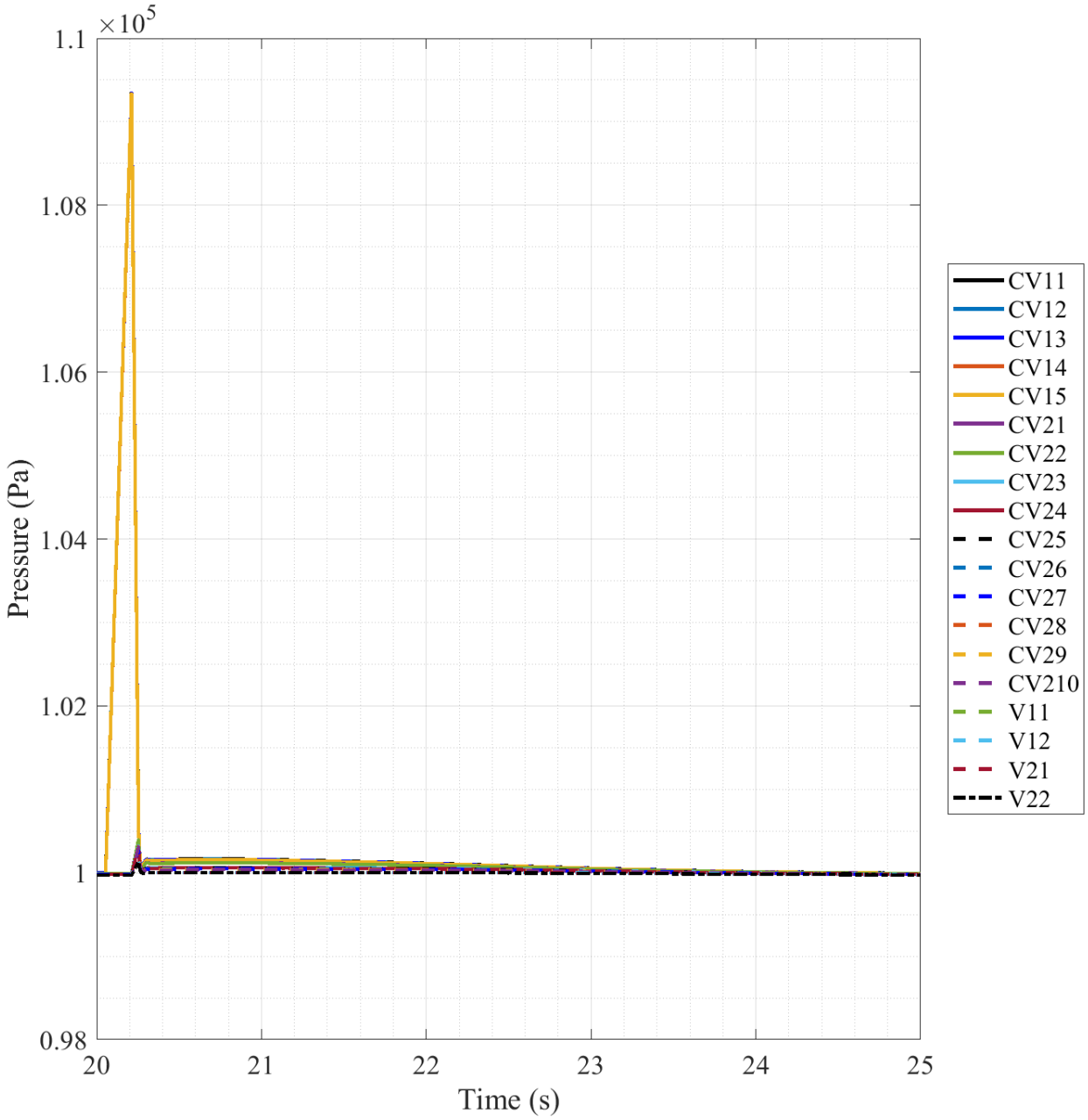

Fig. D.21. 1/28th-Scale Scenario 3 Pressure, 20-25 second Timescale, Individual Data.

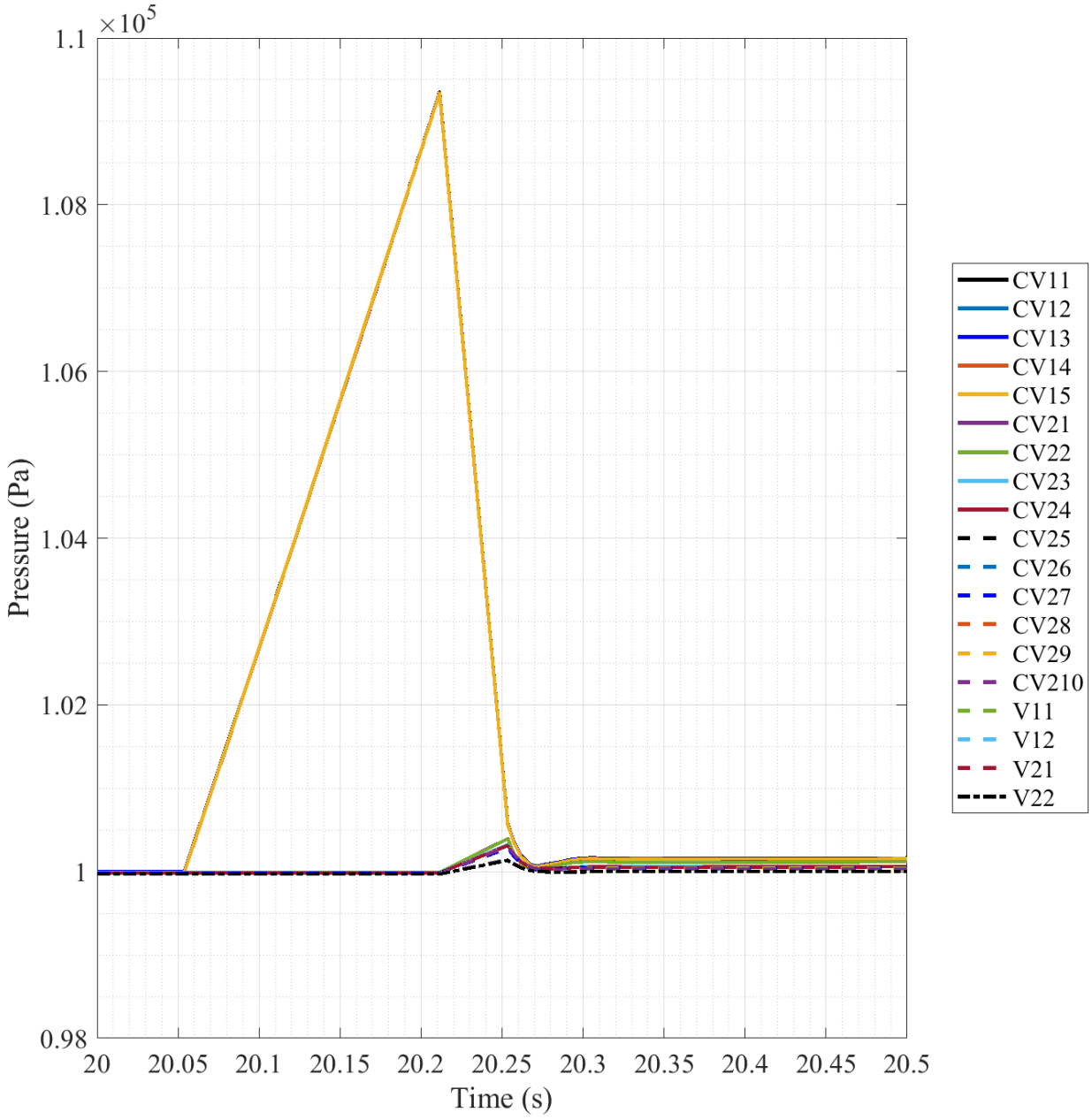

Fig. D.22. 1/28th-Scale Scenario 3 Pressure, 20-20.5 second Timescale.

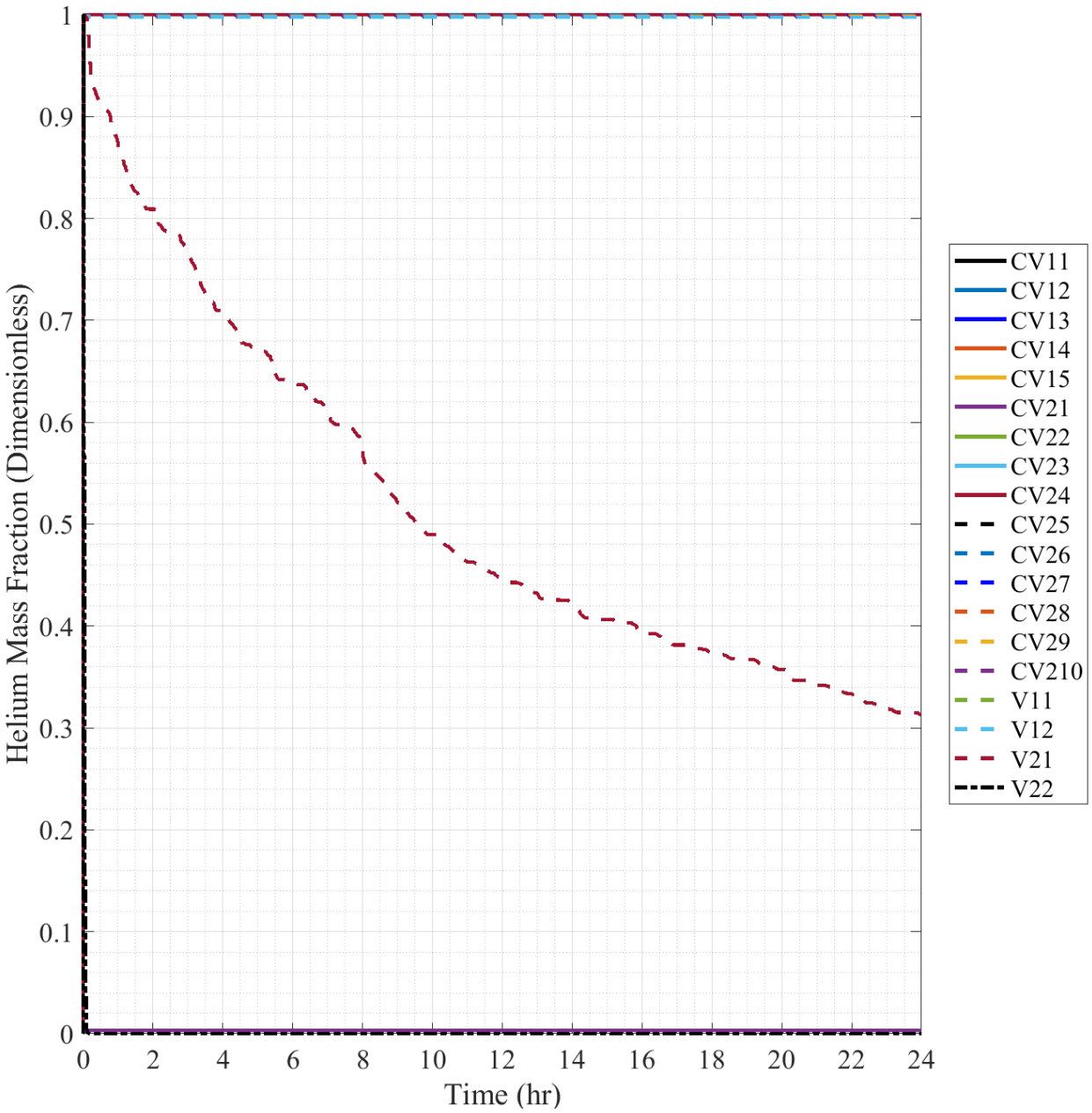

Fig. D.23. 1/28th-Scale Scenario 3 Helium Mass Fraction, Individual Data.

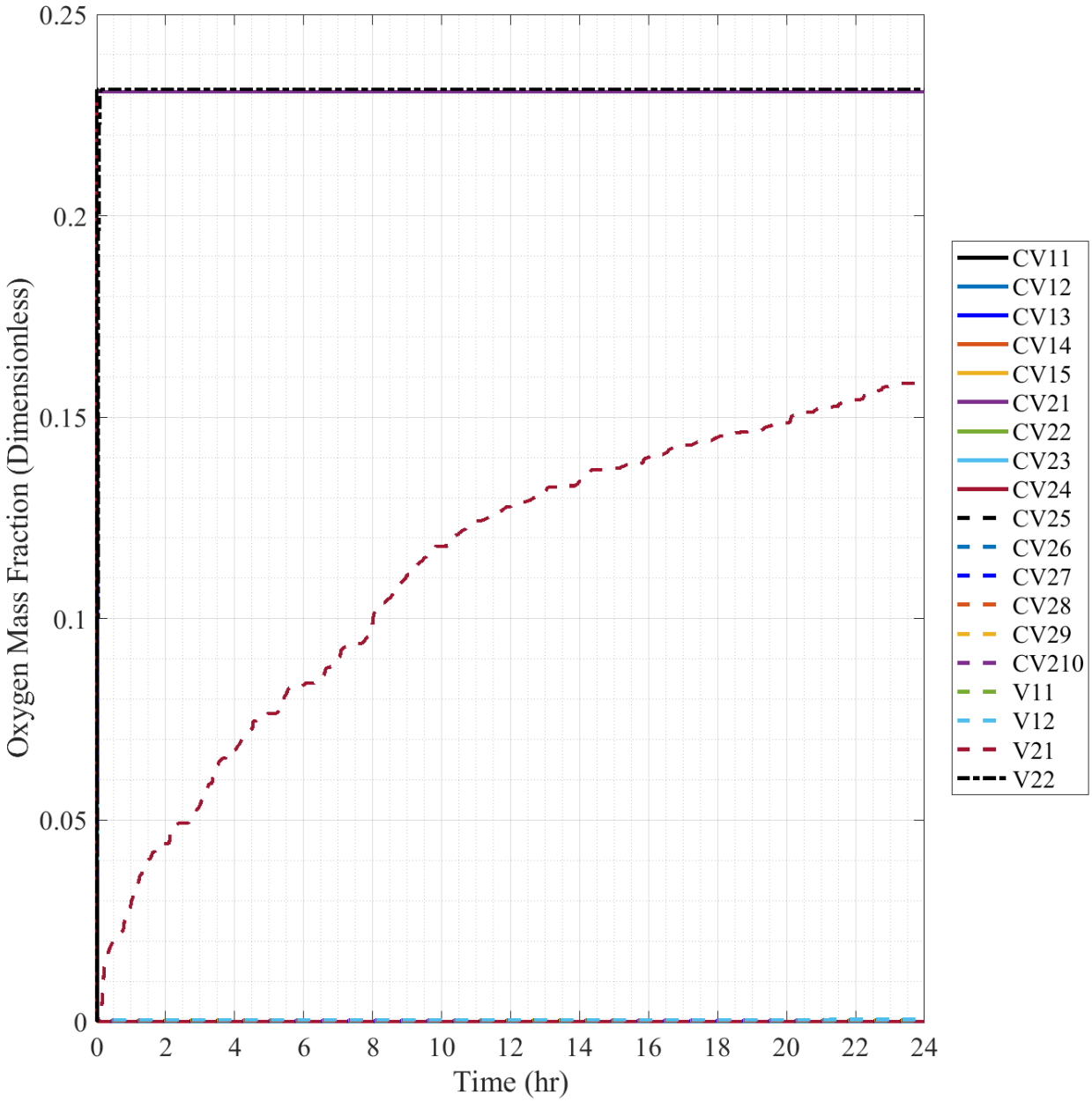

Fig. D.24. 1/28th-Scale Scenario 3 Oxygen Mass Fraction.

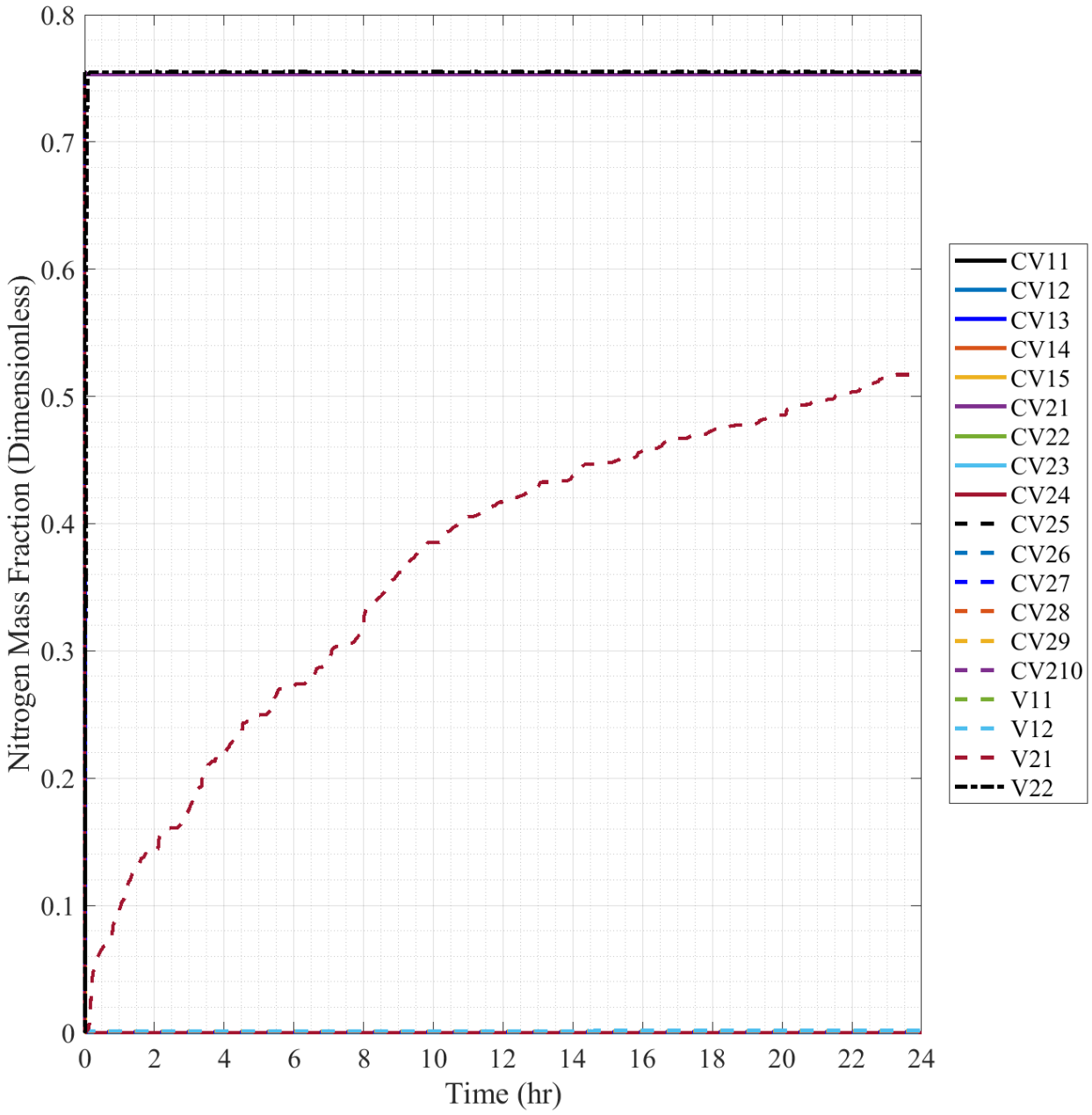

Fig. D.25. 1/28th-Scale Scenario 3 Nitrogen Mass Fraction.

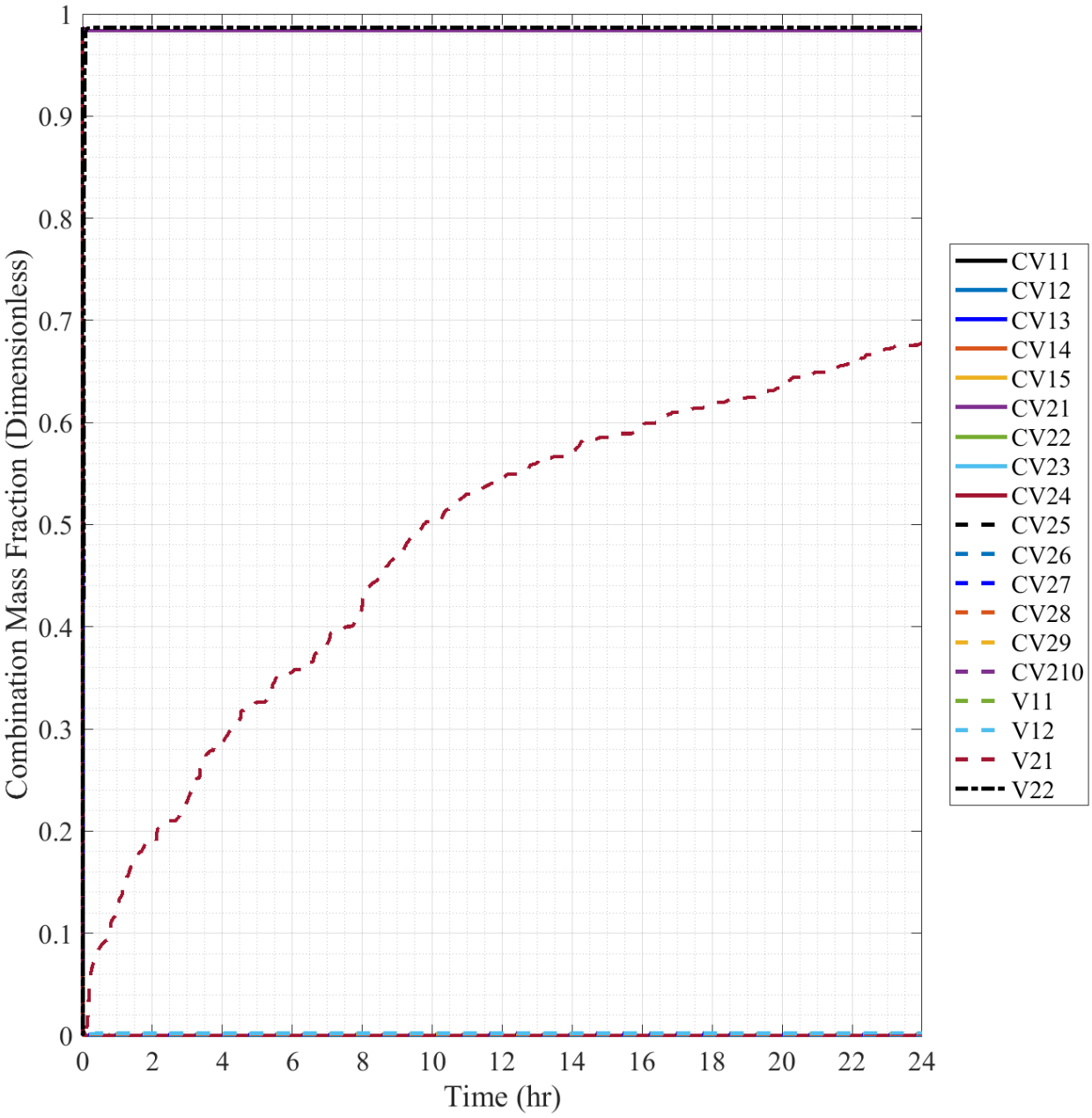

Fig. D.26. 1/28th-Scale Scenario 3 Combination Mass Fraction, Individual Data.

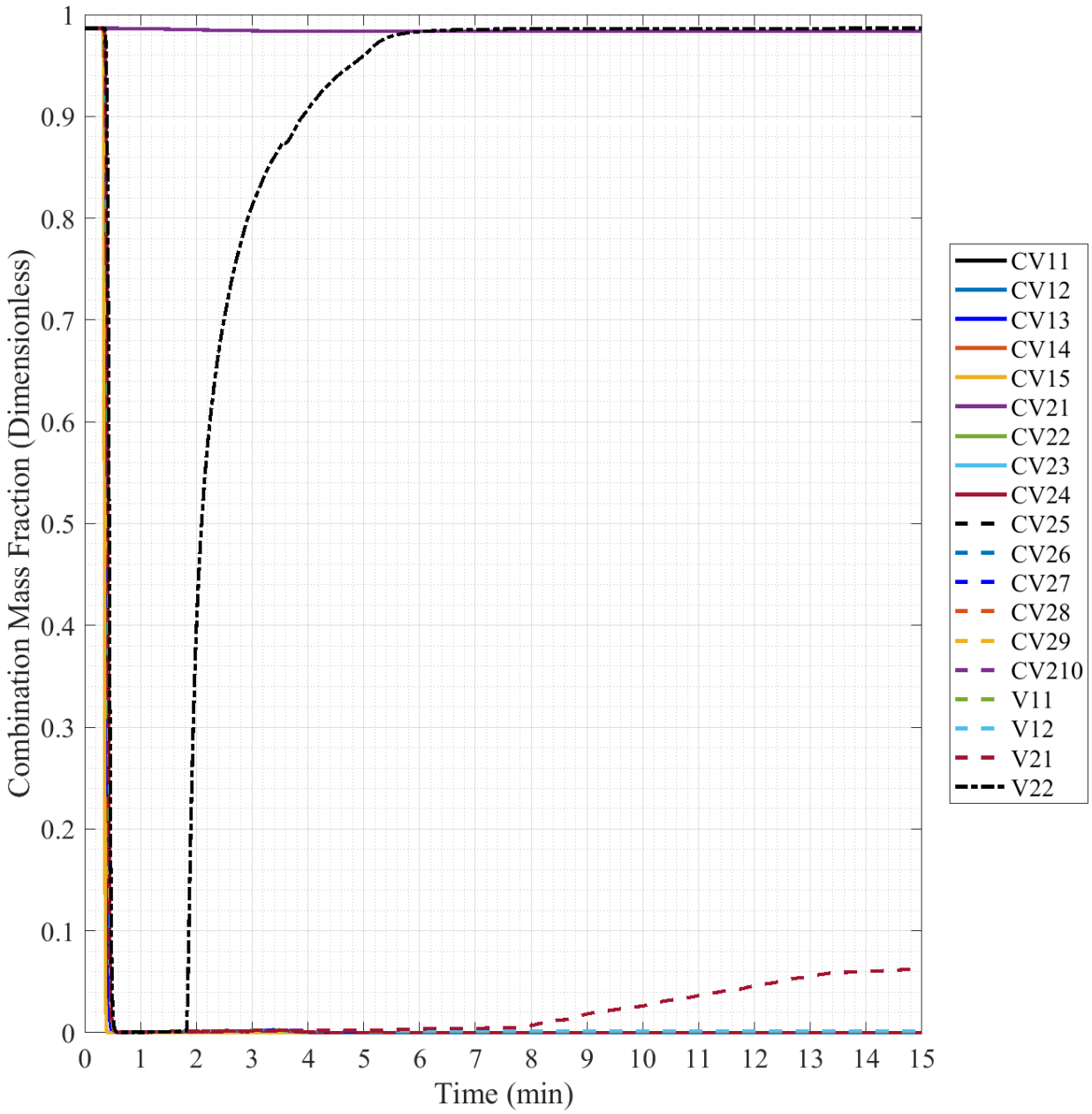

Fig. D.27. 1/28th-Scale Scenario 3 Combination Mass Fraction, 15 minute Timescale, Individual Data.

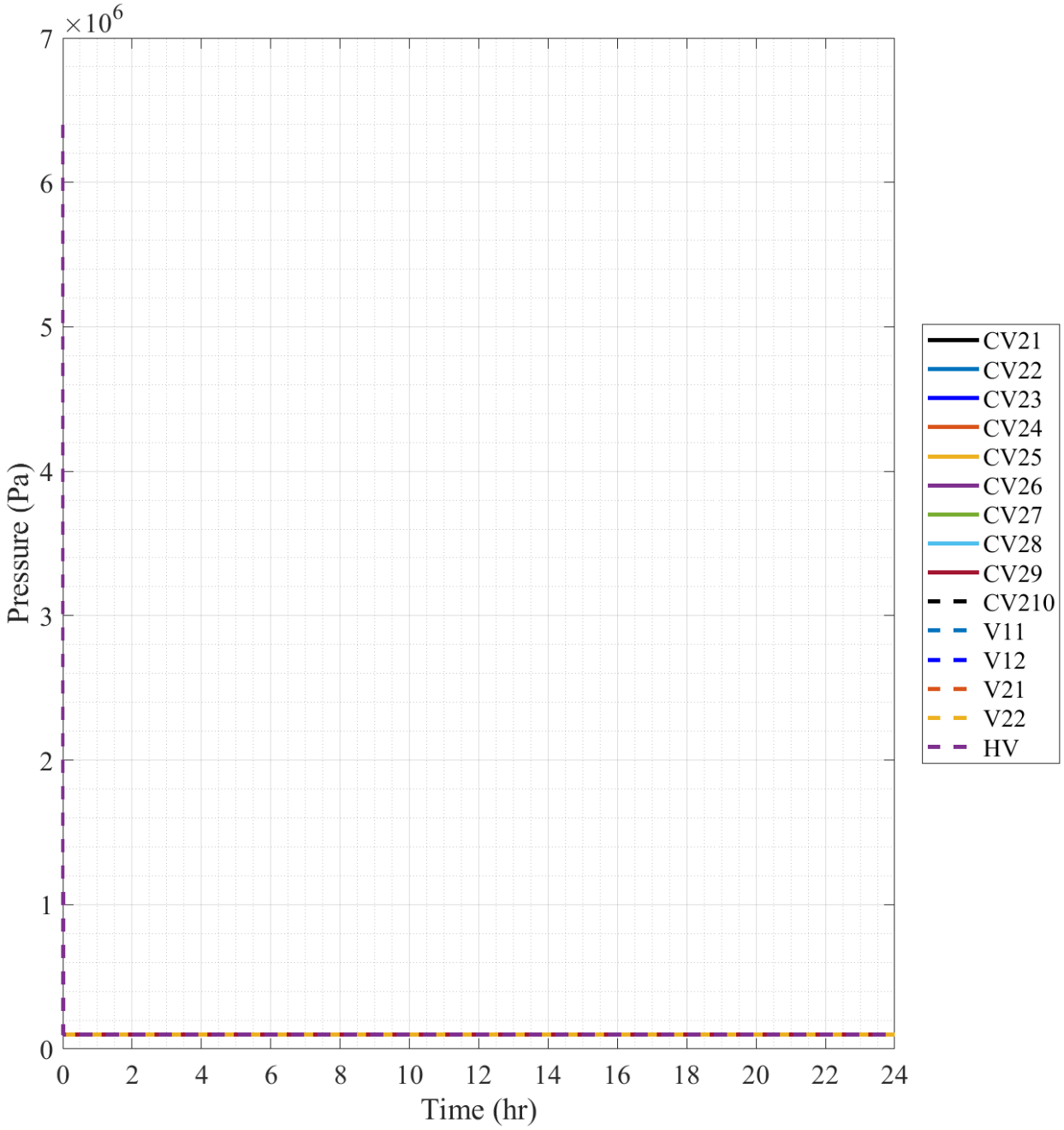

Fig. D.28. 1/28th-Scale Scenario 4 Pressure.

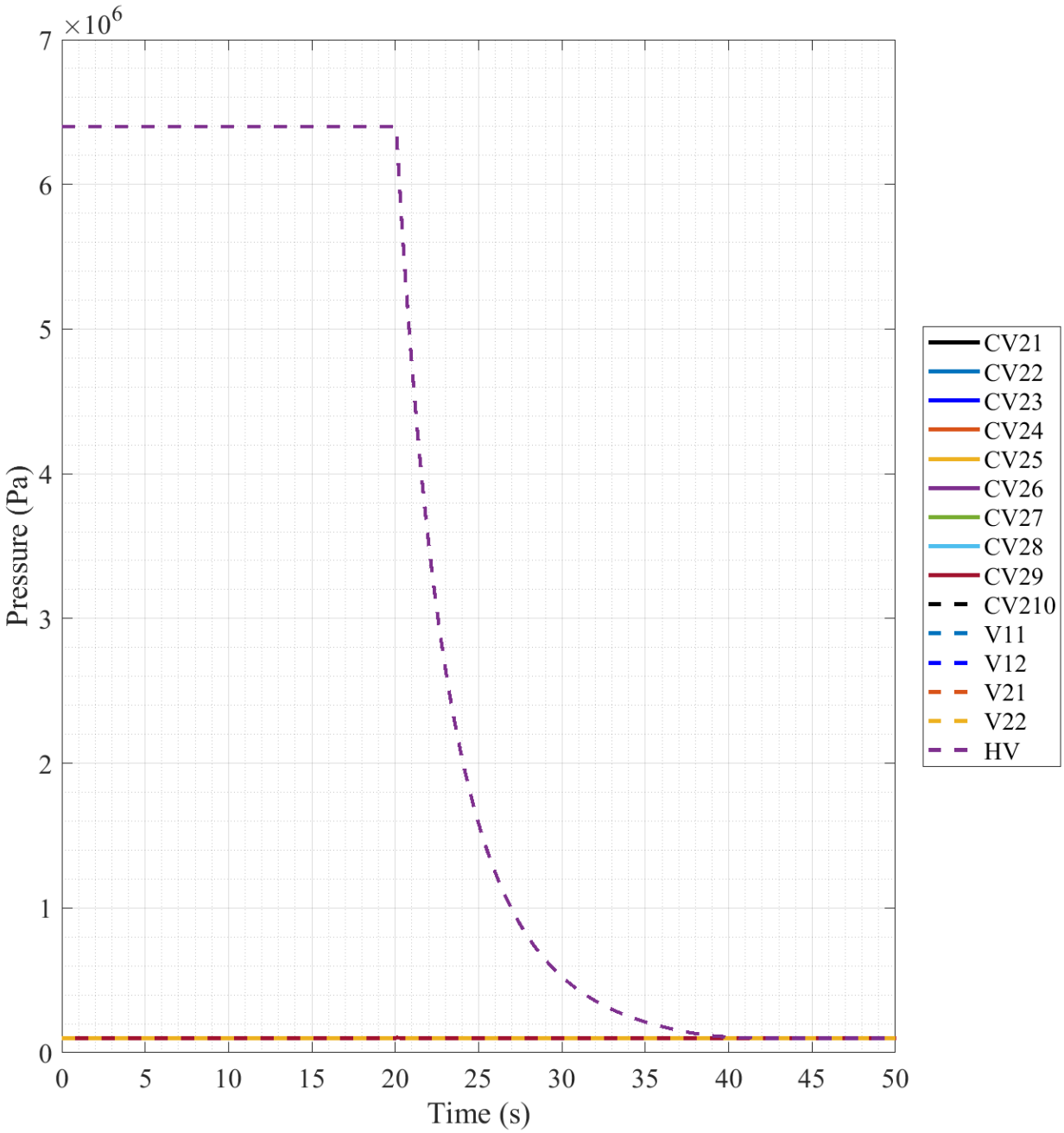

Fig. D.29. 1/28th-Scale Scenario 4 Pressure, 50 second Timescale.

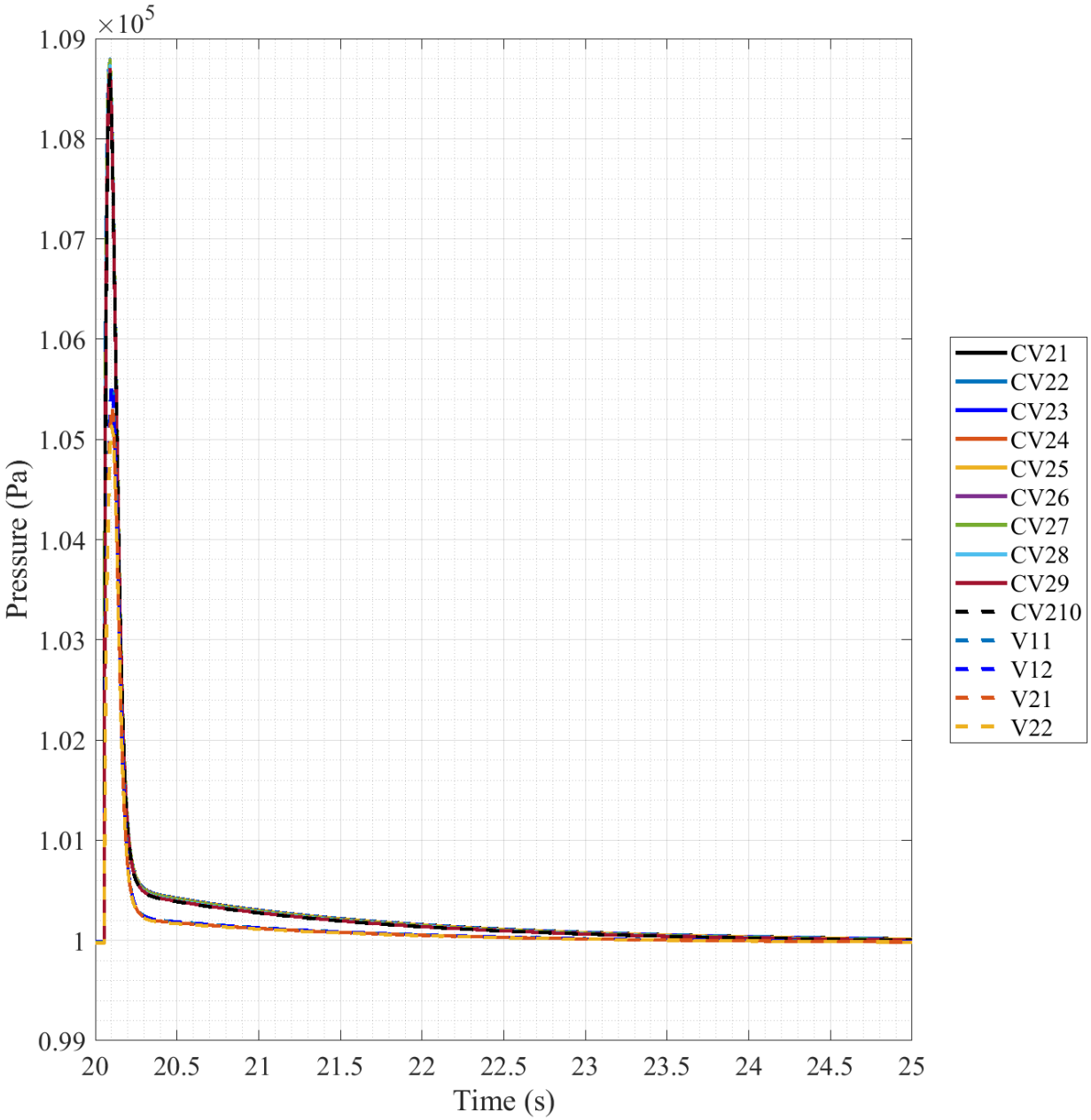

Fig. D.30. 1/28th-Scale Scenario 4 Pressure, 20-25 second Timescale, Individual Data.

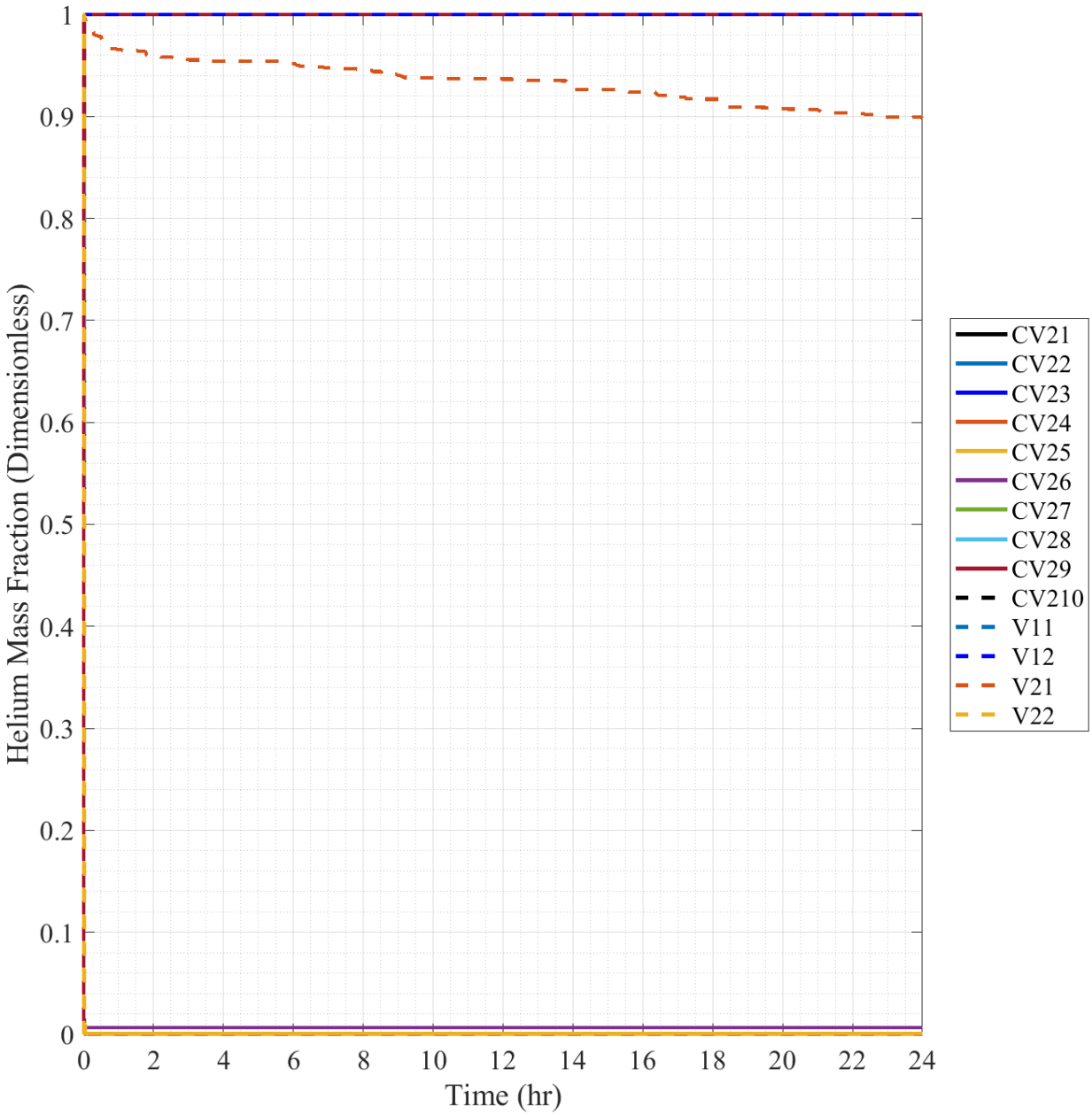

Fig. D.31. 1/28th-Scale Scenario 4 Helium Mass Fraction, Individual Data.

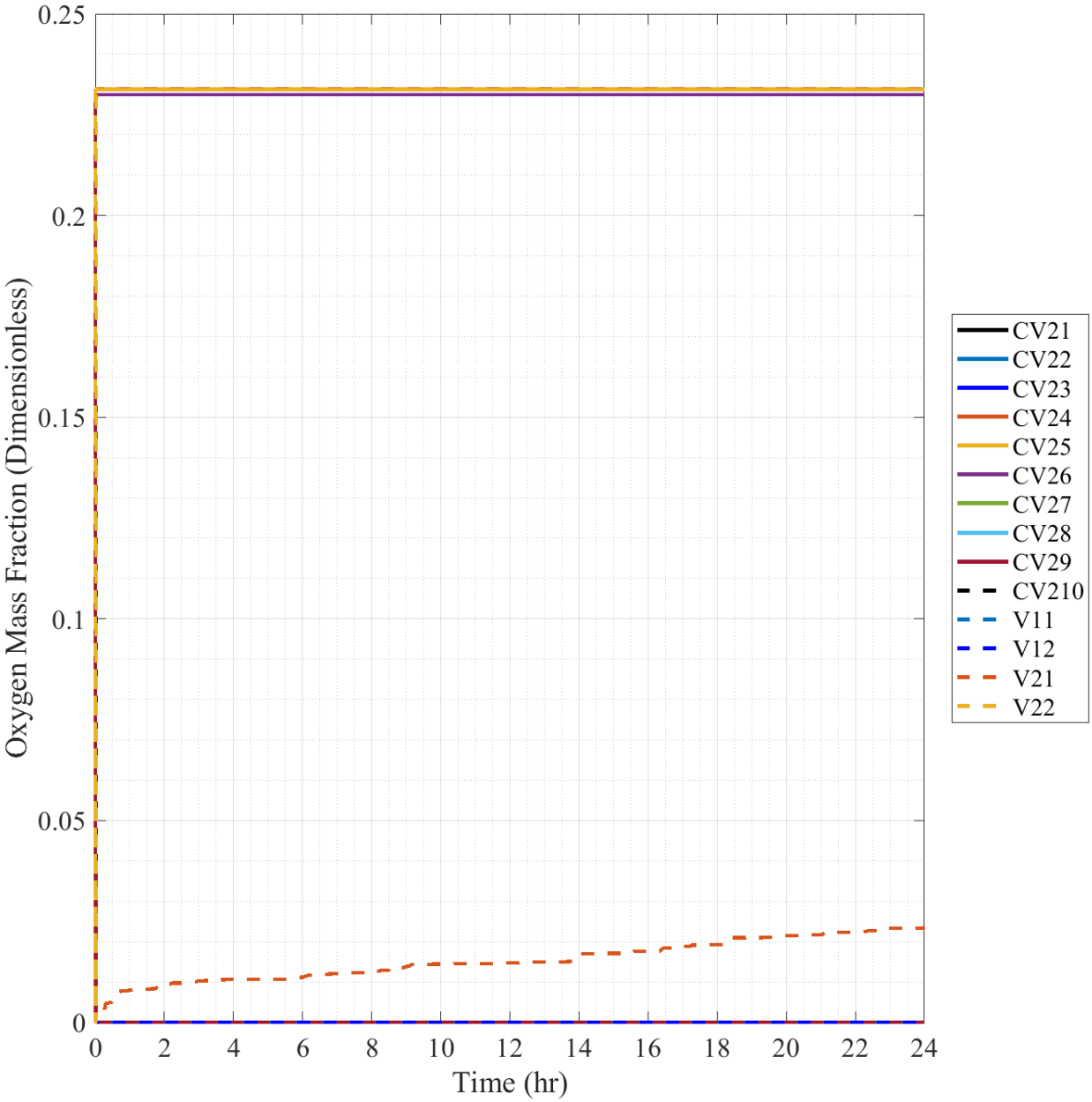

Fig. D.32. 1/28th-Scale Scenario 4 Oxygen Mass Fraction.

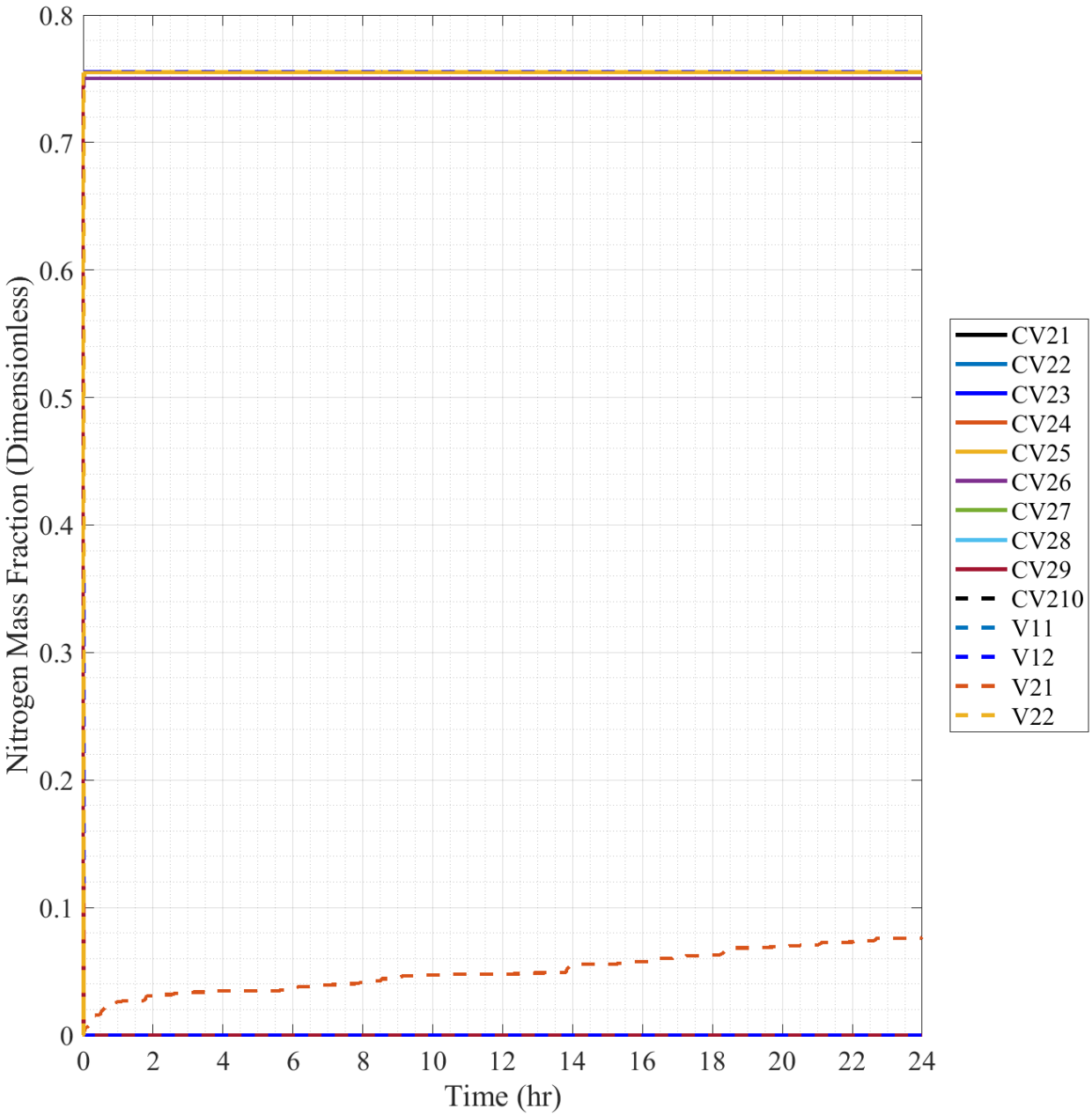

Fig. D.33. 1/28th-Scale Scenario 4 Nitrogen Mass Fraction.

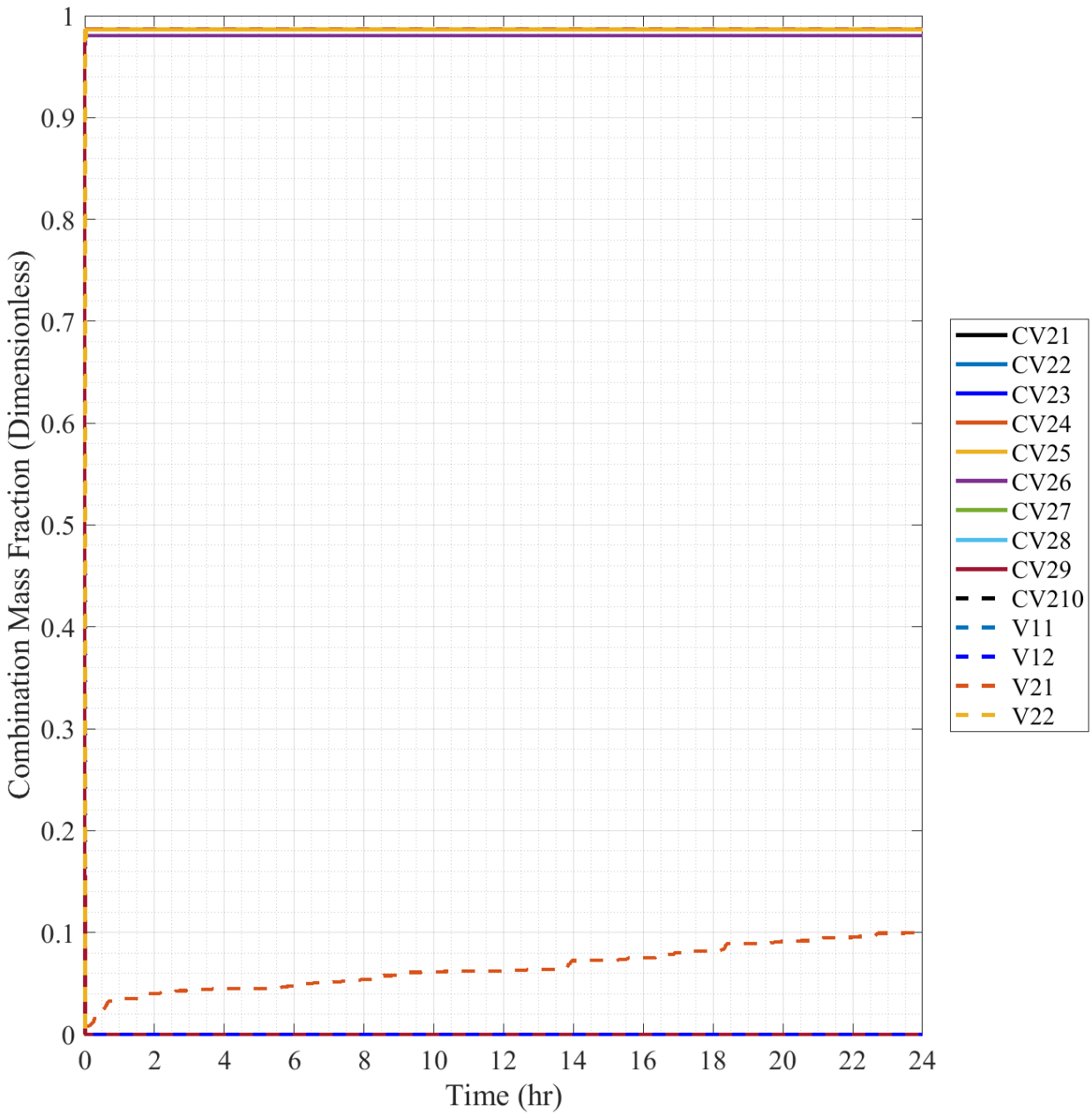

Fig. D.34. 1/28th-Scale Scenario 4 Combination Mass Fraction, Individual Data.

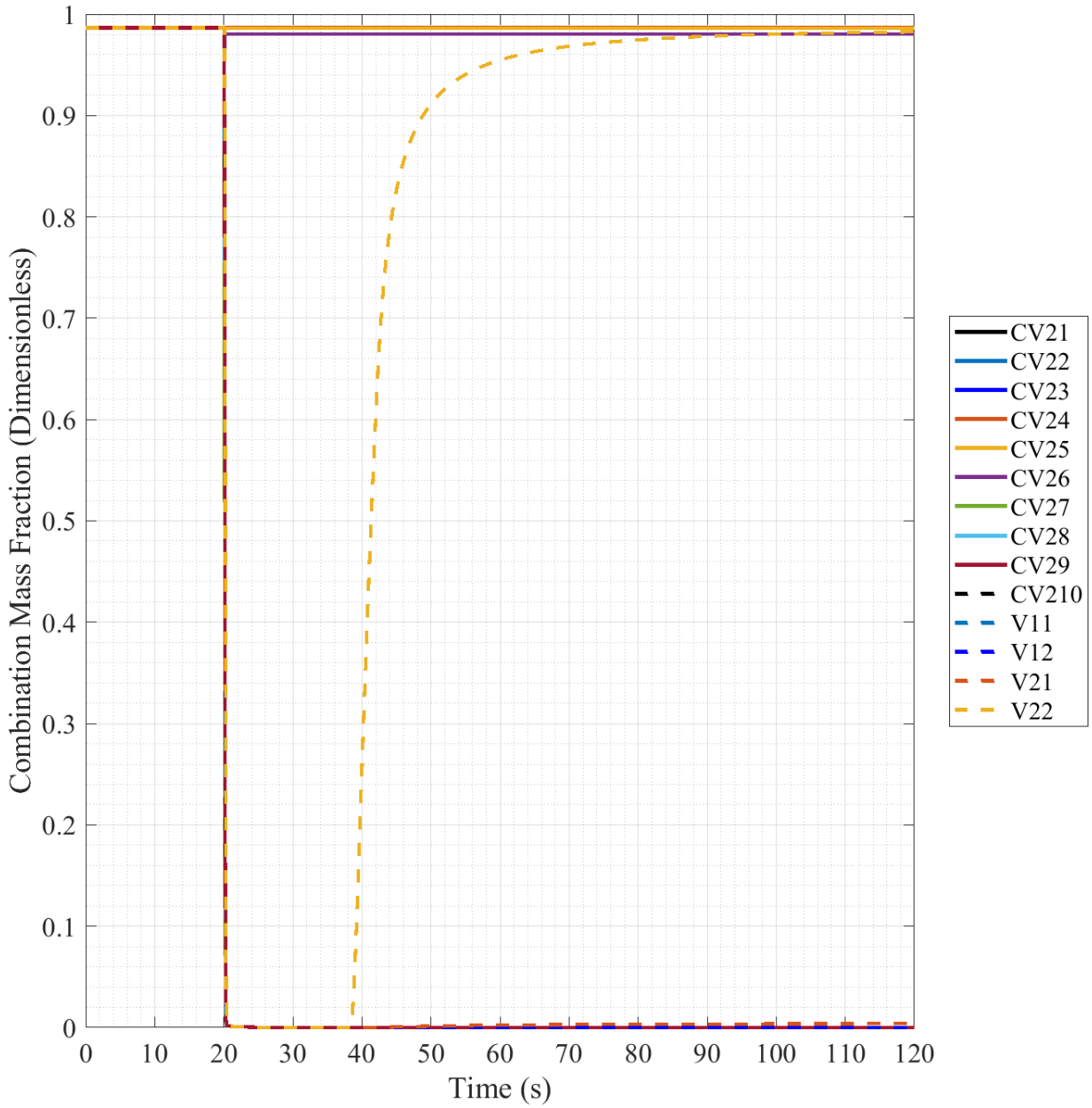

Fig. D.34. 1/28th-Scale Scenario 4 Combination Mass Fraction, 120 second Timescale, Individual Data.

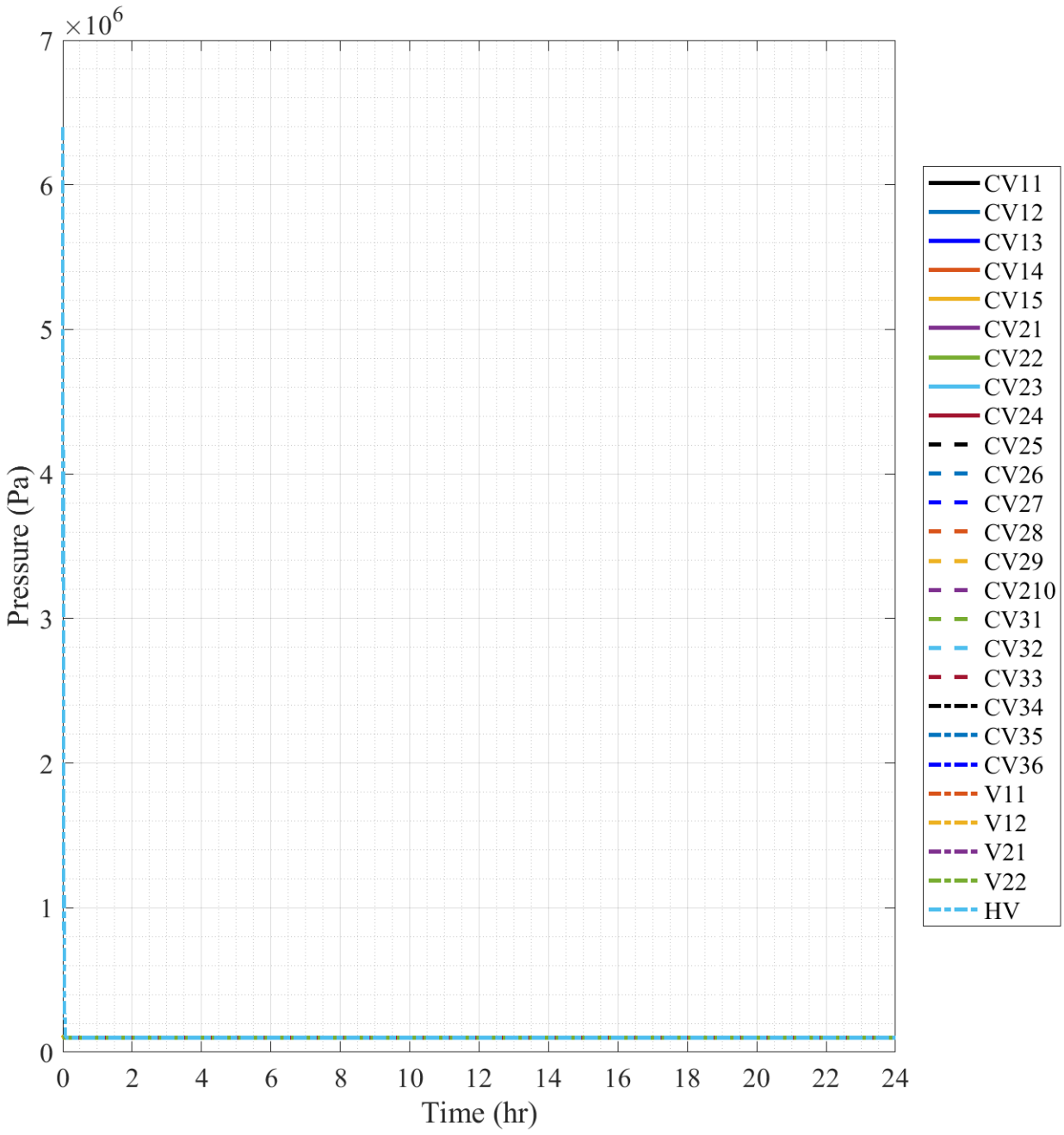

Fig. D.35. 1/28th-Scale Scenario 5 Pressure.

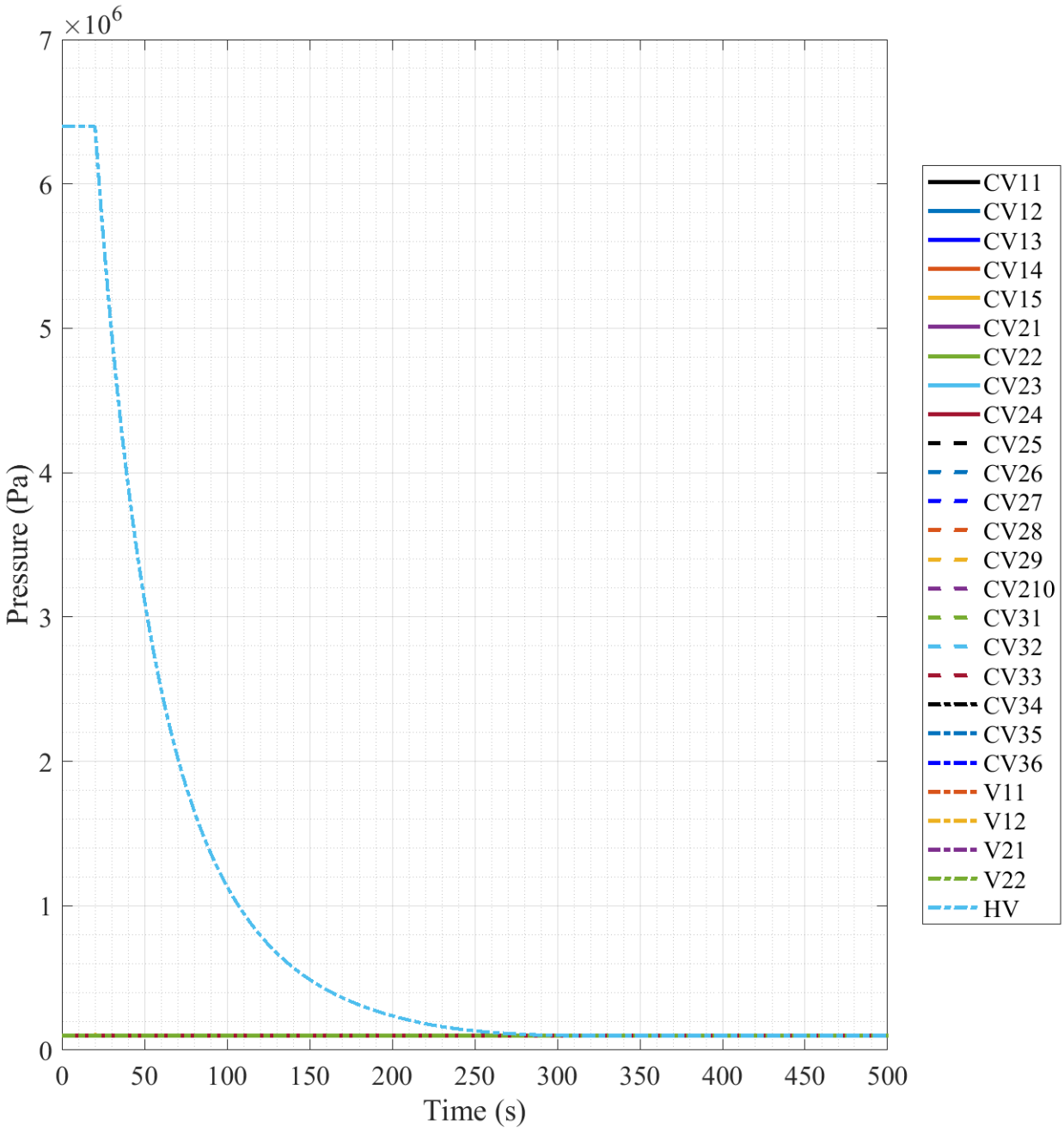

Fig. D.36. 1/28th-Scale Scenario 5 Pressure, 500 second Timescale.

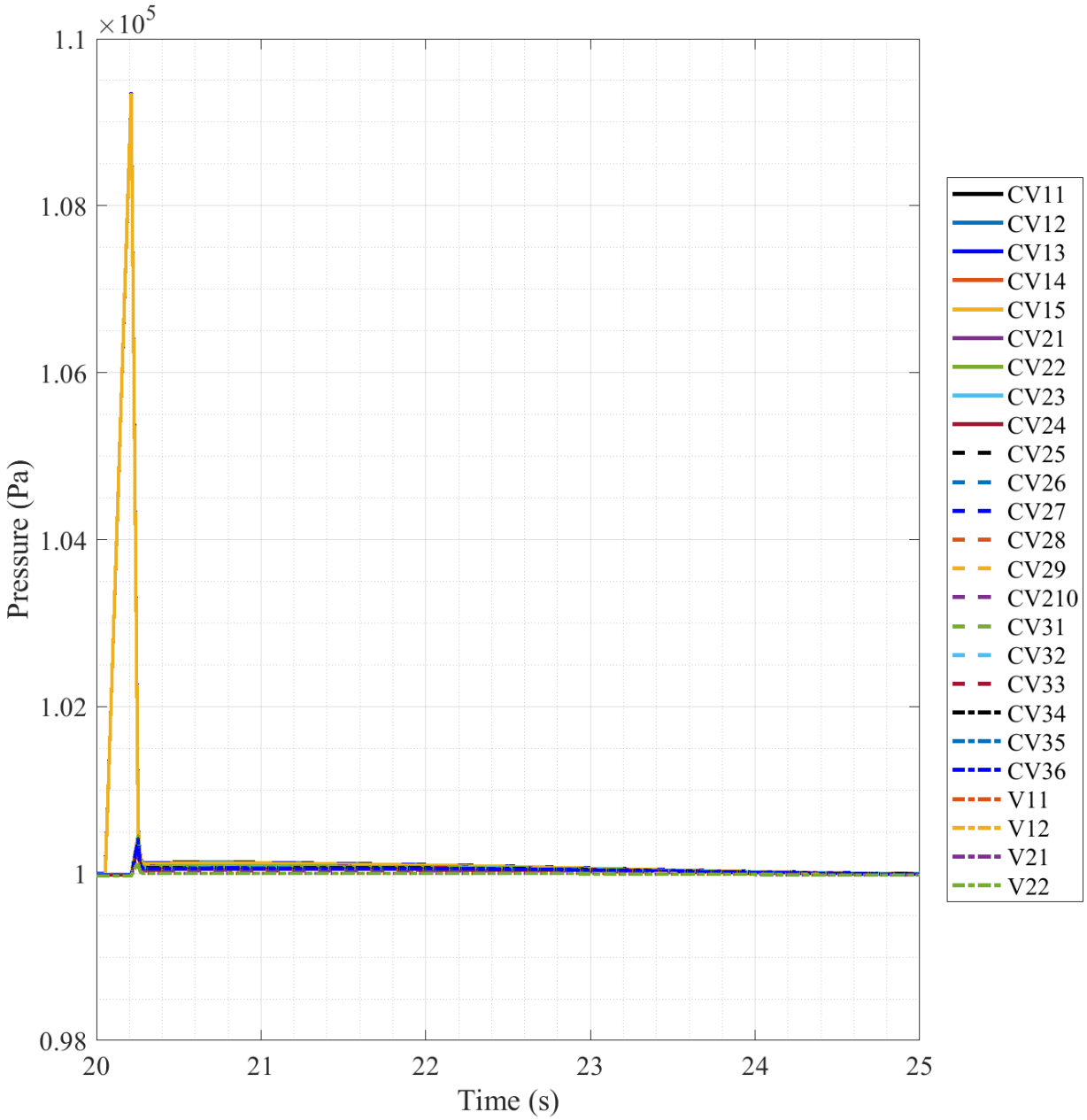

Fig. D.37. 1/28th-Scale Scenario 5 Pressure, 20-25 second Timescale, Individual Data.

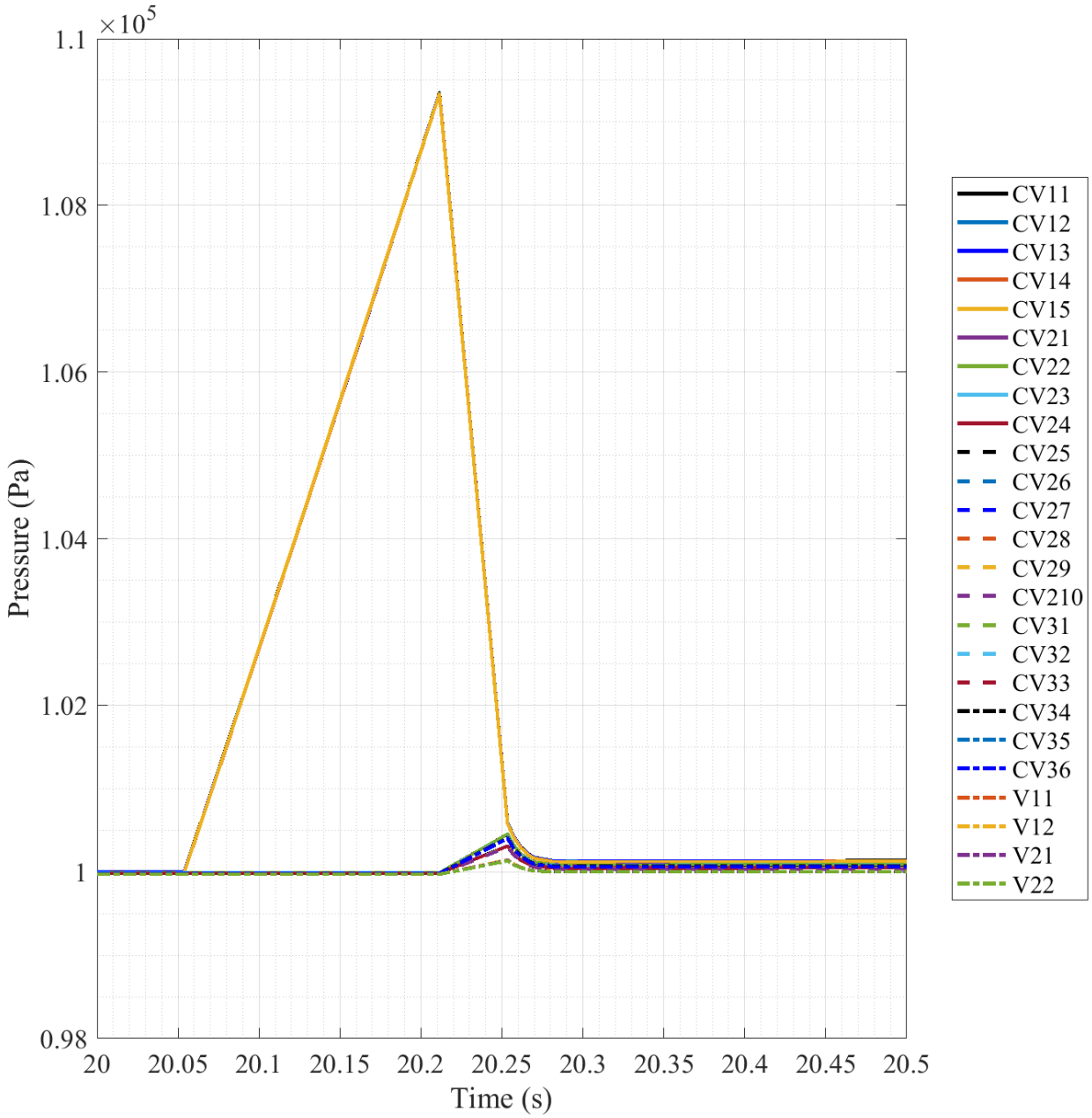

Fig. D.38. 1/28th-Scale Scenario 5 Pressure, 20-20.5 second Timescale, Individual Data.

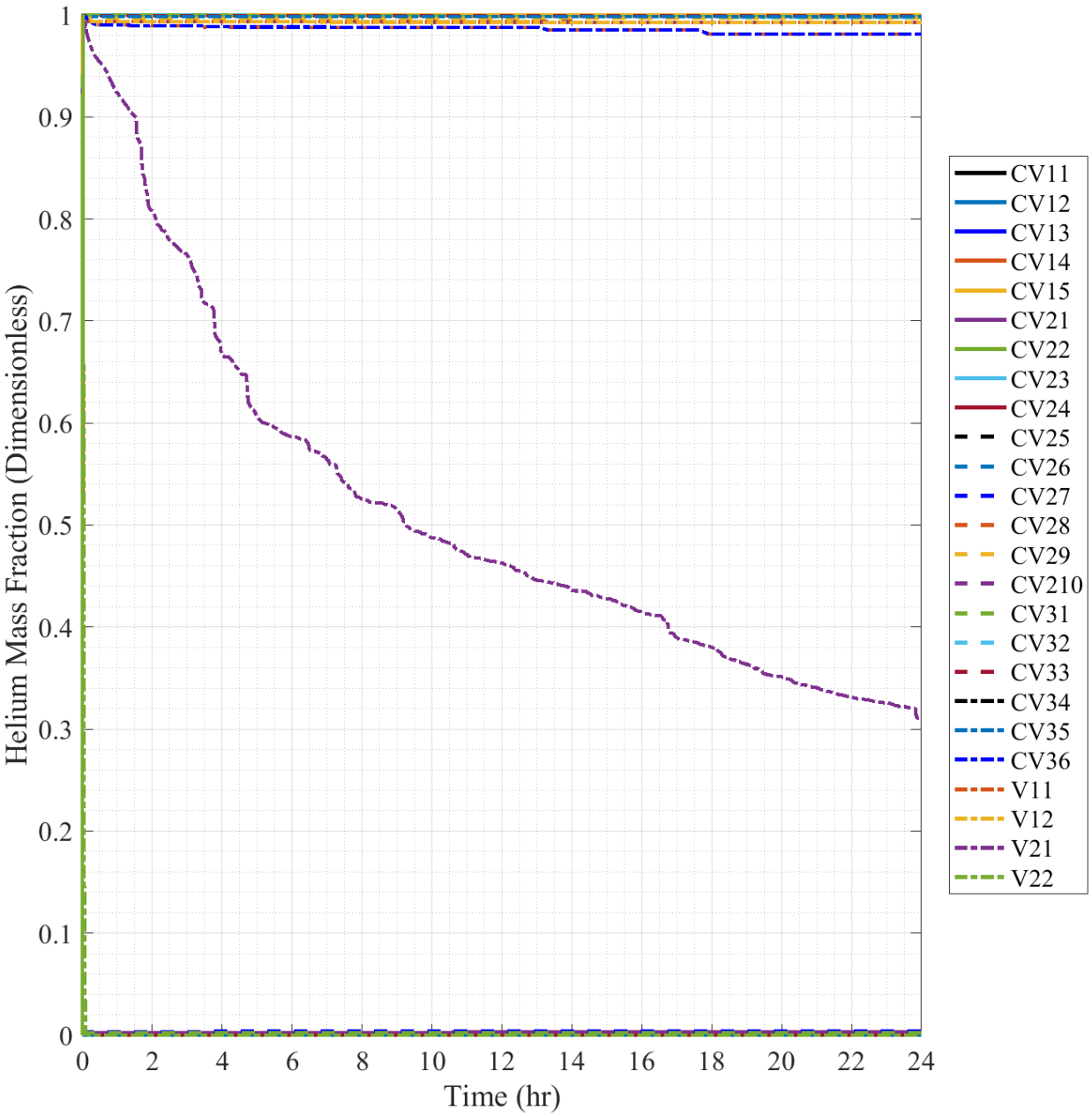

Fig. D.39. 1/28th-Scale Scenario 5 Helium Mass Fraction, Individual Data.

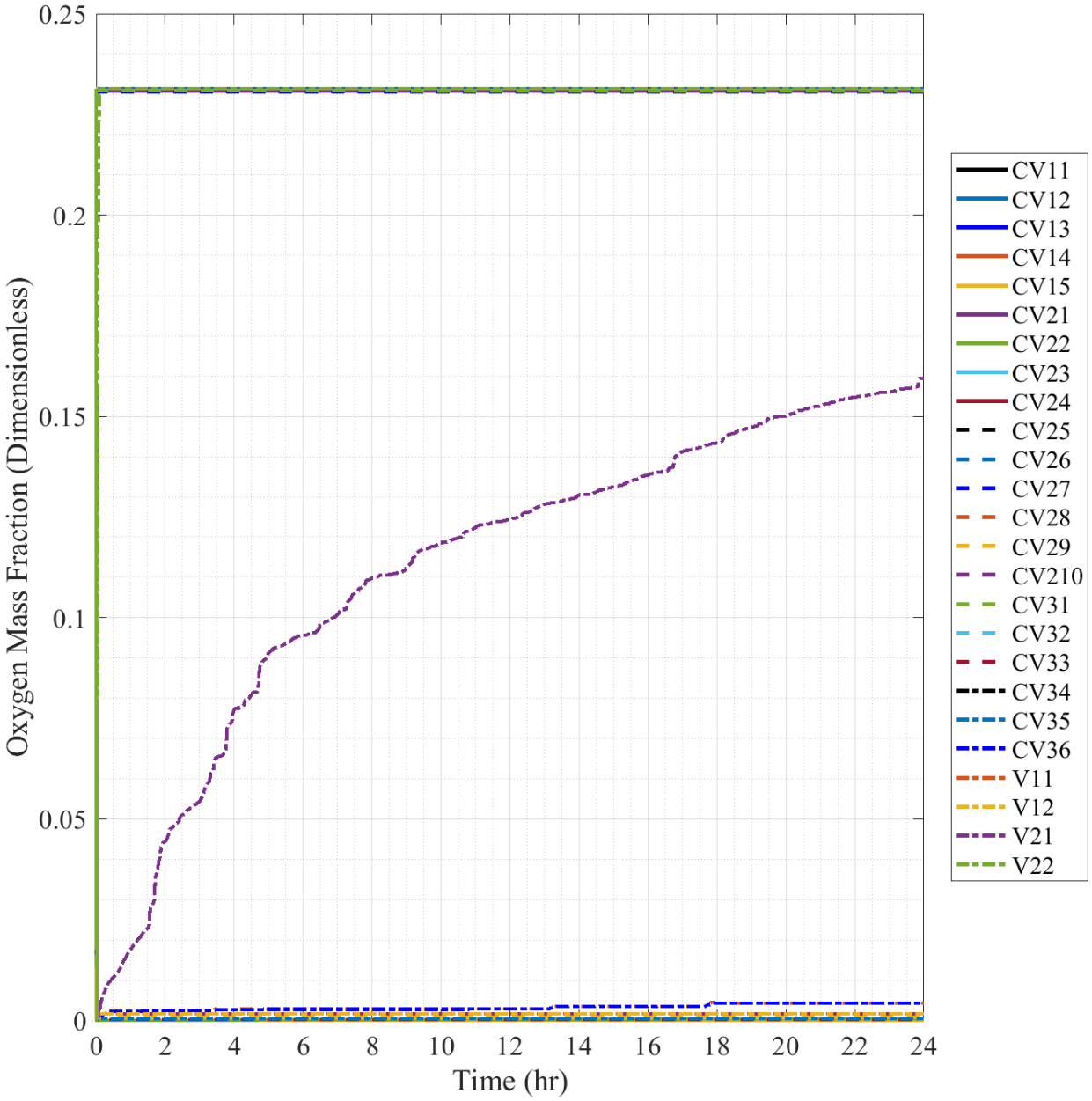

Fig. D.40. 1/28th-Scale Scenario 5 Oxygen Mass Fraction.

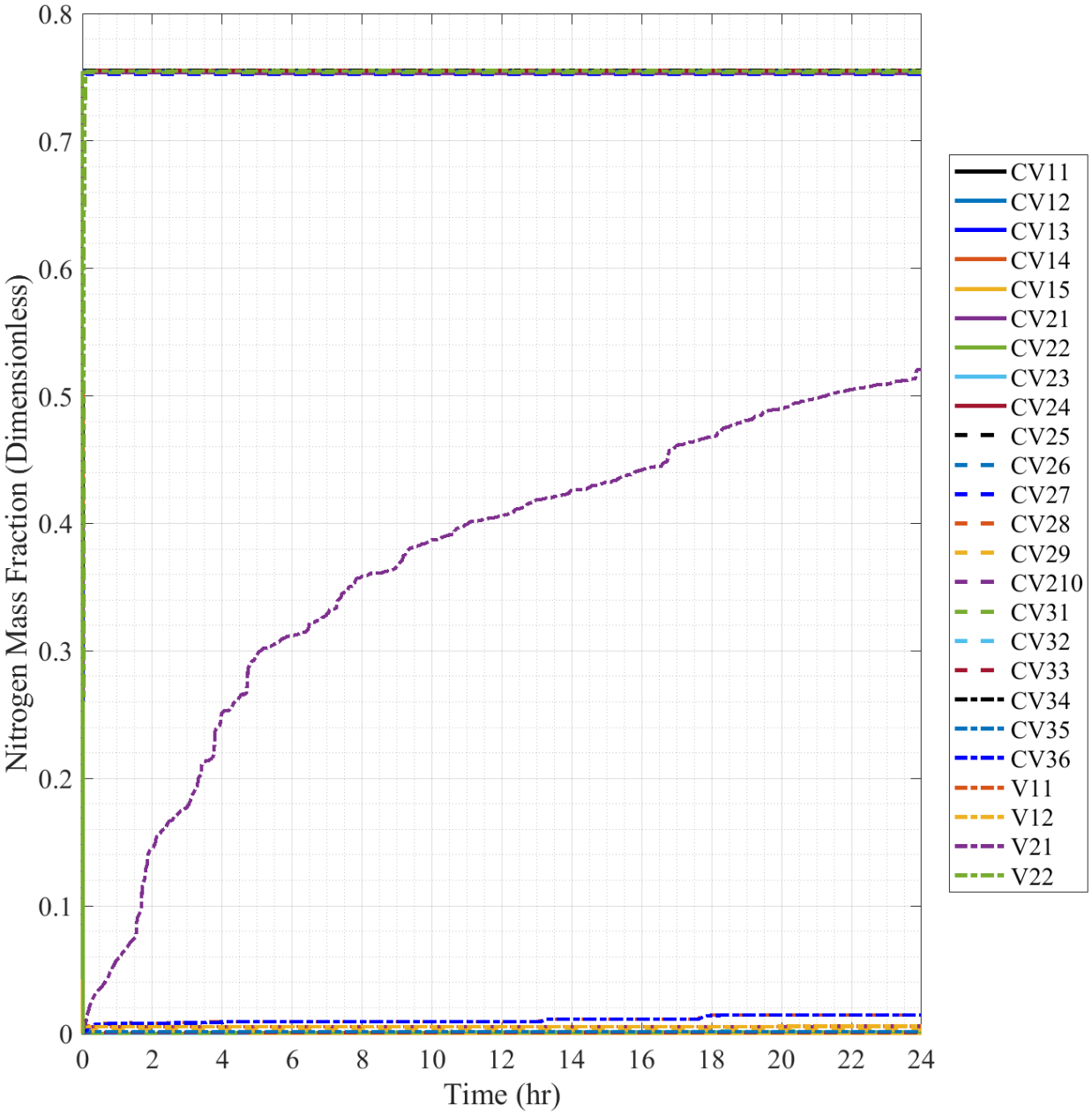

Fig. D.41. 1/28th-Scale Scenario 5 Nitrogen Mass Fraction.

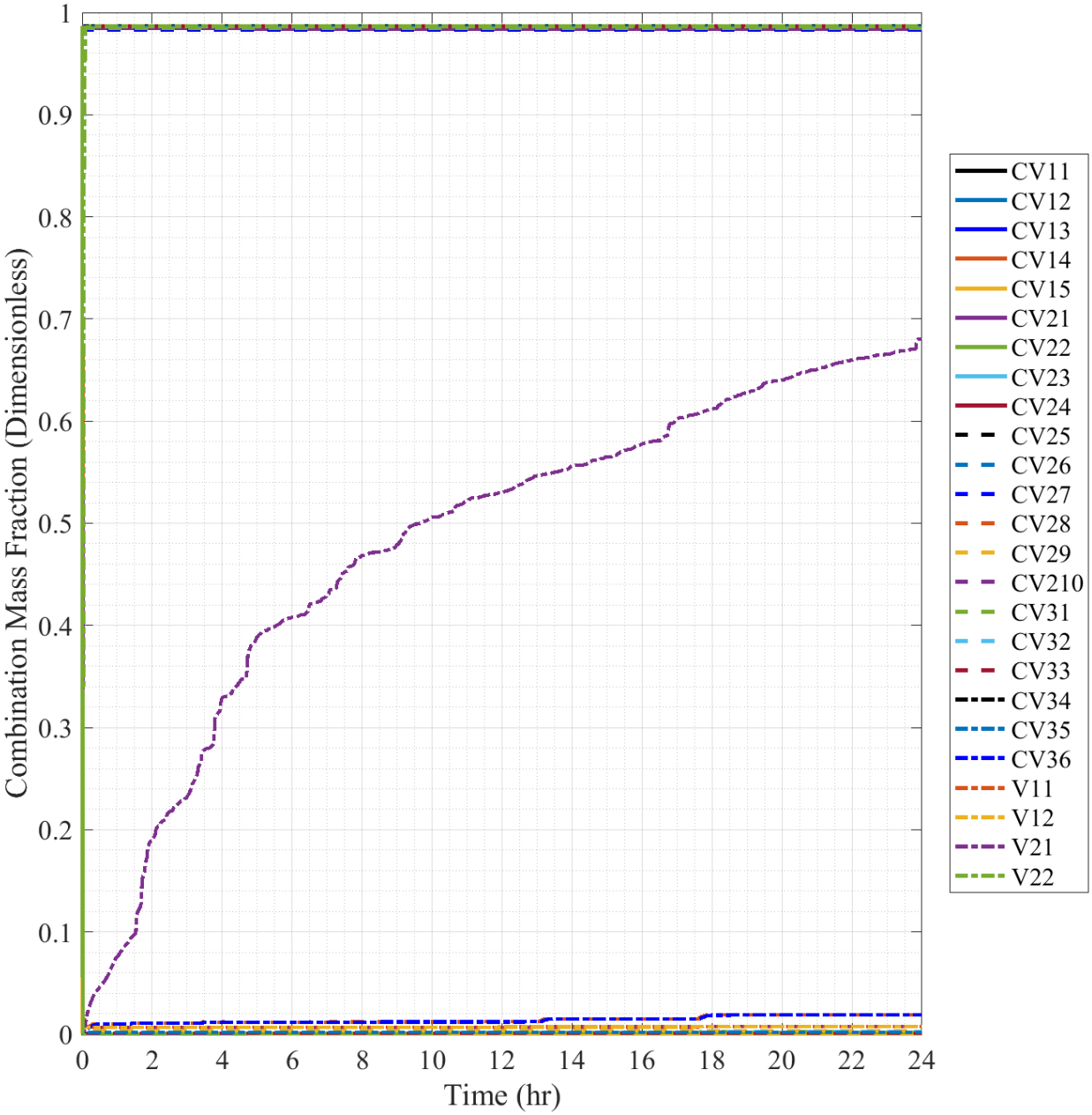

Fig. D.42. 1/28th-Scale Scenario 5 Combination Mass Fraction, Individual Data.

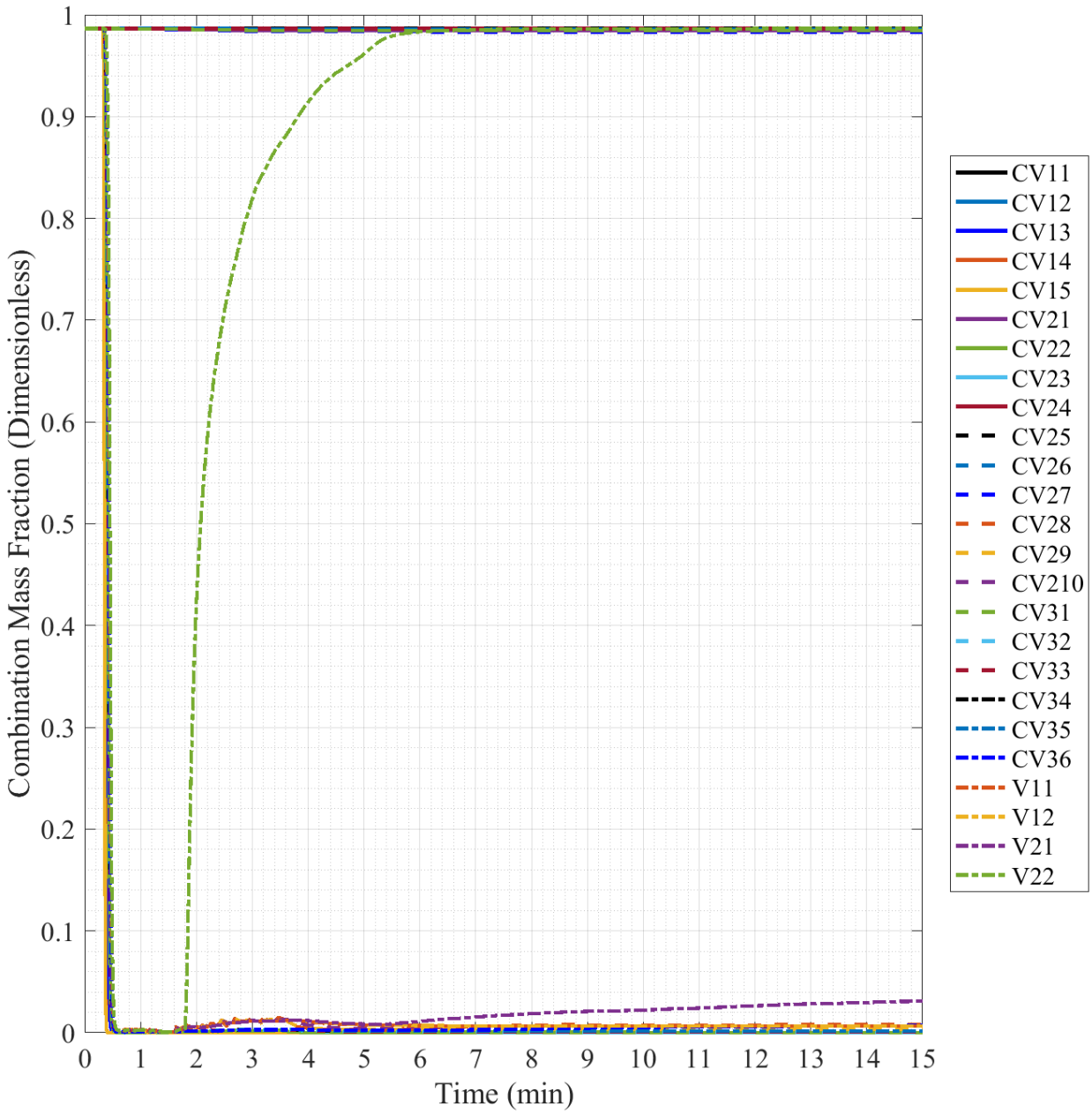

Fig. D.43. 1/28th-Scale Scenario 5 Combination Mass Fraction, 15 minute Timescale, Individual Data.

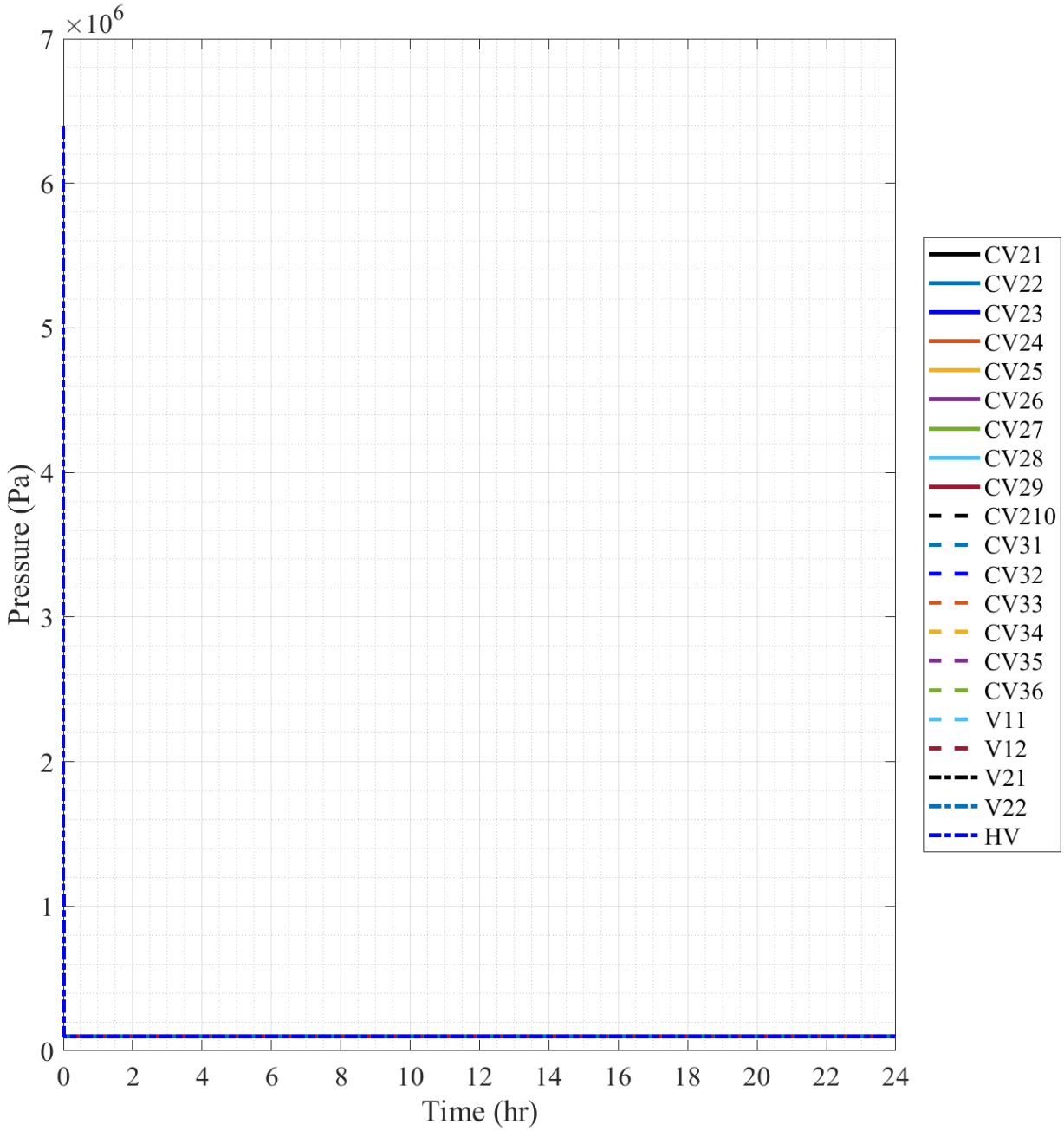

Fig. D.44. 1/28th-Scale Scenario 6 Pressure.

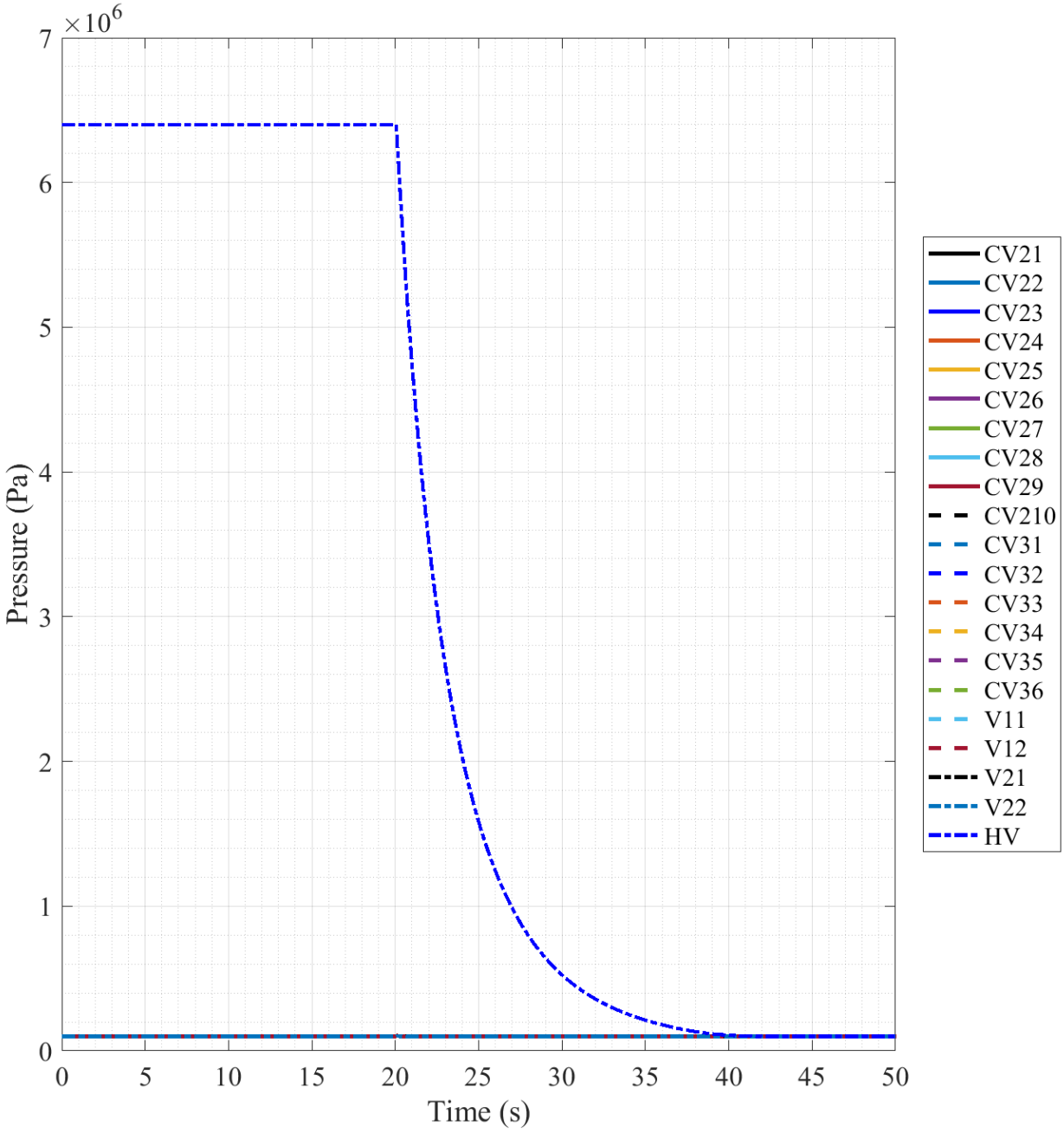

Fig. D.45. 1/28th-Scale Scenario 6 Pressure, 50 second Timescale.

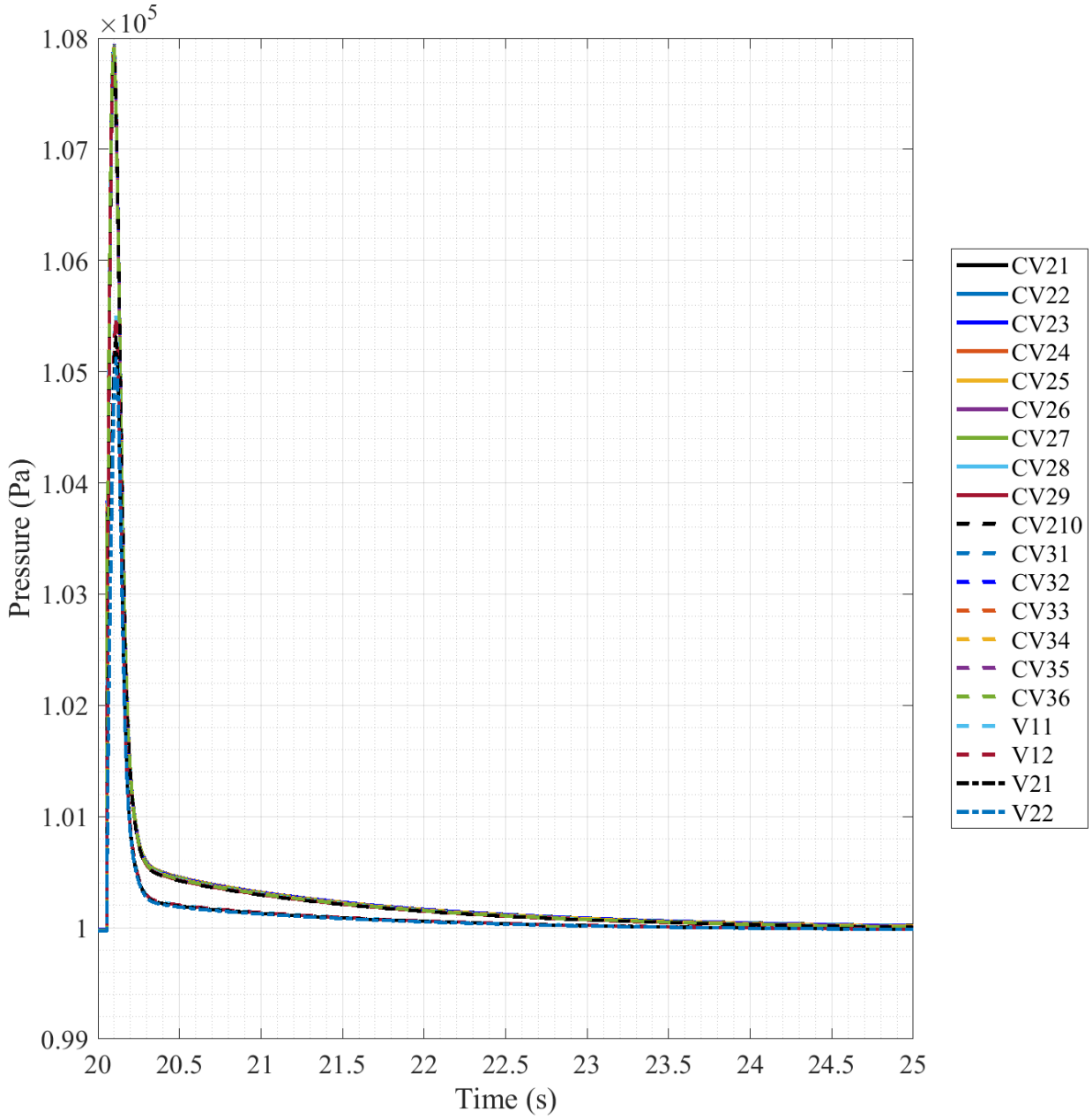

Fig. D.46. 1/28th-Scale Scenario 6 Pressure, 20-25 second Timescale, Individual Data.

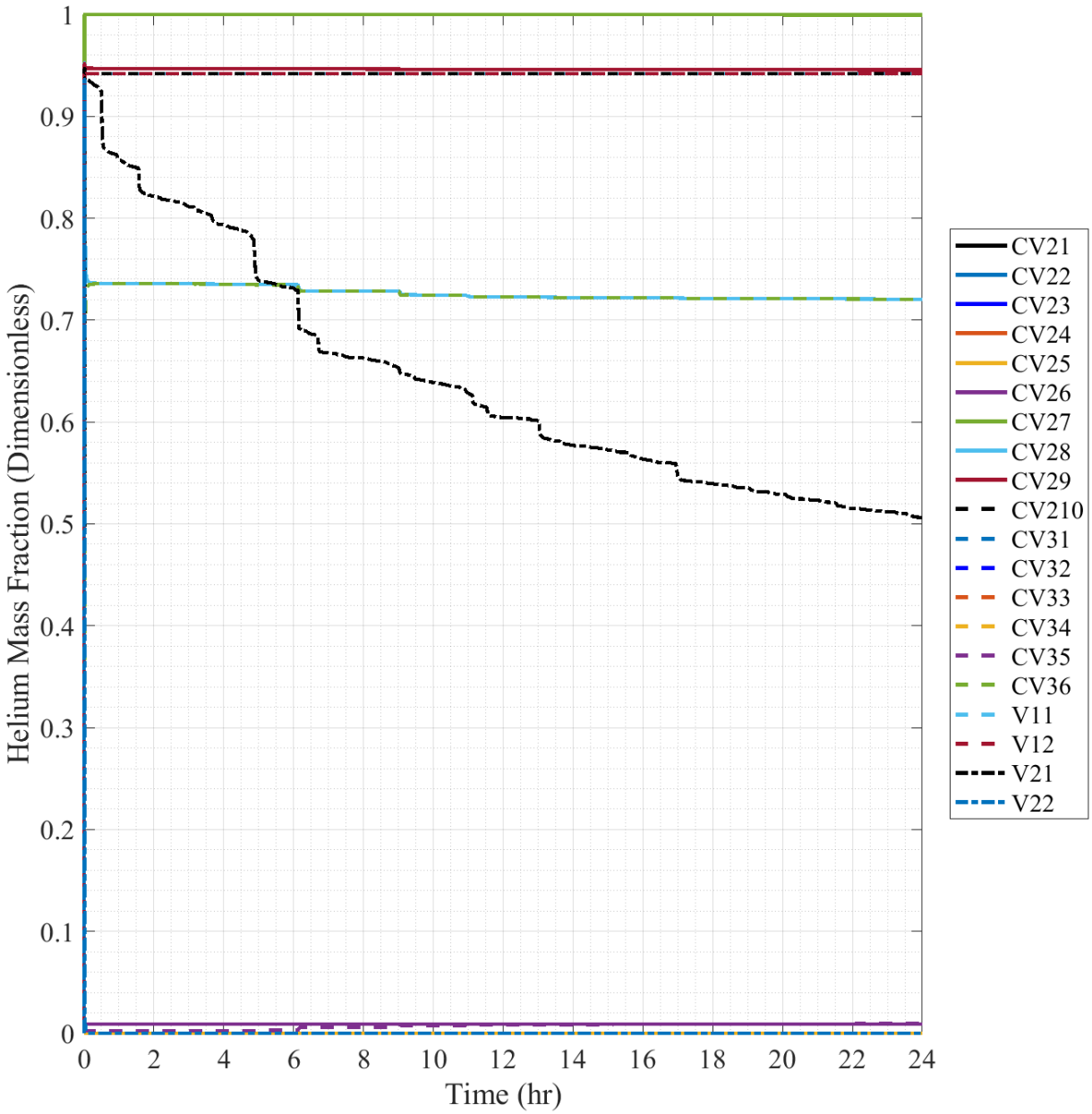

Fig. D.47. 1/28th-Scale Scenario 6 Helium Mass Fraction, Individual Data.

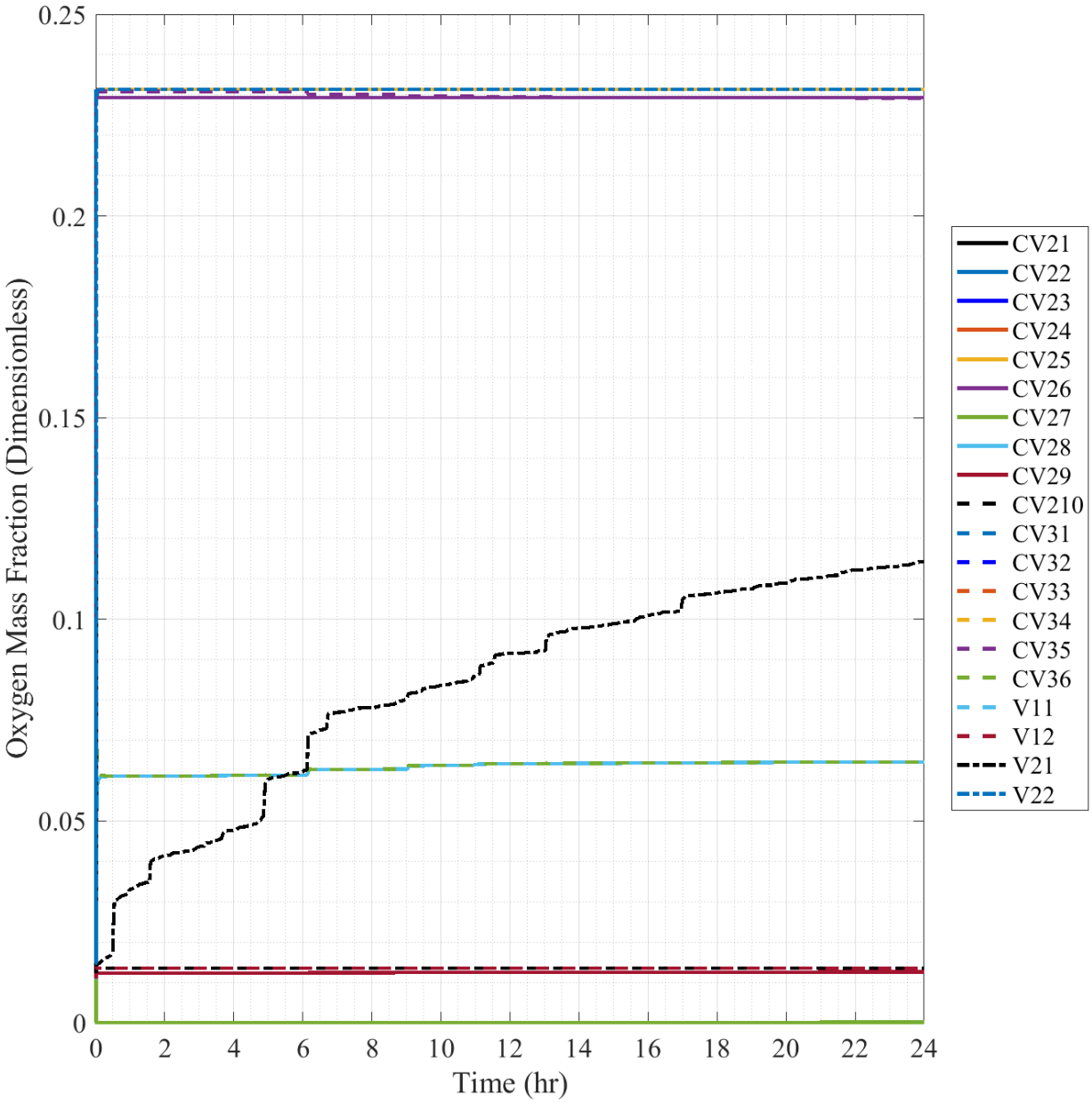

Fig. D.48. 1/28th-Scale Scenario 6 Oxygen Mass Fraction.

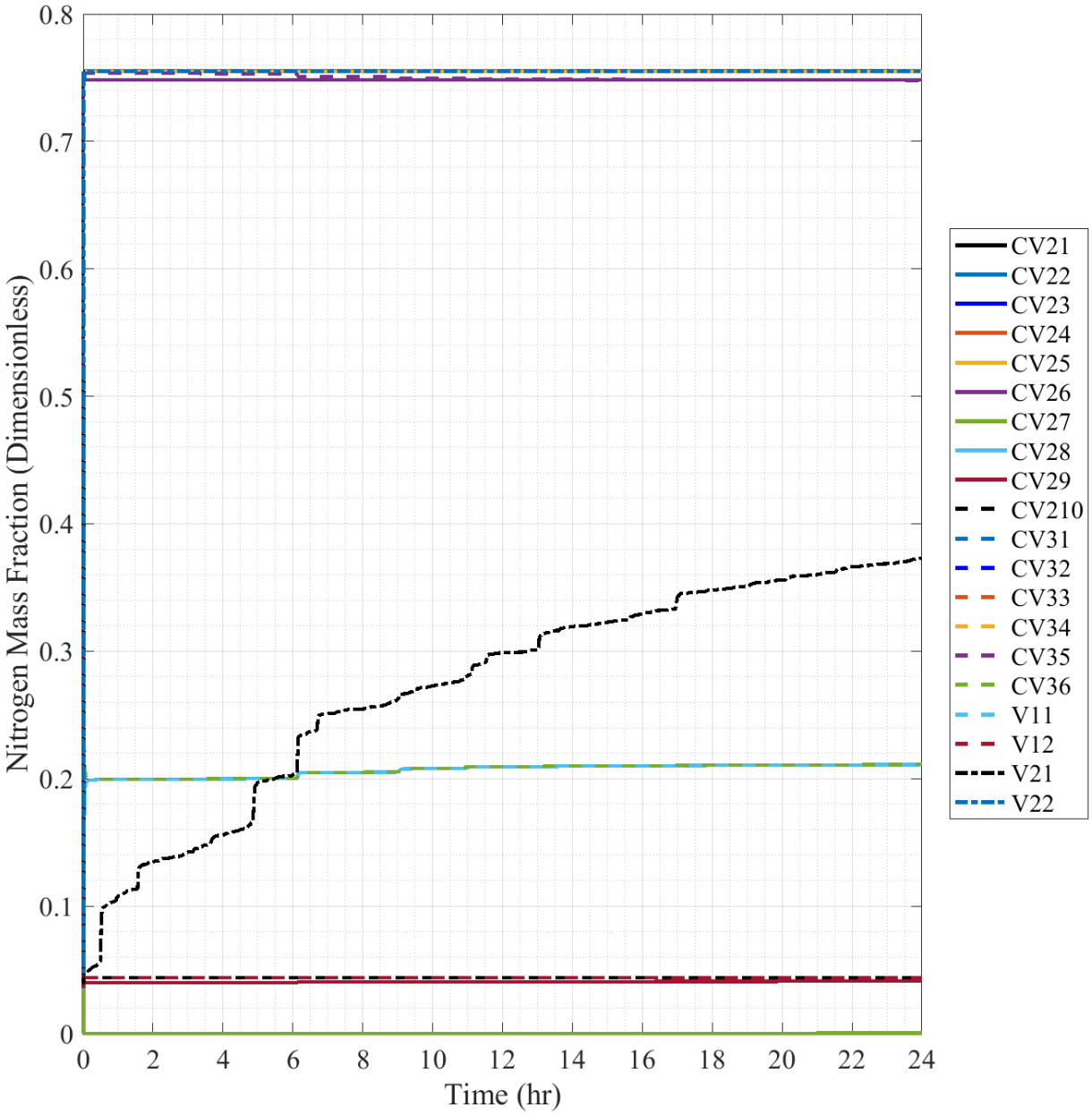

Fig. D.49. 1/28th-Scale Scenario 6 Nitrogen Mass Fraction.

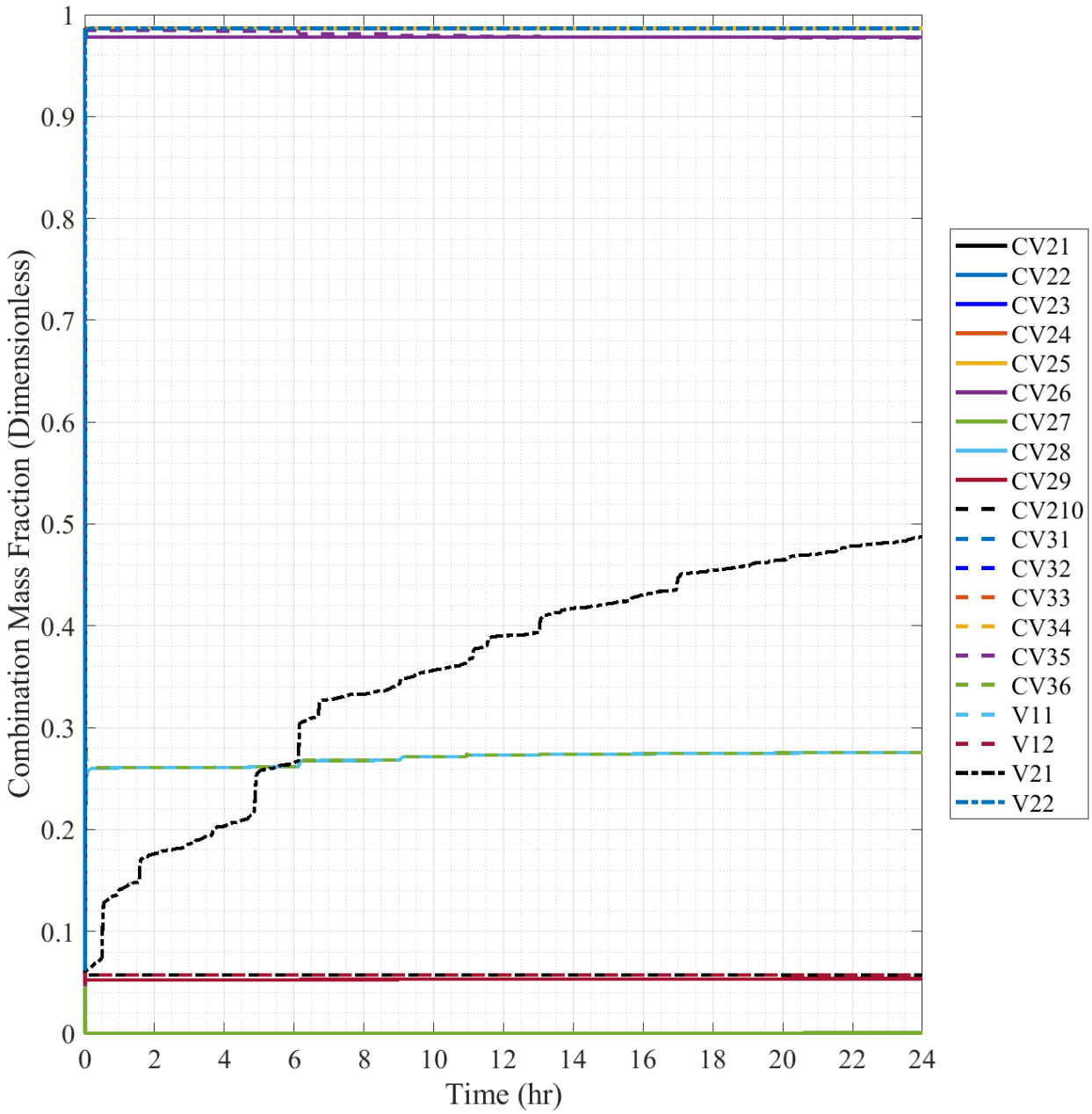

Fig. D.50. 1/28th-Scale Scenario 6 Combination Mass Fraction, Individual Data.

APPENDIX E: FULL-SCALE RESULTS PLOTS

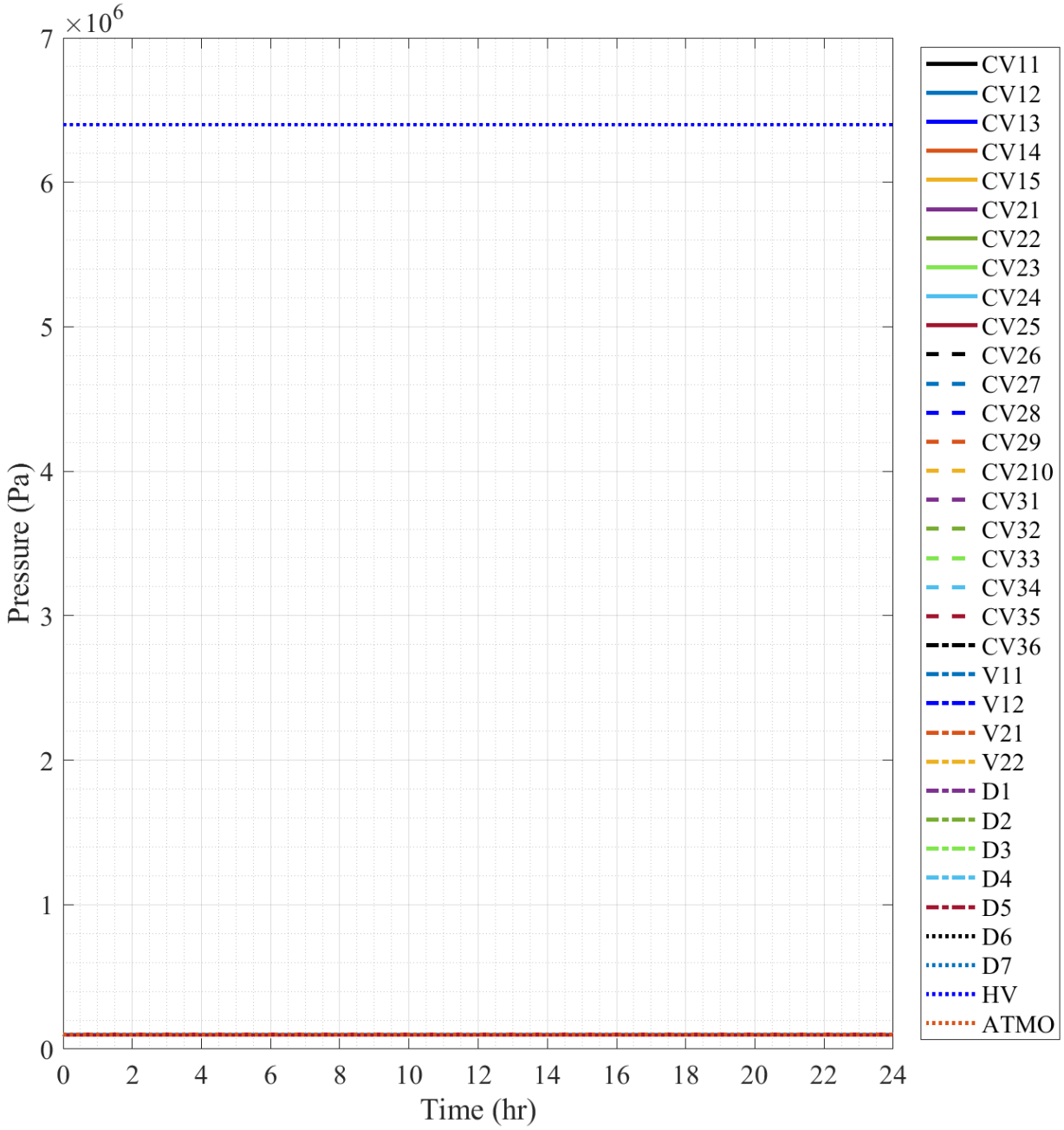

Fig. E.1. Full-Scale Scenario 0 Pressure, Individual Data.

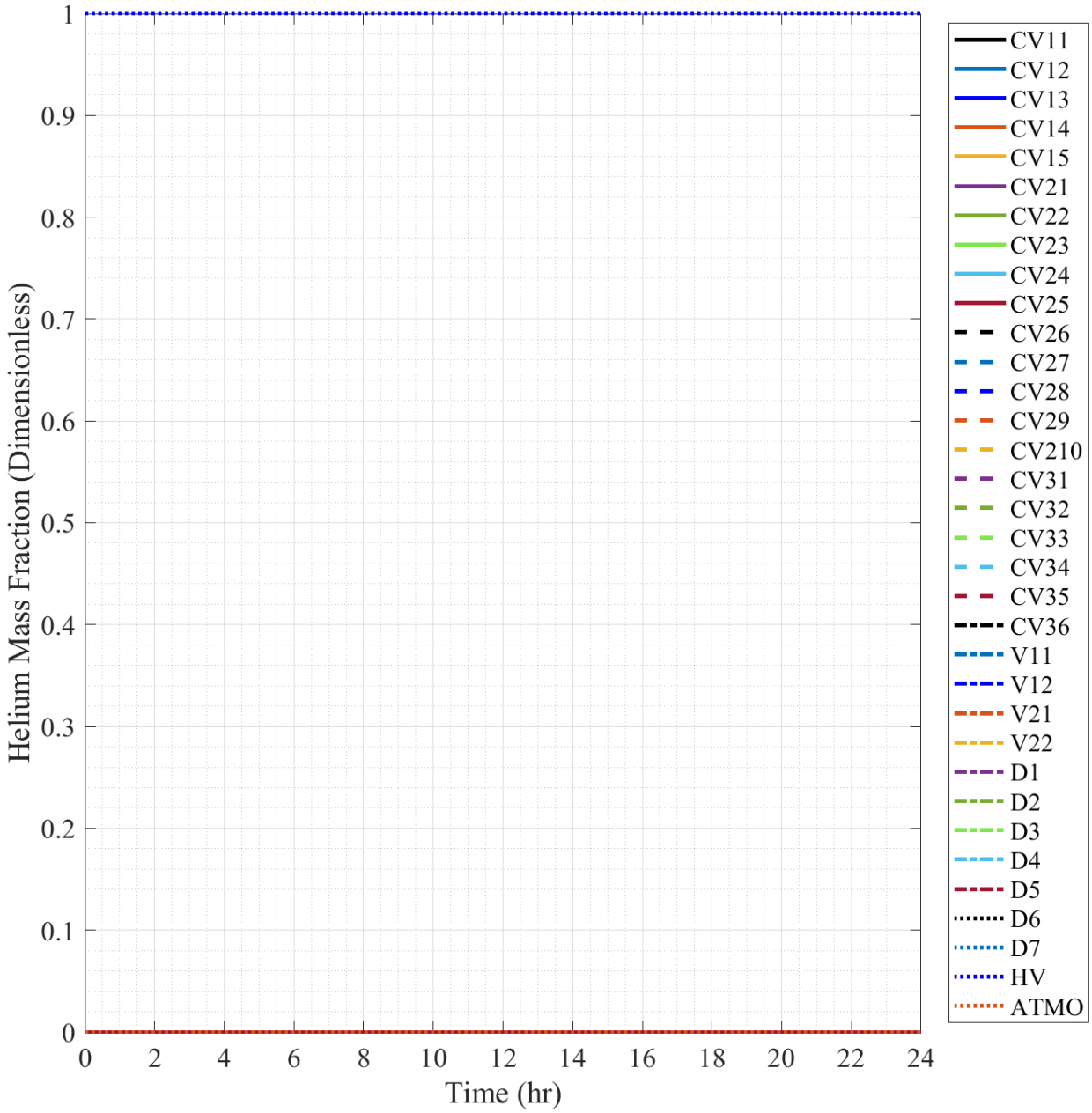

Fig. E.2. Full-Scale Scenario 0 Helium Mass Fraction, Individual Data.

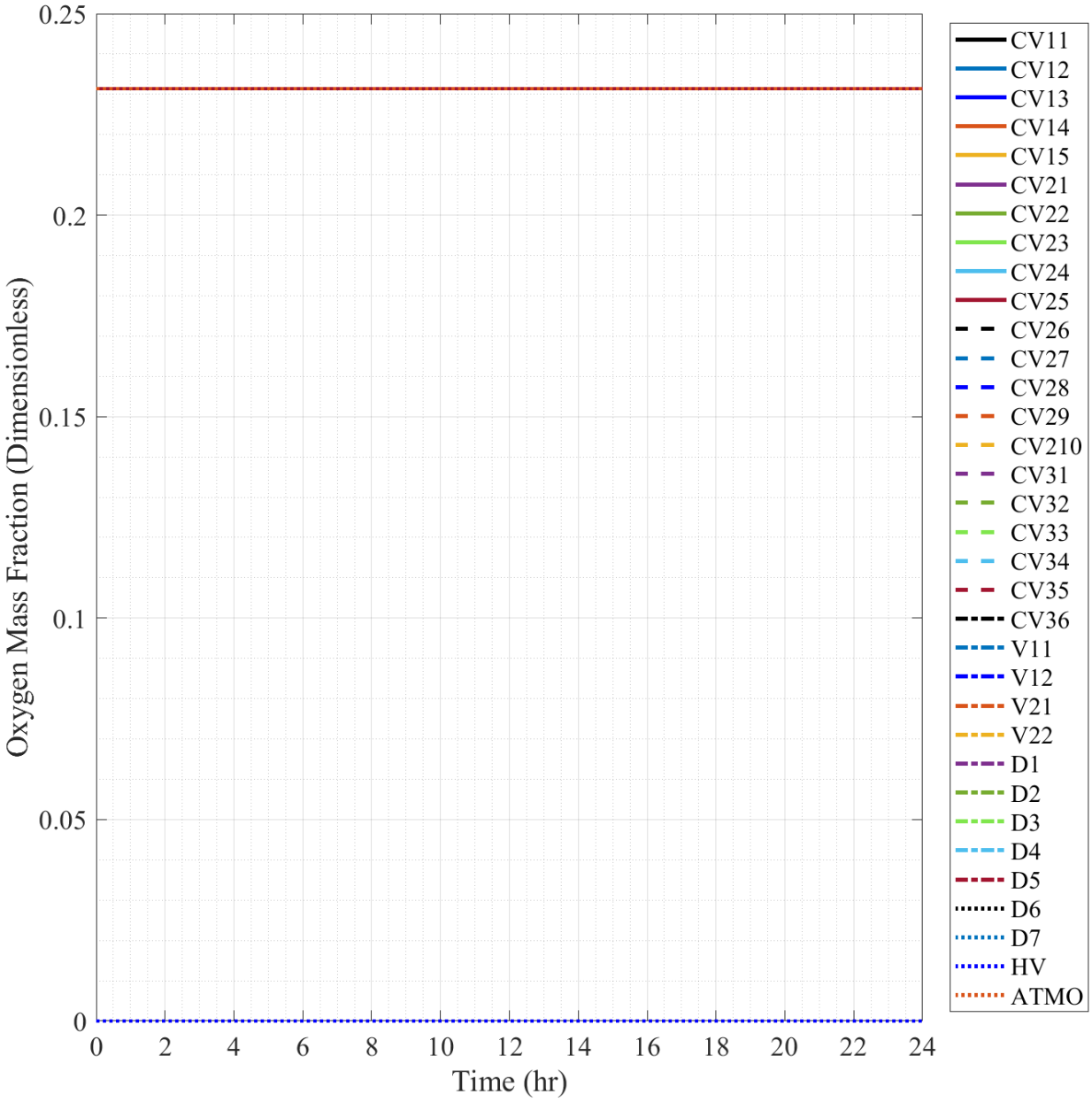

Fig. E.3. Full-Scale Scenario 0 Oxygen Mass Fraction, Individual Data.

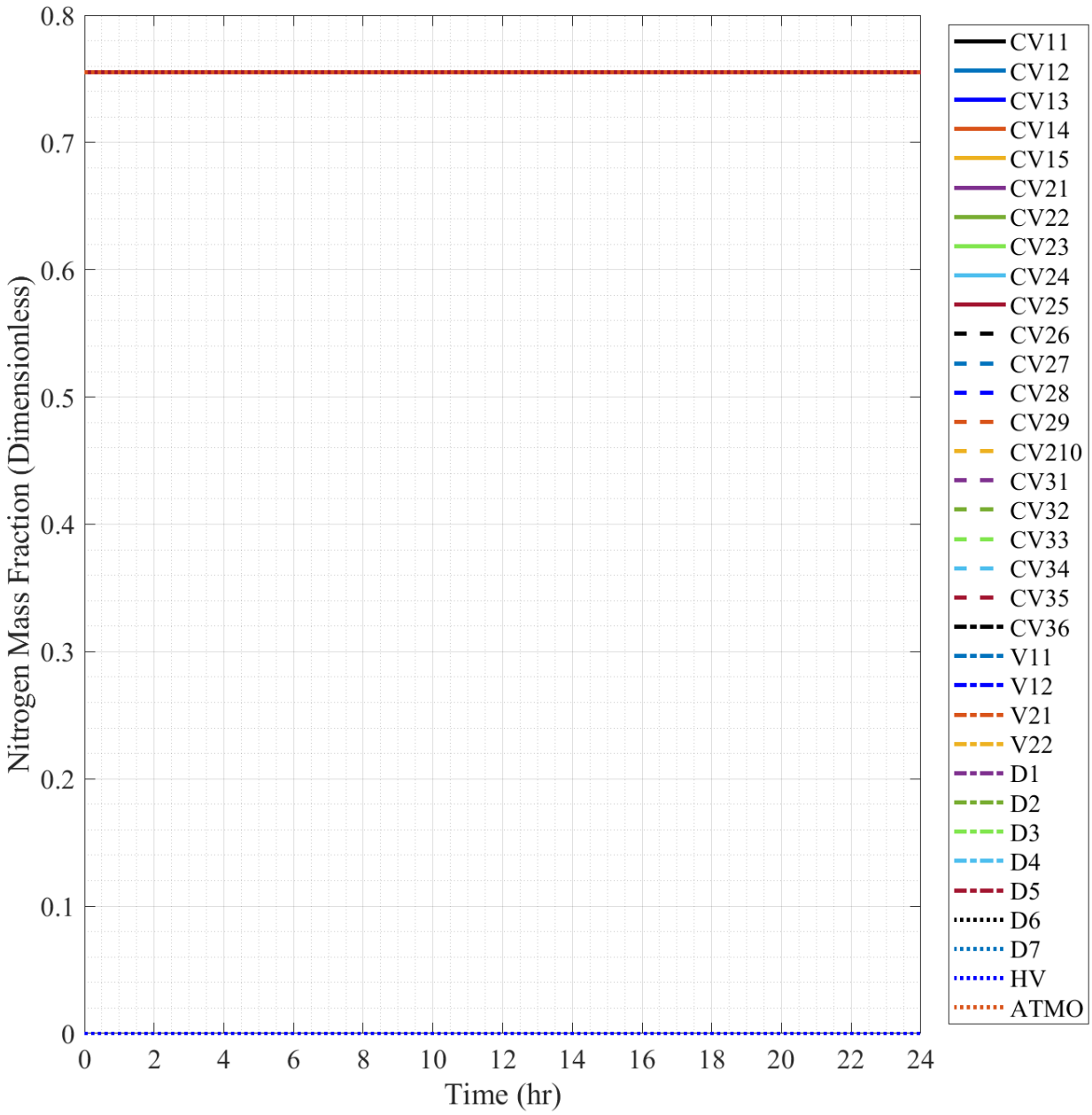

Fig. E.4. Full-Scale Scenario 0 Nitrogen Mass Fraction, Individual Data.

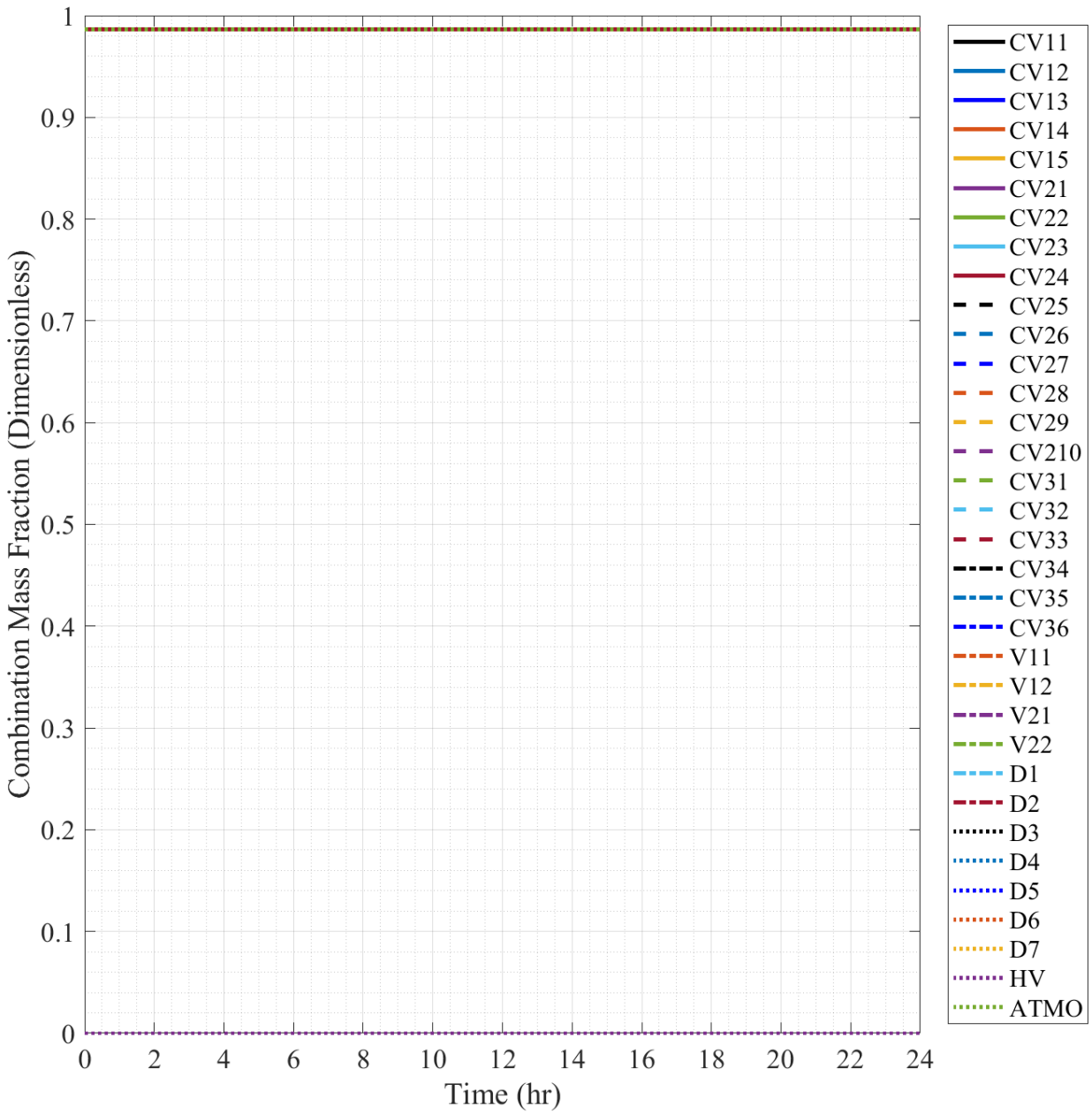

Fig. E.5. Full-Scale Scenario 0 Combination Mass Fraction, Individual Data.

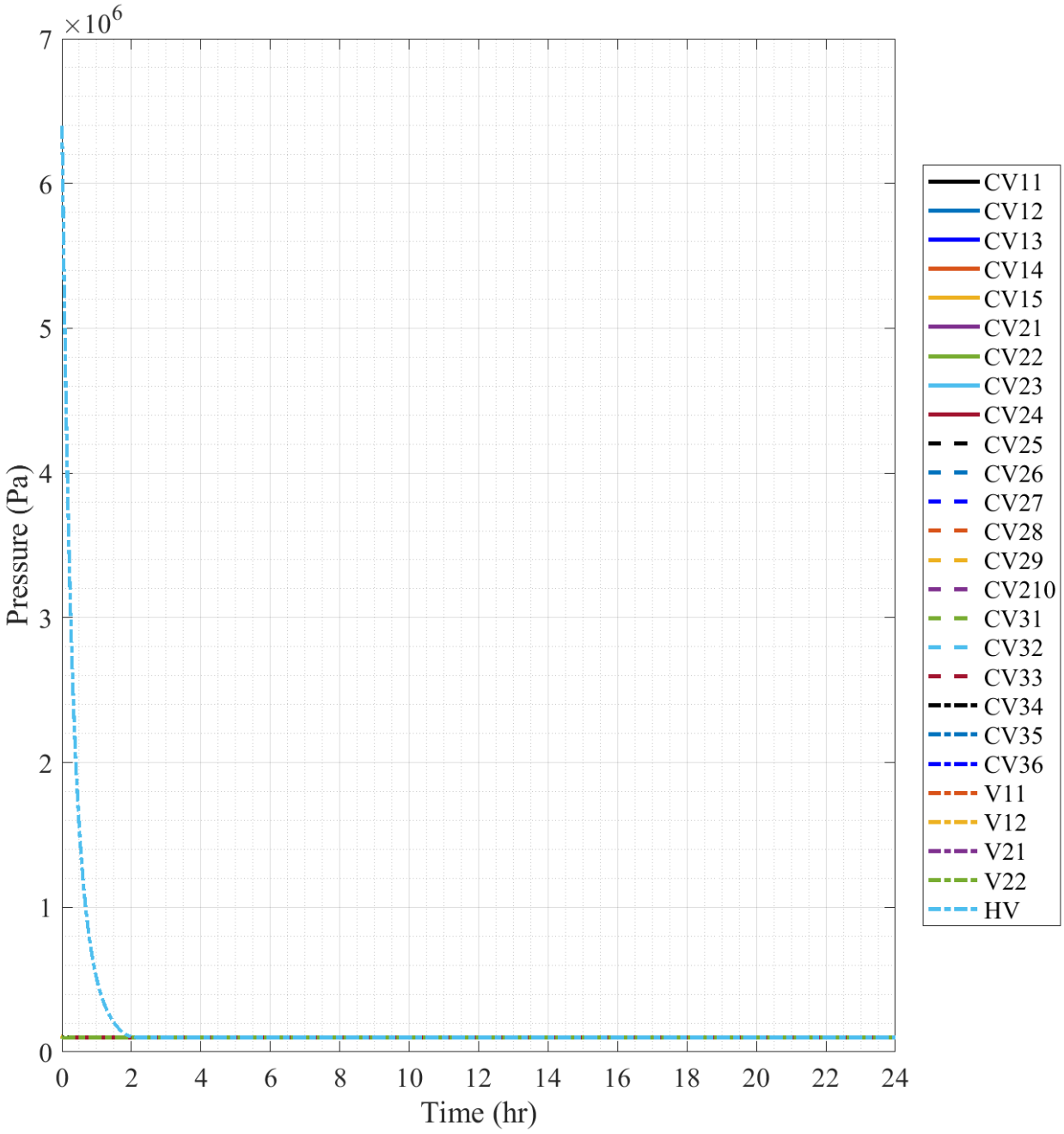

Fig. E.6. Full-Scale Scenario 1 Pressure, Individual Data.

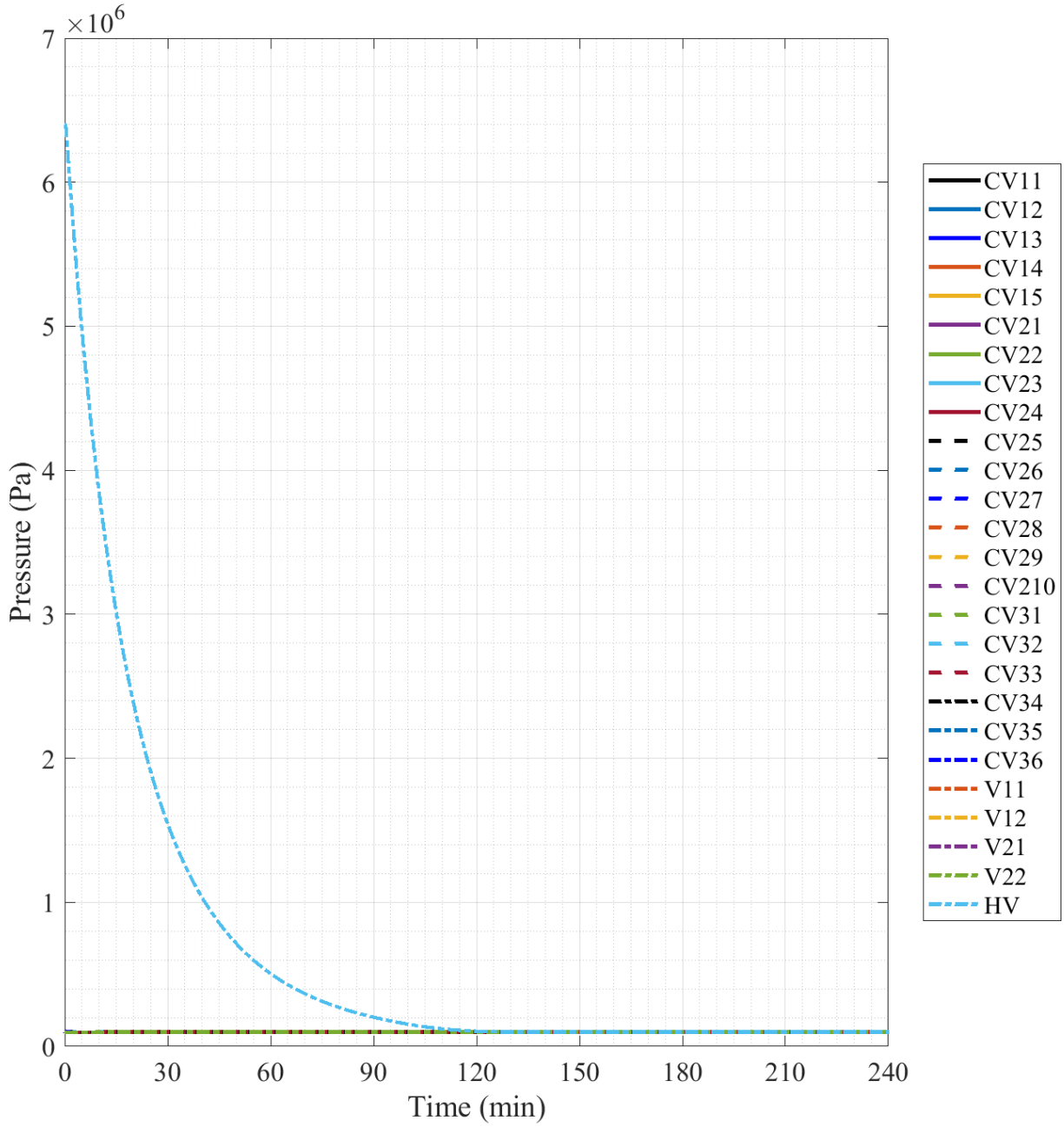

Fig. E.7. Full-Scale Scenario 1 Pressure, 240 minute Timescale, Individual Data.

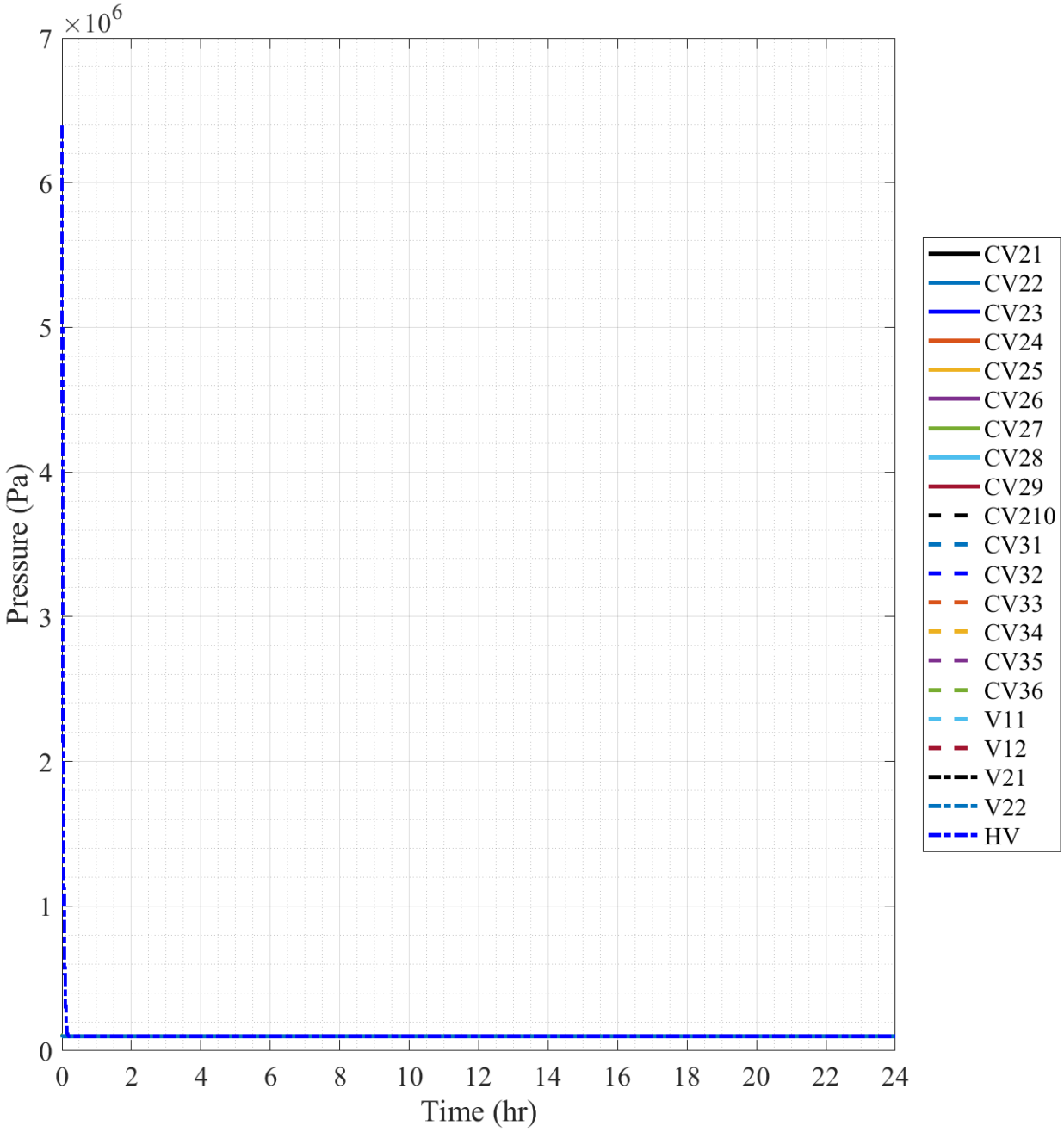

Fig. E.8. Full-Scale Scenario 2 Pressure, Individual Data.

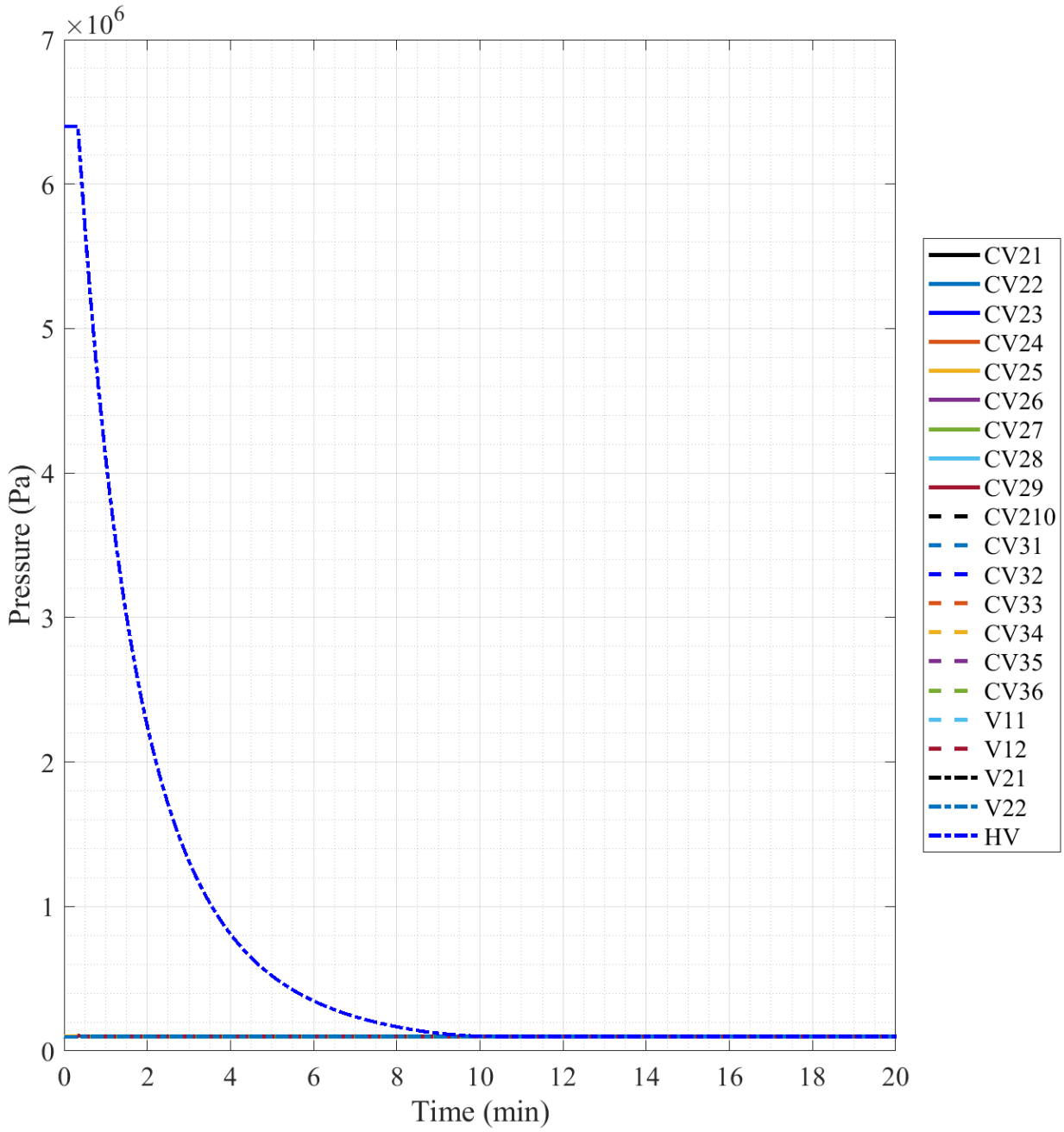

Fig. E.9. Full-Scale Scenario 2 Pressure, 20 minute Timescale, Individual Data.

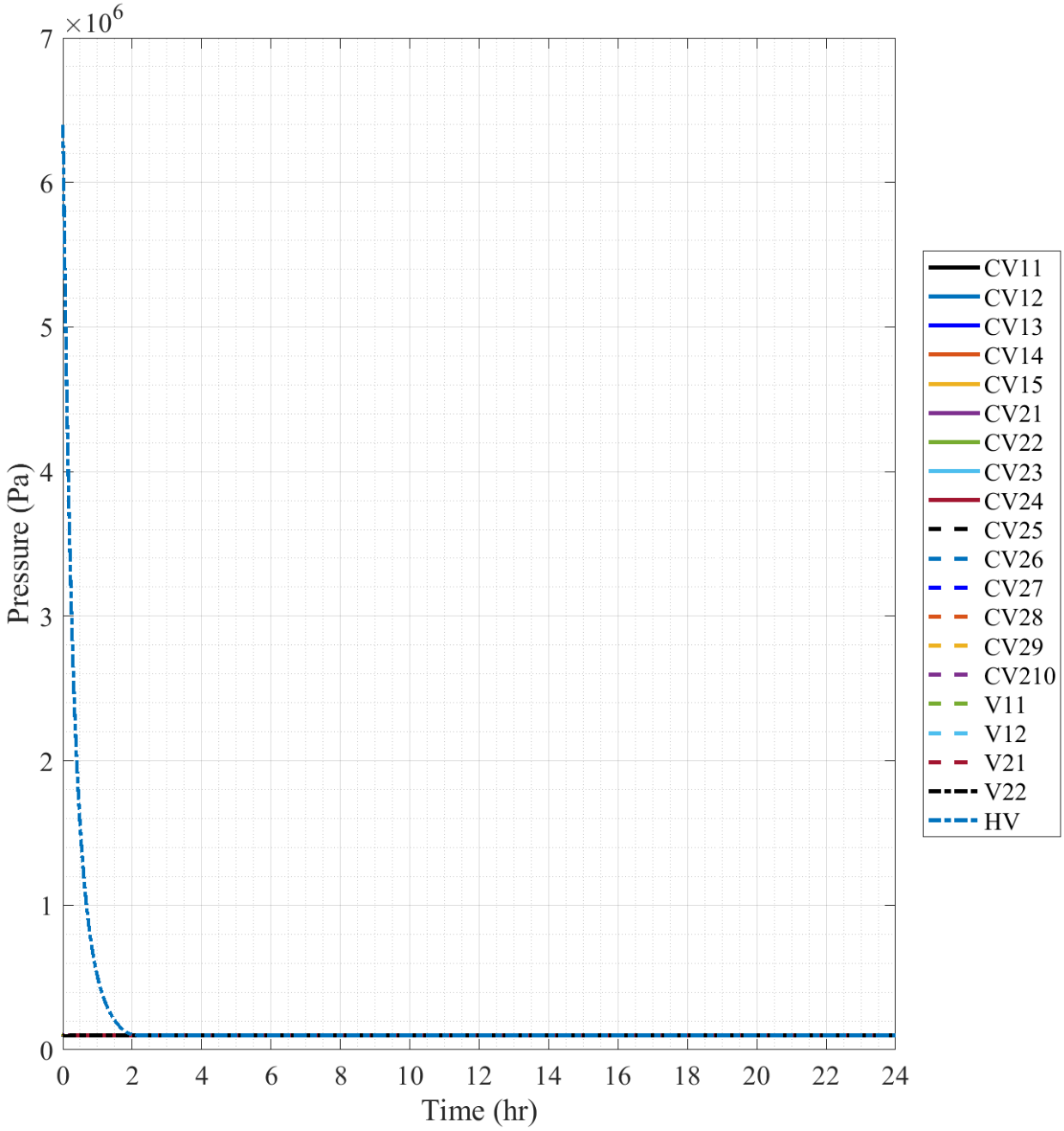

Fig. E.10. Full-Scale Scenario 3 Pressure.

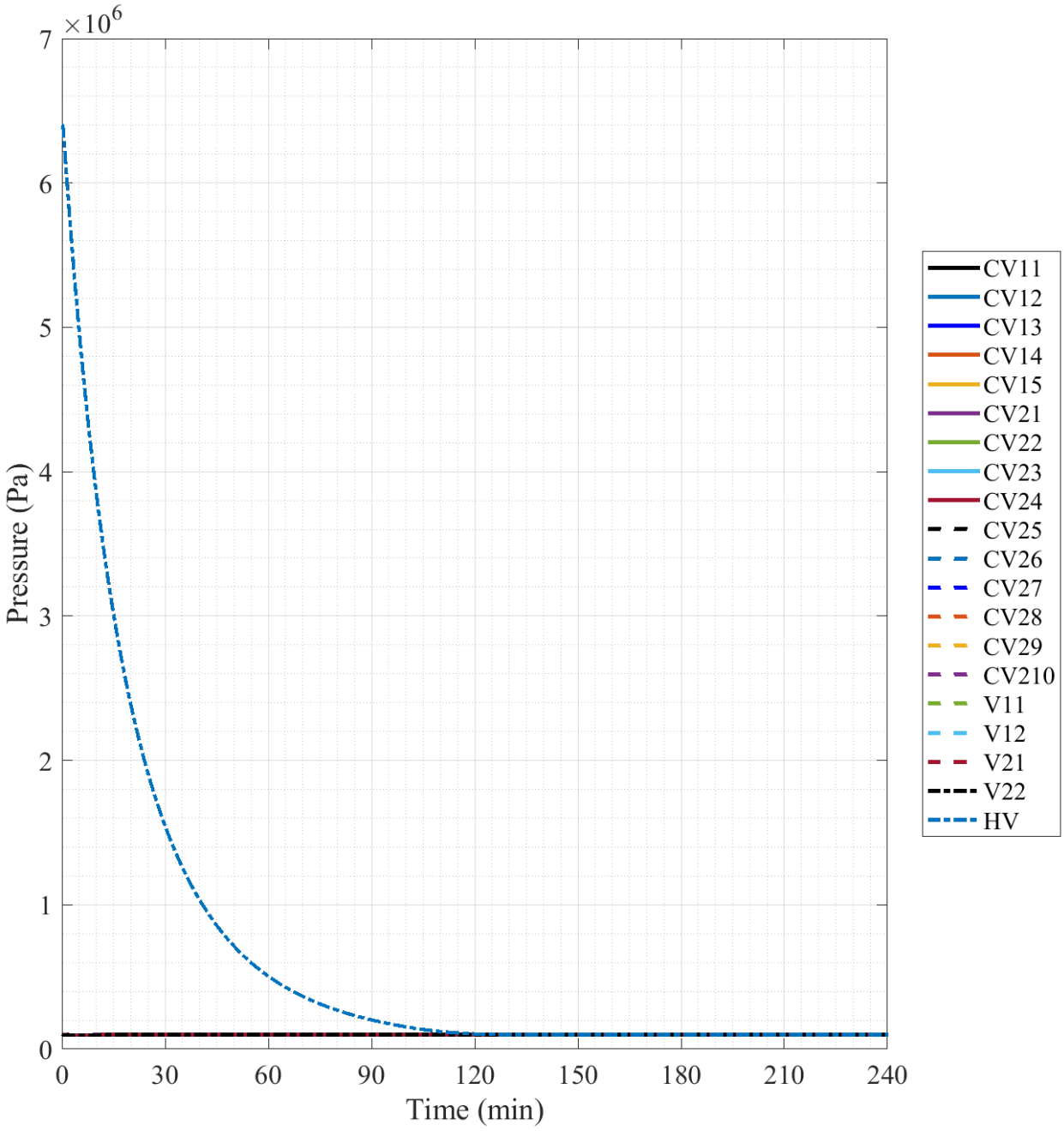

Fig. E.11. Full-Scale Scenario 3 Pressure, 240 minute Timescale.

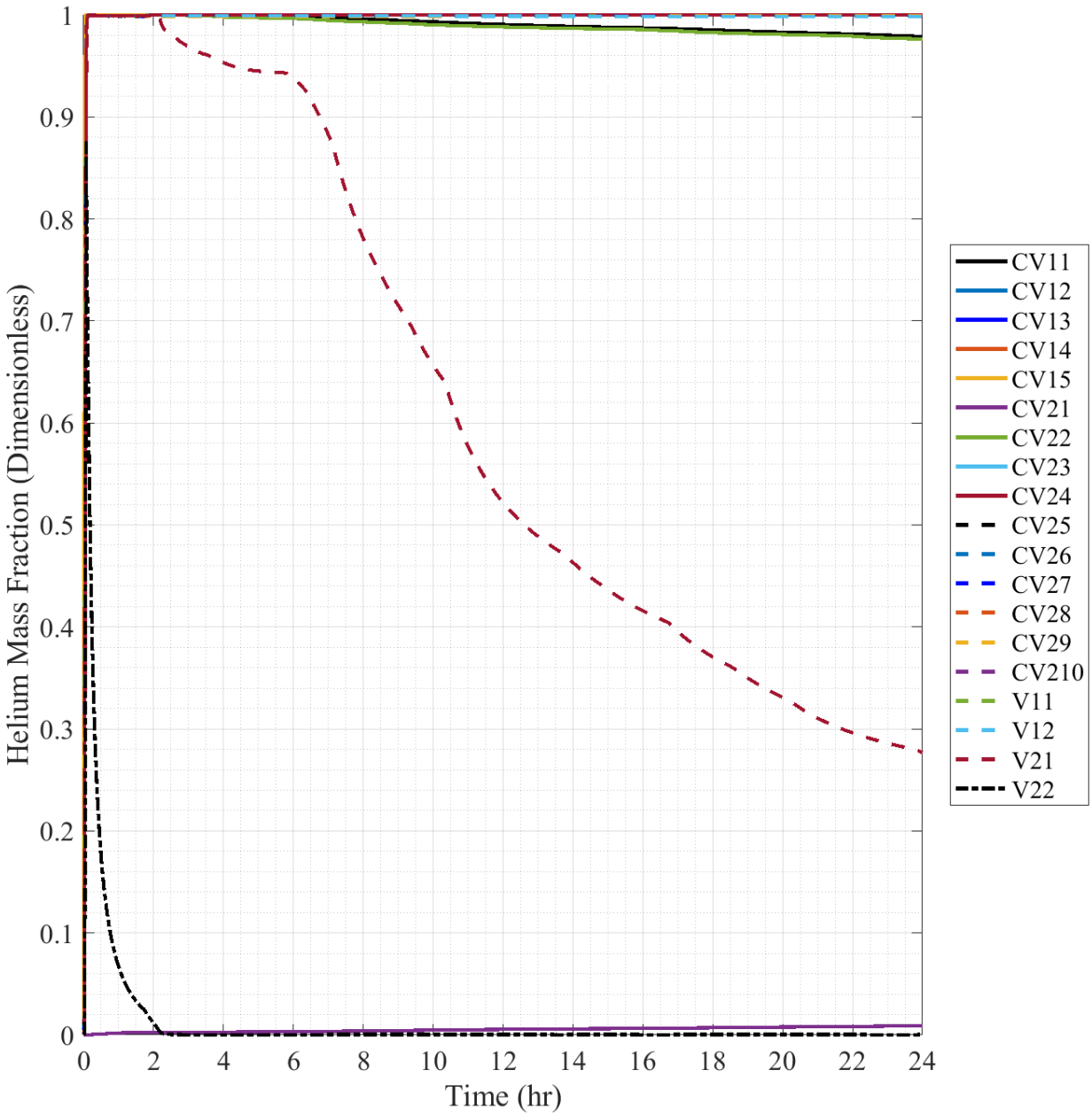

Fig. E.12. Full-Scale Scenario 3 Helium Mass Fraction, Individual Data.

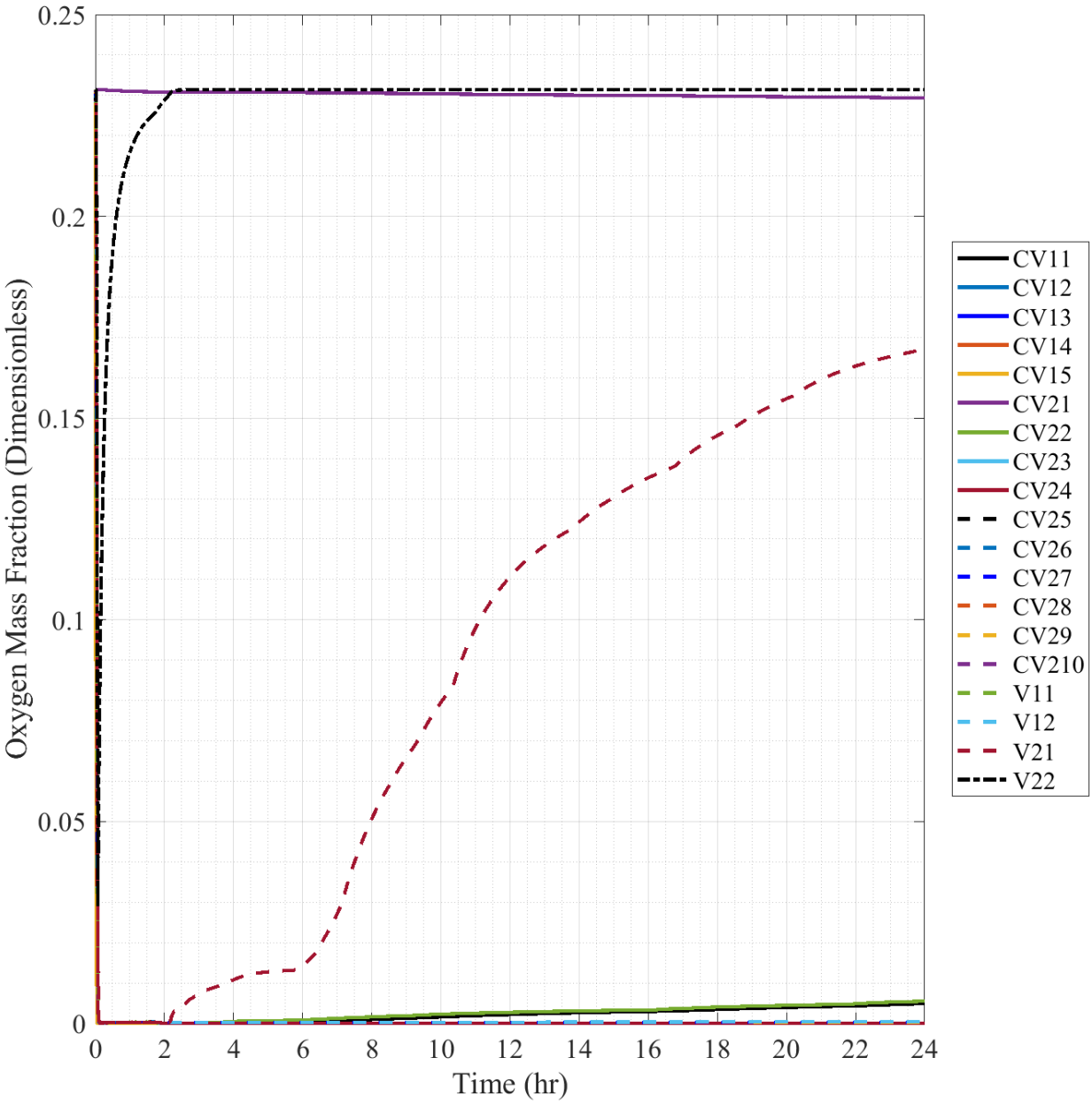

Fig. E.13. Full-Scale Scenario 3 Oxygen Mass Fraction.

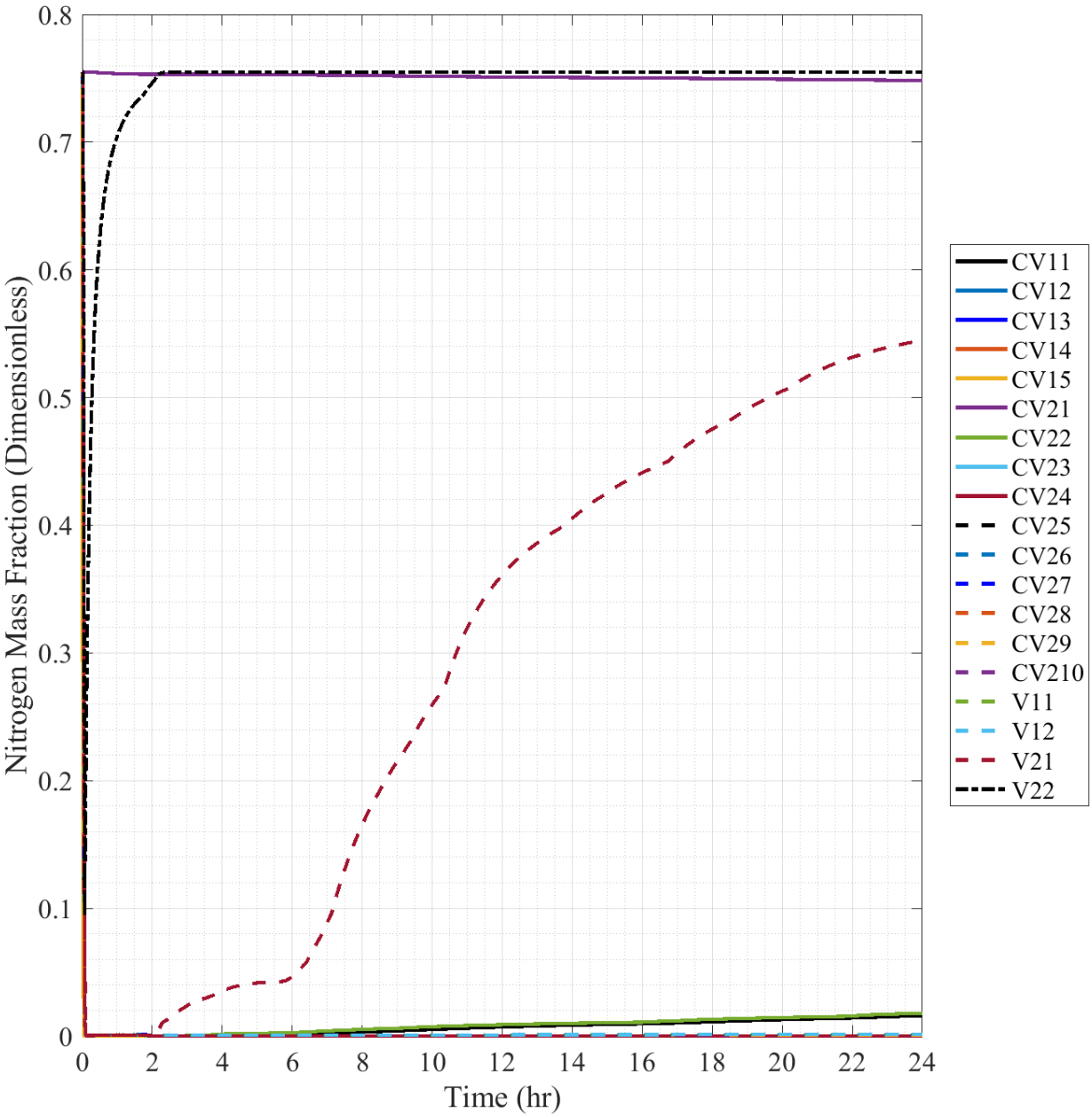

Fig. E.14. Full-Scale Scenario 3 Nitrogen Mass Fraction.

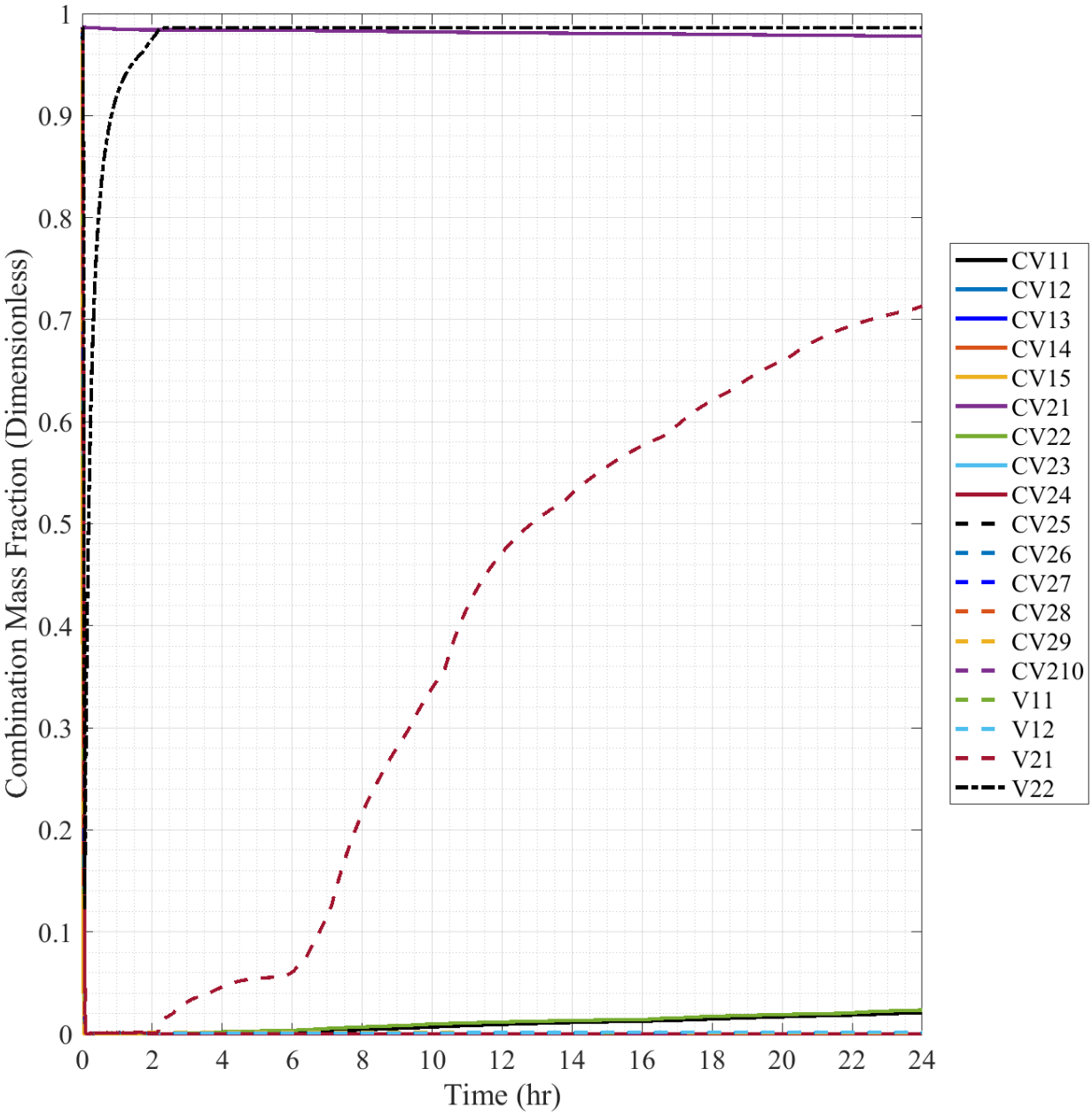

Fig. E.15. Full-Scale Scenario 3 Combination Mass Fraction, Individual Data.

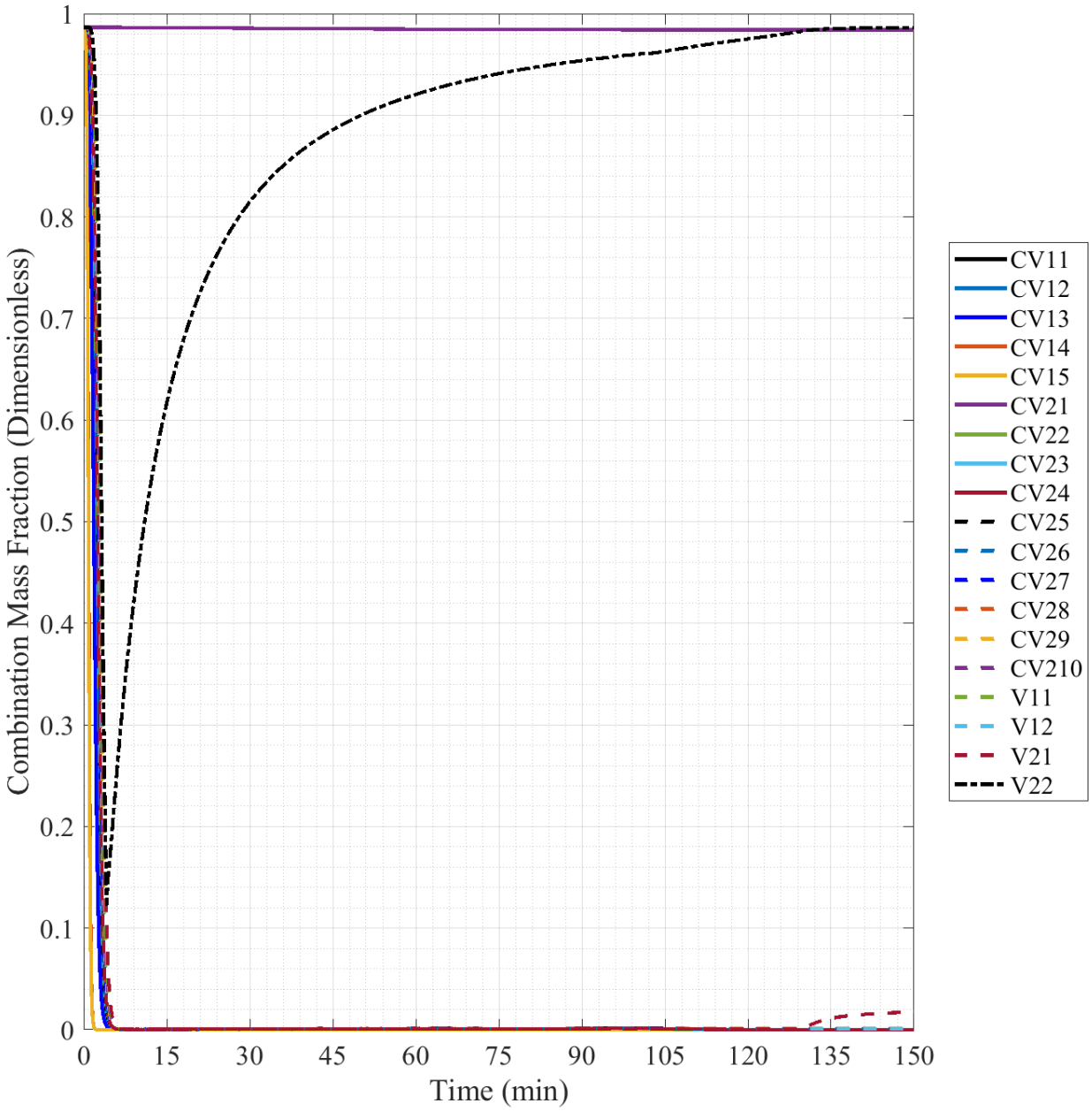

Fig. E.16. Full-Scale Scenario 3 Combination Mass Fraction, 150 minute Timescale, Individual Data.

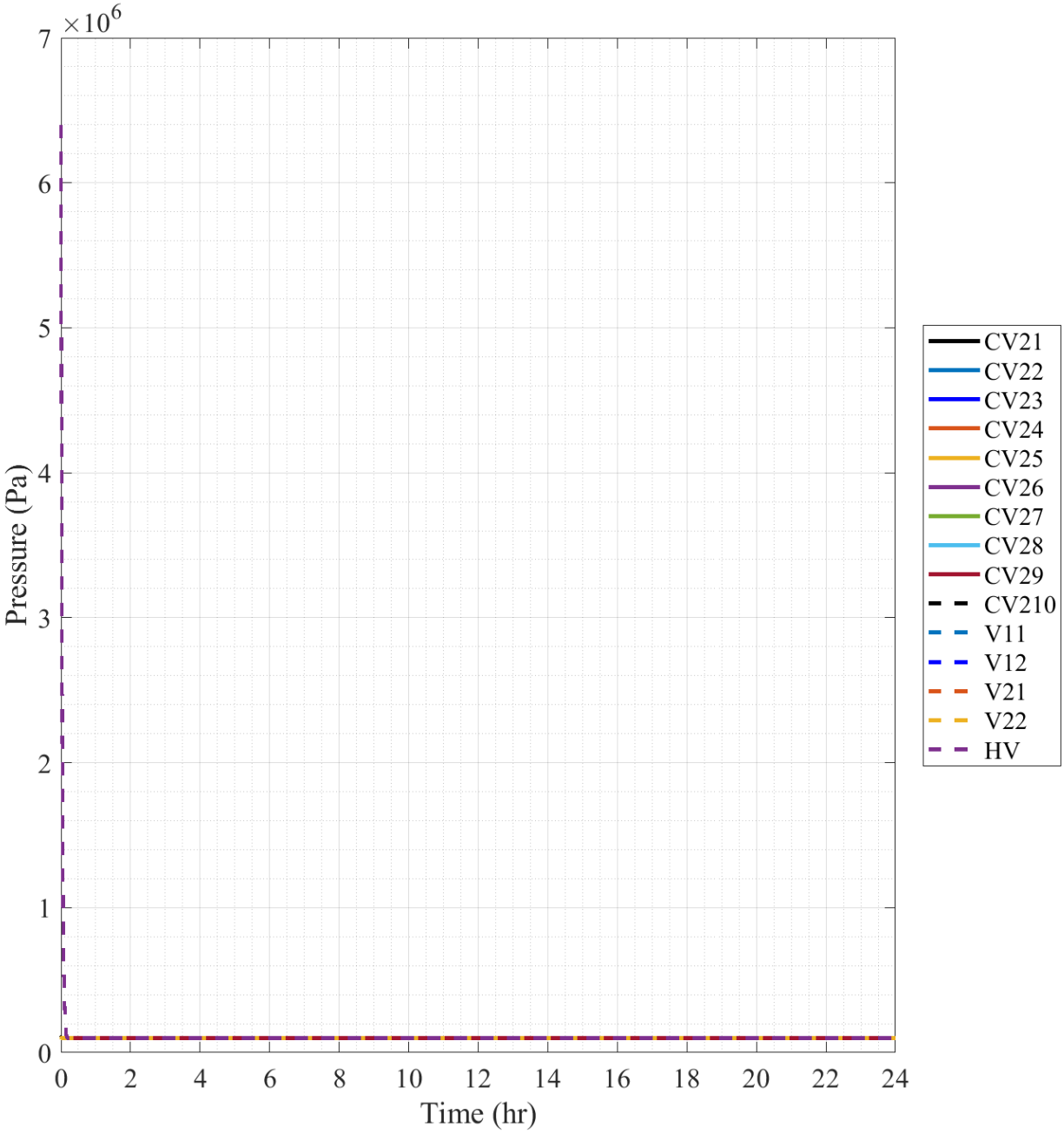

Fig. E.17. Full-Scale Scenario 4 Pressure.

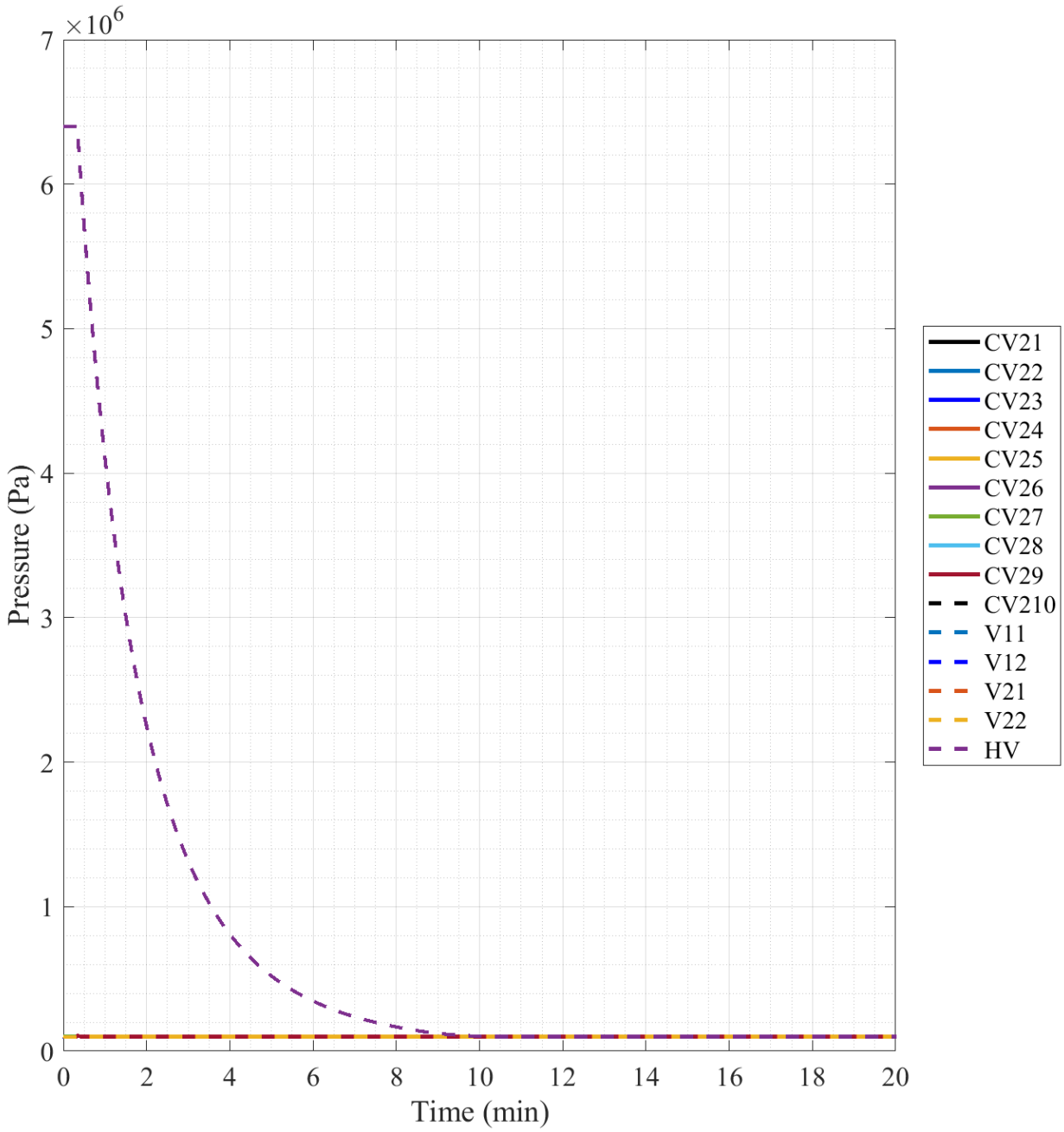

Fig. E.18. Full-Scale Scenario 4 Pressure, 20 minute Timescale.

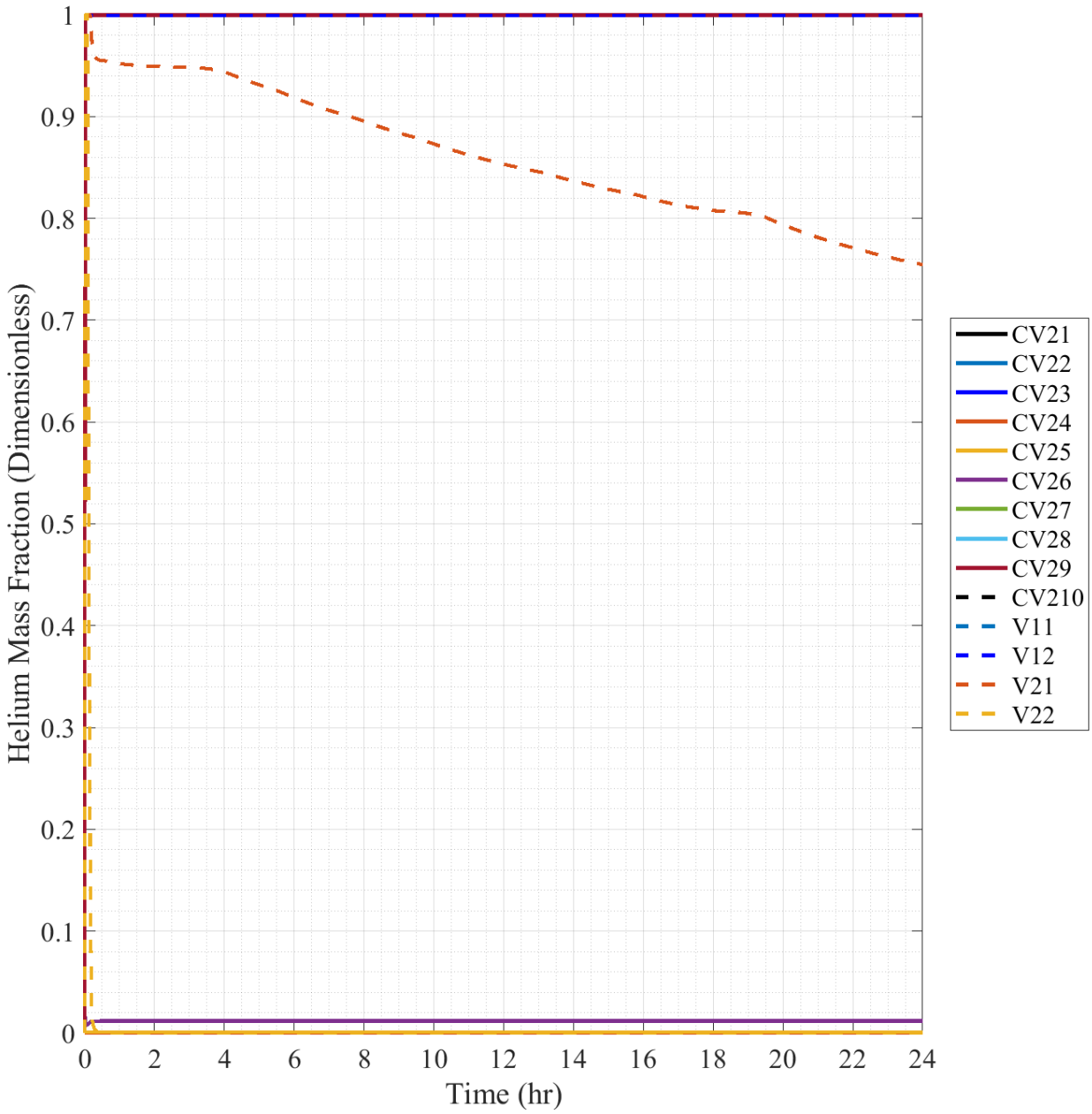

Fig. E.19. Full-Scale Scenario 4 Helium Mass Fraction, Individual Data.

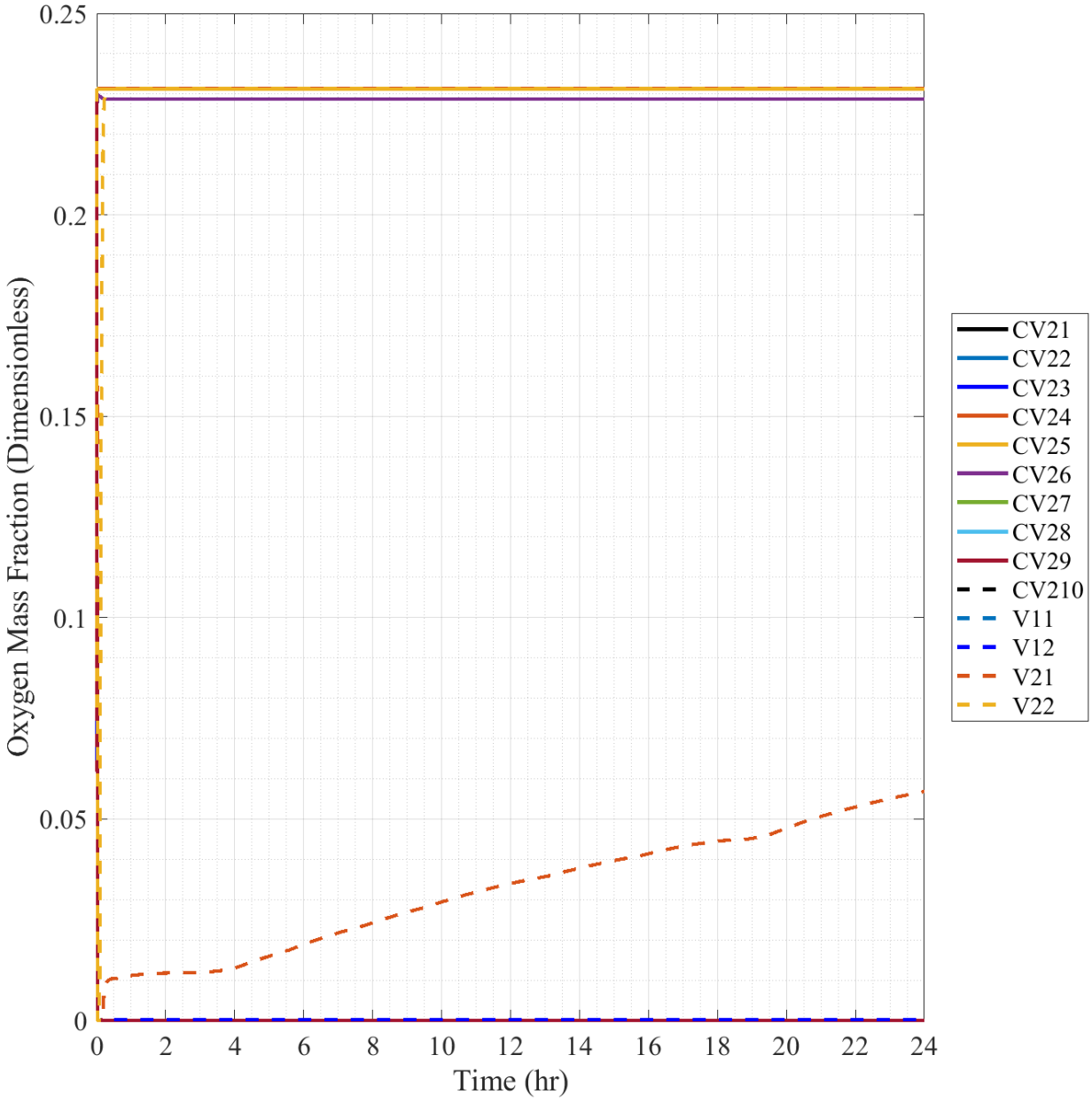

Fig. E.20. Full-Scale Scenario 4 Oxygen Mass Fraction.

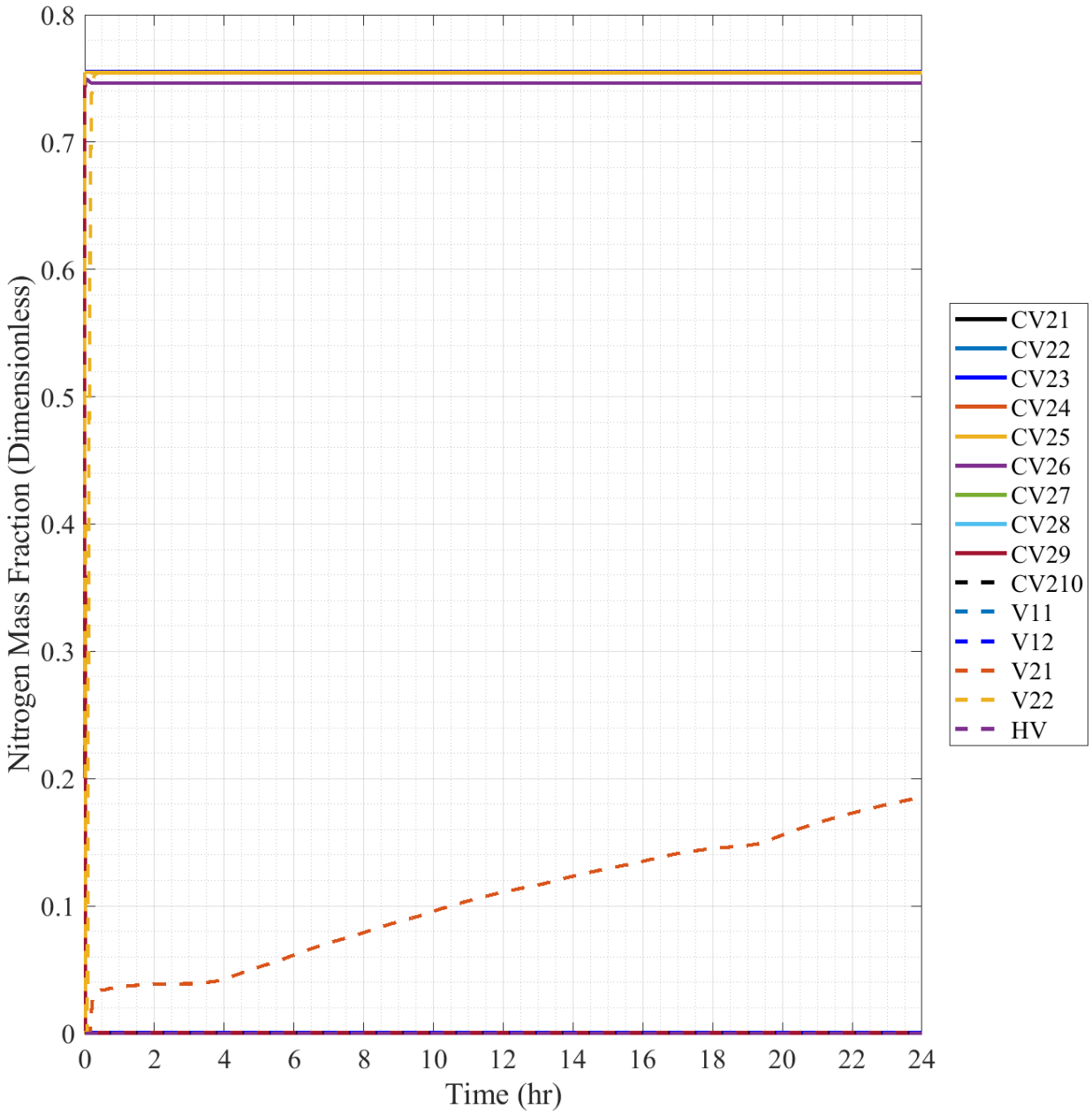

Fig. E.21. Full-Scale Scenario 4 Nitrogen Mass Fraction.

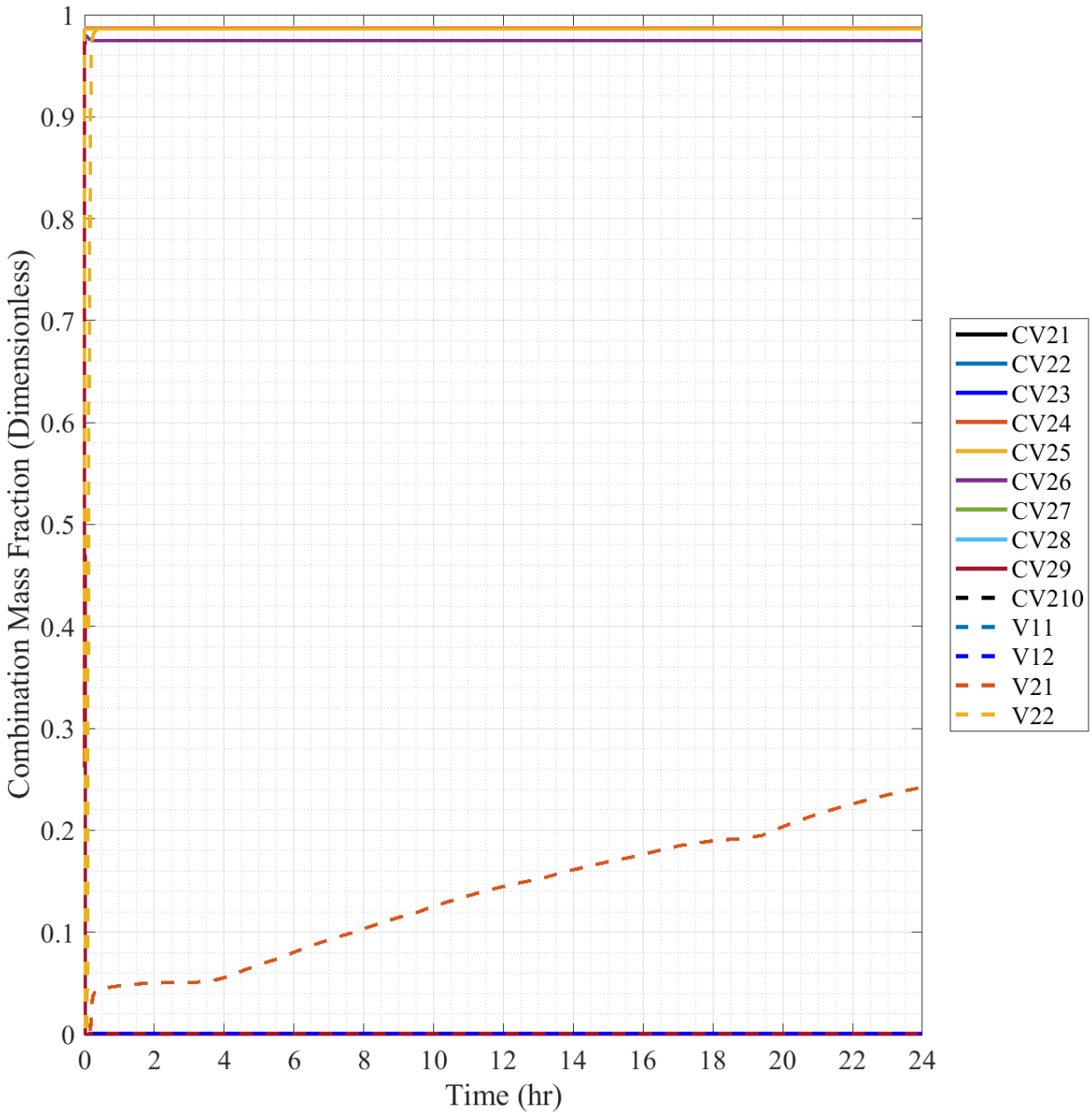

Fig. E.22. Full-Scale Scenario 4 Combination Mass Fraction, Individual Data.

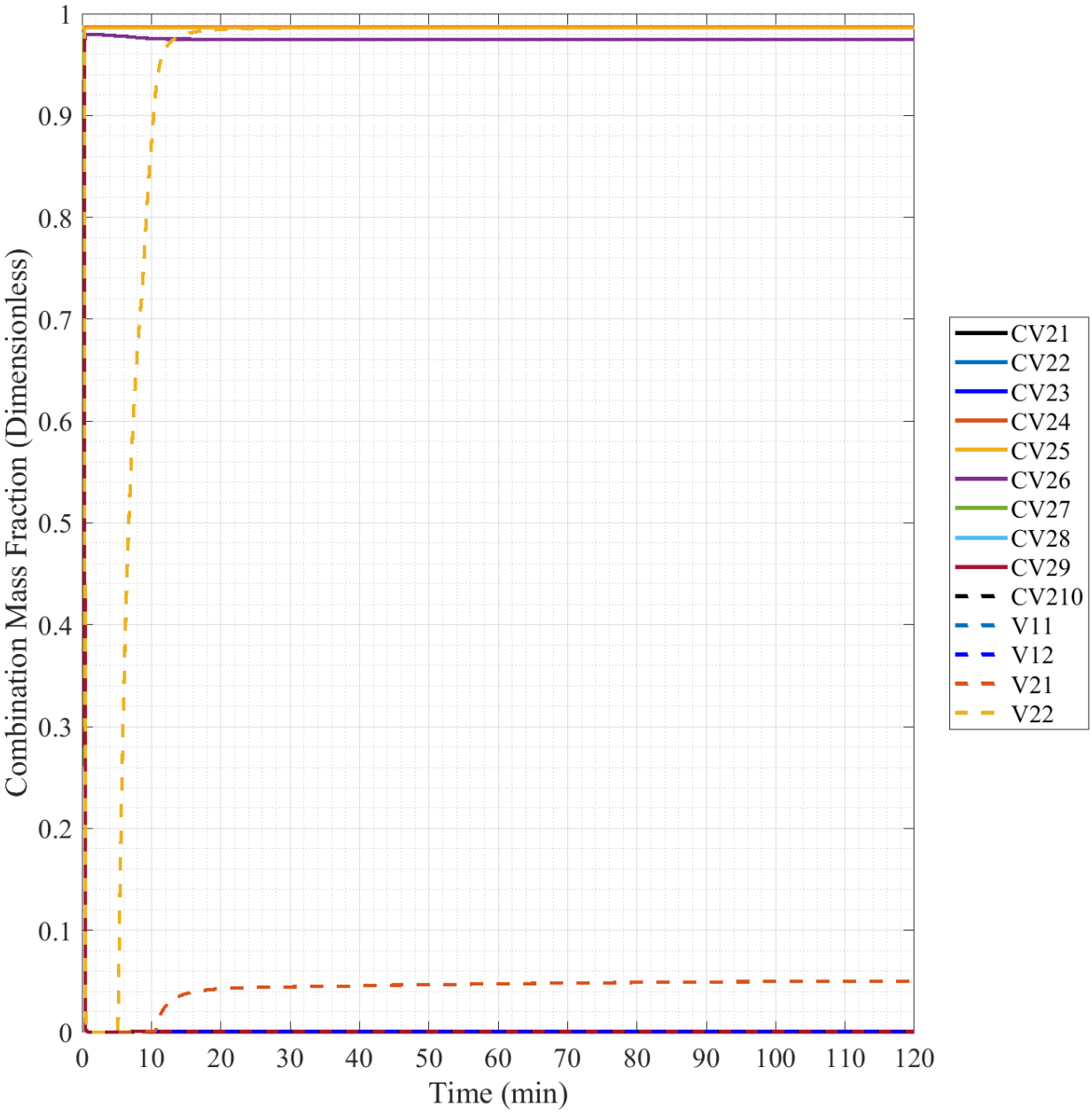

Fig. E.23. Full-Scale Scenario 4 Combination Mass Fraction, 120 minute Timescale, Individual Data.

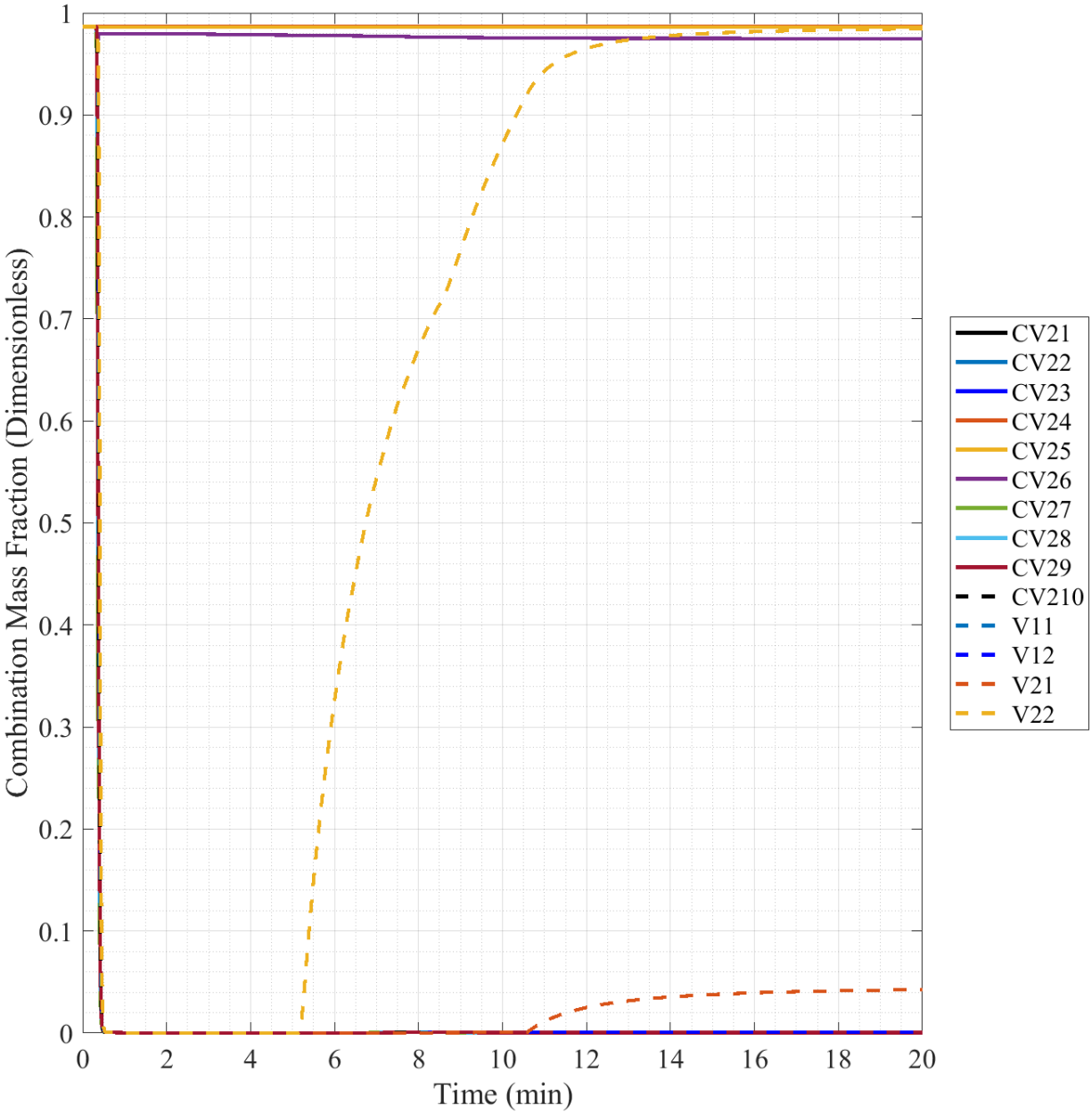

Fig. E.24. Full-Scale Scenario 4 Combination Mass Fraction, 20 minute Timescale, Individual Data.

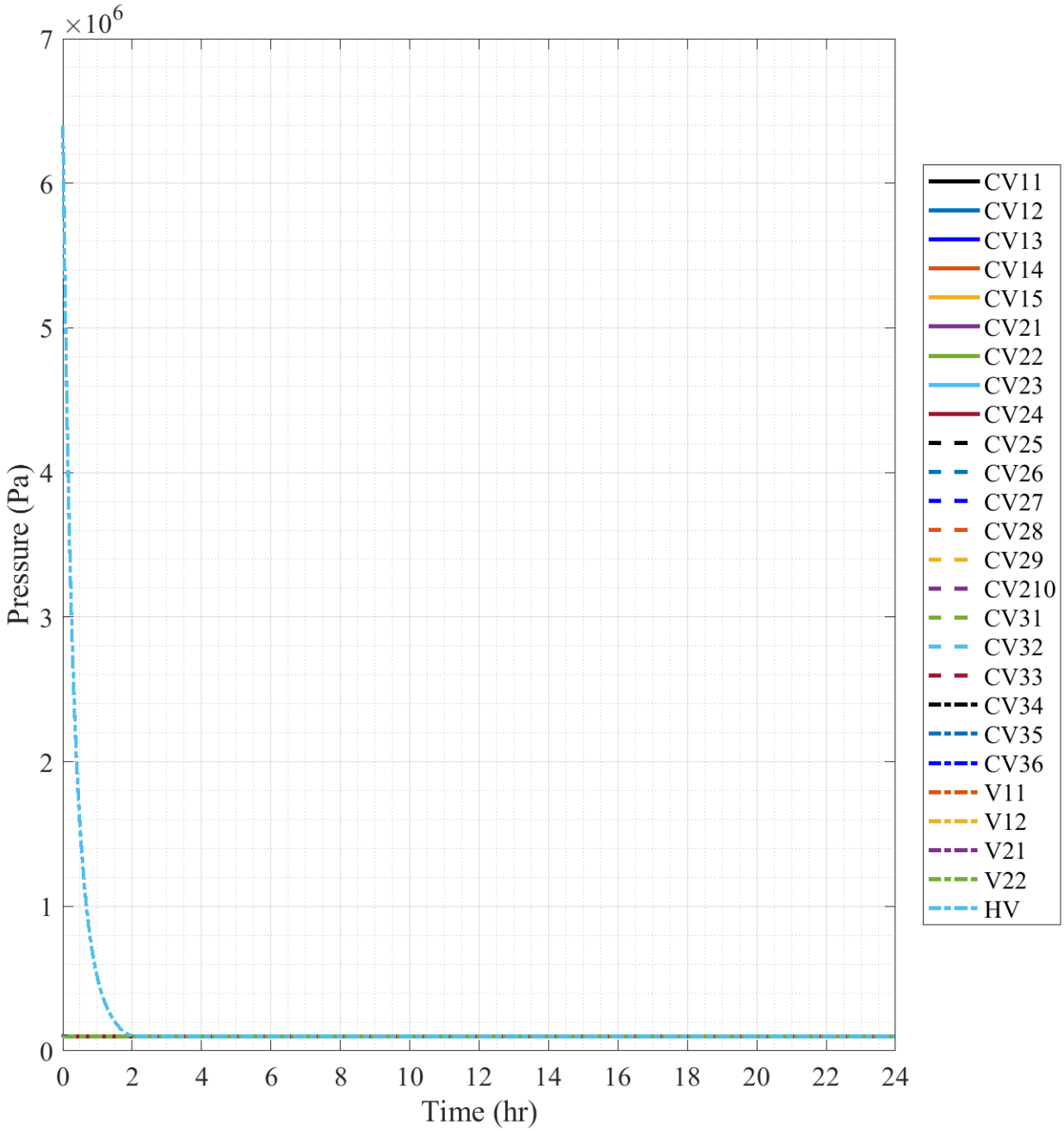

Fig. E.25. Full-Scale Scenario 5 Pressure.

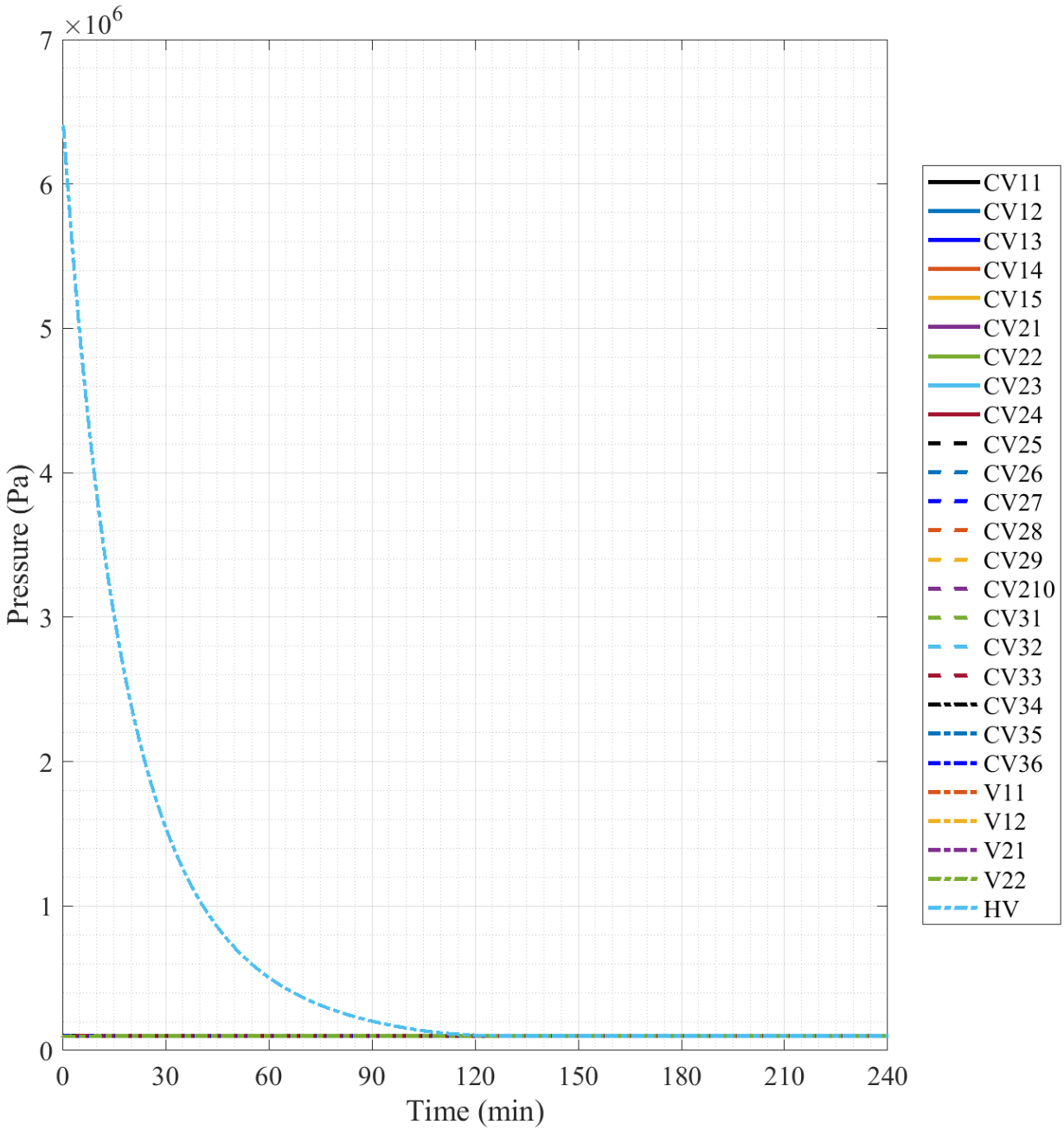

Fig. E.26. Full-Scale Scenario 5 Pressure, 240 minute Timescale.

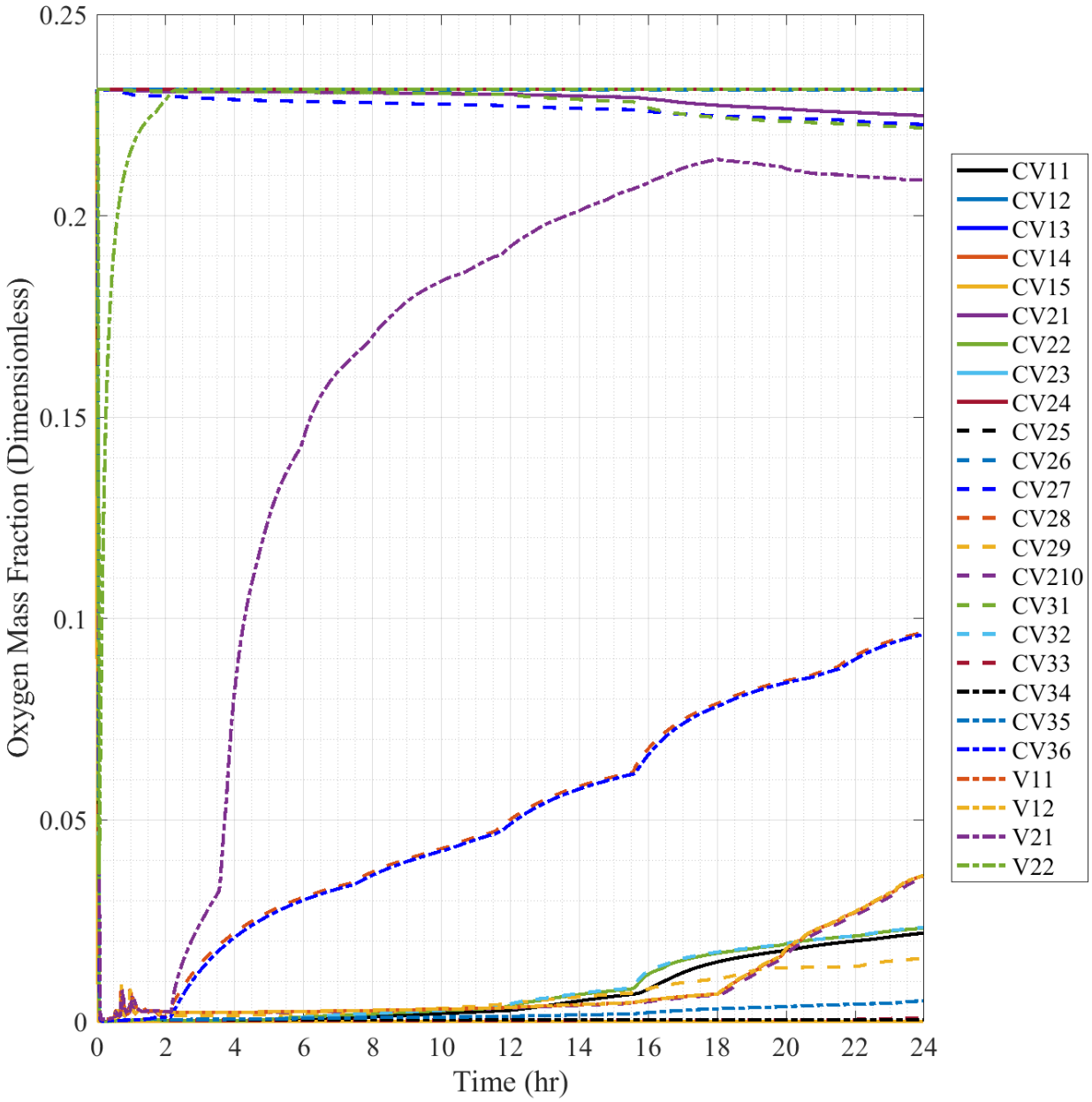

Fig. E.27. Full-Scale Scenario 5 Oxygen Mass Fraction.

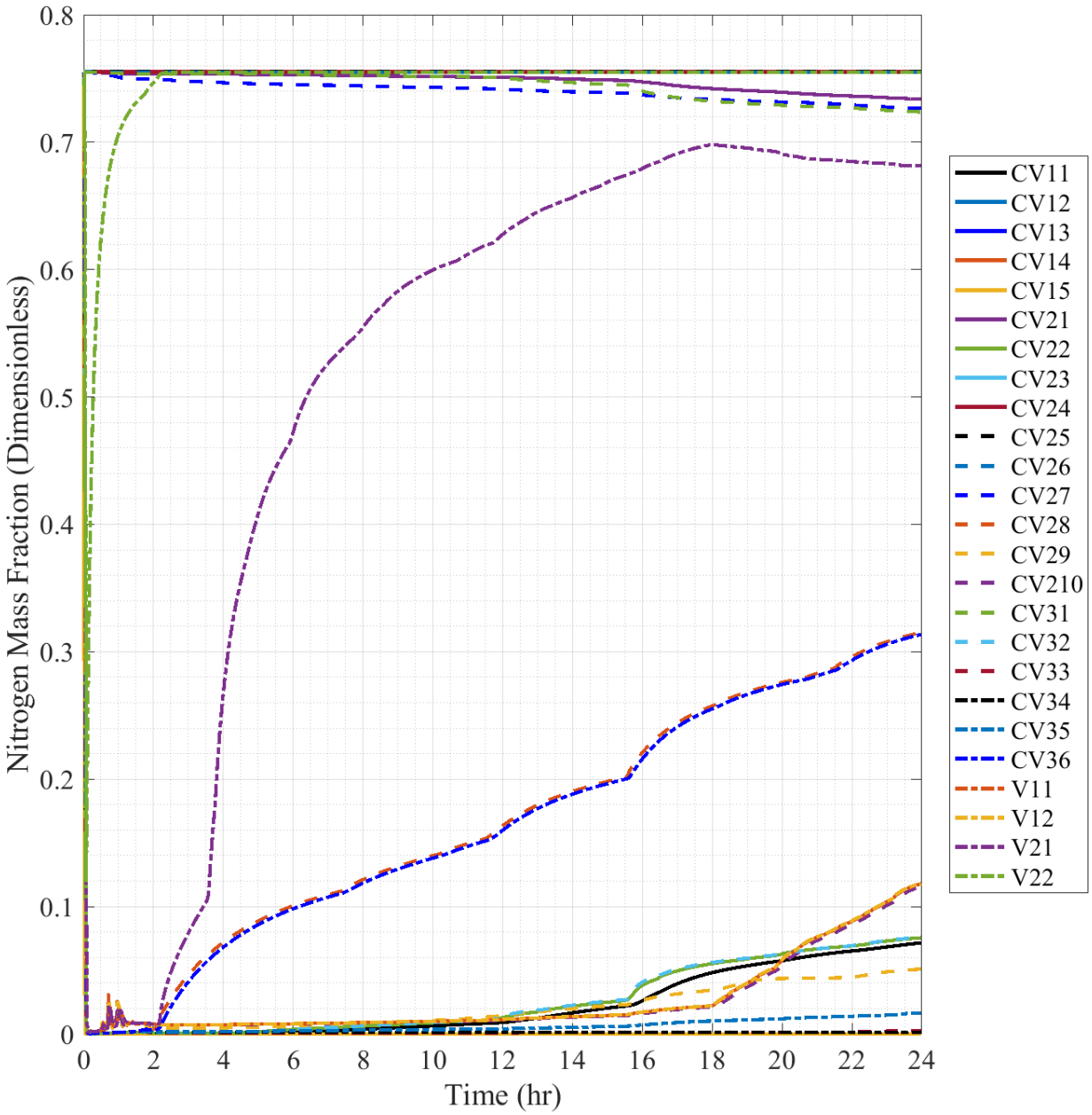

Fig. E.28. Full-Scale Scenario 5 Nitrogen Mass Fraction.

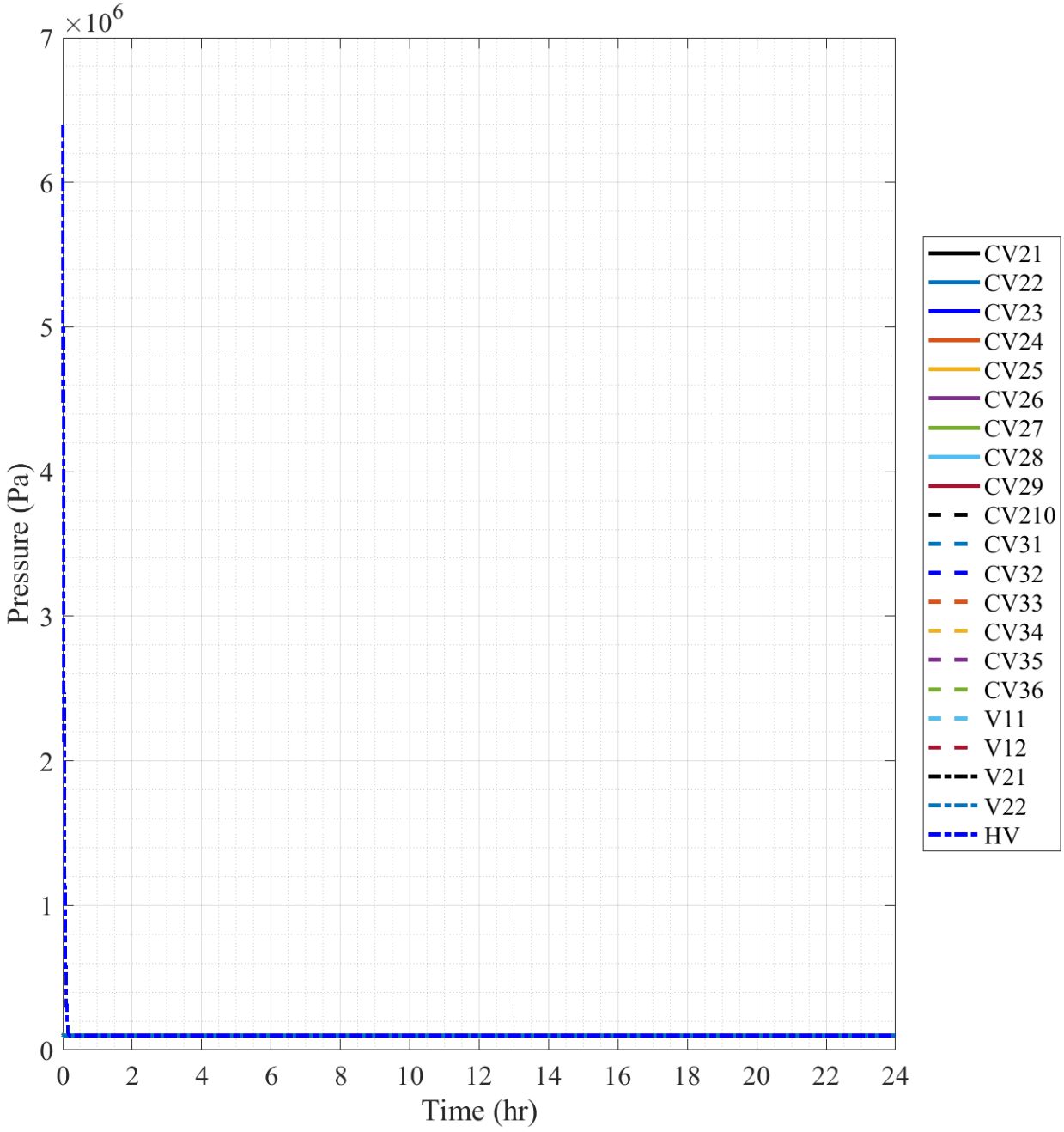

Fig. E.29. Full-Scale Scenario 6 Pressure.

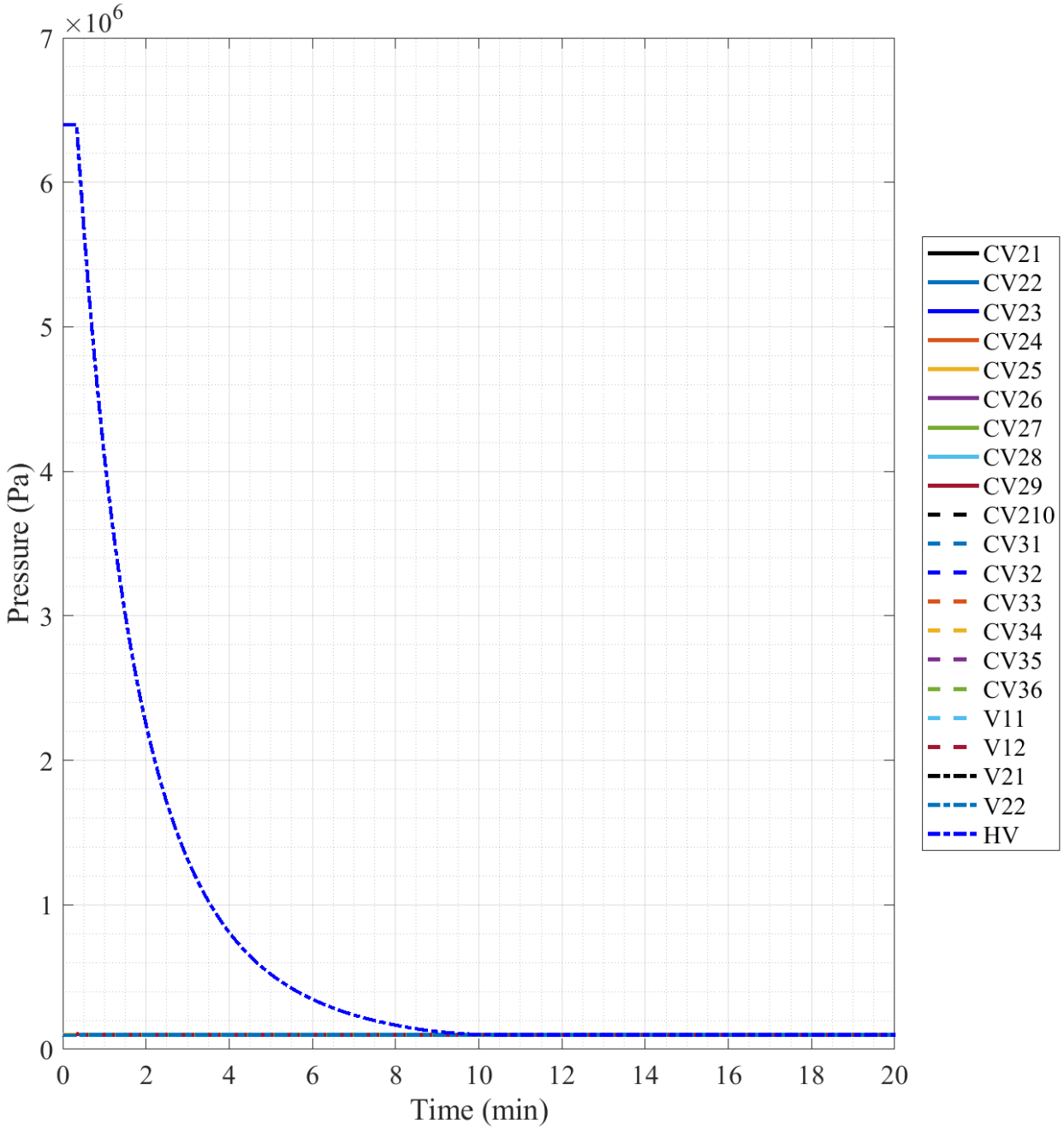

Fig. E.30. Full-Scale Scenario 6 Pressure, 20 minute Timescale.

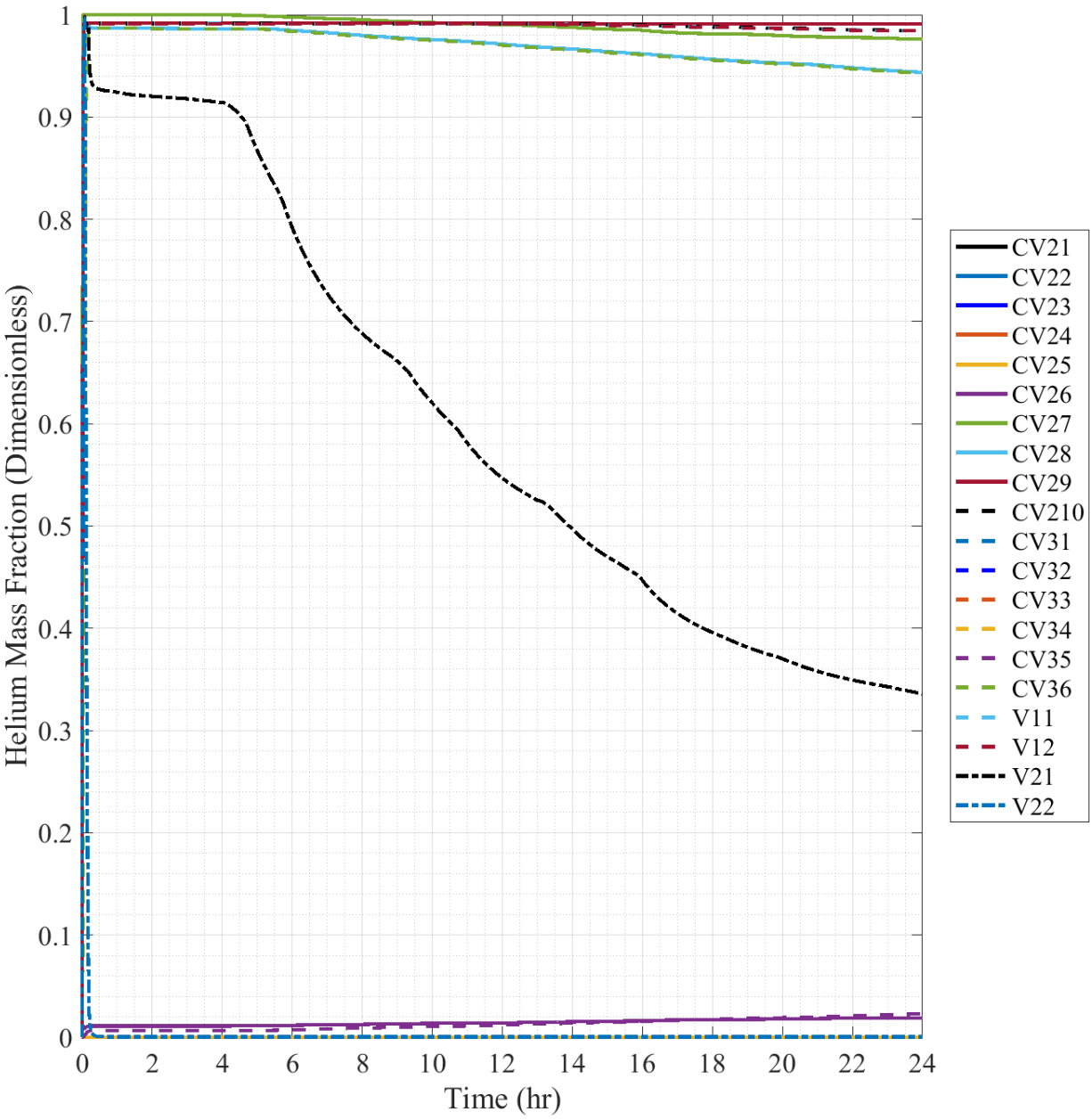

Fig. E.31. Full-Scale Scenario 6 Helium Mass Fraction, Individual Data.

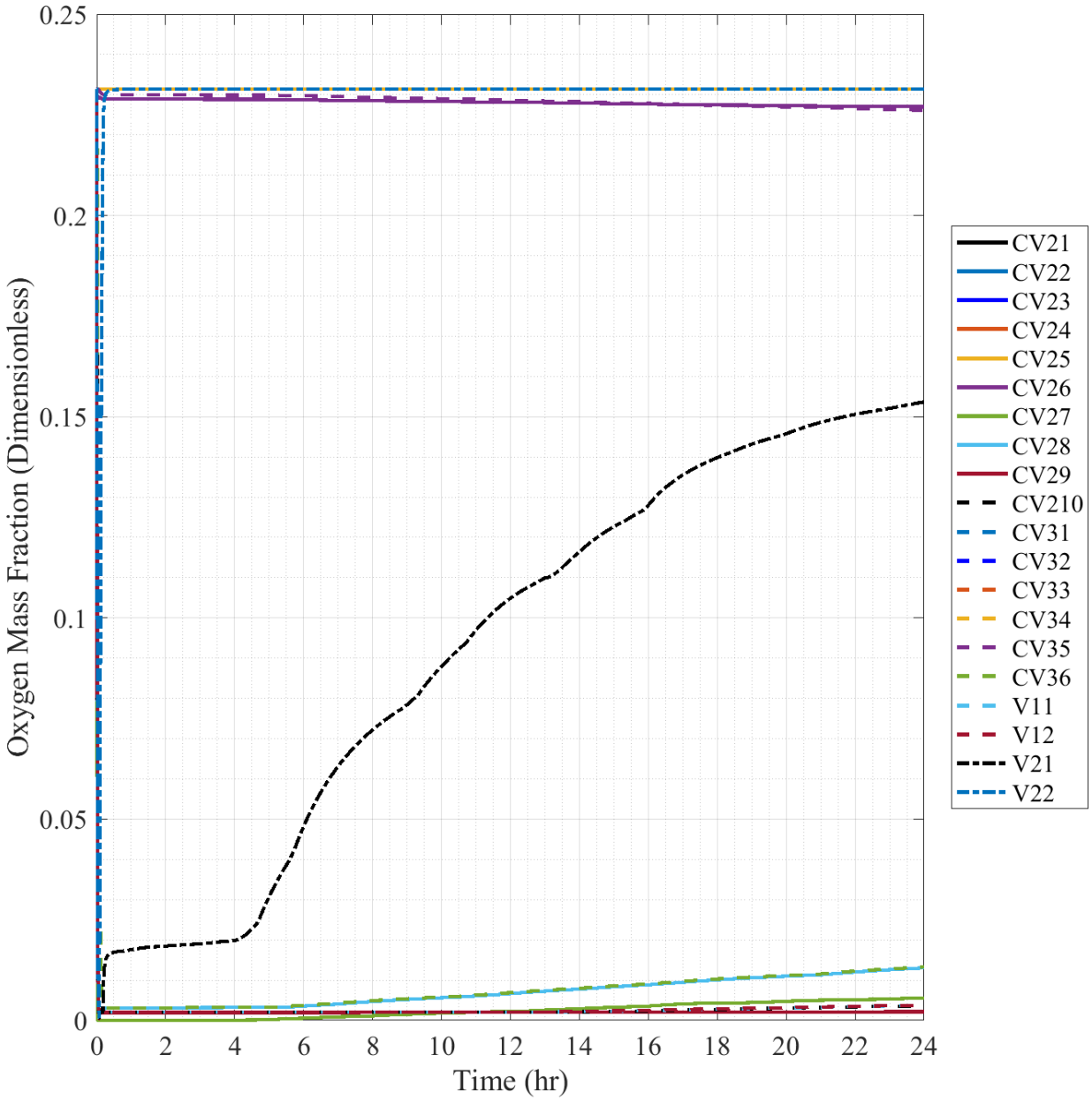

Fig. E.32. Full-Scale Scenario 6 Oxygen Mass Fraction.

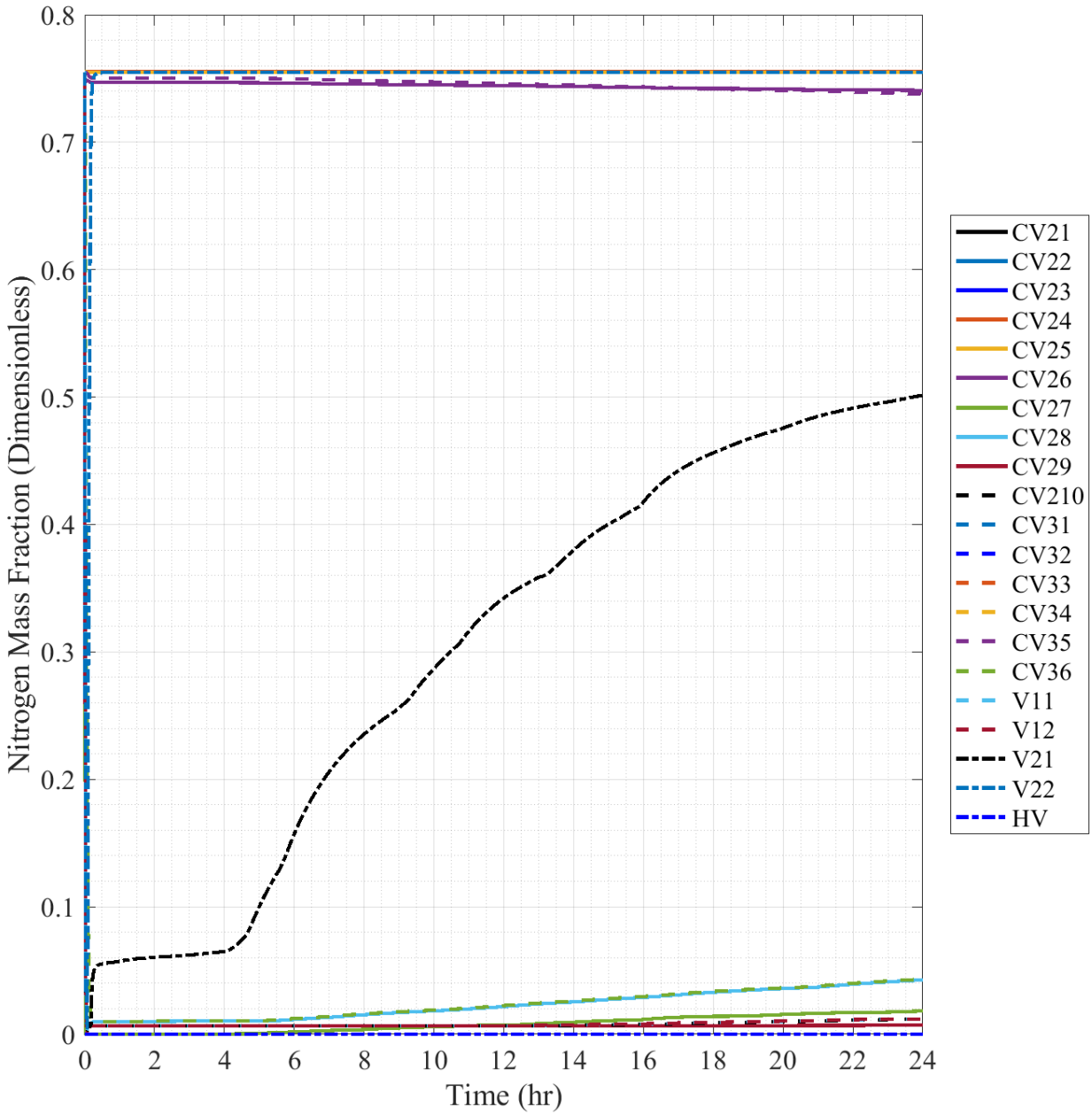

Fig. E.33. Full-Scale Scenario 6 Nitrogen Mass Fraction.

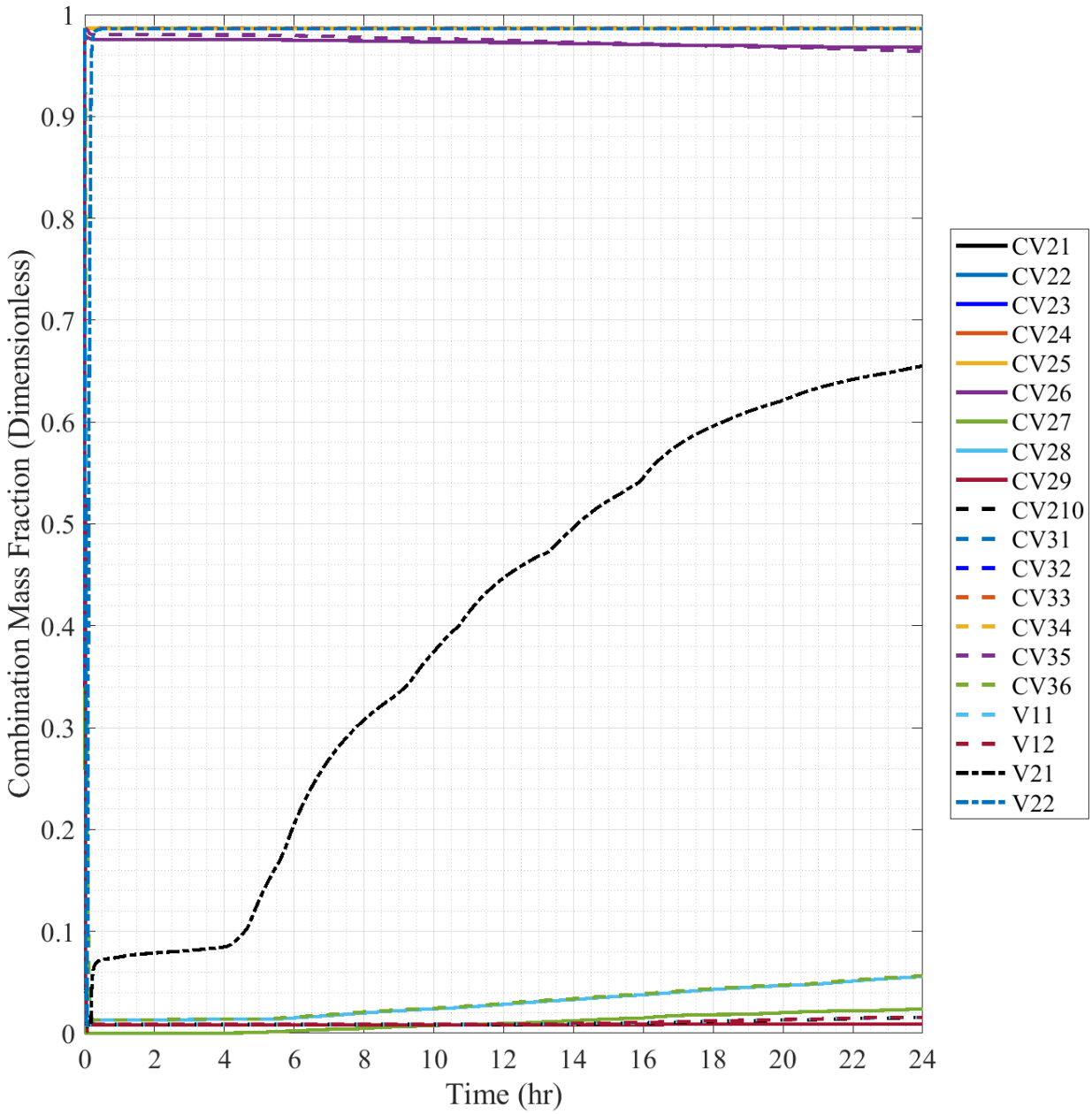

Fig. E.34. Full-Scale Scenario 6 Combination Mass Fraction, Individual Data.